FOSSIL ENERGY

DOE/BC/14896-24
(OSTI ID: 788089)

GEOLOGICAL AND PETROPHYSICAL CHARACTERIZATION OF THE FERRON SANDSTONE FOR 3-D SIMULATION OF A FLUVIAL-DELTAIC RESERVOIR

Final Report
September 29, 1993-September 28, 1996

By:
Thomas C. Chidsey, Jr.

Date Published: October 2001

Work Performed Under Contract No. DE-AC22-93BC14896

Utah Geological Survey
Salt Lake City, Utah

National Energy Technology Laboratory
National Petroleum Technology Office
U.S. DEPARTMENT OF ENERGY
Tulsa, Oklahoma

DISCLAIMER

This report was prepared as an account of work sponsored by an agency of the United States Government. Neither the United States Government nor any agency thereof, nor any of their employees, makes any warranty, expressed or implied, or assumes any legal liability or responsibility for the accuracy, completeness, or usefulness of any information, apparatus, product, or process disclosed, or represents that its use would not infringe privately owned rights. Reference herein to any specific commercial product, process, or service by trade name, trademark, manufacturer, or otherwise does not necessarily constitute or imply its endorsement, recommendation, or favoring by the United States Government or any agency thereof. The views and opinions of authors expressed herein do not necessarily state or reflect those of the United States Government.

This report has been reproduced directly from the best available copy.

DOE/BC/14896-24
Distribution Category UC-122

Geological and Petrophysical Characterization of the Ferron Sandstone for 3-D Simulation of a Fluvial-Deltaic Reservoir

By
Thomas J. Chidsey, Jr.

October 2001

Work Performed Under DE-AC22-93BC14896

Prepared for
U.S. Department of Energy
Assistant Secretary for Fossil Energy

Robert Lemmon, Project Manager
National Petroleum Technology Office
P.O. Box 3628
Tulsa, OK 74101

Prepared by
Utah Geological Survey
P.O. Box 146100
Salt Lake City, UT 84114-6100

CONTENTS

ABSTRACT xxix

EXECUTIVE SUMMARY xxxi

ACKNOWLEDGMENTS xxxv

CHAPTER I - INTRODUCTION 1-1
Introduction 1-1
Purpose and Objectives 1-3
Approach 1-4
Synopsis of Ferron Stratigraphy and Depositional History 1-5
Paleogeography 1-5
Ferron Architecture 1-8
Parasequences and Parasequence Sets 1-8

CHAPTER II - PREVIOUS STUDIES 2-1
Stratigraphy 2-1
Early Studies of the Ferron 2-1
Regional Stratigraphy 2-5
Paleogeography 2-6
Study of the Ferron Accelerates 2-6
Ferron Deltas 2-10
Details Emerge 2-17
Ferron Reservoir Analogs and Sequence Stratigraphy 2-27
Sequence Boundaries and the Introduction of Chaos into Ferron Stratigraphy 2-36
Coal in the Ferron 2-39
Petroleum in the Ferron 2-44
Coalbed Methane Development in the Ferron Sandstone 2-45

CHAPTER III - FACIES OF THE FERRON SANDSTONE 3-1
Introduction 3-1
Offshore-Marine Deposits 3-1
Shelf Sand Deposits 3-1
Shoreline Deposits 3-2
Wave-Dominated Shorelines 3-5
Shoreface 3-5
Transition zone 3-5
Lower shoreface 3-6

Middle shoreface 3-6
Upper shoreface 3-6
Foreshore 3-9
Tidal Inlet 3-11
Distribution of Wave-Dominated Deposits 3-12
Fluvial-Dominated Delta 3-15
General Characteristics 3-15
Distribution of Fluvial-Dominated Deltaic Deposits 3-18
Wave-Modified Delta -- Intermediate Shoreline Types 3-19
General Characteristics 3-19
Distribution of Wave-Modified Deltaic Deposits 3-20
Bay and Lagoon 3-20
Marsh and Swamp 3-24
General Characteristics 3-24
Dynamics of Peat Accumulation 3-25
Coalbeds and Coal Zones 3-26
Alluvial Plain 3-26
Channel Belt 3-26
Overbank Deposits 3-30

CHAPTER IV - REGIONAL STRATIGRAPHY
OF THE FERRON SANDSTONE 4-1
Hierarchy of Stratigraphic Units 4-1
Introduction 4-1
Sequences 4-1
Parasequence Sets 4-1
Parasequences 4-2
Bedsets 4-2
Hierarchical Scheme 4-6
Landward Pinchouts 4-9
Parasequences and Bedsets 4-9
Approach and Terminology 4-9
Kf-Last Chance 4-14
Kf-1 4-15
Kf-1-Limestone Cliffs 4-15
Kf-1-Mussentuchit 4-16
Kf-1-Indian Canyon-a 4-16
Kf-1-Indian Canyon-b 4-17
Kf-1-Indian Canyon-c 4-18
Kf-1-Ivie Creek 4-18
Kf-1-Cowboy Canyon 4-19

Kf-2 4-19
Kf-2-Ivie Creek-a 4-21
Kf-2-Ivie Creek-b 4-21
Kf-2-Ivie Creek-c 4-21
Kf-2-Miller Canyon-a 4-22
Kf-2-Miller Canyon-b 4-24
Kf-2-Muddy Canyon-a 4-25
Kf-2-Muddy Canyon-b 4-25
Kf-2-Dry Wash 4-26
Kf-2-Rochester 4-26
Kf-2-Molen Seep Wash 4-26
Kf-3 4-28
Kf-3-Molen Amphitheater 4-28
Kf-3-Molen Reef 4-29
Kf-4 4-30
Kf-4-Miller Canyon 4-30
Kf-4-Molen Reef 4-30
Kf-5 4-33
Kf-6 4-33
Kf-7 4-34
Kf-8 4-35
Analysis 4-35
Applicability of Sequence Stratigraphic Terminology 4-35
Progradation Styles 4-38
Regional Reservoirs 4-38

CHAPTER V - GEOLOGIC FRAMEWORK OF
WILLOW SPRINGS WASH CASE-STUDY AREA 5-1
Introduction 5-1
Location of the Case-Study Area 5-2
Regional Setting 5-2
Methods 5-2
Lithofacies 5-6
Lithofacies 1: Interbedded Siltstone and Shale 5-6
Lithofacies 2: Hummocky Cross-Stratified Sandstone and Siltstone 5-6
Lithofacies 3: Inclined, Medium-Bedded, Planar-Laminated Sandstone 5-8
Lithofacies 4: Thick-Bedded, Trough and Tabular Cross-Stratified Sandstone
. 5-8
Lithofacies 5: Thick-Bedded, Inclined Planar-Laminated Sandstone 5-9
Lithofacies 6: Sigmoidal-Bedded, Cross-Stratified Sandstone 5-9
Lithofacies 7: Shale with Interbedded Sandstone 5-11

Lithofacies 8: *En Echelon* Sandstone Bedsets and Interbedded Shales 5-11
Lithofacies 9: Multistory, Lensoidal Sandstone 5-12
Lithofacies 10: Multilateral, Lensoidal Sandstone 5-12
Lithofacies 11: Planar-Bedded, Cross-Stratified Sandstone and Siltstone 5-14
Depositional Systems 5-14
Sequence Stratigraphy 5-15
Depositional History 5-16
Kf-1-Indian Canyon-a 5-16
Kf-1-Indian Canyon-b 5-21
Kf-1-Indian Canyon-c 5-21
Stage 1. Barrier-tidal inlet 5-21
Stage 2. Wave-dominated shoreline 5-21
Stage 3. Strand plain 5-24
Stage 4. Interdistributary bay 5-24
Stage 5. Crevasse splay-minor mouth bar 5-24
Stage 6. Distributary channel 5-27
Discussion 5-27
Variations in Depositional Models 5-27
Barred and non-barred shoreline models 5-28
Ebb-tidal delta model 5-28
Sequence Stratigraphic Implications 5-30
Reservoir Quality 5-31
Conclusions 5-32

CHAPTER VI - GEOLOGIC FRAMEWORK OF
MUDDY CREEK CANYON CASE-STUDY AREA 6-1
Introduction 6-1
Location 6-1
Methods 6-5
Facies of Kf-2 in Muddy Creek Canyon 6-5
Kf-2-Miller Canyon-a 6-5
Kf-2-Miller Canyon-b 6-11
Kf-2-Muddy Canyon-a 6-11
Kf-2-Muddy Canyon-b 6-11
Stratigraphy and Depositional History of Kf-2 in Muddy Creek Canyon 6-38
Kf-2-Miller Canyon-a 6-38
Kf-2-Miller Canyon-b 6-45
Kf-2-Muddy Canyon-a 6-53
Kf-2-Muddy Canyon-b 6-63

CHAPTER VII - GEOLOGIC FRAMEWORK OF
IVIE CREEK CASE-STUDY AREA 7-1
Introduction 7-1
Location 7-2
Methods 7-2
Field methods 7-3
Drill-hole program 7-3
Surface elevation and isopach maps 7-4
Stratigraphy 7-4
Kf-1-Iv[a] Bedset 7-6
Subcycle definition 7-9
Clinoform definition 7-9
Bounding layer definition 7-10
Clinoform characteristics 7-11
Characteristics of clinoform bounding layers 7-12
Kf-1-Iv[c] Bedset 7-16
Kf-2-Iv-a Parasequence 7-17
Kf-2-Iv-b Parasequence 7-18
Kf-2-Iv-c Parasequence 7-18
Facies 7-19
Distributary Complex 7-19
Distributary Channel 7-19
Distributary-Mouth Bar 7-22
Clinoform Facies 7-22
Clinoform proximal (cp) 7-22
Clinoform medial (cm) 7-23
Clinoform distal (cd) 7-23
Clinoform cap (cc) 7-23
Brackish-Water Bay/Bay Fill 7-25
Coastal Plain/Swamp 7-25
Transgressive 7-25
Shoreface 7-25
Lower shoreface 7-27
Middle shoreface 7-27
Upper shoreface 7-27
Foreshore 7-27
Paleogeography and Depositional Processes 7-29
Kf-1-Iv[a] Bedset 7-29
Kf-1-Iv[c] Bedset 7-36
Kf-2-Iv-a Parasequence 7-37
Kf-2-Iv-b Parasequence 7-39

Kf-2-Iv-c Parasequence 7-40

CHAPTER VIII - PETROPHYSICAL CHARACTERISTICS
OF THE IVIE CREEK CASE-STUDY AREA 8-1
Introduction 8-1
Mini-Permeameter Measurements 8-1
Methods 8-1
Kf-1-Iv[a] Bedset 8-5
Kf-2 Parasequence Set 8-5
Petrophysics: Overview 8-5
Sampling and Measurements 8-8
Analysis of Ferron Well Logs 8-9
Diagenesis and Porosity of the Ferron Sandstone 8-10
Petrography 8-10
Controls on Porosity: Evidence from Ivie Creek Core Plugs 8-16
Effects of Exhumation on Ferron Porosities 8-17
Secondary Porosity in the Ferron Sandstone 8-19
Velocity of the Ferron Sandstone 8-21
Controls on Velocity: Evidence from Ivie Creek Core Plugs 8-21
Effects of Exhumation on Ferron Velocities 8-23
Do Velocity Logs See Secondary Porosity? 8-25
Permeability of the Ferron Sandstone 8-26
Controls on Permeability: Evidence from Ivie Creek Core Plugs 8-26
Effects of Exhumation and Outcrop Exposure on Ferron Permeability 8-27
Permeability Anisotropy 8-28
Implications for Estimating Amount of Exhumation from
Velocity or Porosity Changes with Depth 8-29
Conclusions 8-30

CHAPTER IX - STATISTICAL ANALYSIS,
IVIE CREEK CASE-STUDY AREA 9-1
Introduction 9-1
Characterization of Geology and Permeability 9-2
Methods 9-2
Kf-1-Iv[a] Bedset Geologic Summary 9-4
Kf-2 Parasequence Set Geologic Summary 9-12
Permeability Summary 9-17
Kf-1-Iv[a] Bedset Permeability Analysis 9-17
Kf-2 Parasequence Set Permeability Analysis 9-19
Controls on Permeability 9-26
Kf-1-Iv[a] Bedset vs. Kf-2 Parasequences: Comparison of Characteristics 9-31

Conclusions 9-34

CHAPTER X - RESERVOIR MODELING AND FLUID-FLOW SIMULATION, IVIE CREEK CASE-STUDY AREA 10-1
Introduction 10-1
Two-Dimensional Modeling 10-4
Developing a Gridded Architecture Model 10-4
Distributing Permeability Within Clinoforms 10-8
Petrophysical Models Used for Flow Simulation 10-13
Two-Dimensional Flow Simulation Studies 10-15
Permeability Upscaling (Homogenization) 10-22
Summary and Conclusions 10-25
Three-Dimensional Modeling 10-27
Model Domain 10-27
Production Strategies and Wellbore Configurations 10-27
Physical Properties 10-27
Initial Conditions 10-27
Absolute Permeability 10-29
Porosity 10-33
Relative Permeability 10-33
Fluid Properties 10-34
Three-Dimensional Flow Simulation Results 10-34
Discussion 10-41
Quantitative Comparison of 3-D Simulation Results 10-41
Comparing 2-D and 3-D Simulation Results 10-46
Conclusions 10-46
Recommendations 10-50
Implications of Reservoir Analog Modeling Results for Oil Reservoir Exploration and Development 10-51
Spacing of Vertical Wells 10-52
Viability of Horizontal Wells 10-52
Oil Recovery Estimates 10-53
Application to Reservoir Studies 10-53
Outcrop-Based Reservoir Analog Studies 10-54

REFERENCES R-1

APPENDIX A - FERRON SANDSTONE STRATIGRAPHIC NOMENCLATURE A-1

APPENDIX B - FIELD METHODS B-1

Digital Measured Sections B-1
Photomosaics B-3
Scaling B-3

APPENDIX C - RESERVOIR MODELING C-1
Estimating the Effect of Bounding Layers on Grid-Block Anisotropy C-1
Step 1 . . . . . C-1
Step 2 . . . . . C-2
Step 3 . . . . . C-2
Step 4 . . . . . C-3
Relative Permeability Relationships: 3-D Modeling C-3
Fluid Properties C-4
Fluid Compressibility, Density, and Viscosity C-4
Pressure-Volume-Temperature Data C-5
Oil and Water Formation Volume Factors vs Pressure C-5
3-D Gridded Data Set C-6

FIGURES

Figure 1-1. Location map of the Ferron Sandstone project area 1-1
Figure 1-2. Diagrammatic cross sections of Cretaceous stratigraphy and Ferron parasequence sets 1-2
Figure 1-3. Paleogeography of North America during Early Turonian time 1-5
Figure 1-4. Isopach map of Cenomanian strata 1-5
Figure 1-5. Isopach map of Turonian strata 1-6
Figure 1-6. Isopach map of Coniacian and Santonian strata 1-6
Figure 1-7. Map of Cretaceous outcrops in Utah 1-7
Figure 1-8. Paleogeography of Utah during Early Turonian time 1-7
Figure 1-9. Paleogeography during Middle Turonian time 1-7
Figure 1-10. Paleogeography during Coniacian time 1-7
Figure 2-1. Taft's 1906 map of coal-bearing rocks in Castle Valley 2-2
Figure 2-2. Lupton's 1916 cross section showing Cretaceous stratigraphy in Castle Valley 2-4
Figure 2-3. Lower part of Spieker and Reeside's 1925 cross section of Cretaceous stratigraphy 2-5
Figure 2-4. Paleogeography of the Ferron Sandstone as reconstructed by Spieker and Reeside in 1926 2-7
Figure 2-5. Katich's 1953 reinterpretation of Ferron paleogeography 2-8
Figure 2-6. Hale's 1972 interpretation of early Ferron paleogeography. 2-11
Figure 2-7. Hale's 1972 interpretation of late Ferron paleogeography. 2-12
Figure 2-8. Cotter's 1975 cross section of the Lower Ferron in Castle Valley 2-13
Figure 2-9. Diagram showing the relationship between Lower and Upper Ferron strata 2-14
Figure 2-10. Paleogeography of the Lower Ferron as interpreted by Cotter in 1976 2-15
Figure 2-11. Diagrammatic cross section showing basic facies and style of cyclicity in the Ferron 2-16
Figure 2-12. Interpretion of the Last Chance delta 2-16
Figure 2-13. Early generalized cross section of Ferron delta-front units. 2-18
Figure 2-14. Generalized cross section of Ferron delta-front units 2-18
Figure 2-15. Shoreline sandstone bodies and laterally equivalent coastal-plain and offshore-marine strata constituting parasequences 2-19
Figure 2-16. Comparison of Ferron paleogeography in Utah with the present-day drainage pattern on the eastern flank of the Andes in northern South America 2-20
Figure 2-17. Ternary diagram of the Last Chance delta 2-21
Figure 2-18. Ferron Sandstone outcrop belt in Castle Valley, location of Ferron drill holes and surface sections, and cross section 2-22
Figure 2-19. Reconstruction of Ferron depositional environments 2-23
Figure 2-20. Depositional model of a shelf sand plume off the mouth of the Damietta Branch of the Nile River 2-24

Figure 2-21. Vernal delta and its shelf sand plume 2-25
Figure 2-22. Possible smaller-scale sand plumes
deposited in front of prograding delta lobes 2-26
Figure 2-23. Stratigraphy of the Ferron Sandstone along the Castle Valley outcrops 2-28
Figure 2-24. Facies that occur within the landward pinchout
of Kf-2 near the mouth of Willow Springs Wash 2-29
Figure 2-25. Four sequences in Turonian-Coniacian strata in central Utah 2-31
Figure 2-26. Facies interpretion of Ferron shoreline sandstones 2-32
Figure 2-27. Diagram showing the partitioning of
sediment in various facies tracts of the Ferron 2-33
Figure 2-28. Ferron depositional episodes equated to parasequences within Kf-2 2-35
Figure 2-29. Ferron stratigraphic framework grouped into 11 parasequence sets 2-37
Figure 2-30. Comparison of thickness of the C coal bed and of
laterally equivalent fluvial deposits 2-41
Figure 2-31. Diagrammatic cross section showing
the depositional history of the C coal bed 2-42
Figure 2-32. Relationships between Ferron coals
and shoreline sandstones in the Price area 2-43
Figure 2-33. Association of thick pods of coal and
landward pinchouts of shoreline sandstone units 2-43
Figure 2-34. Location of gas fields productive from the Ferron Sandstone and
net sandstone-thickness map, Wasatch Plateau/Castle Valley 2-44
Figure 2-35. Location of fields producing coalbed methane in east-central Utah and
the Ferron Sandstone coalbed gas “fairway” 2-46
Figure 3-1. Section exposed on Molen Reef between “Molen Point” and Dry Wash 3-2
Figure 3-2. Diagram showing range of shoreline types present in the Ferron Sandstone 3-3
Figure 3-3. Ternary diagram showing the principal forces that shape delta morphology 3-3
Figure 3-4. Shoreline types recognizable in the Ferron 3-4
Figure 3-5. Diagram showing the three basic categories
of shoreline types distinguished in the Ferron 3-4
Figure 3-6. Diagram distinguishing facies and subfacies within a depositional
sequence formed by progradation of a wave-dominated coast 3-5
Figure 3-7. Shoreface sequence of parasequence
Kf-2-Miller Canyon-b, Muddy Creek Canyon 3-5
Figure 3-8. Middle shoreface, parasequence Kf-1-Indian
Canyon-c, Willow Springs Wash case-study area 3-6
Figure 3-9. Swaley cross-stratification, middle shoreface, parasequence
Kf-2-Muddy Canyon-b, Muddy Creek Canyon case-study area 3-6
Figure 3-10. Middle shoreface, parasequence
Kf-1-Indian Canyon-c, Willow Springs Wash case-study area 3-7

Figure 3-11. Middle shoreface, parasequence
Kf-1-Indian Canyon-a, Willow Springs Wash case-study area 3-7
Figure 3-12. Planar lamination, middle shoreface, parasequence
Kf-2-Muddy Canyon-b, Muddy Creek Canyon case-study area 3-8
Figure 3-13. Thalassinoides burrow form in middle shoreface deposit of the Ferron 3-8
Figure 3-14. Upper shoreface, parasequence
Kf-2-Miller Canyon-b, Muddy Creek Canyon case-study area 3-9
Figure 3-15. Trough cross-stratification, upper shoreface 3-10
Figure 3-16. Laminated sandstone, foreshore, parasequence Kf-1-Indian
Canyon-c, Willow Springs Wash case-study area 3-10
Figure 3-17. Shoreface sequence, parasequence Kf-1-Indian Canyon-c,
Willow Springs Wash case-study area 3-11
Figure 3-18. Tidal inlet deposits, Muddy Creek Canyon,
parasequence Kf-2-Muddy Canyon-b 3-11
Figure 3-19. Upper shoreface facies and tidal inlet deposits,
parasequence Kf-2-Muddy Canyon-b 3-12
Figure 3-20. Tidal inlet facies 3-13
Figure 3-21. Inclined bedsets of the tidal inlet facies 3-14
Figure 3-22. Pelecypod escape burrows in tidal inlet facies 3-14
Figure 3-23. Diagram distinguishing facies within the depositional sequence
formed by progradation of a fluvial-dominated delta 3-16
Figure 3-24. Typical fluvial-dominated deltaic
deposits in parasequence Kf-1-Ivie Creek 3-16
Figure 3-25. Fluvial-dominated deltaic facies,
Kf-1-Ivie Creek [a] bedset, Ivie Creek case-study area 3-17
Figure 3-26. Steeply inclined beds of a fluvial-dominated delta deposit,
Kf-1-Ivie Creek [a] bedset, Ivie Creek case-study area 3-17
Figure 3-27. Fluvial-dominated facies of parasequence
Kf-1-Indian Canyon-c[d] bedset, Coyote Basin 3-18
Figure 3-28. Wave-modified deltaic facies, parasequence
Kf-2-Ivie Creek-a, Ivie Creek case-study area 3-19
Figure 3-29. Distributary complex facies and lower
shoreface/distal-deltaic facies, Ivie Creek case-study area 3-20
Figure 3-30. Bay deposits with *Thalassinoides* burrows,
parasequence Kf-2-Muddy Canyon-a 3-21
Figure 3-31. Burrowing in bay deposits, Miller
Canyon, parasequence Kf-2-Muddy Canyon-a 3-22
Figure 3-32. Lagoonal deposits in Miller Canyon, Kf-2 parasequence set 3-23
Figure 3-33. Tidal channels in Kf-3 at Dry Wash 3-24
Figure 3-34. Swamp deposits associated with the
C-coal zone in the Molen Amphitheater 3-25

Figure 3-35. A-coal zone in upper Quitchupah Creek 3-26
Figure 3-36. Uni-directional trough cross-stratified channel sandstone, Dry Wash 3-27
Figure 3-37. Meanderbelt deposits, parasequence Kf-2-Muddy Creek-a, Muddy Creek Canyon case-study area 3-27
Figure 3-38. Channel belt along the Molen Reef 3-28
Figure 3-39. Lateral accretion in the meanderbelt facies, parasequence Kf-2-Muddy Canyon-a 3-28
Figure 3-40. Channel belt cut into the top of parasequence Kf-2-Ivie Creek-b 3-29
Figure 3-41. Channel cut into the top of the Kf-2 parasequence set, Rock Canyon 3-29
Figure 3-42. Multilateral and multistoried channel belts, Limestone Cliffs 3-31
Figure 4-1. Diagram of hypothetical prograding strand plain 4-3
Figure 4-2. Diagram of continued progradation of the strand plain 4-4
Figure 4-3. Diagram of progradation of a wave-modified delta 4-4
Figure 4-4. Diagram of continued progradation of wave-modified delta 4-5
Figure 4-5. Symbols/patterns used to represent the various sandstone body types in figures 4-6 and 4-9 4-5
Figure 4-6. Diagram showing the arrangement of parasequences within a forward-stepping parasequence set and, within the parasequences, the arrangement of bedsets 4-6
Figure 4-7. Hierarchical scheme of stratigraphic units 4-6
Figure 4-8. Ferron Sandstone nearshore marine facies arrangement 4-7
Figure 4-9. Landward pinchout into coastal-plain or delta-plain deposits 4-10
Figure 4-10. Landward pinchout of parasequence Kf-1-Iv, Coyote Basin 4-10
Figure 4-11. Landward pinchout of parasequence Kf-2-Rochester, Dry Wash 4-11
Figure 4-12. Landward pinchout of Kf-6 in the uppermost part of Muddy Creek Canyon 4-11
Figure 4-13. Closer view of the landward pinchout of Kf-6 shown in figure 4-12 4-12
Figure 4-14. Uppermost sandstone is the Kf-2-Iv-c thinning toward pinchout, I-70 4-12
Figure 4-15. Landward and seaward pinchouts of all the parasequences in the study area 4-13
Figure 4-16. Kf-LC just north of Last Chance Creek, along the Limestone Cliffs 4-14
Figure 4-17. Parasequence Kf-1-Indian Canyon-b and a near landward pinchout of Kf-1-Indian Canyon-c parasequence, Willow Springs Wash case-study area 4-17
Figure 4-18. Middle sandstone package, parasequence Kf-1-CC, Quitchupah Canyon 4-20
Figure 4-19. Parasequence Kf-2-Miller Canyon-a with sand-rich rotated blocks 4-23
Figure 4-20. Parasequence Kf-2-Miller Canyon-b, Muddy Creek Canyon 4-24
Figure 4-21. Parasequence Kf-2-Rochester, Molen Seep Wash 4-27
Figure 4-22. Two upward-coarsening cycles in parasequence Kf-2-Molen Seep Wash 4-27

Figure 4-23. View to the west of the landward pinchout of parasequence Kf-3-Molen Amphitheater 4-29
Figure 4-24. Kf-4-Miller Canyon marine or marginal marine sandstone, Quitchupah Canyon 4-31
Figure 4-25. Kf-4-Molen Reef near the landward pinchout along the edge of the Molen Amphitheater 4-32
Figure 4-26. Kf-5 in Muddy Creek Canyon 4-34
Figure 4-27. Kf-8 channel deposits in Coal Wash 4-36
Figure 4-28. Cobble-sized clasts and oyster-shell hash in Kf-8, Quitchupah Canyon area 4-36
Figure 4-29. Top of stacked packages of coarsening-upward successions 4-37
Figure 5-1. Location map of the Willow Springs Wash case-study area 5-1
Figure 5-2. Detailed map of the Willow Springs Wash case-study area 5-3
Figure 5-3. Diagrammatic cross section showing relative positions of Ferron parasequence sets, Willow Springs Wash case-study area 5-4
Figure 5-4. Map showing the locations of measured sections and the extent of photomosaic coverage, Willow Springs Wash case-study area 5-5
Figure 5-5. Maps showing outcrops of prodelta, lower shoreface, middle shoreface, and upper shoreface/ebb-tidal delta facies within depositional units A, B, and C, Willow Springs Wash case-study area 5-7
Figure 5-6. Maps showing outcrops of foreshore, tidal-inlet, interdistributary bay-fill, and crevasse splay/distributary-mouth bar facies, Willow Springs Wash case-study area 5-10
Figure 5-7. Maps showing outcrops of multistory channel, multilateral channel, and strand plain facies, Willow Springs Wash case-study area 5-13
Figure 5-8. Uninterpreted and interpreted photomosaics of parasequences Kf-1-Indian Canyon-a, -b, and -c, Willow Springs Wash case-study area 5-17
Figure 5-9. Uninterpreted and interpreted photomosaics showing depositional units C and D within parasequence Kf-1-Indian Canyon-c, Willow Springs Wash case-study area 5-18
Figure 5-10. Generalized southwest-northeast cross section along “The Wall” showing parasequences Kf-1-Indian Canyon-a, -b, and -c, Willow Springs Wash case-study area 5-19
Figure 5-11. Paleogeographic maps of the Willow Springs Wash case-study area during deposition of parasequences Kf-1-Indian Canyon-a 5-20
Figure 5-12. Paleogeographic maps of the Willow Springs Wash case-study area during deposition of parasequence Kf-1-Indian Canyon-c 5-22
Figure 5-13. Paleocurrent map and paleocurrent directions of deposits of depositional units C and D within parasequence Kf-1-Indian Canyon-c, Willow Springs Wash case-study area 5-23

Figure 5-14. Palegeographic maps of the Willow Springs Wash case-study area during deposition of parasequence Kf-1-Indian Canyon-c 5-25
Figure 5-15. Paleogeographic maps of the Willow Springs Wash case-study area during Stage 5 and Stage 6 of parasequence Kf-1-Indian Canyon-c 5-26
Figure 5-16. Vertical sequence of sedimentary structures observed within non-barred and barred shorelines 5-29
Figure 6-1. Location map of the Muddy Creek Canyon case-study area. 6-2
Figure 6-2. Muddy Creek Canyon cliffs formed by parasequences in Kf-2, Kf-4, Kf-5, Kf-6, and Kf-7 6-2
Figure 6-3. Generalized cross section showing the four parasequences in Kf-2 in Muddy Creek Canyon 6-3
Figure 6-4. Diagrammatic cross section showing relative positions of Ferron parasequence sets, Muddy Creek Canyon case-study area within the Ferron Sandstone 6-3
Figure 6-5. Topographic map of the Muddy Creek Canyon case-study area 6-4
Figure 6-6. Map showing the locations of drill holes, measured sections, and photo sections in the Muddy Creek Canyon case-study area 6-6
Figure 6-7. Coring operations during the drilling of Muddy Creek drill holes. 6-7
Figure 6-8. Cross section showing stratigraphy and facies of Kf-2 along Muddy Creek Canyon and in the subsurface, as represented by the photomosaics 6-8
Figure 6-9. Cross section showing stratigraphy and facies of Kf-2 along Muddy Creek Canyon and in the subsurface, as represented by the core interpretation from drill holes 6-8
Figure 6-10. Climbing oscillation ripples in middle shoreface strata in rotated slump block, parasequence Kf-2-Miller-a, Muddy Creek Canyon 6-9
Figure 6-11. Large, rotated slump block in delta-front deposits, parasequence Kf-2-Miller-a, Muddy Creek Canyon 6-9
Figure 6-12. Normal faulting of middle shoreface strata in rotated slump block, parasequence Kf-2-Miller-a Muddy Creek Canyon 6-10
Figure 6-13. Small-scale syndepositional faulting associated with a rotated slump block, parasequence Kf-2-Miller-a, Muddy Creek Canyon core 6-10
Figure 6-14. Shoreface deposits, parasequence Kf-2-Miller-b, Muddy Creek Canyon 6-12
Figure 6-15. Storm sandstones and fair-weather mudstones, lower shoreface, parasequence Kf-2-Miller-b, Muddy Creek Canyon core 6-12
Figure 6-16. Middle shoreface, parasequence Kf-2-Miller-b, Muddy Creek Canyon 6-13
Figure 6-17. Hummocky cross-stratified sandstone, middle shoreface, parasequence Kf-2-Miller-b, Muddy Creek Canyon core 6-13
Figure 6-18. Planar lamination and “ball-and-pillow” structures, middle shoreface, parasequence Kf-2-Miller-b, Muddy Creek Canyon 6-14

Figure 6-19. Oscillation ripples, middle shoreface of parasequence
Kf-2-Miller-b, Muddy Creek Canyon core 6-14
Figure 6-20. Vertically aggraded oscillation ripples, middle shoreface,
parasequence Kf-2-Miller-b, Muddy Creek Canyon core 6-15
Figure 6-21. Current ripples, middle shoreface, parasequence Kf-2-Mi-b,
Muddy Creek Canyon core 6-15
Figure 6-22. Planar laminated sandstone, middle shoreface,
parasequence Kf-2-Miller-b, Muddy Creek Canyon core 6-16
Figure 6-23. Bioturbated sandstone, middle shoreface,
parasequence Kf-2-Miller-b, Muddy Creek Canyon 6-16
Figure 6-24. Bioturbated middle shoreface, parasequence
Kf-2-Miller-b, Muddy Creek Canyon core 6-17
Figure 6-25. Bioturbated middle shoreface, parasequence
Kf-2-Miller-b, Muddy Creek Canyon core 6-17
Figure 6-26. Vertical burrows, middle shoreface, parasequence
Kf-2-Miller-b, Muddy Creek Canyon core 6-18
Figure 6-27. Soft-sediment deformation, middle shoreface,
parasequence Kf-2-Miller-b, Muddy Creek Canyon core 6-18
Figure 6-28. Multi-directional trough cross-stratificatione, upper
shoreface, parasequence Kf-2-Miller-b, Muddy Creek Canyon 6-19
Figure 6-29. Trough cross-stratification, upper shoreface,
parasequence Kf-2-Miller-b, Muddy Creek Canyon core 6-19
Figure 6-30. Small channel cut into the top of parasequence
Kf-2-Miller-b, Muddy Creek Canyon 6-20
Figure 6-31. Clay drapes on cross-stratification sets, parasequence
Kf-2-Miller-b, Muddy Creek Canyon 6-20
Figure 6-32. Top of the shoreface deposits, parasequence
Kf-2-Miller-b, Muddy Creek Canyon 6-21
Figure 6-33. Storm layers of sandstone, lower delta front, parasequence
Kf-2-Muddy Canyon-a, Muddy Creek Canyon 6-21
Figure 6-34. Parasequence Kf-2-Muddy Canyon-a, Muddy Creek Canyon 6-22
Figure 6-35. Erosional contact at the base of a storm bed shown in figure 6-34. 6-22
Figure 6-36. Erosional contact separating meanderbelt and underlying delta-front
deposits of parasequence Kf-2-Muddy Canyon-a, Muddy Creek Canyon core 6-23
Figure 6-37. Erosional contact between cross-stratified
meanderbelt sequence and underlying lower delta-front, parasequence
Kf-2-Muddy Canyon-a, Muddy Creek Canyon core 6-23
Figure 6-38. Mudstone rip-up clasts from meanderbelt, parasequence
Kf-2-Muddy Canyon-a, Muddy Creek Canyon core 6-24
Figure 6-39. Mudstone clasts from meanderbelt, parasequence
Kf-2-Muddy Canyon-a, Muddy Creek Canyon core 6-24

Figure 6-40. Cross-stratification sets, meanderbelt deposit, parasequence
Kf-2-Muddy Canyon-a, Muddy Creek Canyon 6-25
Figure 6-41. Trough cross-stratification, meanderbelt deposit, parasequence
Kf-2-MC-a, Muddy Creek Canyon 6-25
Figure 6-42. Current ripples with mud drapes, meanderbelt sequence, parasequence
Kf-2-Muddy Canyon-a, Muddy Creek Canyon core 6-26
Figure 6-43. Clay plug with the meanderbelt of parasequence
Kf-2-Muddy Canyon-a, Muddy Creek Canyon 6-26
Figure 6-44. Full thickness of parasequence Kf-2-Muddy Canyon-a,
west wall, Muddy Creek Canyon 6-27
Figure 6-45. Bioturbated lower delta-front deposits, parasequence
Kf-2-Muddy Canyon-a, Muddy Creek Canyon core 6-27
Figure 6-46. Lateral accretion within the meanderbelt truncated by the transgressive disconformity,
parasequence Kf-2-Muddy Canyon-a, Muddy Creek Canyon 6-28
Figure 6-47. Closer view of truncation of lateral
accretion surfaces shown in figure 6-46. 6-28
Figure 6-48. Transgressive surface separating parasequence
Kf-2-Muddy Canyon-a from overlying shoreface of parasequence
Kf-2-Muddy Canyon-b, Muddy Creek Canyon 6-29
Figure 6-49. Transgressive surface of erosion separating parasequences Kf-2-Muddy
Canyon-b and Kf-2-Muddy Canyon-a, Muddy Creek Canyon core 6-29
Figure 6-50. Sandstone of parasequence Kf-2-Muddy Canyon-b isolated
from underlying meanderbelt deposit, Muddy Creek Canyon 6-30
Figure 6-51. Hummocky cross-stratification, middle shoreface, parasequence
Kf-2-Muddy Canyon-b, Muddy Creek Canyon 6-30
Figure 6-52. Remnant storm layer in bioturbated middle shoreface deposits,
parasequence Kf-2-Muddy Canyon-b, Muddy Creek Canyon 6-31
Figure 6-53. Single storm layer containing climbing oscillation ripple, middle
shoreface, parasequence Kf-2-Muddy Canyon-b, Muddy Creek Canyon 6-31
Figure 6-54. Vertically climbing oscillation ripples in storm-layered, middle
shoreface, parasequence Kf-2-Muddy Canyon-b, Muddy Creek Canyon core 6-32
Figure 6-55. Bioturbated middle shoreface, parasequence Kf-2-Muddy
Canyon-b, Muddy Creek Canyon core 6-32
Figure 6-56. *Thalassinoides* in middle shoreface sandstone,
parasequence Kf-2-Muddy Canyon-b, Muddy Creek Canyon 6-33
Figure 6-57. Opposed directions of lateral accretion in the meanderbelt,
parasequence Kf-2-Muddy Canyon-a and tidal inlet, parasequence
Kf-2-Muddy Canyon-b, Muddy Creek Canyon 6-33
Figure 6-58. Large-scale, planar-tabular cross-stratification, tidal inlet facies,
parasequence Kf-2-Muddy Canyon-b, Muddy Creek Canyon 6-34

Figure 6-59. Large-scale, planar-tabular cross-stratification, tidal inlet facies, parasequence Kf-2-Muddy Canyon-b, Muddy Creek Canyon 6-34
Figure 6-60. Planar-tabular cross-stratification representing large-scale, lateral accretion surfaces of tidal inlet facies, parasequence Kf-2-Muddy Canyon-b, Muddy Creek Canyon core 6-35
Figure 6-61. Trough cross-stratification among large-scale, planar tabular sets of the tidal inlet facies, parasequence Kf-2-Muddy Creek-b, Muddy Creek Canyon 6-35
Figure 6-62. Trough cross-stratification within tidal inlet facies, parasequence Kf-2-Muddy Creek-b, Muddy Creek Canyon 6-36
Figure 6-63. Closer view of trough cross-stratification shown in figure 6-62. 6-36
Figure 6-64. Planar-laminated bearing coalified plant fragments, tidal inlet sequence, parasequence Kf-2-Muddy Canyon-b core 6-37
Figure 6-65. Current ripple cross-lamination of Kf-2 channel, Muddy Creek Canyon core 6-37
Figure 6-66. Map showing the area in which rotated slump blocks are abundant in parasequence Kf-2-Miller Canyon-a, Miller Canyon 6-40
Figure 6-67. Diagrammatic cross section showing final stage of progradation of parasequence Kf-2-Miller Canyon-a. 6-41
Figure 6-68. Early stage of progradation of the shoreline of parasequence Kf-2-Miller Canyon-a 6-42
Figure 6-69. Late stage of progradation of parasequence Kf-2-Miller Canyon-a prior to transgression 6-43
Figure 6-70. Transgression of the sea southward across parasequence Kf-2-Miller Canyon-a prior to progradation of parasequence Kf-2-Miller Canyon-b 6-44
Figure 6-71. Progradation of the older, wave-dominated part of parasequence Kf-2-Miller Canyon-b 6-46
Figure 6-72. Paleogeography early in the progradation of parasequence Kf-2-Miller Canyon-b into the Muddy Creek Canyon case-study area 6-47
Figure 6-73. Paleogeography at the end of progradation of the older, wave-dominated unit of parasequence Kf-2-Miller Canyon-b 6-48
Figure 6-74. Progradation of parasequence Kf-2-Miller Canyon-b beyond the northeastern edge of the Muddy Creek Canyon case-study area 6-49
Figure 6-75. Paleogeography at boundary between the older, wave-dominated and younger, extremely wave-dominated parts of parasequence Kf-2-Miller Canyon-b 6-50
Figure 6-76. Paleogeography of the later, extremely wave-dominated parasequence Kf-2-Miller-b in Muddy Creek Canyon 6-51
Figure 6-77. Transgression of the sea across parasequence Kf-2-Miller Canyon-b prior to progradation of parasequence Kf-2-Muddy Canyon-a 6-52

Figure 6-78. Areas where the meanderbelt deposits of parasequence Kf-2-Muddy Canyon-a are known to be present, Muddy Creek Canyon 6-54
Figure 6-79. Paleogeography very early in the progradation of parasequence Kf-2-Muddy Canyon-a across Muddy Creek Canyon case-study area 6-55
Figure 6-80. Paleogeography near the end of progradation of parasequence Kf-2-Muddy Canyon-a, Muddy Creek Canyon 6-56
Figure 6-81. Progradation of parasequence Kf-2-Muddy Canyon-a through Muddy Creek Canyon case-study area 6-57
Figure 6-82. Paleogeography of parasequence Kf-2-Muddy Canyon-a at the time of emplacement of the northern meanderbelt, Muddy Creek Canyon case-study area 6-58
Figure 6-83. Emplacement of the northern meanderbelt of parasequence Kf-2-Muddy Canyon-a, Muddy Creek Canyon case-study area 6-59
Figure 6-84. Paleogeography of parasequence Kf-2-Muddy Canyon-a at the time of emplacement of the southern meanderbelt, Muddy Creek Canyon case-study area 6-60
Figure 6-85. Emplacement of the southern meanderbelt of parasequence Kf-2-Muddy Canyon-a, Muddy Creek Canyon case-study area 6-61
Figure 6-86. Paleocurrent data fromtrough cross-stratification in northern meanderbelt of parasequence Kf-2-Muddy Canyon-a, Muddy Creek Canyon case-study area 6-61
Figure 6-87. Paleocurrent data derived from trough cross-stratification in southern meanderbelt of parasequence Kf-2-Muddy Canyon-a, Muddy Creek Canyon case-study area 6-62
Figure 6-88. Transgression sea across deposits of parasequence Kf-2-Muddy Creek-a and beginning of progradation of parasequence Kf-2-Muddy Canyon-b, Muddy Creek Canyon case-study area 6-62
Figure 6-89. Direction of inclination of large-scale, planar-tabular cross-stratification representing lateral migration of tidal inlets in parasequence Kf-2-Muddy Canyon-b, Muddy Creek Canyon case-study area 6-64
Figure 6-90. Transport direction indicated by trough cross-stratification in tidal inlets of parasequence Kf-2-Muddy Canyon-b, Muddy Creek Canyon case-study area 6-64
Figure 6-91. Paleogeography at peak transgression and beginning of progradation of parasequence Kf-2-Muddy Canyon-b, Muddy Creek Canyon case-study area 6-65
Figure 6-92. Paleogeography of the earliest phase of progradation of parasequence Kf-2-Muddy Canyon-b, Muddy Creek Canyon case-study area 6-66
Figure 6-93. Emplacement of inlet bodies in landward part of parasequence Kf-2-Muddy Canyon-b, Muddy Creek Canyon case-study area 6-67
Figure 6-94. Paleogeography of prograding, wave-dominated shoreline of parasequence Kf-2-Muddy Canyon-b, Muddy Creek Canyon case-study area 6-68
Figure 6-95. Areas where tidal inlets occur in parasequence Kf-2-Muddy Canyon-b and location of a channel belt, Muddy Creek Canyon case-study area 6-69
Figure 6-96. Paleogeography of parasequence Kf-2-Muddy Canyon-b, Muddy Creek Canyon case-study area 6-70

Figure 6-97. Emplacement of the channel belt that cross-cuts parasequence Kf-2-Muddy Canyon-b, Muddy Creek Canyon case-study area 6-71
Figure 7-1. Location map of the Ivie Creek case-study area 7-1
Figure 7-2. Diagrammatic cross section showing relative positions of Ferron parasequence sets, Ivie Creek case-study area 7-2
Figure 7-3. Data collection point locations in the Ivie Creek case-study area 7-2
Figure 7-4. Ivie Creek case-study area stratigraphy 7-5
Figure 7-5. Stratigraphic section from the Ivie Creek amphitheater of Kf-1 7-5
Figure 7-6. Stratigraphic section from Ivie Creek Canyon of Kf-1 and Kf-2 7-6
Figure 7-7. Photomosaic of Ferron parasequence sets, Ivie Creek case-study area displaying contrasting delta-front architectural styles 7-7
Figure 7-8. Structure and isopach maps of Kf-1-Ivie Creek [a] bedset 7-8
Figure 7-9. Low-angle cross-beds the proximal portions of the Kf-1-Ivie Creek [a] bedset 7-9
Figure 7-10. Stratigraphic nomenclature and hierarchical units of the Kf-1-Ivie Creek [a] bedset, Ivie Creek case-study area 7-9
Figure 7-11. Inclined bedforms (clinoforms) in Kf-1-Ivie Creek [a], Ivie Creek case-study area 7-10
Figure 7-12. Scaled cross sections of Kf-1-Ivie Creek [a] bedset, Ivie Creek amphitheater showing clinoform lithofacies, dominant sedimentary structures, average grain size 7-11
Figure 7-13. Low-angle cross-beds in proximal portion of Kf-1-Ivie Creek [a] bedset cut into the underlying bounding layer 7-12
Figure 7-14. Bounding layer measurement locations and clinoform facies distribution, Ivie Creek amphitheater 7-13
Figure 7-15. Ivie Creek, 40-acre spacing model estimated bounding layer thicknesses 7-15
Figure 7-16. Photomosaic of Ferron parasequences in the Ivie Creek case-study area displaying clinoforms and distributary channel 7-16
Figure 7-17. Isopach map of Kf-1-Ivie Creek [c] bedset 7-17
Figure 7-18. Photomosaic of Ferron parasequences in Ivie Creek case-study area displaying distal, delta-front deposits of the Kf-1 and distributary-mouth-bar deposits of the Kf-2 7-18
Figure 7-19. Structure and isopach maps of parasequence Kf-2-Ivie Creek-c, Ivie Creek case-study area 7-20
Figure 7-20. Photomosaic near I-70 showing both Kf-1 and Kf-2 and major distributary channel associated with the Kf-2-Ivie Creek-c parasequence 7-20
Figure 7-21. Example of Ferron Sandstone reservoir gamma-ray type log and core description for distributary complex facies 7-21
Figure 7-22. Distributary complex facies cut into the shoreface near the mouth of Corbula Canyon 7-21

Figure 7-23. Example of Ferron Sandstone reservoir gamma-ray type log and core description for distributary-mouth bar, distributary channel, middle shoreface, and lower shoreface facies 7-22
Figure 7-24. Example of the Ferron Sandstone reservoir gamma-ray type log and core description for the clinoform distal, medial, proximal, and cap facies; and brackish-water bay/bay fill, coastal plain/swamp, and transgressive facies 7-23
Figure 7-25. Clinoform medial facies at Ivie Creek amphitheater 7-24
Figure 7-26. Clinoform distal facies at Ivie Creek amphitheater 7-24
Figure 7-27. Clinoform cap facies with trough cross-bedding at Ivie Creek amphitheater 7-24
Figure 7-28. Oyster coquina containing brackish-water fauna within carbonaceous mudstone, Ivie Creek core 7-25
Figure 7-29. Thin transgressive Kf-2 above Sub-A coal zone, Ivie Creek amphitheater 7-26
Figure 7-30. Lower shoreface facies found just above the Kf-1/Kf-2 parasequence set boundary, Ivie Creek case-study area 7-26
Figure 7-31. Middle shoreface facies, parasequence Kf-2-Ivie Creek-a, Ivie Creek case-study area 7-27
Figure 7-32. Upper shoreface and foreshore facies, Ivie Creek Canyon 7-28
Figure 7-33. Example of Ferron Sandstone reservoir gamma-ray type log and core description for upper shoreface and foreshore facies 7-28
Figure 7-34A-E. Paleogeographic interpretation of five time steps of the Kf-1-Ivie Creek [a] bedset . . . . . 7-30 through 7-34
Figure 7-35. Diagrammatic cross sectional view of clinoform depositional time steps, Ivie Creek case-study area 7-35
Figure 7-36. Plan view of eight time steps during deposition of Kf-1-Ivie Creek [a] bedset. 7-36
Figure 7-37. Ferron-Tununk contact in upper Quitchupah Canyon 7-37
Figure 7-38. Paleogeographic interpretation of the Kf-2-Ivie Creek-a parasequence 7-38
Figure 7-39. Paleogeographic interpretation of the Kf-2-Ivie Creek-b parasequence 7-39
Figure 7-40. Soft-sediment deformation from parasequence Kf-2-Ivie Creek-b, Quitchupah Creek 7-40
Figure 7-41A-D. Paleogeographic interpretation of four time steps of the Kf-2-Ivie Creek-c parasequence . . . . . 7-41 through 7-44
Figure 8-1. Location of 22 permeability transects in Ivie Creek case-study area 8-2
Figure 8-2. Electronic miniprobe permeameter measuring permeability, Ivie Creek case-study area 8-3
Figure 8-3. Comparison of mini-permeameter tests on core plugs collected from holes where in-situ tests were also conducted 8-4
Figure 8-4. Comparison of permeability and porosity values obtained from core plugs collected from outcrop 8-4

Figure 8-5. East-west permeability distribution along transects in clinoform facies of Kf-1-Ivie Creek [a] bedset, Ivie Creek amphitheater 8-6
Figure 8-6. North-south permeability distribution along transects distributary-mouth bar and upper shoreface/foreshore deposits of the Kf-2-Ivie-b and c parasequences, Ivie Creek case-study area 8-7
Figure 8-7. East-west permeability distribution along transect in distributary-mouth bar and upper shoreface/foreshore deposits and in middle shoreface deposits, Kf-2-Ivie Creek-b and c parasequences, Ivie Creek case-study area 8-7
Figure 8-8. Map of the Ivie Creek case-study area showing drill-hole locations and outcrop sampling traverses 8-8
Figure 8-9. Map of east-central Utah, showing Ferron Sandstone locations of wells with geophysical logs 8-9
Figure 8-10. Polarized-light photomicrographs of fluvial-dominated Kf-1 sandstone 8-15
Figure 8-11. Cross plots of total carbonate and porosity, and total porosity versus percentage of the porosity that is secondary 8-16
Figure 8-12. Fractional porosity and velocity of individual Ferron beds 8-18
Figure 8-13. Comparison of lowest-pressure and highest-pressure measurements of compressional-wave velocity of core plugs, and pressure dependence of velocity 8-22
Figure 8-14. Velocity/porosity patterns from core-plug and log measurements 8-23
Figure 8-15. Comparison of log and core measurements for density and velocity at Ivie Creek drill hole IC-3 8-25
Figure 8-16. Porosity/permeability pattern for core-plug samples from the Ferron Sandstone 8-27
Figure 8-17. Relationship between horizontal permeability and both vertical and diagonal permeability, based on 3-D sets of adjacent core-plug samples 8-29
Figure 9-1. Ivie Creek case-study area, database locations 9-3
Figure 9-2. Typical clinoform facies distribution 9-4
Figure 9-3. Diagram of measurements used for clinoform characterization and bedform thickness vs. position along clinoforms, Kf-1-Ivie Creek [a] bedset, Ivie Creek amphitheater 9-7
Figure 9-4. Kf-1-Ivie Creek [a] bedset detail model, summary of facies and lithology 9-8
Figure 9-5. Kf-1-Ivie Creek [a] bedset detail model, summary of average grain size and sedimentary structure 9-9
Figure 9-6. Statistical analyses of clinoform facies from Kf-1-Ivie Creek [a] bedset 9-10
Figure 9-7. Kf-1-Ivie Creek [a] bedset detail model, summary of bed size and induration 9-11
Figure 9-8. Kf-2 local model, summary of facies and lithology 9-13
Figure 9-9. Statistical analyses of the Kf-2 parasequence set as a whole and parasequences within it 9-14

Figure 9-10. Kf-2 local model, summary of
average grain size and sedimentary structure 9-15
Figure 9-11. Kf-2 local model, summary of bed size and induration 9-16
Figure 9-12. Kf-1-Ivie Creek [a] bedset detail model, permeability vs.
percent sandstone for geometric mean and arithmetic mean 9-18
Figure 9-13. Kf-1-Ivie Creek [a] bedset detail model, cumulative
probability curves for facies vs. permeability 9-20
Figure 9-14. Kf-1-Ivie Creek [a] bedset detail model,
cumulative probability curves for average grain size vs. permeability 9-21
Figure 9-15. Kf-1-Ivie Creek [a] bedset detail model, cumulative
probability curves for sedimentary structure vs. permeability 9-22
Figure 9-16. Kf-1-Ivie Creek [a] bedset detail model, cumulative probability
curves for facies vs. permeability for model and raw data 9-23
Figure 9-17. Ivie Creek amphitheater two-dimensional deterministic
model for the Kf-1-Ivie Creek [a] bedset 9-24
Figure 9-18. Kf-2 local model, permeability vs. percent sandstone 9-25
Figure 9-19. Kf-1-Ivie Creek [a] bedset and Kf-2 detail and local models,
cumulative probability curves for parasequence vs. permeability 9-27
Figure 9-20. Kf-2 local model, cumulative
probability curves for facies vs. permeability 9-28
Figure 9-21. Kf-2 local model, cumulative probability curves for
average grain size vs. permeability 9-29
Figure 9-22. Kf-2 local model, cumulative probability curves for
sedimentary structure vs. permeability 9-30
Figure 9-23. Kf-2 and Kf-1-Ivie Creek [a] bedset potential,
reservoir facies vs. cumulative grain size 9-32
Figure 9-24. Kf-2 and Kf-1-Ivie Creek [a] bedset potential,
reservoir facies vs. permeability 9-33
Figure 10-1. Location of Ivie Creek case-study area 10-1
Figure 10-2. Linework interpretation of Ivie Creek case study architecture 10-2
Figure 10-3. Digitized linework repair in a portion of the modeling domain 10-6
Figure 10-4. Extracting the boundary of an
individual clinoform from the digitized linework 10-7
Figure 10-5. Sub-domain showing closed polygons enclosing
individual clinoforms and gridded clinoforms 10-9
Figure 10-6. Method used to subdivide each clinoform into
distinct facies, and histograms of permeability measurements pooled by facies 10-11
Figure 10-7. Method of populating a clinoform with permeability 10-12
Figure 10-8. Permeability models used in subsequent flow-simulation study 10-14
Figure 10-9. Oil saturation at 180 days after the start of water injection along
the left-hand side of the modeling domain 10-17

Figure 10-10. Oil saturation at 365 days after the start of water injection along the left-hand side of the modeling domain 10-18
Figure 10-11. Oil saturation at 547 days after the start of water injection along the left-hand side of the modeling domain 10-19
Figure 10-12. Oil saturation at 730 days after the start of water injection along the left-hand side of the modeling domain 10-20
Figure 10-13. Cumulative production and water cut curves for the four petrophysical models 10-21
Figure 10-14. Results of permeability upsealing experiments 10-24
Figure 10-15. Schematic diagram showing well patterns used in simulated reservoir production 10-28
Figure 10-16. Location map showing the relationship between the 3-D simulation volume, cliff-face outcrops, drill holes, and geological cross sections 10-29
Figure 10-17. Schematic diagram showing the four permeability structures considered in the 3-D reservoir simulations, Reference case 10-30
Figure 10-18. Isotropic permeability structure used in 3-D simulation studies 10-30
Figure 10-19. Anisotropic permeability structure used in 3-D simulation studies 10-31
Figure 10-20. Plan view comparisons of layer corresponding to z = 34 feet for each of the permeability models used in the 3-D simulations 10-32
Figure 10-21. Simple layered permeability structure used in 3-D simulation studies 10-33
Figure 10-22. Computed oil saturation at 1, 3, and 10 years after the start of water injection, layer z = 34 feet, isotropic permeability model 10-35
Figure 10-23. Computed oil saturation at 1, 3, and 10 years after the start of water injection, vertical section along northwest-southeast diagonal, isotropic permeability model 10-36
Figure 10-24. Computed oil saturation at 1, 3, and 10 years after the start of water injection for the 9-spot production scenario, layer z = 34 feet, isotropic permeability model 10-37
Figure 10-25. Computed oil saturation at 1, 3, and 10 years after the start of water injection for the 9-spot production pattern, isotropic permeability model 10-38
Figure 10-26. Computed oil saturation at 1, 3, and 10 years after the start of water injection for 5-spot production scenario, layer z = 34 feet, layered permeability model 10-39
Figure 10-27. Computed oil saturation at 1, 3, and 10 years after start of water injection for 5-spot production patter layered permeability model 10-40
Figure 10-28. Computed oil saturation at 1, 3, and 10 years after start of water injection for 5-spot production scenario, layer z = 34 feet, anisotropic permeability model 10-42
Figure 10-29. Computed oil saturation at 1, 3, and 10 years after start of water injection for 5-spot production pattern, anisotropic permeability model 10-43

Figure 10-30. Plot of cumulative oil production against time for each permeability model used in the 3-D simulations 10-44
Figure 10-31. Plot of water cut against time for each permeability model used in the 3-D simulations 10-44
Figure 10-32. Comparison of the permeability structures for corresponding 2-D and 3-D modeling domains 10-47
Figure 10-33. Comparison of oil saturations computed in the 2-D and 3-D simulations 10-48
Figure C-1. Schematics showing assumed orientation of permeability tensor with respect to geometry of depositional system and computed permeability tensors used in 3-D simulations C-1
Figure C-2. Approach used to compute permeability tensor from the 2-D domain C-2

TABLES

Table 5-1. Lithofacies within the Willow Springs Wash case-study area 5-15
Table 7-1. Bounding layer measurements and characteristics 7-14
Table 7-2. Tabulation of thickness changes along specific bounding layers 7-14
Table 8-1. Compositional estimates for selected permeability plug thin sections from Kf-1, Ivie Creek case-study area 8-11
Table 8-2. Summary porosity estimates with permeability measurements for drill-hole samples and permeability plugs of table 8-1 . . . . . 8-12, 8-13
Table 9-1. Clinoform facies summary 9-5
Table 10-1. Facies preservation in model domain clinoforms 10-10
Table 10-2. Key reservoir and fluid properties 10-16
Table 10-3. Permeability and porosity for each clinoform facies 10-33
Table 10-4. Cumulative oil production after 10 years of waterflooding 10-42
Table B-1. Sample measured section form. B-1
Table C-1. Relative permeability and water capillary pressure as a function of water saturation. C-4
Table C-2. Oil viscosity as a function of reservoir pressure. C-5
Table C-3. Oil and water formation volume factors as a function of pressure. C-5

ABSTRACT

The objective of the Ferron Sandstone project was to develop a comprehensive, interdisciplinary, quantitative characterization of a fluvial-deltaic reservoir to allow realistic inter-well and reservoir-scale models to be developed for improved oil-field development in similar reservoirs world-wide. Quantitative geological and petrophysical information on the Cretaceous Ferron Sandstone in east-central Utah was collected. Both new and existing data were integrated into a three-dimensional model of spatial variations in porosity, storativity, and tensorial rock permeability at a scale appropriate for inter-well to regional-scale reservoir simulation. Simulation results could improve reservoir management through proper infill and extension drilling strategies, reduction of economic risks, increased recovery from existing oil fields, and more reliable reserve calculations.

The project was divided into four tasks: (1) regional stratigraphic analysis, (2) case studies, (3) reservoirs models, and (4) field-scale evaluation of exploration strategies. The primary objective of the regional stratigraphic analysis was to provide a more detailed interpretation of the stratigraphy and gross reservoir characteristics of the Ferron Sandstone as exposed on outcrop. The primary objective of the case-studies work was to develop a detailed geological and petrophysical characterization, at well-sweep scale or smaller, of the primary reservoir lithofacies typically found in a fluvial-dominated deltaic reservoir. Work on tasks 3 and 4 consisted of developing two- and three-dimensional reservoir models at various scales that incorporated the data and results of the regional stratigraphic analysis (task 1) and case-studies tasks (task 2).

Regionally, the Ferron Sandstone consists of at least nine delta-front sandstone bodies or parasequence sets. Our work focused on two parasequence sets (Kf-1 and Kf-2) in the lower part of the Ferron. The Kf-1 represents a river-dominated delta deposit which changes from proximal to distal. The Kf-2 contains more and cleaner sand, indicating a more wave-influenced environment of deposition.

Lithofacies, measured sections, and other data were plotted on photomosaics of the Ferron Sandstone outcrop belt within the study area for both units examined in the regional analyses. Detailed interpretive work was conducted in three case-study areas: Willow Springs Wash, Muddy Creek Canyon, and Ivie Creek. This work included describing the lithofacies found in each parasequence, constructing stratigraphic cross sections, and producing paleogeographic maps.

In the Ivie Creek case-study area, the bounding surfaces between delta-front clinoform deposits were investigated in detail to fully understand how such features might affect fluid flow in a reservoir. Data from permeability transects and measured sections in the Kf-1 and Kf-2 were used to determine the statistical structure of the spatially variable permeability field within the delta front, and to investigate how geological processes control the spatial distribution of permeability.

Reservoir modeling was conducted on data collected from, and geological interpretations of, the Kf-1-Iv[a] bedset. The modeling effort concentrated on: (1) variations in fluid flow between the lithofacies, (2) the amount of communication between each bed, and (3) the effects the various bounding surfaces within the beds would have on fluid flow. These models were used for two- and three-dimensional reservoir simulations. All simulations involved two fluids, oil and water.

Thus, the Ivie Creek site provides an outcrop-to-simulation case study that adds to the growing suite of reservoir analogs available to constrain geological and petrophysical models used in reservoir simulation studies.

EXECUTIVE SUMMARY

Understanding reservoir heterogeneity is the key to increasing oil recovery from existing fields in the United States. Fluvial-deltaic reservoirs have the largest developed oil reserves, and due to the high degree of reservoir heterogeneity, the largest amount of untapped and unrecovered oil within developed reservoirs. Reservoir heterogeneity is dramatically exposed in the fluvial-deltaic Ferron Sandstone Member of the Cretaceous Mancos Shale in east-central Utah.

The Utah Geological Survey (UGS) led a multidisciplinary team to develop a comprehensive and quantitative characterization of the Ferron Sandstone which allowed realistic modeling of a fluvial-deltaic reservoir at both the interwell and reservoir scale. These models may be used for improved oil-field development in similar reservoirs world-wide. The Ferron Sandstone project team consisted of the UGS (prime contractor), University of Utah, Brigham Young University, Utah State University, Amoco Production Company, Mobil Exploration and Producing Company, and several geologic contractors. This research is performed under the Geoscience/Engineering Reservoir Characterization Program of the U.S. Department of Energy, National Petroleum Technology Office, Tulsa, Oklahoma.

The project was divided into four tasks: (1) regional stratigraphic analysis, (2) case studies, (3) development of reservoirs models, and (4) field-scale evaluation of exploration strategies. The primary objective of the regional stratigraphic analysis was to provide a more detailed interpretation of the sequence stratigraphy and gross reservoir characteristics of the Ferron Sandstone as exposed on outcrop. This regional study included determining the dimensions and depositional environments of important sandstone reservoir bodies and the nature of their contacts with adjacent rock units. The primary objective of the case-studies work was to develop a detailed geological and petrophysical characterization of some of the primary reservoir lithofacies typically found in a fluvial-dominated deltaic reservoir. Tasks 3 and 4, (reservoir models and field-scale evaluation of exploration strategies), incorporated the data and results of Tasks 1 and 2 (the regional stratigraphic analysis and case-studies tasks).

Regionally, the Ferron Sandstone consists of at least nine delta-front sandstone bodies or parasequence sets. These were mapped from over 150 photomosaics and described from field investigations. The depositional environments of the majority of Ferron sand bodies that could constitute important reservoirs and be utilized as reservoir analogs were: (1) prograding shorelines, and (2) fluvial channels that supplied the sediment to the shorelines. The focus of our work was on two parasequence sets in the lower part of the Ferron, designated as the Kf-1 and Kf-2. The Kf-1 represents a river-dominated delta deposit which changes from proximal to distal. The Kf-2 contains more and cleaner sand, indicating a more wave-influenced environment of deposition.

The application of sequence stratigraphic terminology in this study was driven by two factors: (1) the hope that its models and terms would enhance our understanding of the packages of Ferron rocks and increase our ability to predict the occurrence and distribution of reservoir quality facies, and (2) its popularity at the time. A hierarchical system of abbreviations is used to designate each mappable body of rock. Kf designates Cretaceous Ferron Sandstone. The first dash designates the next hierarchical subdivision or parasequence set, for example Kf-2. The next dash in the UGS hierarchical scheme designates a higher frequency stratigraphic unit which is mappable and is separated from the rocks above

and below by a flooding surface and/or transgressive surface of erosion, and makes up the highest frequency unit mapped within each larger stratigraphic unit or parasequence set. These units fit the definition of a parasequence.

The study of the regional stratigraphy helped to put the smaller scale case studies into a larger scale context. One important conclusion related to regional reservoirs was the recognition that all initial progradations begin as wave-dominated. From work in this study we know that the wave-influenced facies generally have better porosity and permeability than the fluvial-dominated facies (there are exceptions), therefore, the landward pinchouts of wave-influence parasequences make good reservoir rocks. Seaward-stepping parasequence sets have much greater dip length than do the vertically aggrading and landward-stepping parasequence sets. A significant portion of the volume of rock within any seaward-stepping parasequence set consists of fluvial channel and meanderbelt facies which have incised older or relatively contemporary shoreface deposits. These channel facies are some of the best reservoirs in the system.

Three project case-study areas were chosen: Willow Springs Wash, Muddy Creek Canyon, and Ivie Creek, in the southern, northern, and central parts respectively of the study area. Lithofacies were described and paleogeographic maps constructed for each parasequence in these areas. Exposures of the Ferron Sandstone in Muddy Creek Canyon offered excellent examples of a variety of facies that accumulated in fluvial-deltaic settings. Various side canyons compliment the Muddy Creek Canyon exposures, allowing a three-dimensional depositional model to be constructed. Access to drilling sites immediately west of Muddy Creek Canyon was excellent compared to most other Ferron outcrop areas.

The Willow Springs Wash area was the largest of the case-study areas and was selected for the excellent three-dimensional aspect of exposures along Willow Springs Wash and Indian Canyon. The focus of the work in the Willow Springs Wash area was on parasequences of the regional Kf-1 delta-front sand. The deposits exposed along Willow Springs Wash and Indian Canyon consist of eleven depositional facies in four distinct, mappable depositional units; three deposited along wave-dominated shorelines and one deposited in a lobe of a fluvial-dominated delta. Misidentification of parasequences and failure to distinguish between autocyclic and allocyclic changes involved in a rock succession can result in misunderstanding the depositional history, the distribution of related facies, and the quality and extent of the potential hydrocarbon reservoir. Models based on outcrop analogs such as the Ferron Sandstone in the Willow Springs Wash case-study area can provide insight into the complexities of these reservoir rocks. No reservoir simulations were conducted on data collected from the Willow Springs Wash area; however, the architectural elements interpreted from the outcrops were incorporated into the overall reservoir model for the Ferron Sandstone.

The Ferron Sandstone in the Ivie Creek case-study area consists of two regional-scale parasequence sets, the Kf-1 and Kf-2. The Ivie Creek case-study area was selected since it contains abrupt facies changes in the Kf-1 delta-front sandstones. Five primary activities were performed as part of the geological characterization of the Ferron Sandstone in the Ivie Creek case-study area: (1) construction of elevation and isopach maps, and cross sections, (2) lithofacies and depositional environment determination, (3) clinoform characterization, (4) geostatistical evaluation, and (5) development of three-dimensional facies models. Cross sections were constructed to tie into the regional picture and for use in the case-study based three-dimensional reservoir modeling effort. These cross sections display parasequence and parasequence set boundaries, measured sections, and correlations through geophysical

logs and conventional core from five project drill holes. Depositional trends were estimated from parasequence surface elevation and isopach maps. Elevation and isopach maps provided insight into paleotopography, sediment source, and depositional patterns. Analysis of these two data types reveals delta evolution during the deposition of the Kf-1 and Kf-2 parasequence sets.

The Kf-1-Iv[a] bedset is characterized by clinoform geometries that dip basinward, recording an episode of delta progradation into a deeper water, fully marine bay. The clinoform outcrops together form an arcuate feature, which is interpreted as a delta-complex. Based on the geometry of the clinoform deposits, the source for the delta is believed to be from the southeast where outcrops contain numerous distributary channel deposits at the top of Kf-1. The wave-modified Kf-2 parasequence set in the Ivie Creek case-study area was deposited in seven depositional environments: (1) lower shoreface, (2) middle shoreface, (3) upper shoreface, (4) foreshore, (5) distributary complex, (6) distributary channel, and (7) distributary-mouth bar. The gamma-ray log characteristics of each facies were tied to core taken from project drill holes in the area.

The clinoform section of Kf-1-Iv[a] bedset was classified into four lithofacies: clinoform proximal, medial, distal, and cap. Descriptive field data were gathered to better define the flow characteristic across clinoform-to-clinoform boundaries. To characterize the clinoform bedforms, measurements were taken of the overall length of the clinoform body, the inclination angle from datum at quartiles along the bedform, and the bedform thickness at quartiles along the bedform. A large quantity of permeability and other petrophysical data was collected and analyzed from outcrop exposures in the Ivie Creek case-study area. These data were integrated into a complete reservoir characterization product that can assist in subsequent reservoir-simulation work.

Spatial variations in lithofacies, stratigraphic thickness, sedimentary structures, and permeability data were quantified through geostatistical analysis. Geostatistical work was devoted to: (1) deriving relationships between permeability and geology, (2) testing the permeability data set for log normality, (3) analyzing permeability controls for both the Kf-1-Iv[a] bedset and Kf-2 parasequence set, (4) establishing an architectural framework based on facies maps, (5) studying the spatial distribution of various parameters, and (6) mapping variables in both a stochastic and deterministic manner.

Reservoir modeling was conducted on data collected from and geological interpretations of the Kf-1-Iv[a] bedset. The modeling effort concentrated on: (1) variations in fluid flow between the lithofacies, (2) the amount of communication between each bed, and (3) the effects various bounding surfaces within bedsets would have on fluid flow in these units. The modeling strategy was finalized following completion of the field-based characterization activities needed to develop input to both geostatistical models and fluid-flow simulators. Model input parameters for both fluid and rock properties have been finalized for a plausible set of reservoir conditions.

The vertical, two-dimensional model domains capture important elements of the transition from proximal to distal fluvial-deltaic lithofacies. In particular, these model domains enable one to explore how clinoform geometry and the inferred properties of the intervening bounding layers might influence the flow of oil and water at the interwell scale. Detailed geological mapping and the results of outcrop-based permeability testing provide a foundation for assigning petrophysical properties within the model domains.

The three-dimensional model domain measures 2,000 feet by 2,000 feet horizontally and 80 feet vertically (610x610x24 m). Within this volume, the detailed distribution of lithofacies types of the Kf-1-

Iv[a] bedset was inferred from a three-dimensional grid of 20 feet by 20 feet by 4-feet (6x6x1.2 m) cells using discretized cross sections. Simulations were made to explore the way that outcrop-based data might be used to improve predictive simulations that, in turn, are needed to plan reservoir development.

Three, three-dimensional models were developed for the project. The first model was obtained by estimating three-dimensional permeability anisotropy from the two-dimensional permeability modeling and applying the result to the facies-based model described above. The second model was a simple, isotropic, layered model. Using only these data represented a conventional, and simplified, approach to building a reservoir model given borehole data obtained at a 40-acre (16.2-ha) spacing. The third, and simplest model was constructed by assigning a single value of isotropic permeability throughout the model domain.

Numerical simulations were performed using the TETRAD-3D finite-difference reservoir simulation software. All simulations involved two fluids, oil and water. Oil production by waterflooding the analog reservoir volume using a 5-spot pattern of wells was simulated for four, three-dimensional permeability/porosity structures. Each permeability/porosity structure represented different approaches taken to preserve the measured geologic details that might influence oil production.

The results of the simulations indicate that every effort should be made to develop permeability models that preserve the effect of the clinoform-related facies observed on outcrop. Even without attempting to incorporate the effect of shale drapes within each clinoform-related facies, it is clear that the overall facies geometry exerts a significant impact on oil production. Analogous fluid-flow simulations performed with the more finely gridded two-dimensional permeability models indicate that relatively thin shale drapes within each clinoform-related facies can have a significant impact on oil production and water cut. The three-dimensional simulation results show that creating a 9-spot pattern through infill drilling within our analog reservoir significantly boosts oil recovery at the expense of increased water cut. If shale drapes could be explicitly included in the three-dimensional model, as they are in the two-dimensional models, we would expect to see a different response because interwell connectivity would likely be reduced. Thus, the Ivie Creek project provides an outcrop-to-simulation case study that adds to the growing suite of reservoir analogs available to constrain geological and petrophysical models used in reservoir simulation studies.

ACKNOWLEDGMENTS

Project Financial Support

The Ferron Sandstone project was performed under the Geoscience/Engineering Reservoir Characterization Program of the U.S. Department of Energy (DOE), National Petroleum Technology Office, Tulsa, Oklahoma, contract number DE-AC22-93BC14896. The Contracting Officer's Representative was Robert Lemmon. The Utah Geological Survey was the prime contractor. Both financial and technical support was also provided by Mobil Exploration/Producing Technical Center and Amoco Production Company during the investigation period of the project (1993 to 1998).

Project Contributors

Principal Investigators:

M.L. Allison; Utah Geological Survey, Salt Lake City, UT, 1993-98, (now with the Kansas Geological Survey, Lawrence, KS); T.C. Chidsey, Jr.; Utah Geological Survey, Salt Lake City, UT, 1998-present

Program Manager:

T.C. Chidsey, Jr.; Utah Geological Survey, Salt Lake City, UT

Financial Officers:

Werner Haidenthaller (1993-96, now with Utah Department of Workforce Services) John Kingsley (1998-present), Dan Kelly (1993-present); Utah Geological Survey, Salt Lake City, UT

Task Contributing Scientists and Organizations:

R.D. Adams (now with A & R Resources, LLC, Salt Lake City, UT), R.L. Bon, T.C. Chidsey, Jr., Janet Gillette, Brigitte Hucka, M.D. Laine, Kevin McClure, S.N. Sommer, D.A. Sprinkel, D.E. Tabet,, K.A. Waite; Utah Geological Survey, Salt Lake City, UT

P.B. Anderson; Geologic Consultant, Salt Lake City, UT

T.A. Ryer; The ARIES Group, Louisville, CO (now with Geoquest Int., Houston, TX)

M.A. Chan, C.B. Forster, Richard Jarrard, Ann Mattson, S.H. Snelgrove; University of Utah, Salt Lake City, UT

J.A. Dewey, Jr., and T.H. Morris; Brigham Young University, Provo, UT

J.V. Koebbe; Utah State University, Logan, UT

Don Best, J.R. Garrison, Jr. (now with the Ferron Group Consultants, LLC., Emery, UT) Bruce Welton, F.M. Wright III; Mobil Exploration/Producing Technical Center, Dallas, TX

R.L. Chambers, Chandra Rai, and Carl Sondergeld; Amoco Production Company, Tulsa, OK

Utah Geological Survey *Petroleum News* was edited by Tim Madden and Roger Bon. The project Internet Homepage was managed by Christine Wilkerson. Jim Parker, Vicky Clarke, Cheryl Gustin, Michele Hoskins, Kevin McClure, Carolyn Olsen, and Ron Neeley (Utah Geological Survey) drafted figures, designed displays, photographed core, and assembled reports. This report was desktop published by Cheryl Gustin.

Mobil Exploration/Producing Technical Center supplied the mini-permeameter and technical training and field assistance was provided by J.R. Garrison, Jr.

This report was reviewed by Bryce Tripp, Dave Tabet, and Mike Hylland, Utah Geological Survey, and Viola Schatzinger and Robert Lemmon, National Petroleum Technology Office, U.S. Department of Energy.

Muddy Creek Canyon Case-Study

The study of Kf-2 in Muddy Creek Canyon was conducted by Thomas A. Ryer of The ARIES Group, Inc. Original funding for that effort was provided by BP Exploration, Anchorage. Edmund R. Gustason's arranging of BP funding and his continued support and many helpful comments throughout the course of the project are gratefully acknowledged. Wellsite geology was done by Rick Geesaman and Paul B. Anderson, Consulting Geologists. The cores were slabbed at the Utah Geological Survey Sample Library. Anderson oversaw the slabbing work and labeled the slabbed cores for depth. Robert P. Fillmore measured ten detailed stratigraphic sections on vertical or near-vertical exposures. Mihaela S. Ryer lent capable support to many phases of the project, particularly those involving computer applications, including preparation of the logs and photo sections.

The Muddy Creek cores were described by Edmund R. Gustason of BP Exploration together with Janok Battacharya and Robert S. Tye of ARCO. They used graphical software to compile the descriptions. Their descriptions are not included in this report: they were published previously in Gustason and others, 1993.

Work in Muddy Creek Canyon was continued under the Utah Geological Survey's DOE-funded study of the Ferron. This work involved integration of the findings of the Muddy Creek study into the broader, regional analysis of the Ferron. This continued work facilitated the refinement of paleoenvironmental interpretations for Kf-2 in the Muddy Creek Canyon area.

CHAPTER I
INTRODUCTION

T.C. Chidsey, Jr., T.A., Ryer, and T.H. Morris

Introduction

River and wave-dominated deltaic reservoirs have the largest developed oil reserves, and due to their high degree of reservoir heterogeneity, the largest amount of untapped and unrecovered oil within developed reservoirs. The Ferron Sandstone Member of the Cretaceous Mancos Shale is a deltaic deposit with excellent exposures of a variety of delta facies which accumulated along the margins of a rapidly subsiding basin (figures 1-1 and 1-2A). The Ferron Sandstone is an analog for many of the highly productive oil and gas reservoirs in the Gulf Coast, Rocky Mountain basins, Alaskan North Slope, North Sea, and many others worldwide. In addition to its value as a reservoir analog, sands and coalbeds of the Ferron Sandstone produce gas in the Wasatch Plateau and along the west-northwest flank of the San Rafael uplift. The Ferron coalbed methane play is currently the most active gas play in Utah. Initial production began in 1992; as of January 1, 2000, 117 billion cubic feet (BCF [3.3 billion m^3]) of gas have been produced from three new fields and an estimated 10 trillion cubic feet (TCF [283 billion m^3]) of in place gas reserves are identified in the trend (Utah Division of Oil, Gas and Mining, 2000; Tabet. 1995a, 1995b; Tabet and others, 1995, 1996).

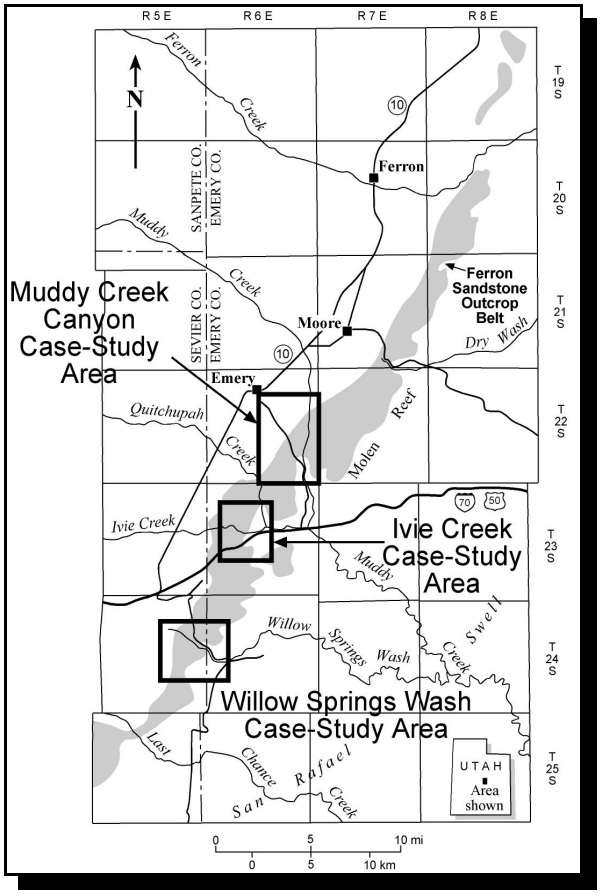


Figure 1-1. Location map of the Ferron Sandstone project area (outcrop belt is shaded) showing the Willow Springs Wash, Muddy Creek Canyon, and Ivie Creek case-study areas.

The Ferron accumulated on a deltaic shoreline in a rapidly subsiding portion of the Cretaceous foreland basin and consists of a series of stacked, transgressive-regressive cycles (deltaic-front sets) which are spectacularly displayed on outcrop. These various deltaic-front sets define a hierarchical pattern of seaward-stepping, vertically-stacked, and landward-stepping depositional geometries. On outcrop each deltaic-front set displays all, or portions, of each of the complex lithofacies that make up typical fluvial-dominated and wave-modified deltaic deposits. The excellent

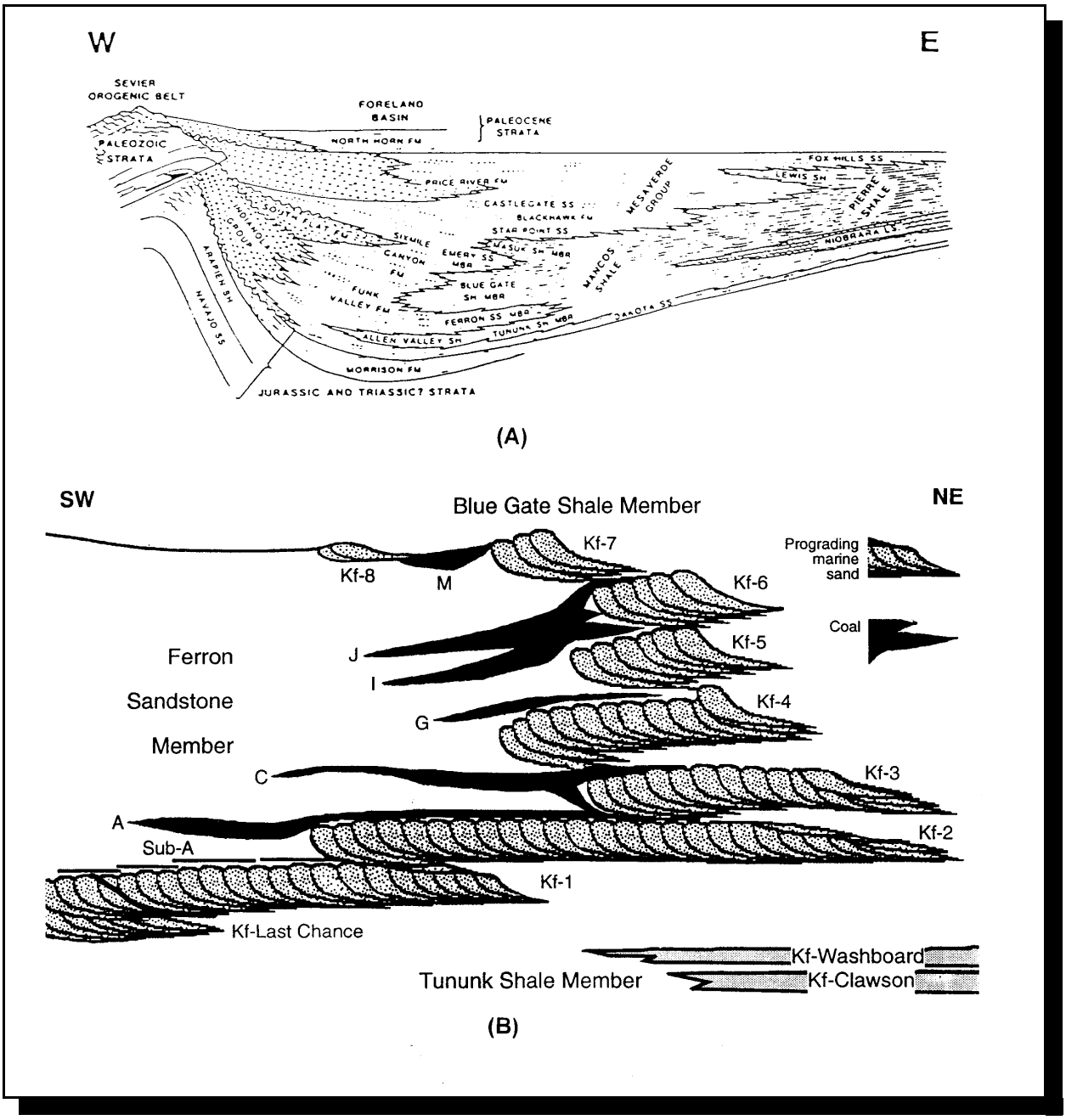


Figure 1-2. (A) Diagrammatic cross section showing the stratigraphy of Cretaceous strata from the Sevier orogenic belt of western Utah eastward to western Colorado (modified from Ryer, 1981a; originally modified from Armstrong, 1968). (B) Diagrammatic cross section in Castle Valley showing relative positions of Ferron parasequence sets with their associated coal zones (black), and the relative stratigraphic position within the Ferron Sandstone. The diagram has no scale.

exposures and accessibility of the three-tiered, hierarchical stacking pattern, and associated complex lithofacies of the deltaic-front sets make the Ferron Sandstone of Utah one of the best analogs for petroleum reservoirs in fluvial-dominated deltas throughout the world.

Efficient development of hydrocarbon reserves depends on a thorough knowledge of the characteristics of the rock units serving as the reservoir. Information about a reservoir is commonly acquired through wireline logs, cores, drill cuttings, and seismic data. The utility of these methods is attested to by the success of petroleum geologists in finding and developing hydrocarbon reservoirs.

In recent years, emphasis has been placed on applying computer simulations to establish reservoir development strategies. These simulations attempt to describe conditions within the reservoir and to predict fluid behavior under the influence of different development strategies. However, without an accurate knowledge of the actual characteristics of the reservoir rock, these models are only marginally useful. In an attempt to overcome this difficulty, modelers are taking into account the various scales of heterogeneity within reservoir rocks. Study of outcrop analogs is a means of identifying and quantifying these heterogeneities. Data obtained from the outcrop can be incorporated into the reservoir model to create a geologically realistic and potentially more accurate predictor of reservoir fluid behavior.

Heterogeneities within clastic rock reservoirs are essentially the result of depositional features, with some diagenetic overprint. Successful identification and prediction of reservoir heterogeneities becomes a matter of correctly identifying the geometry and scale of depositional features. The reservoir heterogeneity of the Ferron Sandstone is dramatically exposed, often in three dimensions, on outcrop. This study attempts to identify the types and scale of heterogeneities within rocks of the Ferron fluvial-deltaic system through sedimentologic and sequence stratigraphic analysis in order to formulate accurate reservoir development strategies.

To evaluate the Ferron Sandstone as a model for fluvial-deltaic reservoirs, the Utah Geological Survey (UGS), University of Utah, Brigham Young University, Utah State University, Amoco Production Company, Mobil Exploration/Producing Technical Center, The ARIES Group, and geologic consultant Paul B. Anderson entered into a cooperative agreement with the U.S. Department of Energy as part of its Geoscience/Engineering Reservoir Characterization program. The geological and petrophysical properties of the Ferron Sandstone were quantitatively determined and incorporated in reservoir models and fluid-flow simulations by this multidisciplinary team. This report summarizes the results of this seven-year project and provides recommendations for applying the results in producing fluvial-deltaic reservoirs (including the Ferron Sandstone itself).

Purpose and Objectives

The purpose of this multi-year project was to use the Ferron Sandstone to develop a comprehensive, interdisciplinary, and quantitative characterization of a well-exposed fluvial-deltaic reservoir to allow realistic inter-well and reservoir-scale modeling for improved oil-field development in producing reservoirs world-wide. This information should help to improve reserve estimates in fluvial-dominated deltaic reservoir systems and aid in designing more efficient production strategies.

Complex reservoir heterogeneities on both interwell and field scales are difficult to resolve during reservoir exploration and development activities. Standard industry approaches rely on

generic depositional models constrained primarily by data obtained from petrophysical (logging and coring) evaluations of exploration and development wells. The quantity, quality, and distribution of these data are typically insufficient to adequately model the reservoir. Work on the Ferron Sandstone assumed that detailed mapping of petrophysical and geological properties of this exposed reservoir would provide a more comprehensive model for reservoir simulation. Improved simulation results can be used to guide exploration and development strategies in reservoirs found in similar depositional environments.

The objectives of the project were: (1) **increase recoverable reserves** by identifying untapped compartments created by reservoir heterogeneity, (2) **reduce development costs** by more efficiently siting infill drilling locations, (3) **increase deliverability** by exploiting the reservoir along optimal fluid-flow paths, (4) **enhance the application of new technologies**, such as horizontal drilling, by identifying optimal drilling directions to maximize fluid-flow, and (5) **identify reservoir trends** for field extension drilling.

Approach

The primary approach of the study was to quantitatively determine the nature and variability of geological and petrophysical reservoir properties as displayed on the extensive exposures of the Ferron Sandstone. The project was divided into four tasks: (1) regional stratigraphic analysis, (2) case studies, (3) development of reservoirs models, and (4) field-scale evaluation of exploration strategies. Both new and existing data were integrated to create a three-dimensional database of spatial variations in porosity, storativity, and tensorial rock permeability at scales appropriate for inter-well and regional reservoir simulation.

Extensive vertical and lateral exposures offered an excellent opportunity for mapping the architecture, geometry, distribution of lithofacies, and for refining current models of the Ferron Sandstone. Case-study areas provided more detailed mapping and analysis of specific lithofacies important to reservoir production (figure 1-1). The existing database was augmented with additional detailed mapping of the three-dimensional geologic structure and determination of petrophysical properties of various lithofacies at case-study locations within the Ferron Sandstone outcrop belt which served as reservoir analogues. Determining permeability anisotropy within each facies was an important task that was accomplished by mapping lithofacies, grain sizes, and sedimentary structures.

Information was collected to identify flow units within each case-study area at the scale of a single production well. Three-dimensional gridded databases were developed that estimate the distributions of both scalar (porosity and storativity) and tensorial (permeability) petrophysical properties of flow units found within the various lithofacies of the Ferron Sandstone. Standard geostatistical approaches were used to extrapolate between the detailed study areas and other observation points.

Reservoir modeling at the field scale was performed to evaluate how a detailed understanding of the geological and petrophysical structure of the Ferron Sandstone will enhance exploration and development strategies in similar reservoir systems. Numerical simulations of reservoir response to multiple-well production strategies were used to quantitatively assess the effectiveness of both standard and modified strategies.

Synopsis of Ferron Stratigraphy and Depositional History

The Ferron Sandstone Member of the Mancos Shale is an eastward-thinning clastic wedge deposited during Turonian-Coniacian (Upper Cretaceous) time. Lower and upper parts of the Ferron are distinguished. The Lower Ferron consists, on outcrop, of shelf sandstones that were transported generally from north to south; the Upper Ferron consists of deltaic deposits that prograded from southwest to northeast. Eight correlatable and mappable units, designated Kf-1 through Kf-8 (figure 1-2B), are recognized in the Upper Ferron. Each unit records a transgressive-regressive cycle of sedimentation. The shoreline sandstone units that define the cycles are characterized by an initial forward-stepping arrangement, followed by vertical-stacking and then back-stepping arrangements. This architecture indicates an initial strong supply of sediment relative to the rate of creation of space within which sediment could accumulate, followed by near-balance, and then a relative decrease in sediment supply. The older shoreline units have much greater lengths along the Ferron outcrop belt, which roughly parallels deposition dip, than do the younger units. Some of the delta-front units can be subdivided into parasequences; several constitute parasequence sets.

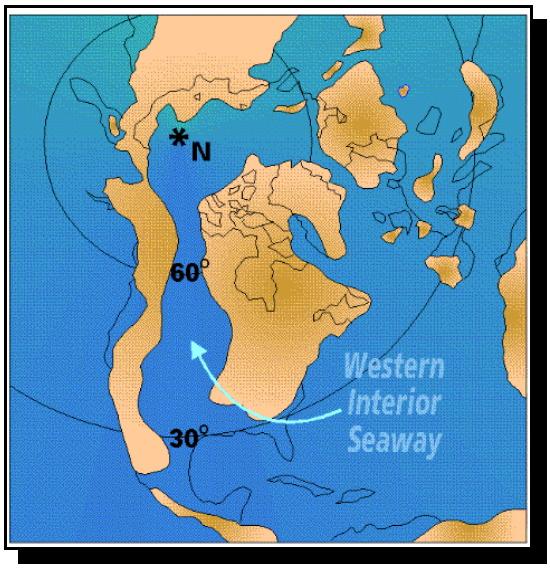


Figure 1-3. Paleogeography of North America during the peak of Cretaceous transgression during early Turonian time (modified from Hay and others, 1993).

Paleogeography

The Ferron Sandstone Member (figure 1-2A) of the Mancos Shale and equivalent parts of the Frontier Formation in northern Utah and Wyoming record a pronounced and widespread regression of the Western Interior Cretaceous seaway (figure 1-3) during middle Turonian through early Coniacian time. Rapid subsidence of a foredeep immediately east of the Sevier orogenic belt began in late Early Cretaceous time and continued through early Late Cretaceous time. Subsidence, however, was not uniform: during the Cenomanian (figure 1-4), the foredeep was strongly elongate and extended

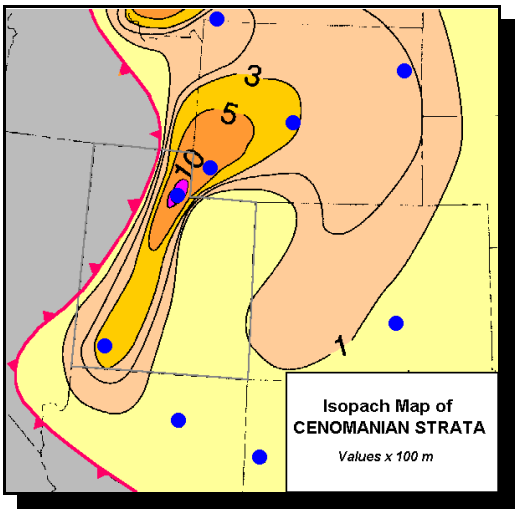


Figure 1-4. Isopach map of Cenomanian strata. A pronounced foredeep lies east of and parallels the Sevier orogenic belt, whose eastern edge is approximated by the thrust fault symbol (modified from Roberts and Kirschbaum, 1995).

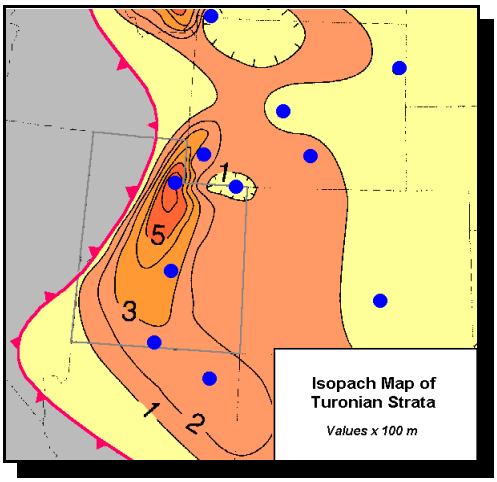


Figure 1-5. Isopach map of Turonian strata. The foredeep remains apparent, but subsidence became concentrated in northeastern Utah and southwesternmost Wyoming (modified from Roberts and Kirschbaum, 1995).

throughout Utah; during Turonian (figure 1-5) and Coniacian through Santonian time (figure 1-6), subsidence became concentrated in northern Utah and southwestern Wyoming and decreased in southern Utah. The relatively straight, north-trending western shoreline of the seaway had reached as far west as the Wasatch Range, the Gunnison Plateau, and the western side of the Markagunt Plateau during middle Turonian time (figures 1-7 and 1-8). The shoreline encroached to within tens of miles of the Sevier orogenic belt in some areas, the closest that it was to come during the Cretaceous. The Tununk Shale accumulated at sub-wave-base depths in central Utah at this time. As the shoreline prograded eastward during middle Turonian time (figure 1-9), the shoreline configuration changed. A pronounced curve of the shoreline developed, reflecting interaction between sediment supply and subsidence. This regression is represented by the Ferron Sandstone in central Utah and by the Frontier Formation in northeastern Utah. In northern Utah and southwestern Wyoming, subsidence was rapid, but sediment supply was more than enough to fill the depositional space created by subsidence. In central and southern Utah, subsidence and sediment supply were more nearly balanced. The embayment that developed in central Utah during Turonian time reflects the northward shift of subsidence during the Turonian.

Hale (1972) and later Cotter (1975a, 1975b) interpreted the bulges of the shoreline that developed in Utah during middle Turonian time to represent deltas, the Vernal delta to the north and the Last Chance delta to the south. Ryer and Lovekin (1986) argued that the embayment in central Utah was caused primarily by very rapid subsidence, that is for a given volume of sediment, the shoreline was able to prograde farther in the more slowly subsiding areas that lay to the north and south, less far in rapidly-subsiding central Utah. The question of just what constitutes an ancient delta aside, all previous investigators have agreed that the Ferron in Castle Valley accumulated on a deltaic shoreline in a rapidly subsiding portion of the Cretaceous foreland basin.

Transgression occurred during Coniacian time (figure 1-10). The sea transgressed rapidly across the Ferron coastal plain to a position near the western edge of the Wasatch Plateau. Coniacian strata are not known in the Henry Mountains basin, indicating that an unconformity exists between continental

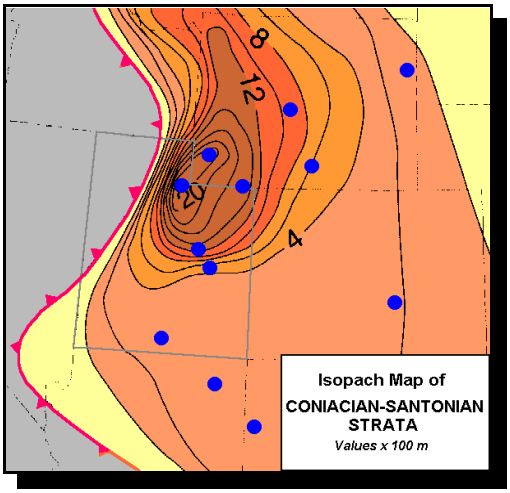


Figure 1-6. Isopach map of Coniacian and Santonian strata. Subsidence became strongly focused in northeastern Utah and southwestern Wyoming (modified from Roberts and Kirschbaum, 1995).

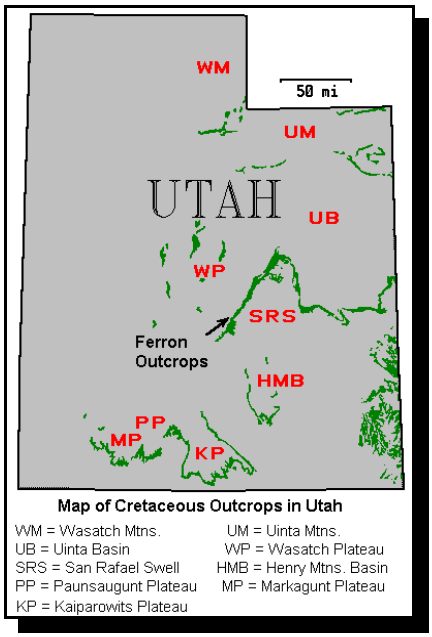


Figure 1-7. Map of Cretaceous outcrops in Utah. The Ferron outcrops lie on the west flank of the San Rafael Swell.

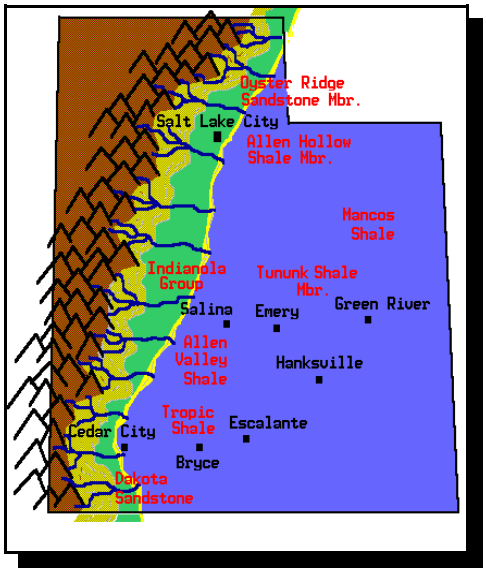


Figure 1-8. Paleogeography of Utah during early Turonian time. Labels identify principal stratigraphic units deposited at this time.

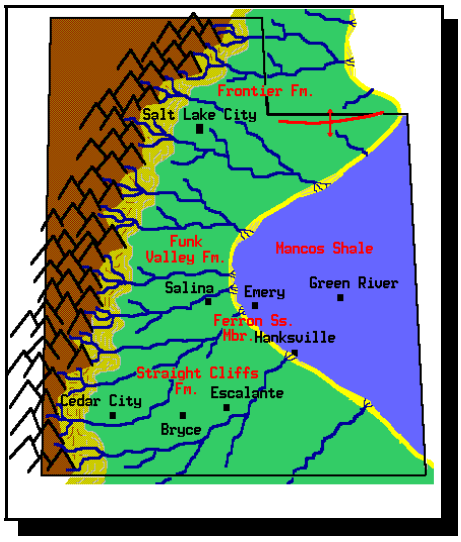


Figure 1-9. Paleogeography during middle Turonian time.

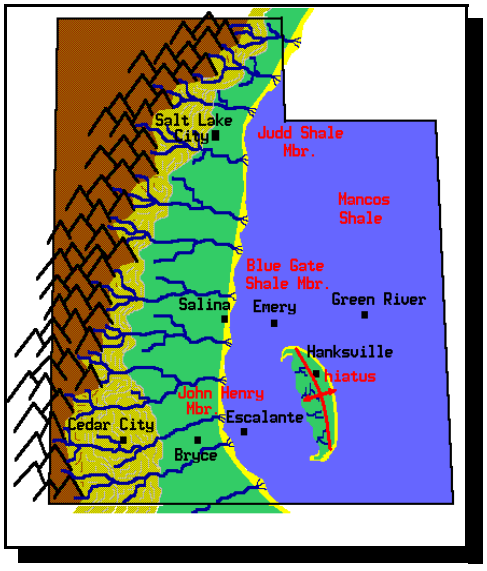


Figure 1-10. Paleogeography during Coniacian time. Coniacian strata are missing in the Henry Mountains basin of southeastern Utah (Peterson and others, 1980). This is interpreted as evidence of subaerial erosion on an island located along the crest of a peripheral bulge.

strata of the Ferron and overlying marine shales of the Blue Gate Shale. This unconformity may represent uplift of and erosion on a peripheral bulge. The erosion may have occurred subaerially, as pictured in figure 1-10, or entirely in marine environments.

Ferron Architecture

Ferron stratigraphy and architecture is shown in diagrammatic cross section figure 1-2. The Clawson and Washboard units, which constitute the Lower Ferron, are shelf sandstones that drifted southward along the hinge of the foreland basin, sourced from the shoreline in the vicinity of the present-day Book Cliffs. The Upper Ferron consists of fluvio-deltaics that were generally transported from southwest to northeast.

Ryer (1981a) recognized that the Upper Ferron consists of a series of stacked, deltaic units that can be defined in outcrop on the basis of cliff-forming delta-front sandstone bodies. These record transgressive-regressive cycles of sedimentation. Five major, correlatable, sandy delta-front units, Kf-1 through 5 in ascending order, plus three less widespread delta-front sandstones, later designated Kf-6, Kf-7, and Kf-8, were mapped. Each delta-front unit, with the exception of Kf-8, was found to have an associated coal bed. The coals carry letter designations originally assigned to them by Lupton (1916). Gardner (1993, 1995a, 1995b), Barton (1994), and Garrison and others (1997) have completed recent studies of the stratigraphy of the Ferron. The papers by Gardner and Barton provide detailed analyses of facies, stratigraphy, and depositional history. All of the recent authors place the Ferron in sequence stratigraphic frameworks, but with quite different results.

Parasequences and Parasequence Sets

Units Kf-1 through 5 can be subdivided into smaller-scale bodies of sediment that correspond to parasequences of Van Wagoner and others (1987). Each parasequence includes an upward-coarsening, upward-shoaling, progradational body of sediment deposited at the shoreline and is bounded above and below by marine-flooding surfaces. In the largely wave-dominated shoreline facies of Kf-1 and Kf-2, distinguishing parasequences is relatively easy inasmuch as the transgressive surfaces are readily defined in the field. Transgressive surfaces are generally more subtle in Kf-3 through 5, although that they too, can be subdivided into parasequences. Kf-1 and Kf-3 through Kf-5 correspond to parasequence sets of Van Wagoner and others (1987). Kf-6 and Kf-7 prograded shorter distances, and these units must be regarded as individual parasequences. Kf-8 prograded only about a mile (1.6 km) and constitutes a single parasequence. Kf-2 consists of two parasequence sets, presently designated Kf-2 early and Kf-2 late.

An important aspect of Ferron facies architecture is that the configuration of the delta-front sandstone bodies changed through time. The oldest sandstone unit, Kf-1 is widespread, having prograded a distance of 15 to 20 miles (24-32 km), and displays relatively little stratigraphic rise in the seaward direction. The minor amount of stratigraphic rise could be interpreted as evidence that progradation occurred during a period of slowly rising relative sea level compared to younger units, or if the rate of relative sea-level rise was essentially constant during Ferron deposition, that progradation occurred more rapidly than during deposition of the younger units.

The initial phase of progradation of Kf-2 (Kf-2 early) was characterized by a moderate amount of stratigraphic rise. The younger part of Kf-2 (Kf-2 later) plus delta-front units Kf-3 through 5 display larger amounts of stratigraphic rise. They prograded shorter distances, generally on the order of 5 to 10 miles (8-16 km). Either relative sea level rose more rapidly during their deposition, or the rate of sediment supply decreased relative to what it was during deposition of Kf-1 and the older part of Kf-2.

These changes are still more pronounced for sandstone bodies Kf-6, Kf-7, and Kf-8. They display a considerable amount of stratigraphic rise and prograded no more than a few miles. Kf-7 is displaced considerably landward from Kf-6; Kf-8 is likewise displaced landward from Kf-7. The rate of rise of relative sea level during deposition of these units was so rapid, or the rate of sediment supply to the shoreline system so reduced, that the shoreline prograded for only brief periods of time. Progradation of delta-front unit Kf-8 was terminated by an abrupt transgression of the Blue Gate sea. The transgression ultimately pushed the shoreline westward to the eastern flank of the Wasatch Range, the western side of the Wasatch Plateau, and the eastern side of the Kaiparowits Plateau in Coniacian time.

In Ferron deltaic deposits, parasequences may be considered as primary reservoir building blocks because marine and/or delta-plain shales act as laterally extensive permeability barriers and commonly separate parasequences. Fluid-flow communication may occur between parasequences where shales are absent due to erosion or non-deposition. Porosity and permeability values, dependent on lithofacies distribution, vary laterally and vertically within a parasequence. Mouth-bar and proximal-delta-front lithofacies are high quality reservoirs; these lithofacies are related to spatial arrangement of parasequences making up the reservoir. Therefore, the initial stage in reservoir characterization must include an analysis of the architecture of parasequences and of lithofacies within parasequences.

CHAPTER II
PREVIOUS STUDIES

Thomas A. Ryer, David E. Tabet, and Thomas C. Chidsey, Jr.

Stratigraphy

Early Studies of the Ferron

The Ferron Sandstone was described as a member of the Mancos Shale by Charles T. Lupton (1916) in his comprehensive study of the geology and coal resources of Castle Valley. Lupton mentioned the Ferron in an earlier publication (1914), making this the first formal use of the name, but the first meaningful description of the Ferron occurs in his 1916 work. Lupton did not designate a type locality or type section for the Ferron, stating simply that the member "is well developed in the vicinity of Ferron and Emery" (Lupton, 1916, p. 31.) In his description of the Ferron, he included a 475-foot-(145-m-) thick stratigraphic section that he had measured through the Ferron in Ivie Creek Canyon, about 8 miles (13 km) south of the town of Emery (figure 1-1). It is clear that he considered the Ivie Creek section representative of the Ferron and its coalbeds. Had the designation of a type section been required in the naming of a stratigraphic unit then, as it is today, it is likely that Lupton would have chosen the Ivie Creek section as his type section for the Ferron.

At least two geologists, Hoxie (1874) and Taft (1906), had examined the Ferron outcrops in Castle Valley prior to Lupton's study. Both had misinterpreted its stratigraphic position, but in different ways. Hoxie (1874) interpreted the coal-bearing Ferron outcrops in the vicinity of Emery to be a down-faulted block of Montana Group strata (the coals, therefore, belonging to what is now known as the Blackhawk Formation -- see account by Lupton, 1916, p. 9). Taft (1906) believed that the Ferron in Castle Valley belonged to the Jurassic section (what Lupton [1916] and other early workers referred to as the McElmo Formation, which apparently spanned the Carmel through Morrison Formations of today's terminology).

Taft's work was very much reconnaissance in nature, but he did formally name some of the stratigraphic units. The Tununk Shale was designated the "Shale of the San Rafael Swell", the Ferron the "Sandstone of the Red Plateau," and the Blue Gate Shale the "Shale of Castle Valley." According to Lupton (1916), Red Plateau is an antiquated name for Cedar Mountain, at the northwestern edge of the San Rafael uplift. The Ferron is not present on Cedar Mountain. Taft had miscorrelated the Ferron with the Jurassic section. These names were not used by any subsequent authors. Taft produced a generalized map of Castle Valley (figure 2-1). On it is traced the contact between the Blue Gate Shale and the Ferron Sandstone. The contact is more or less correct between Ivie Creek and Ferron Creek, but farther north is misplaced toward the east.

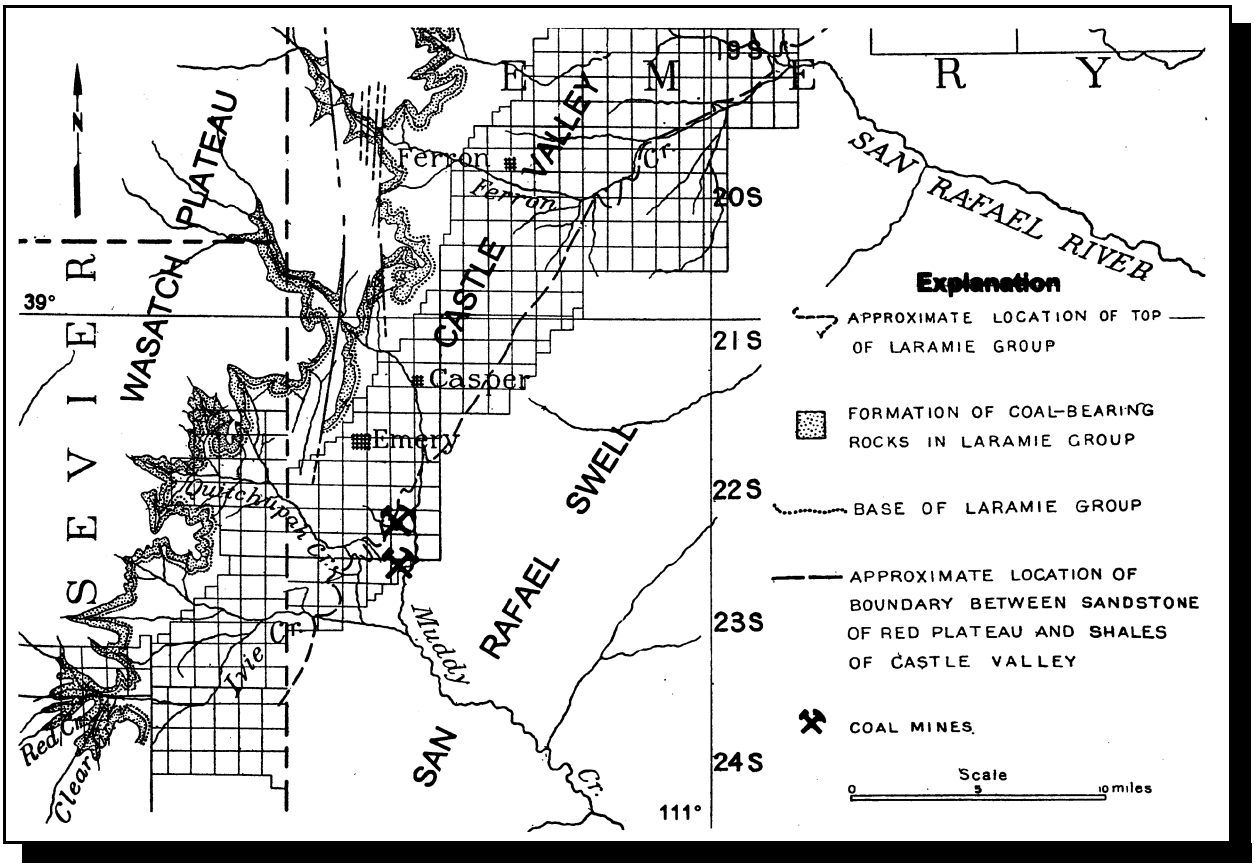


Figure 2-1. Southwestern part of the map included in Taft's (1906) report. The dashed line is the Blue Gate Shale/Emery Sandstone contact (modified from Taft, 1906). The northern of the two coal mines south-southeast of Emery is the Casper mine; the southern is the Bear Gulch mine.

The transgressions responsible for deposition of the Tununk Shale, the regression that led to deposition of the Ferron, and the transgression that marks the change from Ferron to Blue Gate deposition were widespread events in the Western Interior. Sandy strata equivalent to the Ferron had been recognized in the Henry Mountains basin by Gilbert (1877). He named this unit the Tununk Sandstone and the underlying marine shale the Tununk Shale. The marine shale overlying his Tununk Sandstone he named the Blue Gate Shale and the ridge-forming sandstone above that the Blue Gate Sandstone (Gilbert's Blue Gate Sandstone, which is equivalent to the Star Point Sandstone of the Wasatch Plateau, has recently been renamed the Muley Canyon Sandstone by Eaton, 1990). Lupton (1916) miscorrelated the Castle Valley and Henry Mountains basin sections, equating the shale beneath the Ferron in Castle Valley to the Blue Gate Shale, and possibly the Tununk Sandstone and Tununk Shale as well, and the Ferron Sandstone of Castle Valley to the Blue Gate Sandstone of the Henry Mountains basin. The error probably stems from the very similar appearances of the ridges formed by the Ferron along the Molen Reef and Coal Cliffs outcrops on the west flank of the San Rafael uplift and those formed by Gilbert's Blue Gate Sandstone around Caineville, in the northern part of the Henry Mountains basin.

Lupton's (1916) study of the Ferron was very much focused on coal: his description of the rocks of the Ferron is rudimentary and lacks any discussion of facies. Lupton noted the pronounced northeastward thinning and loss of sandstone in the Ferron, but did not offer any interpretation he may have had of how and why such a change takes place. He did comment on the presence of "local unconformities" in the Ferron, one of which he documented in a photograph. The photo (his Plate IIIB) illustrates a fluvial channel scoured into the basal shallow-marine sandstone unit (our Kf-1) on exposures along the west side of Blue Trail Canyon south of I-70. Discordance between the inclined strata of a point-bar deposit within the channel fill and the horizontally bedded sandstone of the underlying shoreface constitutes the evidence for an unconformity. Although Lupton did not discuss the origin of this angular contact in the Ferron, his discussion of a similar feature that he recognized in the Dakota Sandstone makes it clear he understood that the angular "local unconformities" were products of channels cut into pre-existing sediments.

Lupton portrayed Ferron stratigraphy using a series of measured sections (figure 2-2) ranging from the Paradise Lake area of the Fish Lake Plateau on the south to the Castle Valley outcrops south of Wellington on the north. Five of the eight sections are hung on his A coalbed. To the northeast, beyond the limit of deposition of the A coal, carbonaceous shale is identified and used as a datum in sections at Short Canyon and Horn Silver Gulch, east of Ferron. This carbonaceous shale, which forms a conspicuous black band on fresh outcrops, is of marine origin and occupies a position between the top of the Washboard Unit and the base of Kf-2, gradually changing facies to normal silty marine mudstone southward along the Molen Reef. Lupton's northern three sections are hung too high. Although he noted some of the principal lithologic differences between the Ferron sandstones in the northern part of Castle Valley and the coal-bearing Ferron strata in the southern part, he failed to recognized that they occupied slightly different stratigraphic positions.

Despite the above-mentioned correlation problem, plus what we now recognize to be some minor miscorrelations of the coals, Lupton's simple cross section identifies the fact that most of the northeastward thinning of the Ferron is observed in its upper part. It is fairly clear that Lupton did not recognize the lateral equivalence of the upper part of the Ferron and the lower part of the Blue Gate Shale to the northeast. His was a simple, layer-cake stratigraphy with the complication that one of the layers varied in thickness.

Because Lupton (1916) designated the Ferron as a member of the Mancos Shale and because this has become standard U.S. Geological Survey usage, subdivisions of the Ferron must be sub-member-level units. Assignment of the Ferron to member status came about as a result of the westward extension of stratigraphic terminology as geologists moved westward during the course of their early studies. The Mancos Shale was originally named for outcrops in southwestern Colorado (Cross and Spencer, 1899), where the Mancos lacks sandy members. Upon encountering sandstones in the Mancos in Castle Valley, Lupton (1916) chose to distinguish members, rather than to elevate the Mancos to group status and recognize formations within it. In hindsight, this was an unfortunate choice. On the basis of its thickness and wide areal extent, the Ferron Sandstone, the Emery Sandstone, and the marine shale intervals that separate them certainly deserve formation status. Some authors (most notably Hale, 1972) have, in fact, described the Ferron as a formation, but without going through the exercise of formally proposing a change in status.

Although it lacked detailed stratigraphic description, Lupton's (1916) study of the Ferron provided a sound foundation on which subsequent investigators could build.

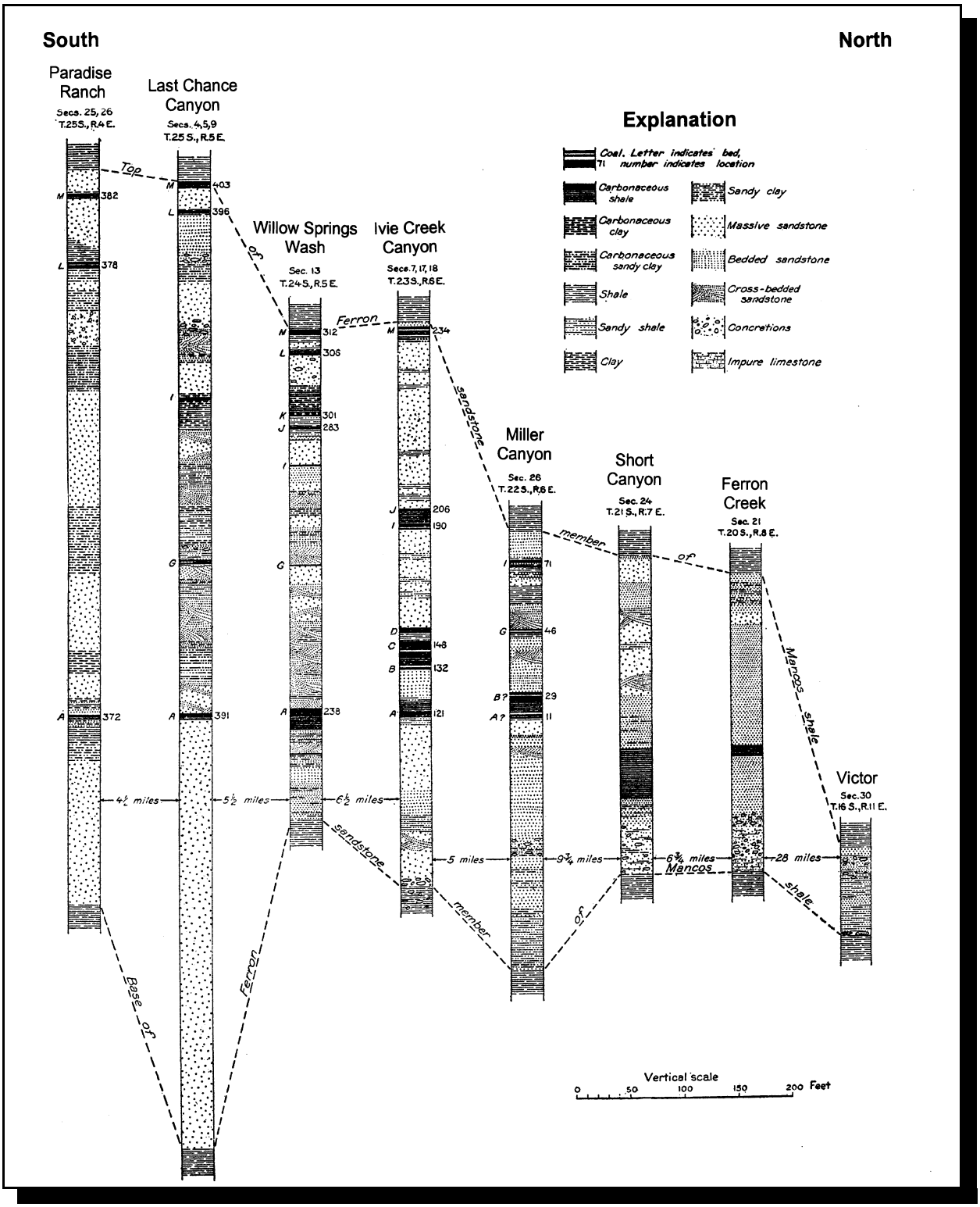


Figure 2-2. Lupton's (1916) cross section showing stratigraphy between Paradise Ranch and Victor (a settlement in Castle Valley, between the towns of Cleveland and Wellington, that does not appear on modern maps). After Lupton, 1916.

The first publications that attempted to place the Ferron Sandstone in a paleoenvironmental setting was authored by Spieker and Reeside (1925, 1926). The earlier publication (Spieker and Reeside, 1925) focused on the stratigraphy of Castle Valley and the eastern side of the Wasatch Plateau; the second attempted to correlate the Castle Valley section westward to isolated Cretaceous outcrops on the western margin of the Wasatch Plateau near the towns of Manti and Salina. The papers are interesting for their descriptions of stratigraphy, but more importantly, represent a significant conceptual advance, portraying lateral as well as vertical relationships between the formations.

Regional Stratigraphy: Spieker and Reeside's 1925 paper portrays northeastward interfingering of the upper part of the Ferron and the lower part of the Blue Gate Shale, the base of the Ferron being drawn as a horizontal surface in Castle Valley. Citing the presence of coal in drill holes near Price, they noted (p. 438) the "regional tendency of the Cretaceous beds to change westward from marine to littoral, to continental and coal-bearing sediments." This is the situation pictured, albeit in a very general way, along the Castle Valley outcrops for the upper part of the Ferron.

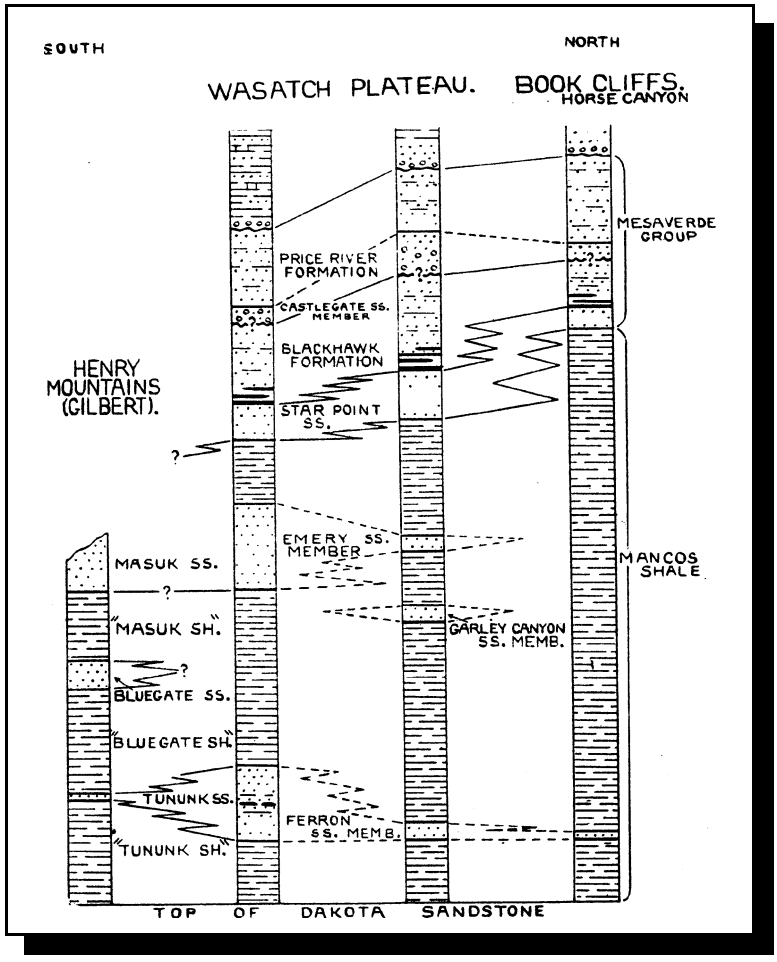


Figure 2-3. Lower part of Spieker and Reeside's (1925) cross section. The Masuk Sandstone of the Henry Mountains basin is miscorrelated with the Emery Sandstone Member of Castle Valley. Modified from Spieker and Reeside (1925).

Spieker and Reeside's correlations between the Henry Mountains basin, Castle Valley, and the western part of the Book Cliffs are shown in figure 2-3. Note the northeastward interfingering of the upper part of the Ferron Sandstone and the lower part of the Blue Gate Shale. Section 1, at the left, is based on Gilbert's (1877) study of the Henry Mountains basin; sections 2 and 3 represent the southern and northern parts of Castle Valley; section 4, at the right, is at Horse Canyon, in the Book Cliffs. Lupton's (1916) miscorrelation of the Ferron Sandstone of Castle Valley with the Blue Gate Sandstone of the Henry Mountains Basin is corrected. The Ferron is properly shown as equivalent to Gilbert's Tununk Sandstone (the name Tununk Sandstone was discarded and replaced with the name Ferron Sandstone Member by Hunt [1946]).

Lupton's miscorrelation between the Castle Valley and Henry Mountains basin sections was the first of several. Although Lupton's Ferron Sandstone-Blue Gate Sandstone miscorrelation is corrected in Spieker and Reeside's cross section, a new miscorrelation was introduced: the Emery Sandstone of Castle Valley is shown as being equivalent to Gilbert's (1877) Masuk Sandstone of the Henry Mountains basin. Hunt (1953) offered a different correlation: they equated the Emery Sandstone of Castle Valley with Gilbert's Blue Gate Sandstone. This correlation, too, was incorrect. Peterson and Ryder (1975; see also Peterson and others, 1980) were the first to interpret the relationships correctly: Gilbert's Blue Gate Sandstone is equivalent to the Star Point Sandstone on the eastern side of the Wasatch Plateau; Gilbert's Masuk Sandstone is equivalent to the Castlegate Sandstone of the Mesaverde Group. The Emery Sandstone of Castle Valley has no sandstone equivalent in the Henry Mountains basin. Eaton (1990) offers a review of the stratigraphic terminology applied to the Cretaceous section in the Henry Mountains basin in recent years. Although the correlation of units between the Castle Valley and Henry Mountains basin sections is now well understood, one serious problem remains: the Masuk Shale Member of the Mancos in its type area in the Henry Mountains basin consists of brackish-water to continental strata and is younger (being equivalent to the Blackhawk Formation) than the Masuk Shale Member as that term is still used in Castle Valley. Revision of the Castle Valley terminology is needed.

Paleogeography: Spieker and Reeside's 1926 paper offers a broader paleoenvironmental interpretation of the Ferron. They interpreted the Ferron Sandstone in Castle Valley to represent a sandy peninsula or shoal area in the sea (figure 2-4) that extended southward from the area of the present-day Wasatch Mountains and Uinta Basin. A unit of marine shale recognized on outcrops along the western side of the Wasatch Plateau, and subsequently named the Allen Valley Shale by Spieker (1946), was correlated with the Ferron, as were shales of the Mancos east of Castle Valley. The correlation across the breadth of the Wasatch Plateau was incorrect, although the error was not recognized until the 1950s (it remains in Spieker's landmark 1946 paper detailing Mesozoic and Cenozoic stratigraphy and paleogeography in central Utah). Spieker and Reeside's (1926) interpretation of Ferron paleogeography is the first of several interpretations in which all or part of the Ferron in Castle Valley was reconstructed as a southward-extending body with a northern provenance surrounded on three sides by shaly strata.

Study of the Ferron Accelerates

Gas was discovered in the Ferron Sandstone at Clear Creek field in the northeastern part of the Wasatch Plateau in 1951 (see **Petroleum in the Ferron** section later in this chapter). The discovery prompted the publication of several studies in the 1950s that led to a great improvement in the understanding of Ferron stratigraphy and depositional history.

Katich (1953, 1954) studied the Ferron in the vicinity of the Wasatch Plateau and came to a very different conclusion about Ferron paleogeography than had Spieker and Reeside (1926). The presence of the ammonite *Collignoniceras woollgari* in both the Allen Valley and Tununk Shales demonstrated their equivalence. The Ferron was shown (Katich, 1953) to be younger than the Allen Valley Shale, being equivalent, instead, to the lower part of the Funk Valley Formation (Spieker, 1946) of the western Wasatch Plateau.

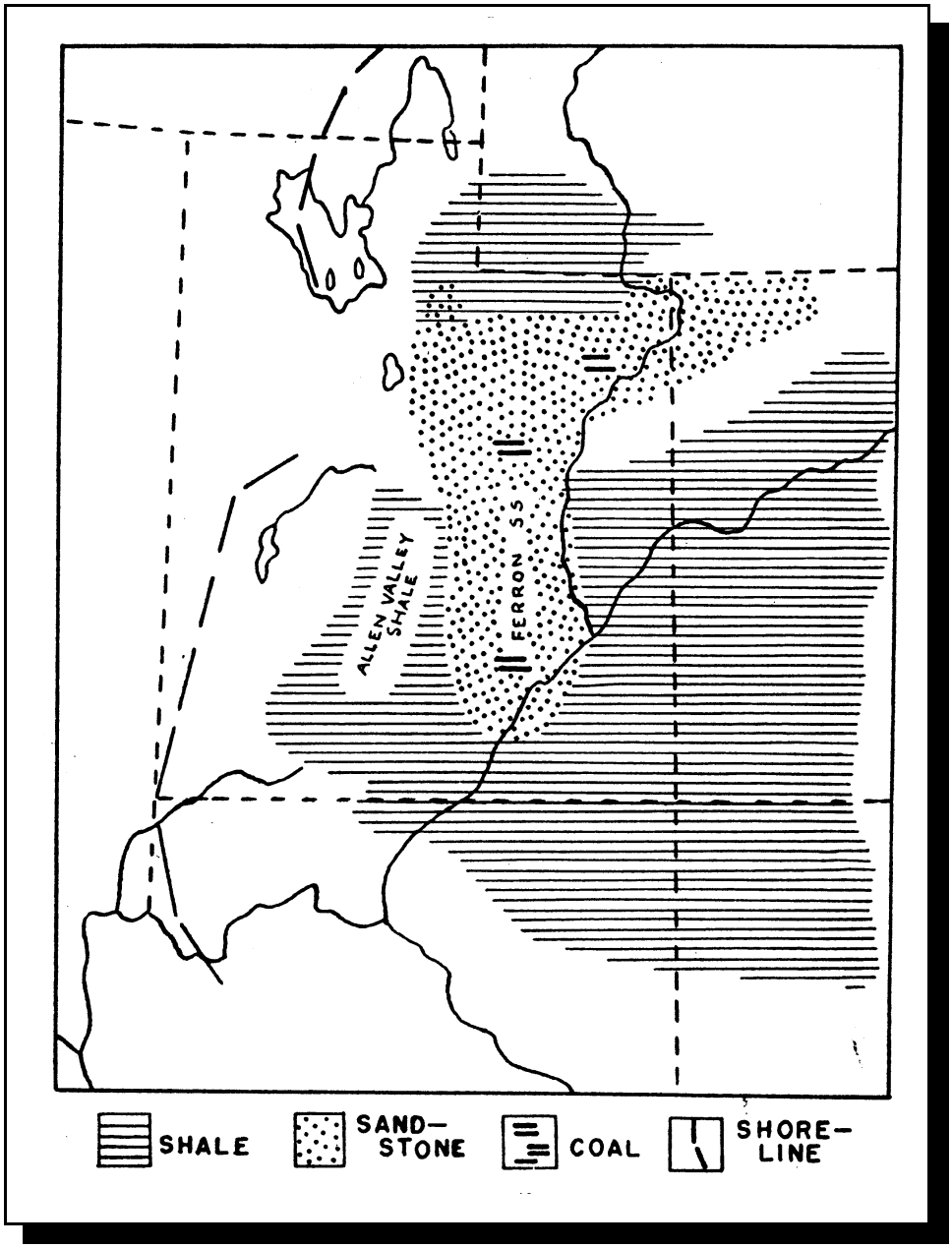


Figure 2-4. Paleogeography of the Ferron Sandstone as reconstructed by Spieker and Reeside (1926), as redrawn by Katich (1953). The Ferron Sandstone and the Allen Valley Shale were interpreted to be age-equivalent. From P.J. Katich, Jr., AAPG Bulletin Vol. 37, No. 4, AAPG ©1953, reprinted by permission of the American Association of Petroleum Geologists; modified from Spieker and Reeside, 1926.

Katich's (1953) paleogeographic map (figure 2-5) represents Ferron paleogeography in a much simpler form and resembles paleogeographic maps produced by most later authors. Analysis of cross stratification in fluvial sandstone of the Ferron further convincingly demonstrated that the Ferron had a western and southwestern, not a northern, source.

Davis (1954) studied the Ferron and reached many of the same conclusions that Katich had. Davis confirmed a concept that had earlier been reached by Katich (1951) in his dissertation, but retracted in his publication (Katich, 1954): that the Ferron consists of two distinct parts. Davis designated these the lower and upper members of the Ferron.

The Lower Ferron consists of gray, fine-grained, calcareous, marine sandstone and siltstone and contains two distinctive horizons bearing large, "cannon-ball" concretions. It extends from "Molen Amphitheater" and the southern part of Molen Reef northeastward to the vicinity of Price, generally varying between 60 and 70 feet (18 and 21 m) in thickness. Davis believed that he could recognize the Lower Ferron on wireline logs run in the gas wells of Clear Creek field. He correlated the Lower Ferron to the uppermost, silty and sandy part of the Tununk

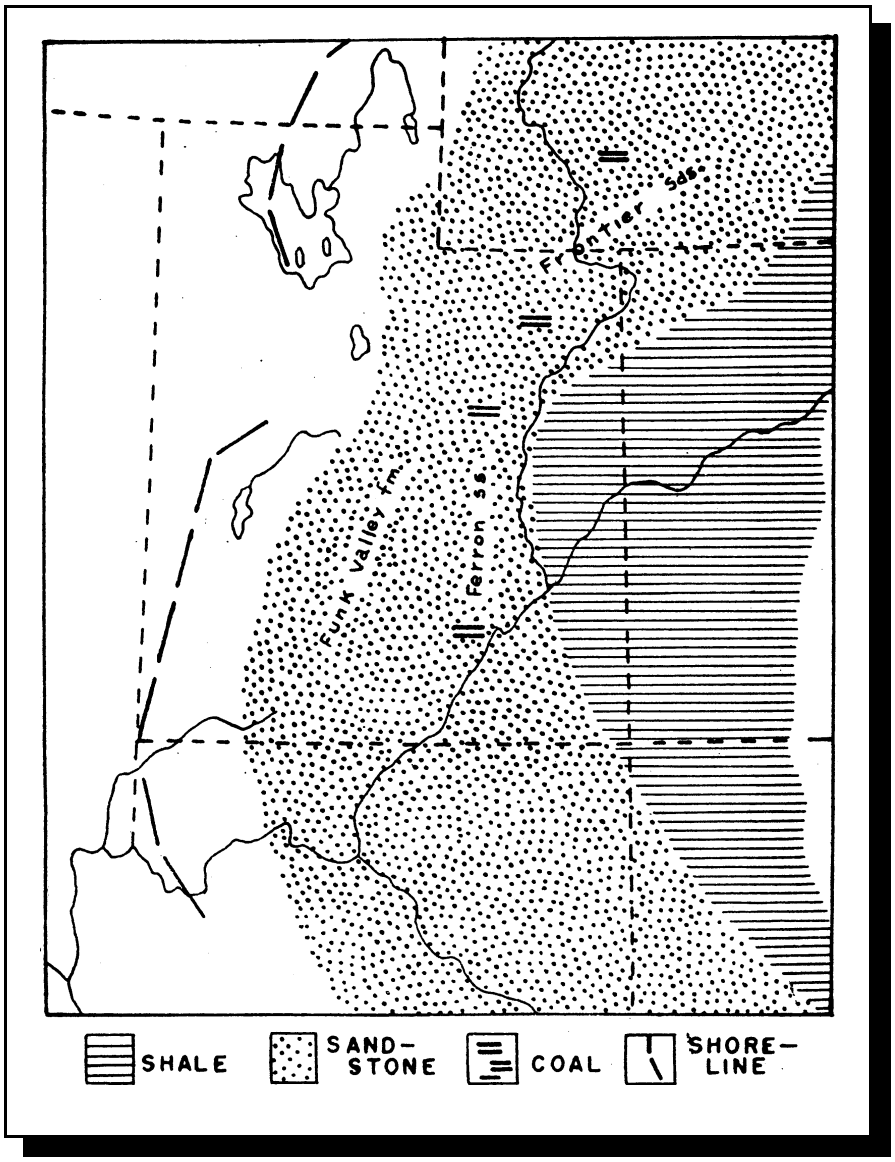


Figure 2-5. Katich's (1953) reinterpretation of Ferron paleogeography. The Ferron is correctly correlated with the basal part of the Funk Valley Formation, eliminating the peninsula and the bay that lay west of it that had been interpreted by Spieker and Reeside (1926). From P.J. Katich, Jr., AAPG Bulletin Vol. 37, No. 4, AAPG ©1953, reprinted by permission of the American Association of Petroleum Geologists; modified from Spieker and Reeside, 1926.

Shale in the Henry Mountains basin. Southward thinning and loss of sandstone suggests a northern or northwestern source, although no paleocurrent or other definitive data was cited in support of this interpretation.

The Upper Ferron comprises a much wider variety of rocks than does the Lower Ferron: shallow-marine sandstone, coal, carbonaceous shale, and fluvial sandstone in highly lenticular bodies are common. The Upper Ferron is about 500 feet (150 m) in thickness south of Emery, feathering out into marine shale northeastward along the Castle Valley outcrops. The paleocurrent data indicating a southwestern source described by Katich (1953) and confirmed by Davis (1954) are all from strata of the Upper Ferron.

Davis' (1954) studies led him to the conclusion that "a decided change in sedimentation took place in the passage from the Lower Ferron to Upper Ferron time. Deposition from the northwest and western sources became practically insignificant as compared with a new strong supply that began to come from the southwest." This conclusion has been borne out by all later studies, with one notable exception discussed later.

Edson and others (1954) described the productive Ferron section in Clear Creek field. Seven sands were recognized in the discovery well, leading to a "1st" (shallowest) to "7th" (deepest) sandstone terminology that was applied throughout the field. Detailed correlation of the well logs indicates that only the 7th sandstone is continuous throughout the field; all of the other sandstones are highly lenticular and their number and positions vary between well bores. Although Edson and others (1954) did not interpret facies and paleoenvironments, it is now clear that the basal sandstone was deposited on the prograding shoreline and that the remaining, shallower sandstones are of fluvial origin.

Knight (1954) studied the heavy mineral content of samples of Ferron Sandstone collected from outcrops and from wells drilled on the Wasatch Plateau. Correlating sandstones between wells at Clear Creek field had proven to be very difficult. Knight's study was undertaken with the purpose of determining whether or not heavy minerals were of value in establishing correlations between individual sandstone beds of the Ferron in the subsurface. His results are negative, with the exception of one general conclusion that lends support to the paleoenvironmental interpretations of Katich (1953) and Davis (1954): that "confinement of ... garnet to the southern area [southern part of Castle Valley] seems to indicate a sedimentary realm separated by one means or another from that in which the rest of the Ferron was deposited and also a separate, local source area."

Important papers describing the petroleum geology of latest Paleozoic through Early Tertiary strata beneath the Wasatch Plateau and on the western flank of the San Rafael uplift were published by Walton (1954, 1955). The bearing of Walton's papers on hydrocarbons in the Ferron is discussed later, but one critical point must be mentioned here because it influenced the paleoenvironmental interpretation of some later investigators. Walton (1955, p. 399), in a brief description of the Ferron, stated that the member "has little or no coal [in the northeastern part of the Wasatch Plateau] and appears mostly marine throughout." Subsequent work has shown that only the basal sandstone section of the Ferron is of shallow-marine origin beneath the northeastern part of the Wasatch Plateau; the remainder is composed of continental strata. Coal is best developed in a position farther to the east. Much the same relationship can be documented on the Ferron outcrops in the southern part of Castle Valley and on the east flank of the Fish Lake Plateau.

Ferron Deltas

Cretaceous paleogeography was reconstructed for a broad area including northeastern Utah, northwestern Colorado, and southwestern Wyoming by Hale and Van De Graaff (1964). Castle Valley lies at the southwestern edge of their maps. Hale and Van De Graaff (1964, p. 129) mapped a large "eastward bulging delta-like feature" centering on what are now the Uinta Basin and Uinta Mountains and extending eastward just beyond the Utah-Colorado state line. They referred to it as the "Vernal delta." Their map shows a narrow embayment on the southern flank of the delta, stretching southwestward from the area north of Price to the vicinity of Clear Creek field. Although Hale and Van De Graaff offered no evidence to support the existence of this embayment, there can be little doubt that it's origin lies in Walton's (1954 and 1955) assertions that the Ferron at Clear Creek field is mostly or entirely of marine origin.

Hale (1972) studied subsurface data from wells drilled during the 1950s and early 1960s in the search for gas beneath the Wasatch Plateau and combined them with original outcrop studies to arrive at a new interpretation of Ferron paleogeography and depositional history. He elaborated on Davis' (1954) concept of two distinct members of the Ferron, although he defined them in a different way. He revived Spieker and Reeside's old idea of a southward-extending peninsula, though in a different location. Two paleogeographic maps (figures 2-6 and 2-7) summarize Hale's concepts.

Hale (1972) recognized two geomorphic features on which predominantly sandy sediments accumulated during early Ferron time: the "Castle Valley bar" in the north, a west-southwestward extending peninsula supplied with sediment from the Vernal delta and fed by long-shore drift, and the "Last Chance delta", a northeastward extending deltaic complex fed from the southwest and named for exposures along Last Chance Creek on the east side of the Fish Lake Plateau. A large inlet situated at the town of Ferron separated the two and allowed exchange of marine water with the "Sanpete Valley embayment," which lay to the west of both features. The Sanpete Valley embayment is the most significant feature in this interpretation, defining the northwestern margin of the Last Chance delta and the western margin of the Castle Valley bar. The only evidence Hale offered for the existence of the Sanpete Valley embayment is Walton's (1954, 1955) statement that the Ferron at Clear Creek field is entirely of marine origin. Aware that the Ferron includes coal in many of the wells that penetrated the embayment section, Hale (1972) rationalized that the "few thin carbonaceous shales and coaly streaks are ... carbonaceous matter derived from [an] adjacent paludal environment."

Hale defined the "Lower Ferron", a member-level unit, to including the deposits of the Castle Valley bar and the Sanpete Valley embayment, plus time-equivalent deposits in the lower part of the Last Chance delta. Rise of relative sea level subsequently submerged the Castle Valley bar and the area of the Sanpete Valley embayment opened to become part of the Mancos seaway. The "Upper Ferron" includes the younger part of the Last Chance delta. Davis (1954; and Katich, 1951, before him) had interpreted the Lower Ferron to be an older, northern depositional system and the Upper Ferron a younger, southern system. Hale's interpretation of contemporaneity of the northern Ferron system and the lower part of the southern deltaic system is quite different. Subsequent work would show the earlier interpretations of Katich and Davis to be the correct one. Although Hale's (1972) interpretation of paleogeography was rejected, his Vernal and Last Chance deltas have been recognized, at least as generalized features, by most students of the Ferron who followed.

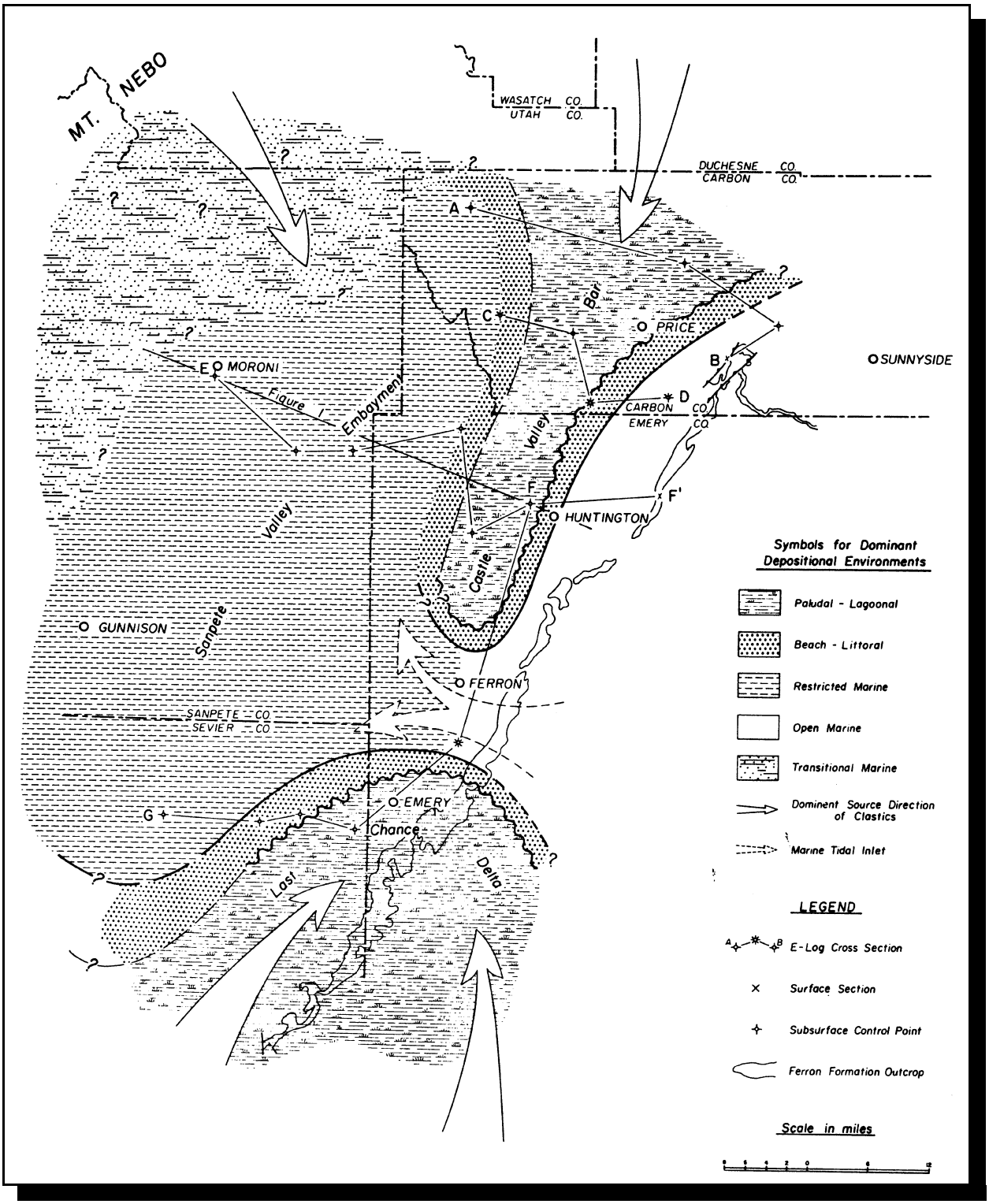


Figure 2-6. Hale's (1972) interpretation of early Ferron paleogeography. The critical feature in this map is the Castle Valley bar, which separated the large Sanpete Valley embayment from the Cretaceous seaway. From Hale, 1972.

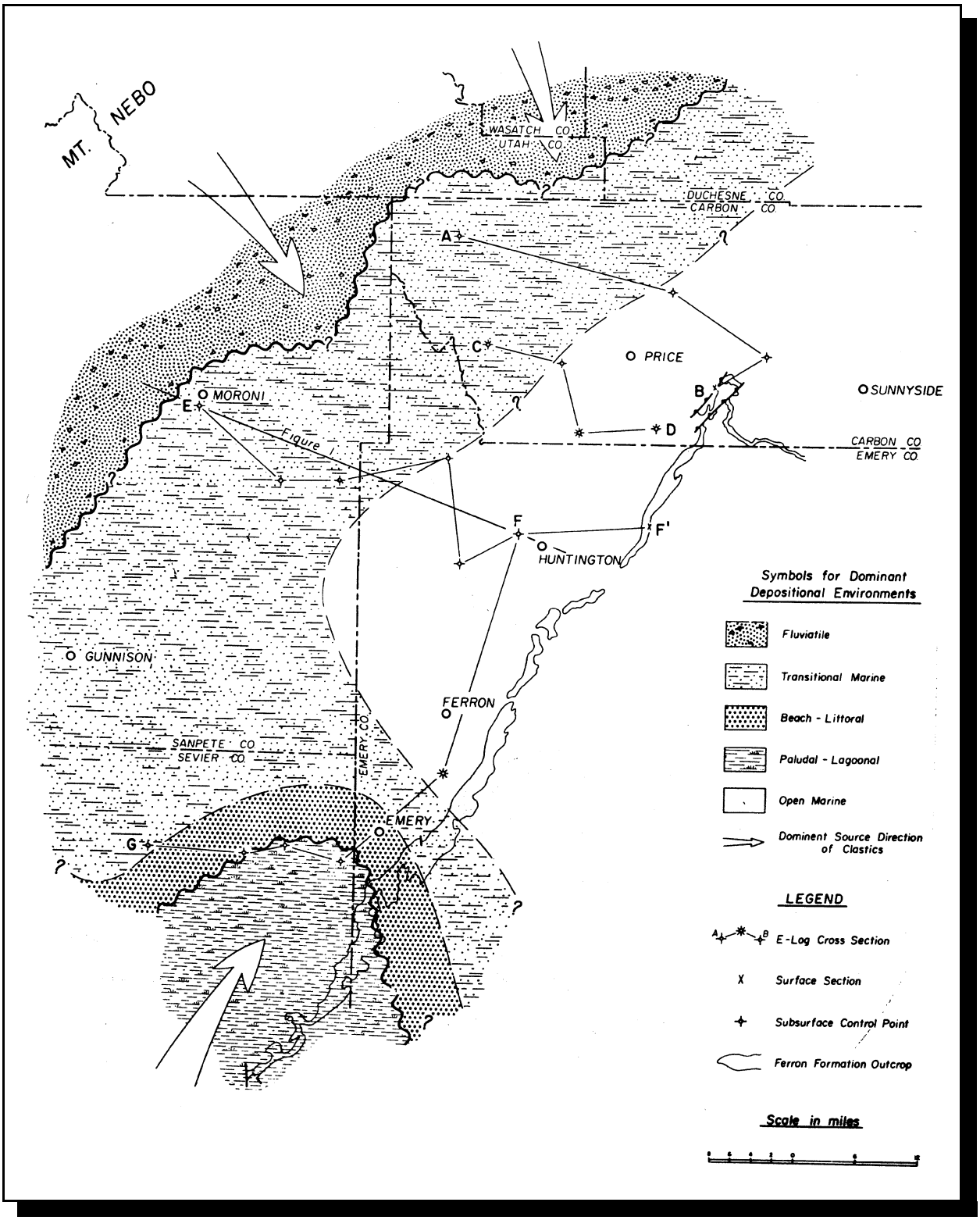


Figure 2-7. Hale's (1972) interpretation of late Ferron paleogeography. Sea-level rise and transgression has obliterated the Castle Valley bar. From Hale, 1972.

Cotter conducted a study of the entire Ferron outcrop belt during the early 1970s. His work culminated in of a series publications (Cotter, 1971, 1975a, 1975b, 1976) that offered interpretations of Ferron stratigraphy and depositional history that were considerably more refined than the preceding interpretations. Cotter's interpretations incorporated important concepts that had evolved from numerous studies of depositional processes in modern alluvial plain, coastal, and shallow-marine settings that had been completed during the 1960s.

Cotter (1975a) defined four mappable "units" (figure 2-8) on the Ferron outcrops of northern Castle Valley. These strata correspond to the Lower Ferron of Davis (1954). Most important are the Clawson Unit and overlying Washboard Unit, which are laterally continuous over most of the length of the Castle Valley outcrops. They constitute two upward-coarsening depositional sequences composed predominantly of very fine to fine-grained, silty sandstone that has been extensively burrowed in most areas. They bear the distinctive "cannon ball" concretions recognized by previous authors. Cotter (1975a, 1975b, 1976) was the first to demonstrate that these two units disappear southward by facies change into normal marine Tununk Shale. He clearly demonstrated that they occupy a position stratigraphically beneath the coal-bearing strata of the Upper Ferron near Emery (figure 2-9). Cotter interpreted the Clawson and Washboard units as representing a low-energy coast where sand, transported southward by longshore drift from the Vernal delta (figure 2-10), accumulated on barrier islands similar to Sapelo Island, Georgia.

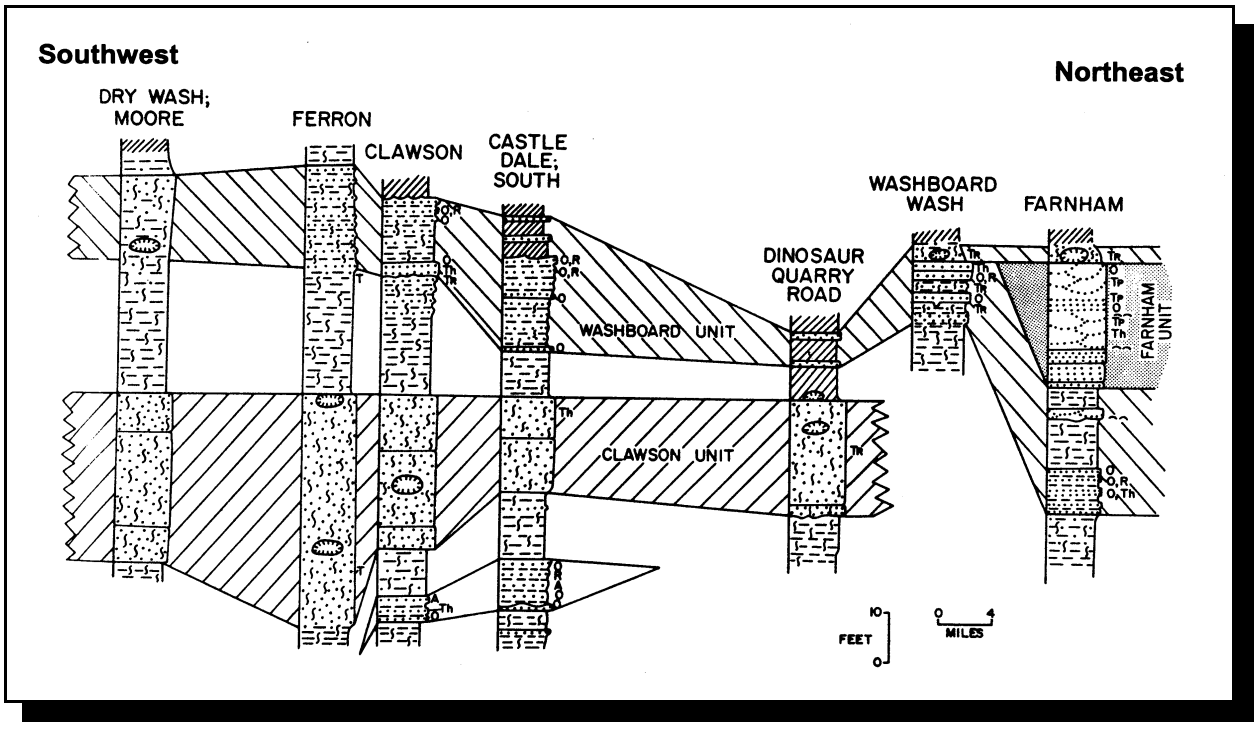


Figure 2-8. Part of Cotter's (1975a) cross section showing the stratigraphy of the Lower Ferron in Castle Valley. The Clawson and Washboard units are the most widespread of the four units he defined. After Cotter, 1975a.

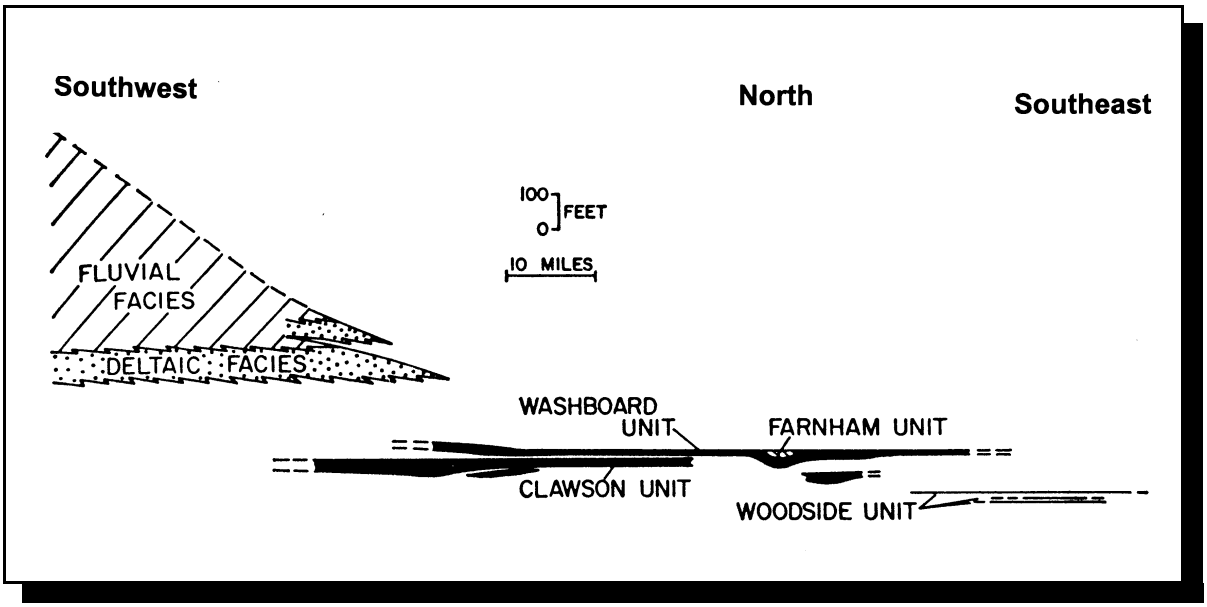


Figure 2-9. Relationship between Lower and Upper Ferron strata (from Cotter, 1975a). The Lower Ferron, composed primarily of the Clawson and Washboard units, is clearly distinguished as older than the Upper Ferron deltaic strata. After Cotter, 1975a.

Cotter (1975b, 1976), like Katich, Davis, and Hale before him, interpreted the coal-bearing strata of the Upper Ferron to represent a northward to northeastward prograding delta, to which he applied Hale's (1972) name "Last Chance Delta." Cotter offered a very specific interpretation of the delta: it "formed as a broad, fan-shaped complex comprising numerous coalescing and overlapping subdelta lobes" (Cotter, 1976, p. 481) representing a high-constructive lobate delta. Cotter recognized the cyclic character of progradation of the Ferron shoreline (figure 2-11) and found in his deltaic interpretation an explanation for the cyclicity: the process of deltaic progradation followed by subsequent abandonment and transgression. His interpretation (figure 2-12) shows two hypothetical delta lobes superimposed on a map of the Ferron outcrops in southern Castle Valley. Although the figure is generalized, it clearly indicates that progradation and abandonment of delta lobes might explain shoreline regressions and transgressions of 5 miles (8 km) or more, enough to explain the second, generalized progradational unit pictured in figure 2-9. Cotter's work contains the first clear conceptualization of cyclicity in the deltaic deposits of the Ferron and represents the first attempt to explain the origin of the cyclicity.

Another important advance in Cotter's work was the recognition that the shoreline of the Last Chance delta did not advance uniformly northward or northeastward. Some of the shorelines prograded northwestward or even westward, and these shoreline deposits share an important characteristic: whereas the shorelines that prograded northward to northeastward display very gentle seaward dips, those that prograded northwestward to westward commonly display much greater dips, in some instances reaching 15 degrees. Cotter (1975b) cited the outcrops along the north side of Ivie Creek (within our Ivie Creek case-study area) as an example of this phenomenon, documenting the steep westward dips with several photographs. He interpreted the steep delta fronts as forming where fresh, sediment-laden water from the Last Chance distributary channels flowed into embayments in which the salinities had been reduced.

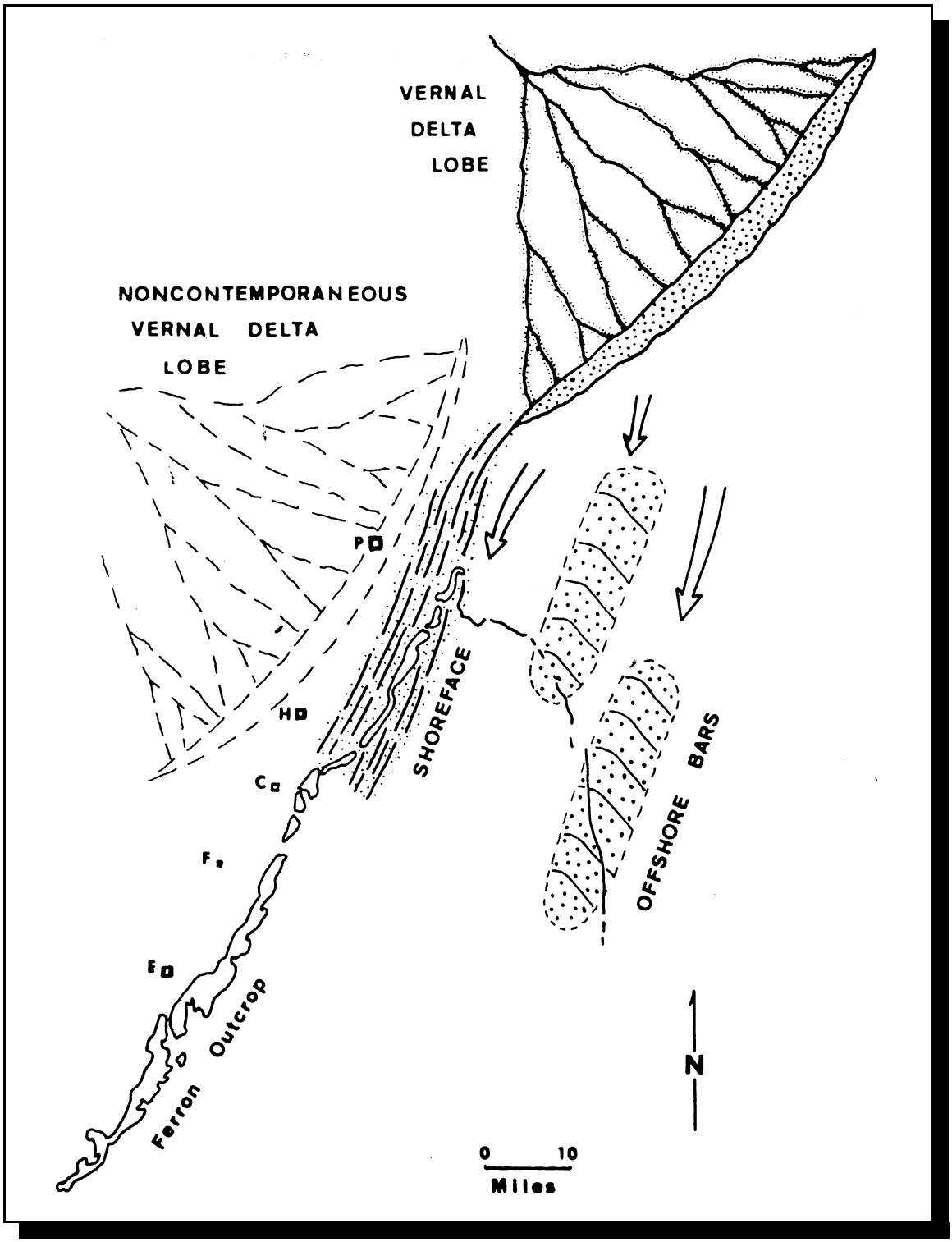


Figure 2-10. Paleogeography of the Lower Ferron as interpreted by Cotter (1976). The Clawson and Washboard units accumulated along a strand-plain/barrier-island coast and nourished by sand transported southward from the Vernal delta. From Cotter, 1976.

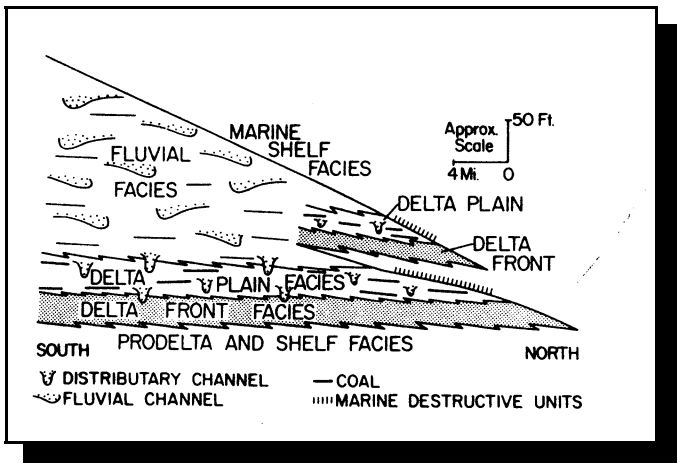


Figure 2-11. Diagrammatic cross section showing basic facies and style of cyclicity in the Ferron, as recognized by Cotter, 1975b. From Cotter, 1975b.

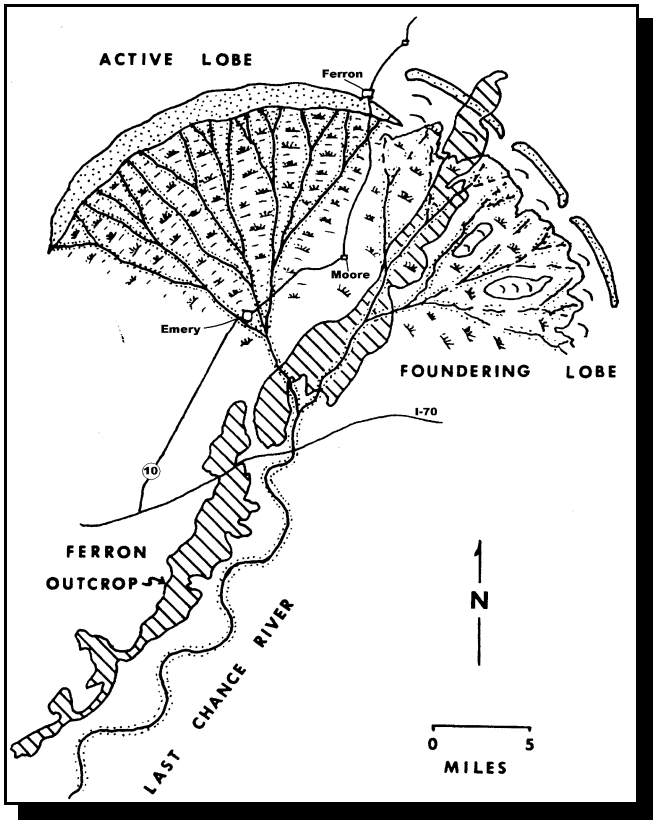


Figure 2-12. Cotter (1976) interpreted the Last Chance delta as a high-constructive, lobate delta system. Lobe progradation and abandonment, pictured diagrammatically here, was offered as an explanation for the transgressive-regressive cyclicity evident in the Ferron. From Cotter, 1976.

Cotter used the term "Gilbert delta" to refer to the steep delta fronts he observed in the Ferron. The term derives from the morphologies of Pleistocene deltas deposited in glacial Lake Bonneville and described by Gilbert (1885). Gilbert deltas are characterized by steep delta-front strata bounded below and above by low-angle to flat "bottom-set" and "top-set" beds. The "type" Gilbert deltas deposited on the shoreline of Lake Bonneville formed where streams characterized by high bed loads reached and rapidly mixed with the fresh water of the lake. Along marine coast, fresh water from river mouths generally overflows the denser, saline water, resulting in salinity stratification and development of a fresh-water plume. Cotter's hypothesis is that a shallow, restricted embayment, perhaps like the Sanpete Valley embayment of Hale (1972), but more likely much smaller, contained (at least periodically) low-salinity water, facilitating rapid mixing and, therefore, steep slopes. This question is addressed further in our description of the Ivie Creek case-study area.

Details Emerge

Ryer conducted a comprehensive study of the Ferron outcrops in the southern part of Castle Valley and available drill-hole data from Castle Valley and the Wasatch Plateau during the late 1970s. The results of this study were presented in a series of papers published by Ryer and various collaborators during the early 1980s. The emphasis of Ryer's work was the recognition and mapping of packages of strata representing "major cycles of sedimentation" in the Ferron (Ryer, 1980, 1981a, 1981b, 1982a, and 1982b). These cycles were designated "4th order" cycles (Ryer, 1984) building on the terminology of Vail and others (1977). Five delta-front units representing 4th order cycles (our Kf-1 through Kf-5) were initially recognized (figure 2-13). Each was distinguished on the basis of an overall upward-coarsening shoreline sandstone unit plus equivalent delta-plain strata. The deposits of each cycle contain a widespread bed of coal, for which the letter designations of Lupton (1916) were retained.

Two additional shoreline sandstone bodies were identified by Ryer in the vicinity of Emery (our Kf-6 and Kf-7), but were not associated with 4th-order because of their very limited dimensions in the depositional dip direction. Kf-6 and Kf-7 were elevated to the same status as Kf-1 through Kf-5 in Ryer's later publications (figure 2-14). Like Cotter, Ryer interpreted the Ferron to be the product of deltaic sedimentation, specifically river-dominated, lobate deltas. Wave-modified deposits of the shorefaces that lay between active delta lobes were also distinguished.

Ryer (1981a) analyzed the relationships between the coalbeds of the Ferron and the equivalent delta-front sandstone units. This subject is described in greater detail in the following section of this chapter. The concept of "stratigraphic rise" played a key part in his analysis, as it has in more recent studies. Progradation of a shoreline during a period of relative rise of sea level results in what can be termed stratigraphic rise of a shoreline sandstone unit. During progradation, the position of recognizable facies boundaries move upward relative to some horizontal datum. Recognizable horizontal data in the rock record are rarities (an example would be a layer of volcanic ash preserved in a peat deposit). In practice, stratigraphic rise is most easily recognized on the basis of seaward thickening of the unit of marine shale beneath and seaward of the shoreline deposit. Greater stratigraphic rise is reflected by more rapid basinward thickening of marine shale unit. In figure 2-15, stratigraphic rise is reflected by the upward shift of the boundary between upper

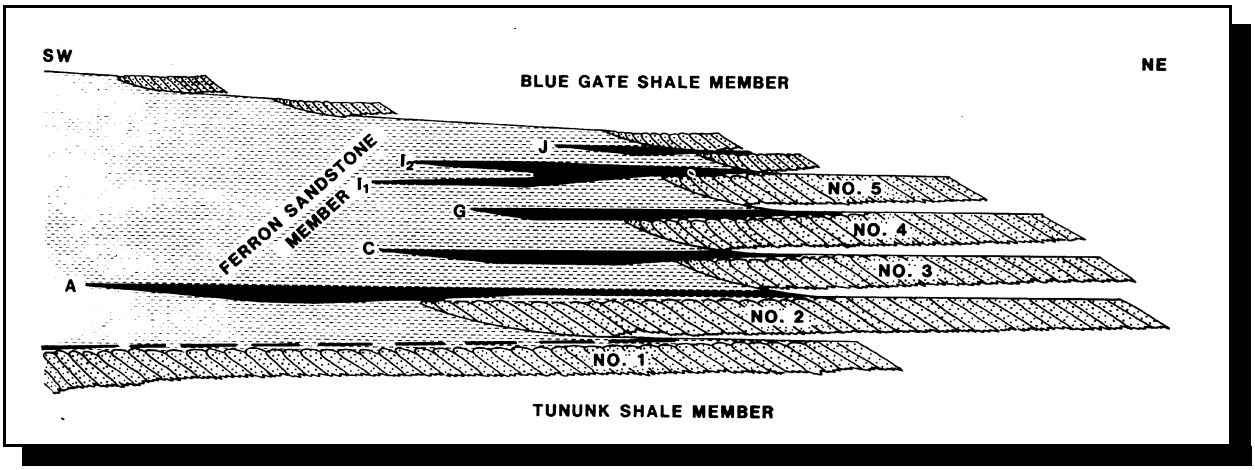


Figure 2-13. Generalized southwest to northeast cross section of the Ferron defining Ryer's (1981a) delta-front units. Two additional delta-front units lying near the landward edge of delta-front unit no. 5 were identified, but were not assigned numbers owing to their small size. The final two units, near the left edge of the diagram, do not exist. From T.A. Ryer, AAPG Bulletin Vol. 65, No. 11, AAPG ©1981a, reprinted by permission of the American Association of Petroleum Geologists.

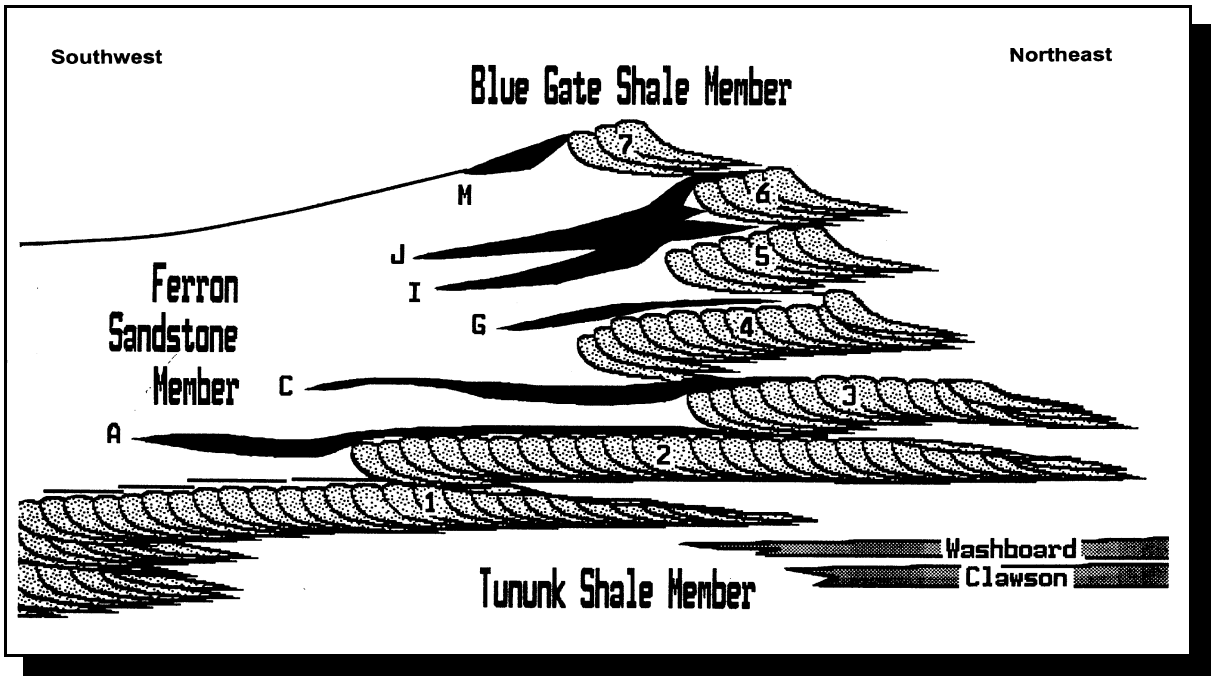


Figure 2-14. Ryer (1991) updated his generalized cross section of the Ferron, recognizing delta-front units no. 6 and no. 7 as of equal importance to nos. 1 through 5. Compare to figure 2-13. After Ryer, 1991.

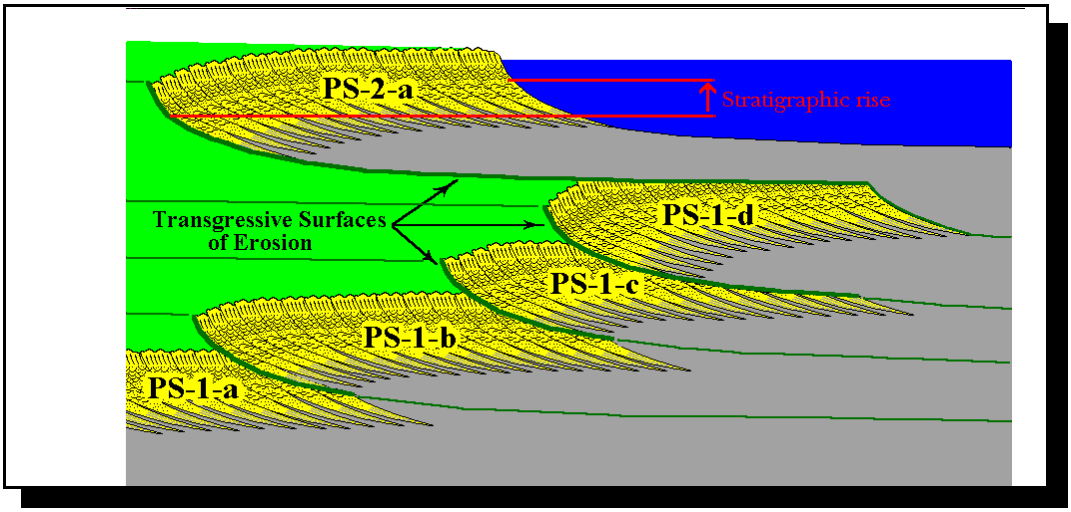


Figure 2-15. Bodies of shoreline sandstone, patterned, record phases of progradation. They are bounded by transgressive surfaces, heavy gray lines, that represent times of erosional transgression of the shoreline. The shoreline sandstone bodies and laterally equivalent coastal-plain and offshore-marine strata constitute parasequences. Facies within each shoreface depositional sequence rise seaward as a result of rise of relative sea level during progradation.

shoreface and middle shoreface strata. The thicknesses of the delta-front sandstone units is closely related to stratigraphic rise: thicker sandstone units record higher rates of relative sea-level rise during progradation; thinner units record lower rates. The older delta-front sandstones of the Ferron (our Kf-1 and Kf-2) are thinner and extend farther basinward than the younger delta-front sandstone units (Kf-3 through Kf-7; figure 2-14), suggesting that the rate of relative sea-level rise in central Utah increased through Ferron deposition. Ultimately, the rate of relative sea-level rise accelerated, resulting in a final, rapid transgression of the sea southwestward across the Last Chance delta. Several subsequent studies by other authors developed these concepts further.

Utilizing outcrop relationships as a guide, Ryer and McPhillips (1983) correlated the Ferron in the subsurface of the Wasatch Plateau. They rejected Hale's (1972) hypothesis of a Castle Valley bar and Sanpete Valley embayment, tying the Lower Ferron sandstone westward and southwestward to the basal sandstone of the Ferron in the subsurface. They interpreted the Clawson and Washboard units of Cotter (1975a) as distal Lower Ferron sands deposited on the shelf. Most importantly, they argued that the Vernal and Last Chance deltas were not true deltas, but larger-scale geomorphic features related to tectonics. The Ferron shoreline, they argued (Ryer and McPhillips, 1983) "received sediment from numerous rivers that built deltas on a much smaller scale than the Last Chance and Vernal deltas as [defined by Hale, 1972]. These small deltas coalesced laterally to produce continuous sheets of delta-front sandstone as the shoreline prograded."

The origin of the Vernal Delta was addressed in greater detail by Ryer and Lovekin (1986). They argued that the conspicuous seaward bulge of the shoreline in northeastern Utah and southwestern Wyoming that had been named the Vernal delta by Hale (1972) owed its origin to movement on the ancestral Uinta Mountain uplift. Uplift of this feature during earliest Late Cretaceous time had earlier been documented by Weimer (1962). As the Ferron-Frontier shoreline prograded eastward to what is now the Uinta Basin and Uinta Mountains, subsidence occurred, but at a slower rate than in areas to the north and south. This differential subsidence, Ryer and Lovekin argued, is the cause of the bulge in the shoreline. A negative line of evidence was also presented. They cited the northern Andes in South America as a modern analog for the Sevier Orogenic Belt in Utah and Wyoming and inferred the spacing of drainages that would have existed in Utah during Ferron-Frontier deposition. Features as large as the Vernal and Last Chance "deltas," they concluded, could not have been deposited by individual rivers (figure 2-16).

A series of seven drill holes cored through the Ferron just west of the outcrop belt by ARCO in 1982 were the subject of a study by Thompson (1985). The principal findings are described in a paper by Thompson and others (1986). The study focused primarily on the interpretation of facies and depositional environments represented in the core. Six outcrop sections located close to the cores were measured in order to augment the core interpretations. Thompson and others (1986), like Cotter (1975b) and Ryer (1981a), interpreted the Ferron to represent lobate, river-dominated deltas (figure 2-17). Although their description and interpretation of sedimentary features in cores are excellent, their study presents only a very general picture of Ferron stratigraphy. A cross section

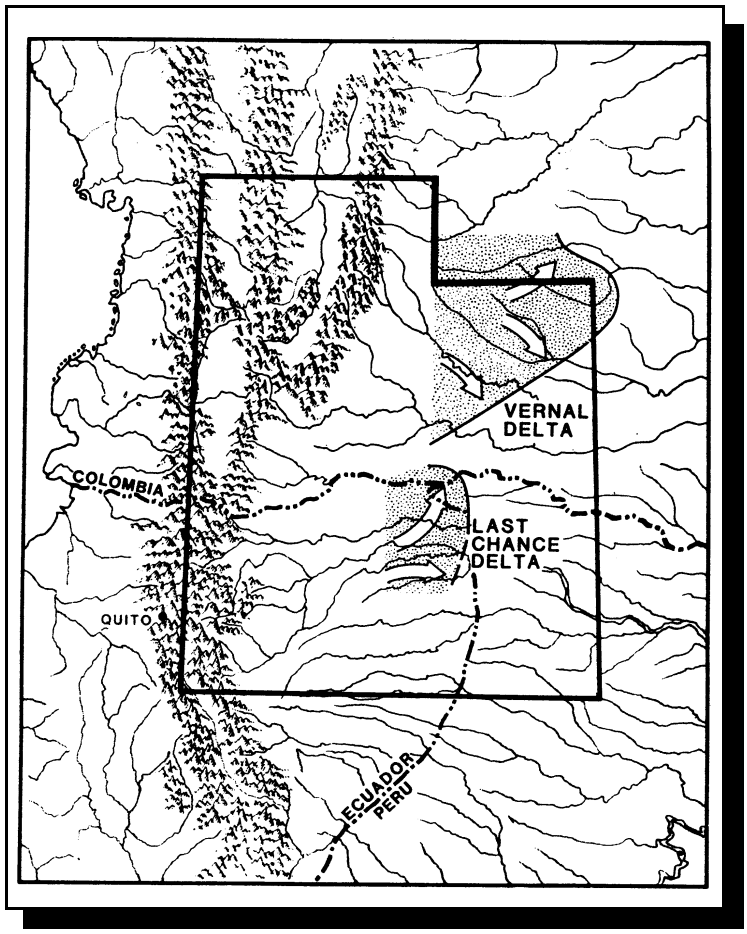


Figure 2-16. Comparison of Ferron paleogeography in Utah with the present-day drainage pattern on the eastern flank of the Andes in northern South America. The Andes are made to coincide with the Cretaceous Sevier orogenic belt. On the basis of this comparison, Ryer and Lovekin (1986) concluded it was unlikely that the Vernal and Last Chance deltas could have been the deltas of individual rivers. From T.A. Ryer and J.R. Lovekin, AAPG Memoir 41, AAPG ©1986, reprinted by permission of the American Association of Petroleum Geologists.

depicting the stratigraphy in and between five of the ARCO drill holes (figure 2-18) distinguishes facies very broadly. No attempt was made to distinguish and correlate the coal seams mapped and named by Lupton (1916) or the individual delta-front sandstone bodies defined by Ryer (1981a).

Of particular interest is Thompson and others (1986) identification of sandy shelf "plume" deposits in the Ferron. Their model, shown in figure 2-19, recognizes bodies of sand deposited on the shelf by a south- or southeast-flowing current and nourished by sediment delivered to a delta front situated up-drift. The model is based on an interpretation by Coleman and others (1981) of a sand body located in the Mediterranean Sea off and down-drift of the mouth of the Damietta Branch of the Nile Delta. They interpreted it as a Holocene deposit formed by transport of sand from the river mouth onto the adjacent shelf by an eastward flowing current. Palmer and Scott (1984) elaborated on the model (figure 2-20) and applied the concept of a sandy shelf "plume" to explain

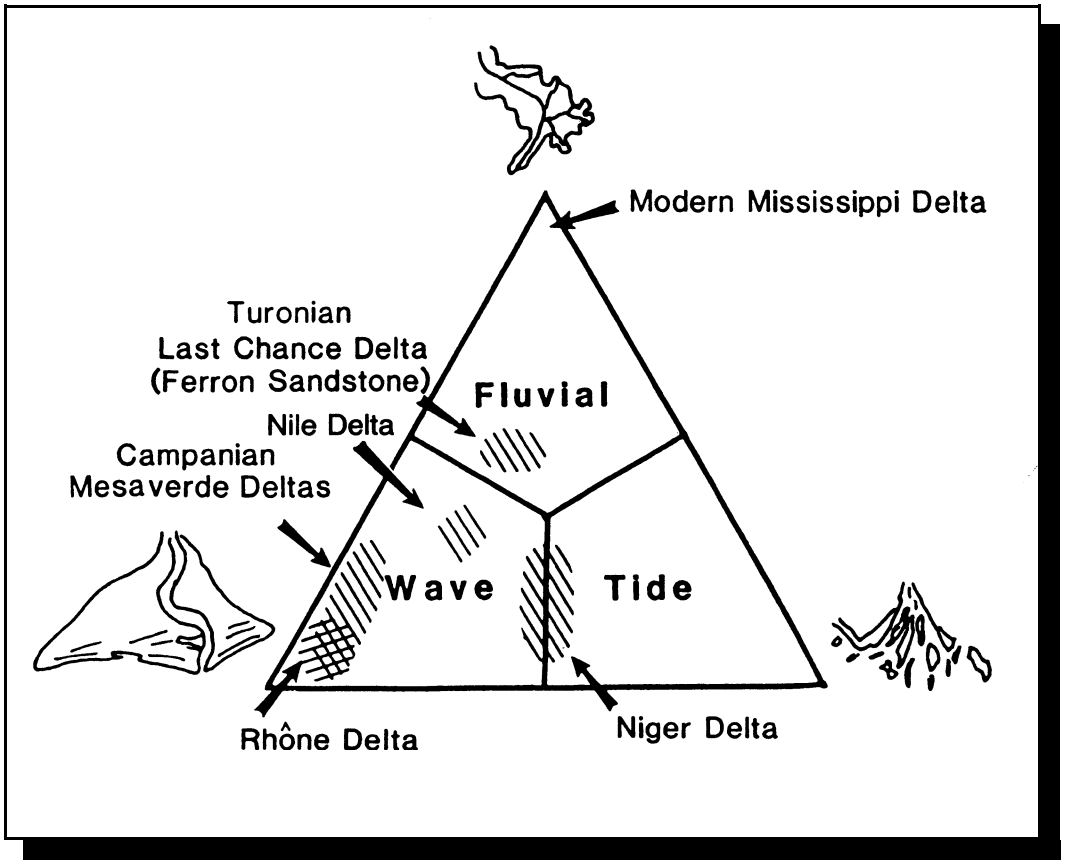


Figure 2-17. The Last Chance delta is interpreted by Thompson and others (1986) to be a river-dominated delta with moderate wave influence (from Thompson and others, 1986). The ternary diagram they used was modified from Galloway, 1975.

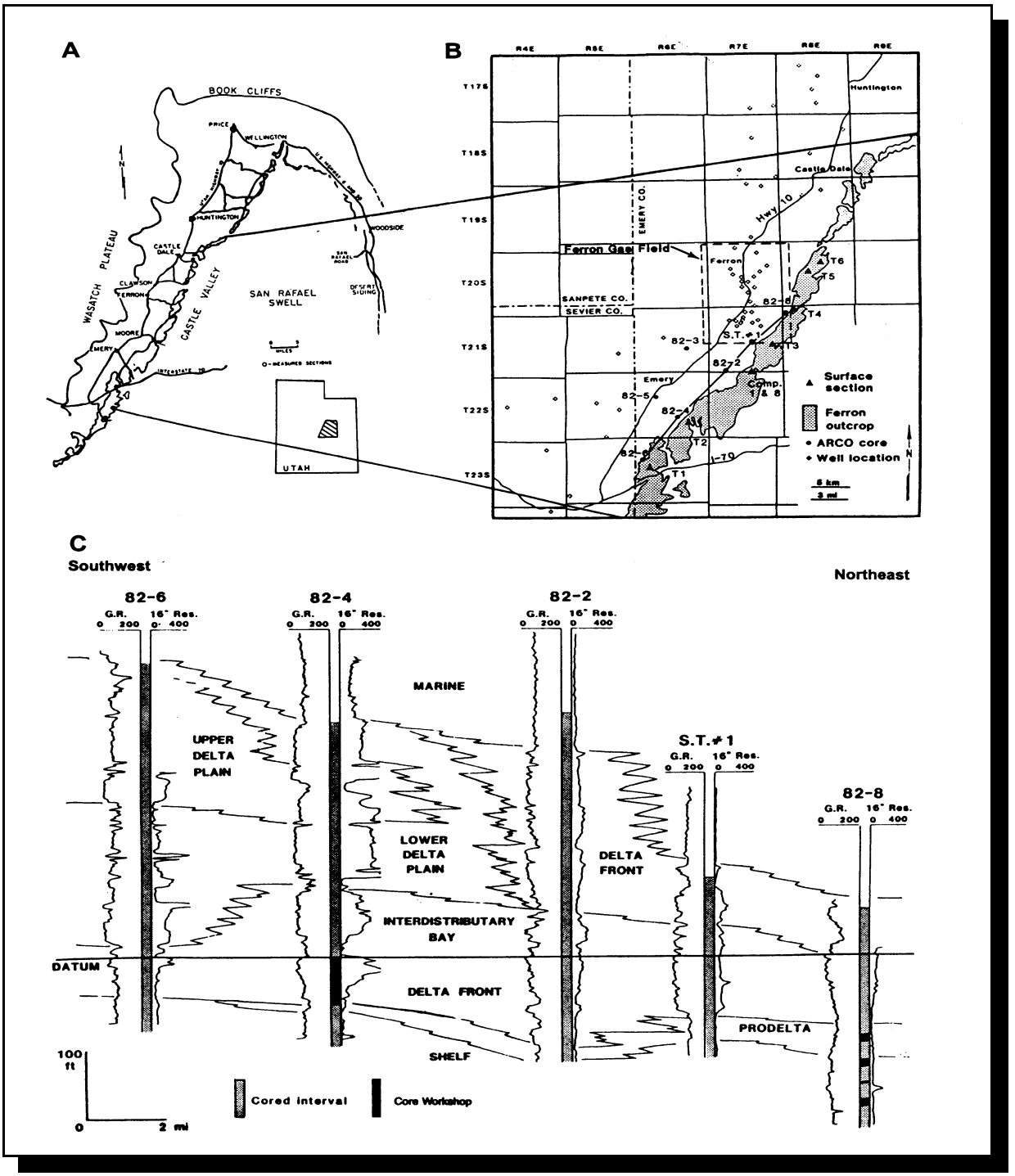


Figure 2-18. A. Ferron Sandstone outcrop belt in Castle Valley (from Cotter, 1975b). B. Location of Ferron drill holes, surface sections, and cross section. C. Southwest to northeast cross section (shown on figure 2-18B)showing correlations between five core holes drilled through the Ferron by ARCO. Drill hole 82-6 is situated near Ivie Creek; 82-8 is southeast of Ferron. Interfingering of facies is shown, but is highly generalized and, in some areas, simply incorrect. Modified from Thompson and others, 1986.

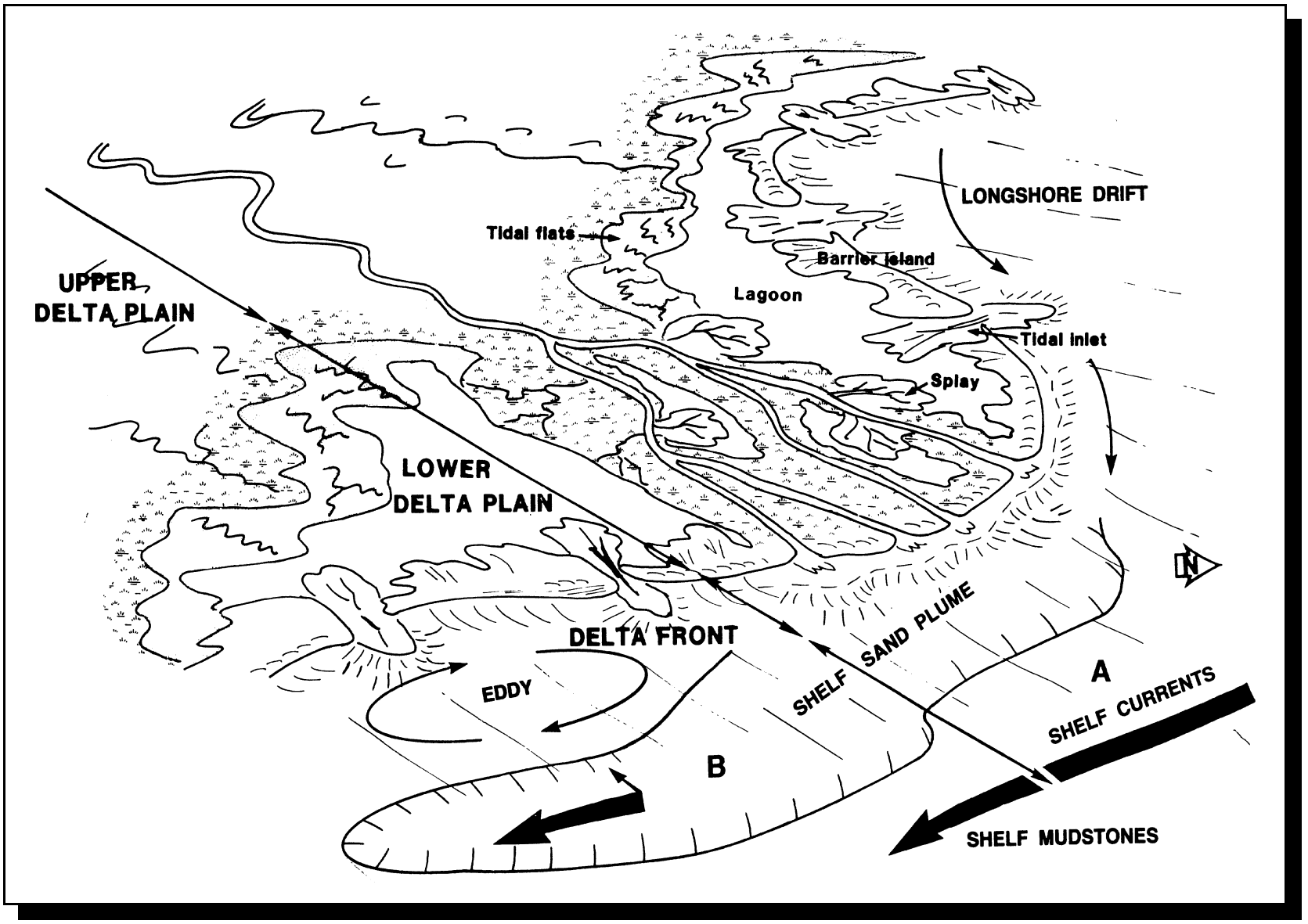


Figure 2-19. Reconstruction of Ferron depositional environments (from Thompson and others, 1986). A -- shelf muds transported from outside immediate area; B -- fine sands transported shelfward from advancing delta.

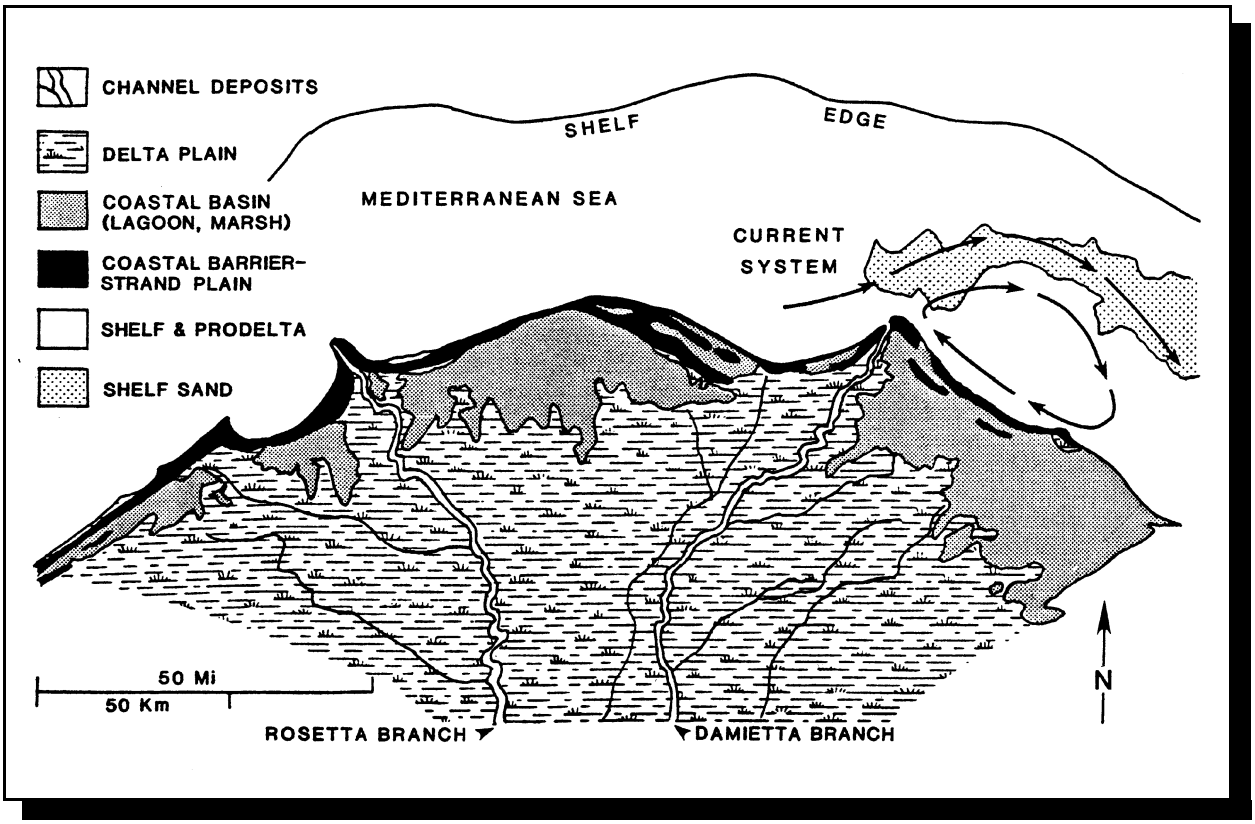


Figure 2-20. Depositional model from Palmer and Scott (1984) showing origin of a shelf sand plume interpreted by Coleman and others (1981) to exist of the Mediterranean shelf off the mouth of the Damietta Branch of the Nile River. From J.J. Palmer and A.J. Scott, AAPG Bulletin Vol. 68, No. 1, AAPG ©1984, reprinted by permission of the American Association of Petroleum Geologists; modified from Fisher and others, 1969; shelf system after Coleman and others, 1981; shelf edge from Said, 1981.

sandstones in the Upper Cretaceous La Ventana Tongue of the Cliffhouse Sandstone in the San Juan Basin. Scheihing and Gaynor (1991) re-examined data for the Damietta shelf "plume" and argued that it is not a Holocene deposit formed on the shelf, but rather a Pleistocene deposit that accumulated along the shoreline, brought by longshore drift from the mouth of the Damietta Branch when sea level was lower. Regardless of whether or not the sand body associated with the Damietta Branch accumulated as a shelf plume, the model itself has merit. We believe that Thompson and other's (1986) explanation of the Lower Ferron is correct, but add another component that they did not consider to explain its location -- the creation of a shoal area on the sea floor that corresponds to a peripheral bulge to the shoreline.

For the Ferron, the sand plume model was invoked to explain the origin of the Lower Ferron, which Thompson and others (1986) interpreted as a large plume derived from the Vernal delta (figure 2-21), and also to explain some more localized sandy strata in the basal part of the Upper

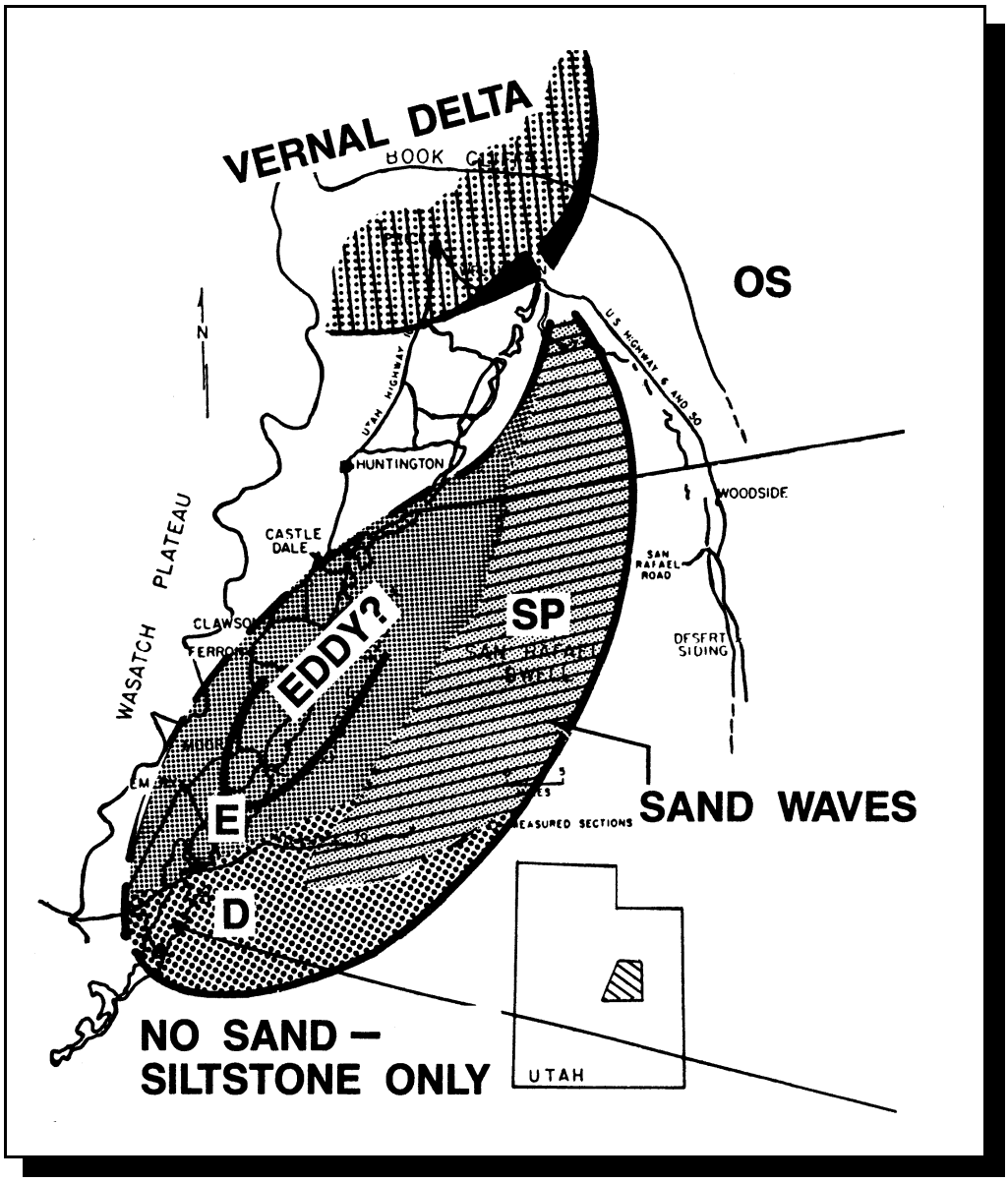


Figure 2-21. Vernal delta and its shelf sand plume from Thompson and others (1986). OS -- open shelf; SP -- sand plume; E -- eddy; D -- distal silty plume. Sandy plume deposits are shown as limited to the San Rafael uplift, from which they were eroded when the structure was uplifted in Tertiary time. For data-point locations see figure 2-18.

Ferron (their Last Chance delta; figure 2-22). In some respects, the shelf plume model of Thompson and others (1986) is strikingly similar to the Castle Valley bar interpretation of Hale (1972) and also resembles the peninsula interpretation of Spieker and Reeside (1925); figure 2-4. The main difference is that the shelf plume is interpreted to have existed mainly to the east of the present-day outcrop belt, on what is now the San Rafael Swell, whereas Hale's Castle Valley bar was located

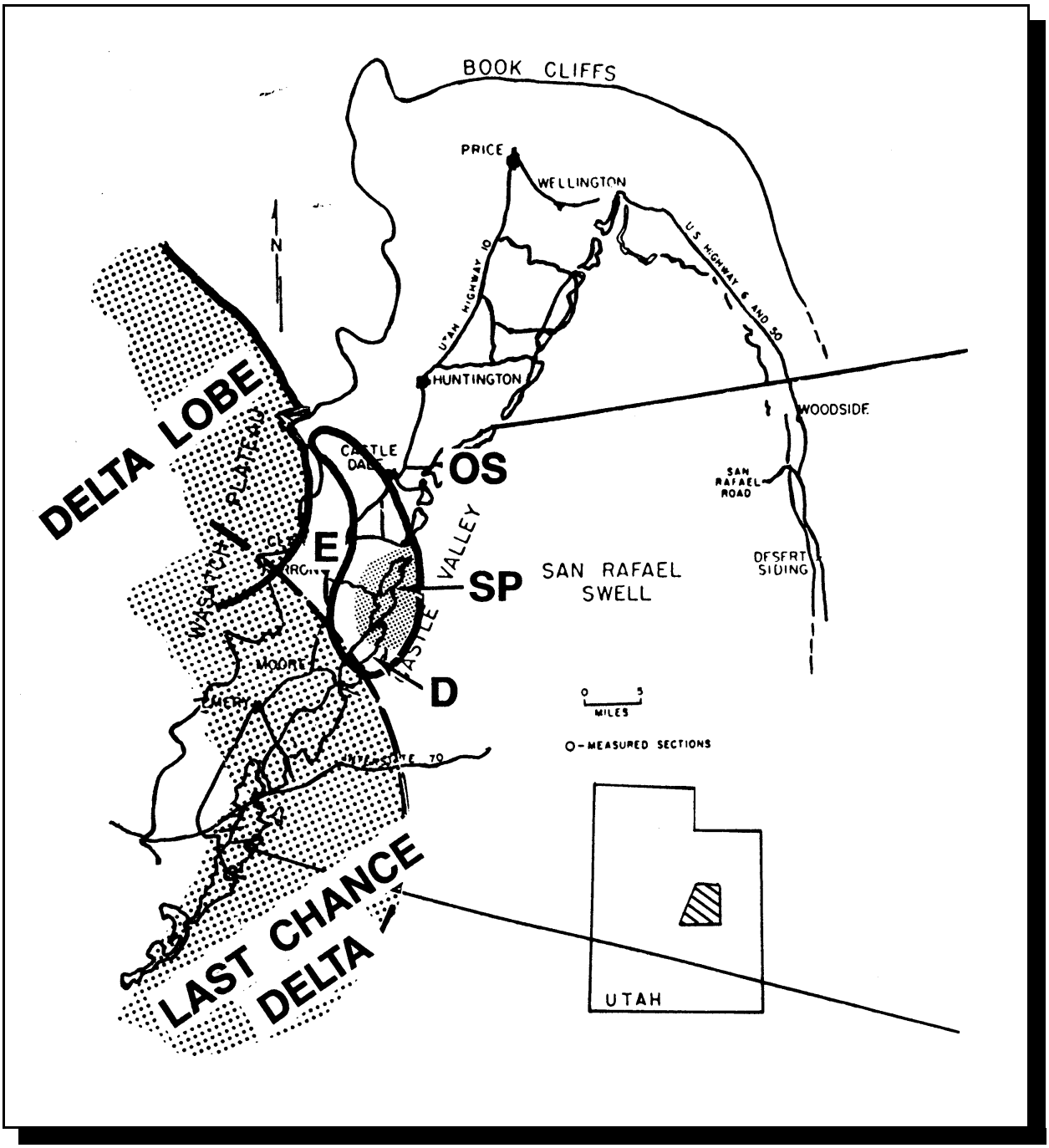


Figure 2-22. Possible smaller-scale sand plumes deposited in front of prograding delta lobes from Thompson and others (1986). OS -- open shelf; SP -- sand plume; E -- eddy; D -- distal silty plume. Note the large size of the hypothetical delta lobe pictured north of the Last Chance delta. It is comparable in size to the lobes pictured by Cotter (1976; see figure 2-12). For data-point locations see figure 2-18.

mainly to the west of the outcrop, in the subsurface. Cotter (1976) (figure 2-10) invoked southward transport on the shelf to explain some lenses of sandstone that he assigned to the Lower Ferron (his Woodside Unit; figure 2-9) on the northeast flank of the San Rafael uplift, but his shelf-sand interpretation was applied at a much smaller scale than was the Vernal delta plume model of Thompson and others (1986).

Ryer (1987) proposed a general model that distinguished different origins for the Lower Ferron and Upper Ferron (the paper was finally published in 1993a; a revised version appeared in 1994.) Ryer argued that the effects of both sea-level change and variations in the flux of clastics from the Sevier Orogenic belt can be distinguished in the Ferron. The Lower Ferron was deposited primarily as the result of a lowering of eustatic sea level. Rise of sea level led to deepening of water and accumulation of marine mudstone above the Washboard Unit. Slowing of subsidence and possibly structural rebound of the foredeep that lay immediately to the east of the Sevier Orogenic Belt led to an increase in the flux of sediment across the foredeep to the shoreline in central Utah during late Turonian time. The coarse-grained Calico Bed of the Kaiparowits Plateau records this event in southwestern Utah. The increased flux of sediment caused progradation of the Upper Ferron shoreline in Castle Valley, despite continued rise of sea level. The distinctive, river-dominated deltas of the Upper Ferron, which are unusual in the Upper Cretaceous section of the Western Interior, are the product of this rapid sediment influx.

Molenaar and Cobban (1991a, 1991b) collaborated to synthesize their knowledge, gained through many years of study, of Cretaceous stratigraphy on the south and east sides of the Uinta Basin. The Ferron outcrops lie at the southwestern margin of the area they considered in their report and there are no findings that altered or significantly added to previous interpretations of the Ferron in Castle Valley. Some of their conclusions regarding areas to the north and east, however, are of interest.

Molenaar and Cobban (1991a, 1991b) named a bed of sandstone that is present near the middle of the Tununk Shale on the northeast flank of the San Rafael uplift and into eastern Utah the Coon Spring Sandstone Bed. Included in it is the Woodside Unit of the Ferron defined by Cotter (1975a) (figure 2-9). The Coon Spring Sandstone Bed contains the ammonite *Collignoniceras woollgari*, dating it as early middle Turonian in age.

A questa-forming unit of black marine shale containing varying amounts of very fine grained, platy, thin-bedded sandstone in eastern Utah had previously been assigned to the Ferron by many workers (for example Hintze and Stokes, 1964). Molenaar and Cobban reassigned it to the Juana Lopez Member of the Mancos, arguing that it is much more like the Juana Lopez of areas to the east and southeast than it is to the Ferron in Castle Valley. Their cross sections, one of which incorporates subsurface data between Emery and the northern plunge of the San Rafael uplift (figure 2-23) show the Juana Lopez Member as being essentially equivalent to the Upper Ferron.

Ferron Reservoir Analogs and Sequence Stratigraphy

Numerous studies of the Ferron undertaken in the late 1980s and early 1990s filled in many of the details that were lacking in earlier studies. Analysis was done at a considerably finer scale and the focus shifted from paleoenvironmental analysis and reconstruction for its own sake to analysis for the purpose of determining the distribution of petroleum reservoir characteristics. This was the

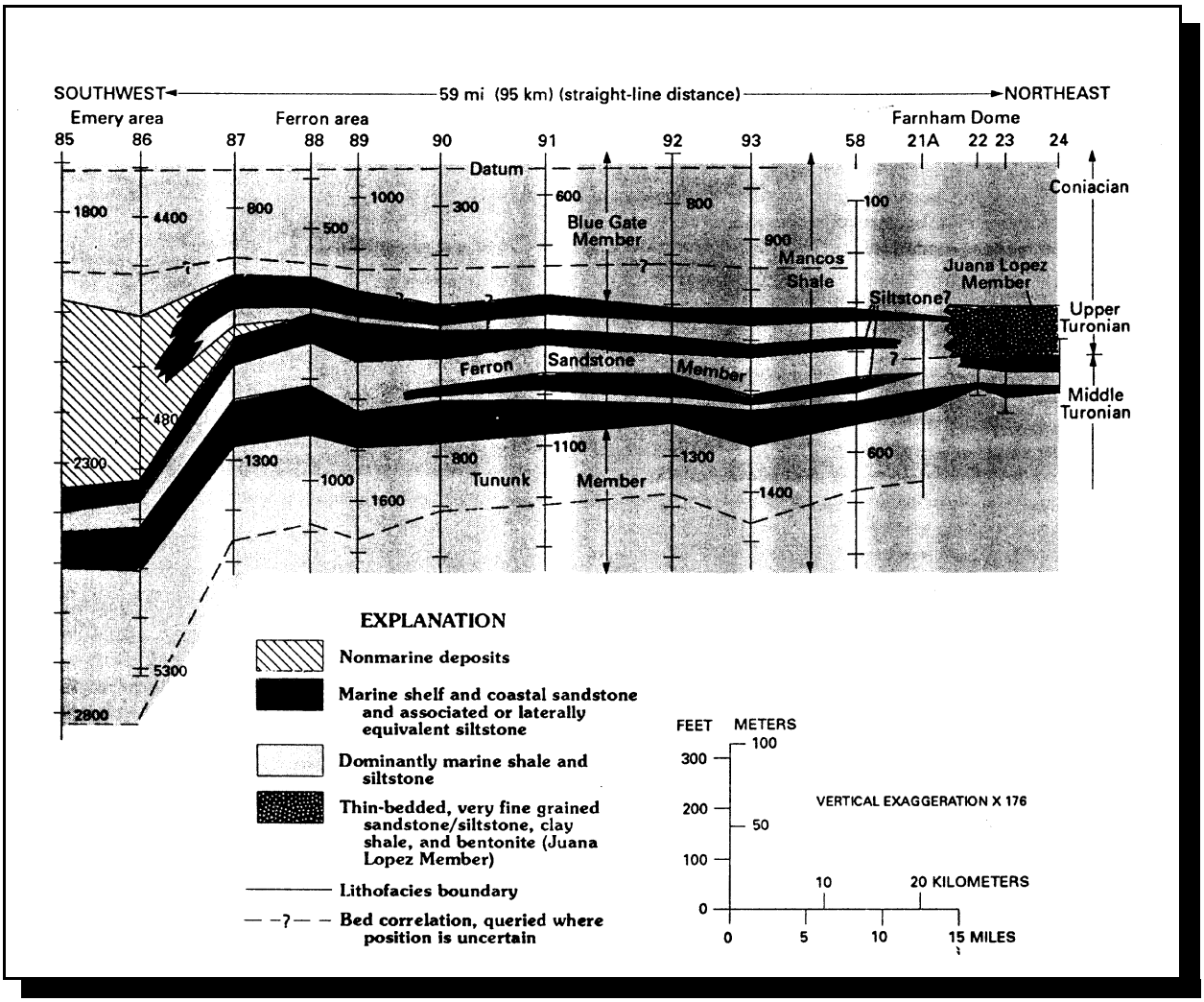


Figure 2-23. Stratigraphy of the Ferron Sandstone along the Castle Valley outcrops from Molenaar and Cobban (1991a).

result of two primary factors: (1) previously completed studies provided a sound stratigraphic framework within which these detailed studies could be efficiently conducted; and (2) analysis of petroleum reservoir types and the amounts of mobile but unrecovered petroleum that they contain pointed to fluvial-dominated sandstones as an important, underdeveloped resource (Tyler, 1988; Ray and others, 1991).

The landward pinchouts of two of the delta-front units of the Ferron, our Kf-2 and Kf-6, were described by Anderson (1991a, 1991b). This study addressed the character of stratigraphic traps that might be formed by these features and compared them with landward pinchouts of highly wave-dominated shoreline deposits of the Blackhawk Formation in the Book Cliffs. Anderson's description of the Kf-2 landward pinchout at the mouth of Willow Springs Wash (figure 2-24) is notable in that it discriminates sub-facies within the landwardmost part of the Kf-2 delta-front sandstone body and characterizes them, at least in general terms, as to their relative reservoir quality.

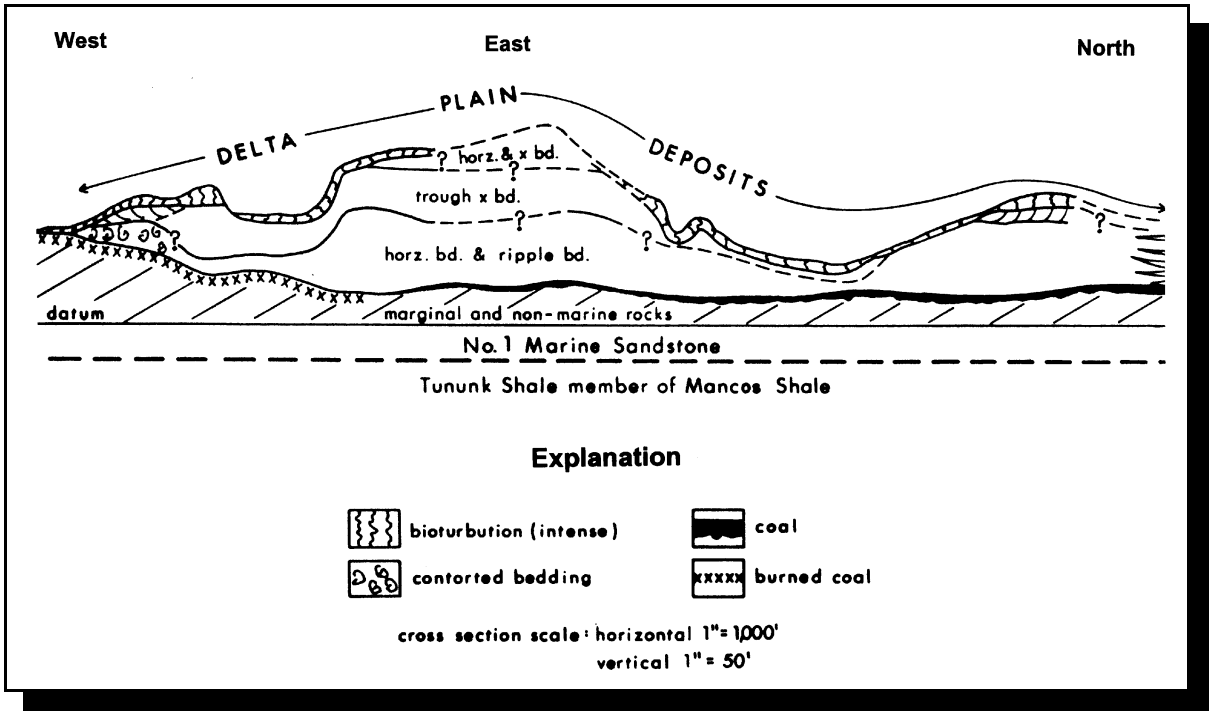


Figure 2-24. Facies that occur within the landward pinchout of Kf-2 near the mouth of Willow Springs Wash (modified from Anderson, 1991b).

Five drill holes were cored southeast of Emery as part of a study of Ferron unit Kf-2 in the Muddy Creek Canyon area by Ryer in 1992. The initial results of the study were presented in a field trip guidebook (Ryer, 1993b; Ryer and Gustason, 1993) and core workshop notes (Gustason and others, 1993). The study addressed the origin of several parasequences in Kf-2 and was the starting point for additional work that is part of this DOE-funded study. Permeability data from the cores and adjacent outcrops in Muddy Creek Canyon were compiled and analyzed by Mobil Exploration, but these results remain proprietary.

Ryer studied outcrops in Indian Canyon, south of Willow Springs Wash, with the purpose of distinguishing autocyclic from allocyclic origins of several parasequence-level units defined there. Preliminary results were reported by Ryer (1993a, 1993b, 1993c). The study was continued as part of this DOE-funded project, our Willow Springs Wash case-study area. Exposures in Indian Canyon record an abrupt change from wave-modified shoreline to fluvial-dominated deltaic deposits. The bedding surface across which this change occurs has many of the characteristics of a marine-flooding surface, yet lacks any evidence of transgression of the shoreline or of relative sea level rise. Ryer interpreted the change to represent autocyclic shifting of a river system into the Indian Canyon area and subsequent progradation of a fluvial-dominated delta. This concept figures prominently in our approach to more regional analysis of the Ferron reported in this study.

Two comprehensive, interrelated studies of the Ferron were conducted by Gardner and geoscientists of the Bureau of Economic Geologists (BEG), The University of Texas at Austin. Gardner's studies of Ferron sedimentology and stratigraphy were conducted primarily as part of a Ph.D. dissertation (Gardner, 1993) at the Colorado School of Mines. Based largely on Gardner's findings, the BEG identified the Ferron as a good analog for a number of important Neogene

reservoirs in the Texas Gulf Coast productive province. The BEG, with funding from the Gas Research Institute (GRI) and DOE, and later with direct financial support from oil and gas companies, focused on the stratigraphy, sedimentology, and permeability structure of a number of stratigraphic units representing important reservoir facies. Previous studies of permeability structure are discussed at length later in this chapter.

Gardner conducted an exhaustive study of the Ferron that contributed a large amount of new data and many innovative interpretations, as well as a complete review and, in some cases, rethinking of previous interpretations. Gardner's studies of the Ferron are summarized in two outstanding papers published in 1995 (Gardner, 1995a, 1995b). Both deal with tectonic and eustatic controls on sedimentation of mid-Cretaceous strata: the first addresses most of the Rocky Mountain region (exclusive of Montana); the second focuses on central Utah. Many of Gardner's detailed stratigraphic descriptions and interpretations of the Ferron remain unpublished and can be found only in his dissertation (Gardner, 1993) and in guidebooks reproduced for various field trips (Gardner, 1992; Gardner and others, 1994).

Gardner (1995b) defined a hierarchy of cycles related to base-level rise and fall (figure 2-25). The Ferron represents the base-level fall-to-rise turnaround of a "long-term cycle" (the 2nd order cycle of Vail and others, 1977). Four "intermediate-term cycles" (3rd order) were distinguished and named for characteristic fossils (Gardner, 1995a). The Lower Ferron of Castle Valley plus a thick, basal sandstone unit included in the Ferron on its southernmost outcrops near Last Chance Creek are assigned to the Hyatti sequence (named for the ammonite *Pyionocyclus hyatti*). The Upper Ferron constitutes the Ferronensis sequence (named for the ammonite *Scaphites ferronensis*).

Gardner designated the level of cyclicity represented by the numbered delta-front sandstones of Ryer (1981a) "short-term cycles" (4th order). Gardner designated these units as genetic sequences (GS) -- GS 1 through GS 7 of the Upper Ferron (figure 2-26) following the numbering system of Ryer (1981a) (the deposits of genetic sequences are referred to in some of Gardner's work as "stratigraphic cycles" [SC], for example SC 1, SC 2, and so forth; in the remainder of this discussion, our Kf- terminology is substituted for the GS or SC designation). Kf-1 through Kf-3 were recognized as displaying a forward-stepping pattern that represents base-level fall; Kf-4 displays a vertically-stacked pattern representing the turnaround and beginning of base-level rise; and Kf-5 through Kf-7 display a backward-stepping pattern representing a sustained period of base-level rise. A smaller level of cyclicity, that is essentially equivalent in scale to the "parasequence" of Van Wagoner (1995), was also distinguished. Gardner's thesis and guidebooks include numerous, very well documented examples of this level of cyclicity.

Gardner, like previous students of the Ferron, recognized that the Ferron consists largely of the deposits of fluvial-dominated deltas. He noted a pattern, however, that previous workers had missed: the shoreline sandstones of Kf-1 through Kf-4 consist largely of fluvial-dominated deltaic deposits, whereas those of Kf-5 through Kf-7 consist predominantly or even entirely of wave-dominated deltaic deposits. One of Gardner's innovative contributions to understanding the Ferron is his analysis of this phenomenon in terms of volumetric partitioning of sediment between various paleoenvironments. Figure 2-27 summarizes the concept of volumetric partitioning. Volumetric partitioning offers an explanation for the distribution of fluvial- and wave-dominated delta-front deposits in the Ferron. Stated in the simplest possible terms, Gardner's explanation for the distribution of fluvial- and wave-dominated deltaic deposits is as follows:

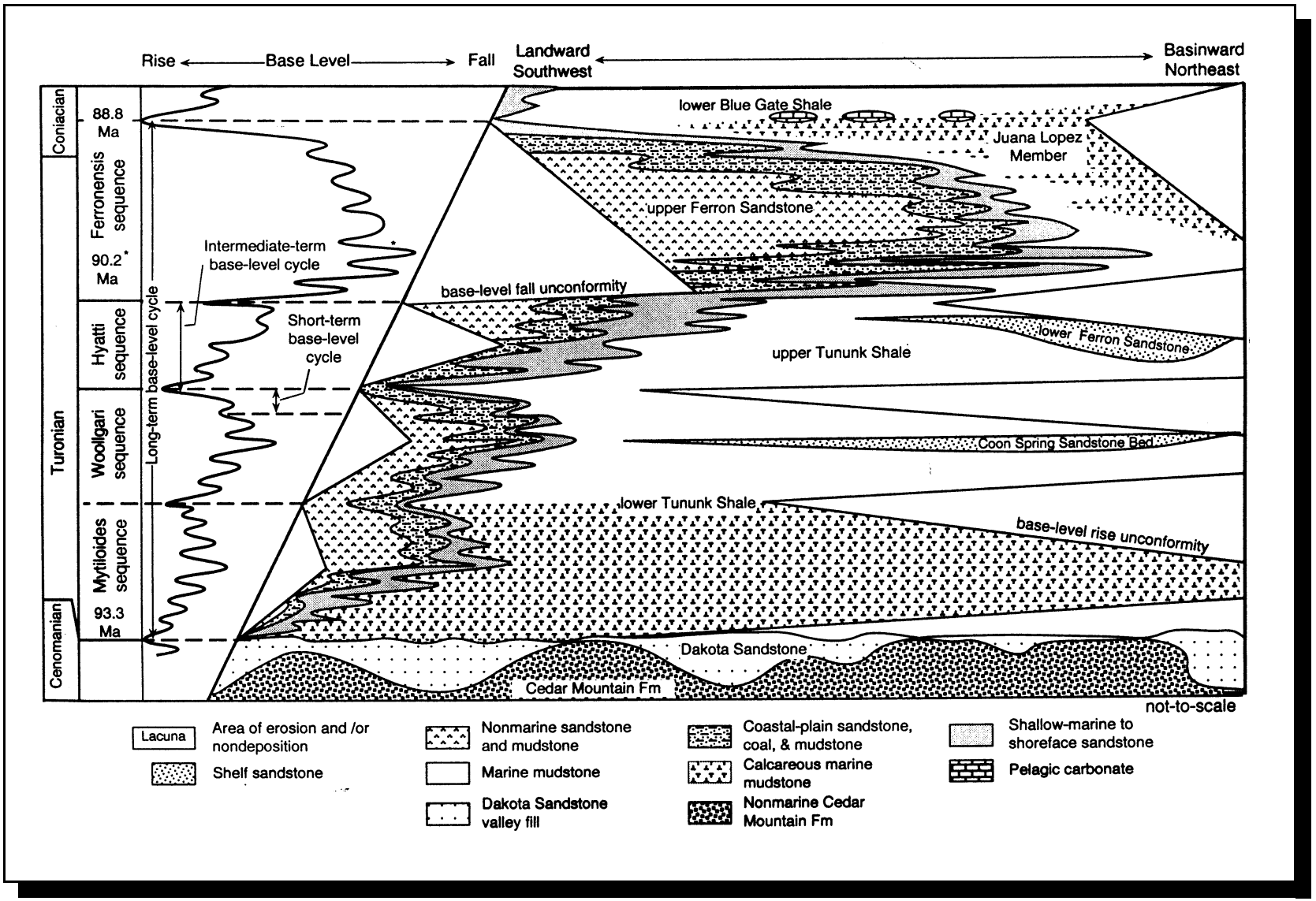


Figure 2-25. Gardner (1995a) distinguished four sequences in Turonian-Coniacian strata in central Utah and named them for diagnostic invertebrate faunas. The Hyatti sequence includes strata of the Lower Ferron; the Ferronensis sequences includes the deltaics of the Upper Ferron (from Gardner, 1995a).

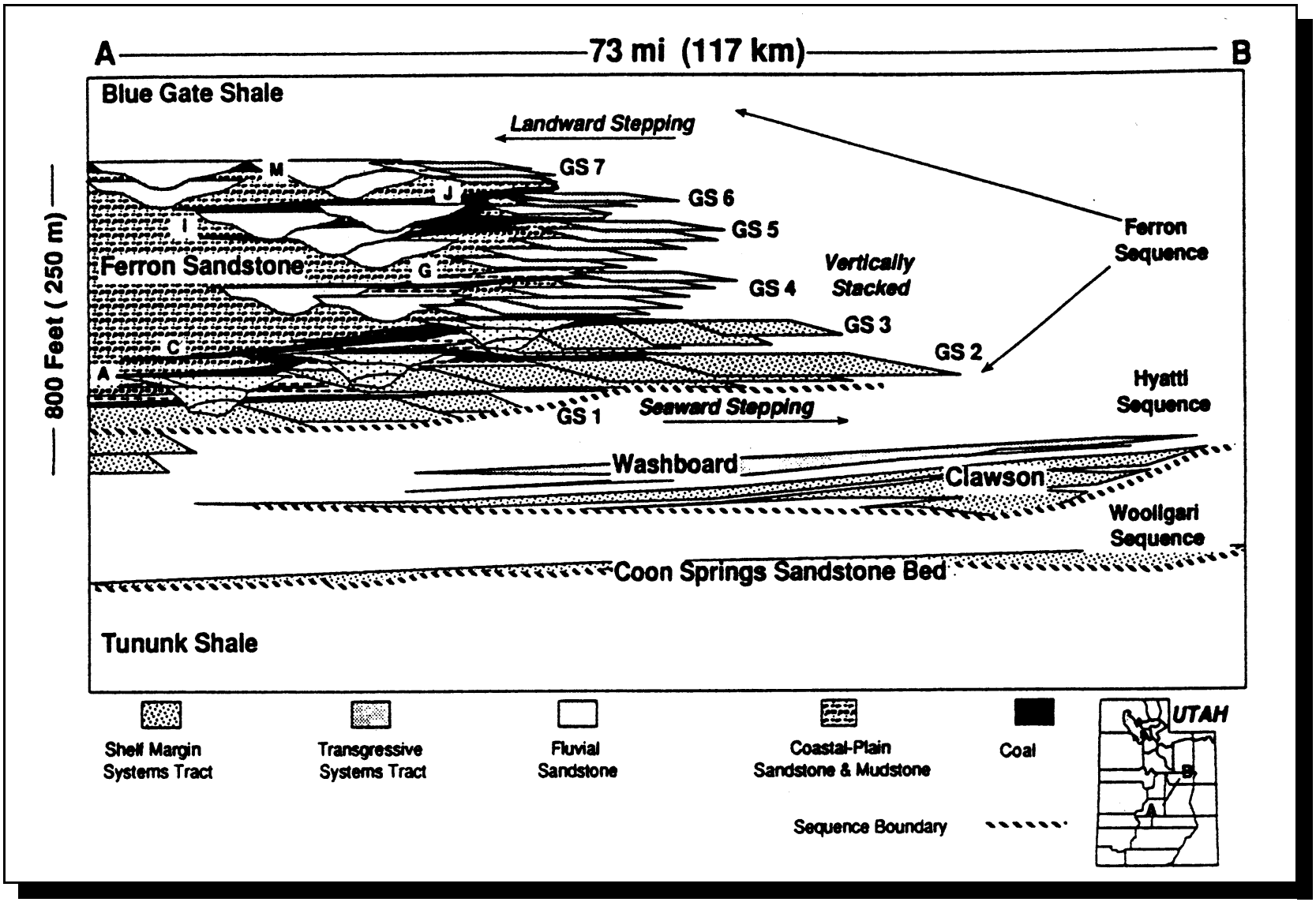


Figure 2-26. Gardner (1993) interpreted the shoreline sandstones of Kf-1 through Kf-4 (GS in this figure stands for "genetic sequence") as deposits of fluvial-dominated deltas and those of Kf-5 through Kf-7 as deposits of wave-dominated deltas (from Gardner and others, 1992).

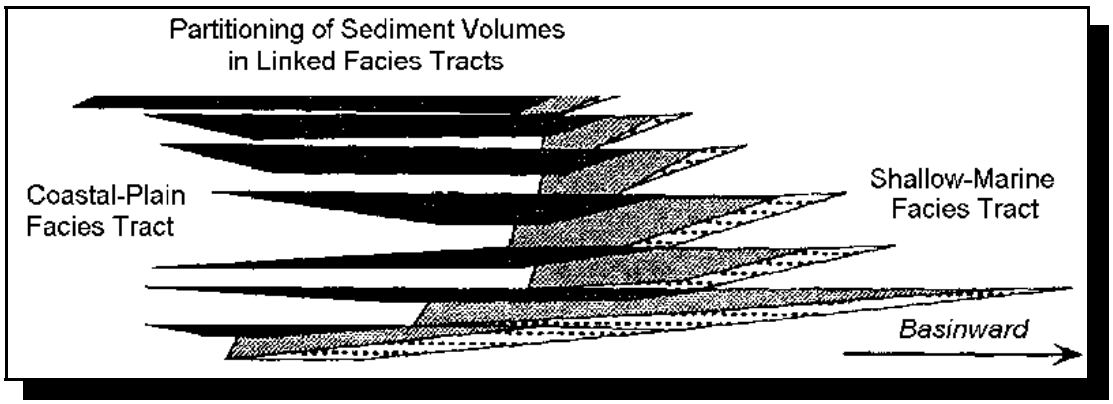


Figure 2-27. Diagram showing the partitioning of sediment in various facies tracts of the Ferron. Rate of rise of relative sea level increased through Ferron deposition, resulting in increasing volumes of sediment deposition in coastal-plain facies tracts and decreasing volumes of sediment deposition in shallow-marine facies tracts (from Gardner and others, 1994).

- During the lowering of base level associated with deposition of Kf-1 through Kf-3 and the turnaround and initial rise associated with deposition of Kf-4, most of the sediment was conveyed through the fluvial systems to the shoreline. Because of the high rate of delivery of sediments at the river mouths, wave energy was insufficient to cause major reworking of the deltaic deposits which, as a result, took on classic lobate to bird-foot, fluvial-dominated forms. Slow aggradation of sediment in the coastal plain behind the shoreline led to accumulation of relatively thin, widespread, largely single-storied meanderbelt deposits.

- During the rising of base level associated with deposition of Kf-5 through Kf-7, rivers aggraded the coastal plain more rapidly. More sediment was tied up in meanderbelt deposits, which are thick and multistoried, and in the fine-grained deposits of the adjacent flood basins. The amount of sediment conveyed throughout the fluvial systems to the shoreline was reduced. Because of the lower rates of accumulation of sediment at the river mouths, wave energy was sufficient to rework the deltas in cuspate, wave-dominated morphologies.

The BEG's study of the Ferron incorporated work previously conducted by Gardner and built upon it. Numerous geoscientists from the BEG contributed to the project. Barton, however, worked on all phases of the project and is the principal contributor of most of the new stratigraphic concepts. These studies focused on units deemed to be good analogs for Gulf Coast reservoirs. Their initial object of study was a sandy meanderbelt deposit plus underlying delta-front strata of Kf-5 exposed in Muddy Creek Canyon (one of our case-study areas). Study of Kf-5 was later extended northward to include all of the Kf-5 outcrops east and north of Muddy Creek Canyon. Additional case studies were initiated in deposits of Kf-2 at Ivie Creek and at Dry Wash. The final phase of the BEG study of the Ferron, now in final stages of compilation, involves the detailed stratigraphy of the entire Ferron section between I-70 and Dry Wash.

The final reports of the BEG's work are in preparation and have yet to be published. Many of their results and conclusions, however, can be found in various interim reports (Barton and Tyler, 1991), in reports published by the GRI (Fisher and others 1993a, 1993b), in the Ph.D. dissertation of Barton (1994), and in unpublished field trip guidebooks (Barton and Tyler, 1995).

The main thrust of the BEG study was to build on Gardner's interpretations of depositional histories, stacking patterns, and facies architecture, and to define the permeability distributions within the recognizable sandstone facies. Detailed studies were focused primarily on Kf-2, which is part of the strongly forward-stepping, lower part of the Upper Ferron, and Kf-5, which is part of the backward-stepping, upper part of the Upper Ferron.

Barton, initially working jointly with Gardner and then independently, compiled very detailed stratigraphic information and large permeability data sets for a number of sites in the Ferron. Working at a more regional scale, Barton (1994) recognized two errors that had initially been made by Ryer and propagated by Gardner: (1) the seaward limit of Kf-1 occurs in the southern part of the Coal Cliffs north of I-70, not in the southern part of Molen Reef as previously mapped; and (2) the seaward limit of Kf-6 occurs just north of Dry Wash, close to the seaward limit of underlying Kf-5, farther northeastward than previously thought. The first of these points had been recognized independently by our UGS project team (Anderson and Ryer, 1995). Both the BEG and UGS teams also independently came to the realization that unit Kf-2, as previously defined, constitutes more than one "4th order" or "short-term" cycle of sedimentation. The approaches used by the two teams to correcting this problem, however, are different and are discussed at length is Chapter IV, Regional Stratigraphy. The details of one of Barton's (1994) subdivisions of Kf-2 is summarized in figure 2-28.

The most recent report by Barton (Barton and Tyler, 1995) includes a new and fundamentally different interpretation of the origins of parasequence-level units in the Ferron. Like many other workers, he interpreted his parasequences as products of fluctuations in relative sea level. Ryer and Gardner had done the same, but both had concluded that rates of lowering of sea level had always been exceeded by the overall rate of basin subsidence. Interpreted this way, eustatic fluctuations are represented by varying rates of relative sea-level rise: falling eustatic sea level results in a slower rate of relative sea-level rise and progradation; rising eustatic sea level results in a more rapid rate of relative sea-level rise and transgression. Barton and Tyler (1995) argued that the Ferron preserves evidence of relative sea-level lowering based on interpretation of sequence stratigraphic relationships within the lower, forward-stepping part of the Ferron deltaic complex. Following a period of progradation under conditions of rising relative sea level, sea level fell, leading to incision of channel systems and seaward shift of the shoreline to a more distal, lower position. Subsequent rise of sea level lead to upward and forward building of the shoreline, formation and filling of a bay/lagoon complex, and filling of valleys. One of the most important implications of this interpretation is that rivers are incised into pre-existing sediments during periods of relative sea-level fall to form valleys: many of the deposits, previously interpreted as channel deposits laid down on an aggrading alluvial plain or delta plain, are reinterpreted as valley fills. We disagree with Barton's new interpretation of the origin of parasequences in Kf-2 and present evidence to support our interpretation in Chapter IV.

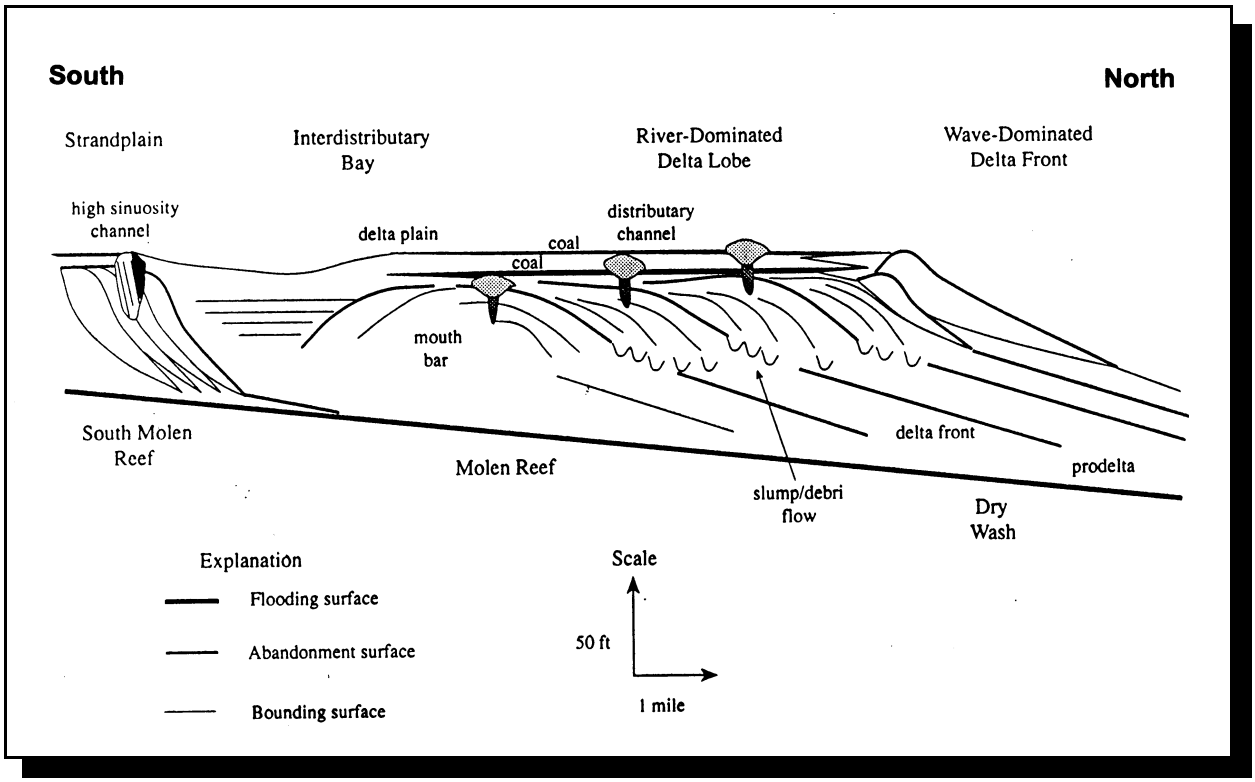


Figure 2-28. Detailed outcrop work and analysis of photomosaics allowed Barton (1994) to distinguish numerous depositional episodes, which he equated to parasequences, within Kf-2 between Miller Canyon and Dry Wash (after Barton, 1994).

An interpretation of Ferron stratigraphy published by Schwans (1995) is different than anything that preceded it. Schwans identified a major unconformity -- a sequence boundary -- on outcrops of the Ferron at I-70. The unconformity lies near the base of Kf-1, such that the Ferron exposed there lies with an erosional, unconformable contact on the Tununk Shale. Carried into the subsurface and through the existing well control, Schwans' unconformity defines a large, east-trending paleovalley. In general terms, Schwans' model calls for a pronounced drop of relative sea level in central Utah during middle Turonian time, an eastward shift in the position of the shoreline to the present-day San Rafael uplift, and fluvial erosion of a broad valley. During a subsequent rise of sea level, the valley flooded to form a large estuary within which the bulk of the Ferron, as exposed in Castle Valley, accumulated.

We disagree with Schwans' interpretation and to fully critique it would require a lengthy discussion. In short, Schwans force fitted a model -- the "slug model" of Vail and others -- that simply doesn't apply to the Ferron. Particularly revealing in understanding the origin of this interpretation is the fact that the list of references cited in the paper (Schwans, 1995) does not include a single one of the studies of the Ferron that have been described here. It includes, instead, references to all of the widely recognized papers defining the principles of sequence stratigraphy, particularly the numerous papers published by Van Wagoner on the Blackhawk Formation in the Book Cliffs.

Preliminary results of a Ferron study that is presently underway by Garrison and van den Bergh have been published in extended abstract form (Garrison and van den Bergh, 1996; van den Bergh and Garrison, 1996) and in a field trip guidebook (Garrison and others, 1997). One of the principal goals of their project is the same as one of ours: to divide the Ferron into genetic units at the level of the parasequence.

Figure 2-29 shows Garrison and van den Bergh's stratigraphic framework. It distinguishes three sequences consisting of 33 parasequences organized into 11 parasequence sets. There are some subtle, but important, differences between this and previous correlations schemes. The two unconformities (sequence boundaries) identified within the Ferron, the earlier within Kf-2 and the later within Kf-4, are entirely new. They are both defined on the basis of erosional relief that is present at the bases of meanderbelts. The relief on the contacts, apparently, is attributed to subaerial erosion and development of topography, rather than to simple local variation in the amount of scouring that occurred during emplacement of the meanderbelts. We disagree with Garrison and van den Bergh's interpretation of these sequence boundaries. The specific reasons for our disagreement will be discussed in Chapter IV, where the stratigraphic units are described. In general, our disagreement stems from two points: (1) we disagree with some of the key correlations that led them to their conclusions, and (2) the absence of appropriately placed low-stand shoreline deposits associated with their sequence boundaries makes the existence of significant subaerial erosional surfaces highly unlikely.

Another new aspect of Garrison and van den Bergh's interpretation is the arrangement of parasequences in Kf-6, Kf-7, and Kf-8 (figure 2-29). Each contains two parasequences and in each the younger parasequence is positioned landward of the older one such that these three parasequence sets are back-stepping or retrogradational parasequence sets. Previous workers who have studied these units have failed to recognize the internal organization described by Garrison and van den Bergh. We, too, have not recognized it in the course of our work and, for this reason, we believe that Garrison and van den Bergh's interpretation is incorrect.

Sequence Boundaries and the Introduction of Chaos into Ferron Stratigraphy

The last few years has seen a fundamental change in how geologists look at the Ferron: not just in how they go about looking at it, but also in what kinds of things they see when they look. This change is a direct result of the rise and widespread acceptance of sequence stratigraphy.

From the early work of Lupton (1916) through the fleshing-out of the details of Ferron stratigraphy provided by Gardner (1993) and Barton (1994), each student of the Ferron essentially built upon the work of his or her predecessors: each publication provided new details and more refined interpretations. During the 1990s, an increasing number of geologists approached study of the Ferron with a different question in mind: How does what we see in the Ferron fit the tenets of sequence stratigraphy? Many geologists have looked at the Ferron in this new way, although only a few have fully documented their conclusions in publications. The new way of looking at things has led to a very different result: each worker sees something different than the other; no two are in agreement.

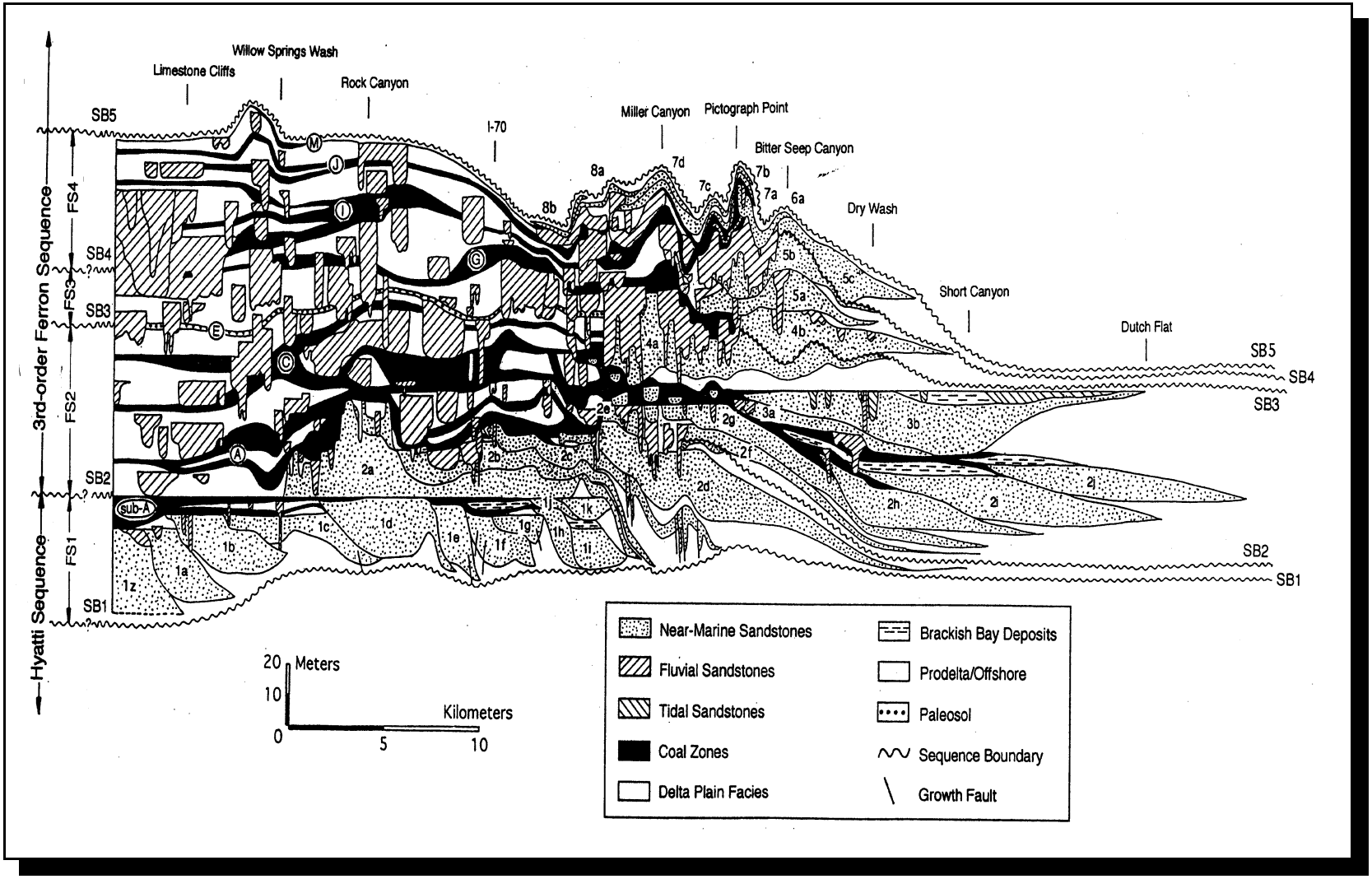


Figure 2-29. Ferron stratigraphic framework from Garrison and others (1997). Two subaerial, erosional unconformities are recognized within the Ferron. They, plus two more undefined unconformities in the underlying Tununk Shale and overlying Blue Gate Shale members, are interpreted to be sequence boundaries that define three sequences within the Ferron. Numerous parasequences are distinguished in the figure. They are grouped into 11 parasequence sets, although the sets are not defined on the figure.

Gardner (1993, 1995a) made the first well documented effort to define the sequence stratigraphy of the Ferron. An essential conclusion of his analysis is that no unconformities exist to define sequence boundaries. The three sequences he distinguished in the Turonian-Coniacian section of central Utah are, instead, based on correlative surfaces. All of the deltaic Upper Ferron strata discussed here belong to the youngest, (Gardner's Ferronensis) sequence. The correlative surface that serves as its base coincides with the top of Kf-Washboard, Kf-Clawson, and Kf-Washboard documenting a period of low sea level. The upper boundary of the sequence remains undefined.

Seven sequence boundaries that correspond to unconformities, listed here in descending stratigraphic order, have been identified recently:

1. Garrison and van den Bergh (1996) and Garrison and others (1997) distinguished an unconformity in Kf-4.

2. Pulham and Pemberton (work in progress) have defined an unconformity at the base of the C coalbed (corresponding to a position that we interpret as belonging to the latest part of Kf-2) in the middle part of Muddy Creek Canyon based primarily on analysis of the trace fossil assemblages present in five cores.

3. Garrison and van den Bergh (1996) and Garrison and others (1997) distinguished an unconformity in Kf-2.

4. van den Bergh and Sprague (1995) recognized an unconformity on the top of Kf-2 in the area south of Coyote Basin (north of Willow Springs Wash).

5. Barton and Tyler (1995) has distinguished several minor erosional surfaces that he believes are characterized by subaerial erosion in Kf-2. Though minor, they would still be considered sequence boundaries.

6. Shanley and McCabe (1991, 1995) extend an unconformity they recognize in the Straight Cliffs Formation of the Kaiparowits Plateau to a position somewhere low in the Ferron in the Castle Valley outcrops. Their initial interpretation (verbal communication, 1998) is that it corresponds to the top of Kf-1 at Ivie Creek.

7. Schwans (1995) defined a sequence boundary corresponding to surface near the base of Kf-1 at Ivie Creek.

Thus, seven studies identified seven unconformities, no two of which are the same. The very fact that there is a total lack of agreement among the practitioners of this approach casts suspicion on its accuracy and usefulness. Our opinion is that there is evidence to support only one of the interpretations, that of van den Bergh and Sprague (1995).

Coal in the Ferron

Coal has long played an important role in the economy of central Utah. The coalbeds of the Ferron have always been of minor importance compared to the coals of the Blackhawk Formation in the nearby Wasatch Plateau, but nonetheless have been important as a source of coal for local use. Only one mine, Consolidation Coal Company's Emery Mine, which was active from the mid-1970s to the mid-1990s, has produced coal on a large, commercial scale from the Ferron (8.5 million tons [7.7 mt]). The following is a brief review of the history of study of coal in the Ferron. Not included are studies addressing geochemical aspects of Ferron coal.

The first written documentation of coal in Castle Valley occurs in a report issued by the Wheeler Survey. R.L. Hoxie of the Army Corps of Engineers recorded in his journal of October 11, 1853 that "specimens of coal were brought in from the hills near the camp." Lupton interpreted the location of the camp as being near the head of the canyon of Muddy Creek. The J coalbed is conspicuously exposed at many localities along the canyon walls in this area, and it is almost certain from this seam that the samples were acquired.

Forrester (1892) collected samples from coalbeds in Ivie Creek and Quitchupah Canyons and published proximate analyses. It is likely that his samples came from the I coalbed and from either the A or C coalbeds of Lupton's (1916) terminology. Forrester interpreted the coal-bearing strata as belonging to the Montana Group (that is the Mesaverde Group), dropped into this position several miles east of the main Mesaverde outcrop belt by faulting. The Joe's Valley-Paradise graben lies between the Ferron and Mesaverde outcrop belts in the area south of Emery, although it is not apparent that the structure was recognized by Forrester. If it was, it would have lent credibility to his interpretation. It is likely, however, that a more important factor was the presence of coal. The presence of coal was known in Mesaverde Group strata throughout much of the Colorado Plateau, whereas strata between the base of the Mesaverde and the top of the Dakota are generally shaly and lack coal. That the coal-bearing strata at Ivie Creek and Quitchupah Canyons do not belong to the Dakota is obvious to anyone visiting the southern Castle Valley outcrops. It is likely that Forrester simply assumed any coal younger than the Dakota must belong to the Mesaverde and devised a structural interpretation to fit his preconception.

Taft (1906) briefly examined some of the Ferron outcrops near Emery. He reached the conclusion that "... coal, which is of little economic importance, is known to occur only to the east and southeast of Emery." His statement that coal is unimportant in the Emery area is surprising inasmuch as his map shows the locations of the Casper and Bear Gulch mines. Taft presumably visited these mines, both of which exploited sections of the C coalbed that exceed 6 feet (2 m) in thickness. Furthermore, he collected a sample of coal from what is now known as the Cowboy mine, south of Emery, where the I coalbed is 5 to 6 feet (1.5-2 m) thick.

Lupton's (1916) study of the coal geology and coal resources of Castle Valley stands as the first of two primary reference on coal in the Ferron. Lupton conducted his field work during two periods: July 17 through October 7, 1911 and September 9 through November 2, 1912. This represents a total of 138 days. His field party consisting of himself plus five other men, several of whom apparently were locals. One cannot help but be impressed by the amount of work completed, particularly given the poor condition of roads in the area at that time and the fact that the party lacked adequate topographic maps and had to survey most of their locations.

Lupton (1916) named the significant coalbeds of the Ferron, assigning them letters of the alphabet, in ascending stratigraphic order. The thickest and, therefore, economically most important coalbeds are the A, C, and I. The C and I coalbeds were being mined at the time of Lupton's visits and he had encountered a prospect dug into the A coal along Quitchupah Creek. Based on his many outcrop measurements of coal thicknesses, Lupton (1916) estimated at total coal resource of 1.43 trillion tons (1.3 trillion Mg).

Lupton's report includes some minor miscorrelation of coalbeds. The most significant miscorrelations involve the A coal, stratigraphically the lowest seam designated. Another coal zone, older than Lupton's A coal, exists in the middle and southern parts of the coal field, but this fact was unrecognized (this lowest coal zone now has the awkward designation "sub-A"). Coal of this zone in the Last Chance Creek and Paradise Lake areas were miscorrelated with the A coal, the miscorrelation occurring in the rugged outcrops of the Limestone Cliffs south of Willow Springs Wash. A second miscorrelation of the A coal, one that remained unrecognized until our study, also occurred at its northeastern limit in the "Molen Amphitheater." Our work, discussed in Chapter IV, shows that the coal that extends northward to Dry Wash is actually the lower part of the C coalbed, not the A coalbed as correlated by Lupton and all subsequent workers.

Lupton documented the fact that coal is a minor component of the Ferron on outcrops north of a line extending east from Emery and becomes absent entirely a short distance north of Dry Wash as the Ferron becomes increasingly dominated by marine facies. Although coal is absent on many of the Ferron outcrops in the middle and northern parts of Castle Valley, it does occur in the Ferron to the west, in the subsurface. The presence of Ferron coal in the Price area was noted by Spieker and Reeside (1925). They reported that drilling along the Rio Grande Railroad about 10 miles (16 km) west of the Ferron outcrops indicated about 200 feet (61 m) of predominantly sandy Ferron section containing several coalbeds, one of them 7.5 feet (2.3 m) thick. Additional data about the thicknesses and stratigraphic positions of the coals near Price were published by Gray and others (1966). Situated at depths too deep for economic mining, these coalbeds would later become the focus of an active program of coalbed methane development.

Doelling (1972) published an analysis of the Emery coal field as part of his comprehensive treatise on coal in Utah. His is the second principal work on Ferron coal. Although it contributes little data on the thicknesses and areal extents of coal seams beyond what can be found in Lupton (1916), it does present a much broader picture of Ferron coal, including considerable information about coal quality. Doelling (1972) confirmed Lupton's estimate of coal resources, and in addition distinguished measured, indicated, inferred, and potential reserves. Measured and indicated reserves total 758 million tons (688 Mg). Color maps corresponding to U.S. Geological Survey 7.5 minute quadrangles (although with different names) portray the surface geology at a scale of approximately 1: 42,000.

Ryer (1981a) placed the principal coalbeds of the Ferron into their depositional setting and recognized an important genetical relationship between coals and their equivalent shoreline sandstone units: the greatest thicknesses of coal is present at and landward of the landward pinchouts of the shoreline sandstone (figure 2-13). Thick coal tends to occur in pods whose long axes are perpendicular to the shoreline trend. These pods represent flood basin and swamp areas bounded along depositional strike by sand-rich meanderbelt deposits. Ryer and others (1980) used laterally continuous beds of altered volcanic ash to document these relationships in the C coalbed of the

Ferron (figures 2-30 and 2-31). The details of the physical and chemical properties of the altered volcanic ash layers are addressed by Triplehorn and Bohor (1981) and Bohor and Triplehorn (1993).

Coal in the Ferron in the subsurface near Price was analyzed by Bunnell and Hollberg (1991). Their work predated the development of coalbed methane in this area and their interest in the coal was from the perspective of a minable resource, rather than in its contained methane. They utilized the model proposed by Ryer (1981a) to explain the thickness distributions of the four to five coal zones recognized there. The Ferron in the area they studied is about 200 feet (60 m) thick. The shoreline orientation was north-northeast to northeast. Of particular interest is the strongly "back-stepping" or "retrogradational" pattern that the shoreline sandstone bodies of the Ferron display (figure 2-32). As is the case on outcrops of the Upper Ferron farther south in Castle Valley, maximum thicknesses of coal occur in the vicinities of landward pinchouts (figure 2-33).

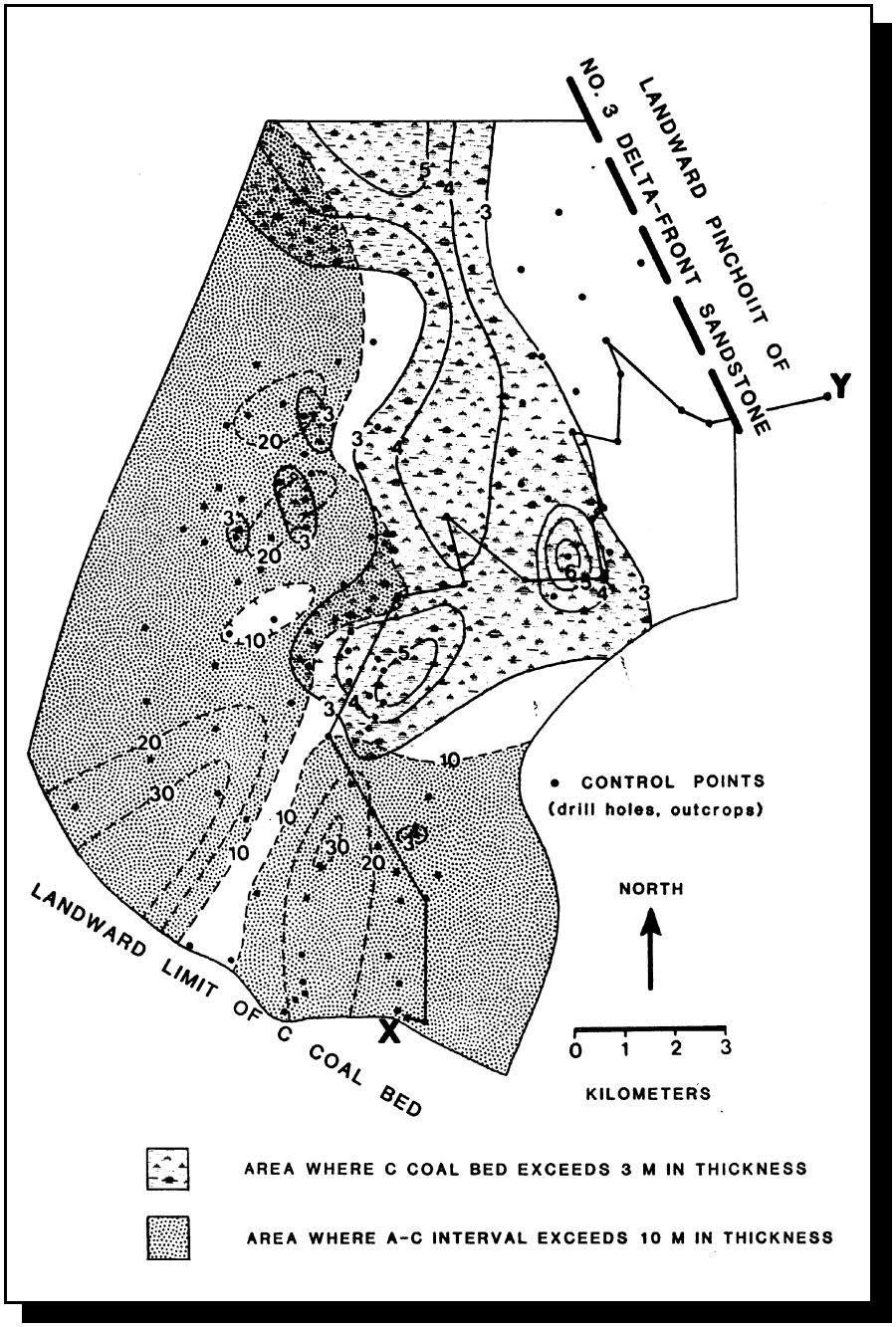


Figure 2-30. Comparison of thickness of the C coalbed and of laterally equivalent fluvial deposits. There is an inverse relationship, peat deposition having been prohibited in areas of fluvial aggradation (from Ryer and others, 1980).

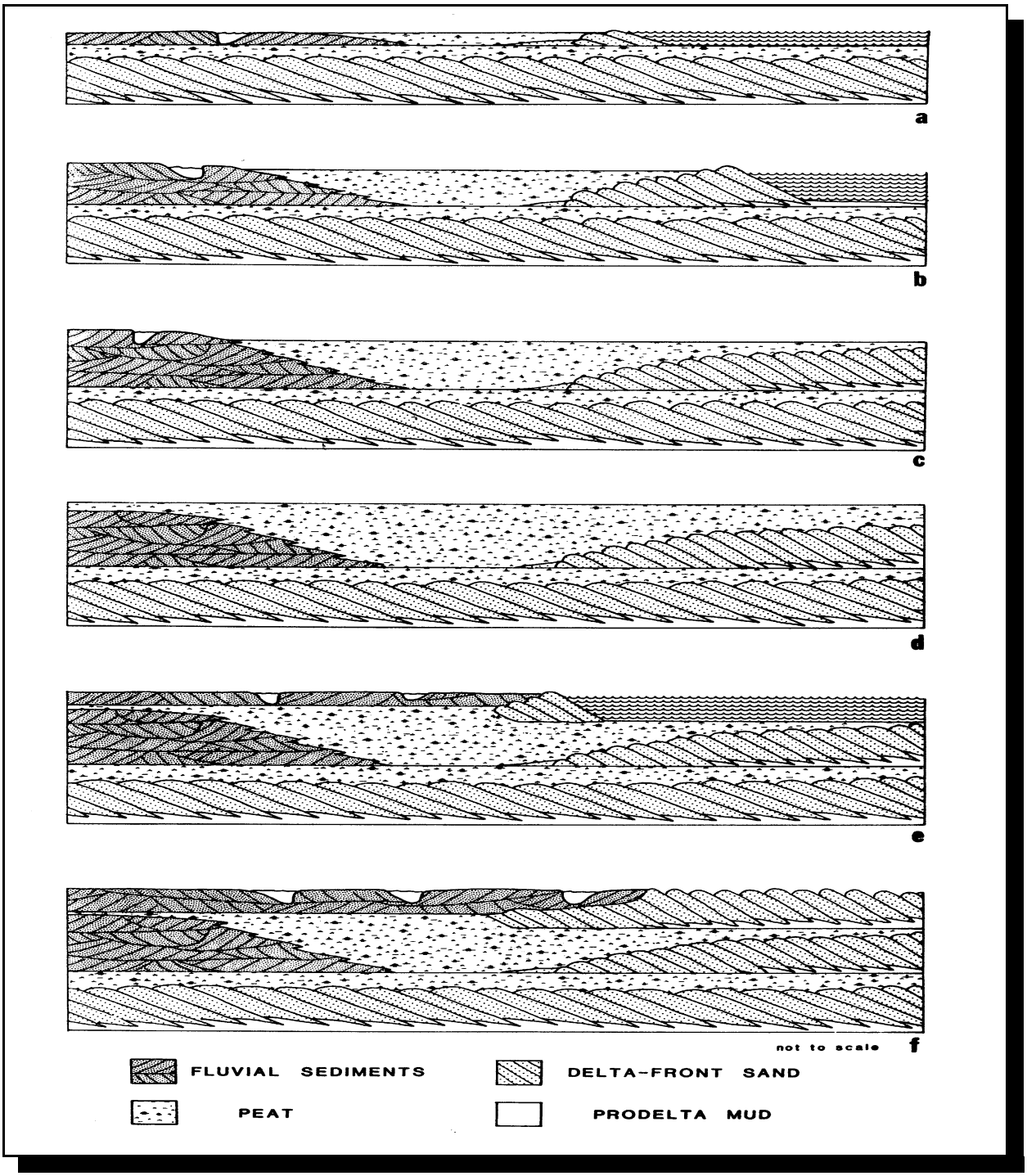


Figure 2-31. Diagrammatic cross section showing the depositional history of the C coalbed and associated units. The C coal was interpreted to have formed entirely during progradation of Kf-3, an interpretation that must be revised following discovery of the fact that the Kf-3 pinches out landward into the C coal, such that its lower part formed during the latest part of deposition of Kf-2 and perhaps partly during the transgression that ended Kf-2 (from Ryer and others, 1980.)

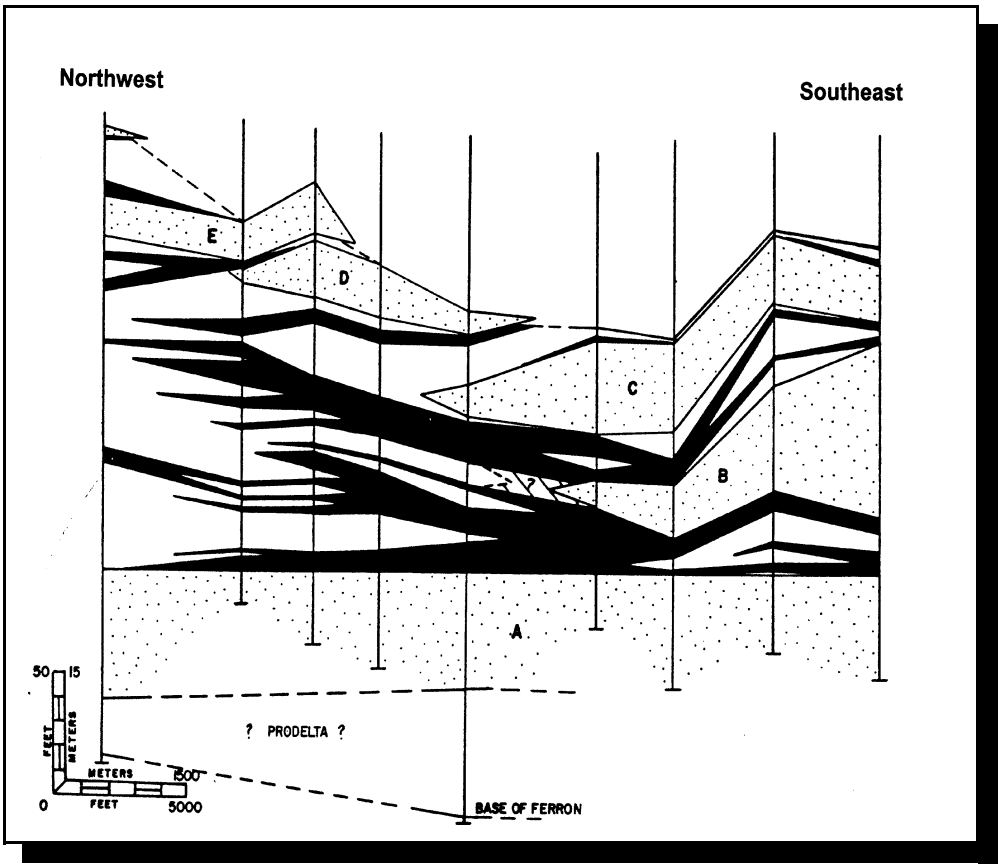


Figure 2-32. Relationships between Ferron coals (black) and shoreline sandstones (stippled) in the Price area. Shoreline sandstones B through E show a strongly back-stepping arrangement (after Bunnell and Hollberg, 1991).

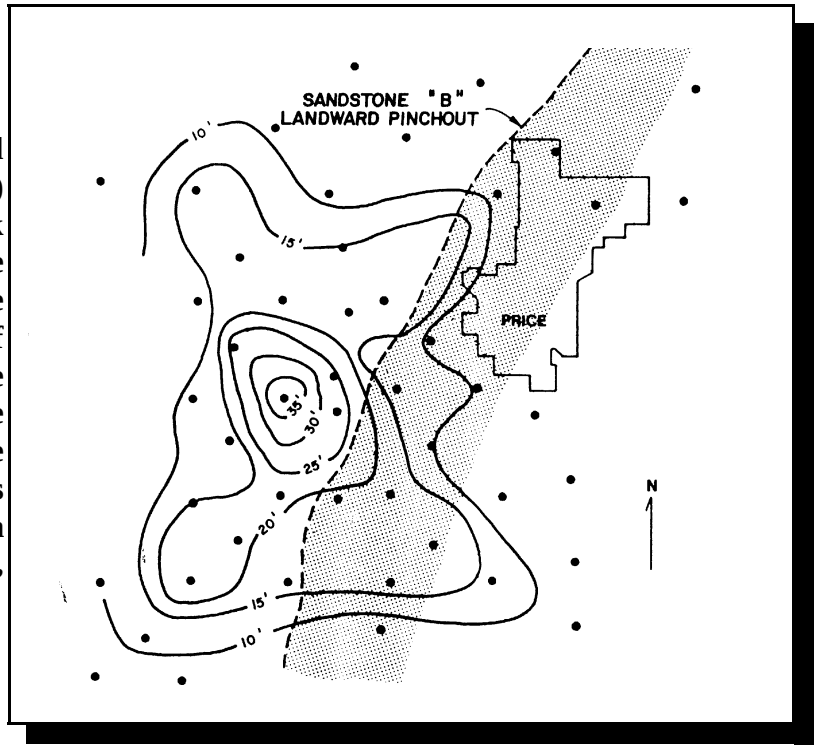


Figure 2-33. Bunnell and Hollberg (1991) demonstrated that thick pods of coal are associated with the landward pinchouts of shoreline sandstone units in the subsurface near Price, as is the case on the Ferron outcrops in Castle Valley (from Bunnell and Hollberg, 1991).

Petroleum in the Ferron

The Ferron Sandstone has been a target of oil and gas exploration since 1921, when the Phillips No. 1 Huntington well was completed as a dry hole on the Huntington anticline, located in Castle Valley near the town of Huntington (Kuehnert, 1954). The first significant shows of oil in the Cretaceous section were reported in the Dakota Sandstone in a well drilled at Gordon Creek in 1922. The first commercial success occurred on the Clear Creek anticline, where Byrd-Front, Inc. discovered gas in the Ferron in 1951 (Edson and others, 1954; Tripp, 1991a, 1993a) (figure 2-34). Gas was subsequently discovered in the Ferron at Flat Canyon anticline (Flat Canyon field) in 1953 (Tripp, 1993b), at Joes Valley in 1953 (Tripp, 1993c), at Ferron anticline in 1957 (Tripp, 1990a, 1990b, 1991b, 1993a) and Indian Creek/East Mountain field, now part of Flat Canyon field, in 1981 (Laine and Staley, 1991) (figure 2-34). The Ferron was found to contain gas and extremely light oil (56E API) on the southern part of the Flat Canyon field, this constituting the only significant occurrence of producible liquids from the member (Laine and Staley, 1991; Sprinkel, 1993).

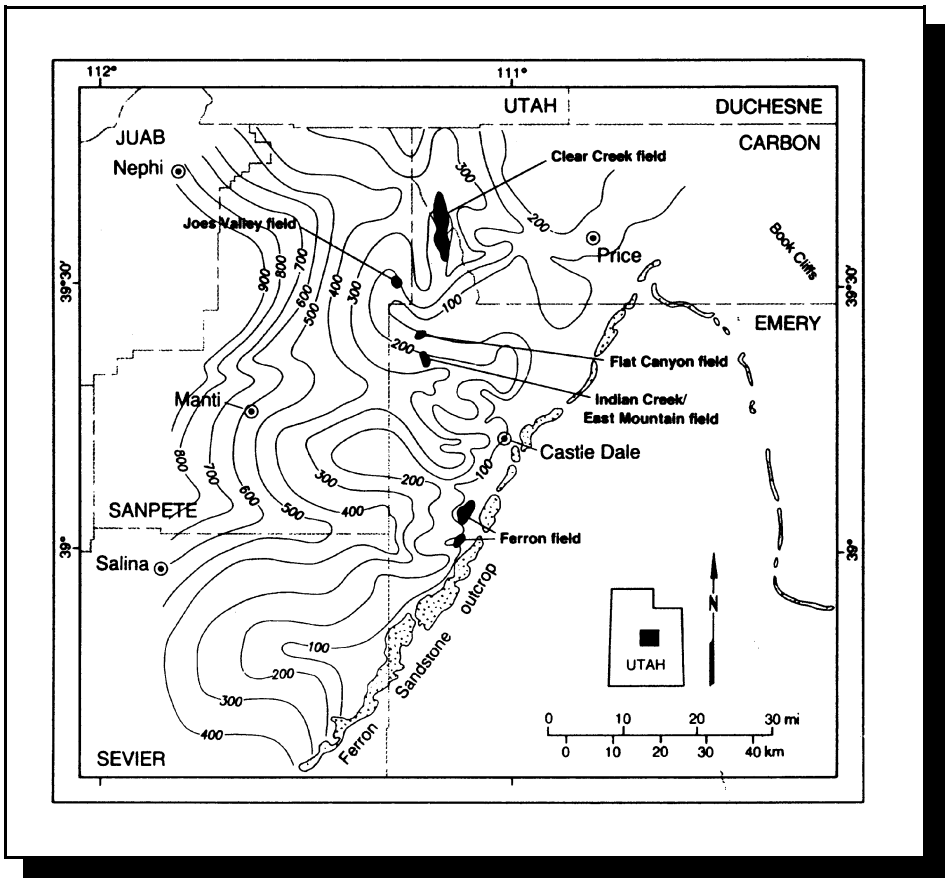


Figure 2-34. Location of gas fields (solid black) productive from the Ferron Sandstone and net sandstone-thickness map, Wasatch Plateau/Castle Valley. Contour interval is 100 feet. Thick lobes of sandstone indicate areas of deltaic deposition (from Sprinkel, 1993; modified from Tripp, 1989).

Of these discoveries, Clear Creek field is by far the most important. Clear Creek field has produced over 114 billion cubic feet (BCF [3.2 billion m^3]) of gas, far surpassing the 11.4 BCF (320 million m^3) of gas produced from Ferron field, the second in importance (Utah Division of Oil, Gas and Mining, 2000). Edson and Scholl (1954) estimated that the Clear Creek field would ultimately produce 700 BCF (20 billion m^3) of gas. Flat Canyon and Joes Valley, fields have produced 8.6 BCF (240 million m^3) and 3 BCF (85 million m^3) from commingled Ferron and Dakota reservoirs of gas respectively as of January 1, 2000 (Utah Division of Oil, Gas and Mining, 2000). Cumulative oil production from Flat Canyon field is 14,719 barrels (2,340 m^3) (Utah Division of Oil, Gas and Mining, 2000). Flat Canyon and Joes Valley fields were abandoned in 1969 and 1976 respectively (Tripp, 1993c).

The discovery of Clear Creek field played a significant role in stimulating study of the Ferron. As discussed earlier, the Ferron at Clear Creek was found to include a basal sandstone unit characterized by good lateral continuity, overlain by a thicker section containing discontinuous sandstones. The difference in these two sandstone types was of considerable interest. The dissertation by Katich (1951), completed in the same year the field was discovered, provided a picture of the Ferron stratigraphy on outcrop. The discovery provided an impetus for studies integrating the outcrop and basic subsurface observations by Katich (1954) and Davis (1954).

Walton, who was instrumental in the discovery of Clear Creek (Edson and others, 1954) summarized the petroleum geology of the Wasatch Plateau and Castle Valley in papers published in 1954 and 1955. Numerous papers published in recent years by Tripp (1990a, 1990b, 1991a, 1991b, 1993a, 1993b, and 1993c), Laine and Staley (1991), and Sprinkel (1993) provide a current review of the status of Ferron oil and gas exploration and production.

Coalbed Methane Development in the Ferron Sandstone

Coal miners long knew that methane in coalbeds posed a serious risk of explosion, and the U.S. Bureau of Mines began research on this problem when it was created in 1910 (Irani and others, 1977). Early research by the U.S. Bureau of Mines focused on quantifying the amount of methane released in active coal mines to alleviate the health and safety problems created by the gas (Diamond and Levine, 1981). In the late 1970s, following two interruptions in petroleum supply from the Middle East, the DOE and the GRI began researching new and unconventional sources of natural gas. Based on the U.S. Bureau of Mines measurements of large volumes of methane in coalbeds, the DOE and the GRI sponsored studies to quantify and develop techniques to economically produce gas from coalbeds. Preliminary coalbed gas resource estimates by the DOE were completed for all major coal basins in the United States by 1982. These early studies focused subsequent research and development efforts on five basins: Black Warrior, central and northern Appalachians, Piceance, and San Juan (ICF, 1990). Utah's coalbed gas potential was discounted because little was known of the deep coal resources.

Early coalbed gas work in Utah, during the late 1970s and early 1980s, consisted of UGS studies to measure the gas content of coals in the major Utah coal fields (Davis and Doelling, 1976; Davis and Doelling, 1977; Doelling and others, 1979; Smith, 1981; Smith, 1986; Keith and others, 1990a, 1990b, 1990c, 1990d; and Keith and others, 1991), and a few individual production test wells drilled in the Book Cliffs coal field by Mountain Fuel (Allred and Coates, 1980, 1982). Recent work

by the UGS has helped define the structure, thickness, depth, extent, and maturity of the coal deposits, and the coalbed gas resources of the Ferron Sandstone Member of the Mancos Shale (Tripp, 1989; Gloyn and Sommer, 1993; Sommer and others, 1993; Tabet and Burns, 1996; Tabet and others, 1996).

The first concentrated attempt to produce coalbed gas in Utah was a 1990 five-well pilot program by Cockrell Oil Corporation testing the Blackhawk Formation coals of the Book Cliffs coal field north of Price, Utah. This initial program led to the development of the 25-well Castlegate coalbed gas field by Pacific Gas and Electric, which purchased Cockrell's project area in 1993. The Castlegate field, was sold in August 1994 to Anadarko Petroleum Corporation, which operated the field until 1998.

Interest in the coalbed gas potential of the Ferron Sandstone in the Emery coal field began with a five-well pilot program by River Gas Corporation and the discovery of Drunkards Wash field near Price in 1992 (figure 2-35). From the initial pilot program River Gas has expanded development to bring a total of 193 wells on-line in the field as of January 1, 2000 (Utah Division of Oil, Gas and Mining, 2000). Further, an environmental impact statement (EIS) was completed by the U.S. Bureau of Land Management (BLM) in May 1997 that will allow River Gas to drill approximately 400

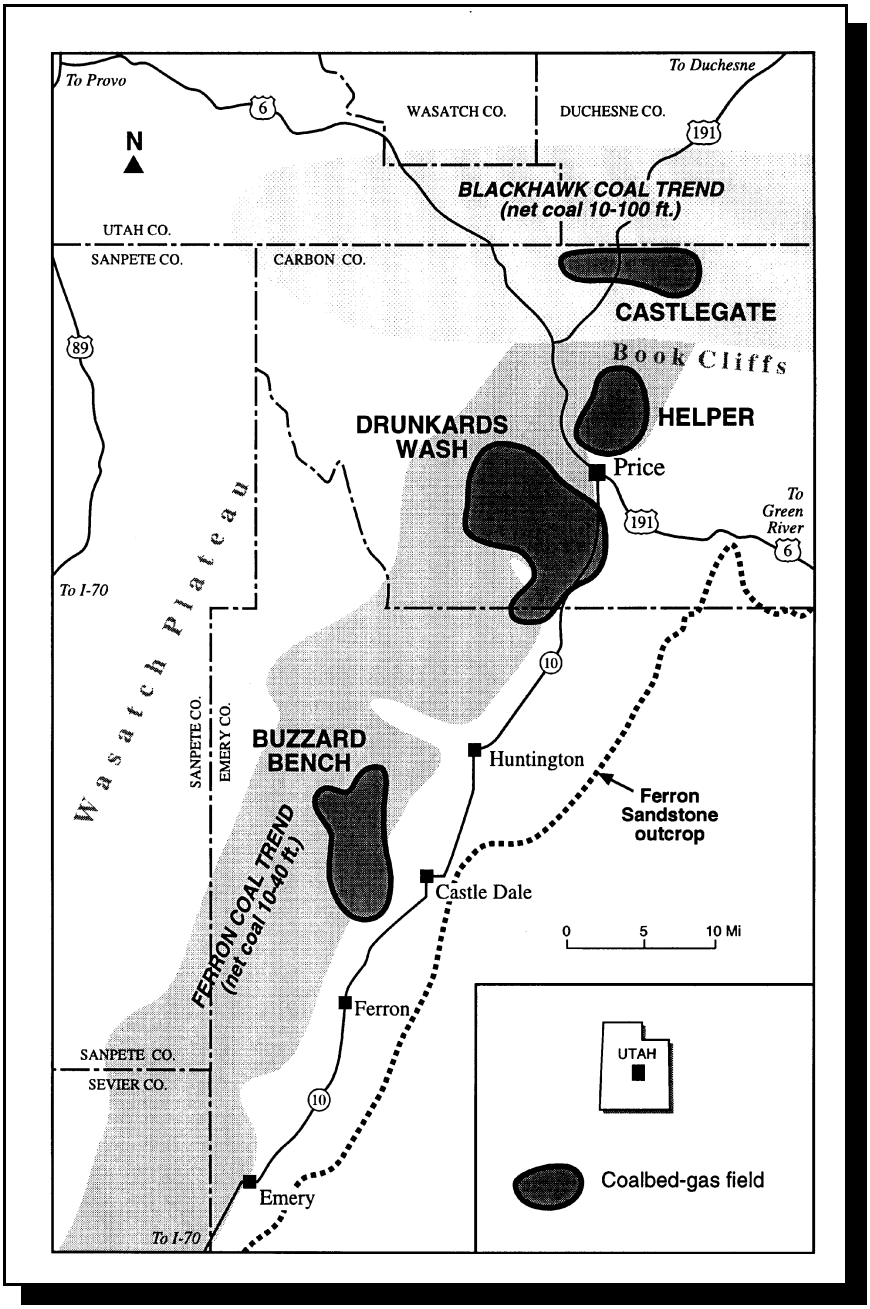


Figure 2-35. Location of fields producing coalbed methane in east-central Utah and the Ferron Sandstone coalbed gas "fairway" Carbon, Emery, Sanpete, and Sevier Counties, Utah (modified from Tabet and others, 1996).

more gas wells. As of January 1, 2000, Drunkards Wash field had produced 118.5 BCF (3.3 billion m^3) of gas and ranks as the Utah's sixth largest gas field in terms of production (Utah Division of Oil, Gas and Mining, 2000).

Development of the Ferron Sandstone coalbed gas play has also expanded as Texaco Exploration and Production, Incorporated and Anadarko Petroleum Corporation have proved up coalbed gas reserves in the Buzzard Bench and Helper fields along the play (figure 2-35). As of January 1, 2000, Texaco had completed and started coalbed gas production from 10 wells in the Buzzard Bench field in the area west of Castle Dale. As of January 1, 2000, Buzzard Bench field had produced 1.9 BCF (53.2 million m^3) of gas (Utah Division of Oil, Gas and Mining, 2000). Anadarko has 67 producing coalbed gas wells in the Helper field to the northeast of Price, Utah. As of January 1, 2000, Helper field had produced 5.4 BCF (151.2 million m^3) of gas (Utah Division of Oil, Gas and Mining, 2000).

Current development of the coalbed gas from the Ferron Sandstone is focused on the shallower, 1,000 to 4,500-foot- (300-1,400-m-) deep, eastern side of the Ferron coalbed gas "fairway" which covers approximately 211,000 acres (85,400 ha) (figure 2-35). If all of this area were drilled on 160-acre (65-ha) centers, and each well was equally productive, then 1,320 gas wells would be drilled. Ultimate recoverable gas reserves for the shallow portion of the "fairway" would be 3.7 TCF (104.8 billion m^3) of gas if each of the 1,320 coalbed-gas wells produced 2.8 BCF (79 million m^3) of gas. Gas is transported to markets in Utah via a 18-inch (45.7-cm) pipeline owned and operated by Questar Pipeline Company. The Drunkards Wash discovery and its proven commercial success has resulted in the most active oil and gas lease play in Utah during the 1990s.

CHAPTER III
FACIES OF THE FERRON SANDSTONE

T.A. Ryer and P.B. Anderson

Introduction

The Ferron Sandstone consists predominantly of fluvial-deltaic deposits. The majority of Ferron sand bodies that could constitute important reservoirs and can, therefore, be regarded as reservoir analogs were deposited: (1) on prograding shorelines, and (2) by the fluvial channels that supplied the sediment to the shorelines. As a whole, the Ferron Sandstone exposures of the study area have roughly equal amounts of these two principal sand-body types, but there is great variation in the abundance of facies along the Ferron outcrop belt: fluvial strata and their associated overbank deposits predominate in the southwest, grading seaward to predominantly shoreline strata in the northeast (see figure 1-2, Chapter I, Introduction).

Gardner (1993) included very detailed discussions of facies, their rock types, sedimentology, and ichnology: his dissertation stands as the most thorough treatment of Ferron facies. Here, we offer a more generalized discussion of Ferron facies, organized generally from seaward to landward, as they would occur in a depositional sequence recording progradation of the shoreline into the sea.

Offshore-Marine Deposits

The Tununk and Blue Gate Shale Members of the Mancos Shale, which under- and overlie, respectively, the Ferron Sandstone Member, were deposited in a offshore-marine paleoenvironments at depths below storm-wave base. Offshore-marine shale is a relatively minor component of the Ferron in the study area, found in increasing amounts toward the northeast (figure 3-1). Units of marine shale in the Ferron that separate the shoreline sandstone units in the northeastern part of the study area (see figure 1-3, Chapter I, Introduction) may be considered as representing southwestward-thinning tongues of the Mancos Shale.

Shelf Sand Deposits

The Clawson and Washboard units of the Ferron (Kf-Clawson and Kf-Washboard, respectively, of our terminology; commonly referred to together as the Lower Ferron) were deposited on the shelf at water depths ranging from about storm-wave base to depths shallower than fair-weather wave base. They represent a plume of sand that was transported southward on the shelf (Thompson and others, 1986; see figure 2-19, Chapter 2, Previous Studies), probably from a bulge of the shoreline commonly referred to as the "Vernal delta."

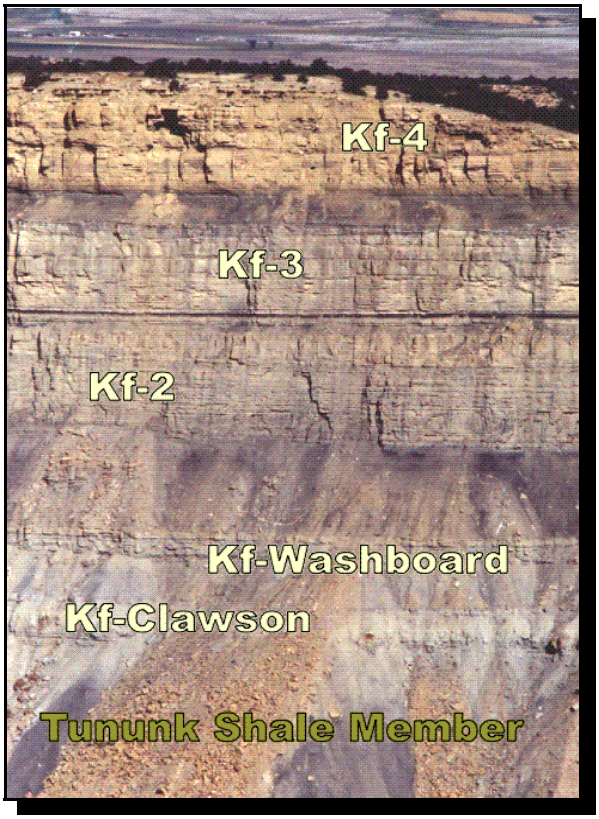


Figure 3-1. Section exposed on Molen Reef between "Molen Point" and Dry Wash. Dark gray units are marine shales. The uppermost part of the Tununk Shale Member is exposed here beneath the Clawson and Washboard shelf-sand units of the Ferron. A unit of marine shale separates the Washboard unit from the basal shoreline unit of the Upper Ferron, represented here by Kf-2. The black band on top of Kf-2 is the A coal bed. The marine shale unit that lies between the shoreline sandstone of Kf-3 and Kf-4, which genetically is part of Kf-4, can be considered to be a southward-extending and thinning tongue of the Blue Gate Shale Member. Kf-5 and Kf-6 have been eroded from the outcrop in this area. The Blue Gate Shale Member forms the flats in the far distance at the top of the photo.

The Clawson and Washboard units consist predominantly of very fine and fine-grained sandstone. Most of the sandstone has been bioturbated. Where they have not been destroyed by burrowing, planar lamination and oscillation ripple lamination are the most common sedimentary structures in these sands. Both units generally coarsen upward from a gradational base overlying marine shale; both have abrupt tops interpreted as marine flooding surfaces.

The Clawson and Washboard units form minor ledges (10 to 20 feet [3-6 m]) beneath the larger cliffs formed by the shoreline sandstone units of the Upper Ferron (figure 3-1). As the sandstones of the Upper Ferron grade northeastward into marine shale, the ledges formed by the Clawson and Washboard units become relatively more significant until, in the northernmost part of the study area, the Clawson becomes the most conspicuous feature of the Ferron outcrop belt. The sandstone content of the units varies: in the north, the Clawson Unit forms a much more prominent ledge than does the Washboard Unit, while in the south the situation is reversed.

Shoreline Deposits

Shoreline types preserved in the Ferron range from wave-dominated to strongly fluvial-dominated. Figure 3-2 shows the range in shoreline types interpreted to have existed in the Ferron. Although highly diagrammatic, this figure shows that the shoreline orientation had a large influence on shoreline type. The western shoreline of the Interior Cretaceous Seaway generally trended northward (see figure 1-4 1-3, Chapter I, Introduction) but, because of an embayment in central to northern Utah that formed as a result of more rapid subsidence in this area (see figures 1-6 and 1-7, Chapter I, Introduction), the shoreline in the study area generally trended north westward (see figure 1-10, Chapter I, Introduction). Ferron shorelines that faced eastward or northeastward were reworked by waves; some of the sand from east-facing, wave-dominated deltas was carried along

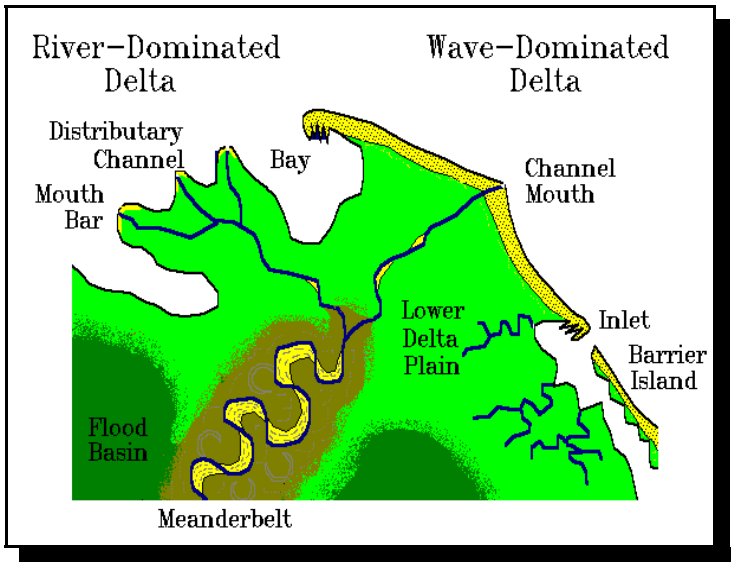


Figure 3-2. Diagram showing range of shoreline types present in the Ferron Sandstone.

shore to accumulate in adjacent shorefaces. Ferron deltas that built northward or north westward, toward the subsiding area, faced the embayment and were sheltered from waves. This explains why the most strongly fluvial-dominated deltaic deposits of the Ferron accumulated on deltas that prograded toward the north or northwest, an observation that was first made by Cotter (1975a, 1975b).

There is clear evidence of tidal deposits preserved in Ferron strata (primarily in deposits of bays, lagoons, and tidal inlets, all of which are discussed later), but no evidence to indicate that the tidal range exceeded low microtidal. Delta types in the Ferron range from wave-dominated to fluvial-dominated (figure 3-3; see also figure 2-17, Chapter II, Previous Studies). Shoreline strata of the Ferron as a whole, therefore, can be considered to lie along a linear axis extending from strongly wave-dominated deposits of the shoreface through wave-dominated deltas to strongly fluvial-dominated deltas (the later two being included as the upper apex and lower left apex in figures 3-4 and 3-5).

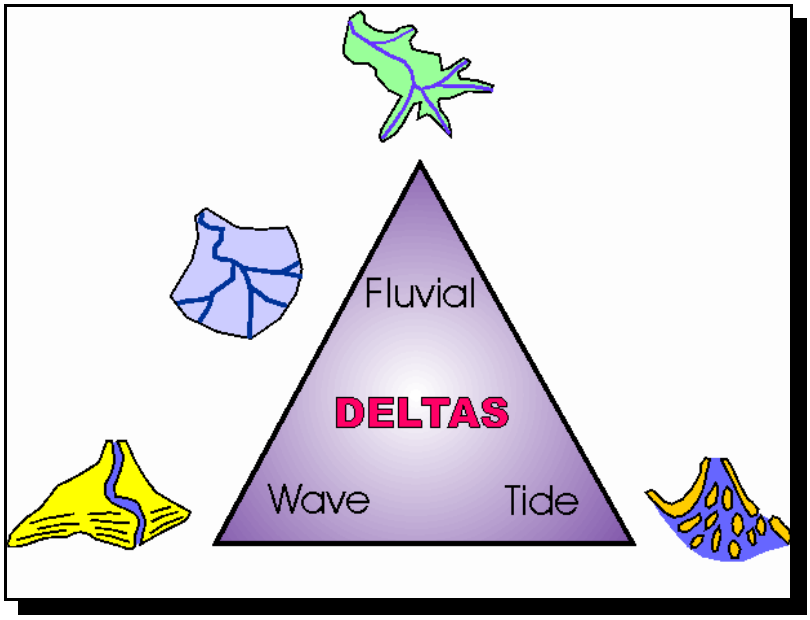


Figure 3-3. Ternary diagram showing the principal forces that shape delta morphology: fluvial input of sediment, wave-reworking of sediment, and reworking of sediment by tidal currents (after Galloway, 1975).

In this study, we distinguish three basic shoreline types in the Ferron: wave-dominated, wave-modified deltaic, and fluvial-dominated deltaic. The boundaries between these categories are arbitrary: examples representing the entire range between the end members can be recognized on the Ferron outcrops. We discuss the end members first, then describe the intermediate, wave-modified deltaic category.

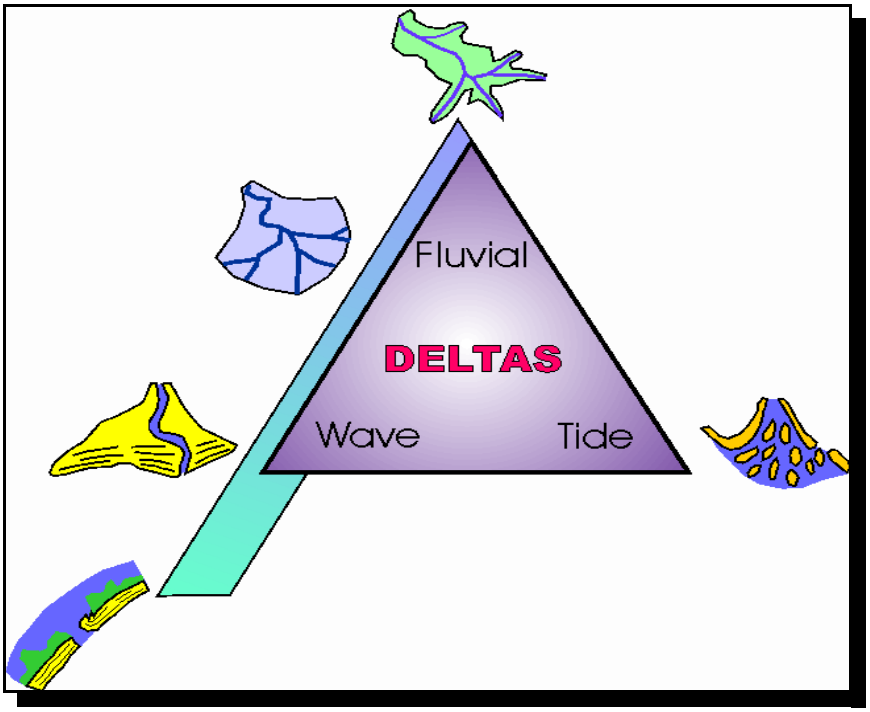


Figure 3-4. Shoreline types recognizable in the Ferron include wave-dominated, non-deltaic shorelines deposited as prograding strand plains and on barrier islands (after Galloway, 1975).

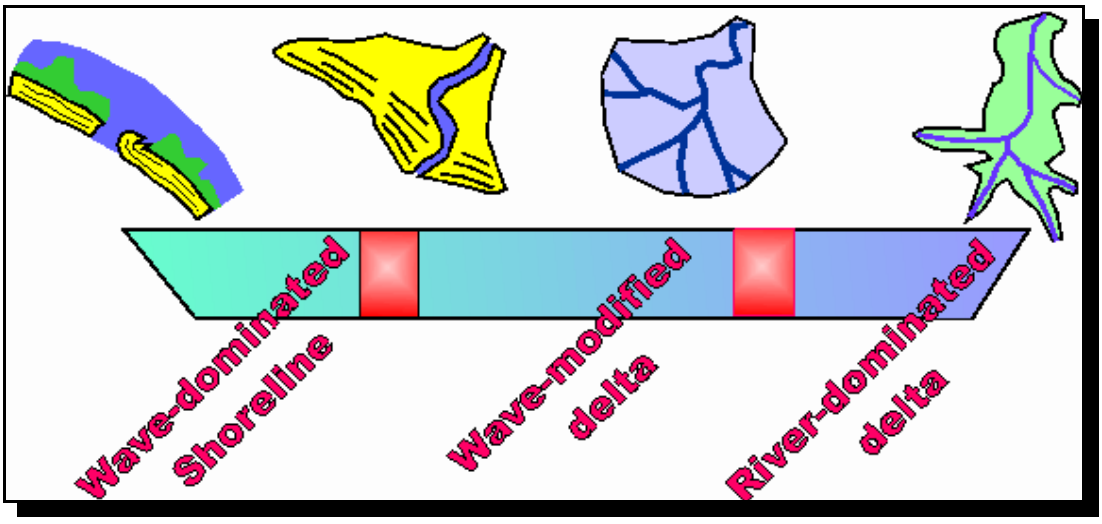


Figure 3-5. Diagram showing the three basic categories of shoreline types distinguished in the Ferron. There a gradation of types over the recognized range and the three types are arbitrarily defined.

Wave-Dominated Shorelines

Shoreface

Deposits of wave-dominated shorelines (figure 3-6) predominate in the Ferron. A typical outcrop of a wave-dominated shoreline deposit is shown in figure 3-7, and their thickness is generally from 30 to 60 feet (9-18 m). Stratigraphic successions of the Ferron deposited on wave-dominated shorelines (both wave-dominated deltas and shorefaces) have one or more shoreface subfacies: transition zone; lower, middle, and upper shoreface; and foreshore.

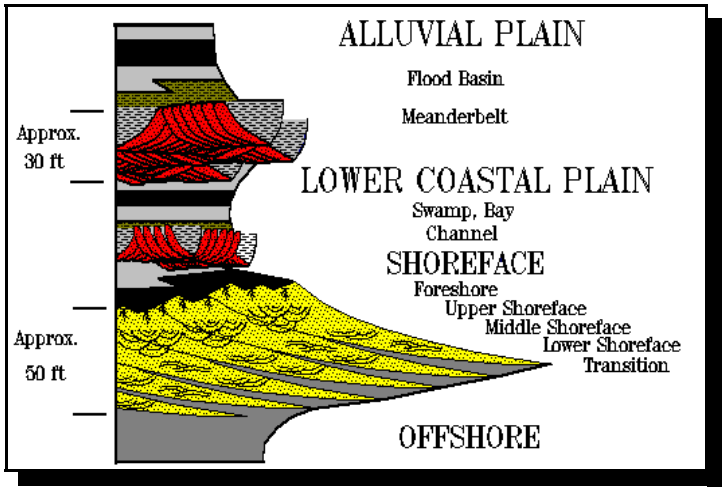


Figure 3-6. Diagram distinguishing facies and, in the shoreface, subfacies within a depositional sequence formed by progradation of a wave-dominated coast.

Most of the shoreline sandstone bodies with these subfacies accumulated on prograding shorefaces that were not directly influenced by rivers, although they were undoubtedly nourished largely with sediment transported by longshore drift from river mouths. Some shoreface deposits of the Ferron are demonstrably associated with barrier islands (for example, the landward pinchouts of Kf-1-Rock Canyon, Kf-2-Muddy Canyon-b, and Kf-6); others are associated with prograding strand plains. Some of the wave-dominated shoreline deposits may represent the margins of strongly wave-modified deltas, areas that morphologically would be included in the delta but which lack active distributary channels and that receive most of their sediment by longshore drift.



Figure 3-7. Thick shoreface sequence of parasequence Kf-2-Miller Canyon-b on the east side of Muddy Creek Canyon. The sandstone has a well-developed "white cap." The abrupt, flat contact at the top of the sandstone is a marine flooding surface.

Transition zone: Strata assigned to the transition zone consist of mudstone with thin beds of sandstone. Sandstone constitutes less than 50 percent of the rock. The sandstone typically outcrops in beds that have abrupt bases, are predominantly planar laminated in their lower parts, commonly grading upward to ripple laminated, with gradational tops. Thicker beds may include hummocky/swaley cross-stratification. The beds generally fine upward to mudstone. Burrowing is generally common and may be abundant. The sandstone beds represent storm layers deposited at depths below fair-weather wave base.

Lower shoreface: The term "lower shoreface," as used here, designates the section of interbedded sandstone and mudstone overlying the transition zone and underlying the middle shoreface. It is characterized by the same style of bedding as the transition zone, but the amount of sandstone exceeds 50 percent and the sandstone beds tend to be thicker and generally contain more hummocky/swaley cross-stratification. The combined transition zone and lower shoreface part of the succession is thin, commonly 10 feet (3 m) or less.

Middle shoreface: The middle shoreface consists of planar laminated and hummocky/swaley cross-stratified sandstone. In the Ferron, the sandstone typically is very fine to fine-grained. Most of the sandstone outcrops in sharp-based beds whose tops are commonly burrowed to bioturbated. Oscillation ripples are commonly present in the upper parts of the beds. These beds represent storm layers deposited above fair-weather wave base. Mudstone layers are generally absent in the middle shoreface, but may constitute up to about 10 percent of the middle shoreface section.

The middle shoreface is thick-15 to 20 feet (5-9 m), representing 50 percent or more of the total thickness of the shoreface succession. Middle shoreface deposits may include abundant burrows. The diversity of burrow types is great, with *Ophiomorpha* and *Thalassinoides* being the most conspicuous forms. Characteristics of middle shoreface deposits are shown in figures 3-8 through 3-13.

Upper shoreface: The upper shoreface is characterized by a distinctly different set of sedimentary structures than the underlying middle shoreface. It consists of trough cross-stratified sandstone with only minor amounts of planar lamination.



Figure 3-8. Predominantly flat-bedded and planar-laminated sandstone of the middle shoreface, parasequence Kf-1-Indian Canyon-c, in Indian Canyon, Willow Springs Wash case-study area.



Figure 3-9. Swaley cross-stratification in middle shoreface strata of parasequence Kf-2-Muddy Canyon-b in the Muddy Creek Canyon case-study area. These strata are only sparsely burrowed.

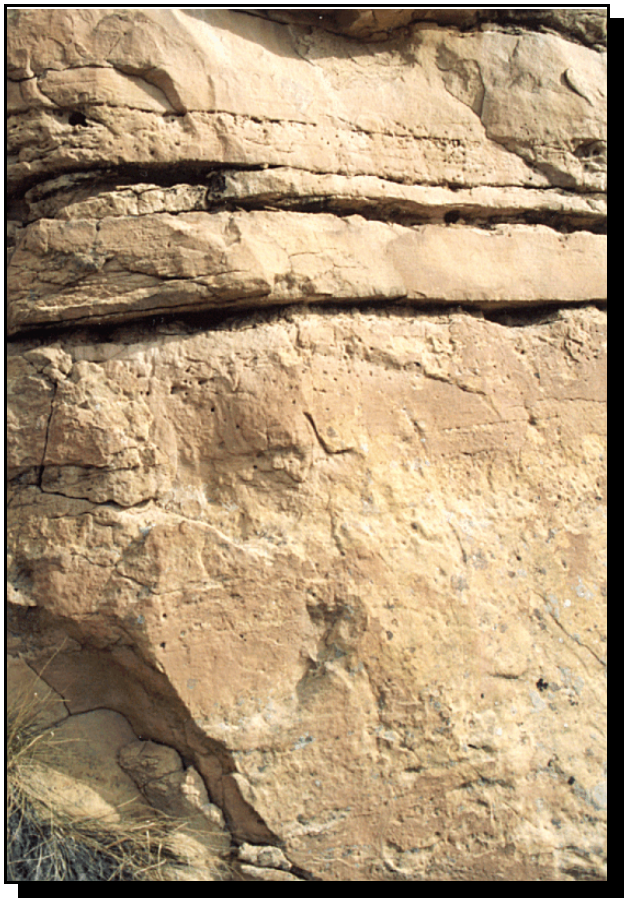


Figure 3-10. Middle shoreface strata of parasequence Kf-1-Indian Canyon-c, in Indian Canyon, Willow Springs Wash case-study area. Beds in the upper part of the photo are planar laminated and sparsely burrowed; those in the lower part are intensely burrowed such that the original physical structures are largely obscured.



Figure 3-11. Middle shoreface strata of parasequence Kf-1-Indian Canyon-a, in Indian Canyon, Willow Springs Wash case-study area. These strata are intensely burrowed to bioturbated. Remnant flat bedding is apparent. The flat top of the sandstone unit is a marine flooding surface overlain by offshore marine mudstone.



Figure 3-12. Planar lamination in a remnant storm layer in the middle shoreface of parasequence Kf-2-Muddy Canyon-b in the Muddy Creek Canyon case-study area. Burrowing has extended downward from fair-weather deposits above the storm bed, totally obscuring its top. The burrows did not extend downward to the abrupt, base of the storm layer, which places laminated sandstone on burrowed, muddy sandstone of the preceding fair-weather deposit.



Figure 3-13. *Thalassinoides* is the most common burrow form in middle shoreface deposits of the Ferron. This example of a bioturbated middle shoreface deposit outcrops in parasequence Kf-2-Muddy Canyon-b in the Muddy Creek Canyon case-study area.

The upper shoreface is usually coarser than the middle shoreface. In the Ferron, upper shoreface strata are typically composed of medium-grained sandstone. The transport directions recorded by the trough cross-stratification are generally highly variable, but oblique onshore directions tend to predominate. The upper/middle shoreface contact is generally abrupt and slightly erosional, probably as a result of scouring by rip-current channels.

The upper shoreface commonly has a thickness of 5 to 10 feet (1.5-3 m) is where it is generally well developed. The thickness may reach 20 feet (6 m) or more near landward pinchouts of parasequence-level shoreline units. Characteristics of upper shoreface strata are shown in figures 3-14 and 3-15.

The upper shoreface, as defined here, is absent in many Ferron shoreline successions. Shorelines on which only fine-grained sand was present lack upper shoreface deposits, indicating that the distinctive trough cross-stratification did not develop in fine-grained sand. In sections where the upper shoreface is not recognized, the middle shoreface extends to the top of the shoreline succession. In such cases, some part of the section designated as "middle" shoreface on the basis of contained physical structures must be equivalent to the "upper" shoreface as it would be recognized on a modern coast.



Figure 3-14. Upper shoreface strata of parasequence Kf-2-Miller Canyon-b in the Muddy Creek Canyon case-study area. The strata are predominantly trough cross-stratified and display high variability in transport direction. Burrows at the top of the photo extend downward from a marine flooding surface: these *Ophiomorpha* and *Thalassinoides* burrows are superimposed from the deeper-water environment that existed during and following the transgression. Strata in the lower, center part of the photo are shown in figure 3-15.

Foreshore: A foreshore can commonly be recognized at the top of shoreline successions that include upper shoreface strata. The foreshore consists of planar-laminated sandstone (figure 3-16) in sets that dip seaward at angles of a few degrees to as much as about 20 degrees. Foreshore deposits in the Ferron are fine- to medium-grained. The lamination is formed under upper flow regime conditions in the swash zone. Foreshore deposits in the Ferron rarely exceed about 5 feet (1.5 m) in thickness. A "white cap" is commonly present, affecting foreshore and upper shoreface strata (see figures 3-7 and 3-16). The top of the succession, except where affected by channels, is abrupt and generally forms a flat bench that is easily traced on outcrops. Such a surface is shown in figure 3-17. Foreshore deposits are also commonly root-penetrated and burrowed at their tops.

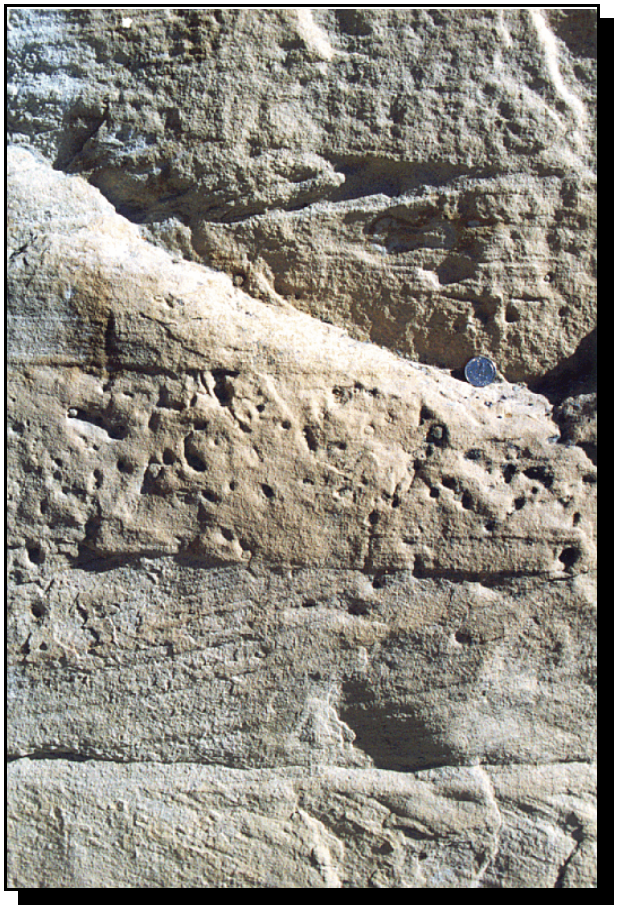


Figure 3-15. Trough cross-stratification of the upper shoreface. The bed in the middle part of the photo has been moderately burrowed. The burrows are truncated at the top of the bed, indicating that they existed in the upper shoreface environment and were not superimposed, as were the burrows at the top of parasequence Kf-2-Miller Canyon-b, as shown in figure 3-14. Contemporaneous burrows are uncommon in upper shoreface deposits.



Figure 3-16. Laminated sandstone at the top of parasequence Kf-1-Indian Canyon-c in Indian Canyon, Willow Springs Wash case-study area, represent the foreshore. The strata have been bleached white, representing a typical "white cap." The area shown here can also be seen at the left side of figure 3-17.



Figure 3-17. Cliff formed by shoreface sequence of parasequence Kf-1-Indian Canyon-c in Indian Canyon, Willow Springs Wash case-study area. The sandstone is extensively rooted at its top and is overlain by carbonaceous shale of the sub-A coal zone. The very flat, abrupt top is typical of wave-dominated shoreline sandstones. Note, also, the presence of a "white-cap."

Tidal Inlet

Tidal inlet deposits have been recognized in two units in the Ferron: the Kf-1-Indian Canyon-c parasequence in Indian Canyon (see Chapter V, Geologic Framework of the Willow Springs Wash Case-Study Area), and the Kf-2-Muddy Canyon-b parasequence in Muddy Creek Canyon (see Chapter VI, Geologic Framework of the Muddy Creek Canyon Case-Study Area). They replace the wave-dominated shoreline deposits locally, removing mostly middle shoreface strata (figure 3-18). Most of the tidal inlet deposits are overlain by normal upper shoreface and foreshore strata (figure 3-19). For this reason, we group tidal inlets as components of the shoreface.

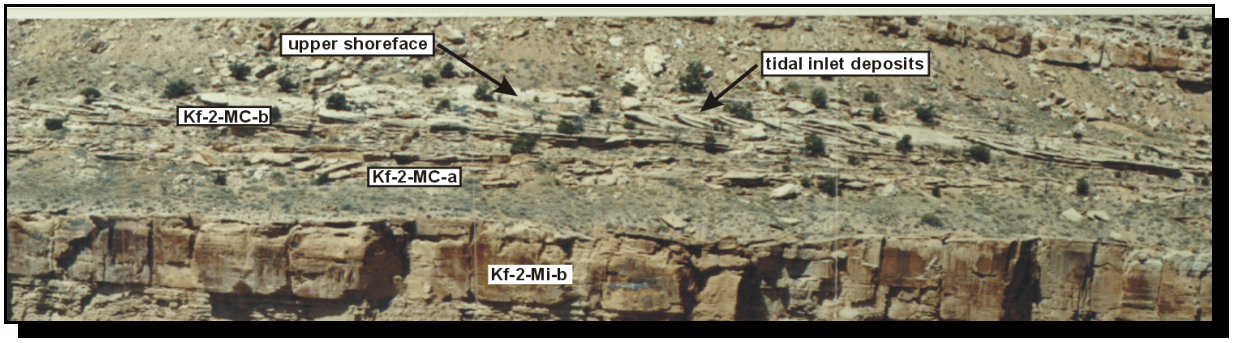


Figure 3-18. Tidal inlet deposits exposed in the west wall of Muddy Creek Canyon, SW1/4NW1/4 section 24, T. 22 S., R. 6 E., of the Salt Lake Base Line, from parasequence Kf-2-Muddy Canyon-b. Note the left to right inclinations of large planar tabular beds. These beds record the lateral migration of the tidal inlet. Although not well exposed here, the upper light-colored sandstone bed is upper shoreface and foreshore environments which migrated across the inlet as it filled. The top of the wave-dominated parasequence Kf-2-Miller Canyon-b forms the vertical cliff at the bottom of the photo.



Figure 3-19. Upper shoreface facies capping the inclined bedding in the tidal inlet deposit of parasequence Kf-2-Muddy Canyon-b (see figure 3-18 for location of photo). Multidirectional thin to medium bedded trough cross-bedding predominates with minor *Ophiomorpha* and some "escape burrows."

Tidal inlet deposits are characterized by conspicuous, sloping bedding surfaces that record migration of the inlets along the coast (figures 3-20 and 3-21). They include fine- to medium-grained, predominantly laminated sandstone. Trough cross-stratification is also present. Burrows are rare, the most distinctive form being *Cylindrichnus* (figure 3-22).

Distribution of Wave-Dominated Deposits

Wave-dominated deposits are present in all nine of the Ferron shoreline units. It is the predominant type of shoreline deposit in Kf-4 through Kf-8, but is also an important component in Kf-Last Chance through Kf-3. The first body of sediment deposited in each of the parasequences distinguished in the Ferron is wave-dominated.



Figure 3-20. Characteristic of the tidal inlet facies is thick-bedded, planar tabular sets (geologist for scale). Occasionally some trough cross-bedding is also present within the inclined bedsets.



Figure 3-21. View north along the tops of the inclined bedsets of the tidal inlet facies. The base of the tree in the mid-ground is about the top of the inclined beds and the base of the upper shoreface (see figure 3-19). Hammer for scale at the center of the photo.

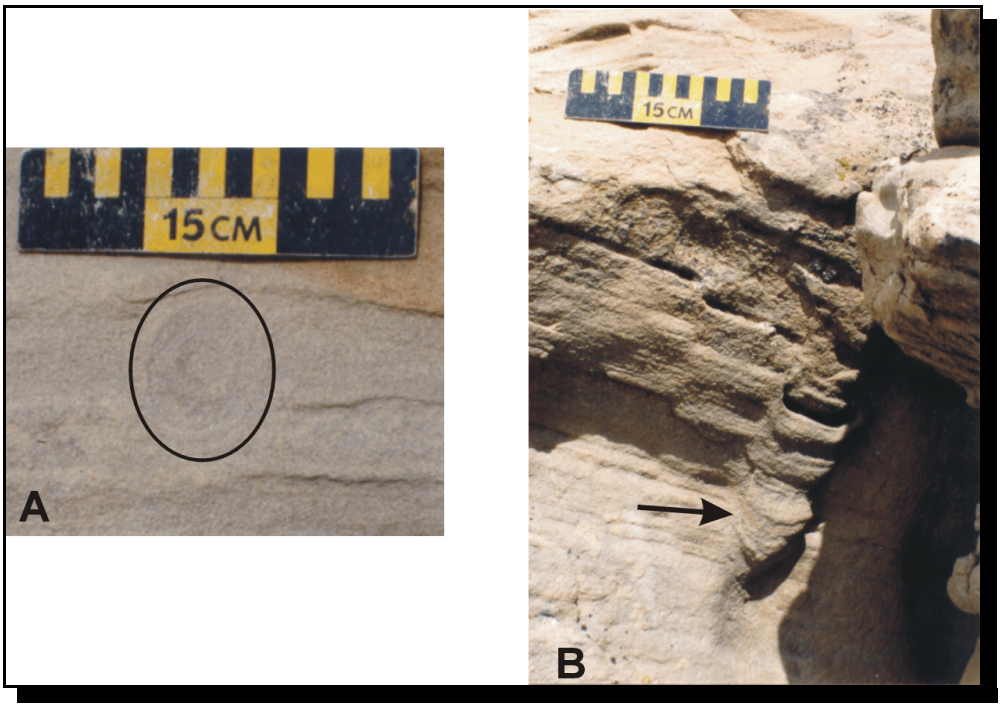


Figure 3-22. Pelecypod escape burrows are common in the tidal inlet facies. (A) is a vertical view of the trace fossil showing the collapse of bedding into the burrow, and (B) is a horizontal section through a burrow showing its concentric nature.

Fluvial-Dominated Delta

General Characteristics

In the Ferron, fluvial-dominated deltaic deposits are generally distinguished by the following characteristics (figure 2-23).

1. Thickness of the delta-front succession is relatively thin, typically about 20 to 30 feet (6-9 m), indicating a shallow "mud line" and low wave energy (figure 3-24).

2. Mudstone interbeds are common through the entire succession, although their number and thickness decreases markedly upward (figure 3-25).

3. Inclination of beds is usually very gentle, but locally may become steep enough to be quite apparent on outcrops (figure 3-26). Where this happens, sandstone beds or bedsets pinch rapidly seaward and interfinger with mudstone.

4. The succession of sedimentary structures in sandstone beds varies greatly, but the most common pattern is upward gradation from storm layers characterized by planar lamination and hummocky/swaley cross-stratification to trough cross-stratification. Where present, trough cross-stratification indicates generally unidirectional flow.

5. Contemporaneous distributary channels and small channels that may represent tidal creeks or distributary channels (see figure 3-26) are very common, replacing the top of the delta-front succession in many or most outcrops. As a result, the top of delta-front successions lack the abrupt, flat top characteristic of wave-dominated shoreline deposits.

6. Burrowing is sparse. *Planolites* and *Arenicolites* are the most common burrow forms. This attests to rapid sedimentation, to reduction of salinities in the vicinity of the river mouth, or to both.

The morphologies of fluvial-dominated deltas in the Ferron cannot be defined precisely. Two of the units in our detailed case-study areas -- Kf-1-Ivie Creek[a] bedset at Ivie Creek and Kf-1-Indian Canyon-c[d] bedset at Willow Springs Wash (Indian Canyon) -- include fluvial-dominated deltaic facies. In both cases the deltas built to the northwest. Kf-1-Ivie Creek[a] has been mapped as having a general lobate form. The delta or deltas included in Kf-1-Indian Canyon-c[d] are less well defined, but probably had a more elongate, possibly even "bird-foot" form.

Perhaps the most distinctive characteristic of fluvial-dominated deltaic deposits in the Ferron is the presence of numerous beds of mudstone throughout much of the thicknesses of the delta-front depositional sequences. This is the characteristic that is most noticeable when viewing outcrops at a distance or when analyzing photomosaics. The presence of the beds of mudstone and the fact that they commonly occur within 10 feet (3 m) of the tops of the sequences indicates that fair-weather

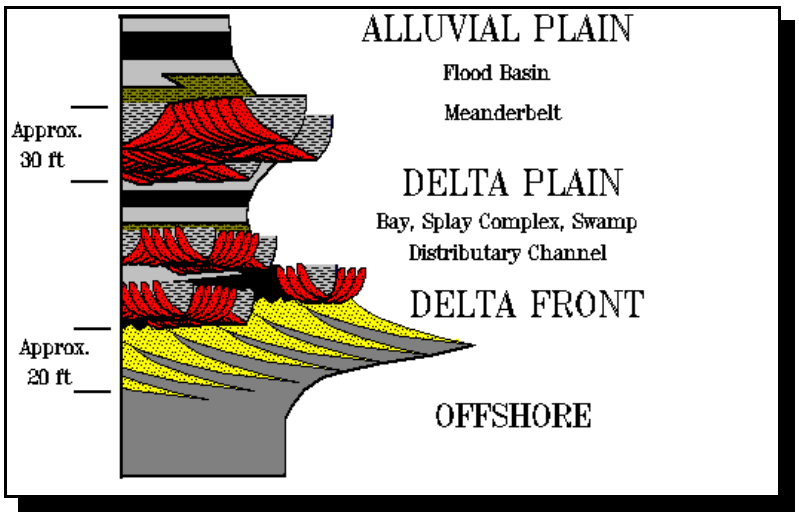


Figure 3-23. Diagram distinguishing facies within the depositional sequence formed by progradation of a fluvial-dominated delta.

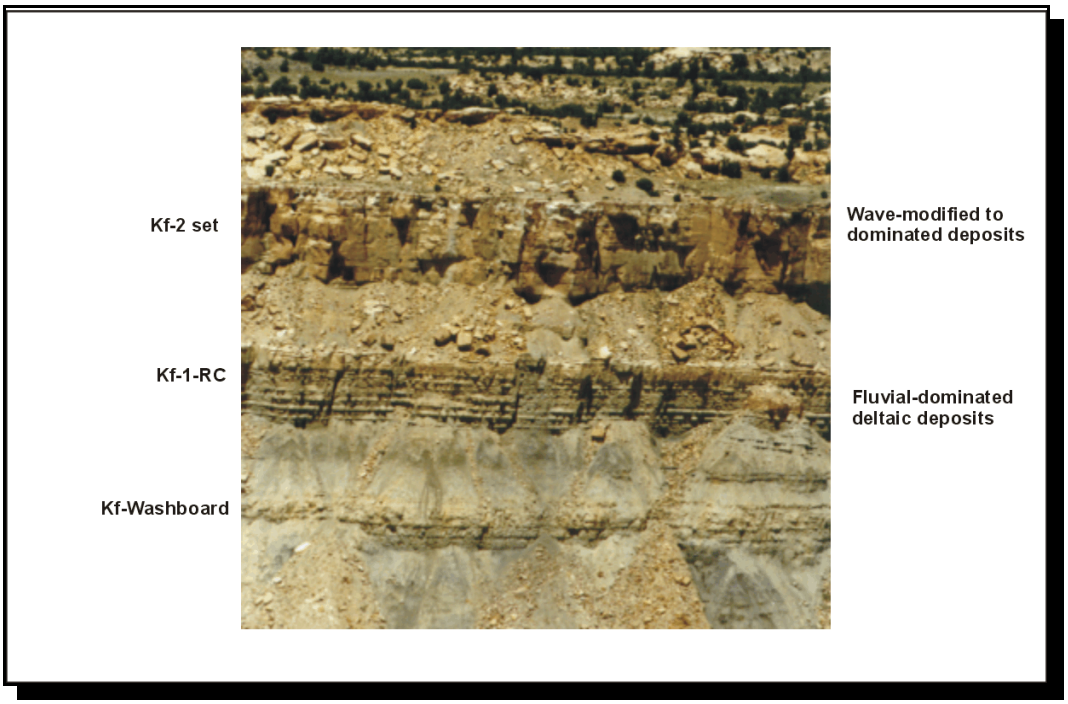


Figure 3-24. Typical fluvial-dominated deltaic deposits are exposed along the south escarpment of Mesa Butte in parasequence Kf-1-Ivie Creek. Mudstone and sandstone are interbedded and the capping sandstone of the unit is typically thicker bedded and often trough cross-bedded. The upper and thicker sandstone cliff is formed by three parasequences of near-shore wave-dominated to wave-modified facies and is easily distinguished on outcrop from the bedding style of the underlying fluvial-dominated delta deposit.



Figure 3-25. Fluvial-dominated deltaic facies represented by typical interbeds of mudstone separating sandstone. The Kf-1-Ivie Creek [a] bedset in the Ivie Creek case-study area, north side, near the junction of Quitchupah Creek.

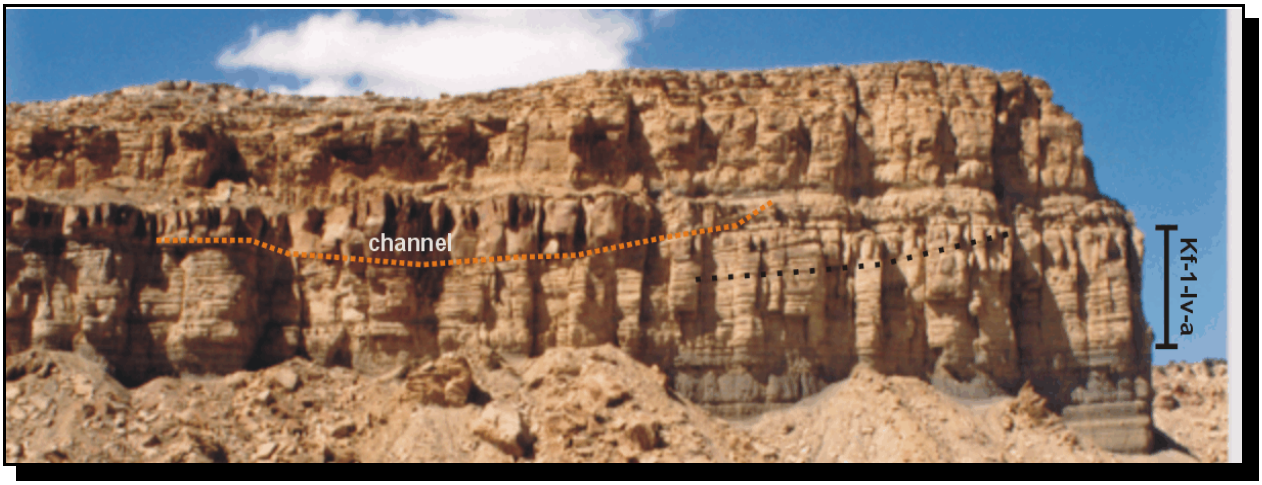


Figure 3-26. Steeply inclined beds of a fluvial-dominated delta deposit from Kf-1-Ivie Creek [a] bedset in the Ivie Creek case-study area. Inclination is from right to left, or to the west. Note the rapid thinning of individual beds as they are followed to the west. A small channel cuts into the deltaic deposits from the overlying unit.

periods were characterized by very low wave energies on these deltas (figure 3-27). By contrast, storm events, represented by the sharp-based, planar laminated to hummocky cross-stratified sandstone beds, impacted the deltas strongly, moving sand to water depths of about 30 feet (9 m).

Distribution of Fluvial-Dominated Deltaic Deposits

Fluvial-dominated deltaic deposits are a significant component of Kf-1 and Kf-2 and are documented through photomosaic mapping of the outcrop of these units within the study area (Anderson and others, in press). They are not recognized in the other units.

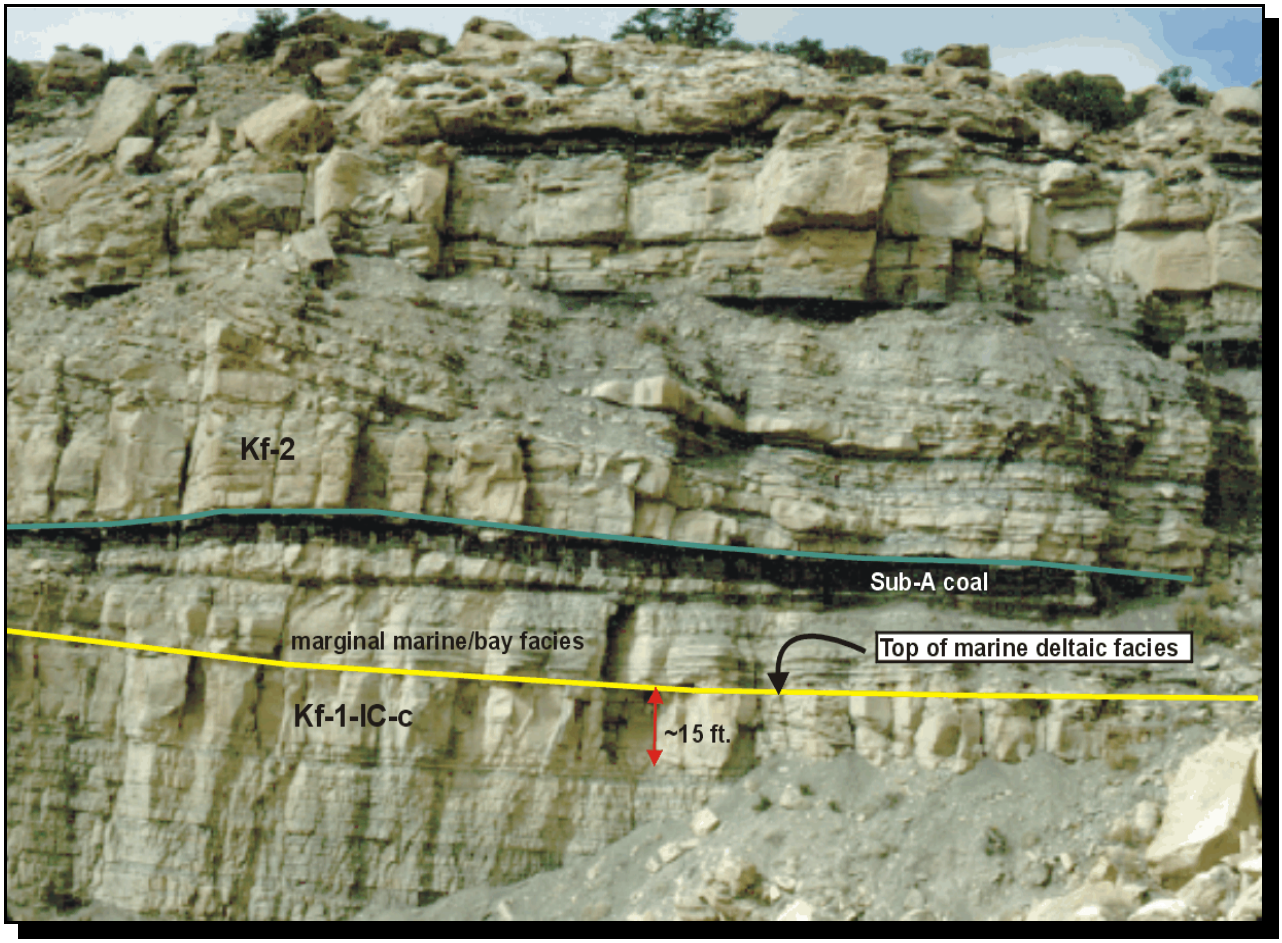


Figure 3-27. Fluvial-dominated facies of parasequence Kf-1-Indian Canyon-c[d] bedset at Coyote Basin showing mudstone layers within about 10 feet (3 m) of the top of the facies. The black layer just above the deltaic facies is the sub-A coal. About 12 feet (3.7 m) of bay deposits lie between the top of the fluvial-dominated deltaics and the coal zone.

Wave-Modified Delta -- Intermediate Shoreline Types

General Characteristics

Many of the shoreline sandstone units of the Ferron correspond to neither the wave-dominated nor the fluvial-dominated categories described above. They are commonly thick, like the shoreface sandstone sequences, but include much more gradational bases and more mudstone interbeds, like the fluvial-dominated deposits. They commonly include distributary channels and associated mouth-bar deposits (collectively referred to as distributary complexes, figure 3-28), indicating that river mouths were present during their deposition. This facies is dominated by trough cross-stratification, particularly in the upper portions of the facies. Stratigraphically lower in the

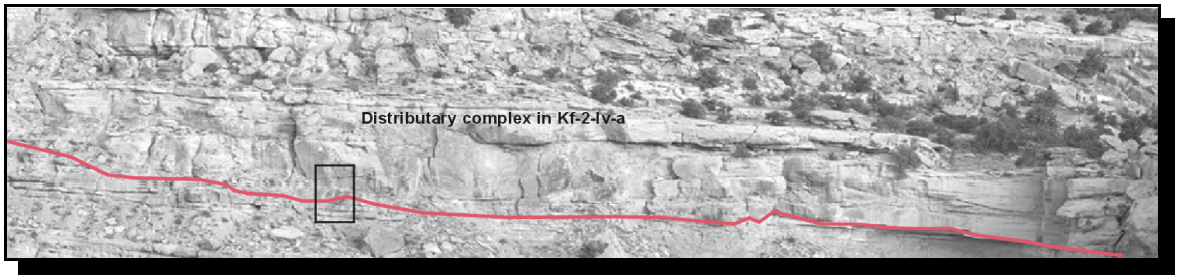


Figure 3-28. Wave-modified deltaic facies of parasequence Kf-2-Ivie Creek-a display a complex of bedforms related to distributary channels and mouth-bars underlain by mud-rich lower shoreface or distal-delta facies, Ivie Creek case-study area. See figure 3-29 for a detailed view.

facies are troughs complexly mixed with parallel and current lamination (figure 3-29). Commonly, these facies grade into more typical wave-dominated shoreface deposits. Included trace faunas are less abundant than in the shoreface deposits, but constitutes the typical shoreface assemblage dominated by *Thalassinoides* and *Ophiomorpha*. We classify these as intermediate deposits representing wave-modified deltas.

Wave-modified deltaic deposits accumulated on delta-fronts that experienced more wave reworking than did the fluvial-dominated delta fronts. We have no examples in the Ferron where the form of a wave-modified delta can be reconstructed with certainty. It is likely that these deltas were broad, lobate forms several miles in width. Some may have been arcuate in form. Where the orientations of inclined strata deposited on the delta fronts can be determined accurately, they indicate that these deltas prograded toward the northeast or east. Oriented in this way, they were strongly affected by waves rolling in from the Interior Cretaceous Seaway.

Another possible origin of these mixed wave- and fluvial-influenced deltas is offered by Bhattacharya (1998). He cites the example of the modern Danube River delta, which shows asymmetry created by wave energy on one side of the delta from longshore drift. On the updrift side of the river mouth, sand is deposited in a sequence of prograding shoreface deposits, while on the down drift side, a barrier-spit system develops from sediments derived chiefly from the river. Lagoons fill by a combination of river, tides, and bay-head deltas. This relatively new model has not been rigorously applied to the Ferron but conceivably fits well with the complexity observed on outcrop.

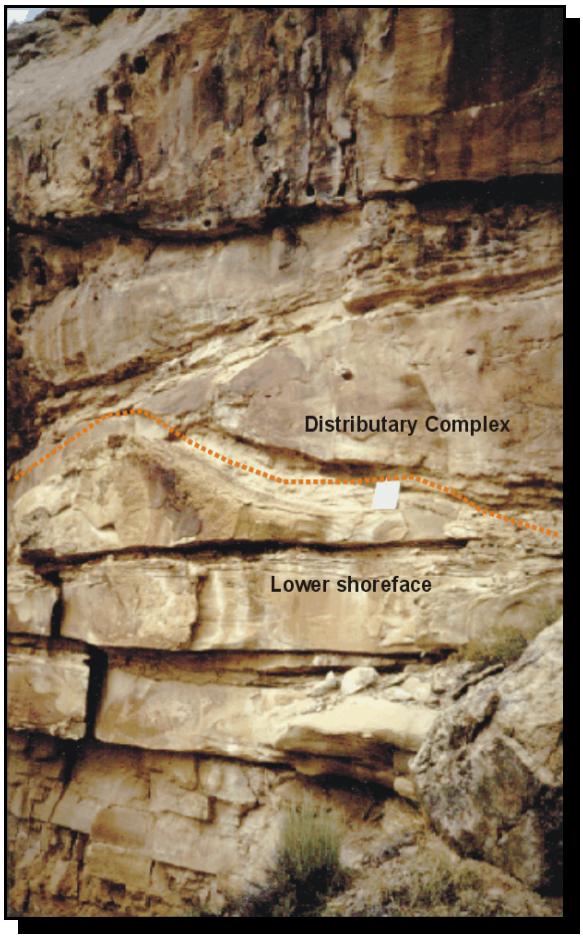


Figure 3-29. Distributary complex facies scour into underlying hummocky cross-bedded lower shoreface or distal-deltaic facies of parasequence Kf-2-Ivie Creek-a (see location on figure 3-28). The clipboard marks the contact. The distributary complex consists of dominantly trough cross-stratified beds with significant parallel laminations and current ripples.

Distribution of Wave-Modified Deltaic Deposits

Wave-modified deltaic deposits are common in Kf-1 through Kf-4 and are documented on photomosaics of the outcrop of these units within the study area (Anderson and others, in press). They are not recognized in Kf-Last Chance or in Kf-5 through Kf-8.

Bay and Lagoon

Mudstone, muddy sandstone, and sandstone were deposited in bays and lagoons associated with Ferron shorelines (figure 3-30). Depositional sequences representing bays and lagoons are usually no more than about 10 feet (3 m) thick. Sandstones are generally sparsely burrowed to bioturbated and contain horizontal bedding, commonly with oscillation ripples. In some cases, the oscillation ripples have flat tops, indicating intertidal to very shallow subtidal settings. Shells, particularly oyster and corbulid bivalve shells, are common locally (figure 3-31). It is generally difficult to distinguish deposits of bays and lagoons from each other on Ferron outcrops. Invertebrate faunas are sometimes of value in distinguishing whether a particular body of water contained brackish water or water of full marine salinity, but whether we call it bay or lagoon is most often based on our interpretations of contemporaneous shoreline deposits: bodies of marine water that lay landward of wave-dominated shorelines, and specifically behind landward pinchouts of these bodies, are interpreted to be lagoons; bodies of brackish to marine water that are associated with fluvial-dominated or wave-modified deltaic deposits are interpreted to be bays. Occasionally we use the modifier "brackish" before bay. This is used only when the bay assemblage of fossils are present in the rocks.

Lagoon deposits are relatively uncommon in the Ferron. We have identified them in only one setting: situated landward of landward pinchouts of the first, wave-dominated body of sediment in a parasequence. The best documented examples are located in Indian Canyon (Willow Springs Wash case-study area) landward of the landward pinchout of Kf-1-Indian Canyon-c, and in the "Bear Gulch" and Miller Canyon exposures (figure 3-32) landward of the landward pinchout of Kf-2-Muddy Canyon-b.



Figure 3-30. Bay deposits typically are lithologically heterogeneous, containing mudstone and siltstone with varying amounts of sandstone. Burrowing is common. In the photo, large *Thalassinoides* burrows have mixed the otherwise well-stratified section. Carbonaceous material is typically present and varies from moderate to high (carbonaceous mudstones). Coaly pods and isolated plant fragments are also common. Photograph taken from near the top of parasequence Kf-2-Muddy Canyon-a, south of "Bear Gulch,"(see photomosaic TC3, Anderson and others, in press).



Figure 3-31. Intense burrowing in these bay deposits just south of the mouth of Miller Canyon in the meanderbelt of parasequence Kf-2-Muddy Canyon-a make the bedding indistinct and difficult to see except in the poorly sorted sandstone bed in the middle of the photograph. Oysters, *Corbula*, and other brackish water fossils are present throughout these beds. Hammer and keys for scale. The dark pods and blobs are coaly material, the remains of plant debris originally deposited in a bay. The presence of brackish water fossils in the meanderbelt indicate the influence of tides or an esturine environment.

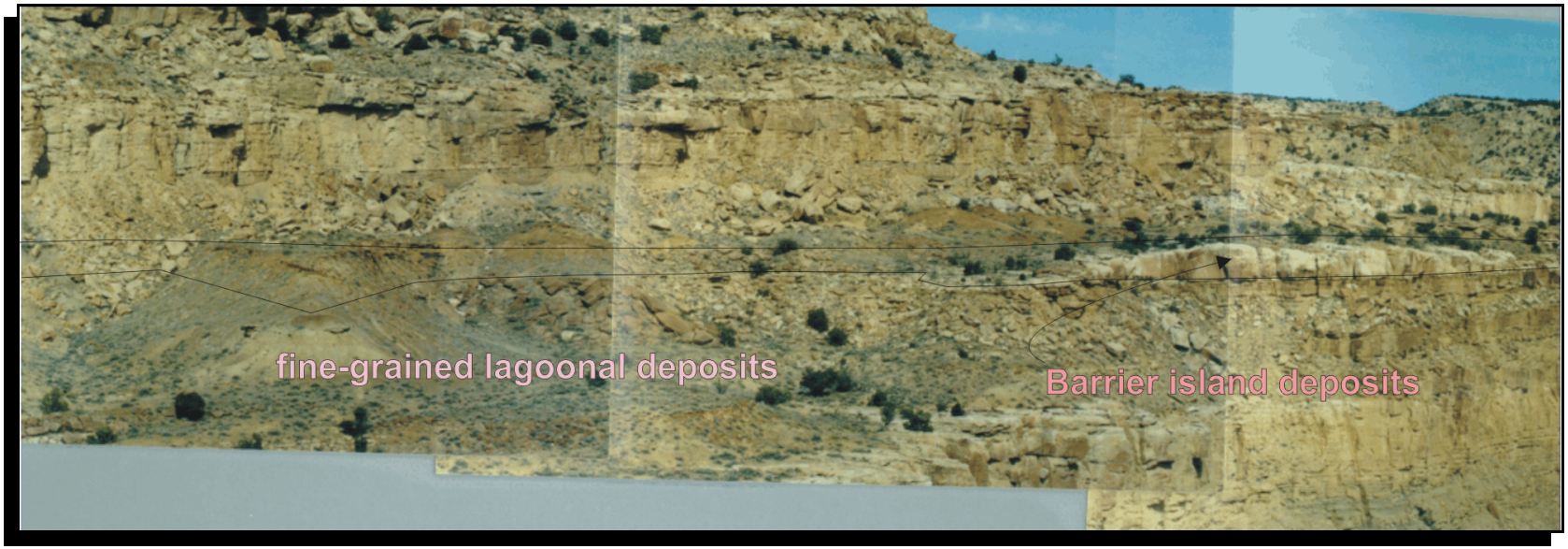


Figure 3-32. Lagoonal deposits are present at the landward side (left side of figure) of shoreface deposits on the north side of Miller Canyon very near the junction with Muddy Creek Canyon. This is the uppermost parasequence of the Kf-2 parasequence set.

Tidal channels occur along the margins of bays and lagoons (figure 3-33). Their size and number are a function primarily of tidal range. Tidal channels can be distinguished from fluvial channels on the basis of higher mudstone content, particularly in the upper parts of the tidal channels sequences, where mud layers fall out of the water column at high tide, and by the presence of burrows and body fossils attributable to marine to brackish-water organisms. The lower, tidally influenced reaches of rivers share many of the characteristics of tidal channels, and the distinction between them cannot be made with certainty. Many small tidal channels deposits are commonly associated with the deposits of shallow bays on the lower delta plain in the Ferron. It is their presence and their fining-upward character that makes the tops of the delta-front sequences difficult to distinguish precisely.

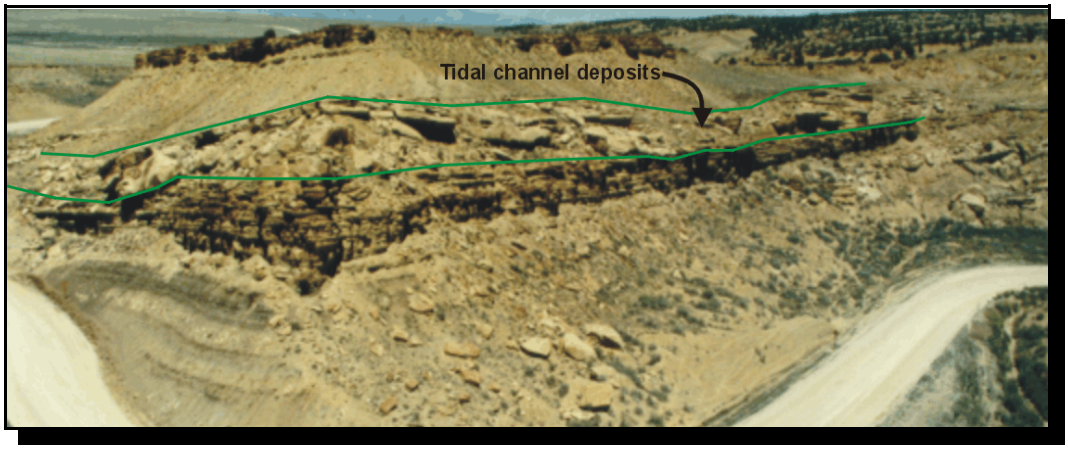


Figure 3-33. Tidal channels (or spit) in Kf-3 at Dry Wash. Note the lateral accreted bed and bedsets inclined away from the photographer. Mudstone is commonly found between the sandstone beds and the laterally accreted sandstone interfingers laterally with fine-grained lagoon or bay deposits.

Marsh and Swamp

General Characteristics

Carbonaceous strata ranging from carbonaceous mudstone to clean coal are common in the Ferron. Coalbeds have been of considerable economic importance in the past; carbonaceous mudstone is presently being mined at two locations near the town of Emery for use as a soil enrichener. From the perspective of stratigraphic studies, coalbeds and associated carbonaceous strata serve as extremely useful stratigraphic markers that allow correlation of shallow-marine and continental strata.

Thick beds of coal in the Ferron (Doelling, 1972; Ryer, 1981a) are the products of coalification of beds of clean peat that accumulated in delta-plain settings and in swamps that lay between the principal meanderbelts in the alluvial plain (figure 3-34). Carbonaceous shales, carbonaceous mudstones, and carbonaceous sandstones formed from peats that included substantial clastic components. These impure peats were deposited in settings were clastics were repeatedly introduced to the swamp, as occurs along the margins of channels.



Figure 3-34. Swamp deposits associated with the C-coal zone in the "Molen Amphitheatre." Geologist's knee is just above a carbonaceous shale split in the coal, representing a period of time when clastics flooded into the swamp in minor amounts.

Dynamics of Peat Accumulation

The dynamics of peat accumulation and preservation are a complicated subject that we will not address in detail here. Distilled to the essentials, thick bodies of clean peat accumulate in settings where the following conditions occur:

1. suitable for growth of vegetation (swamp),

2. swamp environment remains stable (no rapid lateral shift of facies),

3. no deposition of clastics, and

4. water table rises.

The fourth term is probably the most complicated. The rise of the water table, which facilitates the preservation of the peat, must occur at essentially the same rate as the generation of preservable organics by the plants: if the water table rises faster than peat can be produced, the peat swamp is flooded and peat deposition slows and eventually ceases; if the water table rises more slowly than peat accumulates, part of the peat oxidizes prior to burial, yielding a peat that is higher in impurities. In delta plains and in alluvial plains located along the margins of the sea, relative sea level is the factor that controls the rise or fall of water level is swamps. Relative sea level is a function of eustatic sea level and local subsidence. It can be concluded that all of these conditions cited above were met and were optimal during many long spans of time during Ferron deposition.

Coalbeds and Coal Zones

The Ferron includes many correlatable beds of coal. They were originally named by Lupton (1916) and all subsequent workers have followed his terminology. The thickest and most widespread coals constitute the A, C, G, I, and J coalbeds (figure 3-35). Coalbeds commonly split into two or more beds separated by clastics. Traced laterally, coalbeds commonly thin and grade to carbonaceous mudstone. Coals, associated carbonaceous mudstones, plus non-carbonaceous strata included between the various splits of coal and beds of carbonaceous mudstone that are laterally equivalent to a principal coal bed are commonly grouped into a "coal zone" (Doelling, 1972; Garrison and others, 1997) that can be correlated over a wider area than the principal coalbed itself. We designate both coalbeds and coal zones on the photomosaics produced during the course of this study (Anderson and others, in press).

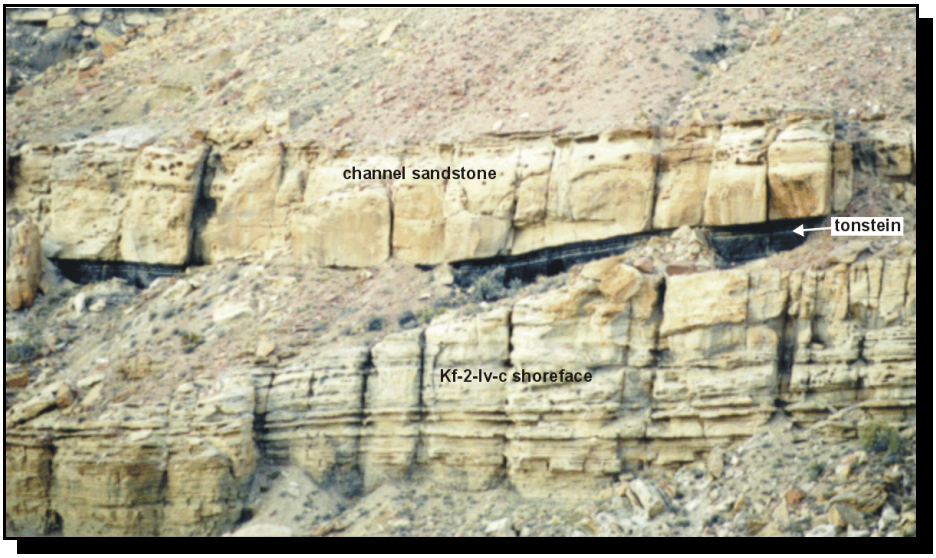


Figure 3-35. The A-coal zone in upper Quitchupah Creek. A thin, light colored bed is found near the top of the seam. This "tonstein" or ash bed can be correlated laterally for some distance. The coal lies in or atop a cut into the shoreface of parasequence Kf-2-Ivie Creek-c and is overlain by a wide channel sandstone.

Alluvial Plain

Alluvial-plain deposits laid down in river channels and in the adjacent flood plains constitute a major part of the Ferron Sandstone. They make up the bulk of the Ferron south of I-70. Channel belt and overbank facies assemblages are distinguished.

Channel Belt

Predominantly sandy sediment deposited within active river channels constitute the channel belt deposits of the Ferron. Sand size generally ranges up to medium, but some coarse- and very coarse-grained sandstone is present, particularly in the channel belt deposits of Kf-4. Trough cross-stratification is the most common sedimentary structure preserved in the channel belt sandstones (figure 3-36). In a typical vertical profile through a channel deposit, the preserved height of the cross-stratification sets decreases upward. Ripple-drift cross-lamination is common in the highest part of the sequence, where the sand fines upward, eventually grading to mudstone (figure 3-37).

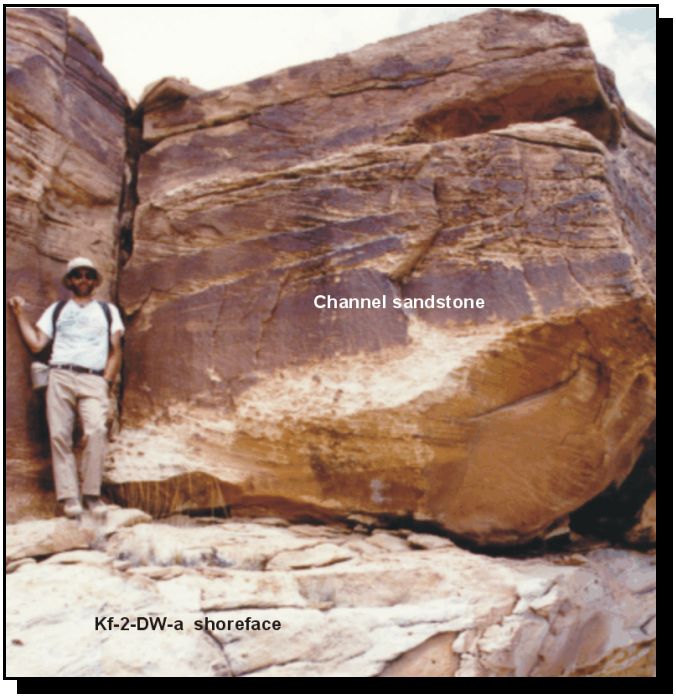


Figure 3-36. Uni-directional trough cross-stratified channel sandstone cutting into the shoreface of parasequence Kf-2-Dry Wash at Dry Wash. The base of the channel is at the geologist's feet. The basal bed is thick while the upper beds of troughs are medium.



Figure 3-37. Meanderbelt deposits of parasequence Kf-2-Muddy Creek-a in the Muddy Creek Canyon case-study area. Geologist feet lie at the top of the deposit where current ripple laminations dominate. The bed size of the underlying troughs generally decrease in thickness upward.

"Channel belt" is a general term that includes the deposits of a variety of channel forms. Many, and probably the majority, of the Ferron channel belts were meanderbelts laid down by highly sinuous rivers. Direct evidence of this can be found in the many lateral accretion surfaces (figures 3-38 and 3-39), representing lateral migration of point bars, in the Ferron channel belts. Lateral accretion surfaces and, locally, abandoned channel fills provide the best evidence for determining

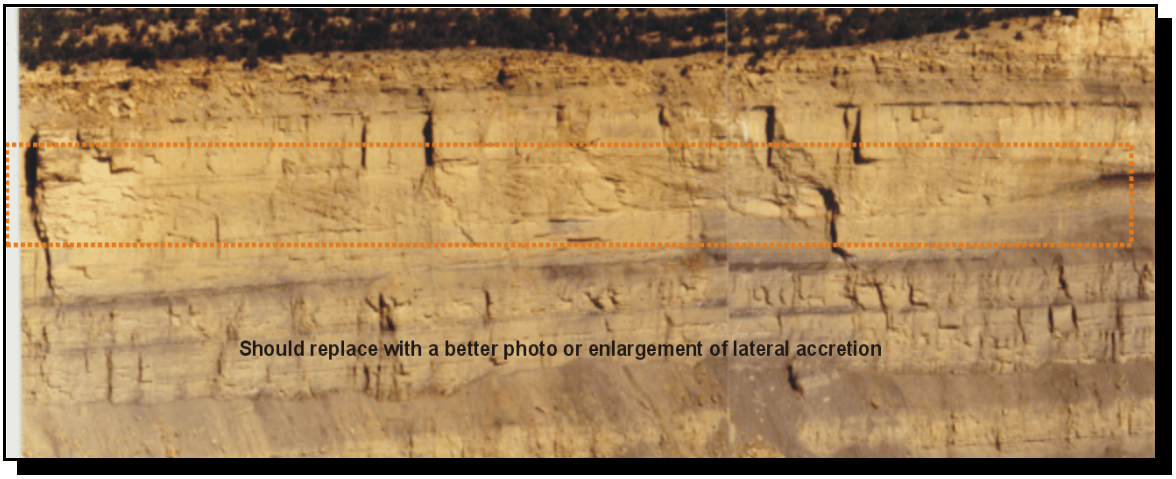


Figure 3-38. Channel belt of laterally accreting deposits exposed near Molen Point along the Molen Reef. This channel belt can be traced along the outcrop for about 2,000 feet (0.6 km) (see photomosaics MR1 and MR2, Anderson and others, in press). On the right the A coal is cut by the channel system. The overlying Kf-3-Molen Reef parasequence then transgressed across the top of the channel belt.

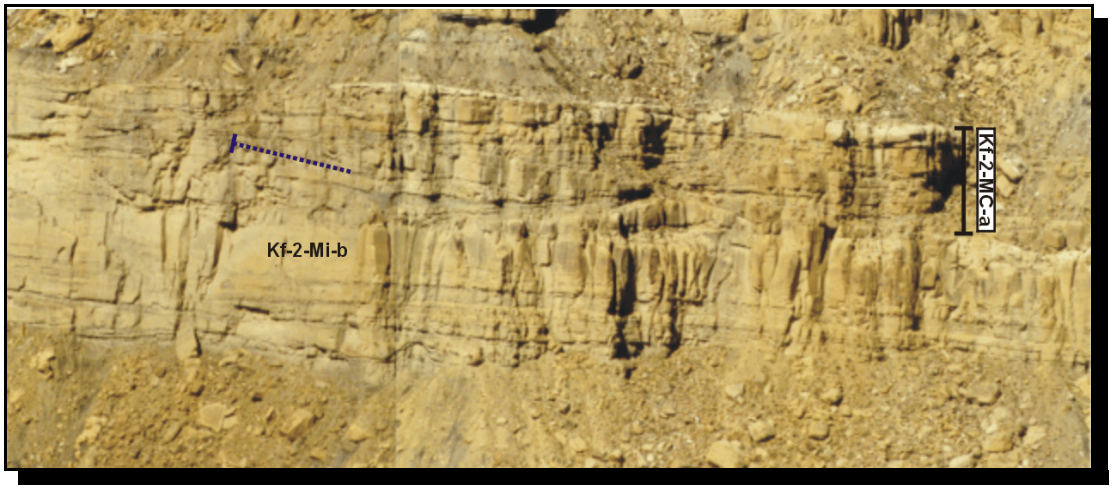


Figure 3-39. Lateral accretion in the meanderbelt facies of parasequence Kf-2-Muddy Canyon-a between Miller Canyon and "Bear Gulch." At this location the meanderbelt cuts into the underlying shoreface of parasequence Kf-2-Miller Canyon-b. Typical of this meandering system, most of the sands are separated by thin muddy to silty beds. Contrast this with the alluvial plain channel systems of the multilateral and multistoried type along the Limestone Cliffs (see figure 3-42).

the size of the rivers that deposited the Ferron. They indicate that the rivers were typically about 30 feet (9 m) in depth and up to a few hundred feet in width where they curved around their point bars (figure 3-40). Variations in size, however, are considerable. This stems from the fact that the Ferron was not deposited by a single river and probably not by a single river system: major rivers draining northeastward from the Sevier orogenic belt as well as smaller rivers that had their headwaters within the alluvial plain east of the orogenic belt all left their records in the deposits of the Ferron (figure 3-41).

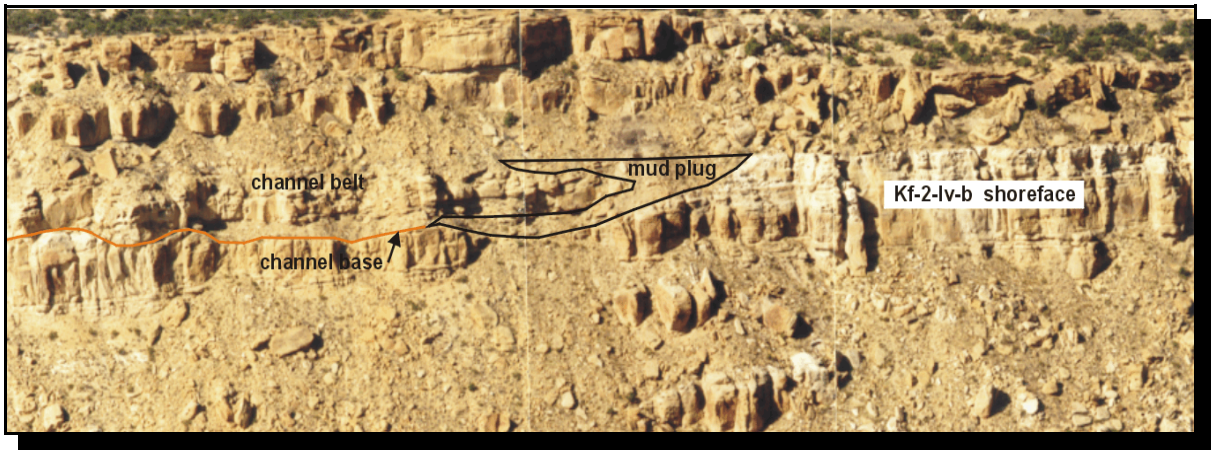


Figure 3-40. Channel belt cut into the top of parasequence Kf-2-Ivie Creek-b, just south of the mouth of Rock Canyon, with a mud plug at the point of its maximum lateral migration. The mud plug is juxtaposed against the white cap of shoreface deposits of Kf-2-Ivie Creek-b.



Figure 3-41. Single channel which migrated laterally only a short distance cut into the top of the Kf-2 parasequence sets on the north side of Rock Canyon, near its mouth. The channel is age equivalent with the coastal plain facies which overlie the near-shore marine unit which it cuts.

Ferron channel belts range up to about 80 feet (24 m) in thickness. Thick channel belts are the result of stacking of individual channel depositional sequences, that is they are "multistoried" deposits. Successive channel bodies rarely stack one body directly above the preceding one. Instead, they tend to be positioned one next to another, adding a "multilateral" component to the channel belt. Continued deposition within the channel belt during rise of base level leads to aggradation and multiple stories of channel bodies. Channel belts deposited during periods of slower base level (relative sea-level) rise tend to be more multi-lateral, whereas those deposited during more rapid periods of base level rise tend to be more multi-storied (figure 3-42).

The amount of mudstone included within Ferron channel belts varies considerably. On outcrops, lateral accretion is most clearly displayed in "inclined heterolithic" channel deposits simply because of the contrast in weathering styles of the sandstone and mudstone interbeds. Lateral accretion can be much more difficult to recognize in point bar deposits that lack shale interbeds.

Gardner (1993) presented a detailed analysis and comparison of the arrangement of depositional "macroforms" (architectural elements representing recognizable bar forms or individual channel forms) within the seaward-stepping, "low-accommodation" units Kf-1 through Kf-3 and the landward-stepping, "high-accommodation" units Kf-4 through Kf-8. He concluded that channel belts associated with seaward-stepping shoreline units contain thinner and more highly interconnected macroforms and include a lower diversity of fluvial facies. The channels themselves were relatively deep and narrow. By contrast, channel belts associated with landward-stepping shoreline units contain thicker macroforms that tend to be separated from one another by fine-grained sediments and are, therefore, less well interconnected. They include a lower percentage of sandstone and a wider variety of fluvial facies. The individual channels were shallower and wider. Finally, channel belts associated with back-stepping shoreline units are flanked by much larger amounts of crevasse splay deposits than are channel belts associated with forward-stepping shoreline units.

Garrison and others (1997) presented an analysis of the width-to-thickness ratios of Ferron channel belts. They utilized data they collected in Willow Springs Wash (van den Bergh, 1995; and van den Bergh and Garrison, 1996), and data gathered from other Ferron outcrops by Barton (1994) and by Lowry and Jacobsen (1993) in their analysis. They generally confirmed the observations of Gardner (1993). Although there is a great deal of overlap of populations in their plot, they were able to demonstrate that width-to-thickness ratios for channels belts generally increase upward in the Ferron passing from seaward-stepping to aggradational to landward-stepping portions of the member.

Overbank Deposits

Overbank deposits in the Ferron consist predominantly of mudstone and sandy mudstone deposited in flood basins as fines that settled from suspension during and following floods. Lenticular bodies of sandstone, generally ripple-drift cross-laminated but also including trough cross-stratification, represent channels that fed crevasse-splay complexes. The crevasse-splay channels generally were much smaller than the principal channels from which they issued. Flood basin clastics interfinger extensively with carbonaceous shales representing swamps formed in areas of lesser clastic input. On outcrop, overbank deposits generally are slope-forming, although the more resistant, sandy crevasse-splay channel deposits locally form ledges (figure 3-42).

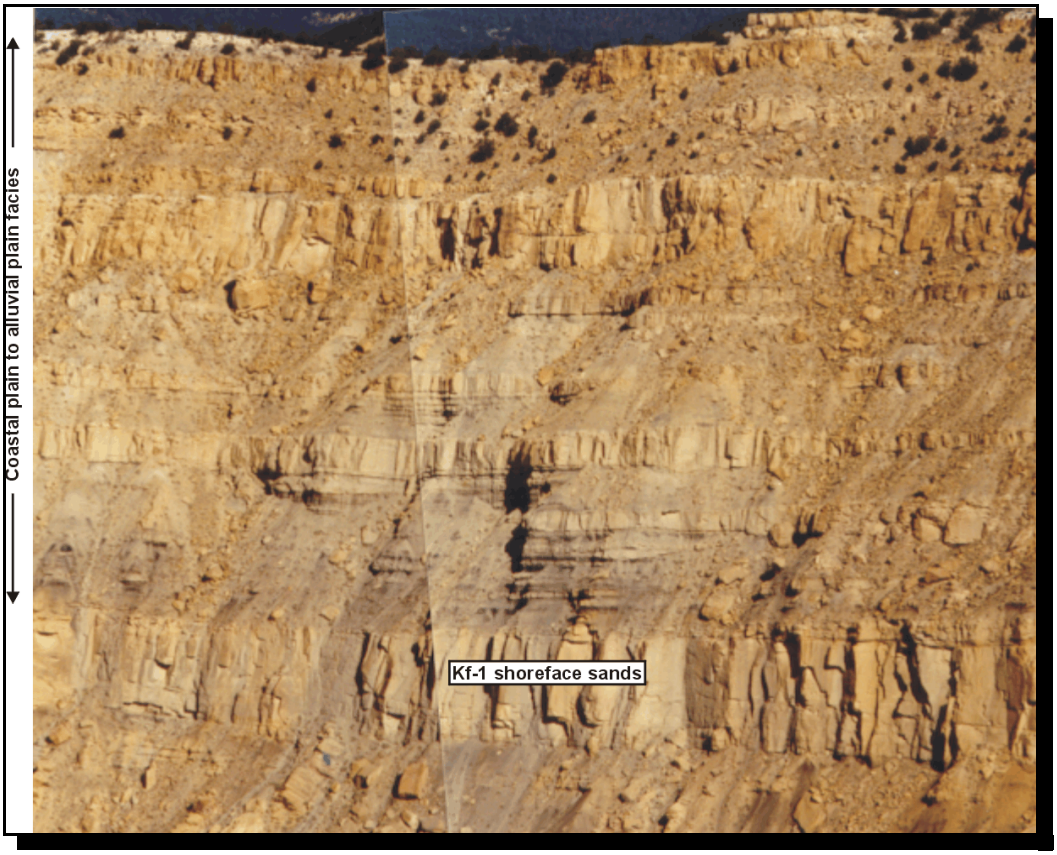


Figure 3-42. Multilateral and multistoried channel belts exposed along the Limestone Cliffs and deposited in the coastal to alluvial plains which followed the progradation of the more seaward nearshore sands of Kf-2 through Kf-8. Note the general upward thickening of the channel sandstone. Channel belts higher in the section are related to aggradational to backstepping patterns observed in nearshore deposits. Higher accommodation space (Gardner, 1993; Gardner and others, 1994; Gardner,1995a, 1995b) in the alluvial plain trapped a greater volume of sediments from the rivers. The tops of these channel belts are often very flat, related to periods of stable base level. Mudstone and interbedded mudstone, siltstone, and sandstone represent crevasse splay and overbank deposits. The massive cliff at the bottom of the photograph is shoreface sands of the Kf-1 parasequence set.

CHAPTER IV
REGIONAL STRATIGRAPHY OF THE FERRON SANDSTONE

T.A. Ryer and P.B. Anderson

Hierarchy of Stratigraphic Units

Introduction

Description of the Ferron Sandstone has reached a level of detail where a variety of types of stratigraphic units have been identified by various authors. They vary considerably in scale. They also vary greatly in the level of confidence that can be assigned to them.

The Ferron was originally defined as a member of the Mancos Shale by Lupton (1914, 1916). Ryer (1981a, 1991) (see figure 2-14, Chapter 2, Previous Studies) recognized a series of seven "delta-front units;" an eighth was designated by Gardner (1993) (see figure 2-26, Chapter 2, Previous Studies) and a ninth was added by the UGS team. We refer to these units as Kf-Last Chance and Kf-1 through Kf-8. Elements of this basic terminology are generally used by all subsequent workers (for a detailed description of previous work see Chapter 2, Previous Studies). Had the Ferron been originally described as a formation, these nine units would constitute members. Should the various members of the Mancos Shale in east-central Utah, the Ferron among them, be elevated to formation status in the future, these nine units should be elevated to member status.

Sequences: The Ferron Sandstone (not including the underlying Washboard and Clawson) contains nine parasequence sets and these sets are bounded by a regional flooding surface (and lag) at the top and a progradation of a regional clastic wedge, marking its base. As discussed in Chapter 2, Previous Studies, several authors have attempted to recognized sequences (in the sense of Mitchum and others, 1977) in the Ferron with different results. Mitchum and others (1977) defined the sequence as: "A depositional sequence is a stratigraphic unit composed of a relatively conformable succession of genetically related strata and bounded at its top and base by unconformities or their correlative conformities." Kamola and Van Wagoner (1995) refine the definition of sequence as: "A sequence is bounded by unconformities defined to be marked by a basinward shift in facies including abnormal subaerial exposure." Normal subaerial exposure is not defined.

Differing sequence stratigraphic interpretations stem from the use of different terms or schemes and the differences involved in applying, often the same scheme. This is a problem that is not unique to the Ferron. We offer our application of sequence stratigraphy to the Ferron Sandstone.

Parasequence Sets: The parasequence set is defined by Van Wagoner and others (1987) as "a succession of genetically related parasequences forming a distinctive stacking pattern bounded by major flooding surfaces and their correlative surfaces." This succession of parasequences is characterized by a recognizable arrangement (Van Wagoner and others, 1990) or stacking pattern. The recognized stacking patterns are: (1) forward-stepping or aggradational, (2) vertically stacked

or aggrading, and (3) back-stepping or retrogradational. Although not included in the definition, it can be inferred that a parasequence set (like any other type of set or group of things) should contain a minimum of two parasequences (however, we have several "sets" that presently contain only one designated parasequence). There is a second part of the definition: a parasequence set is bounded by major marine-flooding surfaces or their correlative surfaces. Two ambiguities enter here. What is a major marine-flooding surface and a change in stacking pattern is not necessarily tied to a major marine-flooding surface. A change in sediment supply, coupled with a constantly rising relative sea-level can dramatically alter the stacking pattern of parasequences. This change in sediment supply may be a local event, not regional.

Parasequences: The parasequence is a smaller-scale depositional unit recognized on the basis of marine-flooding surfaces. Van Wagoner and others (1987) define the parasequence as "a relatively conformable succession of genetically related beds or bedsets bounded by flooding surfaces or their correlative surfaces." They go on to define the marine-flooding surface (now generally shortened to flooding surface) as "a surface separating younger from older strata across which there is evidence of an abrupt increase in water depth." "Marine-flooding surface" is a replacement term for the familiar "transgressive surface;" (Swift, 1967, defined the "ravinement surface," another synonym that is commonly used to describe this same surface in the literature).

The Ferron contains many marine-flooding surfaces and most who have studied the Ferron (but not all) agree on where they are found. In theory, the parasequence includes all strata lying between two marine-flooding surfaces and the correlative surfaces in adjacent continental and offshore marine environments. Unfortunately, the correlative surfaces can very rarely be recognized. As a consequence of this, clastic parasequences are, for all practical purposes, recognized on the basis of bodies of predominantly sandy strata deposited in the nearshore environment.

One of the goals of this study was to define parasequences and parasequence sets in the Ferron. This had not been accomplished at the time the project started. Barton (1994, see figure 2-28, Chapter 2, Previous Studies) and Barton and Tyler (1995), subsequently defined depositional units that are equivalent to parasequences and parasequence sets in the northern outcrops of the Ferron. Garrison and others (1997) (see figure 2-29, Chapter 2, Previous Studies) defined parasequences and parasequence sets over the extent of the Ferron outcrop belt. Garrison had his introduction to Ferron stratigraphy as a Mobil liaison to our project and has adopted a similar approach to ours. Nonetheless, we have fundamental disagreements with Garrison and others (1997) parasequence- and parasequence-set level stratigraphy.

Bedsets: We recognize another area of ambiguity in identifying parasequences. A change from higher energy (sandy) nearshore facies to lower energy (muddy) facies is not always associated with a change in water depth or "flooding event." The Indian Canyon Case-Study area offers an excellent example of a change in shoreline energy, and hence facies, which is unrelated to relative sea level. Because of this ambiguity we have elected to move down in Van Wagoner's hierarchical scheme to the term "bedset." We apply this term for these units that do not clearly indicate marine flooding events, but are mappable, genetically related, and bounded by mappable surfaces. Some of these bedsets may well be parasequences, but until the bounding surfaces can be shown to be marine flooding events the unit remains ambiguous and a bedset in our nomenclature scheme.

The term "bedset" was applied to bodies of rock late in the project. The term is the result of: (1) mapping early in the project of "apparent parasequences" in case-study areas without the regional understanding of the nature of the bounding surfaces in a landward direction, and (2) the recognition that Ferron shoreline progradation is not the result of a single type of deltaic deposition but a complex mix of a variety of styles and some of these styles are recognizable on outcrop as distinct and mappable units but unrelated to marine-flooding surfaces. We chose to call these units bedsets.

In our view, many parasequences identified in the literature have been based on the assumption that a change in sedimentation pattern is always related to a change in water depth or a marine-flooding event. Hence, when stacked coarsening upward rock packages are found in a distal position to a contemporaneous beach, each cycle is presumed to represent a change in water depth or a flooding event. When these "flooding surfaces" are traced up depositional dip they are often lost at about the middle shoreface and multiple "flooding surfaces" are related to a single documented landward pinchout of the beach into coastal plain facies. We would interpret many of these individual sub-parasequence cycles or bedsets as events related to changes in sedimentation patterns, not relative sea-level change. In our own experience we have often identified distinct coarsening upward cycles that when traced landward simply feather to a common stratigraphic horizon with adjacent rock packages above and below, show no intertonguing with coastal plain or marginal marine facies, and no stratigraphic rise (typically associated with progradation in the Ferron). We have interpreted these distinctive sub-parasequence cycles as bedsets, related to changes in sedimentation patterns, not relative sea-level changes.

Sub-parasequence packages of rocks or bedsets can generally be classified on the basis of the three shoreline types described in Chapter 3 (Facies of the Ferron Sandstone): wave-dominated, wave-modified delta, and fluvial-dominated delta. Figures 4-1 through 4-4 show progradation of a hypothetical shoreline. Figure 4-5 displays the symbols used to represent the three shoreline bedset types. Figure 4-6 shows the common arrangement of the three basic shoreline bedset types within the parasequences of a hypothetical parasequence set. This figure emphasizes one of the principal conclusions of our study: the first bedset of each of the parasequences or the first parasequence of the Ferron consists of wave-dominated shoreline deposits.

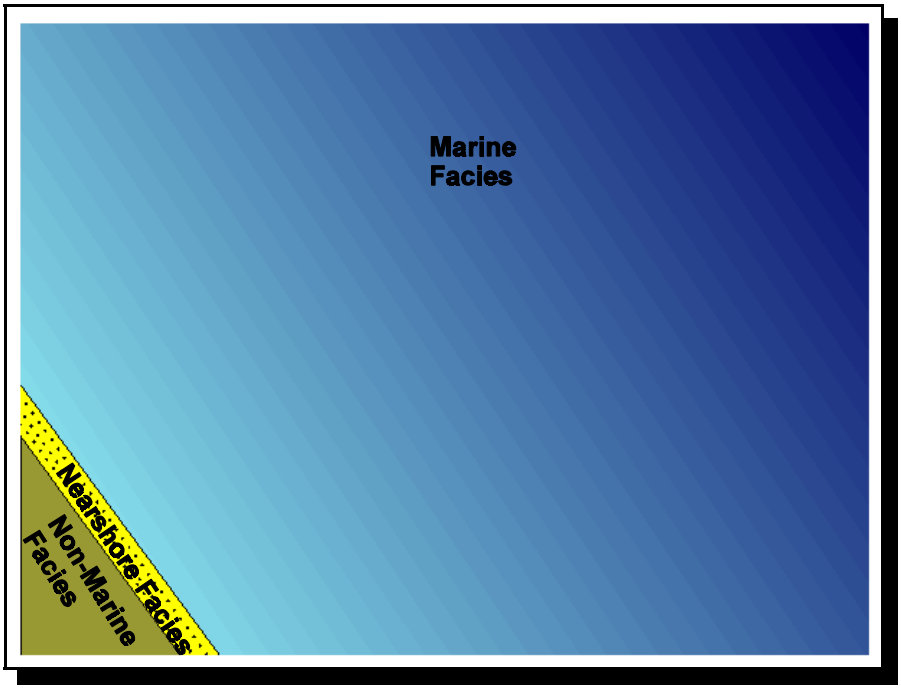


Figure 4-1. Hypothetical prograding strand plain.

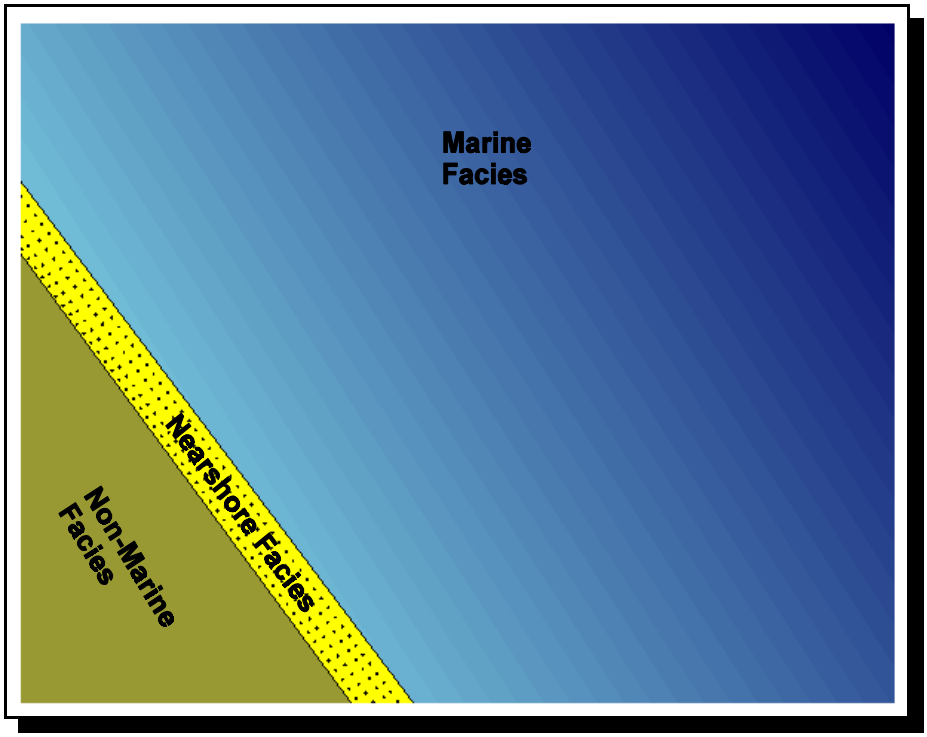


Figure 4-2. Continued progradation of the strand plain. Addition of sediment is by longshore drift, presumably from a deltaic source.

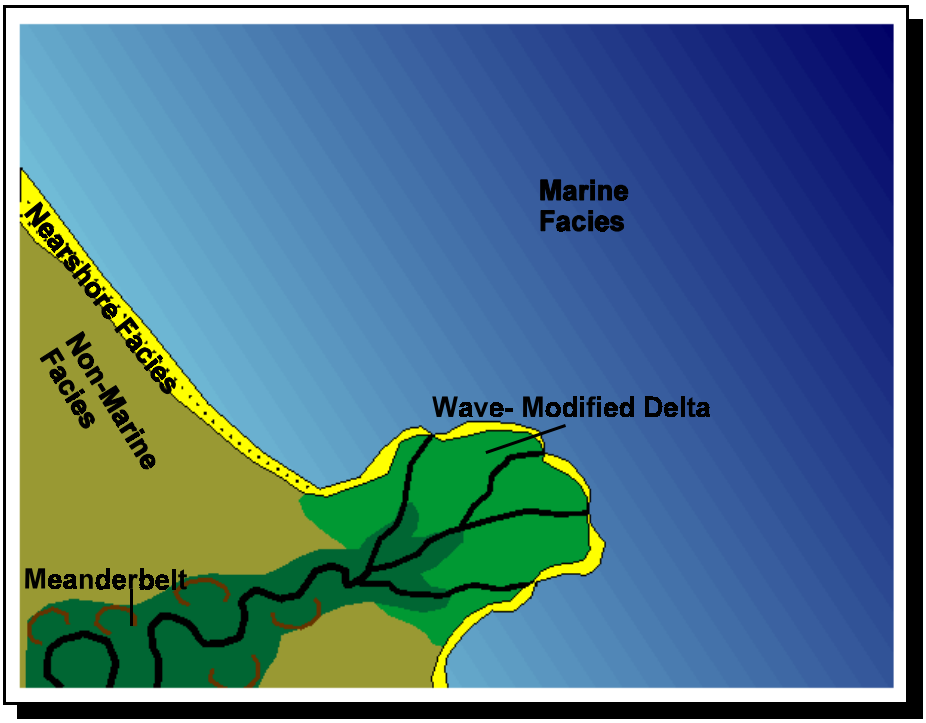


Figure 4-3. Progradation of a wave-modified delta following avulsion of a river system to the segment of coast shown.

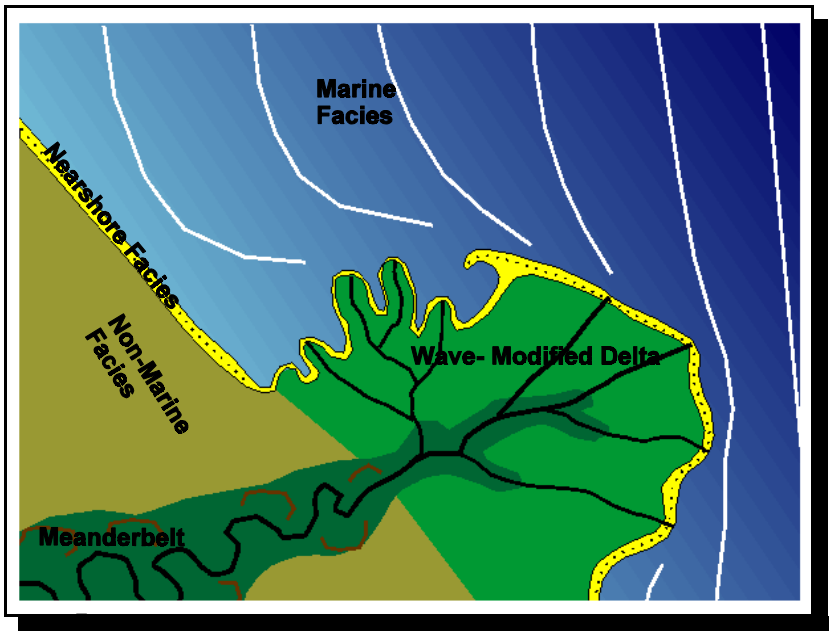


Figure 4-4. Continued progradation of delta. The white lines represent the crests of waves approaching from the east. The northwestern side of the delta experiences lower wave energies and takes on a fluvial-dominated form, whereas the eastern and southeastern sides have a wave-modified form.

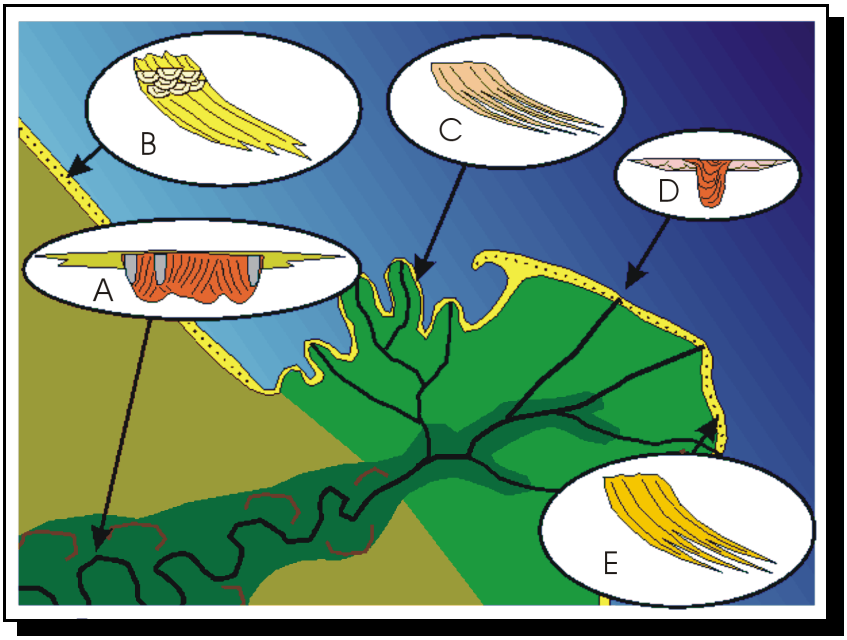


Figure 4-5. Symbols/patterns used to represent the various sandstone body types in figures 4-6 and 4-9. (A) meanderbelts, (B) wave-modified deltaic deposits, (C) fluvial-dominated deposits, (D) distributary channels, and (E) wave-dominated deltaic deposits.

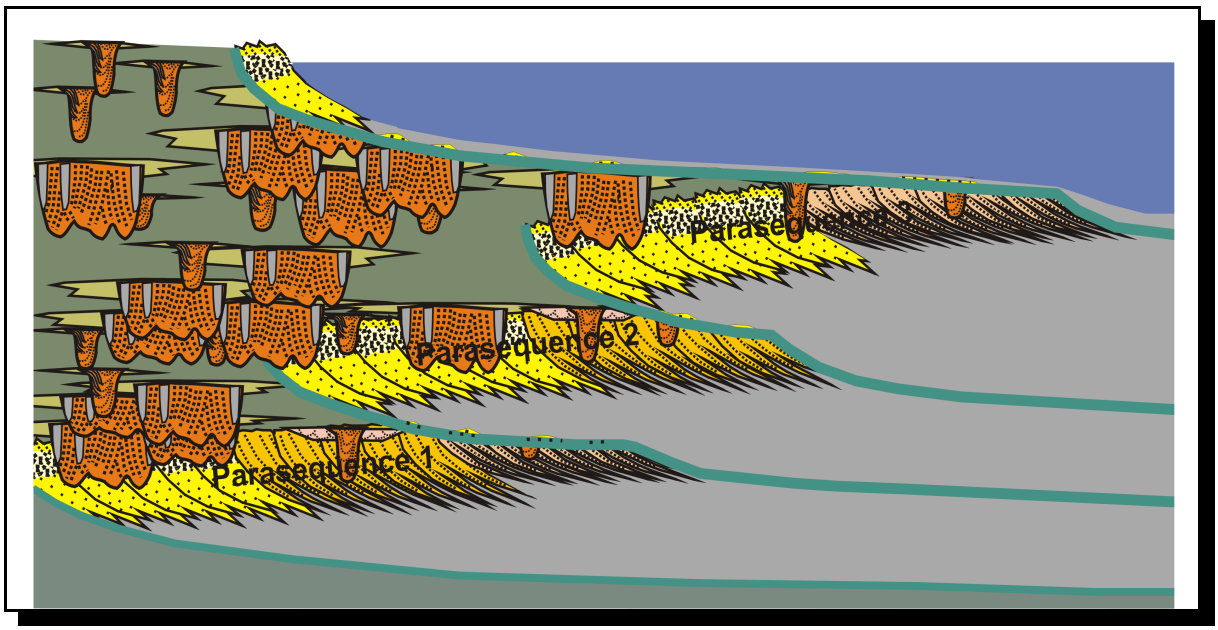


Figure 4-6. Diagram showing the arrangement of parasequences within a forward-stepping parasequence set and, within the parasequences, the arrangement of bedsets. Alluvial plain deposits are in dark gray and offshore marine shale is shown in light gray. Medium gray lines separating parasequences are marine-flooding surfaces. The oldest and youngest of the four shown are major flooding surfaces that bound the parasequence set.

Hierarchical Scheme

We have adopted a hierarchical scheme (figure 4-7) for naming stratigraphic units in the Ferron Sandstone. "Kf" is an abbreviation for the Cretaceous-aged Ferron Sandstone Member of the Mancos Shale. We follow Gardner's (1993, 1995a) interpretation and attribute the Ferron to two sequences. The Lower Ferron lies at the top of Gardner's Hyatti sequence and consists of shelf sandstones; the Upper Ferron constitutes Gardner's Ferronensis sequence and consists of fluvio-deltaics (figure 4-8). However, we would place the thick marine sandstone at the mouth of Last Chance Canyon in the Ferronensis sequence instead of the Hyatti. We do this based on the presence of a rather dark and organic-rich shale zone which consistently lies above the upper shelf sand of the Hyatti sequence along the outcrop and appears to either be equivalent to the lowest Ferronensis marine sandstone at Last Chance Creek or possibly underlie it.

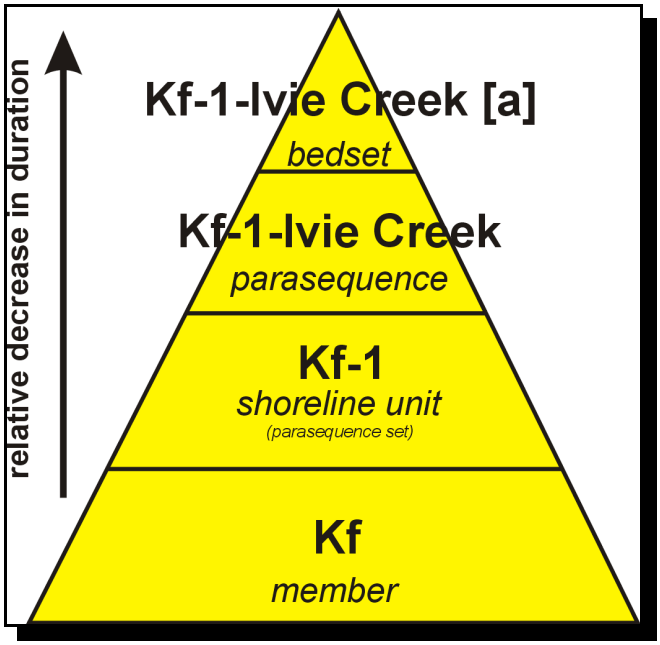


Figure 4-7. Hierarchical scheme of stratigraphic units. Italicized text is the type of stratigraphic unit. The shoreline unit is similar to a parasequence set, but does not rigorously follow published definitions.

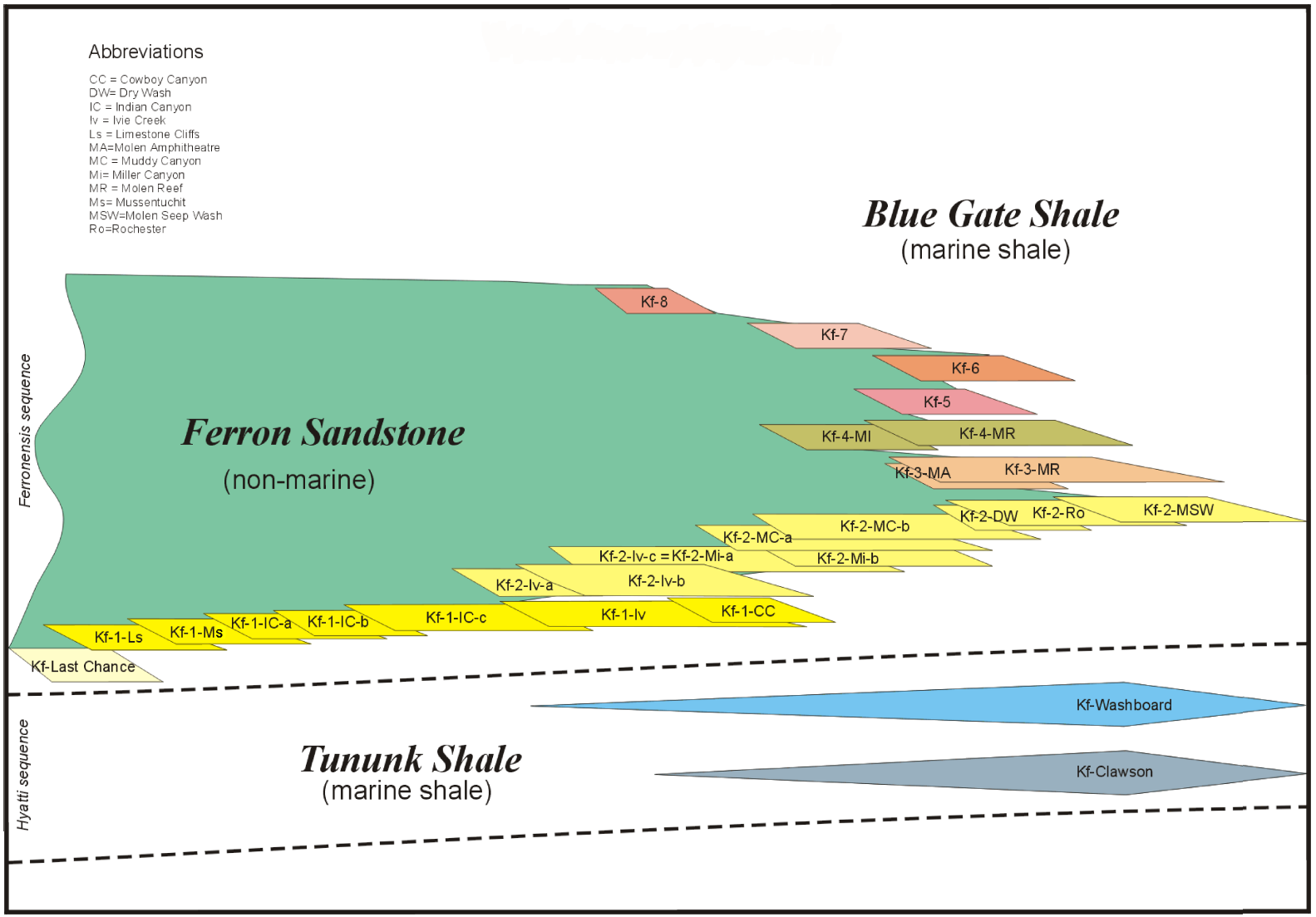


Figure 4-8. Ferron Sandstone parasequence stacking pattern based on nearshore marine facies. Each parallelogram represents a parasequence. The horizontal edges of each parallelogram represents the landward and seaward edges of the nearshore marine sand associated with each parasequence. Sequence boundaries are modified from Gardner (1995a) and are short black dashed line.

The first, second, third, and so forth (Kf-LC, Kf-1, Kf-2, Kf-3, ...) of nine stratigraphic units are identified on the basis of laterally traceable, cliff-forming units composed of shoreline sandstone facies. They are the "delta-front units" of Ryer (1981a), the "genetic units" of Gardner (1993), and the "stratigraphic cycles" of Barton (1994). Some are equivalent to parasequence sets, whereas others include more than one parasequence set. In this report, we refer to them by the very general term "shoreline units" and they are designated by a number or letters after the first dash in the abbreviation. Kf-Clawson and Kf-Washboard are shelf sandstone units in the Lower Ferron that occupy about the same place in the hierarchy. Kf-Last Chance is a unit of uncertain origin that pre-dates Kf-1 and probably post-dates Kf-Washboard. We include it in the Upper Ferron.

At the parasequence level of our hierarchical scheme we add another dash behind the abbreviation that designates the shoreline unit or parasequence set followed by the parasequence name, for example Kf-1-{parasequence name or abbreviation}. Kf-1-Iv is a parasequence defined on the basis of marine-flooding surfaces. We adhere to a rigorous definition of a parasequence: in order to be designated a marine-flooding surface, there must be proof of transgression and deepening of water. The best possible evidence of this is the existence of a landward pinchout, where shoreface sandstone tongues out rapidly into continental facies. The Ferron includes many excellent examples of this phenomenon (such as Kf-1-Limestone Cliffs, Kf-1-Indian Canyon-b, Kf-1-Indian Canyon-c, Kf-1-Ivie Creek, Kf-2-Ivie Creek-a, and -c, Kf-2-Muddy Canyon-a and -b, Kf-2-Dry Wash, Kf-3, Kf-6). Unfortunately we must deal with a common problem in the field application of sequence stratigraphy--incomplete exposures. This necessitates interpreting certain units as parasequence without observing the landward pinchout of the shoreface sandstone. In some cases it could be argued that the parasequences are no more than autocyclic shifts in sedimentation patterns, while in others, Kf-4-Miller for example, a flooding surface must be present, based on the overlying and underlying stratigraphy, but the pinchout is removed by incision of an overlying meanderbelt.

A parasequence is named for a type area. A type area, like Indian Canyon, can be the type area for more than one parasequence, in which case parasequences are labeled sequentially. There is a problem with designating stratigraphic units in the Ferron by means of type areas: there are simply not enough names to go around. We have restricted our names to features that are labeled on the U.S. Geological Survey 7.5 minute quadrangle maps. In some areas, we have identified many more parasequence-level units than we can find unique names for. This necessitates the a, b, c suffix convention. In one case we have two names for the same parasequence; Kf-2-Ivie Creek-c and Kf-2-Miller Canyon-a. Detailed case-study work was completed in both the Muddy Creek Canyon area (Kf-2-Miller Canyon-a) and Ivie Creek area (Kf-2-Ivie Creek-c) before the final regional correlations were complete. To meet project deadlines and budget, the two names for the same parasequence were allowed to stand, hence, when the final correlation of the Ferron units was completed so this parasequence carries one name in the southern area and another name in the northern area. The Muddy Creek Canyon work pre-dates the Ivie Creek work and in future studies we recommend abandoning the term Kf-2-Iv-c.

A bedset is the smallest stratigraphic unit named in this study. A bedset is a relatively conformable succession of genetically related beds bounded by surfaces of erosion, non-deposition, or their correlative conformities (Campbell, 1967). At the bedset level of our hierarchical scheme we attach brackets behind the abbreviation that designates the parasequence with a bedset designation, that is Kf-1-Iv[bedset name or abbreviation]. Bedsets defined in Kf-1 on the basis of lithologic and sedimentologic character and composed of one or another of the three basic shoreline facies are recognized in this study. When a bedset is named, a type area is used. A type area, like

Ivie Creek, can be the type area for more than one bedset, in which case bedsets in the same shoreline unit are labeled sequentially. Some parasequences consist of a single bedset. We have only formally named four bedsets. Numerous bedset bounding surfaces are recognized and mapped on the accompanying photomosaics but the associated bedsets have not been formally named.

Landward Pinchouts

From the perspective of sequence stratigraphic analysis, the landward pinchout of a shoreline sandstone body (shown diagrammatically in figure 4-9) is a distinctive and very important feature. Examples of Ferron landward pinchouts on outcrop are shown in figures 4-10 through 4-14. In each of the outcrop examples shown, the shoreline sandstone body pinches out into strata that clearly were deposited in delta-plain or coastal plain settings. In the examples shown in figures 4-10 and 4-12 through 4-14, the landward pinchouts are both under- and overlain by coal and/or carbonaceous shale. In all four examples, there can be no doubt that a relative rise of sea level accompanied the transgression that preceded progradation of the wave-dominated shoreline sandstone body. The transgressive surface of erosion at the base of each shoreline sandstone body is the landward most part of a marine-flooding surface. Each marine-flooding surface marks a parasequence boundary.

Many landward pinchouts were subsequently eroded and replaced by channel belt deposits (for example parasequence 2 in figure 4-6). Only the more seaward parts of the marine-flooding surfaces remain. In such cases, marine-flooding surfaces must be recognized on the basis of an increase in water depth represented by the deposits above the surfaces relative to the deposits beneath the surfaces. In cases where the increase in water depth is great (such as marine shale overlying coal), marine-flooding surfaces can be recognized with certainty. Where the increase is small (such as marine shale overlying lower shoreface) there is some uncertainty; as demonstrated in our study of the Kf-1 deposits in Indian Canyon, lithologic changes of this type can be produced by purely autocyclic processes that do not involve deepening of water (see Chapter 5, Geologic Framework of Willow Springs Wash Case-Study Area).

The transgressions that ended each of the nine “delta-front units” and preceded the next are represented by major marine-flooding surfaces. Ryer (1981a, 1982a, 1982b) mapped the positions of the pinchouts associated with the major marine-flooding surfaces, although we have reinterpreted the orientations of some of the pinchouts (figure 4-15). Gardner (1993), Barton (1994), and Garrison and others (1997) have mapped the pinchouts associated with “regular” (as opposed to “major”) marine-flooding surfaces. In the following section, we document the bedsets, parasequences, and shoreline units (parasequence sets) that we recognize in the Ferron.

Parasequences and Bedsets

Approach and Terminology

Our analysis of Ferron stratigraphy made extensive use of oblique aerial and ground-based photomosaics. The annotated photomosaics, in CD-ROM format, have been published as an open-file report of the Utah Geological Survey (Anderson and others, in press). Our analysis began with the definition of parasequences within the shoreline sandstone units, each of which was assigned a name based on a type area (for example Kf-1-Indian Canyon-c). The smaller mappable

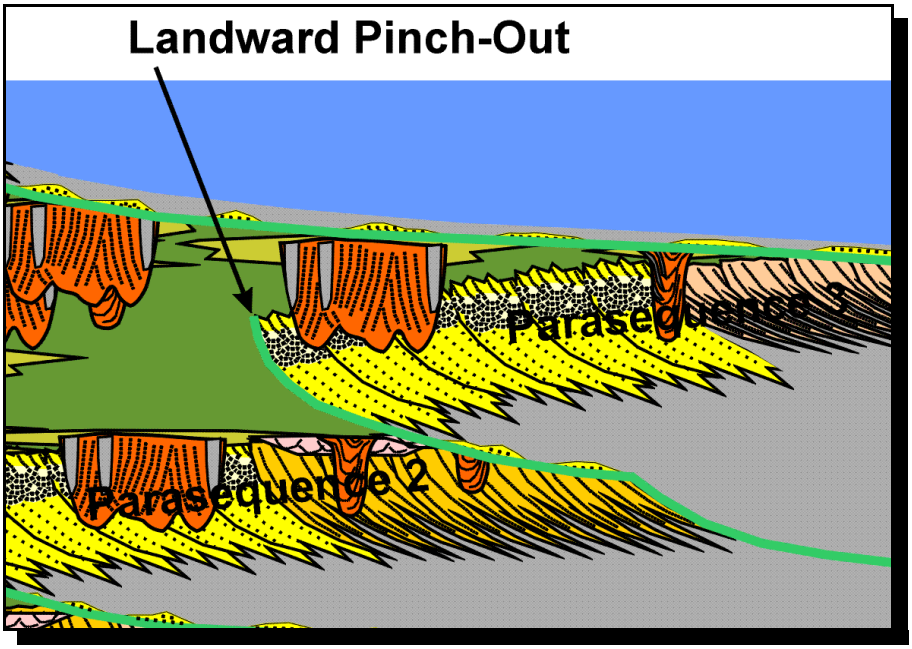


Figure 4-9. Landward pinchout marks point where shoreline sandstone body pinches out laterally into coastal-plain or delta-plain deposits. The pinchout is underlain by the landward most part of the transgressive surface of erosion.

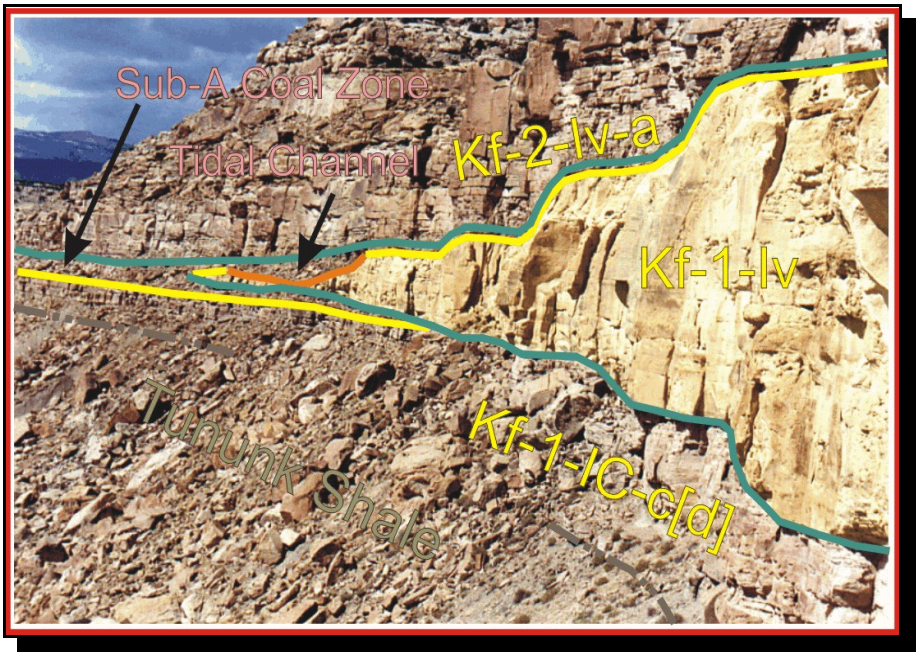


Figure 4-10. Landward pinchout of parasequence Kf-1-Iv on the south-facing cliffs east of Coyote Basin. A small tidal channel filled with muddy sandstone and oyster shells has eroded part of the wave-dominated shoreline sandstone body of Kf-1-Iv near the pinchout.

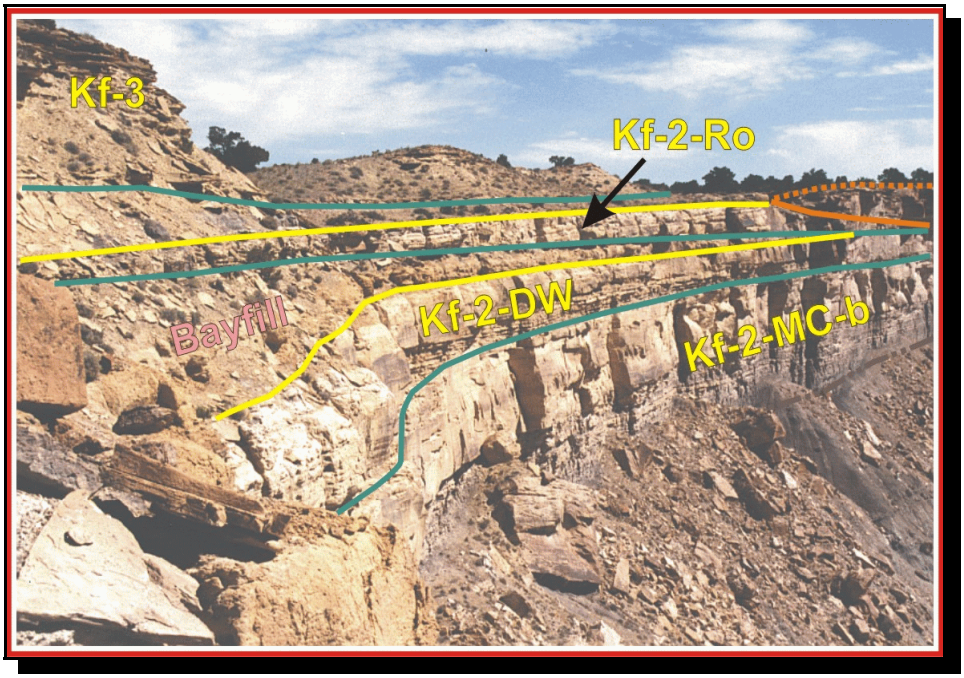


Figure 4-11. Landward pinchout of parasequence Kf-2-Rochester on the northern side of Dry Wash. A fluvial channel belt cuts the wave-dominated shoreline sandstone body near the pinch-out and is outlined in the upper right of the photo. This situation is similar to that shown in figure 4-9.



Figure 4-12. Landward pinchout of Kf-6 in the uppermost part of Muddy Creek Canyon. The white to rusty tan weathering, cliff-forming sandstone was deposited on a strongly wave-dominated shoreline. Carbonaceous shales beneath the transgressive surface of erosion at the base of Kf-6 represent the I coal zone; the bed of coal apparent in the middle of the photo that immediately overlies Kf-6 is the J coal bed. A bed of muddy, burrowed sandstone lies between the I and J coal zone to the south and represents a lagoon that formed during the pre-Kf-6 transgression. The J coal is directly overlain by another transgressive surface of erosion with a thin transgressive lag, which is, in turn, overlain by the Blue Gate Shale.



Figure 4-13. Closer view of the landward pinchout of Kf-6 shown in figure 4-12.



Figure 4-14. The uppermost sandstone is the Kf-2-Iv-c and is rapidly thinning toward the pinchout, which occurs near road level. Carbonaceous-rich sediments from the A coal zone enclose the landward pinchout of this marine sandstone.

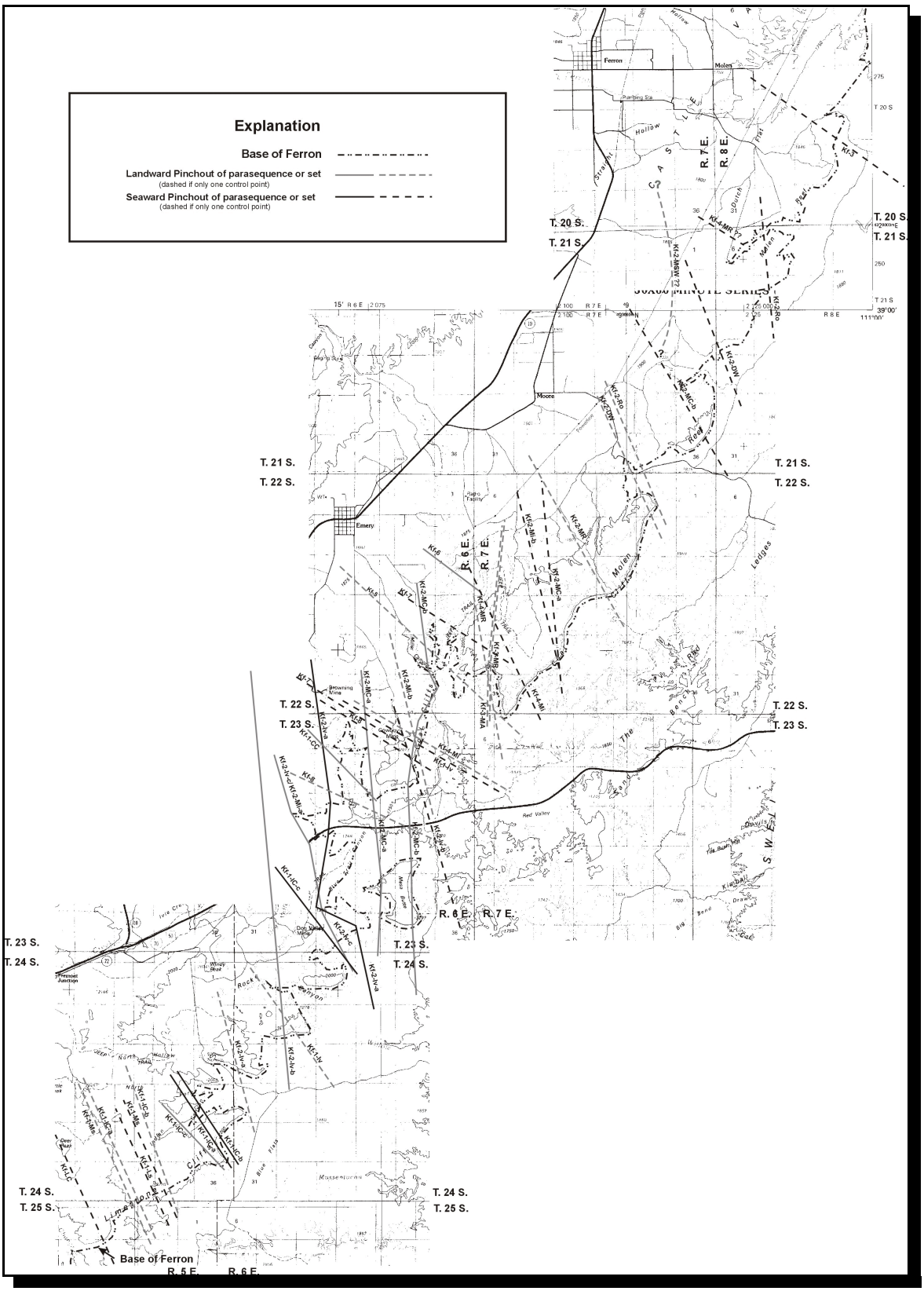


Figure 4-15. Landward and seaward pinchouts of all the parasequences identified in the study area are shown here. The orientation is dashed where only one point of control exists and solid where two or more points have been established on the outcrop.

and genetically related unit is the bedset. The mapping process is interpretive: although the surfaces that bound bodies of sediment with distinct characteristics are clear cut in many instances (such as the boundary between bedsets Kf-1-Ivie Creek[a] and Kf-1-Ivie Creek[c]), they are not clear in many others. We have taken a conservative approach in defining bedsets and parasequences: others would certainly choose to subdivide further or differently.

Choosing a bounding surface between adjacent bedsets from one or another of the three basic shoreline types sometimes had to be done in a somewhat arbitrary fashion, since the change from one type of shoreline to another may be gradational. Numerous transitions, particularly between the wave-dominated and wave-modified shoreline deposits, are observed without a distinct bedset bounding surface. Therefore, every change in shoreline type is not divided by a bedset bounding surface. In some instances (Kf-1-Ivie Creek[a] to Kf-1-Ivie Creek[c]), adjacent bedsets are assigned to the same shoreline type. For deltaic shorelines, the bedsets probably represent different delta lobes; for wave-dominated shorelines, the bedsets probably represent either different wave-energy levels or different rates of sediment supply, both of which are probably a function of changes in nearby deltas.

Next, we located all of the recognizable landward pinchouts of shoreline sandstone bodies and identified the marine-flooding surfaces associated with them. This process is purely descriptive. Then, we defined marine-flooding surfaces that cannot be traced to a landward pinchout owing to fluvial erosion of the underlying shoreline strata in the area that we believed the pinchout originally existed. This process is interpretive, for reasons cited earlier.

Flooding surfaces define parasequences. It must be emphasized that the parasequences we identified on the outcrop encompass only the shoreline and nearshore facies of the parasequence and not the continental and offshore marine facies. With only a few possible exceptions, we did not attempt to trace correlative surfaces for any significant distance landward in the continental deposits nor seaward into prodelta shale.

For detailed descriptions of the stratigraphic units discussed in the following sections, refer to Appendix A. Geographical features used to delineate the locations of these units are shown on figure 1-1 in Chapter 1, Introduction. A detailed, diagrammatic regional cross section and all photomosaics (PM-) are found on CD-Rom in Anderson and others, in press.



Figure 4-16. View of the full sand thickness of Kf-LC just north of Last Chance Creek, along the Limestone Cliffs. Note the thin transition facies at the base of the sandstone and contact with the underlying Tununk Shale. The top of the unit is overlain by a split of the Sub-A coal zone.

Kf-Last Chance

Kf-Last Chance (Kf-LC) is the southern most parasequence and shoreline unit in the study area. The type section of the Last Chance unit of the Ferron is at Last Chance Creek, where the shoreline unit, together with overlying Kf-1-Limestone Cliffs (Kf-1-Ls), forms vertical cliffs approximately 200 feet (50 m) high (figure 4-16). No attempt was made

to trace this unit beyond the outcrop on the north side of the canyon. We tentatively assign this unit the same hierarchical level as the other delta-front units, but we do so based on the anomalous thickness of this unit and its depositional style. As mentioned earlier, we believe this unit belongs to the Ferronensis sequence. No thick coal appears to correspond with the top of the unit, as is the case with many of the other delta-front units. It is possible that a coal does occur at this stratigraphic level farther landward. Kf-Last Chance displays inclined bedsets, stacked en echelon that appear to onlap, or possibly downlap against, a surface that may represent a paleotopographic high in the upper Tununk, resulting in very rapid seaward thinning of this shoreline unit (see PM-LC1). Obviously all or part of these exposures belong to one or more parasequences, but those divisions were not attempted here.

Kf-1

Kf-1 is a seaward-stepping imbricate unit of nearshore marine facies extends on outcrop from south of Last Chance Creek on the south, to the northern portion of Quitchupah Canyon on the north. A seaward pinchout of one of its younger parasequences is well exposed along the east side of "Cowboy Mesa." The Sub-A coal zone is associated with this delta-front unit, overlying the nearshore marine facies across all of its outcrop with the exception of the southern and eastern "Cowboy Mesa" area.

Kf-1 contains the following seven parasequences and three named bedsets, moving from south to north:

1. Kf-1-Limestone Cliffs (Kf-1-Ls)

2. Kf-1-Mussentuchit (Kf-1-Ms)

3. Kf-1-Indian Canyon-a (Kf-1-IC-a)

4. Kf-1-Indian Canyon-b (Kf-1-IC-b)

5. Kf-1-Indian Canyon-c (Kf-1-IC-c)

6. Kf-1-Ivie Creek (Kf-1-Iv)

    Kf-1-Ivie Creek[Rock Canyon] bedset (Kf-1-Iv[RC])

    Kf-1-Ivie Creek[a] bedset (Kf-1-Iv[a])

    Kf-1-Ivie Creek[c] bedset (Kf-1-Iv[c])

7. Kf-1-Cowboy Canyon (Kf-1-CC)

Kf-1-Limestone Cliffs: Kf-1-Limestone Cliffs (Kf-1-Ls) is the oldest parasequence within the Kf-1. The only exposures are along the Limestone Cliffs in an area of very difficult access. Only photo interpretation information was gathered (see PM-LC1). This unit progrades a short distance with relatively steeply inclined bed boundaries, similar in architectural style to the older Kf-LC.

- Type section: southern part of Limestone Cliffs, in the center of section 3, T. 25 S., R. 5 E., Salt Lake Base Line (SLBL).
- Landward limit: south of Last Chance Creek, position not determined.
- Seaward limit: Limestone Cliffs, approximately SE1/4SE1/4 section 34, T. 24 S., R. 5 E., SLBL.
- Facies content of shoreline unit: wave-dominated coast but beginning to show minor wave-modified characteristics in the more distal portions of the outcrops.

Kf-1-Mussentuchit: Kf-1-Mussentuchit (Kf-1-Ms) is the second seaward-stepping parasequence in the Kf-1. Its progradation length on outcrop is the shortest of the parasequences (see PM-LC5), yet it develops a typical thickness of marine delta-front sands.

- Type section: southern part of Limestone Cliffs, along section line between sections 34 and 35, T. 24 S., R. 5 E., SLBL.
- Landward limit: Head of Mussentuchit Wash and Limestone Cliffs, NW1/4NW1/4NW1/4 section 2, T. 25 S., R. 5 E., SLBL.
- Seaward limit: Limestone Cliffs, approximately SW1/4 section 35, T. 24 S., R. 5 E., SLBL.
- Facies content of shoreline unit: wave-dominated, with minor channel deposits cut into the top of the unit and interpreted as bay-fill related to flooding of the overlying parasequence.

Kf-1-Indian Canyon-a: Kf-1-Indian Canyon-a (Kf-1-IC-a) is the third seaward-stepping parasequence in the Kf-1. This unit is also exposed on the Limestone Cliffs (PM-LC6) in the upper reaches of Indian Canyon, where it was first described (see figure 3-11, in the Chapter 3, Facies of the Ferron Sandstone).

- Type section: Indian Canyon, NE1/4NW1/4 section 26, T. 24 S., R. 5 E., SLBL.
- Landward limit: Limestone Cliffs, SE1/4SE1/4 section 34, T. 24 S., R. 5 E., SLBL.
- Seaward limit: Indian Canyon, SW1/4SW1/4 section 24, T. 24 S., R. 5 E., SLBL; Limestone Cliffs, SE1/4 section 25, T. 24 S., R. 5 E., SLBL.

- Facies content of shoreline unit: wave-dominated coast, probably strand plain. Begins to show signs of changing into a wave-modified facies in the Limestone Cliffs.

Kf-1-Indian Canyon-b: Kf-1-Indian Canyon-b (Kf-1-IC-b) is the fourth seaward-stepping parasequence in the Kf-1. This unit is also found in both the Indian Canyon area (figure 4-17) and on the Limestone Cliffs. A definitive landward pinchout into the Sub-A coal zone is well exposed on the Limestone Cliffs (see PM-LC6). The correlation of the unit from the Limestone Cliffs into the Indian Canyon area lacks the assurance allowed by good continuous outcrops.

- Type section: Indian Canyon, east side, just beneath landward pinchout of the overlying parasequence Kf-1-IC-c, SW1/4SW1/4 section 24, T. 24 S., R. 5 E., SLBL.

- Landward limit: Limestone Cliffs, SE1/4 section 34, T. 24 S., R. 5 E., SLBL.

- Seaward limit: Indian Canyon, NE1/4 section 24, T. 24 S., R. 5 E., SLBL; Limestone Cliffs, C section 25, T. 24 S., R. 5 E., SLBL.

- Facies content of shoreline unit: wave-dominated coast, probably strand plain, some indications of transition toward wave-modified in the Limestone Cliffs near the seaward end of the unit.

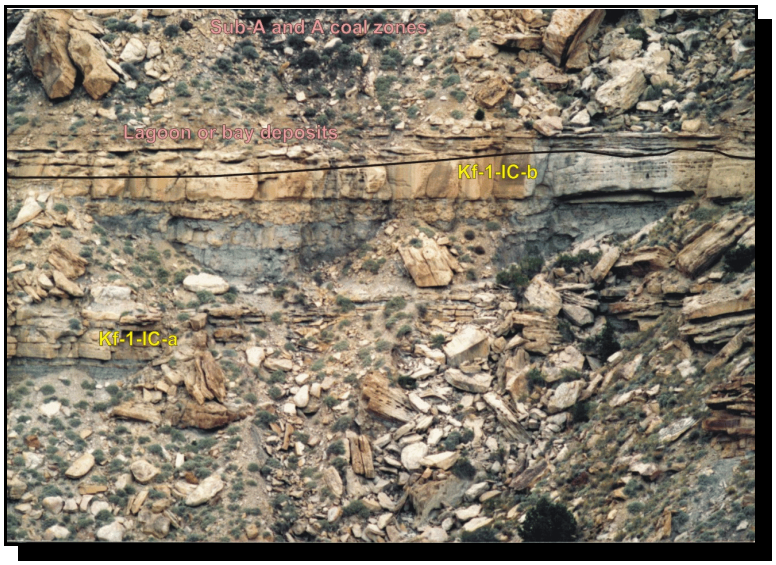


Figure 4-17. Parasequence Kf-1-IC-b is exposed in the east side of Indian Canyon, SW1/4SW1/4 section 24, T. 24 S., R. 5 E., SLBL, with a thin section of parasequence Kf-1-IC-a below. The top of the b unit is scoured by c-aged tidal deposits. This is just landward of the landward pinchout of the overlying Kf-1-IC-c parasequence. The dark coaly material is the Sub-A and A coal zones.

Kf-1-Indian Canyon-c: Kf-1-Indian Canyon-c (Kf-1-IC-c) is the fifth seaward-stepping parasequence in the Kf-1 and its type area is also in Indian Canyon. The unit is exposed on the face of the Limestone Cliffs where much of the delta-front facies have been eroded and replaced by channel facies (see PM-LC13). This unit is discussed in detail in a case study of the Willow Springs Wash, Chapter 5. A bedset of this unit has been designated the Kf-1-IC-c[d] (see PM-BYU1). This parasequence provides the best example of how a change in sediment supply and wave-approach can dramatically change the lithofacies without an associated flooding surface or change in relative sea level. This unit thins initially towards Coyote Basin and "Swell Point," but then begins to thicken into Rock Canyon. In the Rock Canyon area, a younger but unnamed bedset of the parasequence is wave modified (see PM-RC13).

- Type section: (wave-dominated unit) "The Wall" along the west side of Indian Canyon (PM-ICW series from Indian Canyon in the Willow Springs Wash case-study area), SW1/4SW1/4 section 24, T. 24 S., R.5 E., SLBL; (fluvial-dominated unit) mouth of the North Fork of Indian Canyon, north side, NW1/4NE1/4 section 24, T. 24 S., R. 5 E., SLBL. See figure 5-2 for detailed map of the Willow Springs Wash case-study area, including the informally named locations.

- Landward limit: Limestone Cliffs, approximately SE1/4 section 35, T. 24 S., R. 5 E., SLBL.

- Seaward limit: north of Corbula Canyon, SW1/4 section 33, T. 23 S., R. 6 E., SLBL.

- Facies content of shoreline unit: wave-dominated coast, probably, strand plain to fluvial-dominated.

Kf-1-Ivie Creek: Parasequence Kf-1-Ivie Creek (Kf-1-Iv) consists of numerous bedsets (PM-RC38) and extends from a well-exposed landward pinchout (PM-RC) between "Coyote Basin" and "Swell Point" to the seaward pinchout along east "Cowboy Mesa" (see PM-TC2). This outcrop distance is unusually long for a Ferron parasequence and other authors (Garrison and Van den Berg, 1997) have chosen to subdivide the unit into numerous parasequences. No distinct intertonguing of the landward most portion of the nearshore marine facies with non-marine or marginal marine facies of these bedsets were observed on outcrop, hence, the reluctance to call these units parasequences. The first bedset in the parasequence has been named after exposures in Rock Canyon (Kf-1-Iv[RC], see PM-RC8). Two younger named bedsets are the subject of the Ivie Creek case study (Kf-1-Iv[a] and Kf-1-Iv[c], see PM-IC40). Chapter 7 provides additional details on these bedsets.

- Type section: south side of "Swell Point," CSE1/4 section 8, T. 24 S., R. 6 E., SLBL; the unit was studied and named in Ivie Creek before it was correlated to its landward pinchout, hence the name.

- Landward limit: south side of "Swell Point," NW1/4SE1/4 section 8, T. 24 S., R. 6 E., SLBL.

- Seaward limit: north of "Cowboy Point" (S1/2 section 2, T. 23 E, R. 6 E., SLBL) and in the upper portion of Quitchupah Canyon.

- Facies content of shoreline unit: wave-dominated to wave-modified coast; proximal part probably strand plain changing to mainly fluvial-dominated with inclined clinoforms in the distal part.

Kf-1-Cowboy Canyon: Parasequence Kf-1-Cowboy Canyon (Kf-1-CC) type section is at the intersection of "Cowboy Canyon" and Quitchupah Canyon, on the east side (see PM-IC58). The unit has a distinctive thin "white cap" with a thin dirty Sub-A coal above on the east side of Quitchupah Canyon (figure 4-18) and thickens to a thick shoreface near the north end of the Ferron outcrop in Quitchupah (see PM-IC52). The unit's correlation to the southern and eastern portion of "Cowboy Mesa" is unclear. Unlike other parasequences, the landward pinchout is better described as a landward transition into marginal marine beds (see PM-IC46).

- Type section: mouth of "Cowboy Canyon," SE1/4, T. 23 S., R. 6 E., SLBL.

- Landward limit: (gradational with brackish bay) south and west side of Quitchupah Canyon, NE1/4 section 9, T. 23 S., R. 6 E., SLBL.

- Seaward limit: unknown, outcrop ends in northern Quitchupah Canyon.

- Facies content of shoreline unit: wave-dominated.

Kf-2

Kf-2 is a seaward-stepping shoreline unit or parasequence set (figure 4-8). It is the only seaward-stepping unit in which both landward and seaward limits of the units are defined on outcrop (extending 31 miles [50 km] along the outcrop). The landward pinchout is found in Willow Springs Wash (see PM-WS1) and the seaward pinchout is near Ferron Creek. Coals from the A and the lower part of the C coal zones are contemporaneous with this shoreline unit. These coals are not the thickest found in the Ferron, but probably represent the widest spread peat swamp and possibly the greatest volume of coal in the Ferron. Kf-2 contains some of the most internally complex facies arrangements of any parasequence set. The combined thickness of the nearshore marine facies of the unit in the "Tri Canyon" area is thicker (see PM-TC3) than any other parasequence set except the Kf-Last Chance. The top of the shoreline unit is commonly incised by distributary channels and meanderbelts (see PM-RC18 and PM-IC7) which fed continued progradation of the regressive shoreline farther seaward.

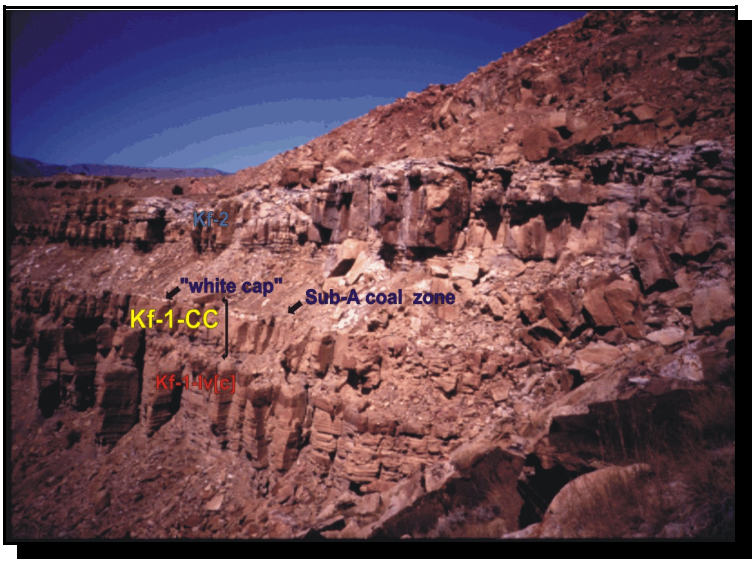


Figure 4-18. The middle sandstone package with the thin white cap is parasequence Kf-1-CC. Just above the white-capped sandstone is a thin Sub-A coal zone. The upper sandstone is the Kf-2 parasequence set and below the Kf-1-CC is the Kf-1-IC[c] bedset. The photo is from Quitchupah Canyon just south of "Cowboy Canyon." The view is to the north.

The parasequence set contains nine parasequences and one unnamed bedset:

1. Kf-2-Ivie Creek-a (Kf-2-Iv-a)
2. Kf-2-Ivie Creek-b (Kf-2-Iv-b)
3. Kf-2-Ivie Creek-c/Kf-2-Miller Canyon-a (Kf-2-Iv-c)/(Kf-2-Mi-a)
4. Kf-2-Miller Canyon-b (Kf-2-Mi-b)
5. Kf-2-Muddy Canyon-a (Kf-2-MC-a)
6. Kf-2-Muddy Canyon-b (Kf-2-MC-b)

   unnamed bedset
7. Kf-2-Dry Wash (Kf-2-DW)
8. Kf-2-Rochester (Kf-2-Ro)
9. Kf-2-Molen Seep Wash (Kf-2-MSW)

Kf-2-Ivie Creek-a: Kf-2-Ivie Creek-a (Kf-2-Iv-a) is the first parasequence in Kf-2 seaward regression of Kf-2. The pinchout is truncated slightly by a scour with muddy fill (see PM-WS1). The unit is wave-dominated in early progradation and later becomes wave-modified. It marks a change in the paleoshoreline of the Ferron from northwest-southeast to north-south (figure 4-15). Another unusual characteristic of this unit is its seaward pinchout. The unit downlaps onto the underlying parasequence set boundary instead of feathering out into prodelta facies (see PM-RC28 and PM-IC40). The name is taken from a locality where the unit was first recognized and described in detail instead of near its landward pinchout.

- Type locality: Ivie Creek Canyon, SE1/4 section 17, T. 23 S., R. 6 E., SLBL.
- Landward limit: mouth of Willow Springs Wash, north side, CSW1/4 section 18, T. 24 S., R. 6 E., SLBL.
- Seaward limit: near "Hoodoo Point" and near "Junction Point;" section 34, T. 23 S., R. 6 E., and section 16, T. 23 S., R. 6 E., SLBL.
- Facies content of shoreline unit: wave-dominated coast probably strand plain, with gradual changes to wave-modified, generally in the more easterly outcrops.

Kf-2-Ivie Creek-b: Parasequence Kf-2-Ivie Creek-b (Kf-2-Iv-b) began its shoreline regression in obscurity. The landward pinchout of nearshore marine facies is poorly exposed and occurs in a bay or brackish water environment (see PM-RC1). It quickly thickens to a well-developed wave-dominated shoreface (see PM-RC3) and often is dominated by middle shoreface facies in much of its outcrop. This unit does feather out into prodelta muds, but in more landward positions exhibits downlap onto the Kf-1 where it is the first progradation of the Kf-2.

- Type section: Ivie Creek Canyon, section 17, T. 23 S., R. 6 E., SLBL.
- Landward limit: near Coyote Basin on the south side of "Swell Point," SE1/4 section 7, T. 24 S., R. 6 E., SLBL.
- Seaward limit: just north of "Cowboy Point," approximately C section 11, T. 23 S., R. 6 E., SLBL.
- Facies content of shoreline unit: wave-dominated to wave-modified delta.

Kf-2-Ivie Creek-c: Kf-2-Ivie Creek-c (Kf-2-Iv-c) is the only parasequence with a stratigraphic equivalent, parasequence Kf-2-Miller Canyon-a (Kf-2-Mi-a). We recommend future workers drop this name and refer to the parasequence as Kf-2-Miller Canyon-a. On its landward side, Kf-2-Iv-c pinches out into delta-plain deposits of the A coal zone in the road cut of I-70 (figure 4-14 and see PM-IC13). No Ferron landward pinchout is more accessible and well exposed. The Kf-2-Iv-c

nomenclature is used for exposures of the parasequence south of I-70 and in the Ivie and Quitchupah Canyon areas. In the Ivie Creek area the unit begins prograding as a wave-dominated shoreline but changes facies to more bay-like deposits (see PM-IC36).

- Type section: Ivie Creek Canyon, NW1/4SE1/4 section 17, T. 23 S., R. 6 E., SLBL.

- Landward limit: Ivie Creek Canyon, C section 17, T. 23 S., R. 6 E., SLBL; 1-70 road cut, SW1/4NE1/4 section 20, T. 23 S., R. 6 E., SLBL.

- Seaward limit: Miller Canyon, NE1/4SW1/4 section 26, T. 22 S., R. 6 E., SLBL; Muddy Creek Canyon, E1/2NW1/4 section 24, T. 22 S., R. 6 E., SLBL (where the unit is designated Kf-2-Mi-a).

- Facies content of shoreline unit: wave-dominated coast, probably shoreface in the proximal part, transforming to low-wave-energy coast, possibly bay shoreline in the east Ivie Creek and west Quitchupah Canyon area, and wave-modified in the "Cowboy Mesa to Tri-Canyon" area.

Kf-2-Miller Canyon-a: Parasequence Kf-2-Miller Canyon-a (Kf-2-Mi-a) is the only unit with a stratigraphic equivalent, the Kf-2-Ivie Creek-c (Kf-2-Iv-c). Kf-2-Mi-a was described in early work in the Muddy Canyon area which pre-dates this study and the name is applied to outcrops on "Cowboy Mesa" and points north and east. The unit is wave-dominated on the south end of "Cowboy Mesa" (see PM-IC15) and continues to diminish in thickness and sand content into Muddy Creek Canyon (see PM-TC7) to the north and eastward into the Molen Amphitheater. Its most distinguishing characteristic is the large slump blocks which are present in several locations in the "Tri Canyon" area (Muddy Creek Canyon, Miller Canyon, and Grassy Canyon junction) (figures 4-19 and 6-12 in Chapter 6, Nix; 1999).

- Type section: Ivie Creek Canyon, NW1/4SE1/4 section 17, T. 23 S., R. 6 E., SLBL.

- Landward limit: Ivie Creek Canyon, C section 17, T. 23 S., R. 6 E., SLBL; I-70 road cut (here designated Kf-2-Iv-c), SW1/4NE1/4 section 20, T. 23 S., R. 6 E., SLBL.

- Seaward limit: Miller Canyon, NE1/4SW1/4 section 26, T. 22 S., R. 6 E., SLBL; Muddy Creek Canyon, E1/2NW1/4 section 24, T. 22 S., R. 6 E., SLBL.

- Facies content of shoreline unit: wave-dominated coast, probably shoreface in the proximal part, transforming to low-wave-energy coast, possibly bay shoreline in the east Ivie Creek and west Quitchupah Canyon area (Kf-2-Iv-c equivalent), and wave-modified in the "Cowboy Mesa to Tri-Canyon" area.



Figure 4-19. Typical of parasequence Kf-2-Mi-a are incongruous sand-rich slumps or rotated blocks. This outcrop is on the south end of "Cowboy Mesa," NW1/4NE1/4 section 15, T. 23 S., R. 6 E., SLBL. Although this is in parasequence Kf-2-Iv-b, the characteristics of these rotated blocks are similar regardless of the stratigraphic unit in which they occur. The scale bar near the bottom of the photo is 5 feet (1.5 m) in length. The tops of these blocks are typically eroded off by the overlying transgression or flooding surface. Dips within the slump blocks are generally steepest near the bottom-center, indicating active sedimentation during rotation.

Kf-2-Miller Canyon-b: Parasequence Kf-2-Miller Canyon-b (Kf-2-Mi-b) marks an important change in deposition of the Kf-2. Some workers (Barton, 1994) have seen this change as important enough to give this stratigraphic boundary a higher rank (parasequence set boundary). The unit is defined in Miller Canyon where it is a thick wave-dominated shoreface with numerous incised channels of contemporaneous and younger age (see figure 6-14 in Chapter 6). Its landward edge is somewhat tentatively identified in the east face of "Cowboy Mesa" (see PM-TC1). The unit feathers out in a seaward direction in the Coal Cliffs. One potential bedset is identified in the unit in the mid-portion of Muddy Canyon (figure 4-20), although we have not chosen to name it at this point.

- Type section: south side of Miller Canyon near its mouth.
- Landward limit: along the east face of "Cowboy Mesa," SW1/4SE1/4 section 2, T. 23 S., R. 6 E., SLBL.
- Seaward limit: Molen Reef, CSE1/4 section 29, T. 22 S., R. 7 E., SLBL.
- Facies content of shoreline unit: wave-dominated, probably stand plain in proximal part; may include deltaic deposits in medial and distal parts.

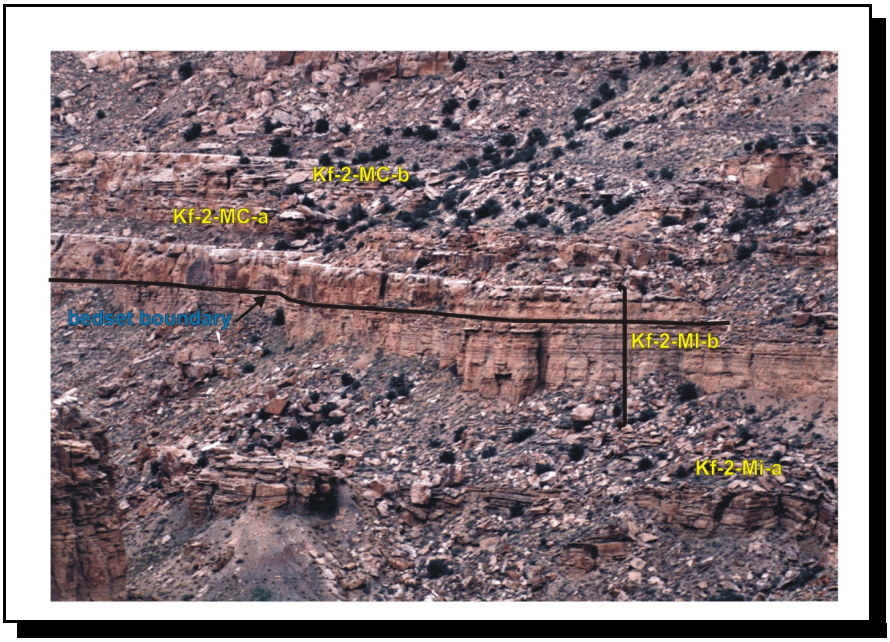


Figure 4-20. The lower cliff-forming sandstone is parasequence Kf-2-Mi-b on the east side of Muddy Creek Canyon, just north of the first meander above the confluence with Miller Canyon. Note the increase in shoreface sand thickness in the upper bedset. This change in deposition is related to an autocyclic event and not to a relative change in sea level.

Kf-2-Muddy Canyon-a: Parasequence Kf-2-Muddy Canyon-a (Kf-2-MC-a) is dominantly meanderbelt facies (see PM-TC7) in the "Tri Canyon" area where it was named, but it begins farther west. Landward pinchouts of the unit have been identified on the south end of "Cowboy Mesa" (see PM-IC63) and on Mesa Butte (see PM-RC42). The paleoshoreline trend is north-south. Along with the overlying Kf-2-MC-b, a couplet is formed in the distal end of their progradation, as they pinchout into the Tununk Shale along the Coal Cliffs (see PM-MR4).

- Type section: southern part of Muddy Creek Canyon, NW1/4SW1/4 section 24, T. 22 S., R. 6 E., SLBL.

- Landward limit: best exposed on Mesa Butte, near "West Point."

- Seaward limit: southern Molen Reef, NE1/4SE1/4 section 29, T. 22 S., R. 7 E., SLBL.

- Facies content of shoreline unit: full range from wave-dominated to fluvial-dominated delta; fluvial-dominated in Muddy Creek Canyon probably represents a low-wave energy delta that prograded into a protected bay.

Kf-2-Muddy Canyon-b: Parasequence Kf-2-Muddy Canyon-b (Kf-2-MC-b) is well exposed in the Tri Canyon area and on Mesa Butte (see PM-RC52 and RC47) where it begins. Flood-tidal deltas and bay deposits are associated with the relative rise in sea level prior to the Kf-2-MC-b regression in the Muddy Creek Canyon area. Dramatic thickening of a wave-dominated shoreline and well-preserved tidal-inlet deposits (see figure 6-57 in Chapter 6) document the beginnings of this parasequence. The unit can be traced along the vertical exposures of the Coal Cliffs north of Dry Wash, making one of the longest outcrop exposures in the Ferron. Along the Coal Cliffs a prominent shaley bedding break occurs in the parasequence. This break is the basis of designation of an unnamed bedset at the end of the progradation of the parasequence.

- Type section: southern part of Muddy Creek Canyon, NW1/4SW1/4 section 24, T. 22 S., R. 6 E., SLBL.

- Landward limit: southern Coal Cliffs north of "Bear Gulch," CSE1/4 section 35, T. 22 S., R. 6 E., SLBL; mouth of Miller Canyon, NE1/4NE1/4 section 35, T. 22 S., R. 6 E., SLBL and SE1/4SE1/4 section 26, T. 22 S., R. 6 E., SLBL; Muddy Creek Canyon, SW1/4SE1/4 section 23, T. 22 S., R. 6 E., SLBL; Mesa Butte SW1/4 section 23, T. 23 S., R. 6 E., SLBL and NW1/4 section 35, T. 23 S., R. 6 E., SLBL.

- Seaward limit: just north of Dry Wash, NE1/4NE1/4 section 36, T. 21 S., R. 7 E., SLBL.

- Facies content of shoreline unit: wave-dominated coast in proximal part, probably strand plain; wave-modified to fluvial-dominated in the north.

Kf-2-Dry Wash: Parasequence Kf-2-Dry Wash (Kf-2-DW) prograded out of a bay created during the flooding event at the close of parasequence Kf-2-MC-b. Exposures of this bay occur along the Moore road through Dry Wash (see PM-DW7). This unit begins as wave-dominated but does not thicken as rapidly as some of the earlier parasequences in this set. This parasequence marks a return to a northwest-southeast trend to the shoreline.

- Type section: cliffs north of Dry Wash, SW1/4 section 35, T. 21 S., R. 7 E., SLBL.
- Landward limit: Dry Wash, SW1/4 section 2, T. 22 S., R. 7 E., SLBL and SE1/4 section 34, T. 21 S., R. 7 E., SLBL.
- Seaward limit: about 0.5 miles (0.8 km) north of Short Canyon, SW1/4 section 18, T. 21 S., R. 8 E., SLBL.
- Facies content of shoreline unit: wave-dominated, probably strand plain in proximal part.

Kf-2-Rochester: Parasequence Kf-2-Rochester (Kf-2-Ro) steps a very short distance seaward (figure 4-11) from the landward pinchout of the underlying parasequence Kf-2-DW (figure 4-15). The geometry of the landward pinchout of parasequences Kf-2-DW and Kf-2-Ro is similar to the two parasequences in the Kf-3 (see below). The seaward edge of the unit is mapped along the Molen Reef, just south of Yellow Seep Wash, and in the small canyon cut by Molen Seep Wash (figure 4-21). This is a slight change in the orientation of the seaward end of parasequences in the set. It indicates a more north-south trend.

- Type section: cliffs north of Dry Wash, S1/2 section 35, T. 21 S., R. 7 E., SLBL.
- Landward limit: Dry Wash, SW1/4 section 35, T. 21 S., R. 7 E., SLBL.
- Seaward limit: about 0.25 miles (0.4 km) south of Yellow Seep Wash, section 8, T. 21 S., R. 8 E., SLBL.
- Facies content of shoreline unit: wave-dominated.

Kf-2-Molen Seep Wash: Kf-2-Molen Seep Wash (Kf-2-MSW) is the last parasequence in the Kf-2 set. It is not clear how this unit relates to the overlying parasequences, but the location of its most proximal facies at the westernmost outcrops in Molen Seep Wash is clearly an indication that the general trend of the shoreline has departed from the trend of the outcrop. This marks the swing of the paleoshoreline to the west and the northern edge of the Last Chance delta of Cotter (1976). From subsurface and outcrop correlations it appears this unit is a new parasequence and is probably related to non-marine to marginal rocks that lie above parasequence Kf-2-Ro in the Dry Wash-Short Canyon area. Two cycles are obvious in Molen Seep Wash (figure 4-22) but it is unclear if they are two parasequences or two bedsets of a single parasequence. Additional outcrop work is needed to clearly understand the correct correlation of this unit.



Figure 4-21. The lowest of the three coarsening-upward cycles is parasequence Kf-2-Ro. The outcrop is located just south and east of Molen Seep Wash (SW1/4NW1/4 section 7, T. 21 S., R. 8 E., SLBL). Correlations are somewhat tentative because of discontinuous outcrops and incomplete photomosaic coverage.



Figure 4-22. Two upward-coarsening cycles in parasequence Kf-2-MSW are exposed on the north side of the wash (NE1/4 section 6, T. 21 S., R. 8 E., SLBL). It is not clear whether these are bedsets or parasequences. Only the upper cycles emerge from the wash onto the main Ferron escarpment. Sandstones in Kf-3 cap the top of the outcrop.

- Type section: Molen Seep Wash at top of Ferron Sandstone, SW1/4 section 6, T. 21 S., R. 8 E., SLBL.

- Landward limit: unknown

- Seaward limit: north of Dutch Flat, beyond the study area.

- Facies content of shoreline unit: proximal facies not exposed, probably wave-dominated.

Kf-3

Two shoreline units or parasequences have been identified in Kf-3. Both of the parasequences exhibit landward pinchouts into the C coal zone. Only a small amount of the C coal lies above the lower parasequence, placing most of the C coal in the Kf-2. Of all the parasequence sets with both the landward and seaward edges defined, the Kf-3 exhibits the greatest amount of horizontal offset on the landward edge with respect to the underlying landward edge of Kf-2. The unit is seaward stepping relative to the underlying Kf-2.

Although Kf-3 contains only two parasequences, it is possible that additional parasequences may be defined with more work along the dip slope of the Ferron between Muddy Canyon and Short Canyon. The parasequences are:

1. Kf-3-Molen Amphitheater (Kf-3-MA)

2. Kf-3-Molen Reef (Kf-3-MR)

Kf-3-Molen Amphitheater: Parasequence Kf-3-Molen Amphitheater (Kf-3-MA) is spectacularly exposed in the "Molen Amphitheater" where the landward pinchout, figure 4-23, is clearly emerging from the upper portion of the C coal (see PM-TC18). The unit is difficult to differentiate from the overlying Kf-3-MR parasequence a short distance from the landward pinchout (see PM-TC20). No exposures of marine facies of the parasequence are found south of the "Molen Amphitheater."

- Type section: at mouth of "Gnat Canyon," NE1/4SW1/4 section 30, T. 22 S., R. 7E., SLBL.

- Landward limit: just west of mouth of "Gnat Canyon:" CSW1/4 section 30, T. 22 S., R. 7 E. SLBL.

- Seaward limit: between Dutch Flat and Ferron Creek, section 22, T. 20 S., R. 8 E., SLBL (this is for the Kf-3 undivided).

- Facies content of shoreline unit: wave-dominated, probably strand plain in proximal part; distal part may include deltaics.

Kf-3-Molen Reef: Parasequence Kf-3-Molen Reef (Kf-3-MR) steps only a few hundred feet seaward from the landward pinchout of the underlying Kf-3-MA (figure 4-23), indicating the change to an aggradational stacking pattern of parasequences (see PM-TC20). The landward pinchout of parasequence Kf-3-MR is clearly into carbonaceous deposits in the upper portion of the C coal and reasonably well exposed in "Gnat Canyon." The combination of the this parasequence and the underlying parasequence Kf-3-MA continue as essentially one massive and undifferentiated cliff former, north along the face of the Coal Cliffs. Several well exposed incisions into the top of the unit outcrop along the Coal Cliffs (see PM-MR7) and in Dry Wash, the top of the unit is incised by tidal channels.

- Type section: "Molen Amphitheater," east of "Gnat Canyon," NE1/4 section 31, T. 22 S., R. 7 E., SLBL.
- Landward limit: at mouth of "Gnat Canyon," NE1/4SW1/4 section 30, T. 22 S., R. 7 E., SLBL.
- Seaward limit: not determined for the parasequence but the Kf-3 set pinches out just southeast f Molen, section 22, T. 20 S., R. 8 E., SLBL .

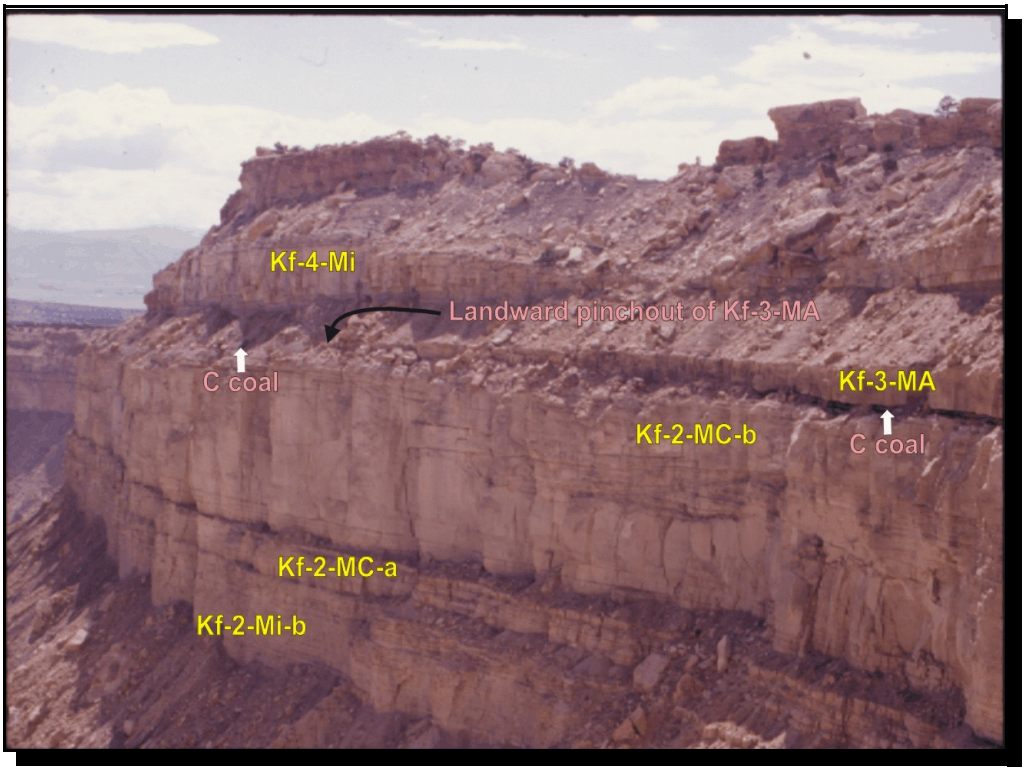


Figure 4-23. View to the west of the landward pinchout of parasequence Kf-3-MA. Note the dark upper split of the C coal under the Kf-3-MA just seaward of the landward pinchout. The landward pinchout of the Kf-3-MR is located about where this photograph was taken and Kf-4-MR landward pinchout is just out of view in the upper right.

- Facies content of shoreline unit: wave-dominated coastline, probably strand plain, in proximal part; distal part includes fluvial-dominated deltaics.

Kf-4

This unit contains two named parasequences which both thicken rapidly within the nearshore facies in a seaward direction. The landward pinchout of the first parasequence is actually landward of the Kf-3 parasequence set. The unit has been characterized as a vertically aggrading part of the overall Ferron cycle. Typical of the back stepping units, the nearshore facies are dominantly wave-dominated. The two named parasequences are:

1. Kf-4-Miller Canyon (Kf-4-Mi)

2. Kf-4-Molen Reef (Kf-4-MR)

Kf-4-Miller Canyon: Parasequence Kf-4-Miller Canyon (Kf-4-Mi) nearshore facies first appears about mid-length of "Cowboy Mesa" where it is cut by a large meanderbelt (see PM-TC2). The unit is wave-dominated and only prograded a short distance. It forms the top of the cliff faces in most of the "Tri Canyon" area. The associated parasequence set boundary at its base is unambiguous with the transgressive deposits and C coal zone below (see PM-TC6). In upper Quitchupah Canyon an *Ophiomorpha*-burrowed sandstone lies above the C coal and is believed to be related to Kf-4-Mi (figure 4-24). Perhaps the burrowed sandstone in Quitchupah Canyon represents a lagoon or bay associated with the turn-around from transgression to regression of the shoreline.

- Type section: southern Coal Cliffs at the mouth of Miller Canyon, SE1/4SE1/4 section 26, T. 22 S., R.6 E., SLBL.

- Landward limit: in Coal Cliffs south of "Bear Gulch," SW1/4NE1/4 section 2, T. 23 S., R. 6 E., SLBL.

- Seaward limit: located about 0.75 miles (1.2 km) northeast of "Molen Point," SE1/4 section 29, T. 22 S., R. 7 E., SLBL.

- Basic facies content: wave-dominated shoreline.

Kf-4-Molen Reef: Parasequence Kf-4-Molen Reef (Kf-4-MR) steps seaward a short distance relative to the underlying Kf-4-Mi parasequence. The landward pinchout is in the "Molen Amphitheater." The unit thickens rapidly to become a distinctive white, semi-resistant step in the topography of the amphitheater (figure 4-25). Exposures of the unit in the cliffs of the Molen Reef are continuous in the south, near the Molen Amphitheater, but become eroded and intermittent to the north (see PM-MR7). In the northern Molen Reef, exposures of this parasequence are in small canyons which cut the top of the Ferron Sandstone on the dip slope west of the cliff escarpment.

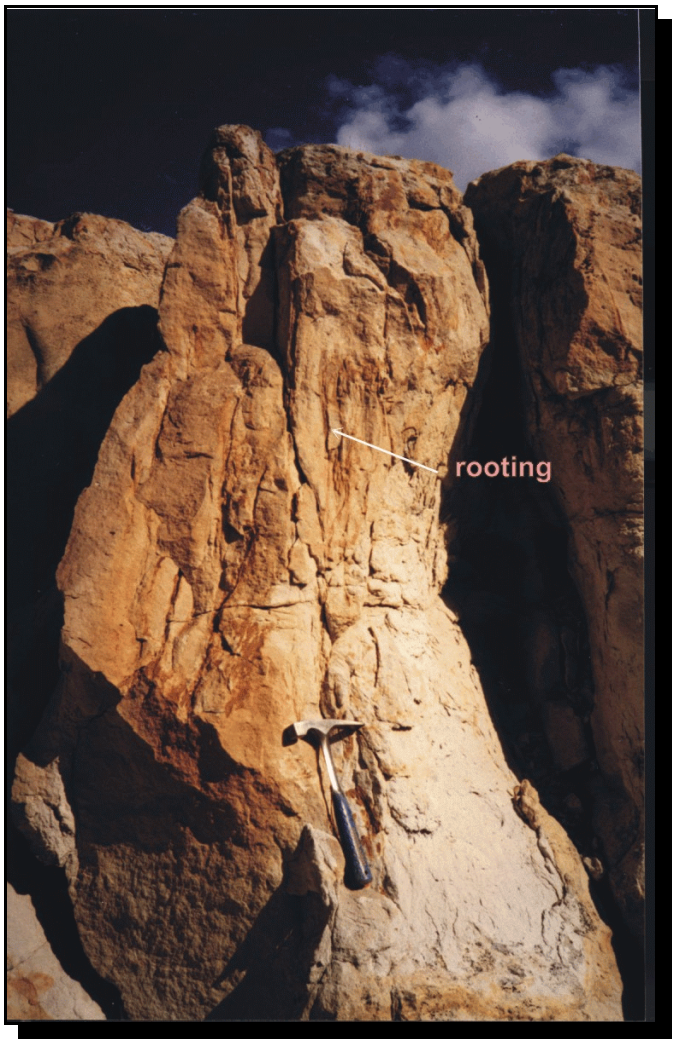


Figure 4-24. Kf-4-Mi marine or marginal marine sandstone in upper Quitchupah Canyon (NE1/4NE1/4 section 4, T. 23 S., R. 6 E., SLBL). The sandstone is moderately burrowed, chiefly *Ophiomorpha*, and here it is rooted from the overlying G coal. The sandstone is 8 to 10 feet (2.4-3 m) thick and lies 20 to 30 feet (6-9 m) stratigraphically above the C coal. Hammer for scale.**Figure 4-24. Kf-4-Mi marine or marginal marine sandstone in upper Quitchupah Canyon (NE1/4NE1/4 section 4, T. 23 S., R. 6 E., SLBL). The sandstone is moderately burrowed, chiefly *Ophiomorpha*, and here it is rooted from the overlying G coal. The sandstone is 8 to 10 feet (2.4-3 m) thick and lies 20 to 30 feet (6-9 m) stratigraphically above the C coal. Hammer for scale.**

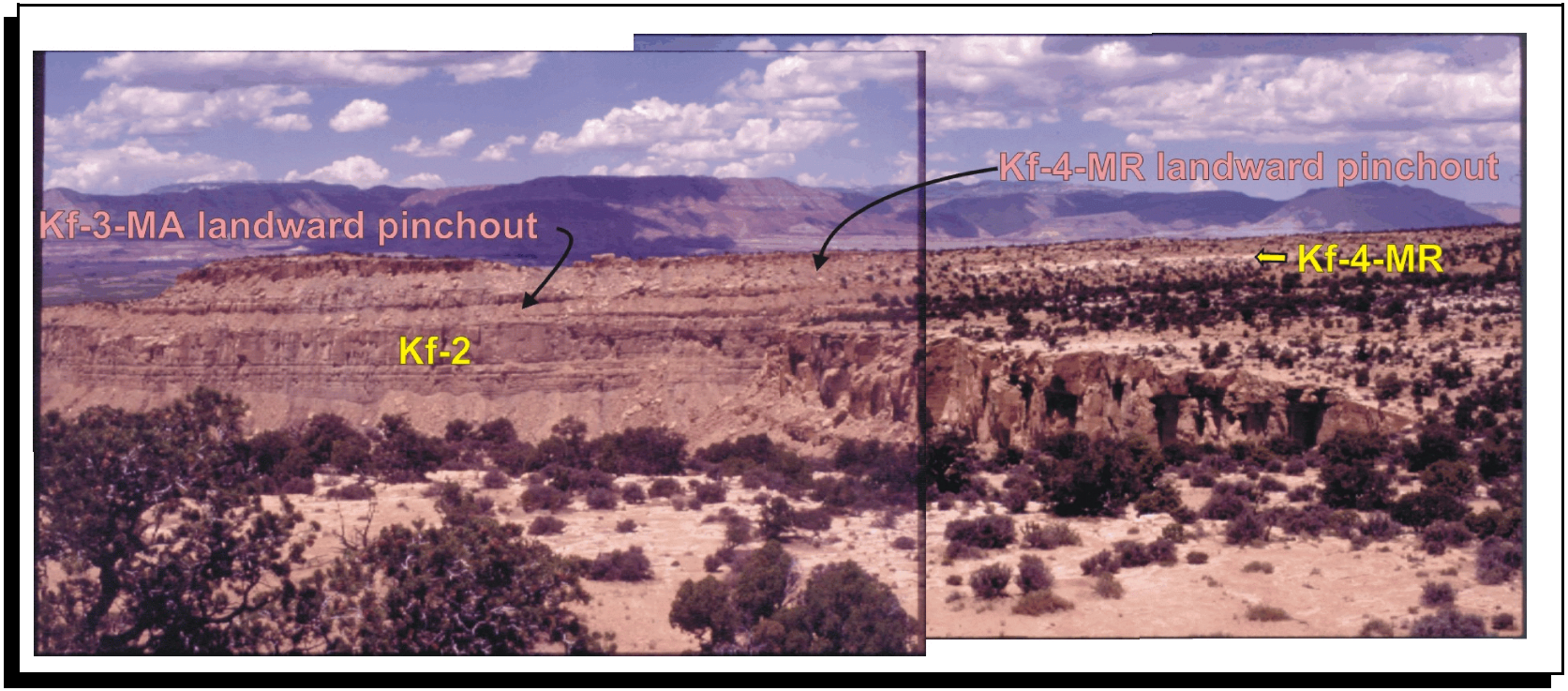


Figure 4-25. Kf-4-MR is conspicuously white on outcrop near the landward pinchout along the edge of the "Molen Amphitheater." The landward pinchout occurs in a marginal exposure. The Kf-3-MA landward pinchout is also clearly visible in this view to the northwest along the east edge of the "Molen Amphitheater."

- Type section: Molen Reef, SE1/4SW1/4 section 29, T. 22 S., R. 7 E., SLBL, or along white, south-facing wall in the "Molen Amphitheater," SE1/4SE1/4 section 30, T. 22 S., R.7 E., SLBL.

- Landward limit: mouth of "Gnat Canyon," NE1/4SW1/4 section 30, T. 22 S., R. 7 E., SLBL.

- Seaward limit: tentatively just north of Molen Seep Wash, section 6, T. 21 S., R. 8 E., SLBL, and at the end of the parasequence set.

- Basic facies content: wave-dominated shoreline-strand plain in proximal part to wave- dominated delta in distal part.

Kf-5

At present this parasequence set has not been divided into parasequences, but this unit has not received as much attention in this study as others and it is likely that it contains more than one parasequence. The landward pinchout of the unit has been removed by younger meanderbelt and channel facies so its position is only approximately located. There is, however, clearly a flooding surface based on the underlying G coal zone and overlying nearshore marine facies of the Kf-5. The top of this wave-dominated unit is scoured in most places where it outcrops (figure 4-26).

- Type section: none; considered to be a parasequence set at present. If Kf-5 is ultimately considered to constitute a single parasequence, a good type section would be the west side of Muddy Creek Canyon, NE1/4SW1/4 section 13, T. 22 S., R. 6 E., SLBL.

- Landward limit: Muddy Creek Canyon, somewhat obscured because of overlying meanderbelt, approximately C section 24, T. 22 S., R. 6 E., SLBL.

- Seaward limit: "Fracture Canyon," SW1/4 section 34, T. 21 S., R. 7 E. SLBL.

- Facies content of shoreline unit: wave-dominated.

Kf-6

Unlike many of the units of the Ferron this one is not exposed on the east-facing Coal Cliffs but is only found at the bottom of the dip slope formed by the Ferron. The landward and seaward limits (figure 4-12) are slightly seaward of the Kf-5, but the unit has been characterized (Gardner, 1993) as the beginning of a back stepping pattern. The unit is wave-dominated reflecting the greater amount of sediments being trapped in the non-marine environment and exposure of the shoreline to wave-energy as the relative rate of sea-level rise overtakes sediment input.



Figure 4-26. Kf-5 on the east side of upper Muddy Creek Canyon. The lower portion of the parasequence consists of very fine- to fine-grained delta-front deposits from a fluvial-dominated delta. This facies is more resistant to weathering and is brown on outcrop. The delta-front facies are cut by more friable distributary channel sandstones which fed younger shoreline deposits somewhere seaward. The contact between the two facies is often preserved in this outcrop.

- Type section: uppermost part of Muddy Creek Canyon, SE1/4NW1/4 section 13, T. 22 S., R. 6 E., SLBL.
- Landward limit: uppermost part of Muddy Creek Canyon, SE1/4NW1/4 section 13, T. 22 S., R. 6 E., SLBL.
- Seaward limit: Dry Wash, NE1/4NW1/4 section 34, T. 21 S., R. 7 E., SLBL.
- Facies content of shoreline unit: wave-dominated coastline, probably strand plain.

Kf-7

Kf-7 is truly a back step from the younger Kf-6. Only one parasequence has been recognized and the landward pinchout is obscured by meanderbelt deposits. The unit is generally thin (5-15 feet) and exposed on the top of the Ferron dip slope (see figure 6-2 in Chapter 6) in discontinuous outcrop making study of this unit difficult.

- Type section: west side of Muddy Creek Canyon, NW1/4SW1/4 section 13, T. 22 S., R. 6 E., SLBL.
- Landward limit: cannot be determined owing to fluvial erosion, approximately at Christiansen Wash, NW1/4 section 33, T. 22 S., R. 6 E., SLBL.
- Seaward limit: upper part of Muddy Creek Canyon, SE1/4NW1/4 section 13, T. 22 S., R. 6 E., SLBL.

- Facies content of shoreline unit: wave-dominated.

Kf-8

Kf-8 represents the last significant regressive nearshore facies sand accumulation in the exposed outcrop of the Ferron. It has not been subdivided into parasequences, but potentially could be. As is the case with the other back-stepping parasequence sets, the exposures of this unit are found at the bottom of the dip slope and top of the Ferron. The unit lies above the "M" coal zone and exposures lie between Quitchupah Creek and Coal Wash (figure 4-27). Cobble-sized rounded clasts of carbonate and quartzite are found within this unit often as a lag at the contact with the Blue Gate Shale (figure 4-28).

- Type section: west side of Quitchupah Canyon, near "Burn Canyon," SE1/4 section 5, T. 23 S., R. 6 E., SLBL.

- Landward limit: approximately at the south line of section 5, T. 23 S., R. 6 E., SLBL, based on drill-hole data and limited outcrops.

- Seaward limit: poorly understood due to the nature of the outcrop, but probably not beyond the Browning Mine/Christensen Wash area; SW1/4 section 33, T. 22 S., R. 6 E., SLBL.

- Facies content of shoreline unit: wave-modified; the presence of large clasts at the base of the unit and the unusual facies arrangement indicate some fluvial influence.

Analysis

Applicability of Sequence Stratigraphic Terminology

The application of sequence stratigraphic terminology in this study was driven by two factors: (1) the hope that its models and terms would enhance our understanding of the packages of Ferron rocks and increase our ability to predict the occurrence and distribution of reservoir quality facies, and (2) its popularity at the time. At the outset of the project the regional stratigraphic focus was on subdividing Ryer's (1981a) previous "deltaic units" into the next logical sequence stratigraphic unit, the parasequence. The key in defining parasequences is the recognition of marine-flooding surfaces. Van Wagoner and others (1990) define these surfaces as, "A surface separating younger from older strata across which there is evidence of an abrupt increase in water depth." The law of superposition makes almost any bedding surface qualify for the first part of the definition, so it is the "evidence of an abrupt increase in water depth" which becomes the important element of establishing a marine-flooding surface or parasequence boundary. It is not clear why a gradual change in water depth is not equally as important to recognize and should not also receive equal status in the hierarchy.

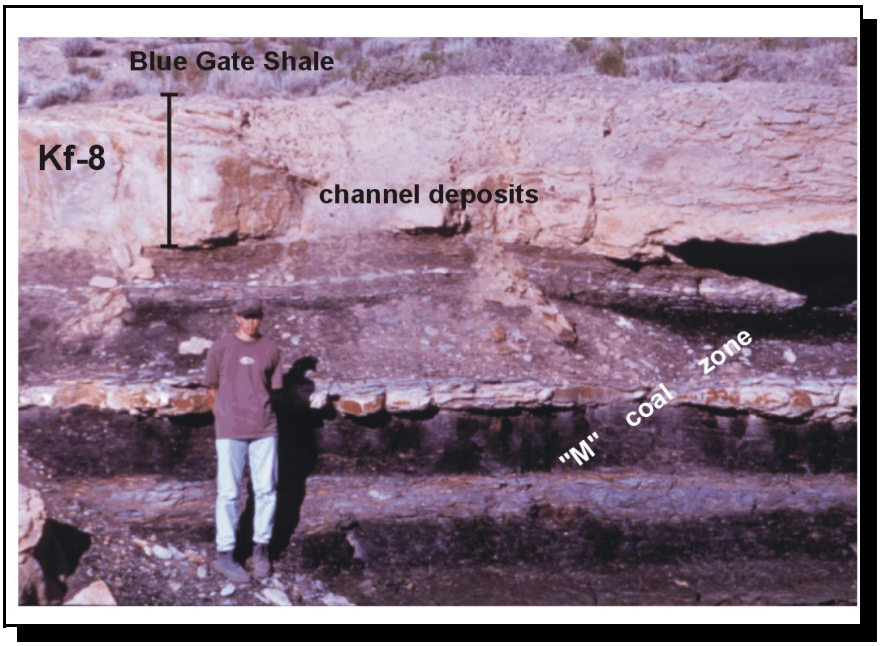


Figure 4-27. Kf-8 channel deposits in Coal Wash lie just south of confirmed marine rocks. This thin back stepping unit lies above the "M" coal zone.

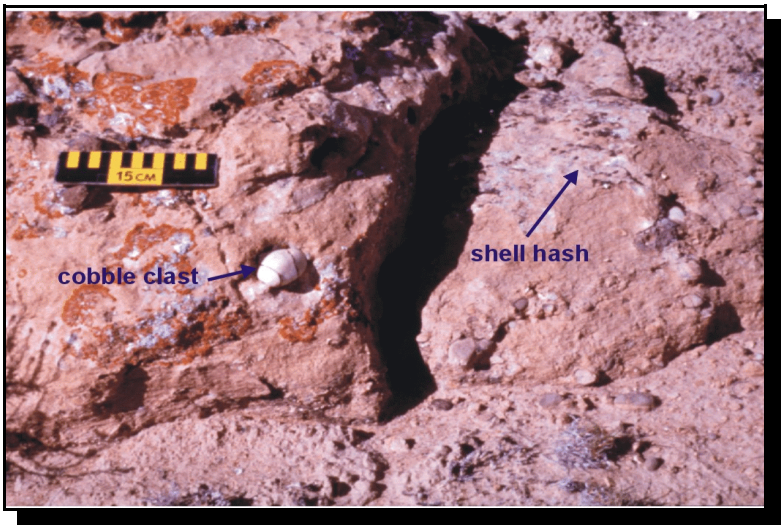


Figure 4-28. Up to cobble-sized clasts and oyster-shell hash are present in thin to medium beds of marine Kf-8 in the west Quitchupah Canyon area, near the contact with the overlying Blue Gate Shale. The clasts are generally carbonate and quartzite. Oyster-shell hash is often associated with the beds containing the large clast size. Similar lithology is found at the contact with the Blue Gate Shale farther south near Coal Wash.

Early in the study numerous coarsening-upward and bed-thickening-upward successions of marine rocks were recognized, and a marine-flooding surface was placed at the top of many of these packages of rocks when they were overlain by another similar succession (figure 4-29). As these units were traced laterally, this "flooding surface" merged with the top of the marine facies with no indication of a vertical offset of the marine into the overlying non-marine or delta-plain facies. This proved there was no relative change in sea level associated with this important bedding surface at this location. The rocks in the package bounded by this bedding surface are genetically related to an event which has differentiated them from rocks above and below.

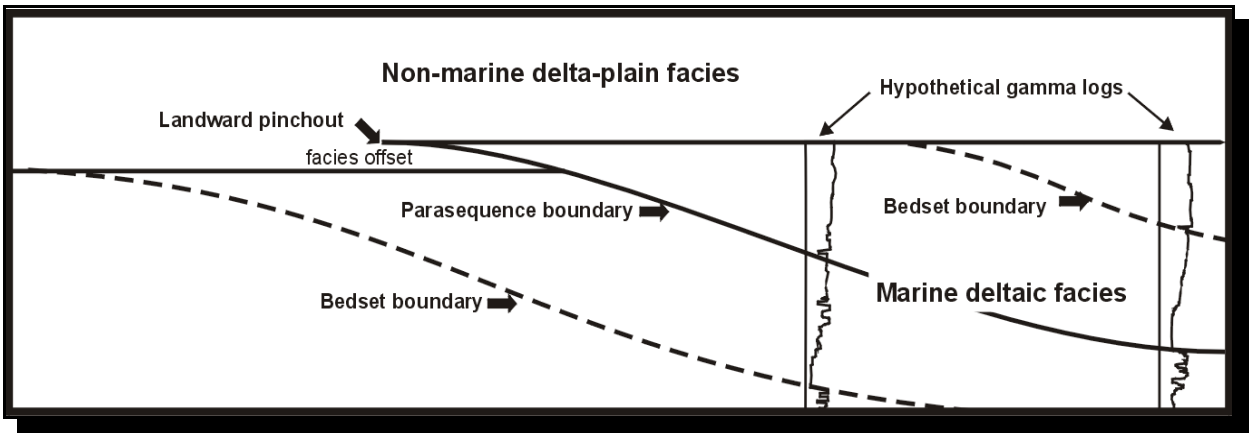


Figure 4-29. In more distal positions relative to the landward pinchout of nearshore marine facies, the top of stacked packages of coarsening-upward successions are easily mistaken for flooding surfaces. These surfaces were designated bedset boundaries because when traced to the marine/non-marine contact no facies offset into the delta plain could found.

A change in sand deposition, in the distal portion of the deltaic shoreface, does not always correspond with a flooding event/relative rise of sea level when traced up depositional dip to the beach. Changes in sediment supply and/or coastline morphology along an actively prograding coast can cause mud deposition to occur where sand previously dominated, without a change in water depth. This change in sediment supply could be accompanied by minor subsidence due either to compaction or tectonics. If so, there is a deepening, but the deepening may not always reach the beach. It seems possible to have a parasequence boundary in the distal portion of genetically related beds but no such boundary (by definition) in the proximal portion of the same chronostratigraphic unit at the beach. Considering the higher compaction ratio of mud to sand, it is likely that the more distal and muddy portions of a delta would compact more than the proximal and sandy facies. No guidance is given for this situation in Van Wagoner's definitions and based on his work in the Book Cliffs (Van Wagoner, 1995) he has chosen to view these minor offshore changes in lithology as always reflecting a "flooding event." We see this as an inherent ambiguity in the application of sequence stratigraphy in high resolution stratigraphic analysis which creates a variety of interpretations for the same stratigraphic interval.

When examining rocks only in the distal portion of the system, it appears hopeless to differentiate a change in sand-shale lithology related to changes in sediment supply or minor compaction-related subsidence, and one of sufficient magnitude to effect sea level at the beach. This fact limits the predictive power of the sequence stratigraphic model in correlating each "parasequence" identified in more distal facies of deltas with corresponding flooding events which effect sedimentation at the beach.

We are aware of two other attempts to apply sequence stratigraphic analysis (terminology) to the Ferron Sandstone (Knox and Barton, 1999) and Garrison and van den Bergh (1996). Many of the interpretations are similar, but there remain many differences. Regardless of who is right or wrong, the noted differences reflect the utility of sequence stratigraphy when applied by various workers. The terms we use in stratigraphy are useful if they enable us to clearly communicate with each other. We see room for improvement by more clearly defining terms.

Progradation Styles

The early progradations of the Ferron (Kf-LC, Kf-1-Ls, Kf-1-Ms) are shorter in length from landward pinchout to seaward pinchout, and the internal inclination of beds are steeper dipping than in later parasequences of seaward-stepping units. The cause of this geometry is not clear, but may be related to more rapid subsidence in the foreland basin locally, creating the steeper inclinations into the basin.

All initial progradations of the Ferron parasequences begin as wave-dominated. With the onset of initial transgression, the sea inundates the low delta-plain and the shoreline moves landward. With this landward transgression of the shoreline, the mouths of rivers are initially flooded and sediment is trapped in the old channel system. During base-level "turns around" and transgression the principal source of sediment at the shoreline is from eroding delta-plain sediments. As waves work the new shoreline, strandline-type deposits are formed.

Progression from one type of delta (wave-dominated, wave-modified, or fluvial-dominated) to another often, but not always, follows a predictable order. Often this change is abrupt and is identified as a bedset, other times the change is gradational. A change from one progradational style to another does not necessary correspond to a new parasequence. The Ferron shorelines prograded as a complex of contemporaneous and diachronous intertonguing delta-types. Bhattacharya (1998) describes Danube River delta as a modern example of various deltaic facies associated with one river along a "wave-influenced" coast. This is a good analogy for portions of the Ferron where a wide variety of facies and architectures are observed within a relatively short distance along the paleoshoreline.

Regional Reservoirs

The study of the regional stratigraphy helps to put the smaller scale case studies into a larger scale context. One important conclusion related to regional reservoirs is the recognition that all initial progradations begin as wave-dominated. From this study we know that the wave-influenced rocks generally have better porosity and permeability than the fluvial-dominated facies, therefore, the landward pinchouts of parasequences make good reservoir rocks. The trends of these reservoirs are shoreline parallel.

Seaward-stepping parasequence sets have much greater dip length than do the vertically aggrading and landward-stepping parasequence sets. A significant portion of the volume of rock within any seaward-stepping parasequence set consists of channel and meanderbelt facies which have incised older or relatively contemporary shoreface deposits. These channel facies are some of the best reservoirs in the system (Barton, 1994, and Chapter 10, this report). Their elongation direction relative to shoreline is orthogonal.

Alluvial-plain deposits consist of a high percentage of sandstone. This is qualitatively obvious when examining the photomosaics along the Limestone Cliffs (see PM-LC1 to LC14). Shale drapes and plugs can create a reservoir which is highly compartmentalized, but individual meanderbelt systems in the alluvial-plain facies have continuity of several miles, based on exposures along the Limestone Cliffs.

Landward-stepping parasequence sets are much smaller in volume of sand because of the relatively short distance they prograded before the continuing rise of sea level overtook sediment supply and the shoreline jumped farther landward. Compared to seaward-stepping units their dip length is short. Landward-stepping units offer the attraction of having an excellent seal of offshore muds stratigraphically above. These units are generally wave-dominated, providing good reservoir sands and are not commonly incised by channel systems which could act as conduit to leak hydrocarbons into the delta-plain and alluvial-plain deposits found landward of these deposits.

CHAPTER V
GEOLOGIC FRAMEWORK OF WILLOW SPRINGS WASH CASE-STUDY AREA

T.H. Morris, J.A. Dewey, Jr., and T.A. Ryer

Introduction

Three-dimensional outcrop exposures of the Ferron Sandstone in east-central Utah illustrate the importance of recognizing autocyclic processes in marine shorelines. In a wave-dominated shoreline, vertical offset between the landward pinchout of two chronostratigraphically distinct marine sandstones demonstrates a marine flooding event. By definition, these individual sandstones would be interpreted as parasequences. However, in a fluvial-dominated shoreline, autocyclic processes may produce no vertical offset between the landward pinchout of two chronostratigraphically distinct marine sandstones. Therefore, a marine flooding event could not have occurred and, by definition, these two sandstones cannot be interpreted as parasequences. Unless the distinction between autocyclic processes and allocyclic processes is recognized, the utility of parasequence correlation is diminished and optimal reservoir development strategies cannot be formulated.

Within the area of the Willow Springs Wash case-study area (figure 5-1), exposures of the Ferron Sandstone permit detailed examination of both macro-and mega-scale features in three dimensions. Observations of lithology, primary sedimentary structures, bedding, bioturbation, and internal architectural elements allow identification of several facies. These facies are grouped into wave-dominated shoreline and fluvial-dominated deltaic depositional systems.

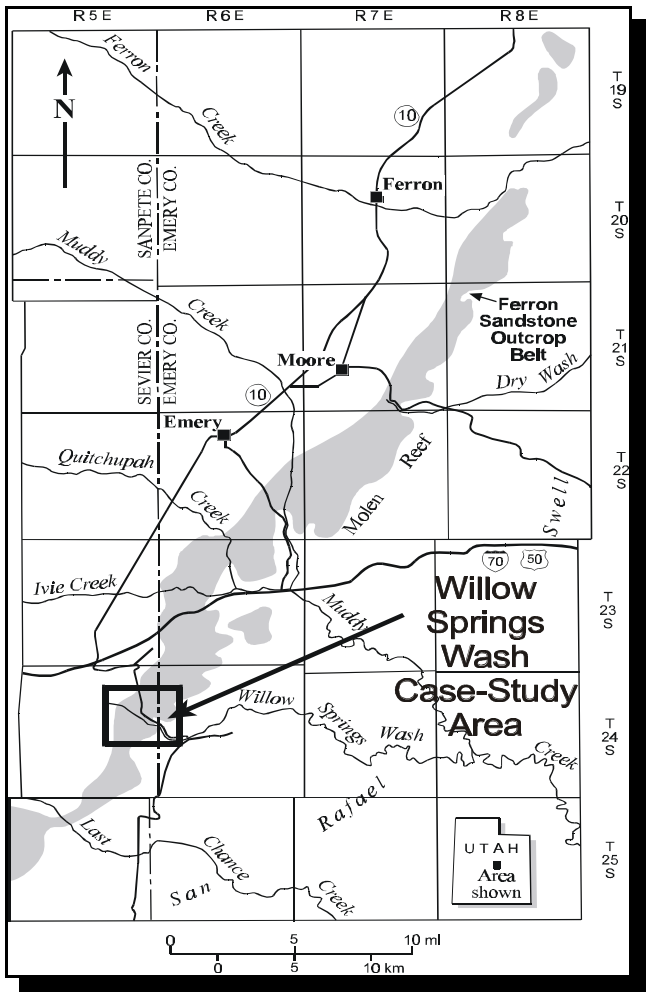


Figure 5-1. Location map of the Ferron Sandstone project area (outcrop belt is shaded) showing the Willow Springs Wash case-study area.

The deposits exposed along Indian Canyon in the Willow Springs Wash case-study area consist of four distinct, mappable **depositional** units; three deposited along wave-dominated shorelines (depositional units A, B, and C) and one deposited in a lobe of a fluvial-dominated delta (depositional unit D). Vertical offsets among the landward pinchouts of these individual depositional units indicate that three parasequences exist, the Kf-1-Indian Canyon (IC)-a, -b, and -c. Parasequence Kf-1-IC-c is composed of two depositional units, C and D, and represents an autocyclic change from wave- to fluvial-dominated deposition. This autocyclic change results in lithologic differences that only resemble a parasequence boundary between the two units.

Misidentification of parasequences and failure to distinguish between autocyclic and allocyclic changes involved in a rock succession can result in misunderstanding the depositional history, the distribution of related facies, and the quality and extent of the potential hydrocarbon reservoir. Models based on outcrop analogs such as the Ferron Sandstone in the Willow Springs Wash case-study area can provide insight into the complexities of these reservoir rocks.

Location of the Case-Study Area

The Willow Springs Wash case-study area is located about 15 miles (24 km) south of the town of Emery, Utah (figure 5-1). Within the case-study area, canyons provide three-dimensional exposures of the rock bodies. The canyons of particular interest are Indian Canyon, the North Fork of Indian Canyon, and Willow Springs Wash. Several locations within the study area are here informally named for convenience of reference (figure 5-2). "The Alcove" is a natural alcove found on the south side of the mouth of Indian Canyon. The North Fork of Indian Canyon has two branches at its head. These are here referred to as the "North Branch"and the "South Branch." "The Wall" refers to vertical exposures along the west and northwest sides of Indian Canyon.

Regional Setting

In the Willow Springs case-study area, Ferron outcrops consist of marine sandstone and shale of the Kf-1 parasequence set, and delta and alluvial-plain deposits associated with the Kf-2 through Kf-8 parasequence sets (refer to Chapter IV, Regional Stratigraphy for an explanation of Ferron sequence stratigraphic nomenclature). The sub-A coal overlying the Kf-1 and underlying the Kf-2 is a carbonaceous shale, which only locally develops into a coal. However, this carbonaceous shale is regionally extensive and serves as an important stratigraphic marker in the area. The landward pinchout of Kf-2 is seen on the north side of the mouth of Willow Springs Wash. Kf-2 is in turn overlain by the A coal zone. The Willow Springs Wash case study focused on deposits within Kf-1 (figure 5-3).

Methods

Data for the study came from measured sections, photomosaic mapping, paleocurrent studies, and facies mapping onto topographic maps. The measured section locations and the photomosaic coverage are shown in figure 5-4. Paleocurrent data locations and facies distributions will be shown below. All of the measured section and paleocurrent data, and interpreted photomosaics are available in Anderson and others (in press).

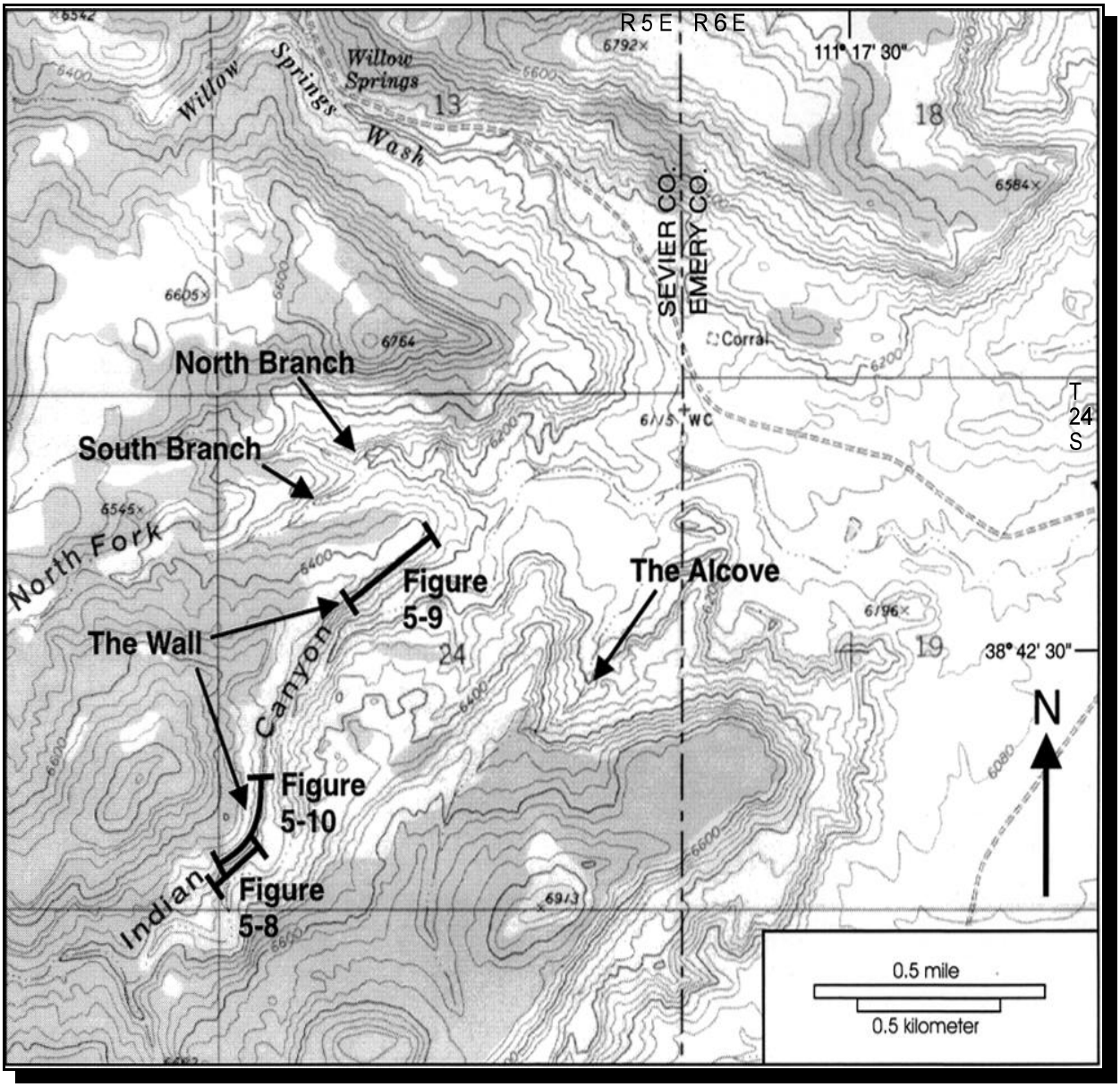


Figure 5-2. Detailed map of the Willow Springs Wash case-study area, including the informally named locations. Modified from the Willow Springs Quadrangle, Utah (U.S. Geological Survey 7.5 minute topographic map).

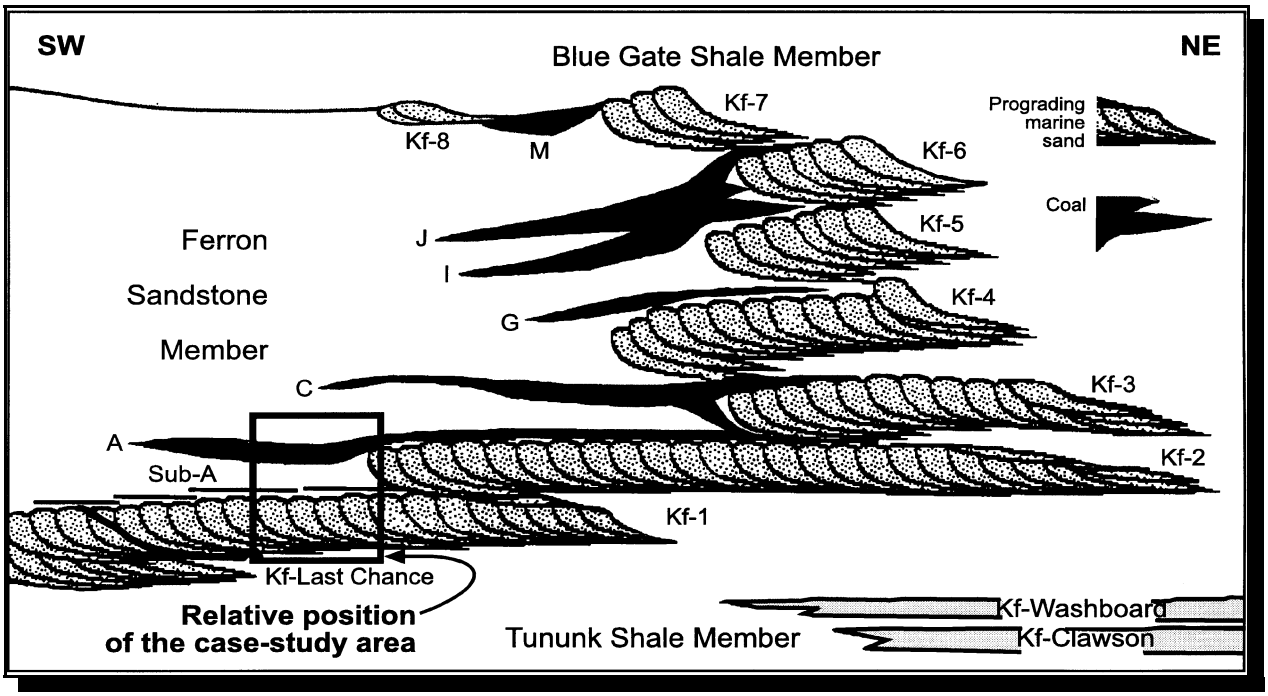


Figure 5-3. Diagrammatic cross section showing relative positions of Ferron parasequence sets with their associated coal zones (black), and the relative stratigraphic position of the Willow Springs Wash case-study area within the Ferron Sandstone (from Ryer, 1991; Anderson and others, 1997). The diagram has no scale.

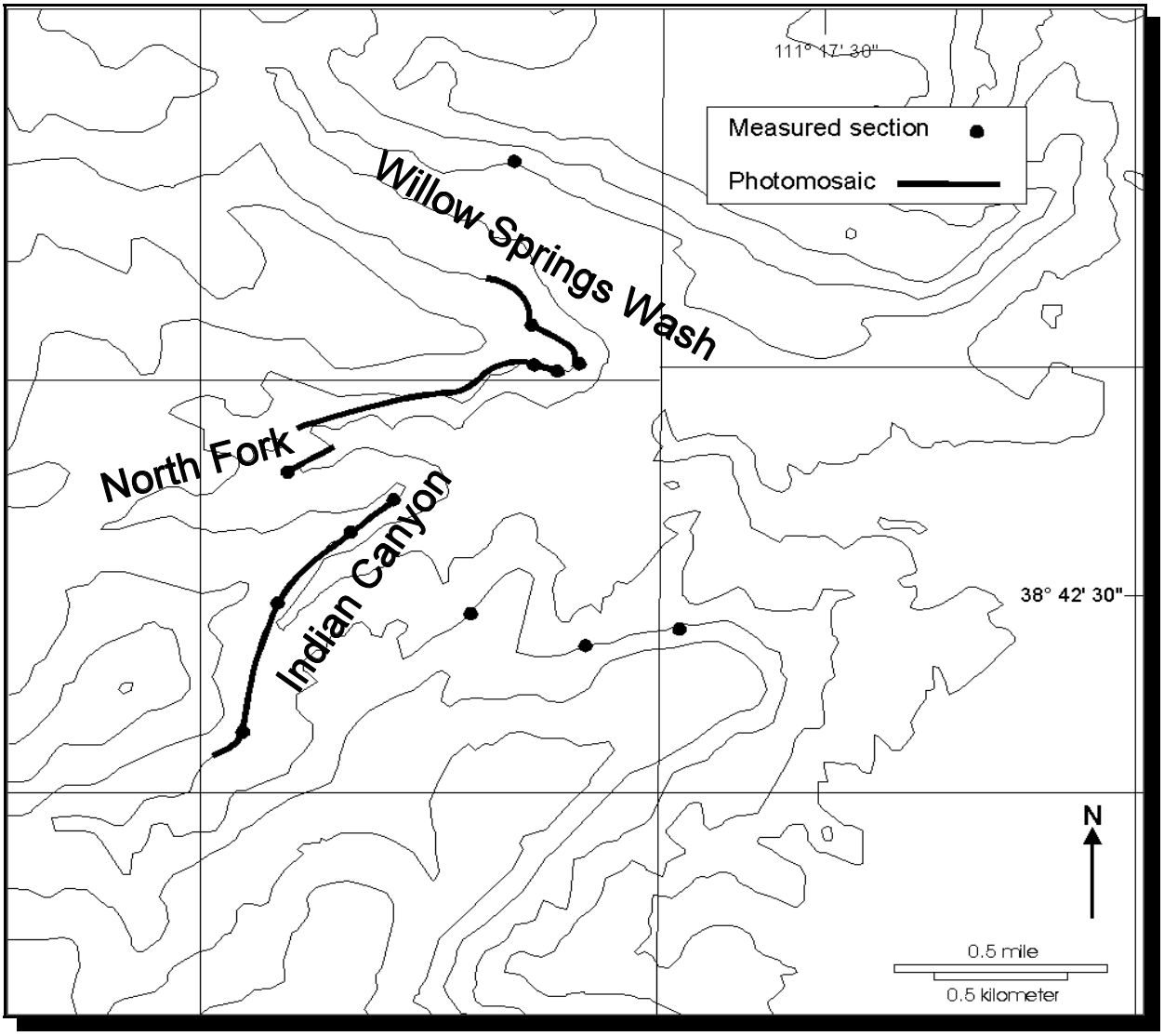


Figure 5-4. Map showing the locations of measured sections and the extent of photomosaic coverage within the case-study area. Refer to Anderson and others (in press) for measured sections and interpreted photomosaics.

Lithofacies

Eleven distinct lithofacies comprise the Kf-1 parasequence set in Indian Canyon of the Willow Springs Wash case-study area. These are distinguished by grain size; type and orientation of sedimentary structures; shape, orientation, and thickness of bedding; bioturbation and ichnofossils; and relationships between bounding surfaces and sedimentary structures (internal architecture). Variation between lithofacies is the direct result of changes in depositional conditions. In this chapter, lithofacies will be referred to by depositional facies names after the characteristics of each individual facies have been described.

In order to break down the outcrop into workable parts, distinct and mappable depositional units were identified. These depositional units are roughly analogous to parasequences as defined by Van Wagoner and others (1990), but differ in the sense that not all are bounded by a marine flooding surface. There are four sets of deposits, or depositional units, within the case-study area. These depositional units are designated A, B, C, and D from base to top, respectively. A sequence stratigraphic interpretation of these depositional units will be discussed later.

In addition, landward and seaward pinchouts of depositional units have been identified. Correlation of landward pinchouts suggests that the shorelines were oriented northwest-southeast during deposition of these units. Land was towards the southwest and the sea was to the northeast. This is in agreement with the observations of Ryer (1981a).

Lithofacies 1: Interbedded Siltstone and Shale

Lithofacies 1 consists of interbedded siltstone and shale. Beds are commonly 1 to 4 inches (3-10 cm) thick. The dominant sedimentary structures are asymmetric ripple lamination, horizontal lamination, and massive bedding. Some of the ripples appear to be starved ripples. Horizontal and vertical burrows of unknown affinity are common. The extent of this lithofacies within the A, B, and C depositional units is shown in figure 5-5A. Internal heterogeneities within this lithofacies are the result of interbedding of siltstone and shale beds, but there is relatively little horizontal variation within the lithofacies.

Lithofacies 1 is interpreted to have been deposited within the prodelta or inner shelf environment. Deposition was probably the result of unidirectional, turbidity currents.

Lithofacies 2: Hummocky Cross-Stratified Sandstone and Siltstone

Lithofacies 2 consists of interbedded very fine-grained sandstone and muddy siltstone. The siltstones are 1 to 6-inch- (3-15 cm-) thick beds and the interbedded sandstones vary in thickness between 4 and 10 inches (10-25 cm). Asymmetric ripple lamination and horizontal lamination are common within the siltstones. Sandstone beds show scoured bases. The sandstones are characterized by hummocky or swaley cross-stratification. The tops are commonly ripple-laminated or rarely show low-angle, small-scale trough cross-stratification. Siltstone is commonly bioturbated and shows both horizontal and vertical burrows. Tops of sandstone beds are also bioturbated, with the degree of bioturbation rapidly diminishing downward. The aerial extent of this lithofacies within the different depositional units is shown in figure 5-5B. Heterogeneity within this lithofacies results from a combination of vertical grain-size variation due to interbedding and horizontal pinch-and-swell of individual hummocky cross-stratified sandstone beds.

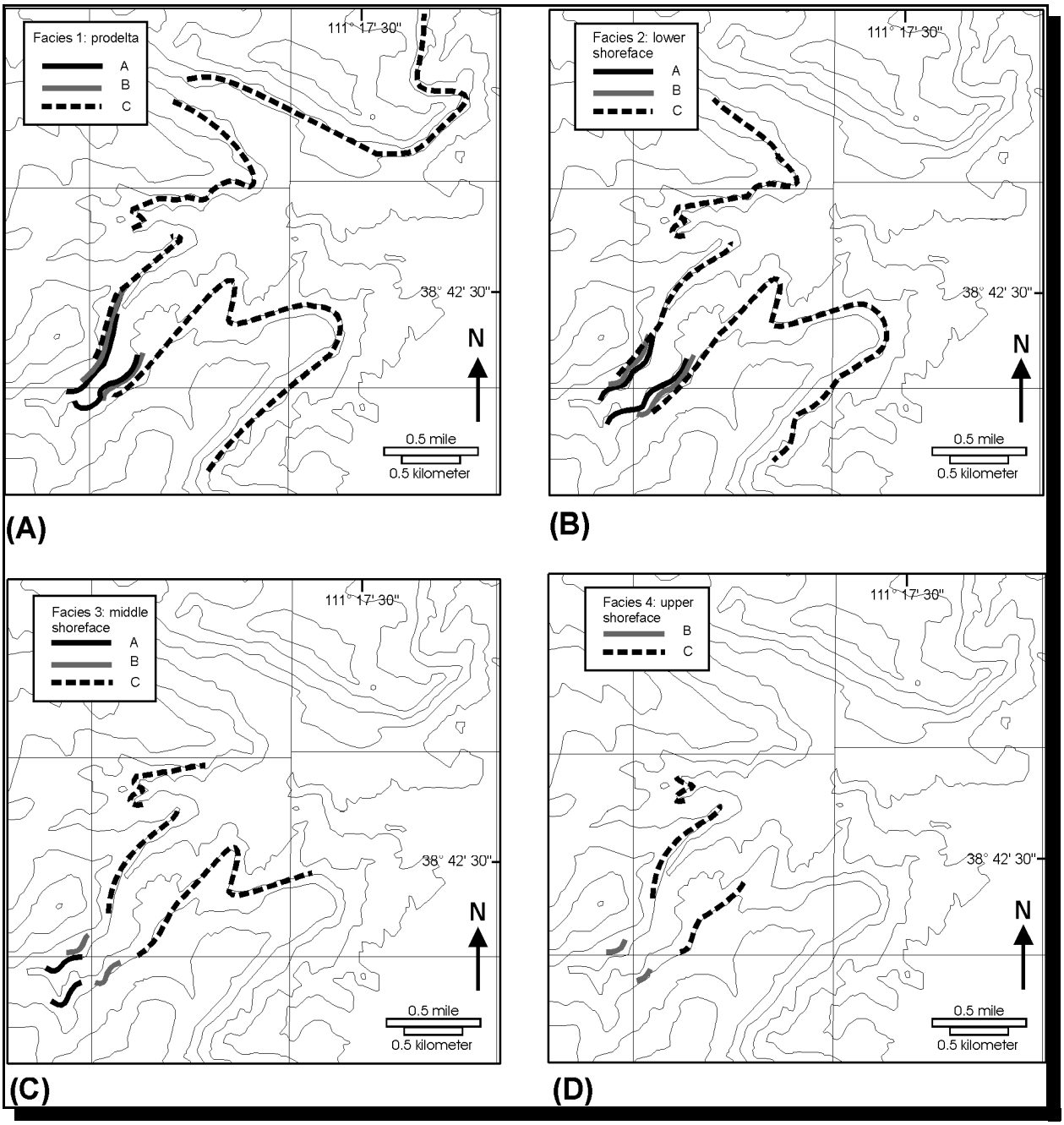


Figure 5-5. Maps showing extent of outcrops of the: (A) prodelta, (B) lower shoreface, (C) middle shoreface, and (D) upper shoreface/ebb-tidal delta facies within depositional units A, B, and C. Depositional unit A is incompletely exposed. Depositional unit B is poorly developed. These facies are absent within depositional unit D.

Lithofacies 2 represents deposition within a lower shoreface environment. Hummocky cross-stratification has been interpreted as forming below fair weather wave-base (Dott and Bourgeois, 1982). Small-scale trough cross-stratification and asymmetric ripple lamination formed as a result of unidirectional currents during the waning of storms. Siltstone deposition and bioturbation represent relatively calm conditions between storms.

Lithofacies 3: Inclined, Medium-Bedded, Planar-Laminated Sandstone

Lithofacies 3 consists of medium-bedded, very fine-grained sandstone with very little siltstone and mudstone. Sandstone beds, 1 to 2 feet (0.3-0.6 m) thick, are inclined to the northeast (seaward). This lithofacies consists of beds with a well-laminated lower portion and a bioturbated upper portion which, from a distance, appear to be alternating well indurated and friable sandstones, respectively. The lower portion shows inclined planar-lamination and ripple-lamination (symmetric and asymmetric) with some scour-and-fill trough cross-stratification. The bioturbated portion of these sandstone beds contain abundant vertical burrows assigned to *Cylindrichnus*, *Ophiomorpha*, and *Thalassanoides*. The aerial extent of this lithofacies within the various depositional units is shown in figure 5-5C. Heterogeneity of this lithofacies results from differences in the amount of bioturbation within individual beds and from the orientation of the beds within the lithofacies. Bedding within the facies is oriented diagonally to bedding within underlying and overlying lithofacies. Any difference in permeability and porosity between the lower, well-laminated portion and the upper, bioturbated portion of individual beds would result in migration of fluids along the bed and diagonally through the facies.

Lithofacies 3 formed within a middle shoreface environment. Deposition was episodic, as evidenced by the presence of discrete zones of bioturbation. The absence of siltstone and mudstone in this environment has two possible causes. First, the energy within the system during "normal" conditions was such that mud and silt were winnowed. Second, the frequency and magnitude of storms was such that any mud and silt that may have been deposited during calm conditions was removed by the next storm.

Lithofacies 4: Thick-Bedded, Trough and Tabular Cross-Stratified Sandstone

Lithofacies 4 consists of very thick beds, 10 to 15 feet (3-5 m) of fine- to very fine-grained sandstone. Internally these beds show abundant trough and/or tabular cross-stratification. Within the lower two-thirds of this lithofacies, the cross-stratification appears to be oriented towards the northeast (seaward). Cross-stratification within the upper one-third is oriented towards the southwest (landward) and shows more variability in paleocurrent direction. Bioturbation is also common within this lithofacies. Vertical burrows (*Ophiomorpha* ?) are present, but for the most part burrow types are not recognizable. The lateral extent of this lithofacies within the various depositional units is shown in figure 5-5D. This lithofacies appears to be relatively homogeneous when compared to the underlying lithofacies 3 (middle shoreface). There are relatively few breaks in bedding and no observable grain size variation.

Lithofacies 4 represents deposition within the upper shoreface of a barred shoreline or within an ebb-tidal delta environment. The details of this interpretation will be discussed later.

Lithofacies 5: Thick-Bedded, Inclined Planar-Laminated Sandstone

Lithofacies 5 consists of thick-bedded, 3 to 5 feet (1-1.5 m), fine-grained sandstone. Internally, the sandstone beds display inclined planar-lamination. The laminae typically dip to the northeast (seaward) but some laminae, though rare, dip to the southwest. The top of this lithofacies also shows minor scour-and-fill with lensoidal geometries and thicknesses up to 1.5 feet (1.2 m). The top of this lithofacies has been rooted by plants from overlying carbonaceous shales. The lateral extent of this lithofacies within the various depositional units is shown in figure 5-6A. As with the upper shoreface, this lithofacies appears to be relatively homogeneous. Lamination within this lithofacies is probably the result of alternating grain-size variation between laminae, however, this variation is not pronounced. In addition, the contact between this lithofacies and the underlying upper shoreface is commonly gradational with no obvious barrier to fluid flow at the boundary.

Lithofacies 5 is interpreted to form within a foreshore or beach environment. Rare, landward-dipping laminae probably formed on the landward side of a berm. Channelization at the top of the facies was possibly caused by minor tidal channels.

Lithofacies 6: Sigmoidal-Bedded, Cross-Stratified Sandstone

Lithofacies 6 consists of sigmoidal beds of fine to medium-grained sandstone. Beds vary in thickness from 0.5 to 2 feet (0.2-0.6 m). Lithofacies 6 shows scour into underlying deposits of lithofacies 4. The depth of scour and overall thickness of the lithofacies increase from about 4 feet (1.2 m) where it begins in "The Wall" to greater than 10 feet (3 m) towards the southwest (landward). Individual beds thin and become tangential to the base of the lithofacies, forming a foreset and a bottomset. Comparison of bedding plane orientations with landward pinchouts shows that the beds dip to the southwest (oblique to shore). Individual beds are probably separated by fine-grained breaks, but this is hard to verify given the inaccessibility of exposure within the study area. Internally, the beds are trough cross-stratified. Paleocurrent orientations of these troughs show movement of sediment perpendicular to the dip direction of the beds, suggesting that this lithofacies developed by lateral accretion rather than downstream accretion (Miall, 1985). The facies is overlain by foreshore deposits that probably eroded any topset bedding. Some bioturbation is present, but burrow types were not recognized. The lateral extent of the lithofacies in depositional unit C is shown in figure 5-6B. Heterogeneity within this facies results from the bedding plain breaks between the sigmoidal-shaped beds. The horizontal variation in thickness of the facies is also a source of heterogeneity.

Lithofacies 6 is interpreted to represent deposits within a tidal inlet. Scour formed as a result of tidal currents passing through the inlet. The inlet was filled by a spit that developed through a combination of longshore drift and tidal currents. Spit development and southeastward inlet migration were followed by development of a foreshore. This lithofacies is differentiated from deposits of meandering fluvial and distributary channels by bioturbation, its position relative to foreshore deposits, and the lack of a spatially-related, lensoidal, channel-sandstone body.

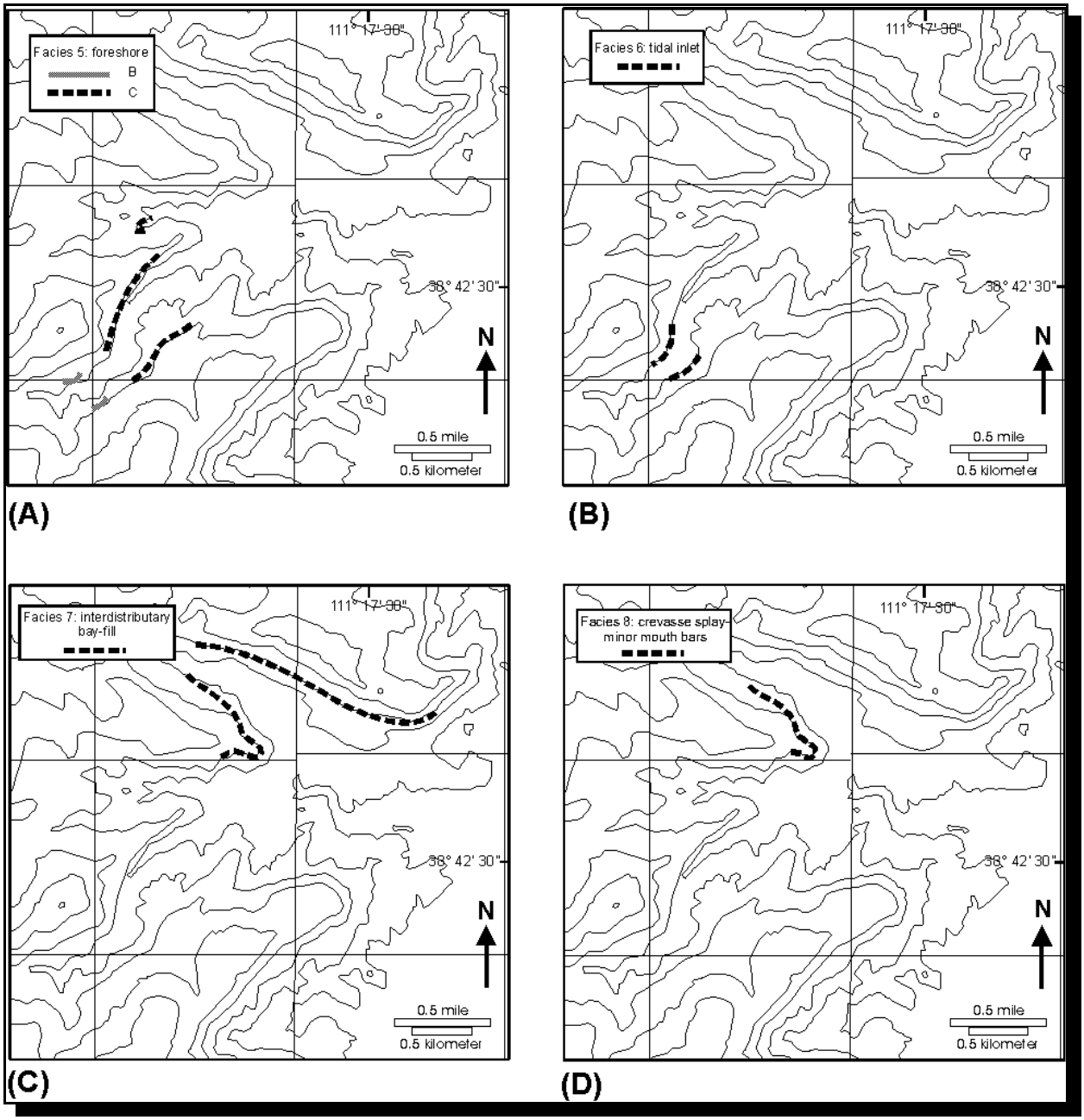


Figure 5-6. Maps showing the extent of outcrops of the: (A) foreshore, (B) tidal-inlet, (C) interdistributary bay-fill, and (D) crevasse splay/distributary-mouth bar facies. Foreshore deposits are present in depositional units B and C. Tidal inlet deposits are only found in depositional unit C. Interdistributary bay-fill and crevasse splay deposits are only found in depositional unit D.

Lithofacies 7: Shale with Interbedded Sandstone

Lithofacies 7 consists of silty shale interbedded with very fine-grained sandstone. Sandstone is relatively minor compared to the siltstones and shales. Shale beds range from 0.5 to 2 feet (0.2-0.6 m) in thickness. Sandstones are typically thin, 0.5 to 1 feet (0.2-0.3 m), but do thicken and become bedsets (grouping of beds that are genetically related as opposed to the use of bedset in our sequence stratigraphic nomenclature; see Chapter IV and discussion later in the chapter) within overlying deposits of lithofacies 8. Ripple-lamination, horizontal lamination, and massive bedding are common within the shales. The sandstones are typically horizontal- or wavy-bedded and ripple-laminated. They are volumetrically minor (less than 10 percent) compared to the shales. Burrowing is abundant, but burrow types were not recognized. The lateral extent of the lithofacies in depositional unit D is shown in figure 5-6C. The lithofacies is not present within depositional units A, B, or C. Lithofacies 7 is heterogeneous vertically and horizontally as a result of interbedding, and the thinning and pinching out of sandstone beds. Furthermore, the fine-grain size should result in poor permeability.

Lithofacies 7 is interpreted as interdistributary bay-fill deposits. These deposits are, in some respects, similar to those of the inner shelf and lower shoreface (lithofacies 1 and 2), and are distinguished in part by their relation to deposits of distributary channels and crevasse splays. In this respect, the distinction between deposits of lithofacies 7 and those of lithofacies 1 and 2 is partly model driven. However, lithofacies 7 does contain less silt and is more aerially restricted than lithofacies 1 and 2. While these observations render an identification within a core difficult, correct identification of the facies does allow estimates of the geographic distribution of the facies.

Lithofacies 8: *En Echelon* Sandstone Bedsets and Interbedded Shales

Lithofacies 8 consists of *en echelon* bedsets of fine- to medium-grained sandstone separated by silty shales. Individual sandstone bedsets start stratigraphically high within the facies as thin units and thicken to about 4 feet (1.2 m). At some point they begin to thin and drop stratigraphically beneath subsequently deposited bedsets. The toes of individual bedsets interfinger with underlying interdistributary bay-fill deposits (lithofacies 7). Sandstone bedsets are isolated from each other by shale and siltstone drapes. These interbedded shales and siltstones range in thickness from less than 1 foot to greater than 2 feet (0.3-0.6 m). Internally, sandstones show a variety of sedimentary structures including trough, tabular, and sigmoidal cross-stratification and planar-lamination. Bedforms appear to be unidirectional and show migration to the northwest. Bedform orientation, in conjunction with northwest-dipping bounding surfaces, suggest that these bedsets grew by "downstream" accretion rather than lateral accretion (Miall, 1985). The tops of sandstone bedsets are locally scoured and filled with trough and tabular cross-stratified sandstone. The total aerial extent of this lithofacies within depositional unit D is shown in figure 5-6D, but it should be noted that the total length of an individual sandstone bedset may only reach 300 to 400 feet (90-120 m). Heterogeneity within this lithofacies results from isolation of sandstone bedsets within silty shales and shale drapes within sandstone bedsets. The *en echelon* stacking pattern of the sandstone bedsets should also affect fluid flow in a manner similar to that of the middle shoreface.

Lithofacies 8 is interpreted to be the deposits of a crevasse splay system that developed within an interdistributary bay. Individual sandstone bedsets are the deposits of minor distributary-mouth bars. Scouring at the tops of these bars was the result of progradation of the minor distributary channels that fed the bars.

Lithofacies 9: Multistory, Lensoidal Sandstone

Lithofacies 9 consists fine- to medium-grained, multistory, lensoidal sandstone bodies. The multistory set reaches a total thickness of 20 to 30 feet (6-9 m). The entire set shows scour down to underlying interdistributary bay-fill (lithofacies 7), crevasse splay (lithofacies 8) and middle shoreface deposits (lithofacies 3). Within this multistory sandstone, multiple episodes of scour-and-fill are evident. Each scour-and-fill set varies in thickness from about 3 to 5 feet (1-1.5 m). Trough cross-stratification is abundant within the scour-and-fill deposits. Thin, fine-grained, ripple-laminated sandstone is common at the top. Extending laterally from the scour-and-fill deposits is a deposit composed of two thick beds of climbing, asymmetric ripple-laminated, very fine to fine-grained sandstone. Ripple-drift direction is away from the multistory channel system. The ripple-laminated deposit has a flat base that appears to have been scoured into underlying interdistributary bay-fill sediments (lithofacies 7). The depth of scour increases towards the multistory scour system. The aerial extent of the combined lithofacies is shown in figure 5-7A. The effect of this facies on heterogeneity within a reservoir is variable. The abundance of scour-and-fill within the lithofacies could be detrimental if there are fine-grained drapes acting as baffles. This type of drape has been observed by the author within other channels in the Ferron Sandstone, but the inaccessibility of the exposure within the Willow Springs Wash case-study area makes this difficult to verify for the North Fork Canyon outcrops. The fact that this lithofacies scours into underlying middle shoreface, interdistributary bay-fill, and other lithofacies suggests that the multistory channel lithofacies could actually serve to enhance the connectivity of otherwise isolated reservoir rock within single or multiple parasequences.

Lithofacies 9 is interpreted to be a distributary channel system. The multistory nature of the channel system suggests that the distributary had a straight reach in contrast to a multilateral, meandering channel. The thick-bedded, ripple-laminated units probably represent deposits within a sub-aqueous levee associated with the distributary channel and are similar to sub-aqueous levees described by Coleman (1976).

Lithofacies 10: Multilateral, Lensoidal Sandstone

Lithofacies 10 crops out along the south wall of Indian Canyon. It consists of two parts: lateral accretion deposits and lensoidal channel deposits. The lateral accretion deposits are exposed within “The Alcove” and consist of westward dipping, medium-thick beds of fine- to medium-grained sandstone. Northward-dipping trough cross-stratification and planar-lamination are abundant and confirm the laterally accreting nature of the beds. These lateral accretion sets terminate laterally into the second type of deposit. The second deposit consists of lensoidal sandstone bodies 15 to 20 feet (5-6 m) thick. These contain fine- to medium-grained sandstone. Like the multistory channel system, this lithofacies shows scour down into middle shoreface deposits. The size of the bedforms and the bedding within the lensoidal bodies decrease upward. The bases of the lensoidal sandstones show large scale, 2 to 3 feet (0.6-0.9 m), trough cross-stratification. The tops of lenses contain abundant asymmetric ripple lamination. The location of the outcrop of this lithofacies is shown in figure 5-7B. As with the multistory channel lithofacies, the effect on reservoir heterogeneity is probably variable. Fine-grained drapes within the lateral accretion sets would act

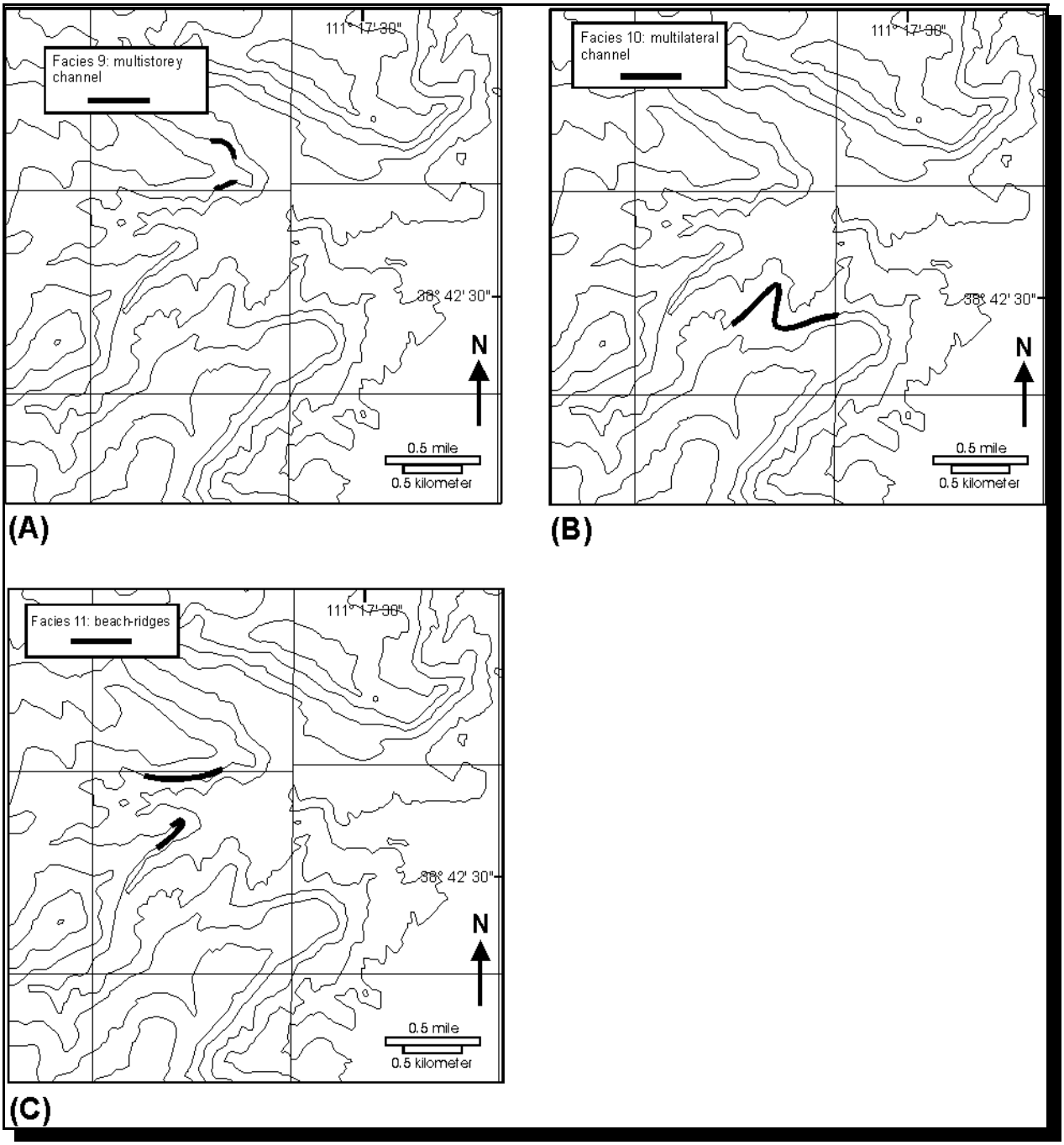


Figure 5-7. Maps showing the extent of outcrops of the: (A) multistory channel, (B) multilateral channel, and (C) strand plain facies. All of these facies are specific to depositional unit D.

as baffles, however, this lithofacies also scours into underlying deposits and connects isolated rock bodies. This lithofacies is more extensive laterally than the multistory channel lithofacies and the deposits within the lensoidal sandstone are as thick as the multistory channel deposits.

Lithofacies 10 is interpreted as a distributary channel system. Unlike the lithofacies 9, this channel system was deposited as a meandering channel system, or meanderbelt, rather than a multistory system with a straight reach. The lateral accretion sets of this lithofacies are distinguished from those of lithofacies 6 (tidal inlet) in that these lateral accretion sets are directly associated with lensoidal channel sandstones. Furthermore, the tidal inlet lithofacies shows evidence of marine bioturbation.

Lithofacies 11: Planar-Bedded, Cross-Stratified Sandstone and Siltstone

Lithofacies 11 is best preserved at the top of the north wall of North Fork and "North Branch" canyons within depositional unit D. The lithofacies consists of interbedded fine sandstone and muddy siltstone. The lithofacies has three distinct, upward-coarsening bedsets. The bedsets are planar and horizontal, and maintain a relatively constant thickness of about 3 feet (1 m). Local scour-and-fill is present, but rare. These scour-and-full structures are never more than about 1 feet (0.3 m) deep, the thickness of any given sandstone bed within the lithofacies. Internally, trough and tabular cross-stratification are the most abundant features within the sandstones. Siltstones are commonly ripple-laminated. Bioturbation is rare. This lithofacies is laterally extensive in the case-study area (figure 5-7C) and fairly homogeneous horizontally. Interbedding of sandstone and siltstone would create barriers to fluids flowing perpendicular to bedding.

This lithofacies is interpreted as cuspate, strand plain/beach ridge deposits extending from the mouths of rivers along wave-dominated shorelines. As a distributary enters a wave-dominated basin, it induces currents that move along shore from the distributary mouth (Heward, 1981). Similar deposits are seen in the modern Sao Francisco delta (Coleman, 1975).

Depositional Systems

These lithofacies can be grouped into two major depositional systems: wave-dominated shoreline and fluvial-dominated delta (table 5-1). Figures 5-5 through 5-7 help to illustrate some of the differences in scale of the deposits within these individual systems. From the above descriptions, it is also apparent that the two depositional systems differ in terms of grain size, bed thickness, bedding orientation, overall lithofacies thickness, and aerial extent of the lithofacies. In general, deposits of the fluvial-dominated delta are thinner, richer in mud, and less laterally extensive than wave-dominated shoreline deposits. These differences come into play when viewed in the context of common well spacings in oil fields.

Recognition of individual facies (lithofacies and depositional) and the depositional systems to which they pertain is important for two reasons. First, correct facies identification will allow more accurate prediction of the locations of adjacent facies. Second, correct facies identification will help to predict the size, shape, and connectivity of different sandstone bodies and the types of barriers to fluid flow within these sandstone bodies. This type of knowledge is useful in planning well spacing, and in secondary and tertiary recovery strategies.

Table 5-1. Lithofacies and depositional within the case-study area and their presence within wave-dominated shoreline or fluvial-dominated deltaic depositional systems.

Lithofacies	Depositional facies	Wave-dominated shoreline	Fluvial-dominated delta
Interbedded silt and shale	Prodelta-inner shelf	x	x
Hummocky cross-stratified sand and silt	Lower shoreface	x	
Inclined bedded, planar-laminated sand	Middle shoreface	x	
Thick-bedded, trough and tabular cross-stratified sand	Upper shoreface/ebb-tidal delta	x	
Thick-bedded, inclined planar-laminated sand	Foreshore	x	
Sigmoidal-bedded, cross-stratified sand	Tidal inlet	x	
Shale and interbedded sand	Interdistributary bay-fill		x
En echelon sand and interbedded silty shale	Crevasse splay-minor distributary-mouth bar		x
Multistory, lensoidal sand	Multistory channel		x
Multilateral, lensoidal sand	Multilateral channel		x
Planar-laminated, cross-stratified sand and silt	Strand plain/beach ridge		x

Sequence Stratigraphy

Sequence stratigraphic concepts allow the geologist to interpret the rock record in a chronostratigraphic context. Rocks can be divided and correlated according to depositional packages that are roughly time equivalent. This approach is a more powerful tool for prediction of facies locations. In the case of the Willow Springs Wash case-study area, the rocks are divided on the basis of temporal changes of relative sea-level. Viewed in terms of relative sea-level change, the difference between autocyclic causes of depositional variation, such as stream avulsion and delta lobe switching, and allocyclic causes, such as eustatic sea-level change or tectonic subsidence, can be determined (Ryer and others, 1995).

The rocks within Indian Canyon can be divided at the parasequence scale of Van Wagoner and others (1990). They defined a parasequence as a "relatively conformable succession of beds and bedsets bounded by marine-flooding surfaces or their correlative surfaces." A marine-flooding surface is defined as a "surface separating younger from older strata across which there is evidence of an abrupt increase in water depth."

Marine-flooding surfaces are commonly interpreted within cores as surfaces below marine shales and above shallower-water sediments. In well logs, marine-flooding surfaces are interpreted on the basis of abrupt decreases in grain size. Identifying marine-flooding surfaces on the basis of grain size changes, however, is not an entirely accurate practice since changes in grain size may be the result of other factors. This being the case, other criteria should be used where possible.

Within Indian Canyon, landward pinchouts of marine sandstones can be identified. These are useful in identifying stratigraphic positions of the marine units relative to each other. Vertical offset between two different landward pinchouts suggests that some amount of change in relative sea-level, whether due to compaction subsidence, local tectonic subsidence, or change in eustatic sea-level, has occurred. If there is no vertical offset between the two pinchouts, then no relative sea-level change has occurred and the surface representing the boundary between the two depositional units is not a marine-flooding surface.

Based on facies stacking patterns, the deposits exposed along Indian Canyon in the Willow Springs Wash case-study area consist of the four distinct, mappable depositional units introduced in the preceeding section; three deposited along wave-dominated shorelines (depositional units A, B, and C) and one deposited in a lobe of a fluvial-dominated delta (depositional unit D). The surfaces between depositional units A and B, and B and C are identified as marine-flooding surfaces, based on vertical offsets between landward pinchouts (figure 5-8). Thus three parasequences exist. However, an examination of the pinchout of depositional unit D shows that this unit pinches out beneath the surface that represents the top of the Kf-1-IC-c parasequence marine sandstone (figure 5-9). In fact, depositional unit D becomes amalgamated with the underlying depositional C close to the pinchout. The coincidence between the stratigraphic positions of the tops and the pinchouts of the two units suggests that no rise in relative sea level occurred and that the surface marking the boundary between the two units is not a parasequence boundary. Thus, Kf-1-IC-c (depositional units C and D) represents an autocyclic change from wave- to fluvial-dominated deposition. This autocyclic change results in lithologic differences that only resemble a parasequence boundary and therefore these depositional units must be considered as a single parasequence.

Based on the relationships between pinchouts, the rocks in the Indian Canyon-Willow Springs Wash are divided into three parasequences (figure 5-10). These are designated from base to top as Kf-1-Indian Canyon (IC)-a, -b, and -c. Parasequence Kf-1-IC-a consists of deposits of depositional unit A. Parasequence Kf-1-IC-b consists of deposits of depositional unit B. Parasequence Kf-1-IC-c consists of deposits of both depositional units C and D. Depositional unit D is therefore a bedset within parasequence Kf-1-IC-c and given the designation Kf-1-IC-c[d].

Depositional History

Kf-1-Indian Canyon-a

The depositional history of the case-study area can now be interpreted on the basis of parasequence formation. Figure 5-11A shows a paleogeographic reconstruction of the case-study area during deposition of parasequence Kf-1-IC-a. Outcrops of this parasequence display a coarsening-upward, progradational succession of beds. The visible facies include prodelta-inner shelf, lower shoreface, and middle shoreface (figure 5-10). This parasequence disappears into the subsurface in Indian Canyon and details of the formation and geometry of this parasequence are speculative. Based on the available outcrop, however, some inferences can be made.

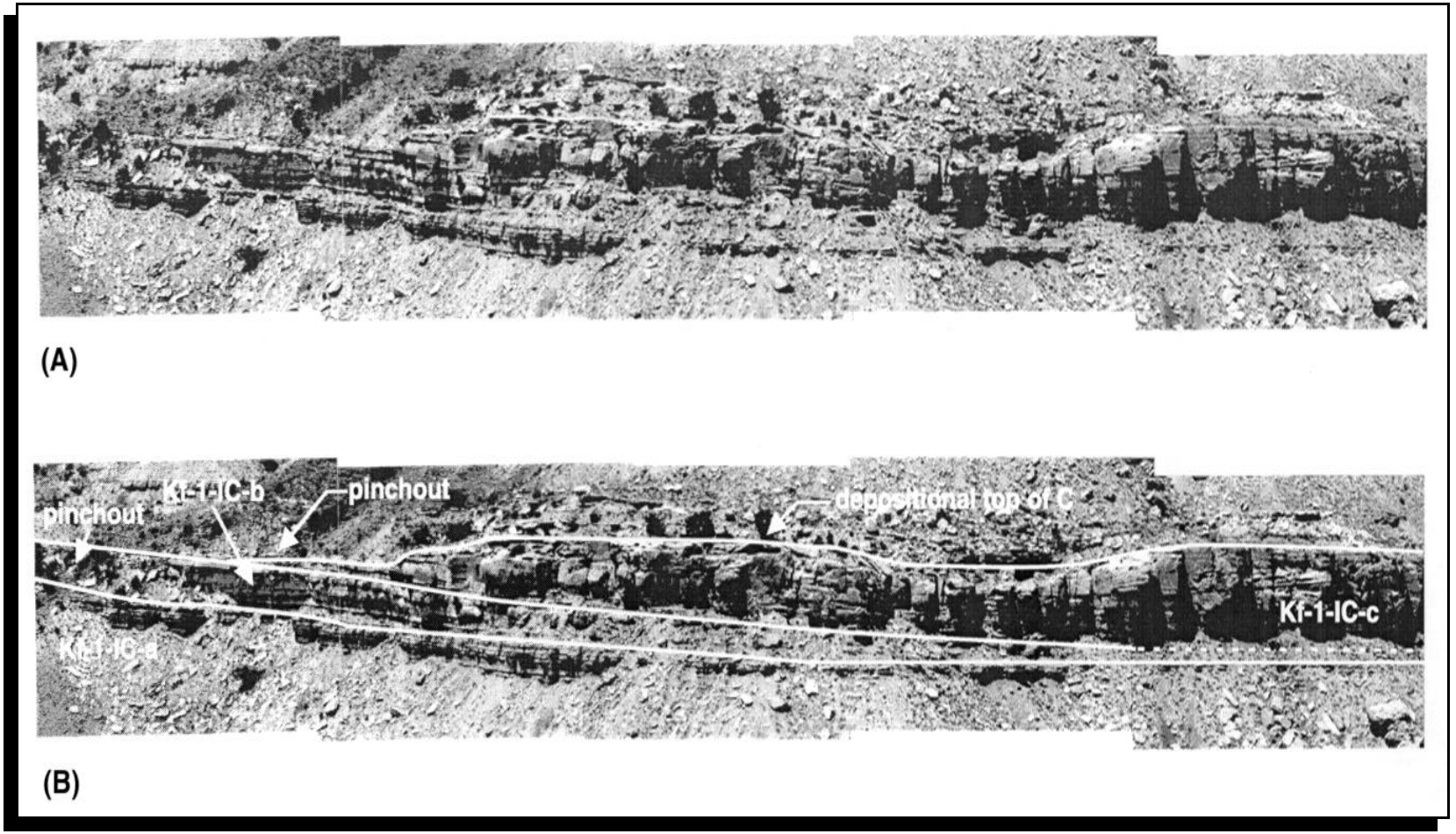


Figure 5-8. Uninterpreted (A) and interpreted (B) photomosaics of parasequences Kf-1-IC-a, -b, and -c. Note landward pinchouts of marine sandstones in parasequences Kf-1-IC-b and -c. Cliff on the right side is approximately 45 to 50 feet (14-15 m) high. The location is at the southwest end of "The Wall," view is to the northwest. See figure 5-4 for location of photomosaic.

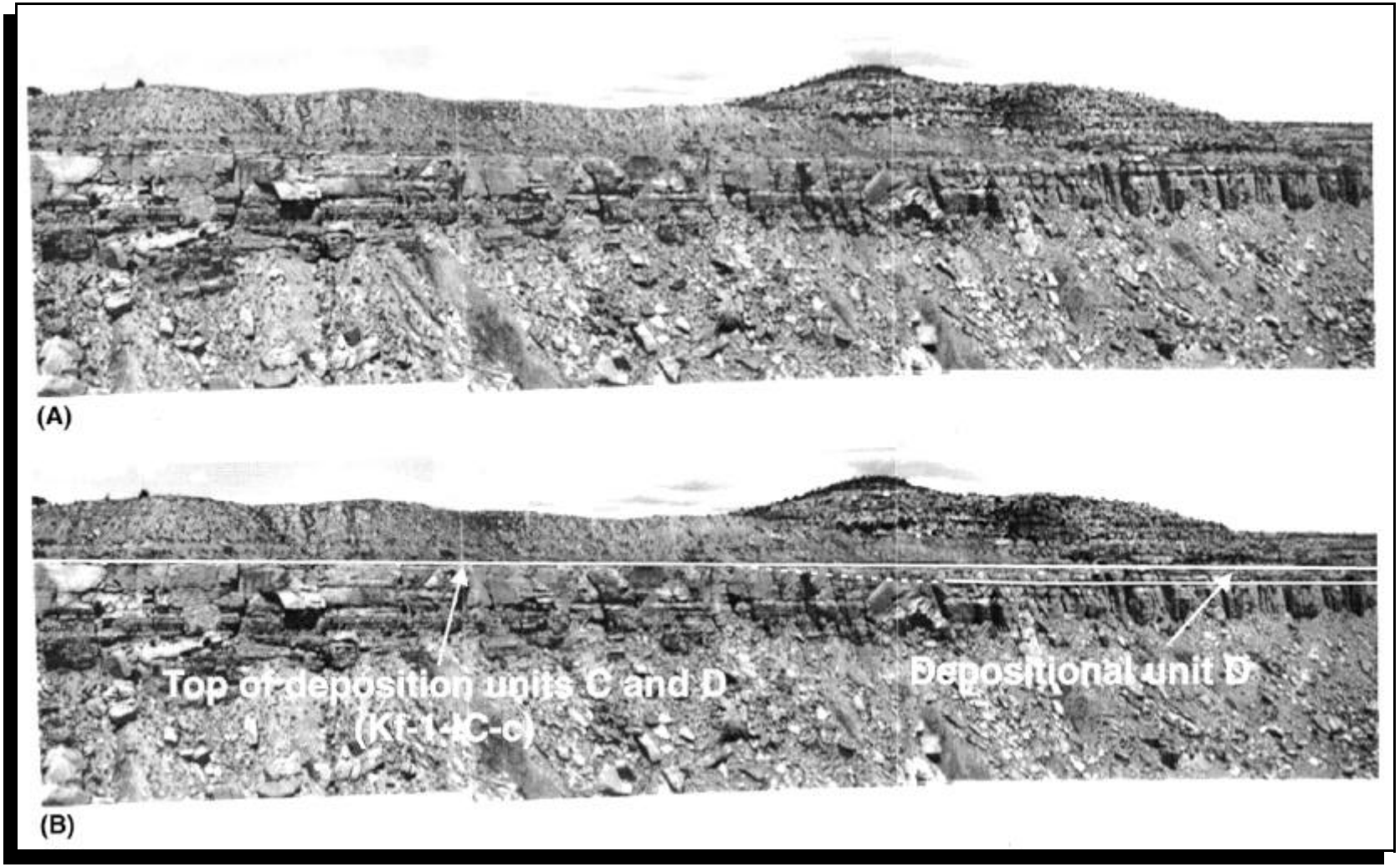


Figure 5-9. Uninterpreted (a) and interpreted (b) photomosaics showing depositional units C and D within parasequence Kf-1-I C-c. This exposure is down depositional dip from the exposure in figure 9. See figure 5-4 for location of photomosaic.

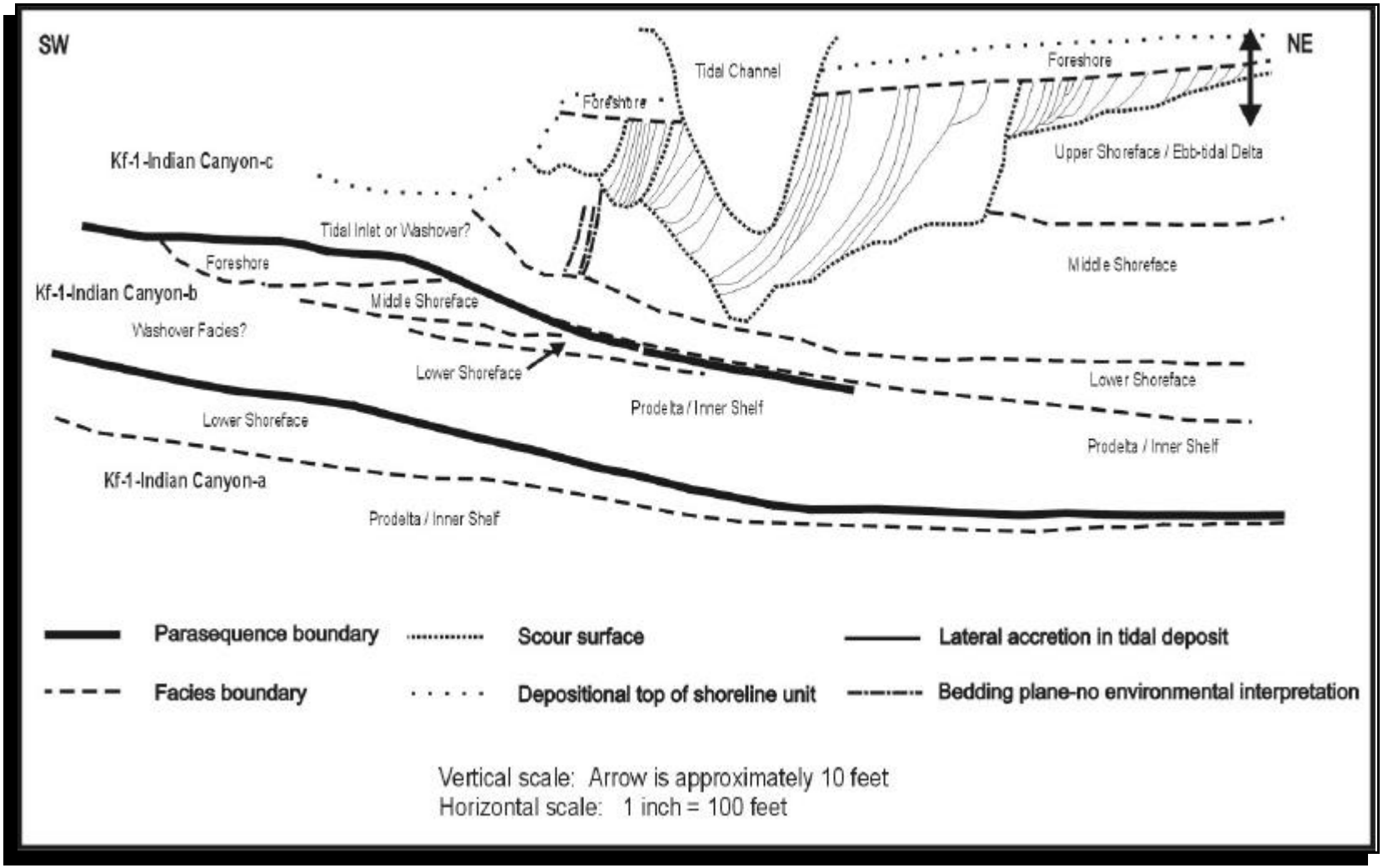


Figure 5-10. Generalized southwest-northeast cross section along "The Wall" showing parasequences Kf-1-IC-a, -b, and -c, and major depositional facies. See figure 5-4 for location of photomosaic.

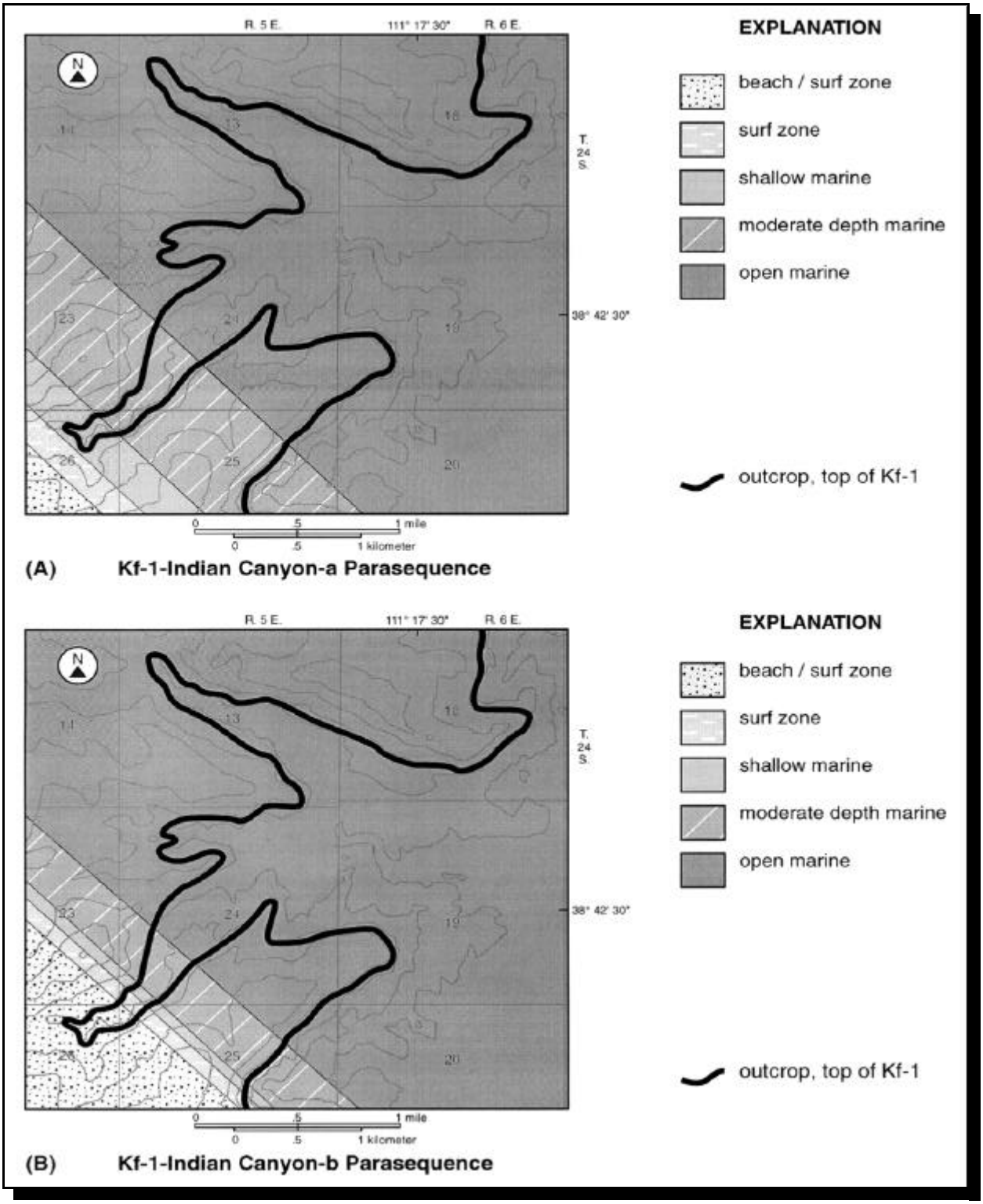


Figure 5-11. Paleogeographic maps of the case-study area during deposition of parasequences Kf-1-IC-a (map A) and -b (map B). These parasequences are characterized by deposition along wave-dominated shorelines. The narrower facies belts of Kf-1-IC-b are possibly the result of a shoreface with a higher gradient than the shoreface of Kf-1-IC-a.

The lower and middle shoreface of the parasequence are very well developed. By comparison with the same facies in other parasequences, we can infer that the Kf-1-IC-a parasequence also contains a well developed upper shoreface and foreshore. The presence of any other facies is uncertain. The shoreline is inferred to have a northwest-southeast orientation. Due to the wave-dominated nature of the shoreline, the deposits within parasequence Kf-1-IC-a are inferred to be linear. The total dimensions of the parasequence are unknown.

Kf-1-Indian Canyon-b

Figure 5-11B shows a paleogeographic reconstruction of the case-study area during deposition of parasequence Kf-1-IC-b. Outcrops of this parasequence display a coarsening-upward, progradational succession of beds and bedsets. Depositional facies observed within this parasequence include the prodelta, a poorly developed lower and middle shoreface, and a foreshore (figure 5-10). The areal extent of this parasequence is very restricted and probably represents only about 500 to 600 feet (150-180 m) of progradation. This parasequence is also inferred to have been deposited along a wave-dominated shoreline. As such, it probably had a morphology similar to that of parasequence Kf-1-IC-a. Mapping of the areal extent of this facies shows facies belts that are narrow compared to those of parasequences Kf-1-IC-a and -c. This suggests that the gradient of the shoreface in parasequence Kf-1-IC-b was probably higher than the gradients of shorefaces in parasequences Kf-1-IC-a and -c.

Kf-1-Indian Canyon-c

The Kf-1-IC-c parasequence had a much more complex history than the previous two parasequences and its development will be considered in various stages.

Stage 1. Barrier-tidal inlet: Figure 5-12A is a paleogeographic reconstruction of the shoreline during deposition of Stage 1 of parasequence Kf-1-IC-c. The base of Kf-1-IC-c is seen at its most landward extent where lower and middle shoreface sandstones overlie planar-laminated foreshore sandstone of Kf-1-IC-b. The tidal channel deposits of facies 6 and medium-bedded, isolated, and mollusk-bearing sandstones located just landward of the landward pinchout suggest that a local embayment existed immediately landward of the shoreline at the beginning of the Kf-1-IC-c parasequence. Southwest-dipping foresets within the tidal inlet suggest that the inlet filled with deposits from a laterally accreting spit. Sediment supply was such that progradation could occur. Seaward of the inlet mouth, ebb-tidal delta deposits may have accumulated with paleocurrent indicators showing northeast-directed flow (figures 5-10, 5-12A, and 5-13A). The embayment itself, however, probably did not last long since such lagoons tend to rapidly fill with sediment (Heward, 1981).

Stage 2. Wave-dominated shoreline: After continued migration of the tidal inlet, wave action was the dominant process affecting the case-study area. Longshore currents might have been important at this time, however, this has not been documented to date. Much of the shoreline progradation occurred at this time. As the shoreline prograded and the embayment behind it filled, tidal channels and creeks increased in their importance in distributing the tidal prism (figure 5-12B).

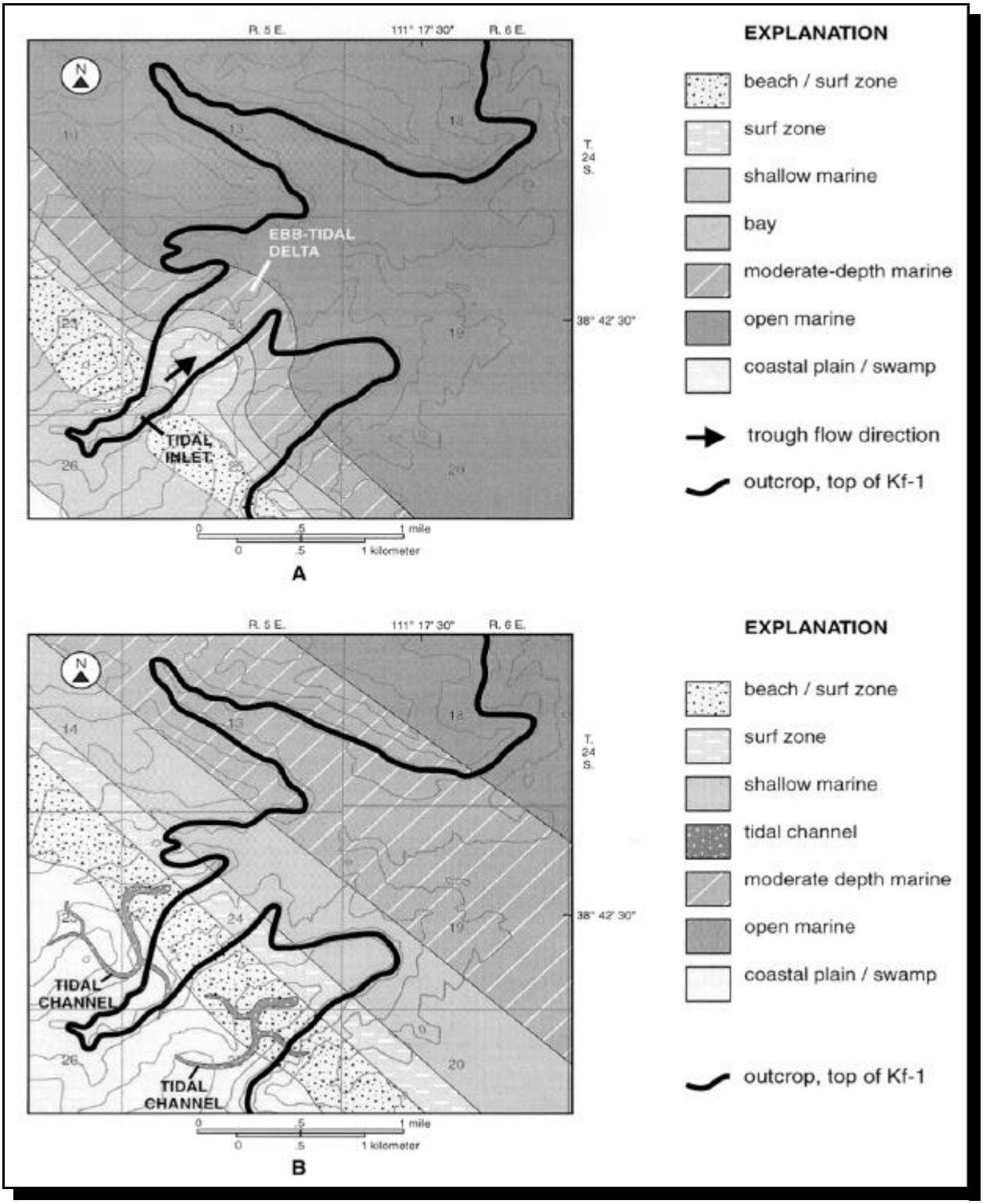


Figure 5-12. Paleogeographic maps of the case-study area during deposition of parasequence Kf-1-IC-c. These deposits are within depositional unit C. (A) shows tidal inlet and possible ebb-tidal delta deposition during Stage 1. (B) shows wave-dominated deposition after the tidal inlet has migrated to the southeast during Stage 2.

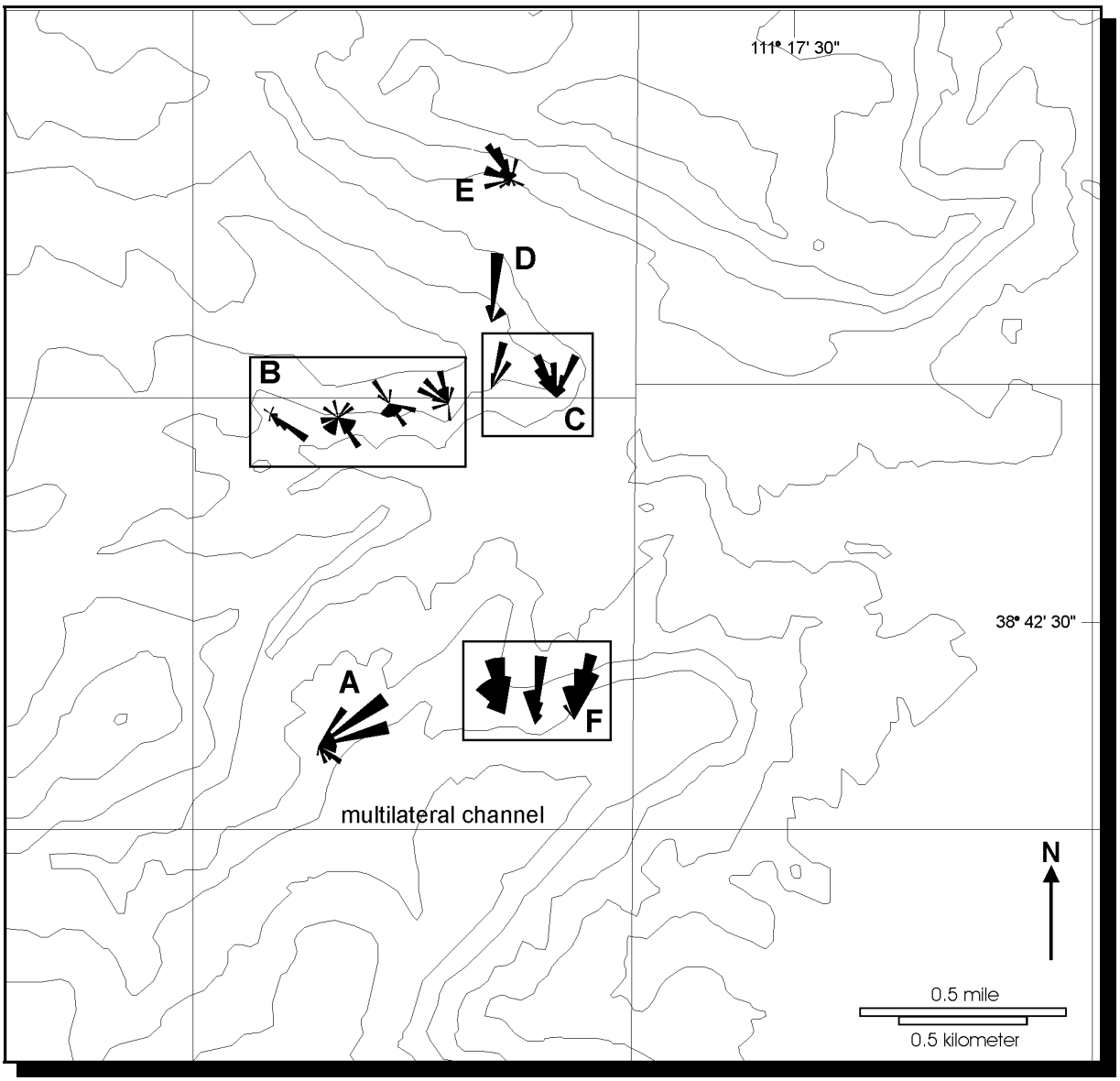


Figure 5-13. Paleocurrent map of deposits of depositional units C and D within parasequence Kf-1-IC-c. (A) Paleocurrent pattern within the upper shoreface/ebb-tidal delta facies of depositional unit C shows northeast-directed flow. (B) Paleocurrent indicators within the strand plain facies of depositional unit D show a change in the dominant current direction from southeast-directed flow to northwest-directed flow. This was the result of a growing distributary system to the southeast of the case-study area. (C) Paleocurrent indicators from the crevasse splay facies (depositional unit D) show northwestward growth into an interdistributary bay. (D) Deposits within the multistory channel facies in Willow Springs Wash show northward flow (depositional unit D). (E) Variable current pattern of distal-mouth bar deposits of depositional unit D. (F) Deposits within the multilateral channel facies show flow to the north, toward the multistory channel in North Fork Canyon (depositional unit D).

Stage 3. Strand plain: At some point during the deposition of the Kf-1-IC-c parasequence, a river system avulsed into the area. Initially, the streams emptying into the area were small and the area was still subject to the effects of wave processes. Sediment that was delivered into the basin was redistributed along cuspate strand lines by longshore drift (figure 5-14A). The initial deposits were amalgamated with the most-recently deposited shoreline sands (depositional unit D/Kf-1-IC-c[d] bedset). Paleocurrent indicators at the head of "North Branch" suggest that sediment derived from the northwest was initially carried by currents towards the southeast (figure 5-13B). Paleocurrent indicators between the head of "North Branch" and the multistory channel system closer to the mouth of North Fork Canyon show that as the strand plain facies grew eastward, northwest-directed currents became dominant. These paleocurrents indicate a source to the southeast. A distributary system near the south end of the case-study area could have provided a sediment source and produced the observed paleocurrent pattern. As the distributaries increased in size, their deposits began to reflect the orientation of the currents that they induced, resulting in northwesterly oriented sedimentary structures.

Stage 4. Interdistributary bay: Subsequent to the initiation of fluvial-dominated processes, the area at the mouth of North Fork Canyon and Willow Springs Wash became isolated and protected from the effects of wave energy (figure 5-14B). The energy of the water in the area decreased and sedimentation was restricted to the deposition of fine clays during calm conditions and very fine sandstone during storms (depositional unit D/Kf-1-IC-c[d] bedset). The cause of the isolation is not directly observable within the case-study area, but several inferences can be made. The last-deposited sandstones within the strand plain facies show transport towards the northwest by longshore currents from the proposed distributary system. Isolation of the case-study area was the result of the formation to the southeast of some type of barrier to these currents. In this case, isolation may have been the result of progradation of a distributary system or sub-delta. As the distributary mouth prograded, longshore currents couldn't carry sediment back into the newly formed interdistributary bay.

This model would suggest two things. First, the distributaries prograded rapidly enough to overcome the effects of wave-reworking. Second, as the distributaries entered the area, the resulting deposits rapidly changed from a cuspate, strand line morphology to a more elongate, possibly shoestring morphology. The outcrops needed to confirm or deny this, however, are non-existent due to local erosion.

Stage 5. Crevasse splay-minor mouth bar: During this stage the sandstones at the mouth of North Fork and Willow Springs Wash were deposited (depositional unit D/Kf-1-IC-c[d] bedset). Northwest-dipping, *en echelon* bedsets of the minor distributary-mouth bar facies suggest that these sandstones were sourced from the east or southeast. Paleocurrent indicators on the ridge separating North Fork and Willow Springs Wash, east of the multistory channel show north and northwestward paleoflow (figure 5-13C). These deposits were the result of a crevasse developing in the inferred distributary to the east (figure 5-15A). Most of the deposits of this crevasse-splay system have been eroded by Holocene erosion, so it is impossible to determine the dimensions of the deposit. It is clear from their absence in the north side of Willow Springs Wash, however, that they did not extend that far north.

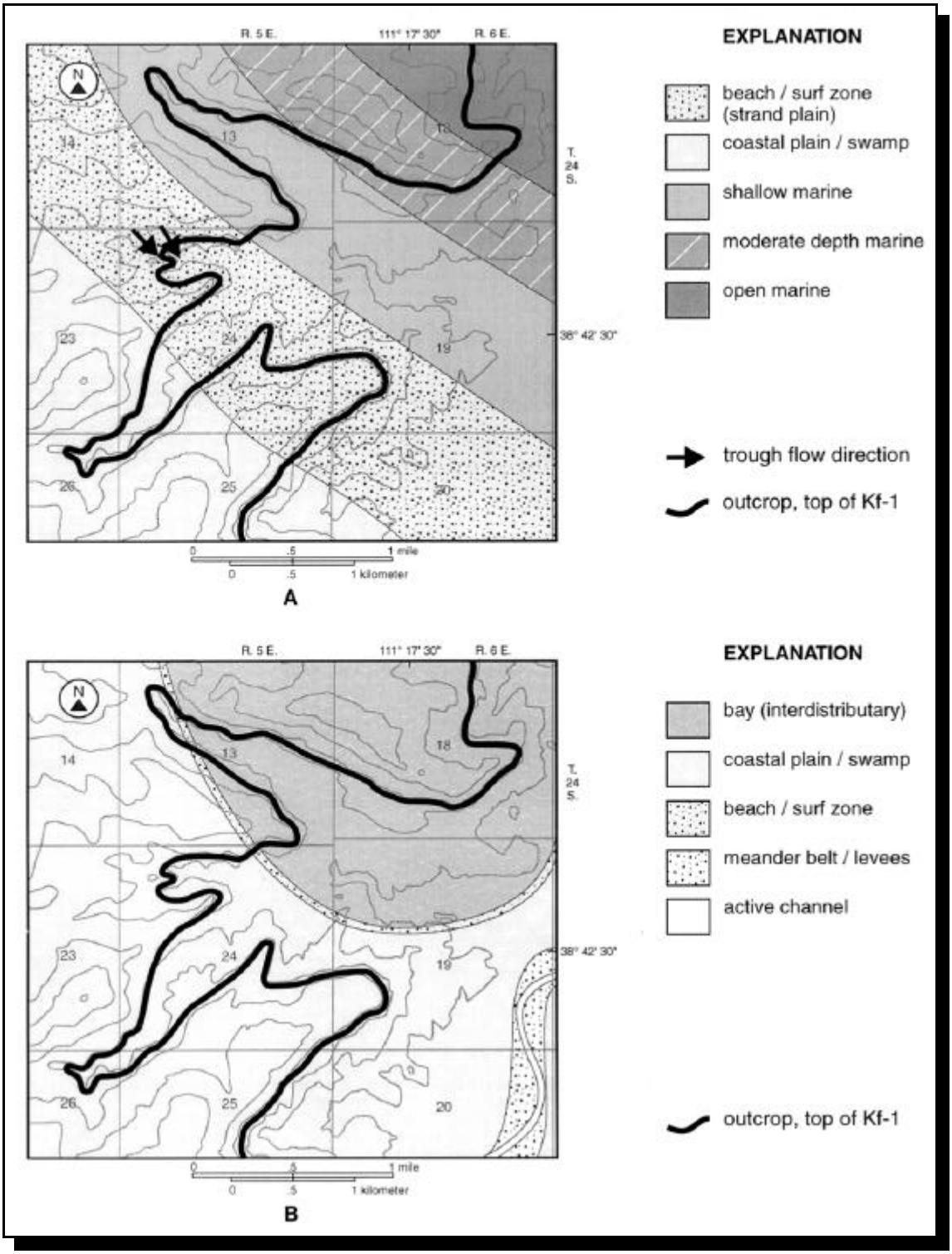


Figure 5-14. Palegeographic maps of the case-study area during deposition of Kf-1-IC-c[d]. (A) shows strand plain deposits alongshore from distributary mouths during Stage 3. (B) shows the interdistributary bay that formed as a result of prograding distributary channels during Stage 4. Both sets of deposits occur within depositional unit D.

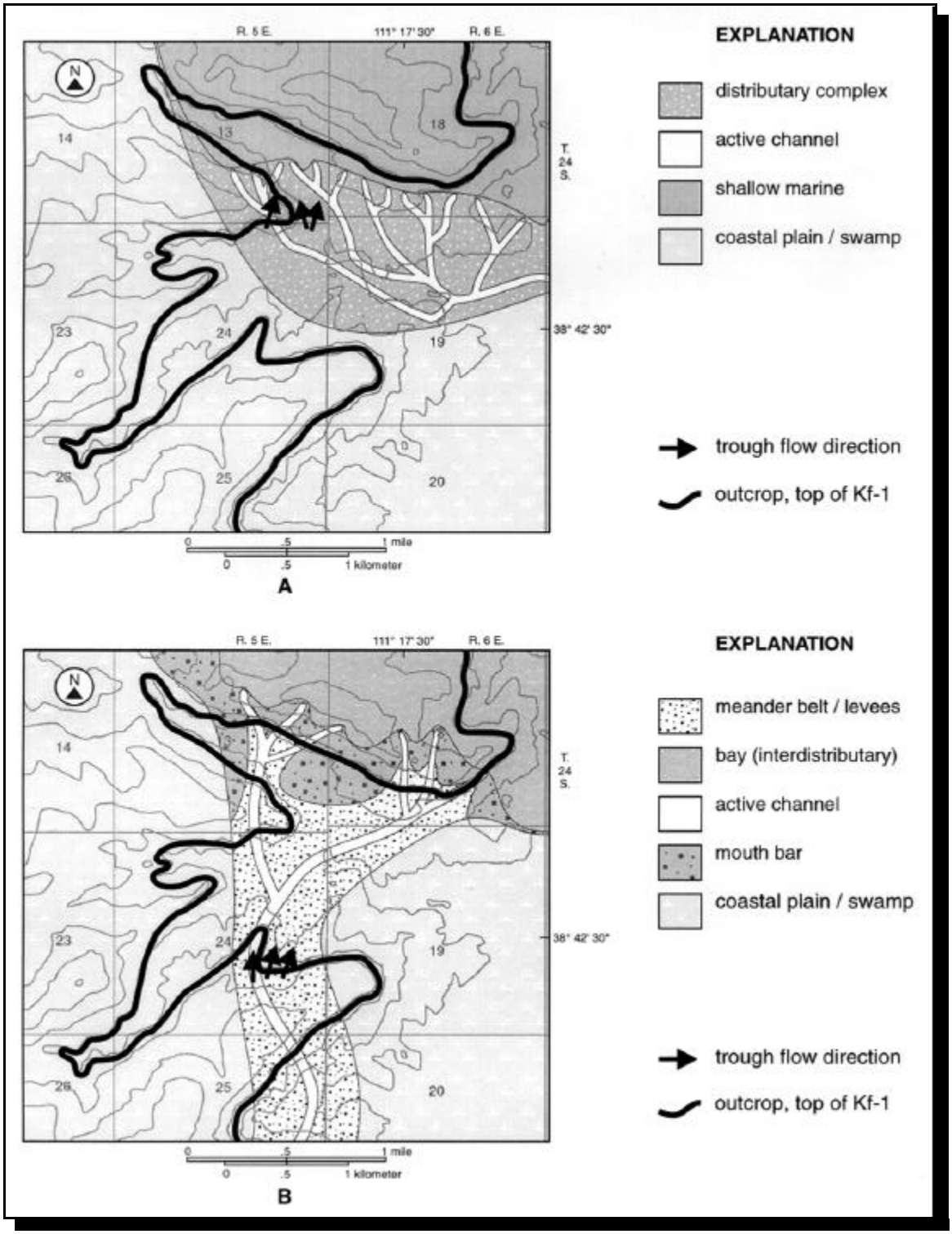


Figure 5-15. Paleogeographic maps of the case-study area during Stage 5 (A) and Stage 6 (B) of parasequence Kf-1-IC-c. (A) shows northwestward progradation of a crevasse splay system into an interdistributary bay. During Stage 6, a distributary avulsed into the immediate case-study area. (B) shows the multilateral channel bifurcating into several smaller multistory channels.

Stage 6. Distributary channel: Finally, a major distributary avulsed into the immediate study area. There are two types of distributary channel deposits. On the north side of North Fork Canyon, a multistory, straight-reach channel system is evident (depositional unit D/Kf-1-IC-c[d] bedset). Straight-reach channel deposits also are present to the north, on the south side of Willow Springs Wash (figure 5-13D). These deposits are not as thick as those in North Fork and they tend to be a little broader. On the north side of Willow Springs Wash, the thick channel sandstone accumulations are gone and in their place are the widely spaced deposits of three or four much smaller channels. These represent bifurcation of the single, large channel into several smaller channels and distributary-mouth bars as the distributary entered the open, distributary bay (figures 5-13E and 5-15B).

To the south, along the south and west walls of "The Alcove," and on the south wall of Indian Canyon, the deposits of a meandering channel system are seen. This channel is not in direct contact with the multistory channel in North Fork and it is not possible to determine the exact relationship between these two deposits. One hypothesis is that the straight-reach system is the distal end of the meandering system and that the two existed simultaneously. Paleocurrent data from "The Alcove" and from the south side of Indian Canyon both indicate northward flow towards the North Fork channel (figure 5-13F). However, comparison of single, lensoidal sandstone bodies in the Indian Canyon exposures with single, lensoidal sandstone bodies within the North Fork exposures suggests that the North Fork channel wasn't large enough to carry the volume of water moving through the meander belt. This problem would be resolved if there were other multistory channels branching from the meander belt.

Another possibility is that the North Fork channel was deposited prior to the development of the meander belt and that the meander belt eroded previously deposited sediment from the straight-reach system. In this, we should expect to find deposits of the meander belt or an associated distributary-mouth bar system in or near Willow Springs Wash. We do not find this in the presently exposed rock, but this may be the result of erosion.

Overlying the bay fill, crevasse splay, and distributary channel deposits are carbonaceous shale and siltstone deposits of the sub-A coal zone which suggest development of peat swamp conditions throughout the area.

Discussion

Variations in Depositional Models

The precise nature of the depositional mechanism that formed the thick-bedded, trough and tabular cross-stratified facies (facies 4) in depositional unit C is not definitely known. Previously, this facies has been interpreted to form within an upper shoreface environment. The close association of this facies with facies that have been interpreted as lower and middle shoreface and foreshore seems to support this interpretation. However, two other important observations need to be addressed. First, paleocurrent data taken from within this facies on the southeast side of Indian Canyon suggests that, with some minor variation, sediment transport was generally in an offshore direction (figure 5-13E). Second, the presence of a tidal inlet in the immediate vicinity suggests that, at least during Stage 1, tides may have affected deposition within this facies.

Barred and non-barred shoreline models: Work by Clifton and others (1971) along the Oregon coast illustrates the types of sedimentary structures, and perhaps more importantly, the orientations of sedimentary structures along high-energy shorelines. They examined non-barred, high-energy shorelines. The vertical sequence of sedimentary structures they describe is shown in figure 5-16A. They divided the high-energy nearshore into five zones. From base to top these zones are: (1) offshore, (2) nearshore-offshore transition, (3) surf zone, (4) swash-surf transition, and (5) swash zone. The surf zone represents the zone of shoaling waves. It is characterized by lunate megaripples and resulting trough cross-stratification. This trough cross-stratification is oriented onshore. This differs from the orientation of the bedforms studied within the trough cross-stratified facies of "The Wall" in Indian Canyon.

Hunter and others (1979) examined the deposits within barred, high-energy systems and found a variety of possible bedform orientations. Bedforms deposited within longshore bars should be oriented onshore or obliquely onshore. Deposits within longshore troughs show longshore orientations. The rip-channel facies contains bedforms oriented offshore or obliquely offshore. Rip-channel mouth bars also show seaward-oriented bedforms. Hunter and others (1979) also predict the vertical sequence of structures that would be produced as a barred shoreline progrades (figure 5-16B). The vertical facies sequence would show a progression from offshore and nearshore-offshore transition facies to rip-channel, longshore trough, and finally, a transition to the swash facies. In general, the grain size would increase upward in the section through the longshore trough facies with an abrupt increase across the base of the rip-channel facies. This abrupt increase in grain size is the result of scour into finer-grained sediments by rip currents and the deposition of a basal lag.

Davidson-Arnott and Greenwood (1976) studied deposits of shore-parallel bars. These deposits vary somewhat from those of oblique bars. Shore-parallel bars contain three facies. The seaward side of the bar contains ripple lamination and seaward-dipping parallel laminations. The bar crest contains horizontal-bedding and trough cross-stratification. The landward facies consists primarily of landward-dipping planar lamination. Successive bars are separated by troughs with current ripples oriented perpendicular to the shoreline. Rip-channel deposits are characterized by seaward-oriented cross-stratification.

The seaward-oriented cross-stratification within facies 4 is consistent with the deposits of rip-channels or rip-channel mouth bars. However, neither the abrupt increase in grain size nor the type of scour that would result from longshore migration of rip-channels have been observed in the case-study area. Furthermore, the landward-dipping, planar lamination associated with the landward side of shore-parallel bars has not been observed. The absence of prominent grain size variations is common within the case-study area. With the exception of fluvial channels, the grain sizes within this system generally range from very fine to upper fine sand and some medium sand. However, the lack of any evidence of landward-oriented or landward-migrating structures within the lower two-thirds of facies 4 is not explained.

Ebb-tidal delta model: An alternative to the barred and non-barred shoreline models is the ebb-tidal delta model. Deposition within an ebb-tidal delta can explain the seaward-oriented cross-stratification within "The Wall." The landward and variably oriented section of cross-stratification overlying this could represent deposits within swash bars flanking and overlying the ebb-tidal delta (M.O. Hayes, verbal communication, 1995).

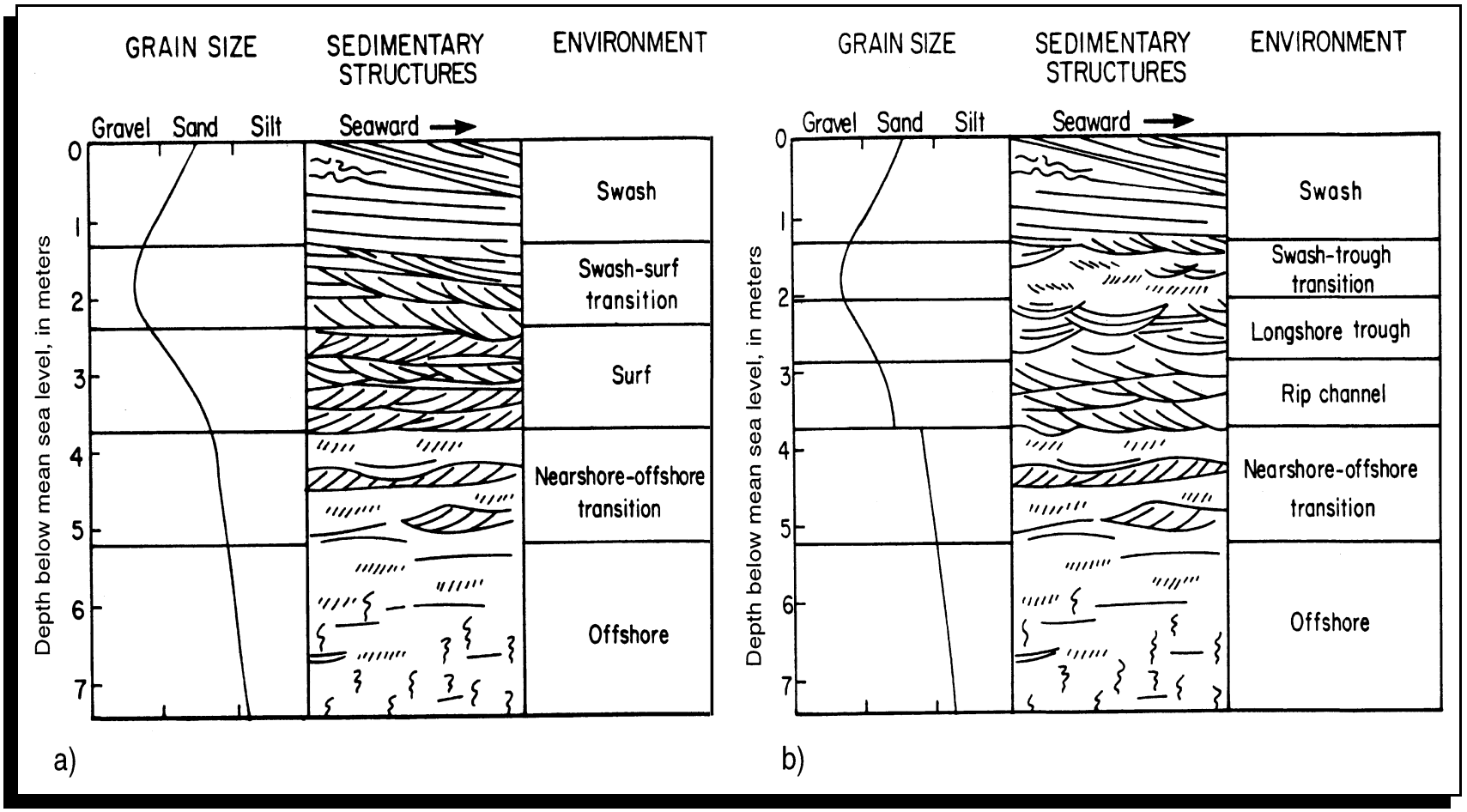


Figure 5-16. Vertical sequence of sedimentary structures observed within (A) non-barred and (B) barred shorelines of the Oregon coast. The orientation of sedimentary structures within "The Wall" eliminates the non-barred shoreline model. The orientation of sedimentary structures in "The Wall" roughly coincides with orientations observed for barred shorelines. The abrupt increase in grain size and the evidence for a significant scoured horizon are not observed. After Hunter and others (1979).

Ebb-tidal deltas develop best under mesotidal conditions, however, they do develop under high microtidal conditions as well (M.O. Hayes, verbal communication, 1995). Davis and Hayes (1984) found the critical condition to be met is not absolute tidal range, but the balance between tidal range and wave energy. If tidal energy and wave energy are balanced, a localized increase in tidal range resulting from local variations in shoreline morphology could result in an increase in the dominance of tidal deposition.

The Ferron Sandstone is generally thought of as having been formed under wave-dominated, microtidal conditions. The importance of waves is certainly evident in the thick, sand-rich deposits forming "The Wall" of Indian Canyon. The existence of ebb-tidal delta deposits would imply tidal ranges that are higher than thought of for the Ferron Sandstone. However, several pieces of evidence suggest that an ebb-tidal delta could exist. First is the observation, already made above, that ebb-tidal deltas can form under microtidal conditions. Second, Hayes has pointed out that along embayments such as the modern Georgia Bight, tidal range increases away from the headlands and towards the apex of the concavity of the bight and that with this increase in tidal range, the dominance of tidal deposits increases as well (M.O. Hayes, verbal communication, 1995). Work by Ryer and McPhillips (1983) has found that during deposition of the lower portion of the upper Ferron Sandstone, such an embayment existed. Third, the presence of a known tidal inlet deposits within Indian Canyon, in conjunction with Walther's Law, suggests that an ebb-tidal delta is a reasonable association of facies. Finally, though it is generally believed that ebb-tidal deltas are usually reworked and redeposited by some other depositional mechanism (that is, longshore drift), some authors suggest that under prograding shoreline conditions, ebb-tidal deposits could be preserved (Heward, 1981). It is certain that as this shoreline prograded, and the upward- and seaward-stepping parasequence architecture suggests that at least on longer scales, sedimentation was overwhelmingly controlled by sea-level rise.

Realistically, a hybrid setting combining both the ebb-tidal delta model and a barred shoreline model may have produced the observed features within Indian Canyon. Slight differences in the depositional model may affect hydrocarbon reservoir potential, however, the evidence to eliminate either model may not exist.

Sequence Stratigraphic Implications

Sequence stratigraphy has become a powerful tool in the interpretation of ancient rock sequences. The use of these concepts has brought new insight into areas of stratigraphy previously thought to be well understood. In light of this, it is appropriate to consider the consequences of the previous discussion on the sequence stratigraphy of the case-study area.

As discussed earlier, the four depositional units are divided into three parasequences: Kf-1-IC-a, -b, and -c. This interpretation is based on the identification of marine-flooding surfaces from vertical offsets of landward pinchouts of marine sandstone bodies. As was previously discussed, the separation of depositional unit D into a distinct parasequence is not warranted, based on the definition given by Van Wagoner and others (1990). It represents a subunit or bedset of parasequence Kf-1-IC-c and is designated as Kf-1-IC-c[d]. This may seem to be an insignificant detail, but it has implications to the positions of adjacent facies.

Let us consider the implications of this interpretation. According to the paleogeographic interpretation stated above, a river system avulsed into the area during deposition of parasequence

Kf-1-IC-c. At that time, deposition within the case-study area changed from wave-dominated deposition to fluvial-dominated deposition. However, there should have existed at the same time some portion of the shoreline that was directly affected by wave energy. This might be some area that was completely unaffected by distributary systems or a portion of a deltaic system that was unprotected from approaching waves. Wave-dominated deposits in this area are within the same parasequence as the fluvial-dominated deposits in Indian Canyon. They are, however, spatially distinct.

One purpose of sequence stratigraphic interpretation and parasequence identification is to identify single, communicable, reservoir quality facies in different wells. Sequence stratigraphic interpretations have the potential of reflecting more accurately, relationships between sandstone bodies that can result in improved production (Van Wagoner and others, 1990). The question now arises, does our sequence stratigraphic interpretation help to achieve that goal? The Kf-1-IC-c parasequence can be "mistakenly" identified as two distinct parasequences, but a "correct" interpretation may cause confusion when identifying reservoir units and interpreting their communicability. In this case, there is nothing gained through a "correct" interpretation.

The benefit of the "correct" interpretation is seen when attempting to predict facies distributions. Taking again the example of parasequence Kf-1-IC-c, we will first predict facies distributions with the "incorrect" interpretation. The coarsening-upwards sequence observable in the interdistributary bay and crevasse splay deposits of depositional unit D or Kf-1-IC-c[d] bedset superficially resembles the coarsening-upwards sequence observed in the transition from prodelta, lower shoreface, and middle shoreface facies of depositional units A, B, and C. If this were the case, we should expect to find a thick, reservoir quality sandstone body landward of the location where we collected our data and at a position stratigraphically higher than the reservoir quality facies within depositional unit C. We see from the outcrop that this is not the case. If we consider the alternative interpretation, the one identified here as "correct," we should expect to find a reservoir quality, shoreline sandstone located in a more seaward direction and at the same stratigraphic interval as the shoreline sandstones of depositional unit C.

Erroneous interpretations of parasequences within the case-study area could also result in miscalculations of rates of sea-level rise (or the rate of subsidence) occurring during a given interval of time and misidentification of channel sandstones and their scoured bases as incised valleys. Subsequent errors in sequence identification and facies location would, in turn, result.

It should be noted that a correct parasequence interpretation is dependent upon correct facies interpretations. In an oil field, the actual amount of data available, regardless of how mature the field, is small in comparison to the data available from outcrop. The ability of the geologist to make detailed interpretations of depositional environments is somewhat limited. This could also limit the ability of the geologist to make a correct sequence stratigraphic interpretation. Hopefully, data such as those presented here will provide an analog that will allow the geologist to formulate more working hypotheses. This may also allow the geologist to come closer to correctly identifying and understanding reality in subsurface reservoir rocks.

Reservoir Quality

Analysis of the facies and depositional environments within Willow Springs Wash case-study area allows us to predict which facies would serve as better hydrocarbon reservoirs. This is done by

identifying those facies which have the thickest accumulations of clean sandstone, the coarsest grain size, the largest areal extent, and the fewest barriers to fluid flow.

Wave-dominated deposits in parasequences Kf-1-IC-a and -c appear to meet the criteria of greater thickness, larger aerial extent, and abundance of coarser grains. The fluvial-deltaic deposits of Kf-1-IC-c are generally finer grained, thinner, less extensive aerially, and typically have more abundant heterolithic breaks (such as the interdistributary bay-fill and crevasse splay/minor distributary-mouth bar deposits). The deposits of medium-grained sandstone are generally thin (1 to 2 feet [0.3-0.6 m]) and not very extensive. Based upon these criteria, we can conclude that the wave-dominated deposits are the better-quality reservoir facies.

In reality, however, the geologist and the reservoir engineer can not chose the type of deposits that hold the hydrocarbon. Indeed, the problem is that the hydrocarbons being targeted are commonly found within the fluvial-deltaic deposits. Because of this circumstance, the geologist and the reservoir engineer need to correctly identify the facies characteristics through the use of detailed facies identification, sequence stratigraphic analysis, and the use of outcrop analogs.

Conclusions

Eleven distinct depositional facies can be identified in the Kf-1 parasequence set in Indian Canyon of the Willow Springs Wash case-study area. These are: (1) prodelta-inner shelf, (2) lower shoreface, (3) middle shoreface, (4) upper shoreface-ebb tidal delta, (5) foreshore, (6) tidal inlet, (7) interdistributary bay-fill, (8) crevasse-splay, (9) multistory channel, (10) multilateral channel, and (11) strand plain/beach ridge facies. These facies can be grouped into two depositional systems: wave-dominated shoreline and fluvial-dominated delta.

Based on lateral and vertical facies associations, the rocks can be divided into four depositional units in ascending order as A, B, C, and D. Marine-flooding surfaces, which are identified on the basis of vertical offset in landward pinchouts, separate the A, B, and C depositional units. There is no flooding surface separating the C and D units. Because of this, the depositional units are divided into three parasequences. These are the Kf-1-IC-a and -b parasequences (which consist of depositional units A and B respectively) and the Kf-1-IC-c parasequence (which consists of depositional units C and D). Depositional unit D is a bedset of the Kf-1-IC-c parasequence.

During the deposition of parasequences Kf-1-IC-a, -b, and early part of Kf-1-IC-c, the case-study area was characterized by northeastward progradation of a northwest-southeast striking shoreline. Parasequence Kf-1-IC-a and the early part of parasequence Kf-1-IC-c represent longer pulses of progradation while parasequence Kf-1-IC-b represents a shorter pulse. During the later part of parasequence Kf-1-IC-c, river avulsion created an autocyclic change in deposition that resulted in an “apparent parasequence.” During this time sedimentation within the case-study area was characterized by deposition within an interdistributary bay, the Kf-1-IC-c[d] bedset.

The interpretations of the case-study area suggest that “apparent parasequences” may result from autocyclic processes. These processes are independent of changes in relative sea-level and as such, they are not parasequences in the *sensu stricto*. Interpretation of these apparent parasequences as true parasequences may help to visualize distinct compartments within a reservoir, but may not be beneficial in predicting facies distributions. Because of this, it is helpful to interpret facies changes and depositional environments and use these conclusions to modify sequence stratigraphic interpretations when possible.

Depositional environments may greatly affect the quality of a sandstone body as a hydrocarbon reservoir. The presence of fine-grained breaks and heterolithic facies will affect the way that fluids flow through a rock body. These characteristics of sandstone bodies are at least partly a direct result of depositional processes. For this reason, detailed facies analysis is a useful tool in oil field development. However, limitations on the available knowledge of rock characteristics (lithology, internal architecture, and so forth) may prohibit a complete interpretation, even in outcrops.

The complex interplay between the environments within a fluvial-deltaic system coupled with the effects of relative sea-level change can make the identification of depositional environments and parasequences a difficult task. Correct interpretations can lead to more detailed information about the types and scale of heterogeneities within a reservoir and the locations of prospective targets. Incorrect interpretations, however, can lead to errors in predicting the distribution of facies with respect to known data points. This in turn may result in incorrect decisions concerning field development strategies.

CHAPTER VI
GEOLOGIC FRAMEWORK OF MUDDY CREEK CANYON CASE-STUDY AREA

T.A. Ryer

Introduction

Exposures of the Ferron Sandstone in Muddy Creek Canyon (figures 6-1 and 6-2) offer excellent examples of a variety of facies that accumulated in fluvial-deltaic settings. This study focused on four parasequences in unit Kf-2 (figure 6-3), the second of the eight major shoreline sandstone units distinguished in the Ferron on the Castle Valley outcrops (figure 6-4) (refer to Chapter IV, Regional Stratigraphy, for an explanation of Ferron sequence stratigraphic nomenclature).

The Muddy Creek Canyon area was chosen for study for the following reasons:

1. Exposures are exceptionally good.

2. A variety of facies of interest are exposed.

3. Other, nearby canyons compliment the Muddy Canyon exposures, allowing a three-dimensional depositional model to be constructed.

4. Access to the outcrops is good, making the locality ideal for field trips.

5. Access to drilling sites immediately west of Muddy Creek Canyon is excellent compared to most other Ferron outcrop areas.

Location

The Muddy Creek Canyon case-study area is located about 3 miles (5 km) southeast of Emery (figure 6-1). Several locations within the are here informally named for convenience of reference (figure 6-5). The name "Muddy Creek Canyon," often shortened to "Muddy Canyon," is used throughout this report. The canyon cut through the Ferron by Muddy Creek, in fact, lacks a proper name. We have seen no published topographic map with any name indicated for it. The larger canyon cut by Muddy Creek into the eastern edge of the Wasatch Plateau is named Muddy Canyon on the topographic maps, and considerable confusion could result from application of the same name to the canyon that was the subject of this study. The name should be used only with an appropriate explanation.

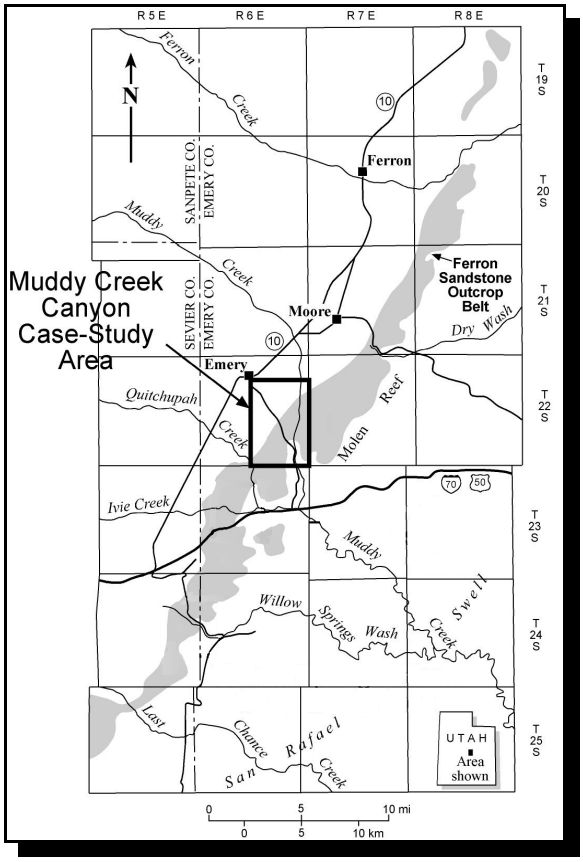


Figure 6-1. Location map of the Ferron Sandstone project area (outcrop belt is shaded) showing the Muddy Creek Canyon case-study area.

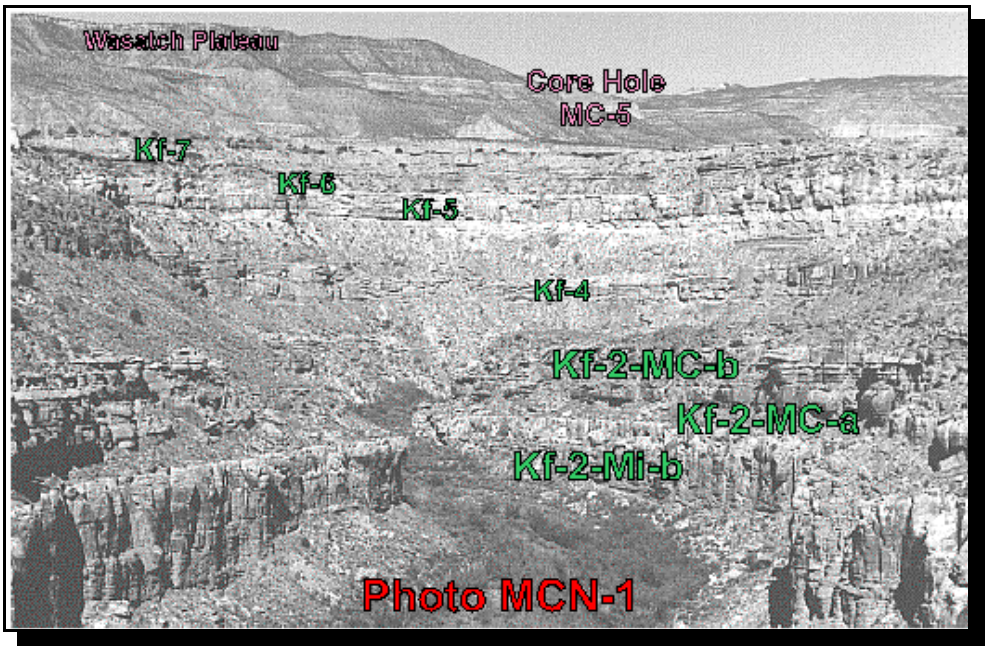


Figure 6-2. View to the northwest in the northern part of the "Middle Reach" of Muddy Creek Canyon. Cliffs formed by parasequences in Kf-2 are labeled, as are younger units Kf-4, Kf-5, Kf-6, and Kf-7. The Tununk Shale crops out in the floor of the canyon. The surface position of core hole MC-5 is on the top of the ledge formed by Kf-7 immediately below the core (drill) hole MC-5 label.

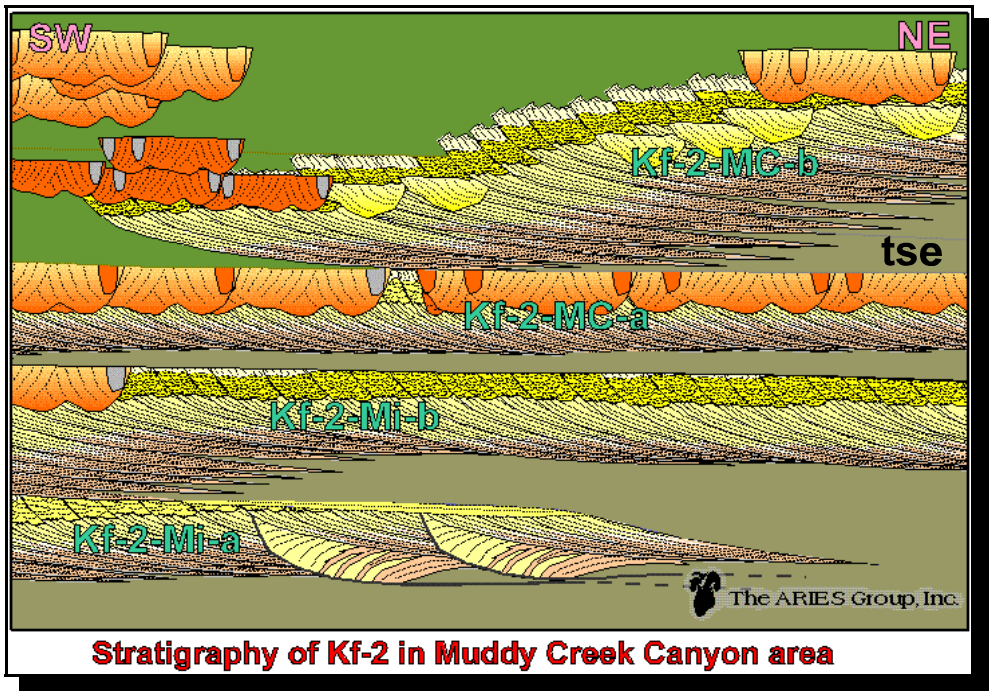


Figure 6-3. Generalized southwest to northeast cross section showing the four parasequences distinguished in Kf-2 in Muddy Creek Canyon and the facies that they contain.

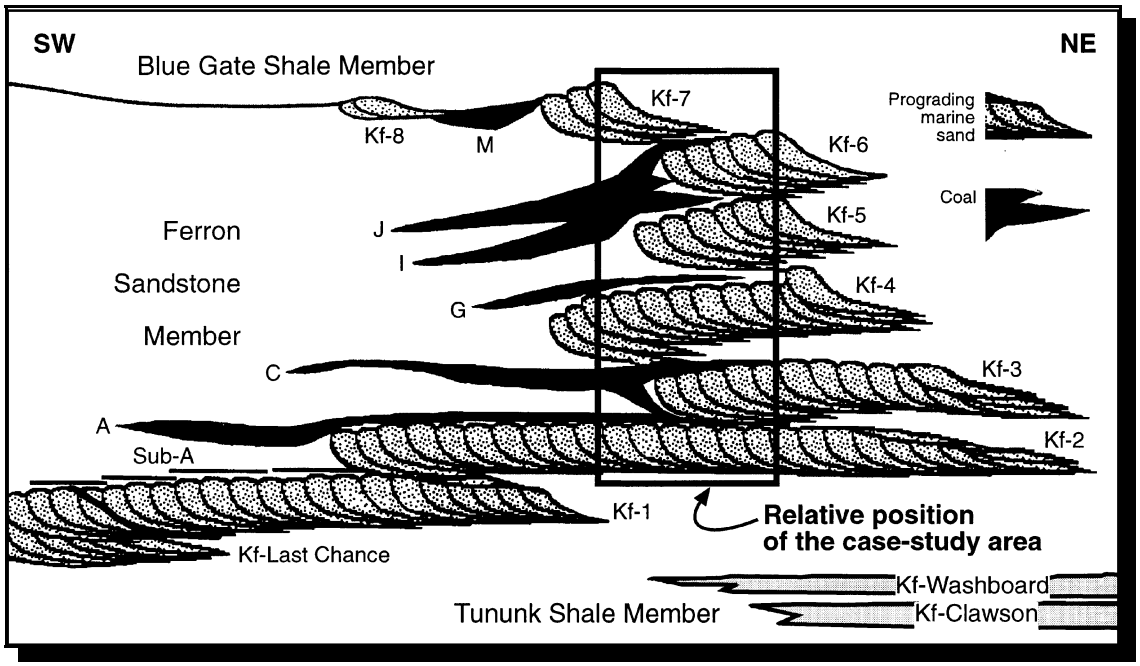


Figure 6-4. Diagrammatic cross section showing relative positions of Ferron parasequence sets with their associated coal zones (black), and the relative stratigraphic position of the Muddy Creek Canyon case-study area within the Ferron Sandstone. The diagram has no scale.

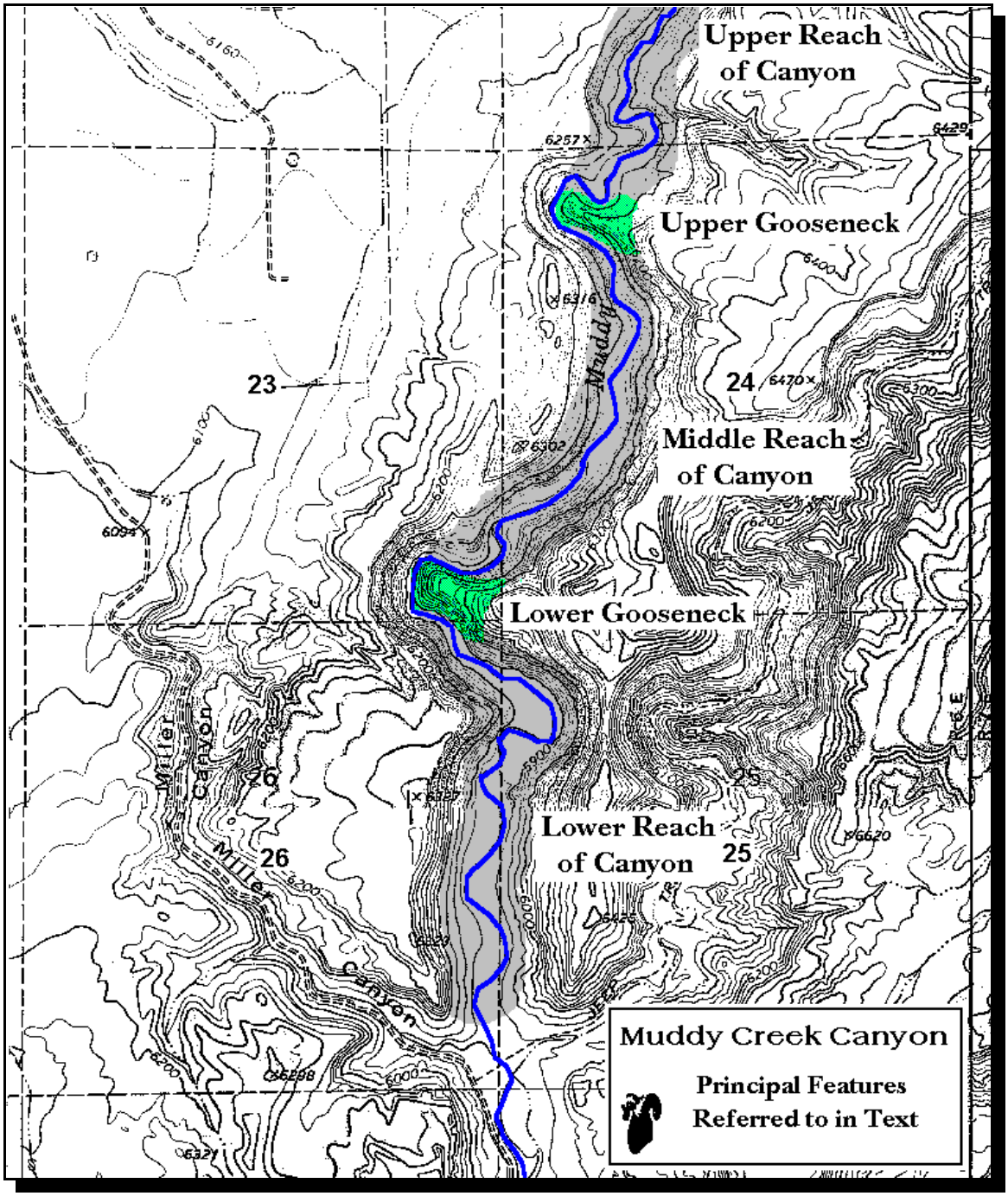


Figure 6-5. Topographic map of the Muddy Creek Canyon case-study area identifying principal features referred to in the text.

Methods

Five drill holes, MC-1 through MC-5 (figure 6-6) were drilled and cored in the summer of 1992 (figure 6-7). Approximately 200 feet (60 m) of core was recovered from each hole, representing all or, in the case of MC-1, almost all of the Kf-2 interval. The cores, which were subsequently slabbed, reside at the Utah Geological Survey Sample Library.

Ten stratigraphic sections (figure 6-6), most located on vertical cliffs, were measured in the summer of 1993. The measured sections are not included in this report and, at this time, remain the proprietary data of BP Exploration. Complete photomosaic coverage of the canyon walls was shot in the summers of 1992 and 1993. The locations of the photomosaics in shown in figure 6-6. The 12 photo sections were constructed combining vertical sections obtained from photos incorporated into the photomosaics and information from nearby measured outcrop sections. The photosections combine interpretations made on both the outcrops and on the photomosaics. They provide the principal control points for a cross section representing the stratigraphy of Kf-2 in Muddy Creek Canyon.

Two diagrammatic stratigraphic cross sections constructed from the photo section and drill-hole data summarize the interpretations. The first (figure 6-8) incorporates the photo sections and observations made on the outcrops and photomosaics; the second (figure 6-9) offers an interpretation of relationships between the five drill holes.

Facies of Kf-2 in Muddy Creek Canyon

Kf-2 in the Muddy Creek Canyon case-study area includes a variety of facies deposited in both shallow-marine and coastal-plain paleoenvironments. The characteristics of Ferron facies are discussed in Chapter III, Facies of the Ferron Sandstone. Here, the parasequences of Kf-2 in Muddy Creek Canyon are discussed and their facies content documented, primarily by means of photographs and their captions. The stratigraphy of these units and their depositional histories are discussed in the following section. Photos of cores begin with P- and the drill-hole number, followed by the depth. The other photos, most of which incorporate an abbreviation of the parasequence name, are outcrop photos. Photos are generally arranged in ascending stratigraphic order.

Kf-2-Miller Canyon-a

Only the distal, seaward part of parasequence Kf-2-Miller Canyon (Mi)-a is present in the Muddy Creek Canyon case-study area. It is likely that it represents a fluvial-dominated deposit, but an insufficient thickness is preserved to allow the making of a firm interpretation (figure 6-10).

The most distinctive feature of Kf-2-Mi-a is the large number of rotated slump blocks (figures 6-11 through 6-13). Other units of the Ferron contain these features, but nowhere is there such a concentration of them as in parasequence Kf-2-Mi-a in Muddy Creek Canyon and the adjacent "Grassy Canyon." The slumps failed toward the northwest or north-northwest, which is interpreted to be the direction of progradation.

A marine flooding surface separates parasequence Kf-2-Mi-a from overlying parasequence Kf-2-Mi-b. There is evidence of erosion of strata on this surface in areas where differential compaction during sedimentation caused areas underlain by the thick, sandy, rotated slump blocks to become highs on the sea floor. Erosion elsewhere appears to have been very minor.

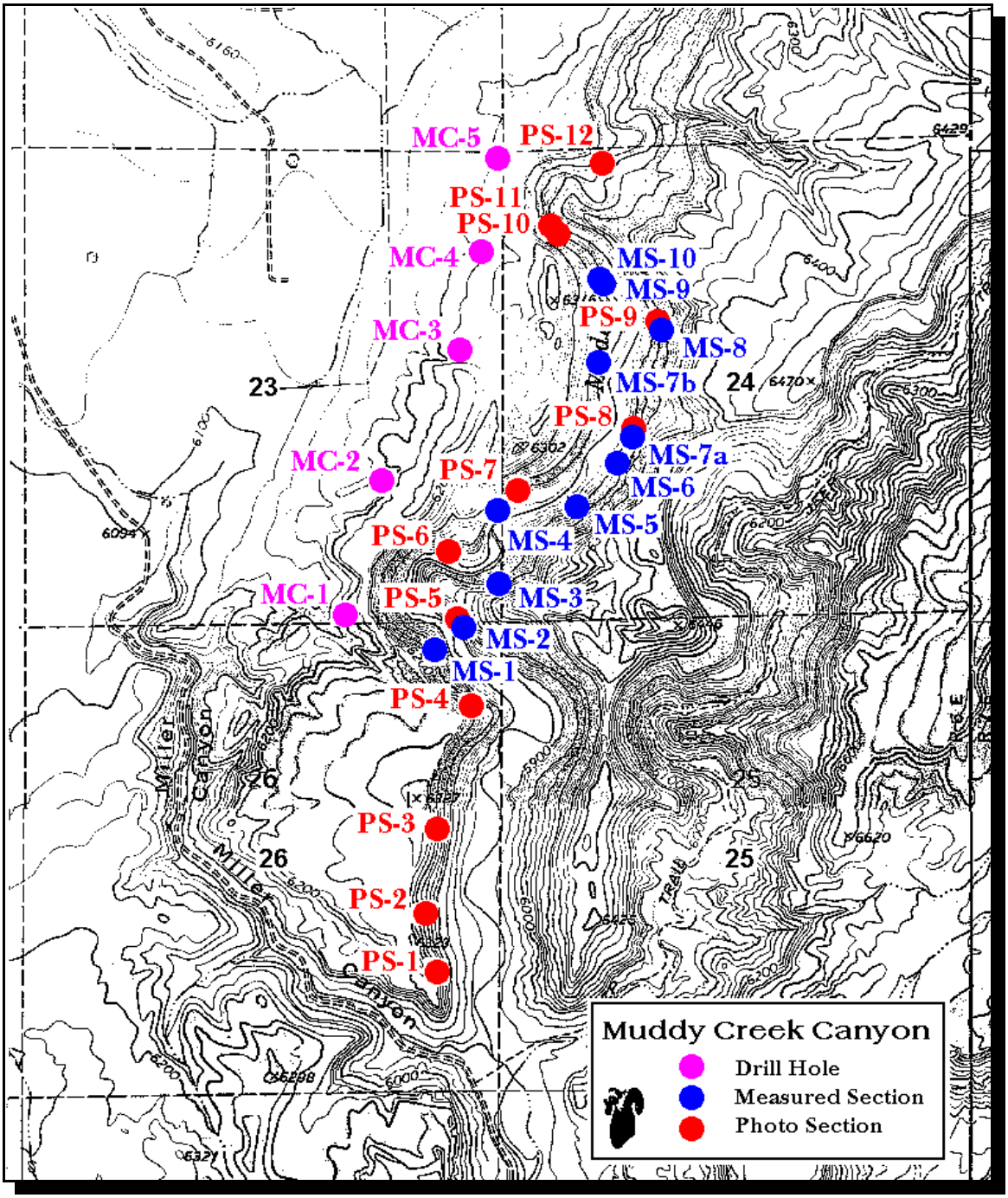


Figure 6-6. Map showing the locations of drill holes (MC1- through MC-5), measured sections (MS-1 through MS-10), and photo sections (PS-1 through PS12) in the Muddy Creek Canyon case-study area.

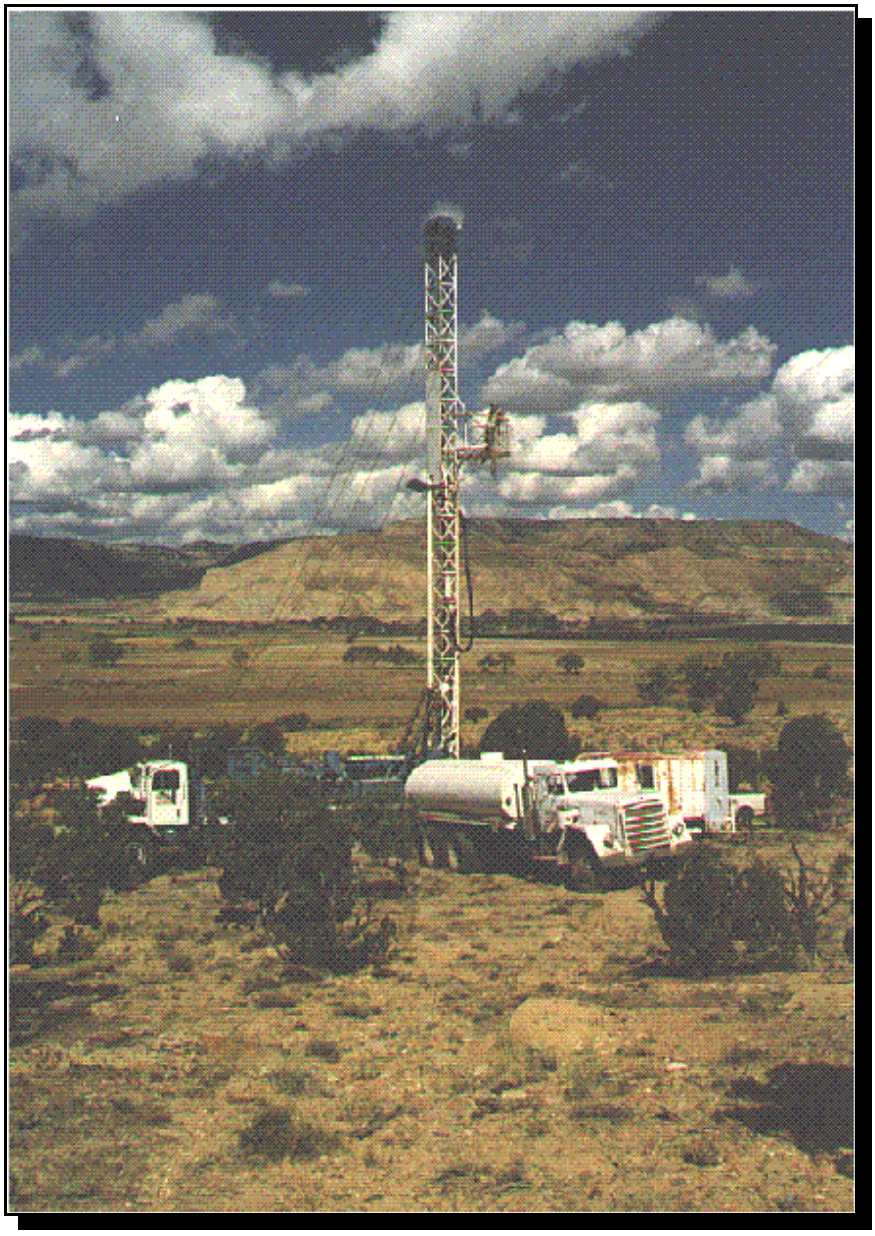


Figure 6-7. Coring operations during the drilling of Muddy Creek drill holes. View is toward the west.

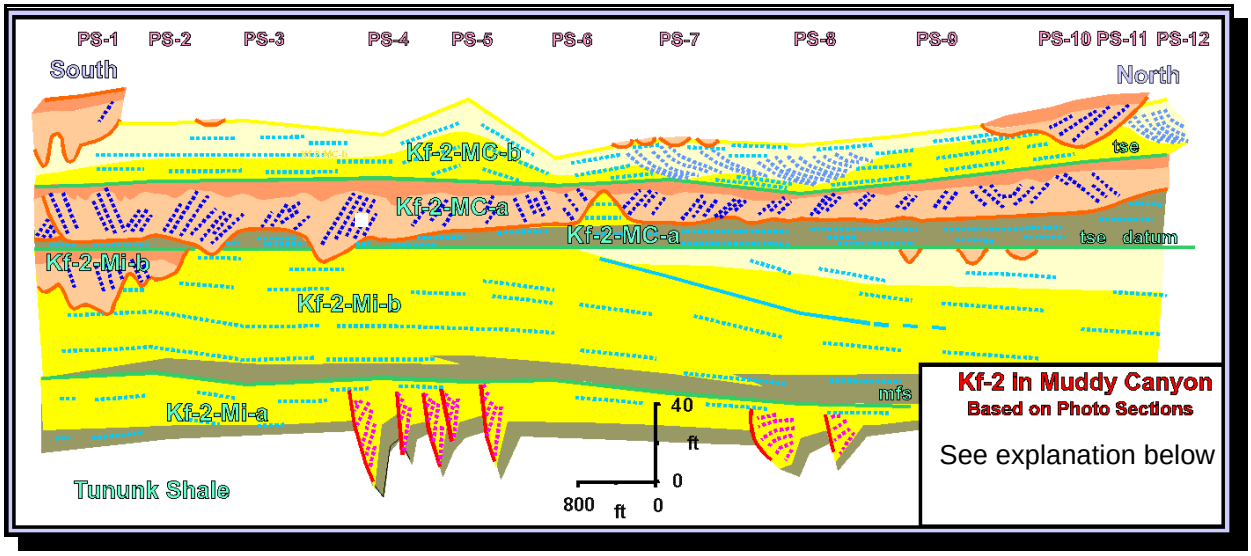


Figure 6-8. Cross section showing stratigraphy and facies of Kf-2 along Muddy Creek Canyon and in the subsurface, as represented by the photomosaics along the "Middle Reach" of Muddy Creek Canyon.

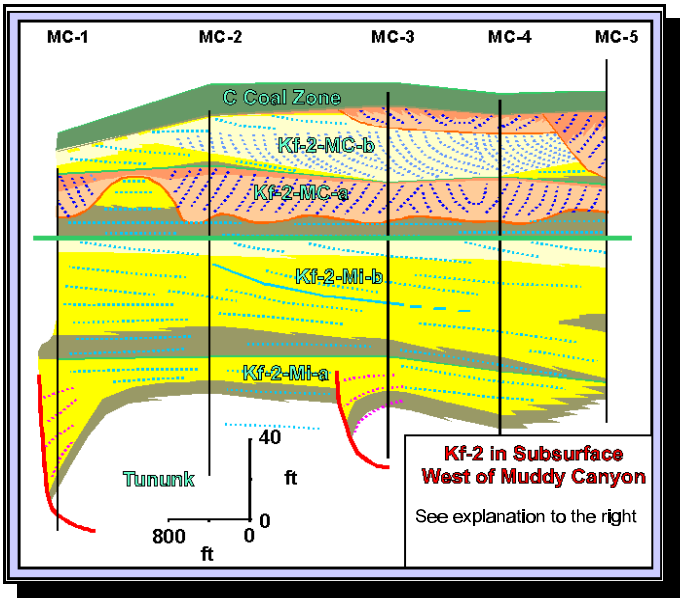
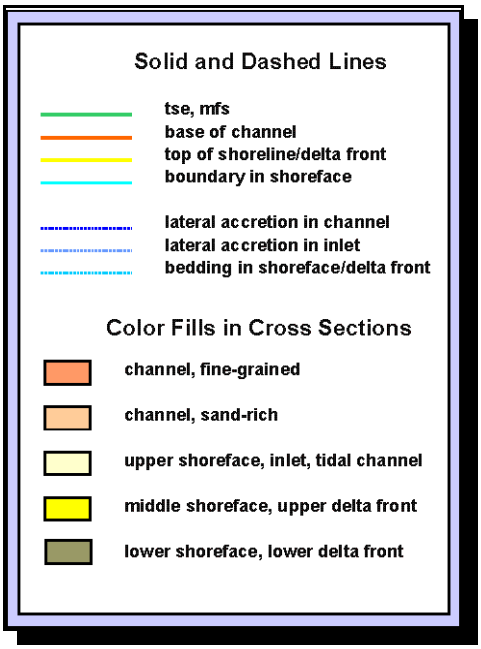


Figure 6-9. Cross section showing stratigraphy and facies of Kf-2 along Muddy Creek Canyon and in the subsurface, as represented by the core interpretation from drill holes, immediately west of the "Middle Reach" of Muddy Creek Canyon.

Explanation



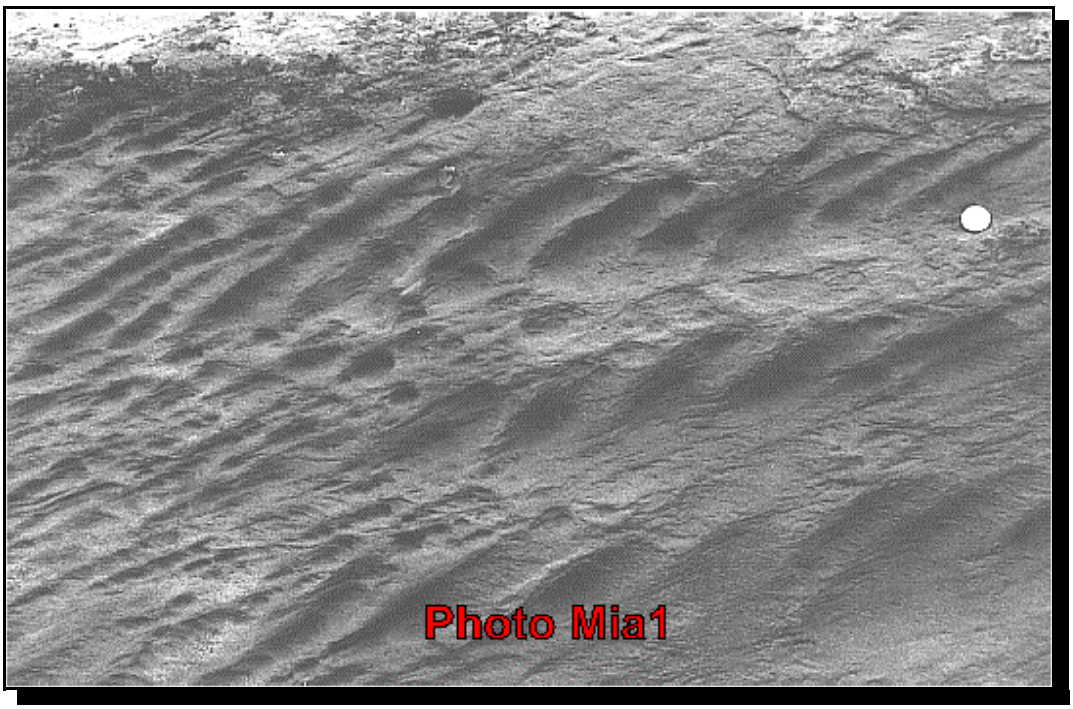


Figure 6-10. Climbing oscillation ripples in middle shoreface strata preserved in a rotated slump block in parasequence Kf-2-Mi-a, "Lower Reach" of Muddy Creek Canyon.

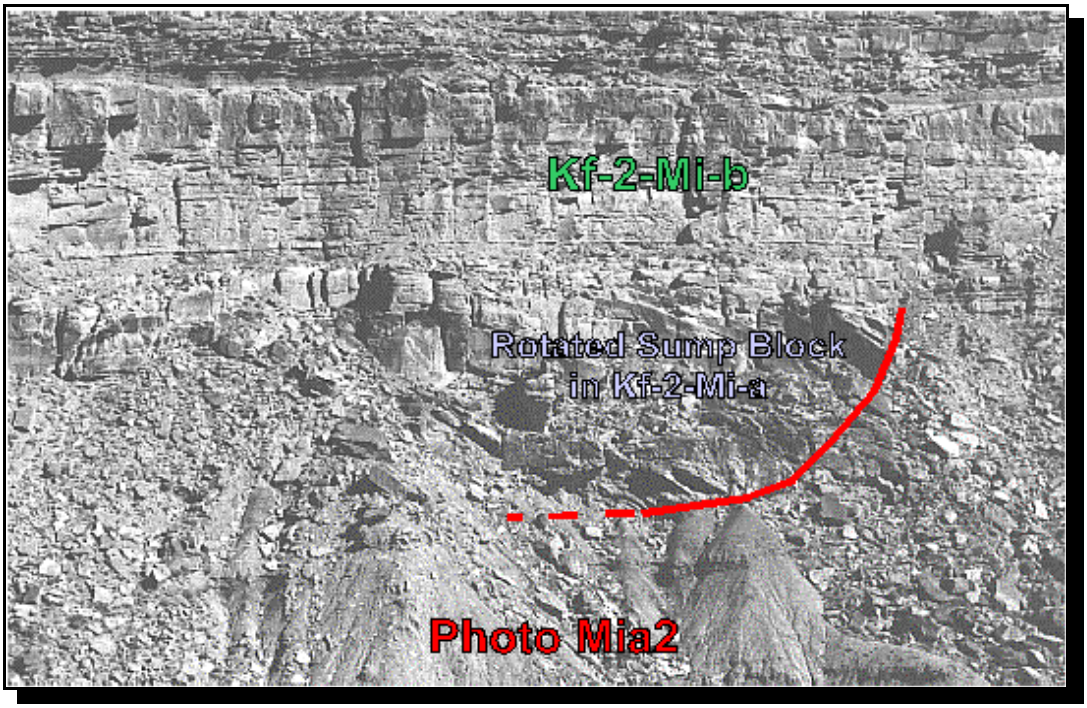


Figure 6-11. Large, rotated slump block in delta-front deposits of parasequence Kf-2-Mi-a, east side of Muddy Creek Canyon.



Figure 6-12. Normal faulting of middle shoreface strata in the landwardmost part of a rotated slump block in parasequence Kf-2-Mi-a in the "Lower Reach" of Muddy Creek Canyon. The faulting records extension in the area of maximum curvature of the master fault plane. Photo by Steven D. Sturm.

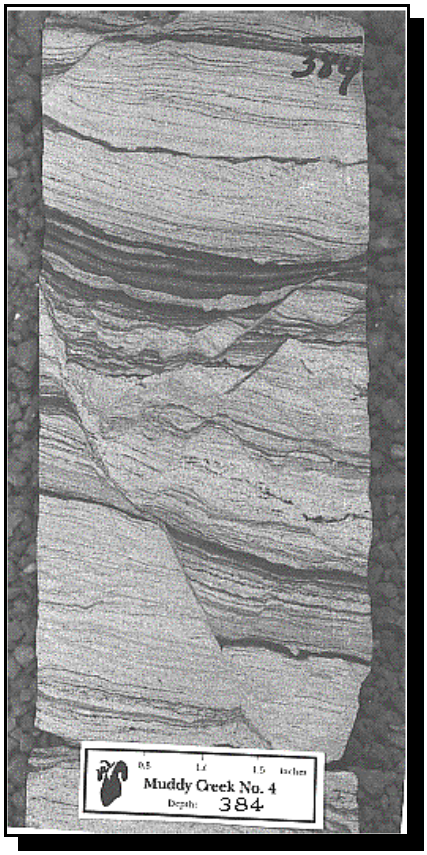


Figure 6-13. Small-scale syndepositional faulting associated with a rotated slump block in parasequence Kf-2-Mi-a. Core from drill hole MC-4 at 384.5 feet.

Kf-2-Miller Canyon-b

With the exception of minor channel deposits at its top, parasequence Kf-2-Mi-b consists entirely of wave-dominated shoreline deposits. It forms vertical cliffs throughout most of the "Middle and Lower Reaches" of the canyon (figure 6-14). The facies characteristics of these three shoreline deposits are shown in figures 6-15 through 6-31. Two subunits are distinguished: a wave-dominated unit in the south and an extremely wave-dominated unit in the north. Although they have not been given separate names, these units are distinguished on the photomosaics. Bedding surfaces in parasequence Kf-2-Mi-b slope gently northeastward.

A transgressive surface of erosion separates parasequence Kf-2-Mi-b from overlying parasequence Kf-2-Muddy Canyon (MC)-a (figures 6-30 and 6-32).

Kf-2-Muddy Canyon-a

Two distinct facies are included in parasequence Kf-2-Muddy Canyon (MC)-a: lower delta front or lower to middle shoreface strata in the lower part (figure 6-33), and meanderbelt deposits in the upper part (figures 6-34 through 6-43). Only in a single small outcrop on the west side of the canyon is a substantial thickness of the original shoreline deposit preserved (figure 6-44). Based on the abundance of mud interbeds in this outcrop, the unit appears to represent a fluvial-dominated shoreline, but the evidence is scanty. The considerable amount and diversity of burrows indicates that this is not an extremely fluvial-dominated deposit (figure 6-45). Lateral accretion is well represented in the meanderbelt deposits (figures 6-46 and 6-47), indicating lateral migration of meander loops in both northward and southward directions. A thin bed of coal and carbonaceous shale representing the seaward most part of the A coal zone overlies that delta-front sandstone unit of parasequence Kf-2-MC-a in the "Lower Reach" of Muddy Creek Canyon.

Parasequence Kf-2-MC-a is separated from overlying parasequence Kf-2-MC-b by a transgressive surface of erosion (figures 6-48 and 6-49). As in the case of parasequence Kf-2-Mi-b, the amount of material removed from the surface by shoreface erosion has not been established, but it is unlikely that it exceeds 10 feet (3 m).

Kf-2-Muddy Canyon-b

A transgressive surface of erosion separates parasequences Kf-2-MC-b and Kf-2-MC-a. In most places in Muddy Creek Canyon, the transgressive surface of erosion lies on the upper part of a meanderbelt sequence. In drill hole MC-2, a thin split of the A coal zone is present beneath the surface. Sand filled burrows, probably *Thalassinoides*, are present in the coal. The fact that they are found in what was certainly a firm substrate (peat) makes them assignable to the *Glossifungites ichnofacies*, the presence of which is commonly invoked as evidence of a parasequence boundary.

Parasequence Kf-2-MC-b (figure 6-50) includes the greatest diversity of facies of the units in the case-study area interval (figures 6-51 through 6-57). Locally, it includes a complete shoreface succession. At many places in the "Middle Reach" of the canyon, and in the vicinity of the "Lower Gooseneck," it includes large-scale, planar-tabular cross-sets that record lateral migration of tidal inlets (figures 6-58 through 6-64). Its top has locally been cut and its uppermost part replaced by fluvial strata (figure 6-65). The shoreface sandstone of parasequence Kf-2-MC-b is conformably overlain by the C coal bed throughout the Muddy Creek Canyon case-study area.

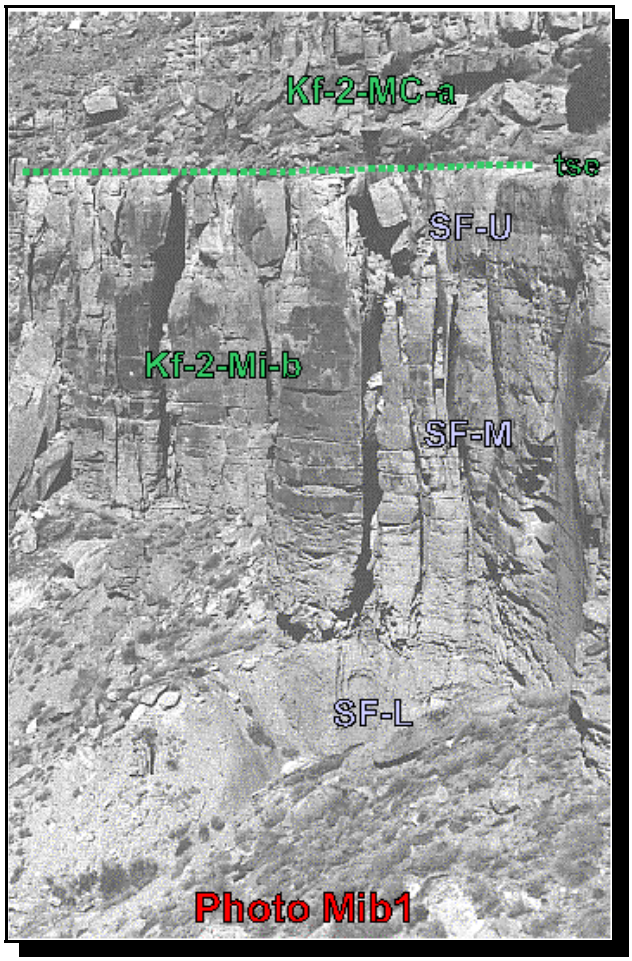


Figure 6-14. Cliff formed by shoreface deposits of parasequence Kf-2-Mi-b on the east side of Muddy Creek Canyon. Lower (SF-L), middle (SF-M), and upper (SF-U) shoreface intervals are marked.

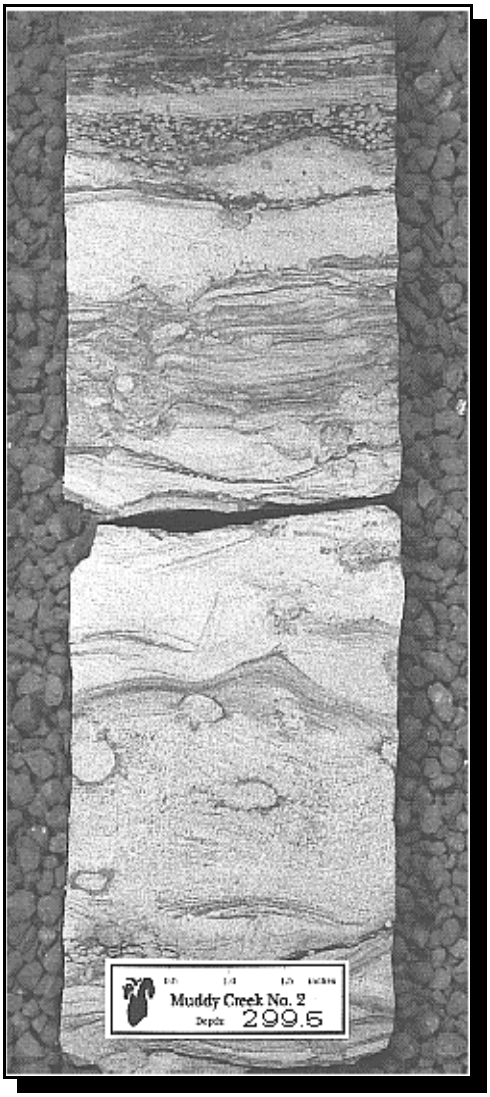


Figure 6-15. Storm sandstones and fair-weather mudstones of the lower shoreface of parasequence Kf-2-Mi-b. *Ophiomorpha* and *Thalassinoides* predominate in the middle and lower part of the cored interval; simple, small, sand-filled tubes representing either *Planolites* or a large form of *Chondrites* are abundant at the top. Core from drill hole MC-2 at 299.5 feet.

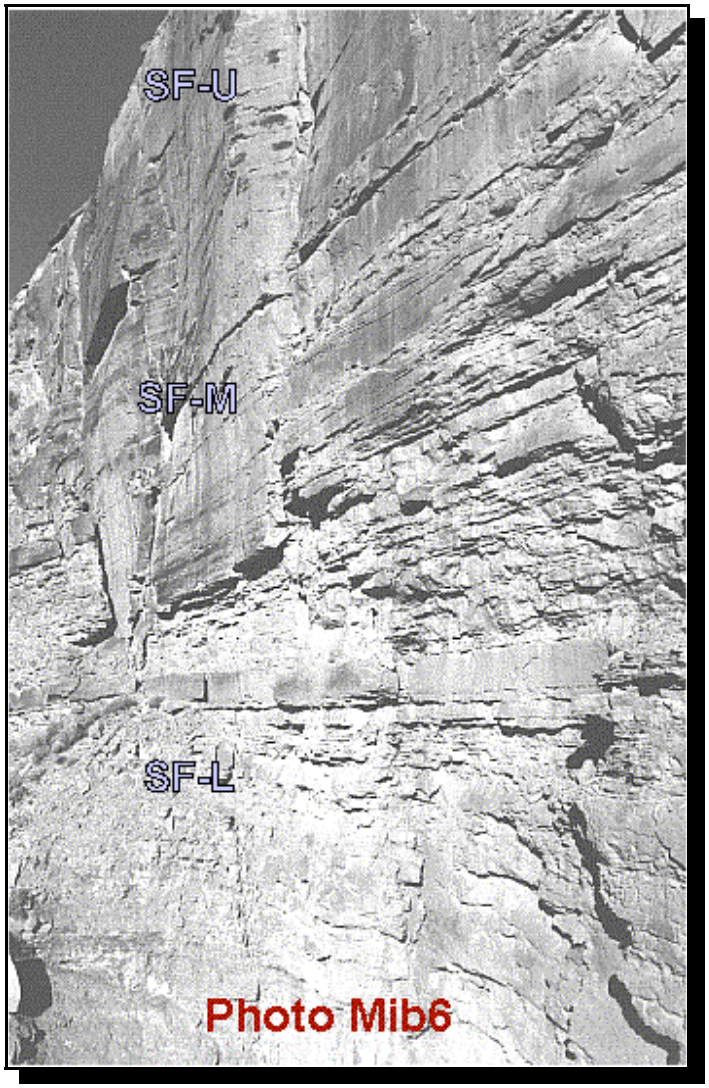


Figure 6-16. The middle shoreface (SF-M) of parasequence Kf-2-Mi-b includes both hummocky to planar-laminated sandstone with minor burrowing and bioturbated fine-grained sandstone, the latter being most common in the lower part of the interval. Exposure on the east side of Muddy Creek Canyon. SF-U = upper shoreface, SF-L = lower shoreface.



Figure 6-17. Hummocky cross-stratified, fine-grained sandstone of middle shoreface of parasequence Kf-2-Mi-b. Note truncation of low-angle laminae against surface immediately beneath the large *Rosselia* burrow. Abrupt contact at the base of the cored interval marks the erosional, basal contact of a storm layer. Note the small mudstone rip-up clasts at the base. Core from drill hole MC-1 at 264 feet.



Figure 6-18. Planar lamination and, at top, "ball-and-pillow" structures in very fine- and fine-grained sandstone of the middle shoreface of parasequence Kf-2-Mi-b, east side of Muddy Creek Canyon.

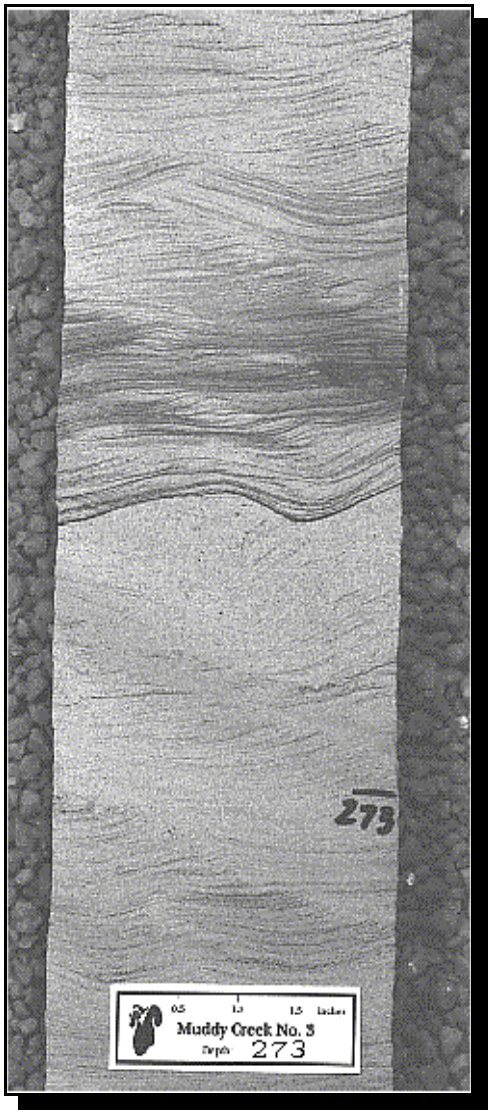


Figure 6-19. Oscillation ripples in middle shoreface of parasequence Kf-2-Mi-b. The rate of climb varies from high to very high. The direction of climb reverses in one thin interval in the upper part of the interval shown. Core from drill hole MC-3 at 273 feet.

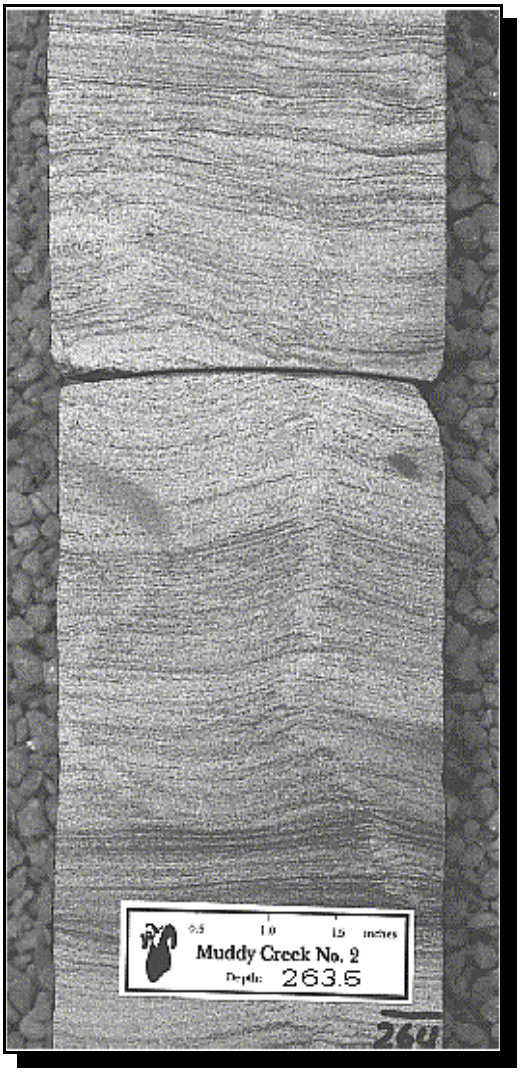


Figure 6-20. Vertically aggraded oscillation ripples in middle shoreface of parasequence Kf-2-Mi-b. Core from drill hole MC-2 at 263.5 feet.



Figure 6-21. Current ripples in middle shoreface of parasequence Kf-2-Mi-b. They display varying degrees of climbing. Based on comparison with the ripples present a foot lower in the core (see figure 6-19), it is likely that these are combined flow ripples. Core from drill hole MC-3 at 272 feet.

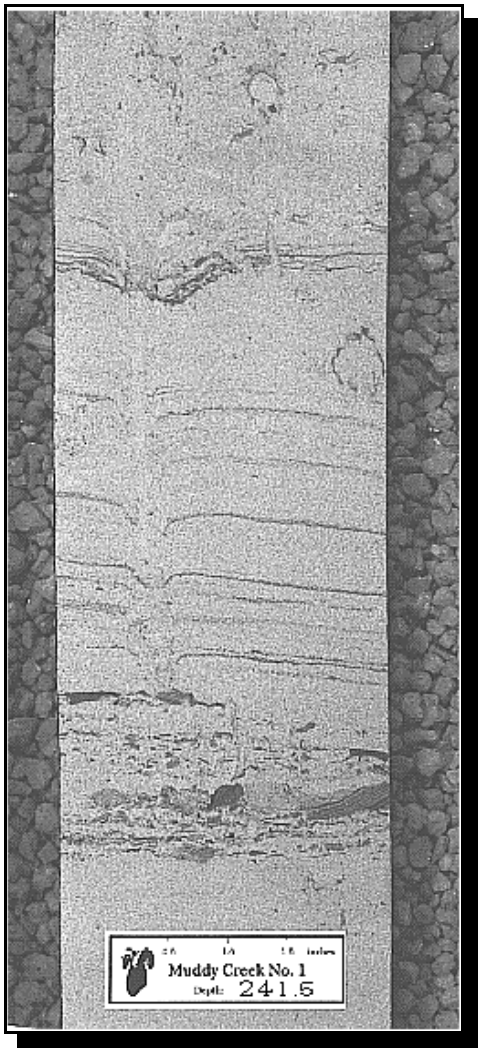


Figure 6-22. Planar laminated, fine-grained sandstone of the middle shoreface of parasequence Kf-2-Mi-b. Prominent, vertically oriented trace along left side displays chevron-shaped deformation of laminae into the burrow, suggesting that it may be an escape structure rather than a dwelling burrow. *Ophiomorpha* are apparent in the upper part of the cored interval. The mudstone rip-up clasts in the lower part of the interval are relatively rare features in middle shoreface sediment. Core from drill hole MC-1 at 241.5 feet.



Figure 6-23. Bioturbated very fine-grained sandstone in the lower part of the middle shoreface interval of parasequence Kf-2-Mi-b, east side of Muddy Creek Canyon.



Figure 6-24. Bioturbated middle shoreface sediment of parasequence Kf-2-Mi-b. Remnant storm layer is recognizable in middle part of interval. Core from drill hole MC-3 at 296 feet.



Figure 6-25. Bioturbated middle shoreface sediment of parasequence Kf-2-Mi-b. There is no trace of any original sedimentary structures. Core from drill hole MC-3 at 300.5 feet.

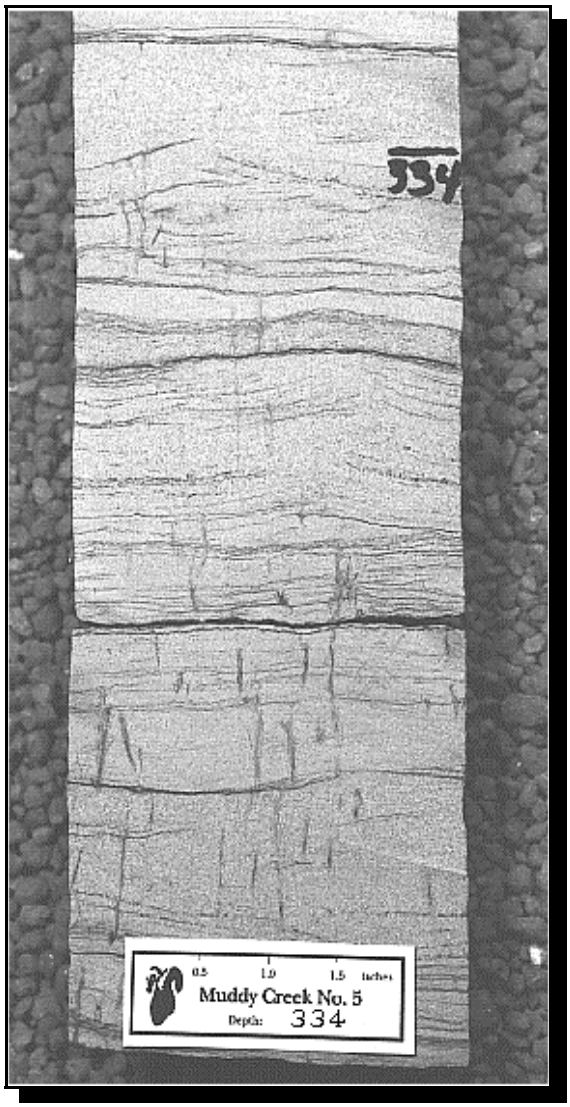


Figure 6-26. Vertical traces (*Trichichnus*?) in middle shoreface of parasequence Kf-2-Mi-b. They bear a striking resemblance to roots (although they lack carbonaceous films commonly present in root traces). Core from drill hole MC-5 at 334 feet.



Figure 6-27. Soft-sediment deformation in middle shoreface of parasequence Kf-2-Mi-b. Core from drill hole MC-1 at 261.5 feet.

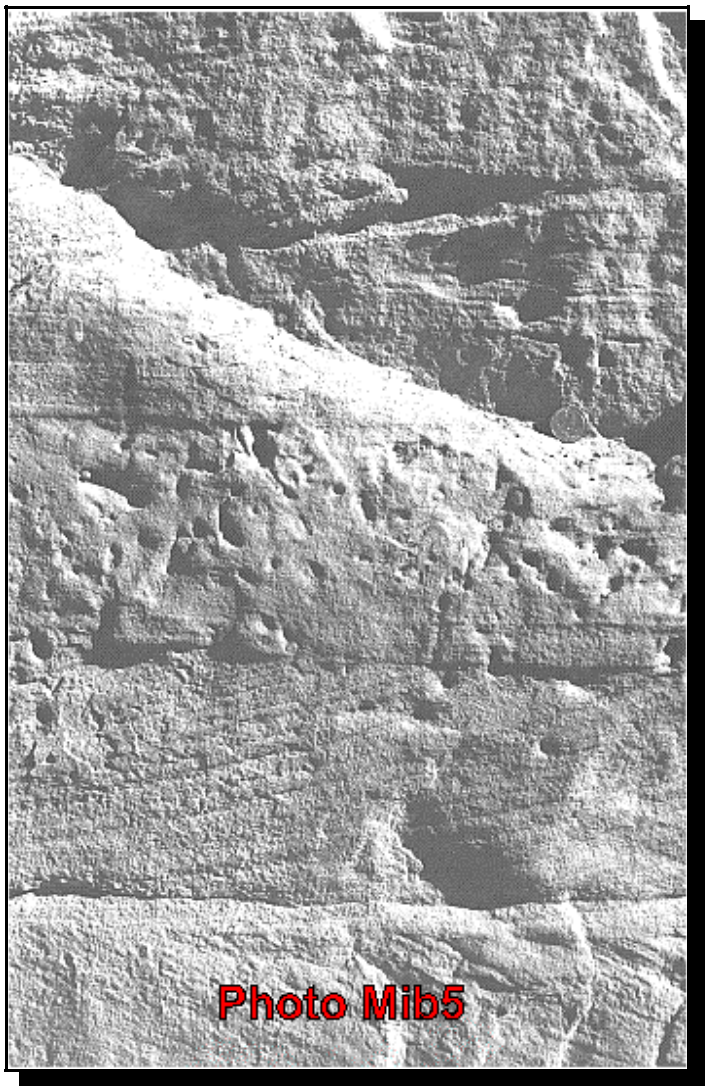


Figure 6-28. Multi-directional trough cross-stratification in beds up to about a foot thick characterizes the upper shoreface of parasequence Kf-2-Mi-b. The sand is moderately well sorted and is medium grained. An interval displaying moderate burrowing by *Ophiomorpha* and *Thalassinoides* is present in the middle part of this photo, taken on the east side of Muddy Creek Canyon.

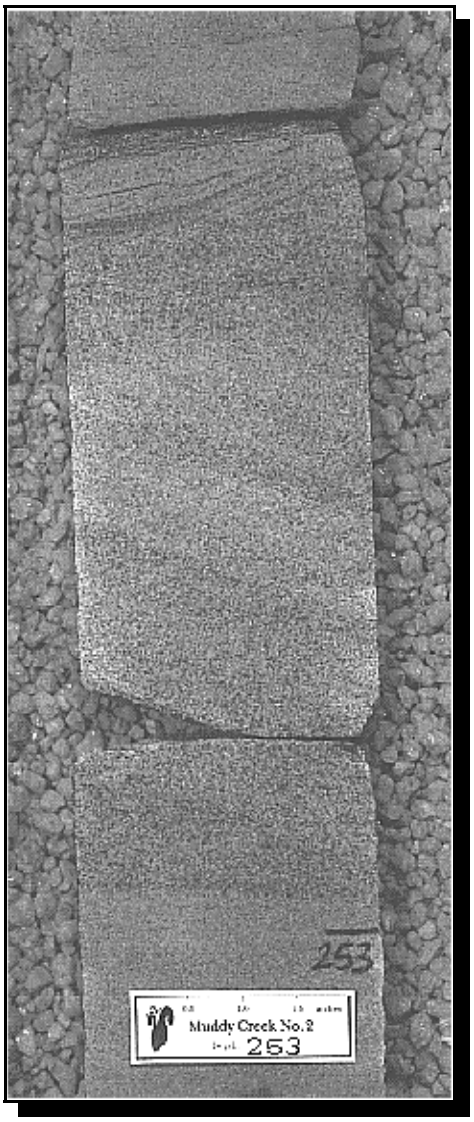


Figure 6-29. Trough cross-stratification in upper shoreface of parasequence Kf-2-Mi-b. Core from drill hole MC-2 at 253 feet.

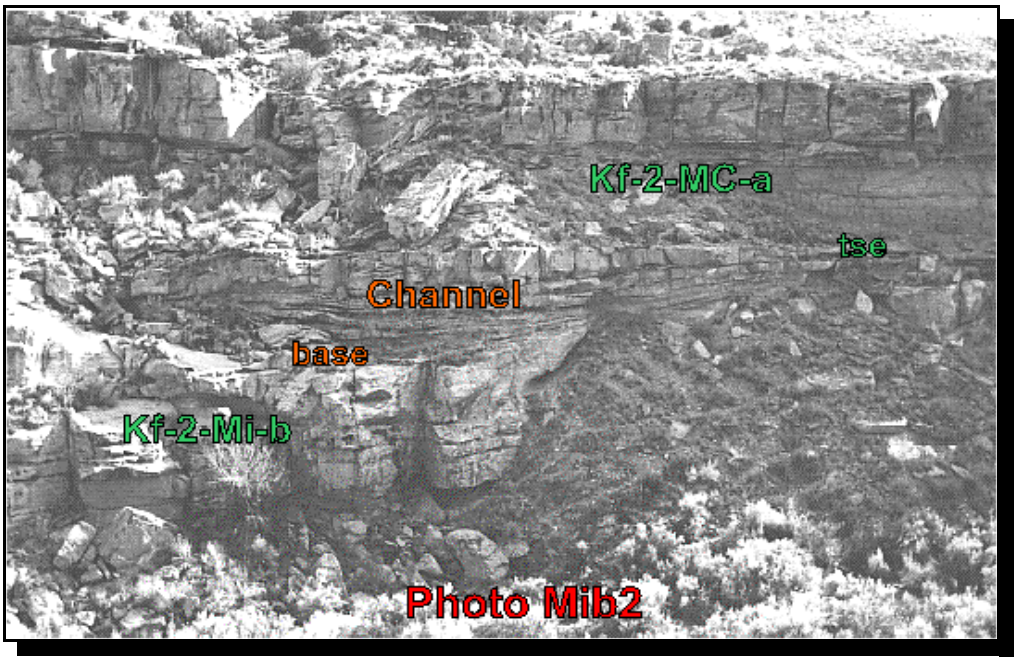


Figure 6-30. One of many small channels cut into the top of parasequence Kf-2-Mi-b is exposed just north of the "Upper Gooseneck" on the east side of Muddy Creek Canyon. As shown in the following figure, this one includes evidence of tidal flow. A transgressive surface of erosion (tse) separates parasequences Kf-2-Mi-b and Kf-2-MC-a.

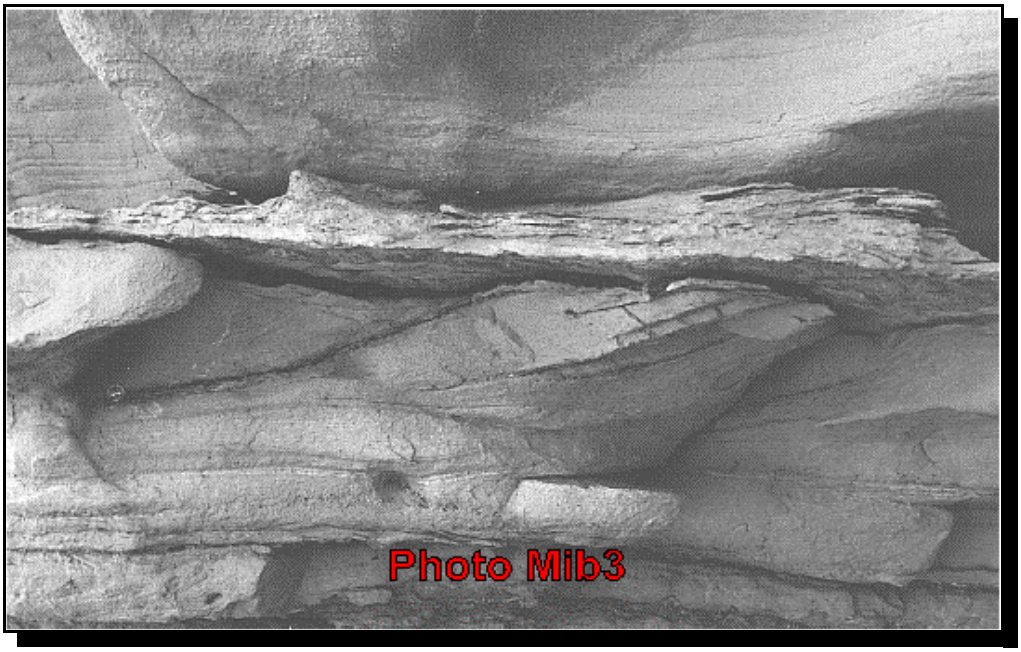


Figure 6-31. Clay drapes on cross-stratification sets in parasequence Kf-2-Mi-b, which have a vaguely sigmoidal form, suggest slack-water deposition of fines as a result of tidal influence. The channel shown here and in the preceding figure may have been a tidal channel on the lower coastal plain, or the lower, tidally influenced part of a small river.

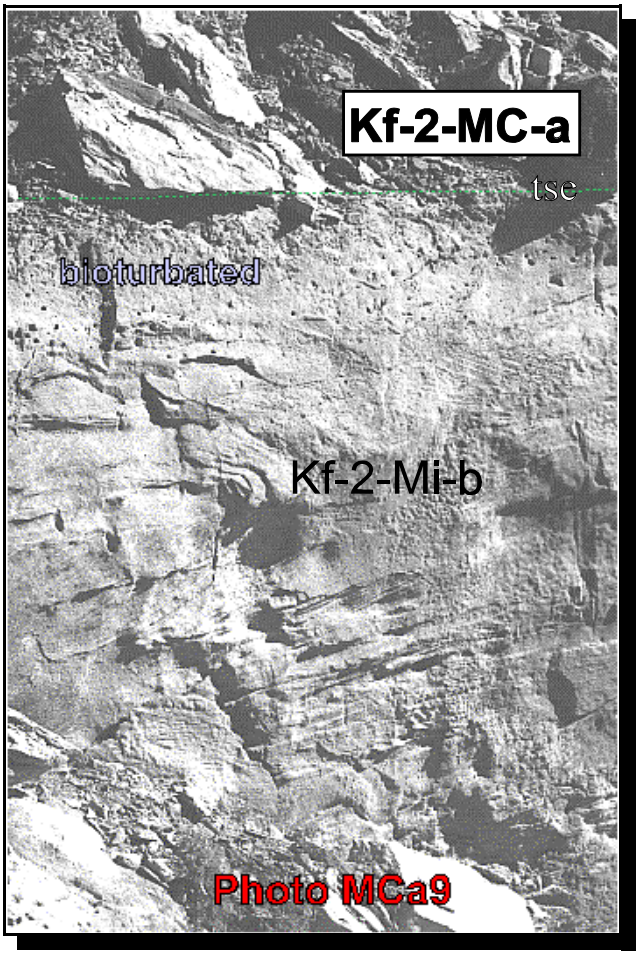


Figure 6-32. The top of the shoreface deposits of parasequence Kf-2-Mi-b is truncated by a transgressive surface of erosion throughout Muddy Creek Canyon. The surface is overlain by marine mudstone of parasequence Kf-2-MC-a. Roughly a foot of sandstone beneath the surface has been bioturbated. Multi-direction trough cross-stratification of the upper shoreface is preserved beneath the burrowed interval.



Figure 6-33. Sharp-based, upward-fining storm layers of sandstone in the lower delta front of parasequence Kf-2-MC-a, east side of Muddy Creek Canyon.

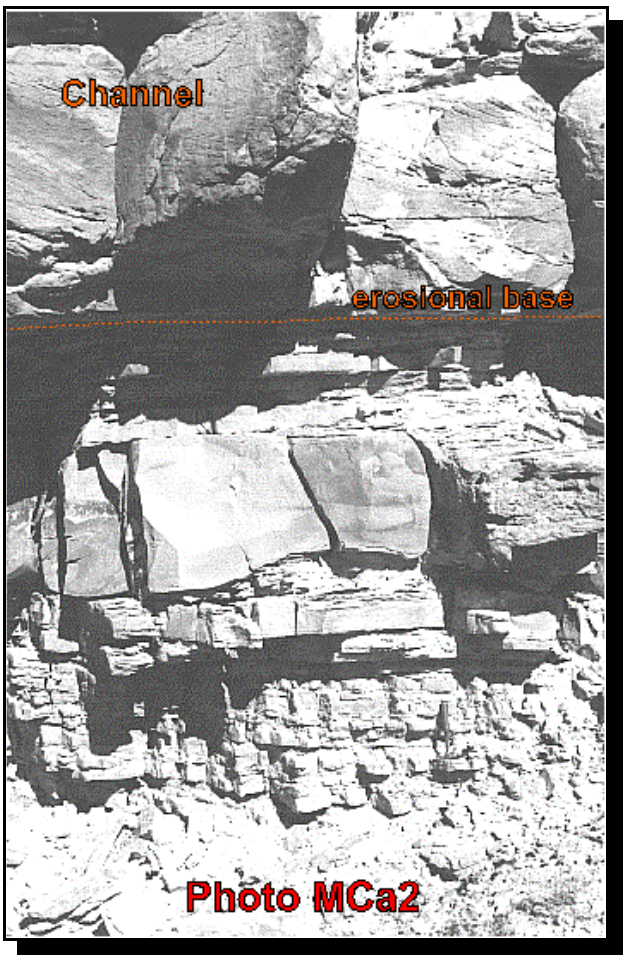


Figure 6-34. Exposure of parasequence Kf-2-MC-a on the east side of Muddy Creek Canyon. The erosional contact between the meanderbelt and the underlying delta-front is indicated. A prominent storm bed in the delta-front interval displays erosional relief, shown in a closer view in figure 6-35.

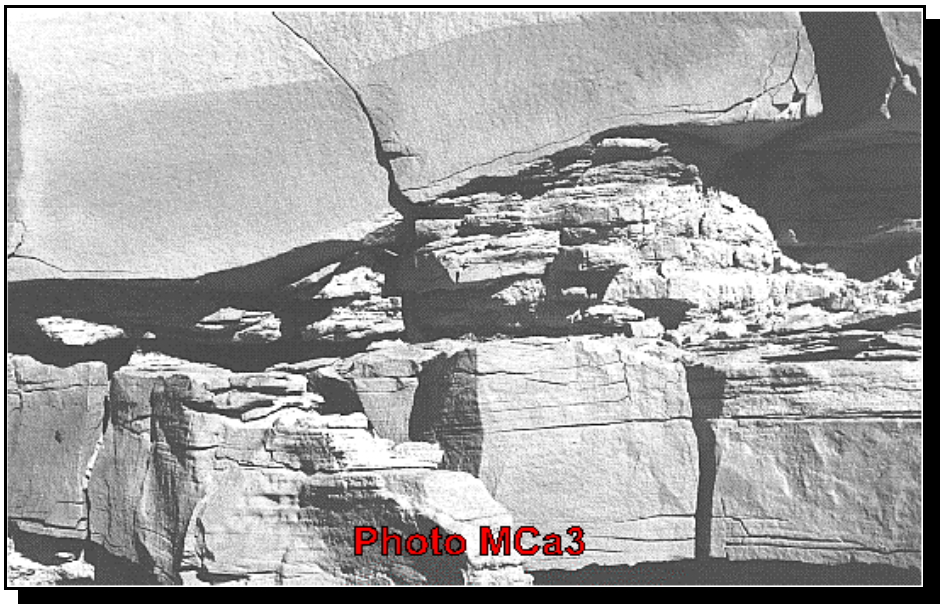


Figure 6-35. Closer view of the erosional contact at the base of a storm bed shown in figure 6-34.

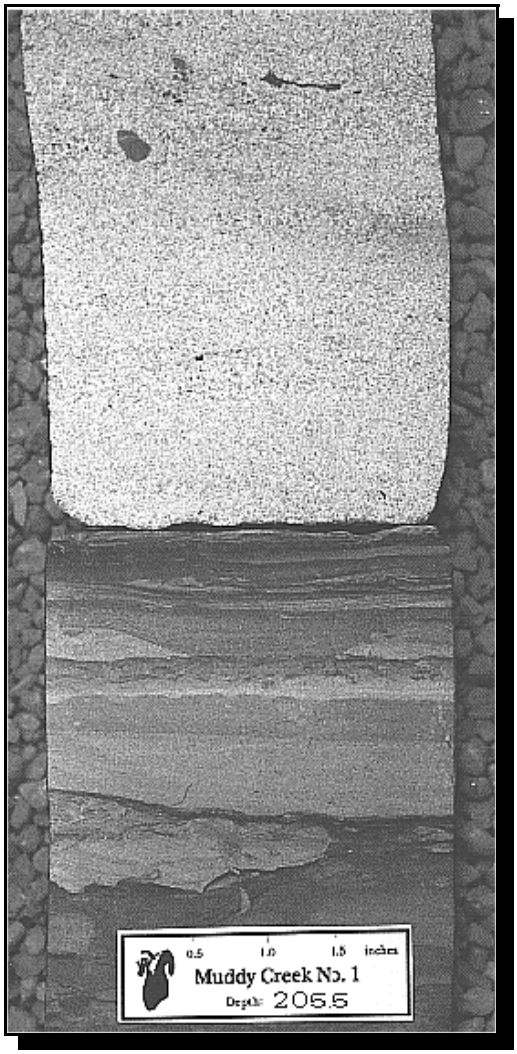


Figure 6-36. Erosional contact separating meanderbelt and underlying delta-front deposits of parasequence Kf-2-MC-a. Core from drill hole MC-1 at 205.5 feet.



Figure 6-37. Erosional contact between cross-stratified, medium-grained sandstone of the meanderbelt sequence and underlying lower delta-front, thinly interbedded sandstone and mudstone of parasequence Kf-2-MC-a. Core from drill hole MC-4 at 273 feet.



Figure 6-38. Large, ragged-edged, mudstone rip-up clasts in the lower part of the meanderbelt of parasequence Kf-2-MC-a. Core from drill hole MC-2 at 235 feet.



Figure 6-39. Mudstone clasts in the lower part of the meanderbelt of parasequence Kf-2-MC-a. Core from drill hole MC-1 at 202 feet.



Figure 6-40. Cross-stratification sets up to three feet thick are present in the meanderbelt deposit of parasequence Kf-2-MC-a, although sets about a foot thick are much more common. The cross-stratification set pictured here is found at the base of the unit.

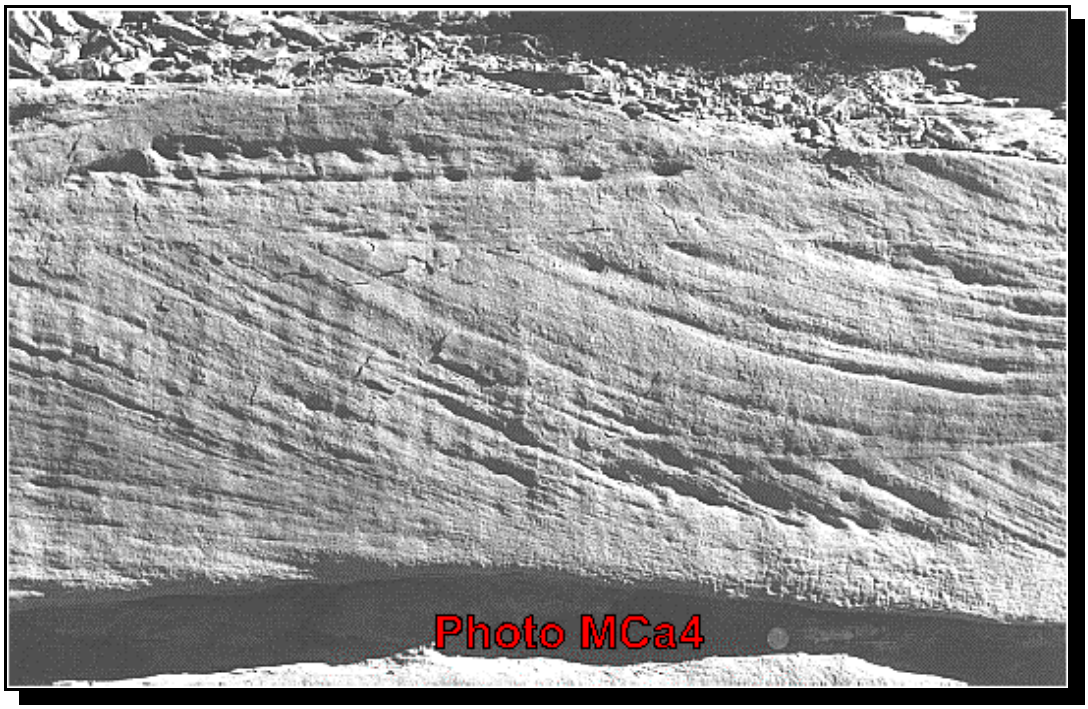


Figure 6-41. Trough cross-stratification in medium-grained sandstone in the meanderbelt deposit of parasequence Kf-2-MC-a, east side of Muddy Creek Canyon.

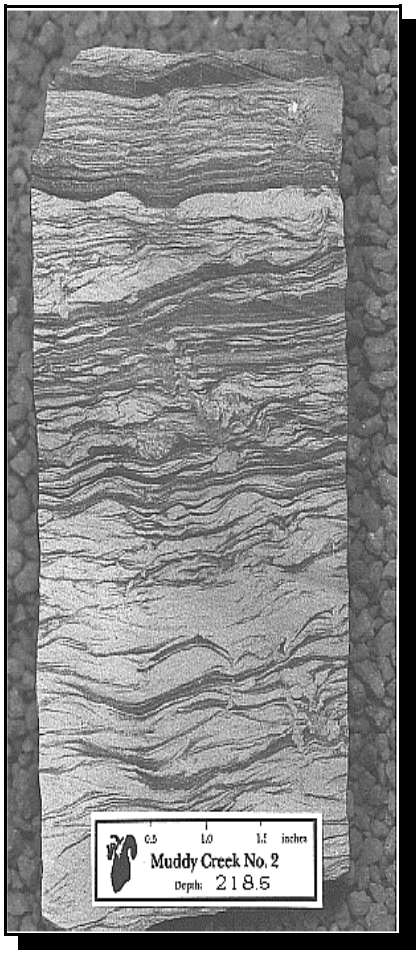


Figure 6-42. Current ripples with mud drapes in the upper part of the meanderbelt sequence of parasequence Kf-2-MC-a. The abundant mud drapes may be evidence of a tidal influence in the channel, whose mouth lay only a few miles or more to the northeast. Burrows are probably *Planolites* and are not diagnostic of a particular paleoenvironment. Core from drill hole MC-2 at 218.5 feet.

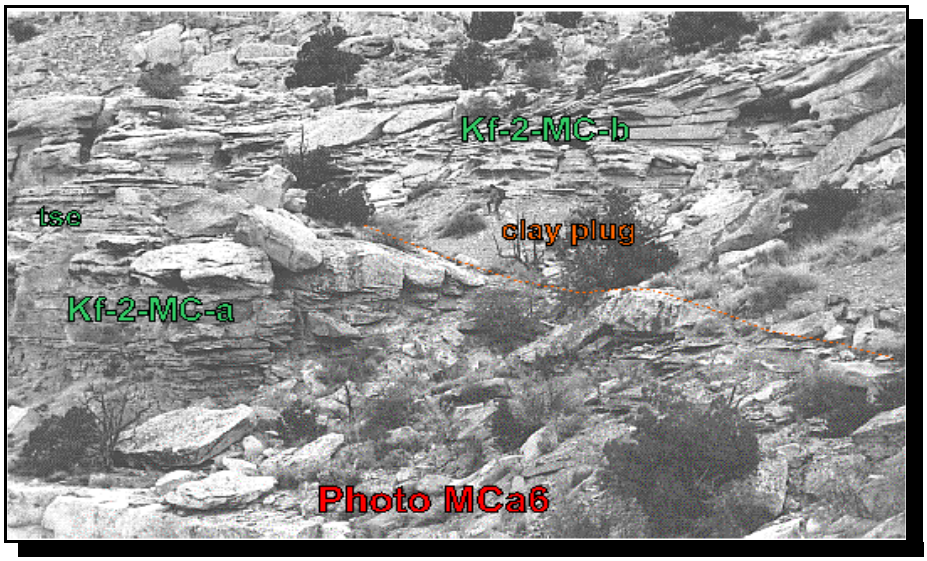


Figure 6-43. Slope on the canyon wall is standing is formed on a clay plug with the meanderbelt of parasequence Kf-2-MC-a. The relatively steep slope on sandstone to the left appears to be the cut-bank side of the channel, indicating that this clay plug belongs to the southern of the two meanderbelt recognized.

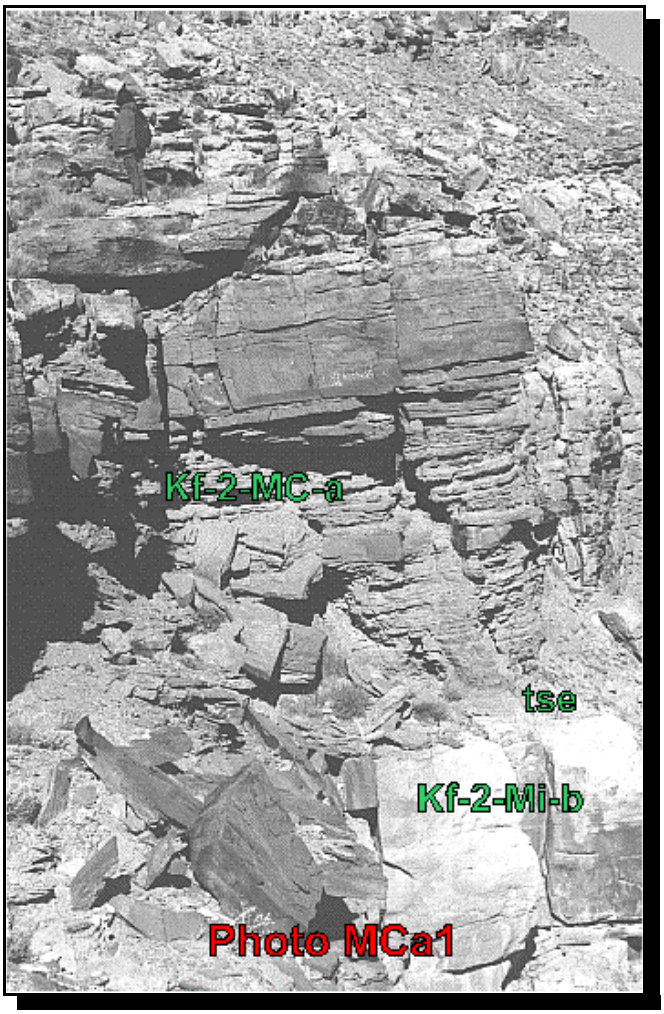


Figure 6-44. Most of the thickness of the delta-front deposit of parasequence Kf-2-MC-a was removed by erosion associated with emplacement of the meanderbelt. In a single, small area on the west wall of the canyon, nearly the full original thickness of the unit is preserved.

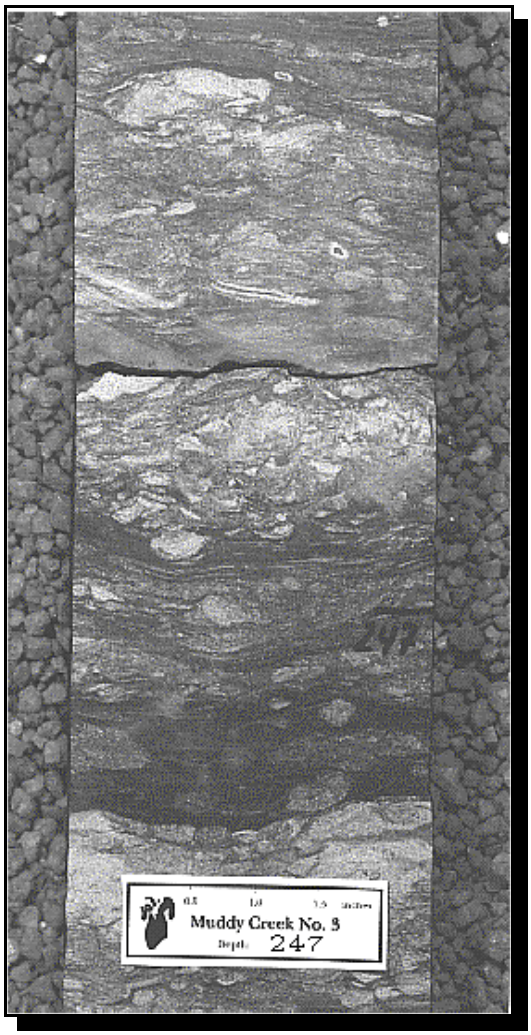


Figure 6-45. Bioturbated lower delta-front deposits of parasequence Kf-2-MC-a. A diverse trace fossil assemblage indicative of normal or near-normal marine salinities is present. Core from drill hole MC-3 at 247 feet.

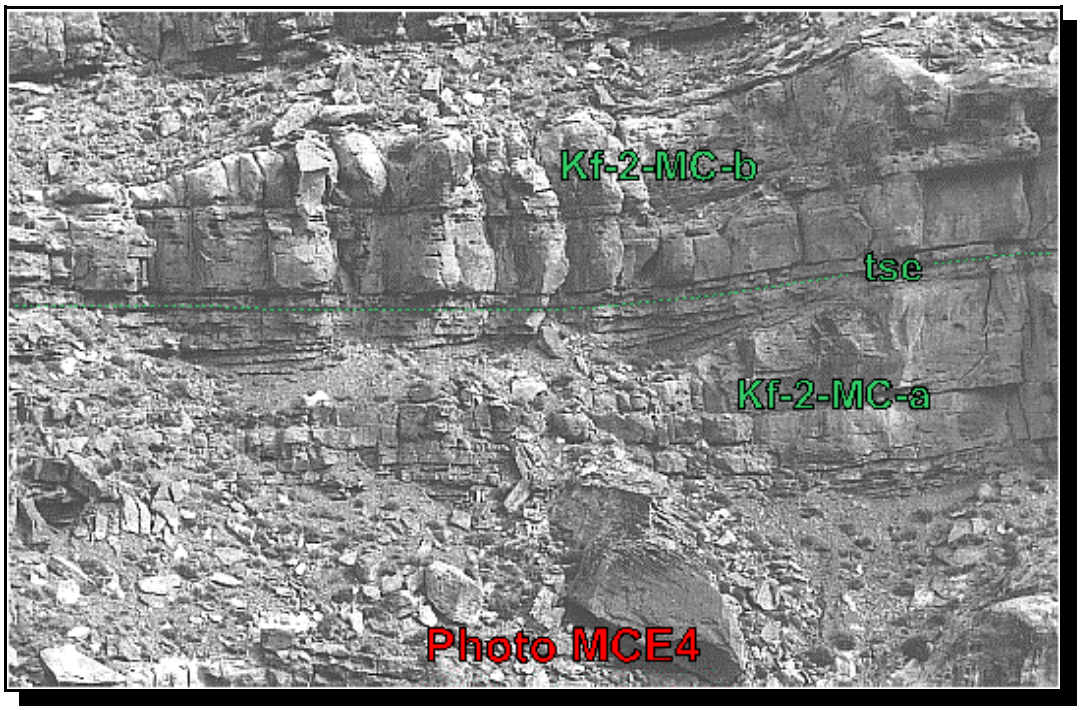


Figure 6-46. Lateral accretion within the meanderbelt of parasequence Kf-2-MC-a truncated by the transgressive disconformity at the base of parasequence Kf-2-MC-b. The later is cut by a fine-grained-filled channel in the left part of the photo. Closer view is shown in figure 6-47. East side of Muddy Creek Canyon upstream of the "Upper Gooseneck."

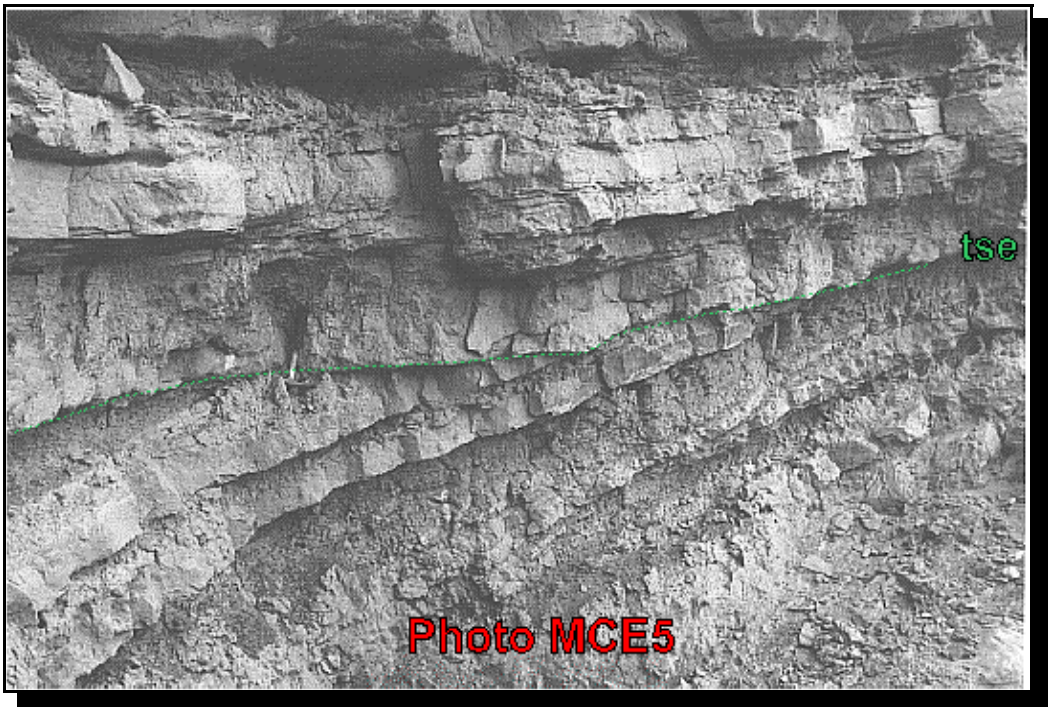


Figure 6-47. Closer view of truncation of lateral accretion surfaces shown in figure 6-46.

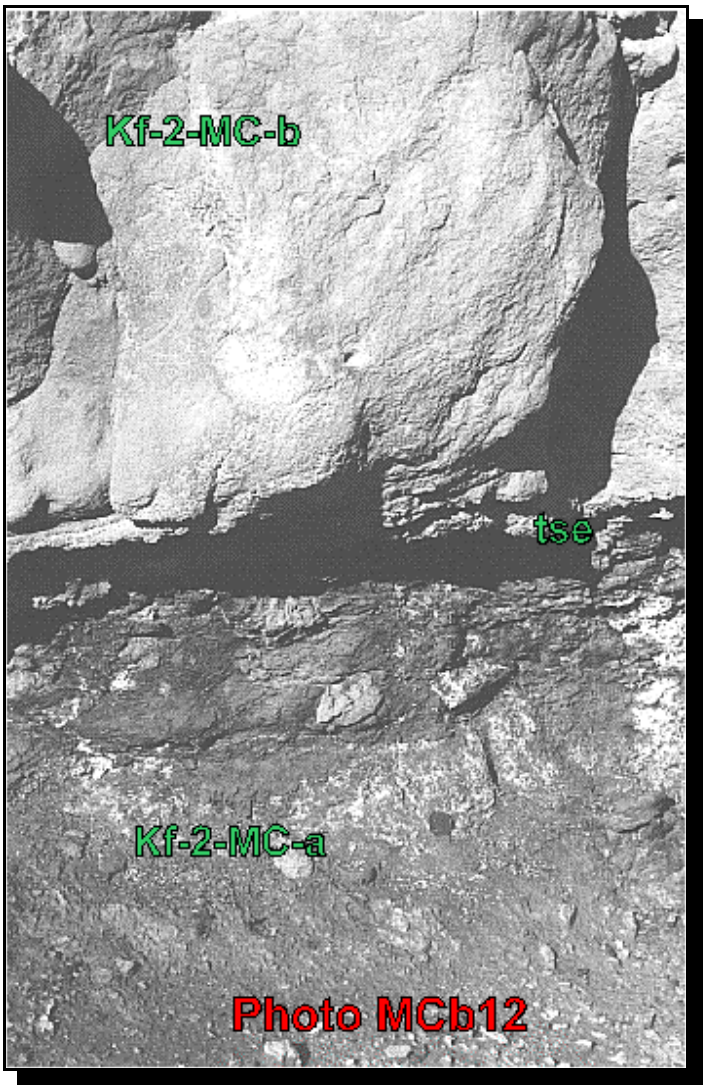


Figure 6-48. Transgressive surface of erosion separates carbonaceous, sandy mudstone of parasequence Kf-2-MC-a from overlying shoreface sandstone of parasequence Kf-2-MC-b. East side of Muddy Creek Canyon.

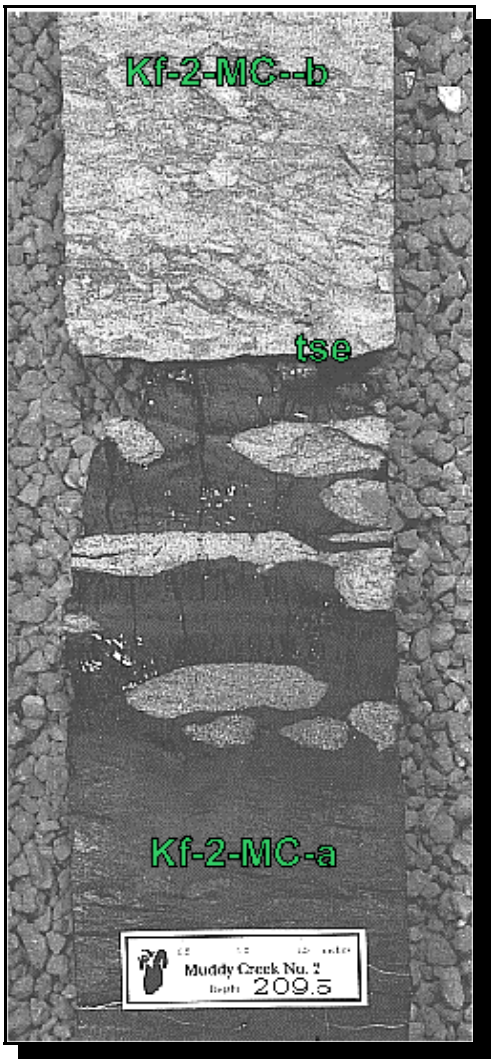


Figure 6-49. Transgressive surface of erosion (tse) separating parasequences Kf-2-MC-b and Kf-2-MC-a. In drill hole MC-2, a thin split of the A coal zone is present beneath the surface. Sand filled burrows, probably *Thalassinoides*, are present in the coal. The fact that they are found in what was certainly a firm substrate (peat) makes them assignable to the *Glossifungites ichnofacies*, the presence of which is commonly invoked as evidence of a parasequence boundary. Core from drill hole MC-2 at 209.5 feet.

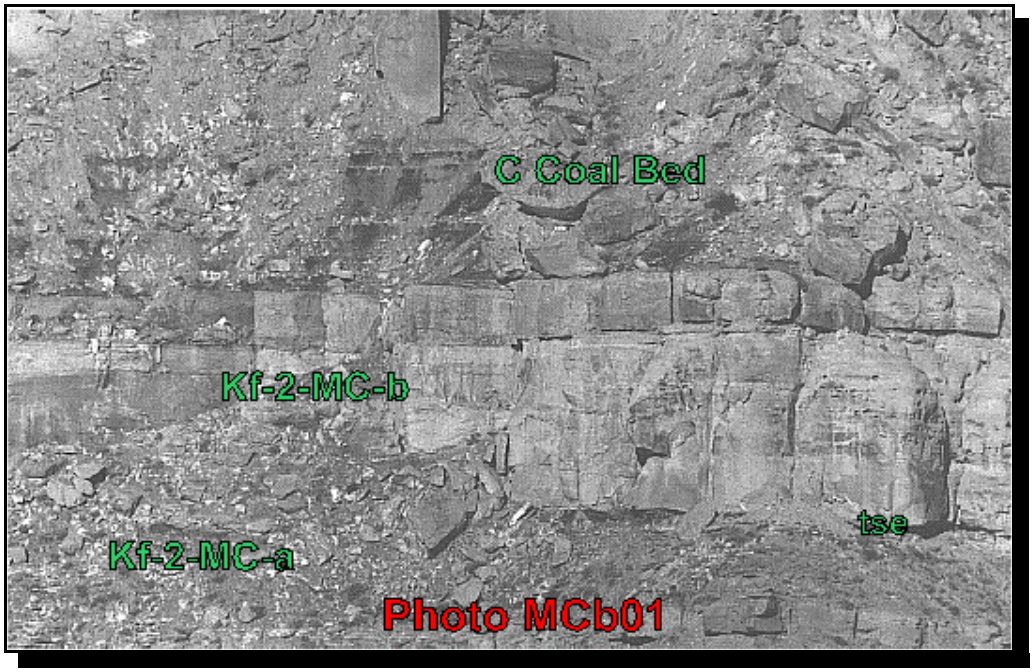


Figure 6-50. Sandstone of parasequence Kf-2-MC-b is isolated from the underlying meanderbelt deposits by an interval of carbonaceous mudstone on the west side of Muddy Creek Canyon in the northern part of the "Lower Reach" of the canyon. Coal was cored in drill hole MC-a at this stratigraphic level. The carbonaceous mudstone and coal represents a lower split of the A coal zone. The C coal is exposed higher in the slope.

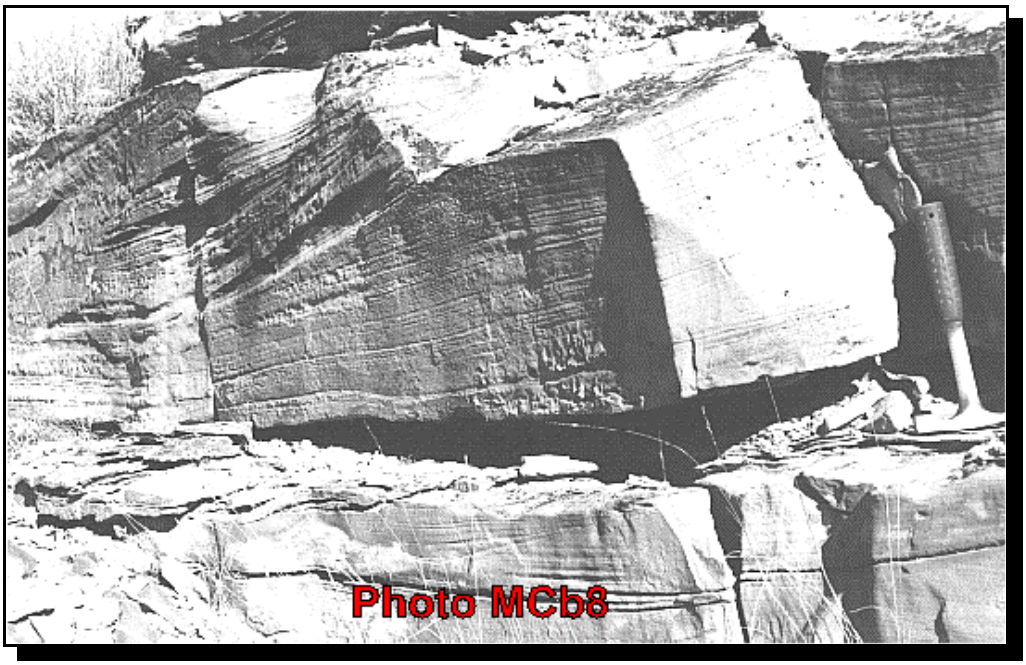


Figure 6-51. Hummocky cross-stratification in very fine to fine-grained sandstone of the middle shoreface of parasequence Kf-2-MC-b, east side of Muddy Creek Canyon.

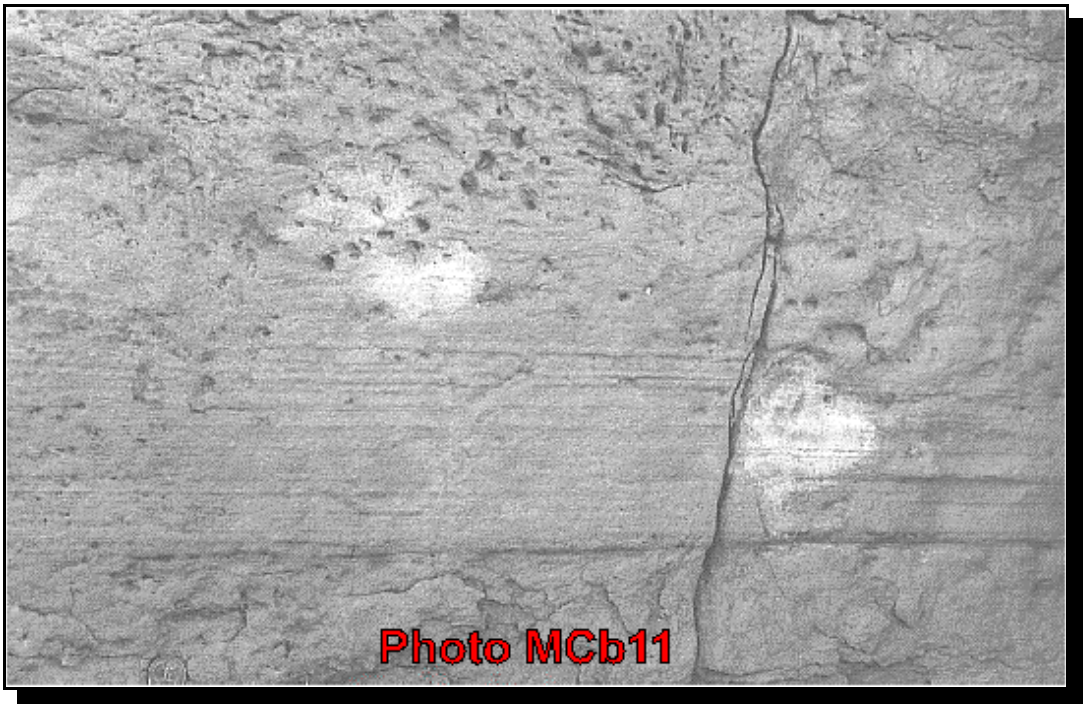


Figure 6-52. Remnant storm layer in bioturbated middle shoreface deposits of parasequence Kf-2-MC-b, east side of Muddy Creek Canyon.

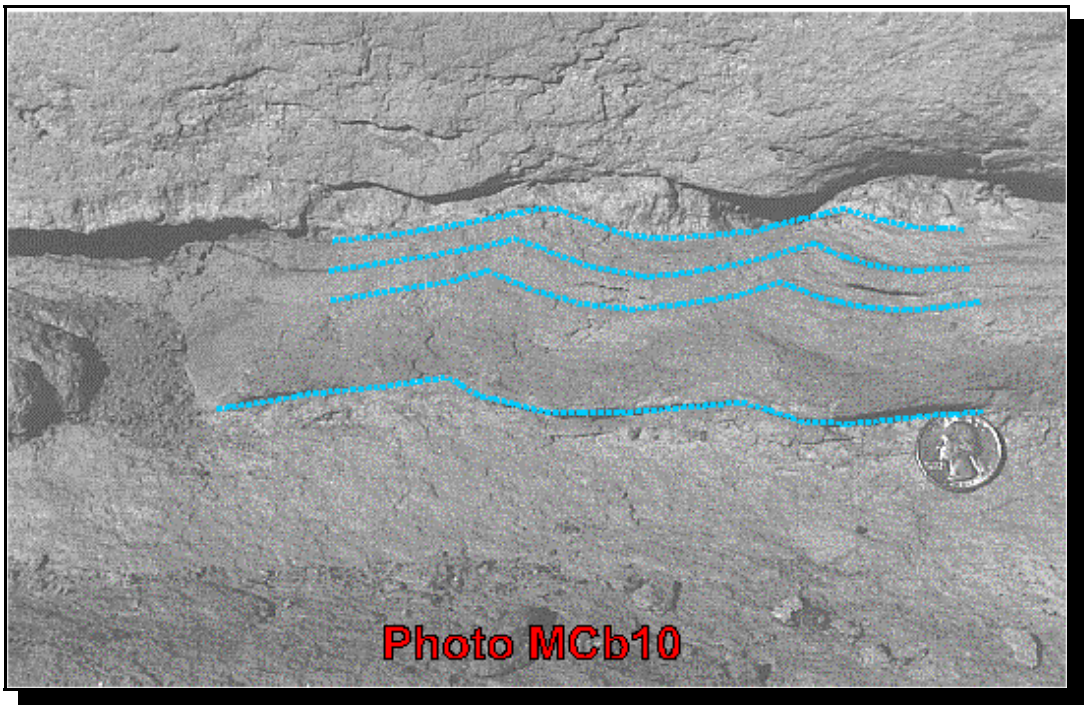


Figure 6-53. Single storm layer containing climbing oscillation ripple stands out in burrowed sandstone of middle shoreface of parasequence Kf-2-MC-b, west side of Muddy Creek Canyon.



Figure 6-54. Vertically climbing oscillation ripples in storm-layered, burrowed middle shoreface deposits of parasequence Kf-2-MC-b. Core from hole MC-5 at 364 feet.

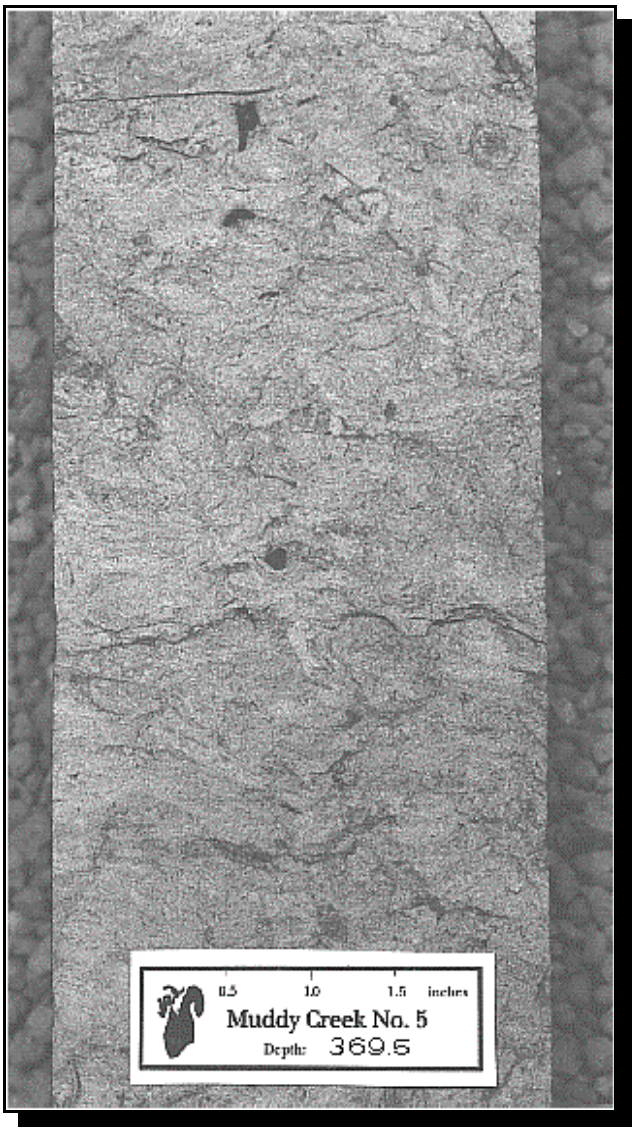


Figure 6-55. Bioturbated sandstone of the middle shoreface of parasequence Kf-2-MC-b. Core from drill hole MC-5 at 369.5 feet.

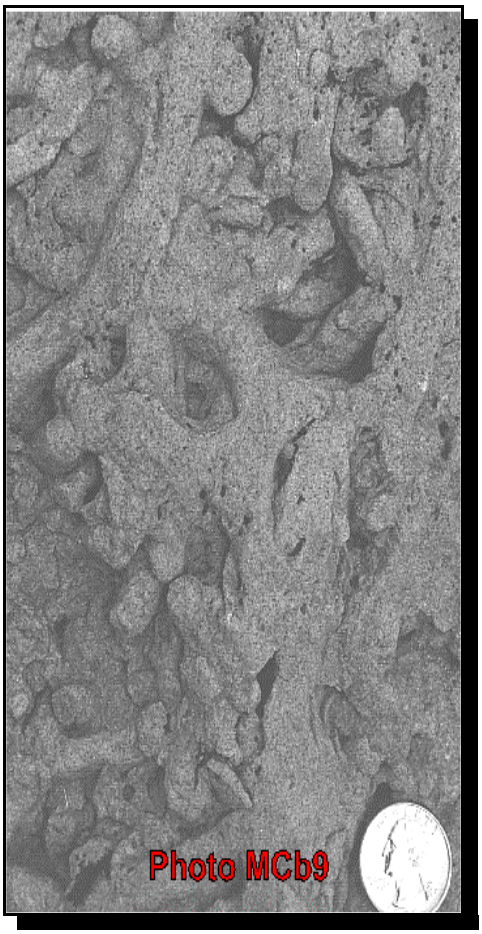


Figure 6-56. ***Thalassinoides*** **in middle shoreface sandstone of parasequence Kf-2-MC-b, east side of Muddy Creek Canyon, southeast of the "Lower Gooseneck."**

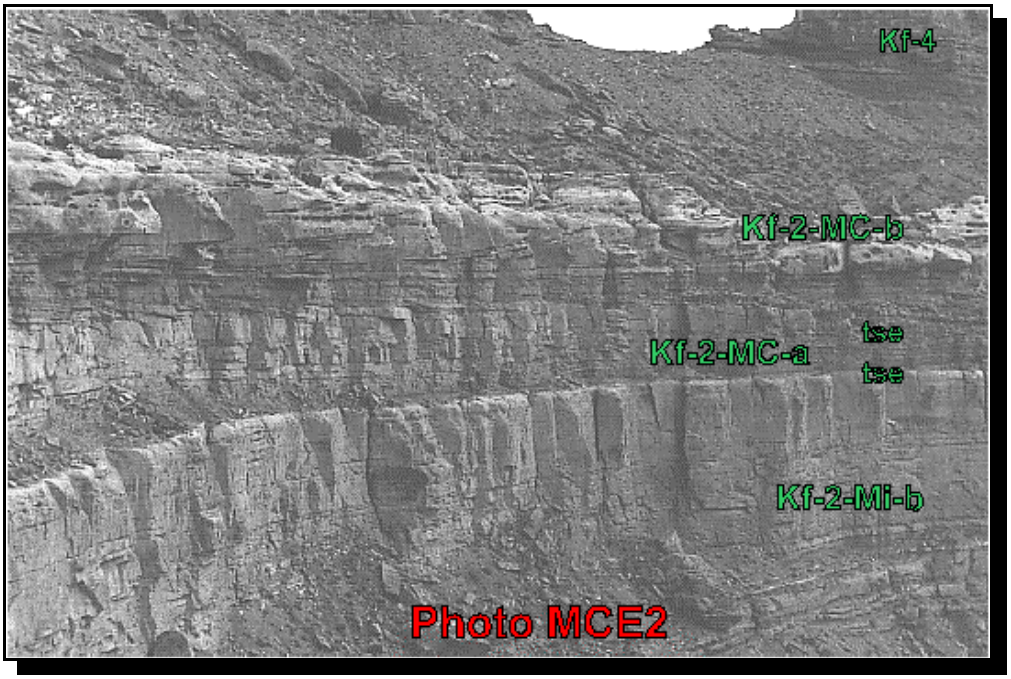


Figure 6-57. Opposed directions of lateral accretion in the meanderbelt of parasequence Kf-2-MC-a and the overlying tidal inlet of parasequence Kf-2-MC-b are evident in the amphitheater just south of the "Lower Gooseneck," east side of Muddy Creek Canyon.

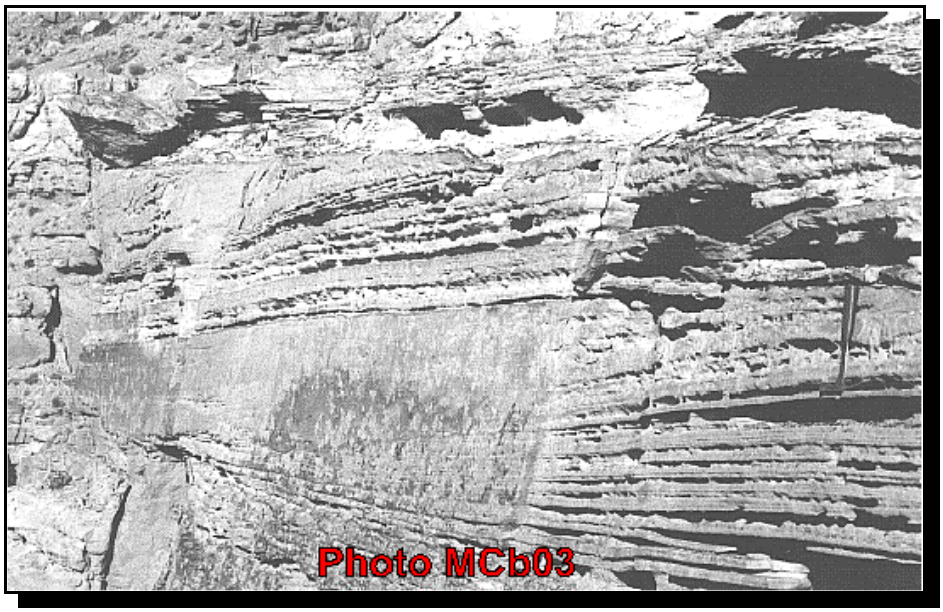


Figure 6-58. Large-scale, planar-tabular cross-stratification is characteristic of the tidal inlet facies of parasequence Kf-2-MC-b. The inclined sets dip toward the north in this exposure on the east side of Muddy Creek Canyon.



Figure 6-59. Large-scale, planar-tabular cross-stratification in the tidal inlet facies of parasequence Kf-2-MC-b, east side of Muddy Creek Canyon. The surfaces become steeper toward the top of the deposit.



Figure 6-60. Planar-tabular cross-stratification representing large-scale, lateral accretion surfaces in the tidal inlet facies of parasequence Kf-2-MC-b. Core from drill hole MC-3 at 198 feet.



Figure 6-61. Trough cross-stratification (X-TR) is present locally among the large-scale, planar tabular sets (X-PT) of the tidal inlet facies of parasequence Kf-2-MC-b.



Figure 6-62. Trough cross-stratification within tidal inlet facies of parasequence Kf-2-MC-b. Figure 6-63 shows closer view of the trough cross-stratification set.

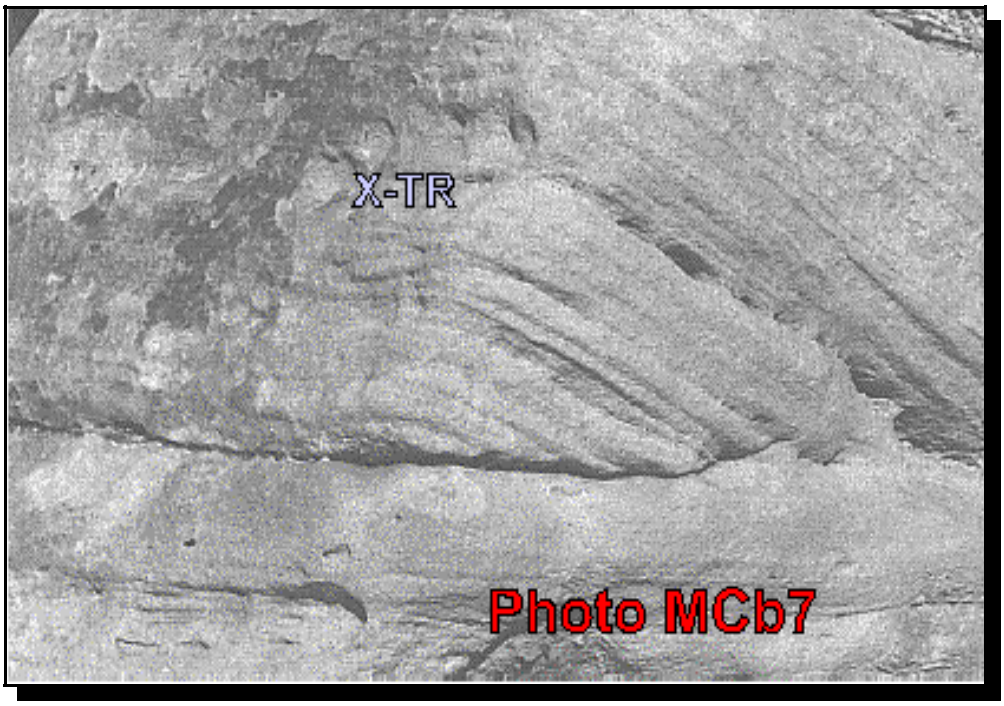


Figure 6-63. Closer view of trough cross-stratification shown in figure 6-62.

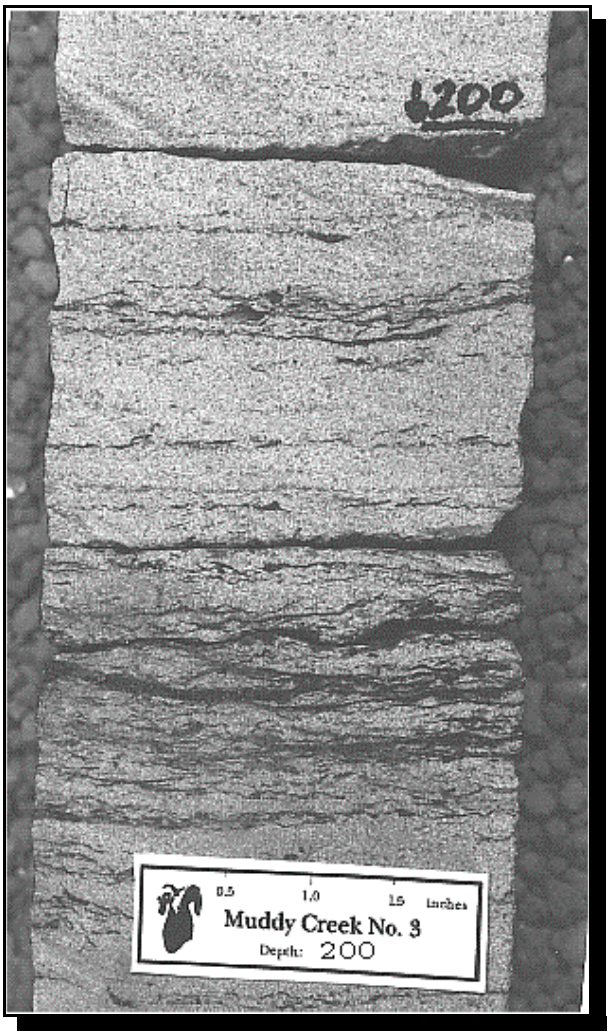


Figure 6-64. Planar-laminated, medium-grained sandstone bearing coalified plant fragments, lower part of tidal inlet sequence, parasequence Kf-2-MC-b. Core from drill hole MC-3 at 200 feet.



Figure 6-65. Current ripple cross-lamination in deposits of a late Kf-2 age channel that locally replaces parasequence Kf-2-MC-b in the vicinity of the "Upper Gooseneck." Core from drill hole MC-5 at 239 feet. This channel deposit has been identified on adjacent outcrops.

Stratigraphy and Depositional History of Kf-2 in Muddy Creek Canyon

The four parasequences distinguished in Kf-2 in Muddy Creek Canyon are shown diagrammatically in the cross section on figure 6-3, which shows these units from the southwest part of the Muddy Canyon area northeastward into "Grassy Canyon." Stratigraphic units in this cross section are not drawn to scale and considerable latitude was taken in drawing the shapes of the sand bodies. This was necessitated by the different shoreline orientations of the units. The surfaces identified were completed from photomosaics throughout the length of the Kf-2 outcrops in Muddy Creek Canyon.

Kf-2 is about 200 feet (60 m) thick in the Muddy Creek Canyon case-study area, which is an exceptionally great thickness. There are three principal reasons for this great thickness.

1. The transgressive surface of erosion (tse) separating parasequence Kf-2-Mi-b and Kf-2-MC-a records a very substantial transgression, one which shifted the shoreline from a position somewhere northeast of Short Canyon at least 12 miles (19 km) southwestward to the mouth of Miller Canyon. It is warranted to consider the part of Kf-2 deposited prior to this transgression and the part deposited following this transgression to be separate parasequence sets. In Muddy Creek Canyon, where the two parasequence sets are vertically juxtaposed, the thickness of Kf-2 represents two parasequence sets, which might, therefore, be expected to be twice as thick as other parasequence sets.

2. A greater amount of space was available to accommodate sediment beyond the seaward limit of underlying unit Kf-1, where existing space had not yet been filled with sediment.

3. Initial progradation of parasequence Kf-2-MC-b (the first parasequence in the younger parasequence set of Kf-2) was slow and was accompanied by substantial rise of relative sea level. Parasequence Kf-2-MC-b increases to a thickness of about 75 feet (23 m) on the east side of "Grassy Canyon," only about a mile seaward from its landward pinchout.

Kf-2-Miller Canyon-a

The seaward part of parasequence Kf-2-Mi-a is present in Muddy Creek Canyon. It is about 60 feet (18 m) thick at the mouth of Miller Canyon and thins north westward up Miller Canyon and northward up Muddy Creek Canyon. Exposures become poor as the unit approaches the canyon floors, but it is apparent that the seaward feather-edge cannot lie far from the outcrops. Traced eastward into Grassy Canyon and the "Molen Amphitheater" beyond, the unit thins and becomes indistinguishable before reaching 'Molen Point." Parasequence Kf-2-Mi-a thickens southward in the Coal Cliffs along the east side of "Cowboy Mesa," constituting about half the thickness of the combined Kf-2-Mi-a and -b interval at "Bear Gulch."

In the Muddy Creek drill holes (figure 6-6), parasequence Kf-2-Mi-a ranges between about 70 feet (21 m) in MC-1, where it is thickened as a result of growth faulting, and a very small thickness (less than 30 feet [15 m]) in MC-5, near what must be its seaward feather-edge.

Parasequence Kf-2-Mi-a shares a transitional base with the underlying Tununk Shale (the stratigraphic position of the Clawson and Washboard units of the Ferron are identifiable in the Muddy Canyon area on the basis of some platy, laminated sandstones, but the units are considered to have feathered out westward into the Tununk in the western part of the "Molen Amphitheater"). Parasequence Kf-2-Mi-a consists of an upward-coarsening succession that grades from mudstone with thin storm layers of sandstone to planar laminated and hummocky/swaley cross-stratified sandstone with only minor interbeds of mudstone. It is capped by a flooding surface, at which the boundary with overlying parasequence Kf-2-Mi-b is drawn. Because parasequence Kf-2-Mi-a is an incomplete shoreline succession, it is difficult to interpret whether it was deposited on a fluvial- or wave-dominated coastline. The fact that it thins toward the northwest in Miller Canyon, coupled with the fact that most or all other units of the Ferron that prograded in this direction display evidence of fluvial domination, suggests that it may be a fluvial-dominated succession. Nothing observable on the outcrops, however, can be cited as clear-cut evidence of this.

Rotated slump blocks (figure 6-11) formed by growth faulting are abundant and well developed in the vicinity of the "Lower Gooseneck" and adjacent parts of the "Lower and Middle Reaches" of the canyon (figure 6-66). Failure occurred toward the northwest in all cases where individual slump blocks and their faults can be traced across the canyon. Failure in this direction is probably related to the pattern of subsidence that existed during Ferron time (see figure 1-6), the area of maximum subsidence lying to the northwest of the case-study area. The sections preserved in these slumps are greatly thickened relative to adjacent, undisturbed sections of parasequence Kf-2-Mi-a. Most of the movement on the faults occurred when progradation had reached middle delta front or upper lower or lower middle shoreface water depths: the thickened sections generally consist predominantly of planar laminated to hummocky/swaley cross-stratified sandstone with minor interbeds of mudstone. Cross-stratification is present in the upper strata of some of the rotated blocks. Cross-stratification sets can, in some cases, be traced laterally into hummocky/swaley cross-stratification. The structures probably formed as storm-driven currents moved sand into the depressions formed by faulting, thus filling the depressions to the level of the shoreface or delta-front profile. Noticeable thinning of parasequence Kf-2-Mi-b above some of the larger rotated slump block attests to differential compaction of the parasequence Kf-2-Mi-a section during loading by overlying sediments of parasequence Kf-2-Mi-b. Drill holes MC-1 and MC-3 are interpreted to have penetrated rotated slump blocks, based on bedding inclination, and the presence of small-scale faulting and deformation structures.

Progradation and contemporaneous growth faulting of parasequence Kf-2-Mi-a are shown diagrammatically in cross section view in figure 6-67. The paleogeography of the early phase of progradation of parasequence Kf-2-Mi-a is shown in figure 6-68. It is probable that the shoreline was wave-dominated at this time, although evidence is sparse. The late phase of progradation is shown in figure 6-69. Thinning of the unit north westward up Miller Canyon and northward up Muddy Creek Canyon is shown to reflect the lobate shape of a subdelta lobe. Channels that fed this lobe must have been small and shallow: sediments that accumulated in them were stripped off during the following transgression, which is shown in figure 6-70.

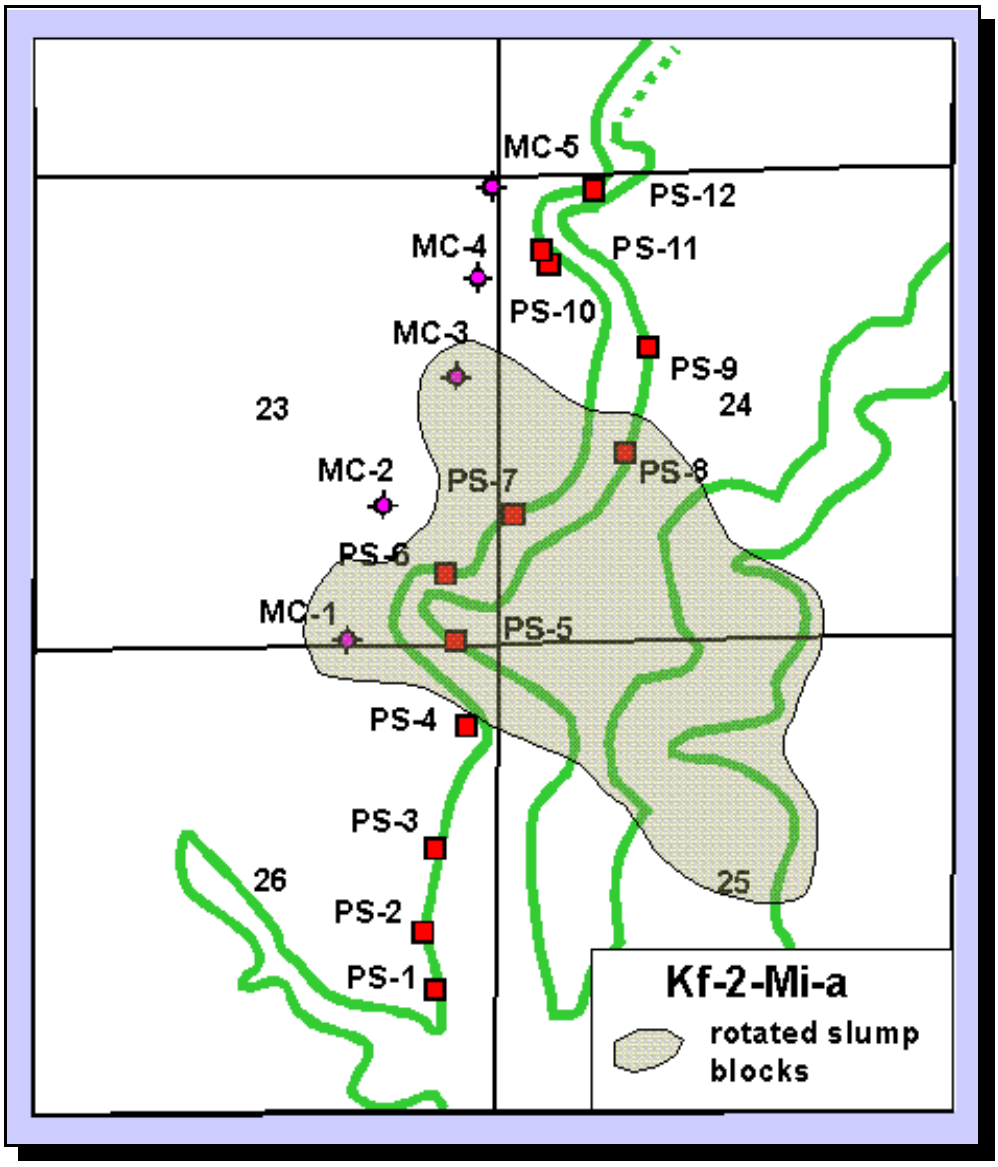


Figure 6-66. Map showing the area in which rotated slump blocks are abundant in parasequence Kf-2-Mi-a.

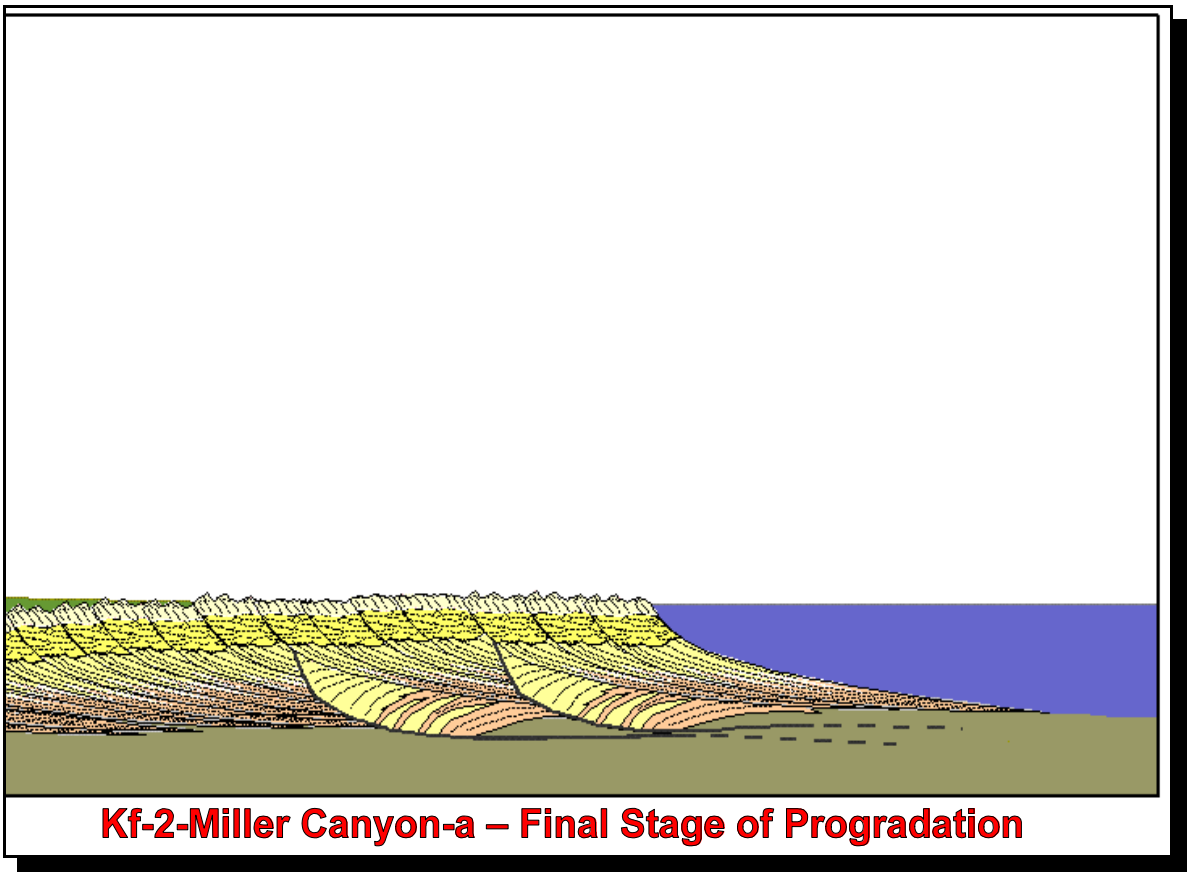


Figure 6-67. Diagrammatic cross section showing final stage of progradation of parasequence Kf-2-Mi-a.

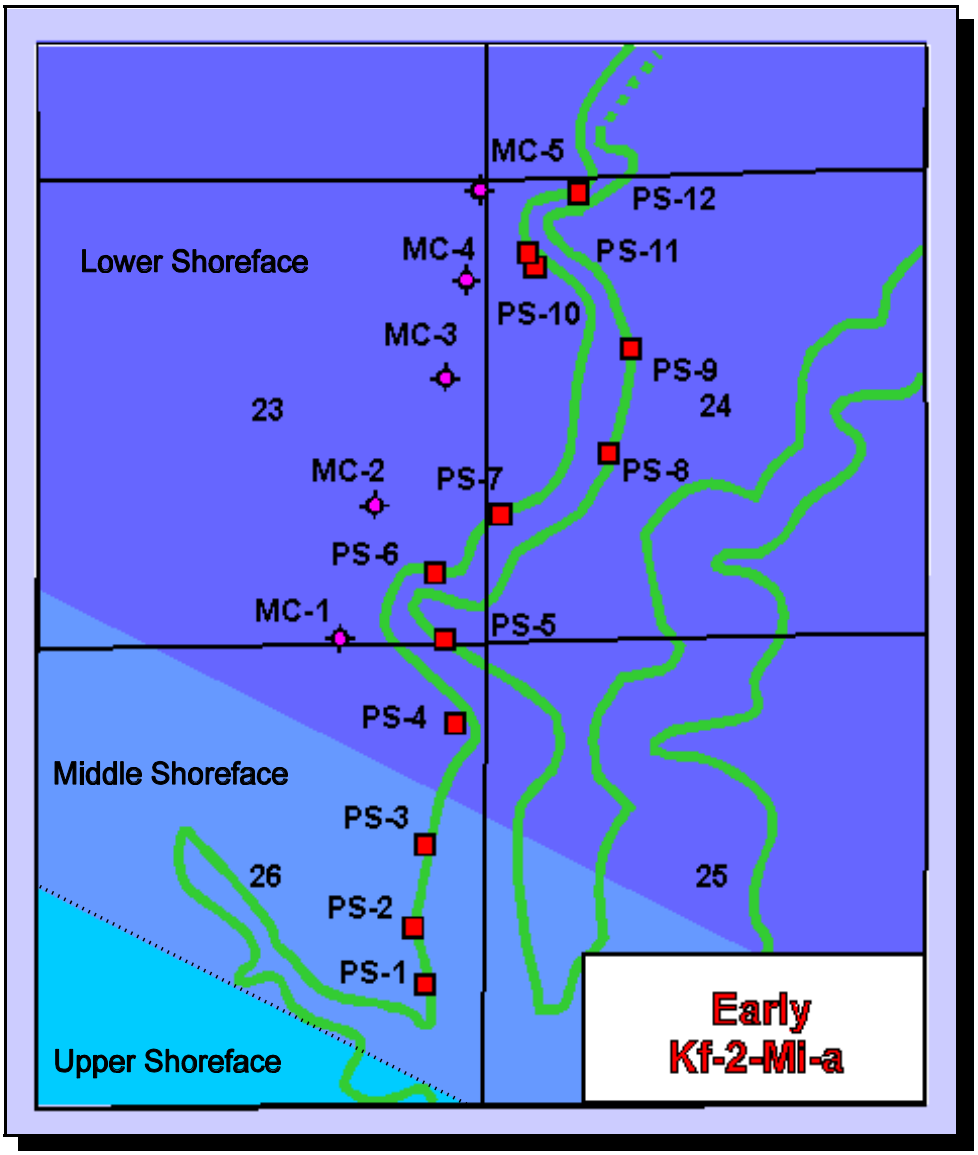


Figure 6-68. Early stage of progradation of the shoreline of parasequence Kf-2-Mi-a, probably as a wave-dominated shoreline. The gray (green) line is the approximate outcrop of Kf-2. The locations of the Muddy Creek drill holes and of the photosections in Muddy Creek Canyon are shown.

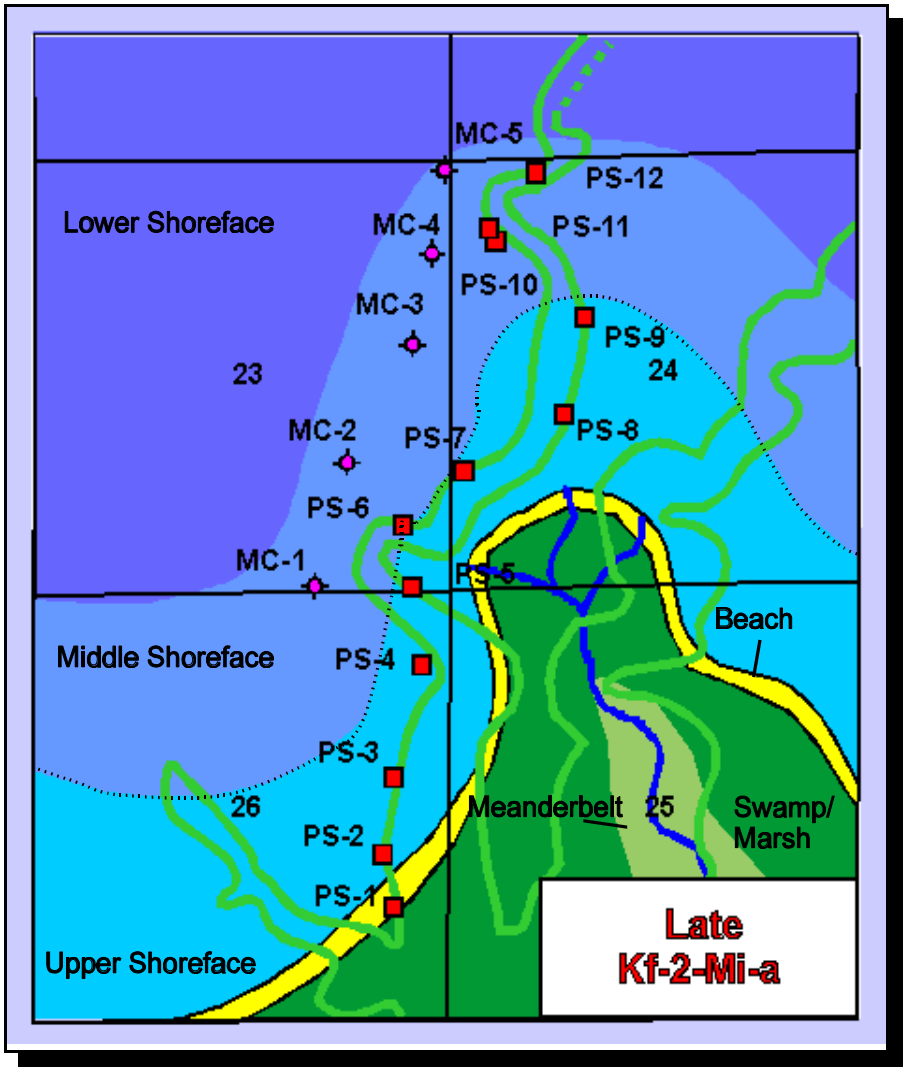


Figure 6-69. Late stage of progradation of parasequence Kf-2-Mi-a, shown here immediately prior to transgression. Although evidence is sparse, it is probable that the final progradation occurred in the form of a fluvial-dominated, lobate delta. Any delta-plain deposits that accumulated in the mapped area were subsequently eroded in the following transgression.

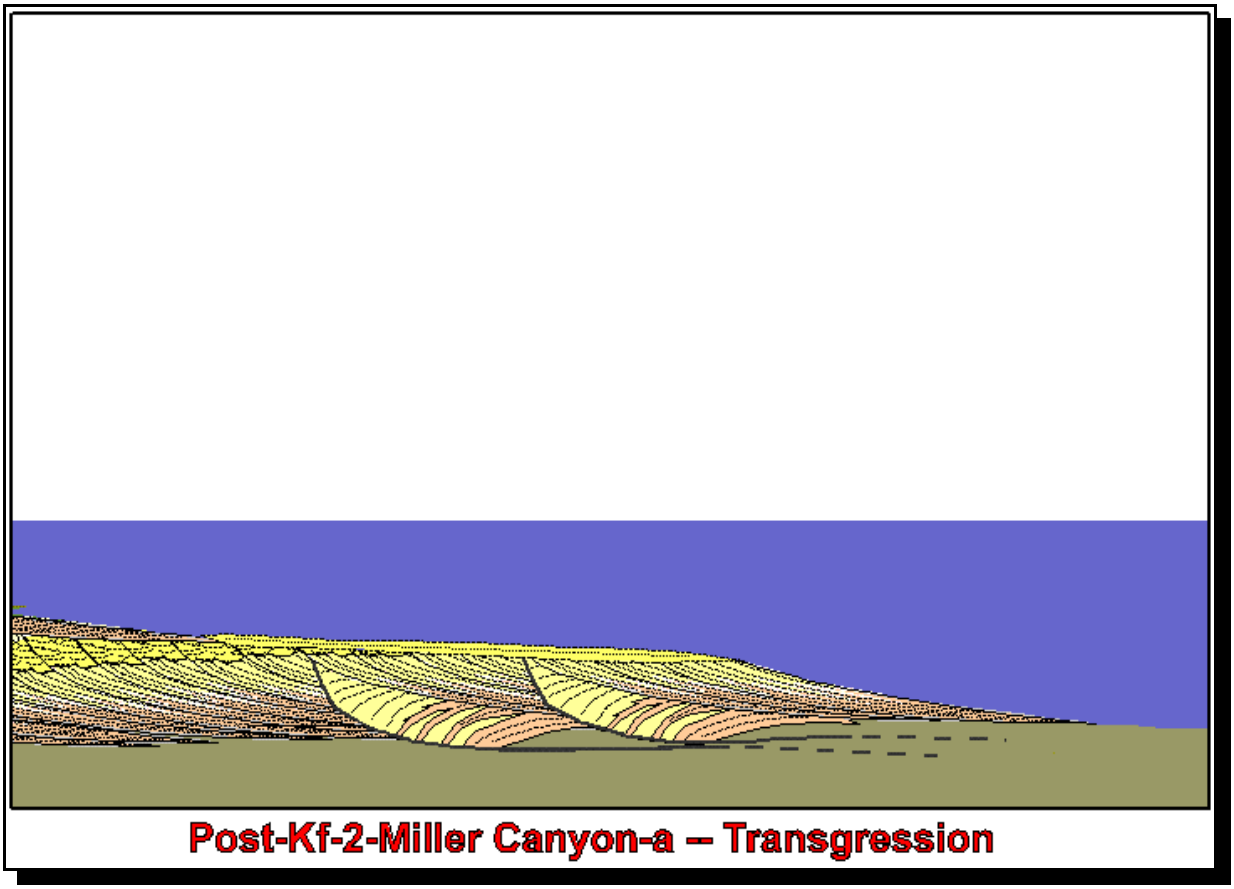


Figure 6-70. Transgression of the sea southward across parasequence Kf-2-Mi-a prior to progradation of parasequence Kf-2-Mi-b. Delta-plain deposits in the Muddy Creek Canyon case-study area were removed by shoreface erosion.

Kf-2-Miller Canyon-b

The high cliffs that rim the "Lower and Middle Reaches" of Muddy Creek Canyon are formed by parasequence Kf-2-Mi-b. The unit is about 70 feet (21 m) thick, displaying only minor variation in thickness within Muddy Creek Canyon (figure 6-8) and in the Muddy Creek Canyon drill holes to the west (figure 6-9). Parasequence Kf-2-Mi-b thins northeastward and eastward into "Grassy Canyon" and the "Molen Amphitheater." Although subdivision may be warranted, the parasequence is presently recognized as extending northward to Dry Wash and Short Canyon, gradually feathering out into the shaly interval above the Clawson and Washboard units of the Ferron in the northern part of Molen Reef. Its landward pinchout has tentatively been identified in the southern part of Cowboy Mesa, in the south-facing outcrops north of Ivie Creek.

Strata contained in parasequence Kf-2-Mi-b are wave-dominated to extremely wave-dominated and are rich in sand. A thick middle shoreface interval is everywhere present. The upper shoreface is best developed in the "Middle Reach" of the canyon, in the younger, extremely wave-dominated part of the unit.

A surface that can be traced through much of the "Middle Reach" of Muddy Creek Canyon separates wave-dominated strata to the south from extremely wave-dominated strata to the north. The surface can be identified on both sides of the canyon. Its orientation indicates that the shoreline prograded toward the northeast following advent of the surface. There are two possible explanations for this surface.

1. The wave energy incident on the coast changed during progradation of parasequence Kf-2-Mi-b, the time of change being marked by the surface. The shoreline may have eroded for a short period of time, followed by renewed progradation under higher wave-energy conditions. This change could have been caused by abandonment of a delta lobe that lay to the east and that provided partial shielding of the Muddy Creek Canyon area from wave energy.

2. A minor drop of relative sea level may have occurred, causing erosion on the shoreface and emplacement of a new, "sharp-based" shoreface against the older shoreface. If such a drop of relative sea level did occur, it probably did not exceed 10 feet (3 m).

Whether or not there was a change in relative sea level associated with the surface in question cannot be determined: the succeeding transgressive surface of erosion has eliminated the evidence that would be necessary to make the distinction between the two proposed series of events. In the first case, the wave-dominated and extremely wave-dominated parts of parasequence Kf-2-Mi-b would be considered subunits of the same parasequence, there being no evidence of a flooding surface between them. In the second interpretation, a sequence boundary would be placed between the two units.

The first model is the simpler of the two and better conforms to the deposition style seen elsewhere in the Ferron. Progradation of the wave-dominated part of parasequence Kf-2-Mi-b is shown in figures 6-71 through 6-73; progradation of the extremely wave-dominated part is shown in figures 6-74 through 6-76. Figure 6-77 shows the following transgression.

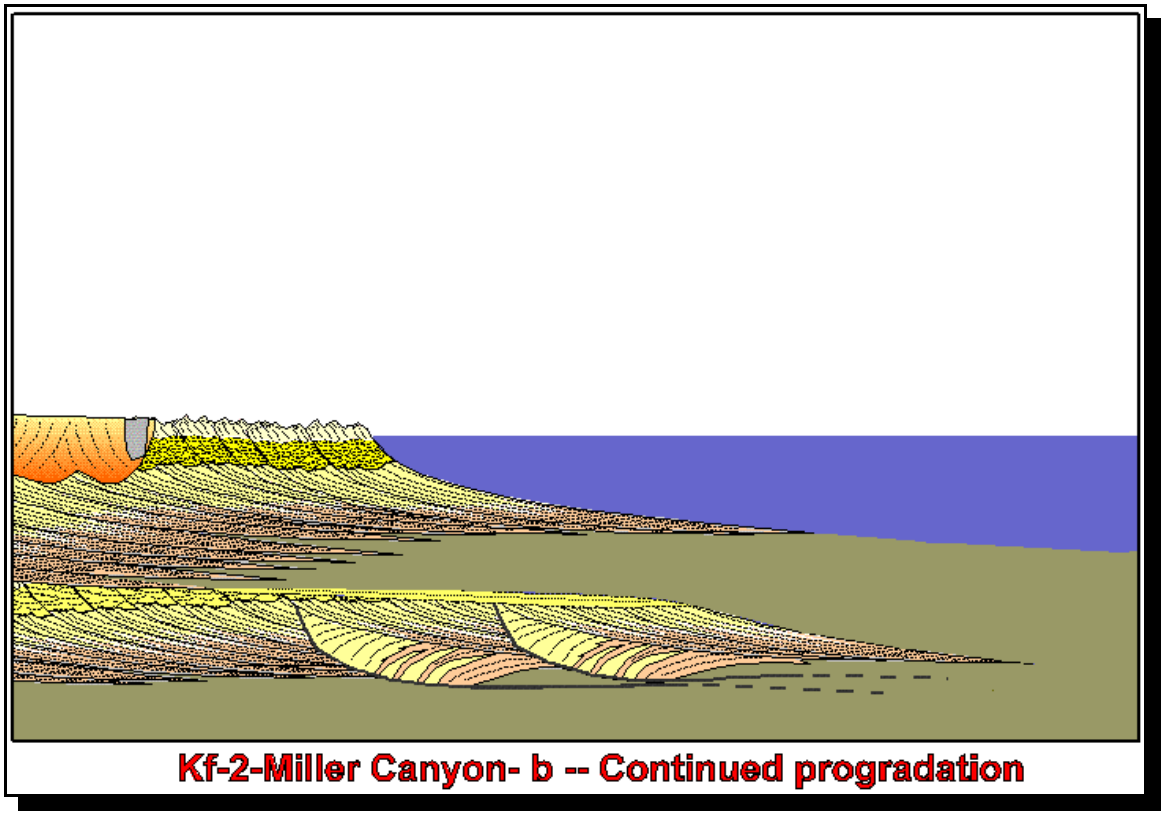


Figure 6-71. Progradation of the older, wave-dominated part of parasequence Kf-2-Mi-b.

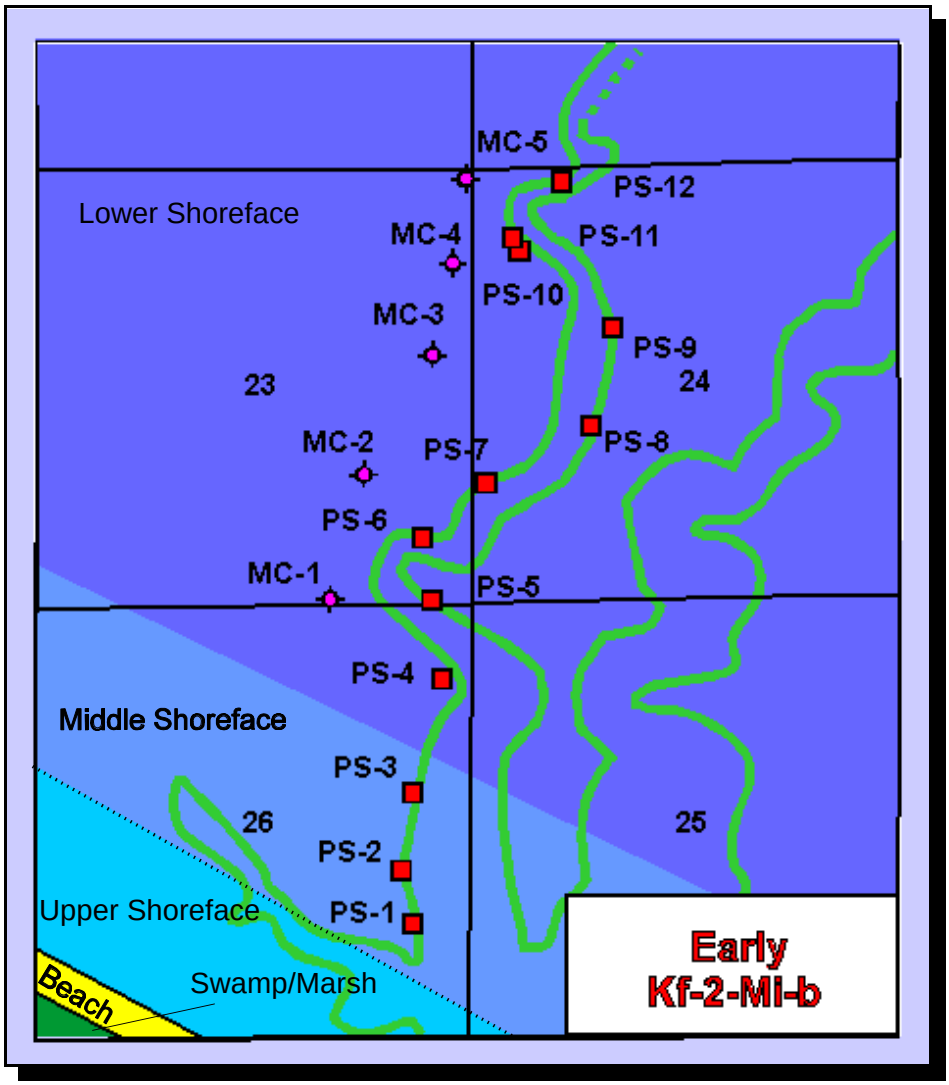


Figure 6-72. Paleogeography early in the progradation of parasequence Kf-2-Mi-b into the case-study area.

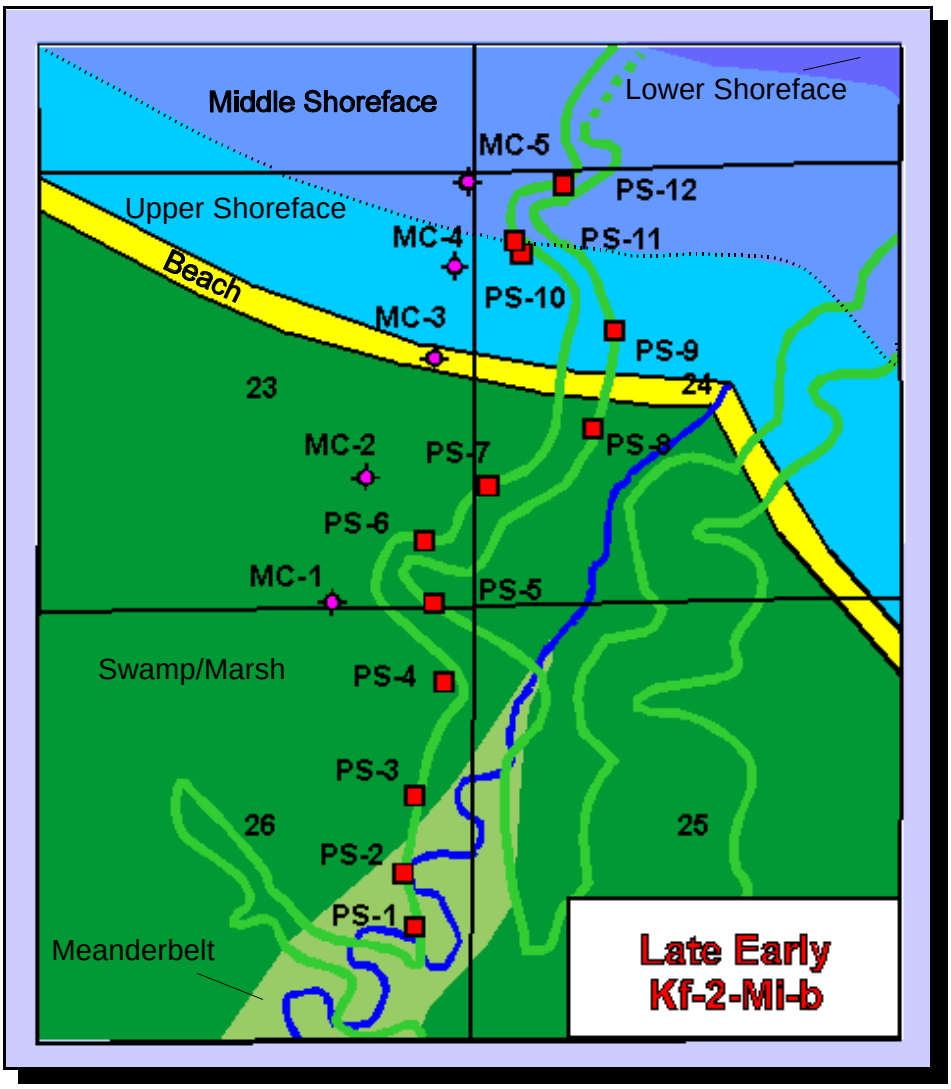


Figure 6-73. Paleogeography at the end of progradation of the older, wave-dominated unit of parasequence Kf-2-Mi-b.

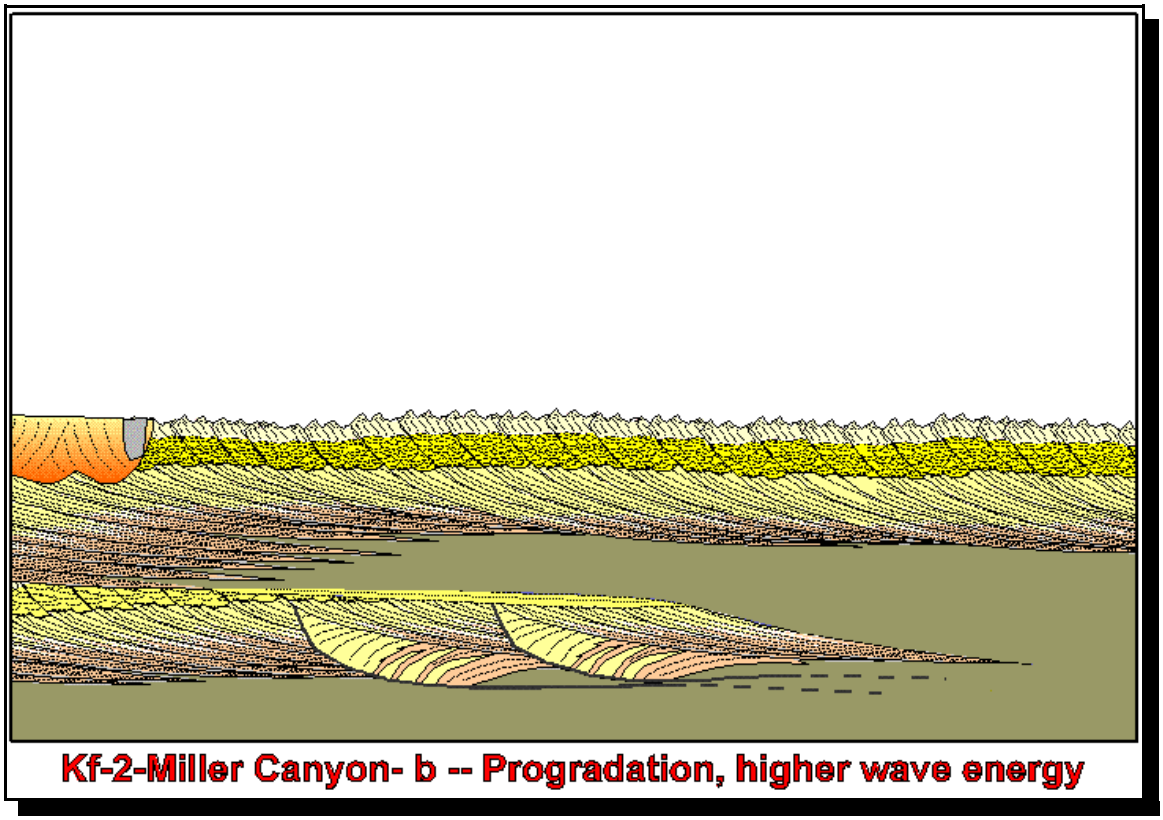


Figure 6-74. Progradation of parasequence Kf-2-Mi-b beyond the northeastern edge of the case-study area.

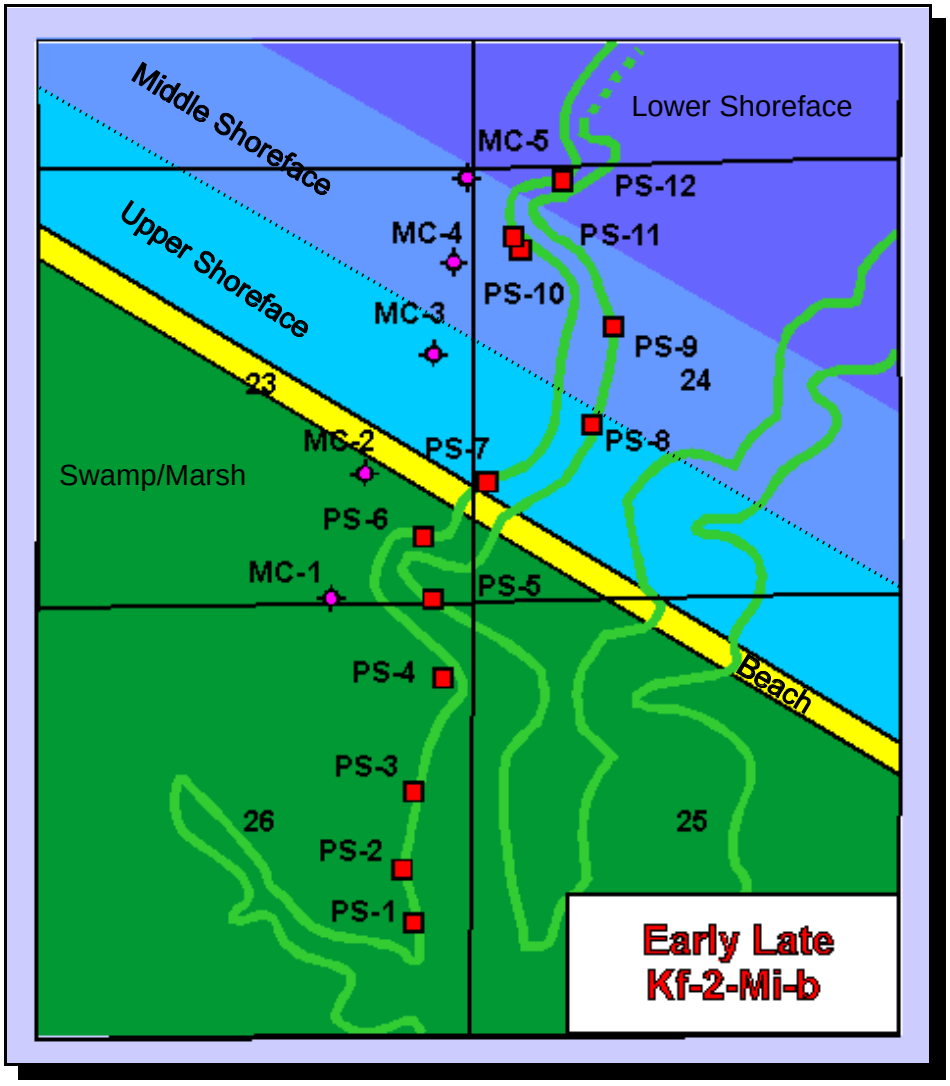


Figure 6-75. Paleogeography at the time of the bedding surface that marks the boundary between the older, wave-dominated and younger, extremely wave-dominated parts of parasequence Kf-2-Mi-b.

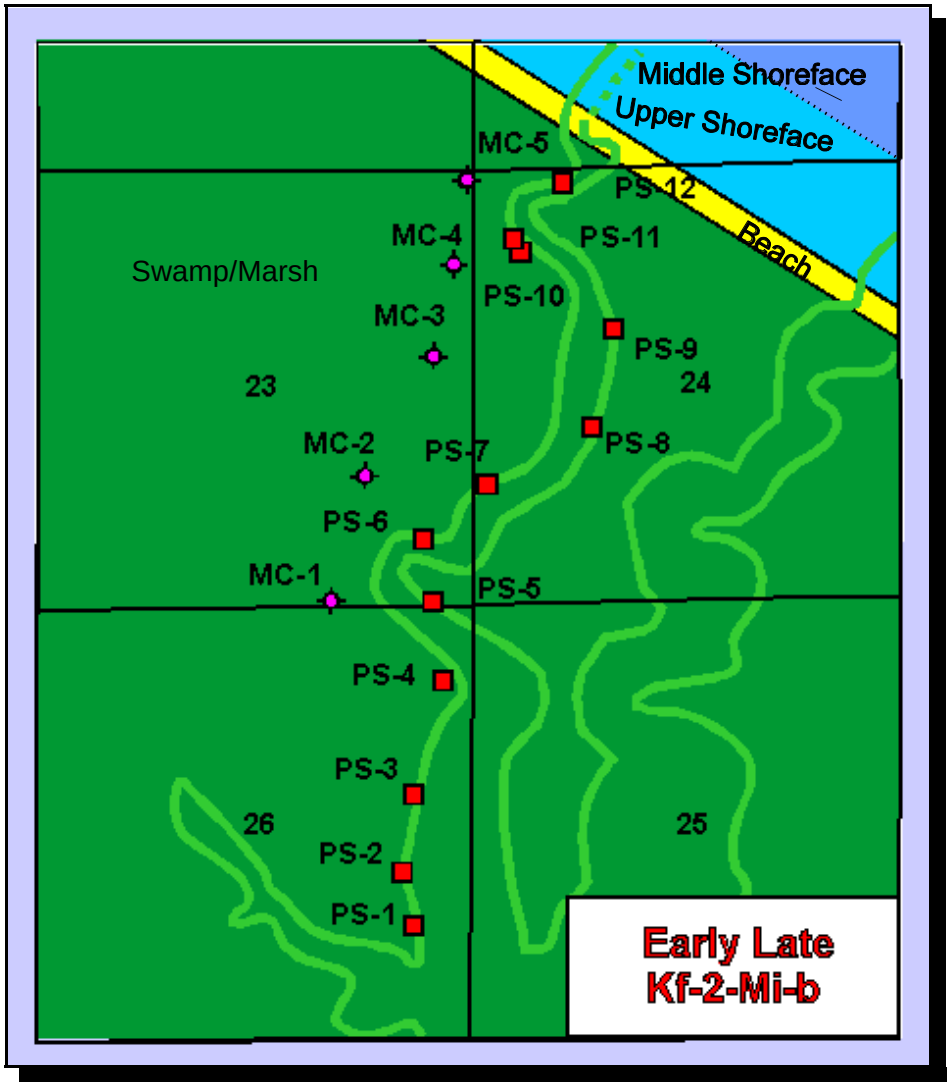


Figure 6-76. Paleogeography of the later, extremely wave-dominated unit of parasequence Kf-2-Mi-b when the shoreline reached the northern limit of exposures in Muddy Creek Canyon.

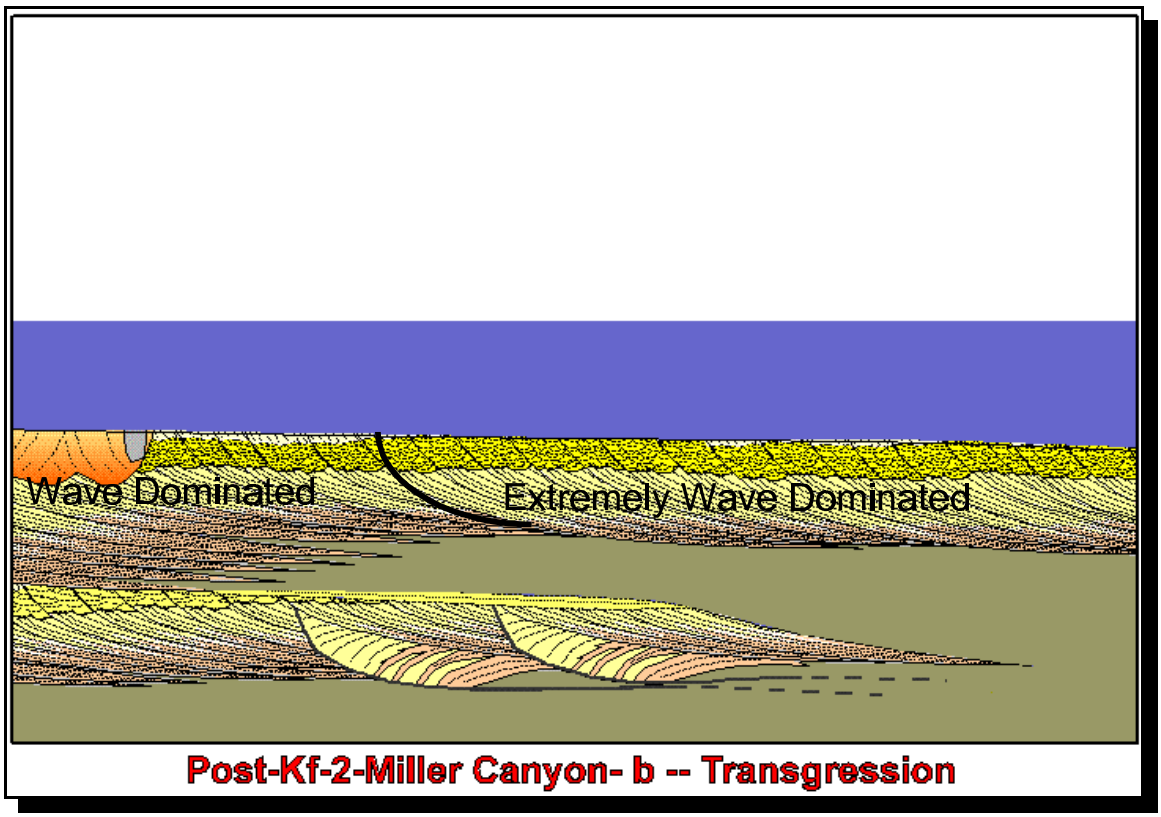


Figure 6-77. Transgression of the sea across parasequence Kf-2-Mi-b prior to progradation of parasequence Kf-2-MC-a.

Fluvial strata make up a minor part of parasequence Kf-2-Mi-b. A channel belt cuts the top of the unit in the southern part of the "Lower Reach" of the canyon and is also present at the mouth of Miller Canyon. It is present along the entire length of the ridge formed by Ferron strata between Muddy Creek and the "Molen Amphitheater." Numerous minor channels scour the top of the unit elsewhere, the most significant of these being in the vicinity of the "Upper Gooseneck." All of the channels were truncated by shoreface erosion during the transgression that ended parasequence Kf-2-Mi-b deposition.

Kf-2-Muddy Canyon-a

A third episode of progradation in the Muddy Creek Canyon area deposited parasequence Kf-2-MC-a, which generally ranges in thickness between 30 and 40 feet (9-12 m). Two channel belts (figure 6-78), a northern belt and a southern belt, include most of the sandstone contained in the parasequence.

Parasequence Kf-2-MC-a can be traced eastward into "Grassy Canyon" and around the promontory that separates "Grassy Canyon" and Muddy Creek Canyon south of the mouth of Miller Canyon from the "Molen Amphitheater." In the northern part of this promontory, the northern edge of southern channel belt has been identified. The delta-front facies, a thin unit of interbedded sandstone and mudstone, continues eastward to "Molen Point." It feathers out seaward in the southern part of Molen Reef.

The delta-front facies of parasequence Kf-2-MC-a is preserved in Muddy Creek Canyon on a single outcrop on the west side of the canyon, just north of the "Lower Gooseneck" (see closer view in figure 6-44). The paleogeography at the beginning of parasequence Kf-2-MC-a progradation is shown in figure 6-79. This map is very interpretive because the position of the landward edge of the parasequence is not known with certainty, most of the strata having been subsequently removed by the channel belts. Early progradation of parasequence Kf-2-MC-a is shown diagrammatically in figures 6-79 through 6-81. Continued progradation of the shoreline and emplacement of the northern meanderbelt is shown in figures 6-82 and 6-83. Emplacement of the southern meanderbelt is shown in figures 6-84 and 6-85.

The contact between the older delta-front and the younger meanderbelt deposits is everywhere erosional and displays up to about 10 feet (3 m) of local relief. The aforementioned outcrop where much of the original delta-front succession is preserved and a clay-plug on the eastern side of the canyon (figure 6-43) together define the boundary between the two meanderbelts.

Transport directions in the two meanderbelts, as determined from trough cross-stratification, varied: transport in the northern meanderbelt, which is interpreted to be the older of the two, was toward the south-southeast (figure 6-86); transport in the southern meanderbelt was toward the northeast (figure 6-87).

Through most of Muddy Creek Canyon, the uppermost beds of the meanderbelt deposits of parasequence Kf-2-MC-a were removed by erosion as a result of transgression of a shoreface (figure 6-88). Subsequent progradation of this shoreface led to deposition of overlying parasequence Kf-2-MC-b. In the "Lower Reach" of the canyon and in drill hole MC-1, which lie near the landward pinchout of parasequence Kf-2-MC-b, carbonaceous shale and coal cap the meanderbelt deposits, indicating that there, the point-bar succession is complete. The carbonaceous units represent a split of the A coal zone.

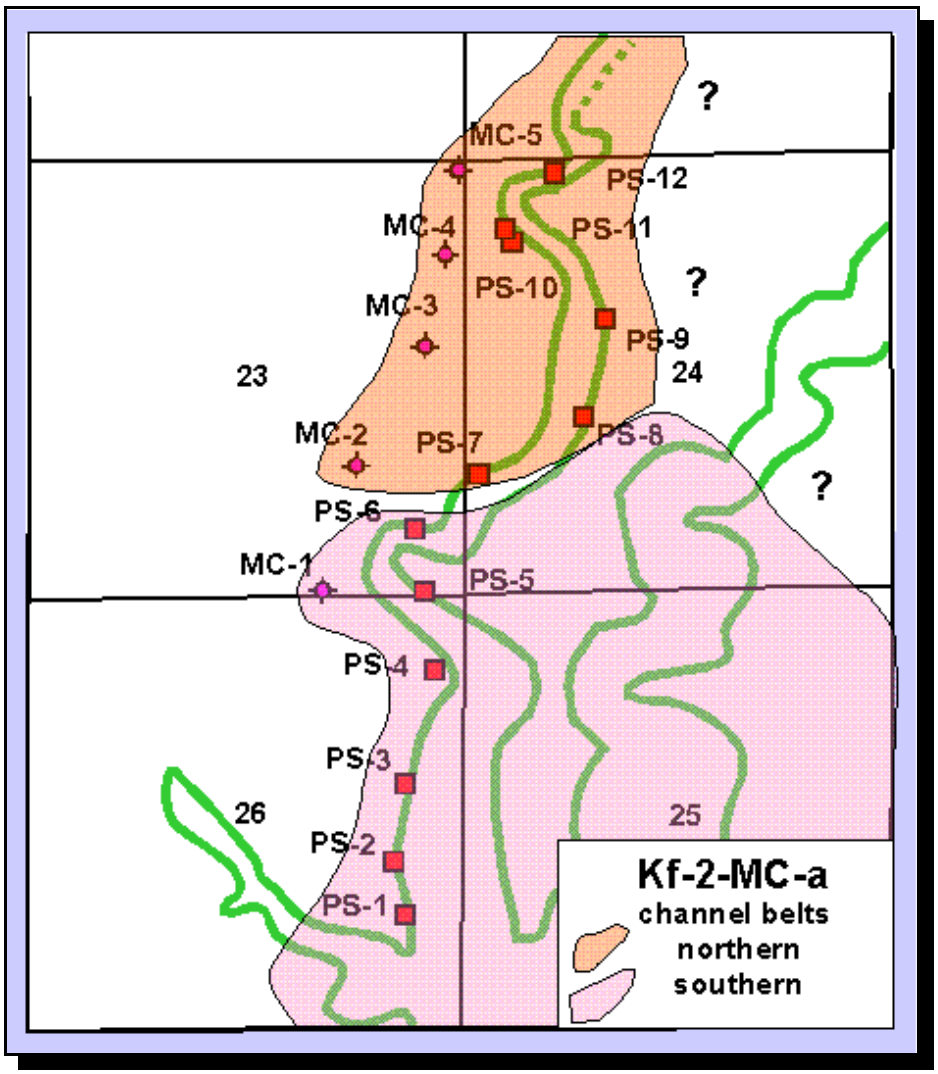


Figure 6-78. Areas where the meanderbelt deposits of parasequence Kf-2-MC-a are known to be present. The position of the northern margin of the southern meanderbelt and the southern limit of the northern meanderbelt can be defined in the Muddy Creek Canyon outcrops; limits shown in the areas where parasequence Kf-2-MC-a is in the subsurface are very approximate.

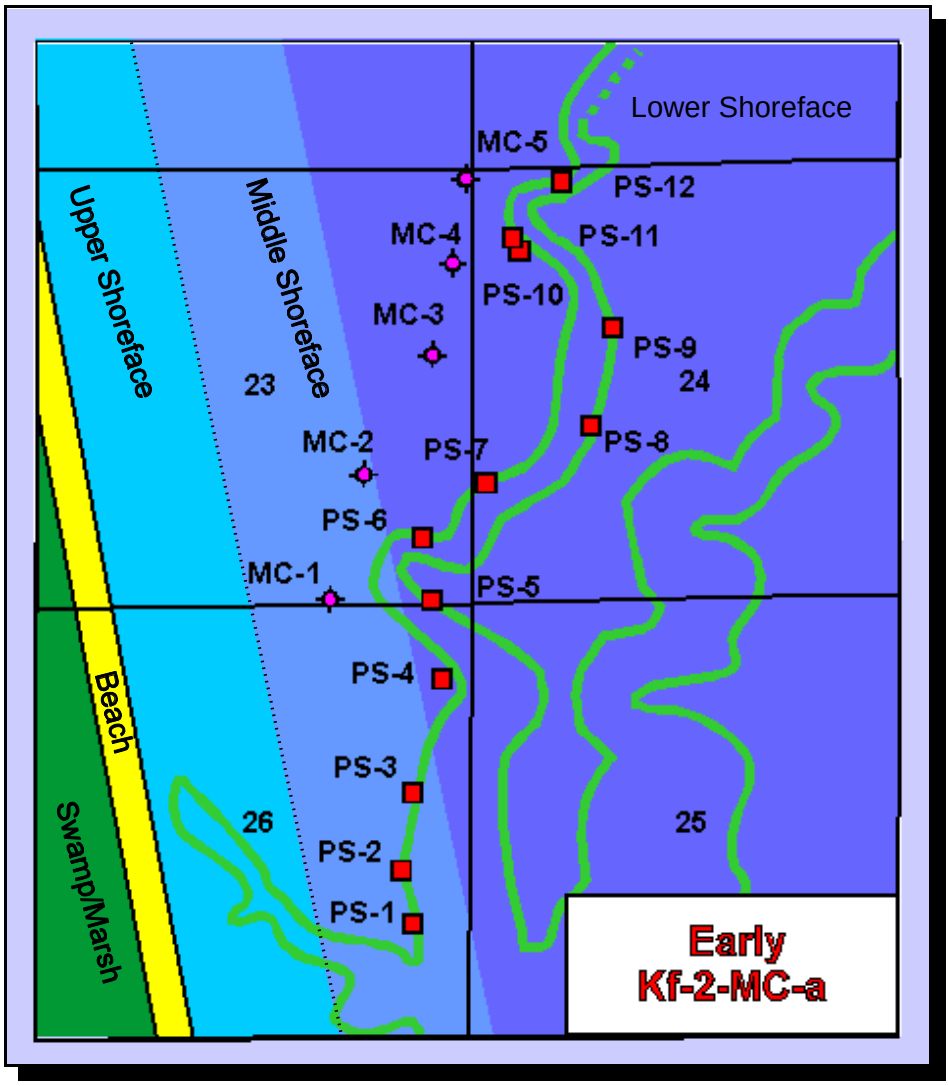


Figure 6-79. Paleogeography very early in the progradation of parasequence Kf-2-MC-a across the case-study area.

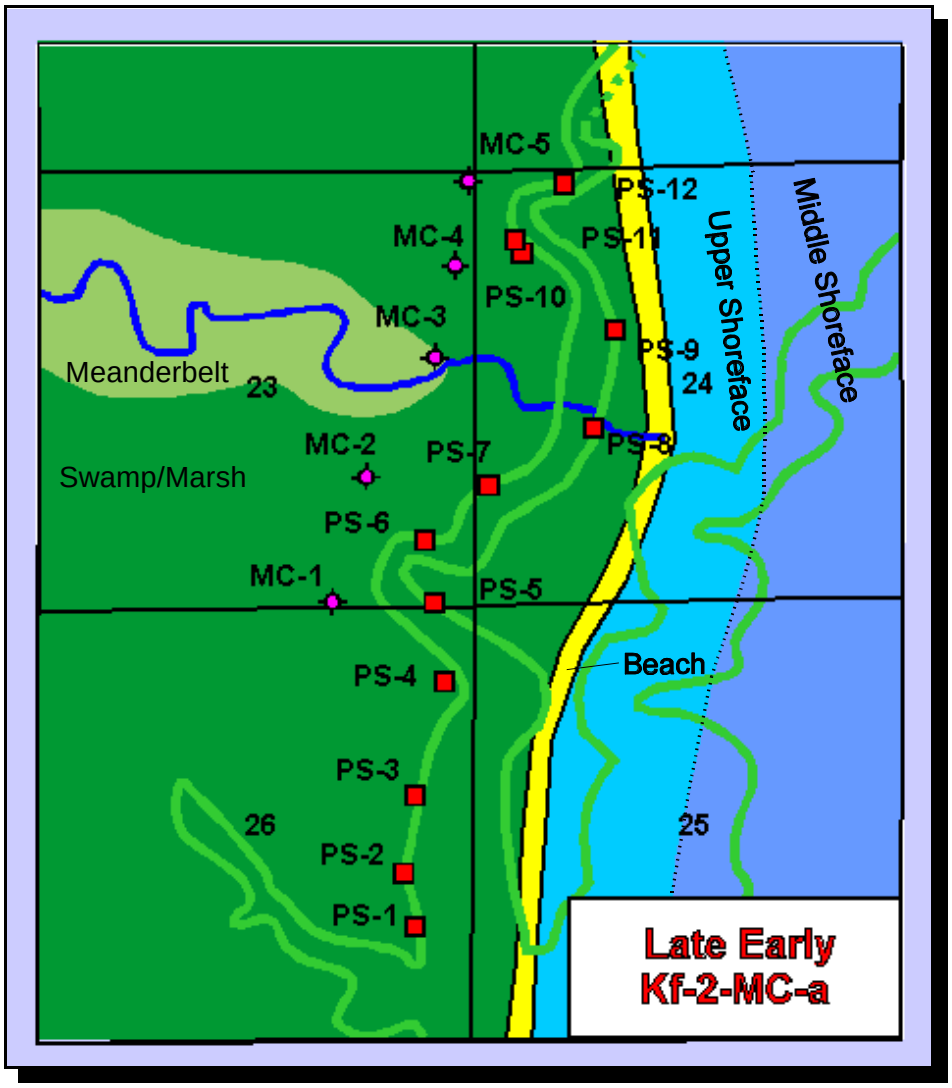


Figure 6-80. Paleogeography near the end of progradation of parasequence Kf-2-MC-a.

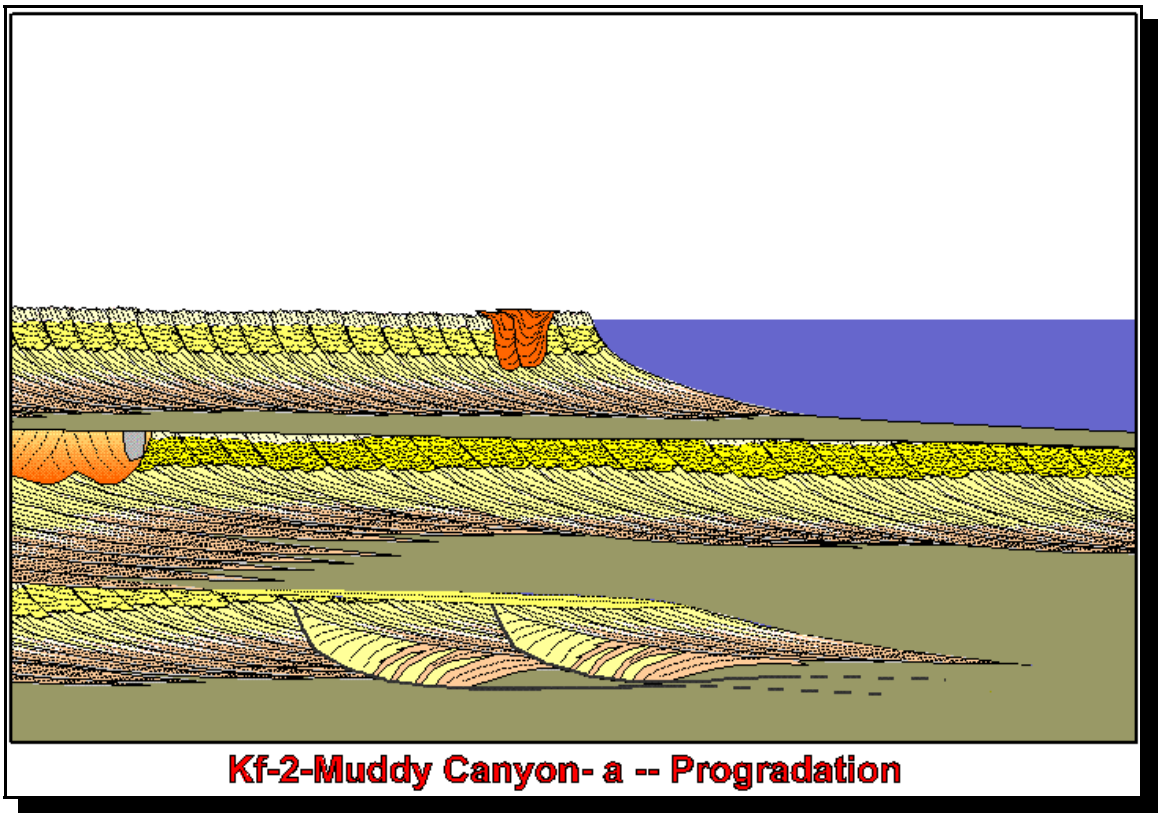


Figure 6-81. Progradation of parasequence Kf-2-MC-a through the case-study area.

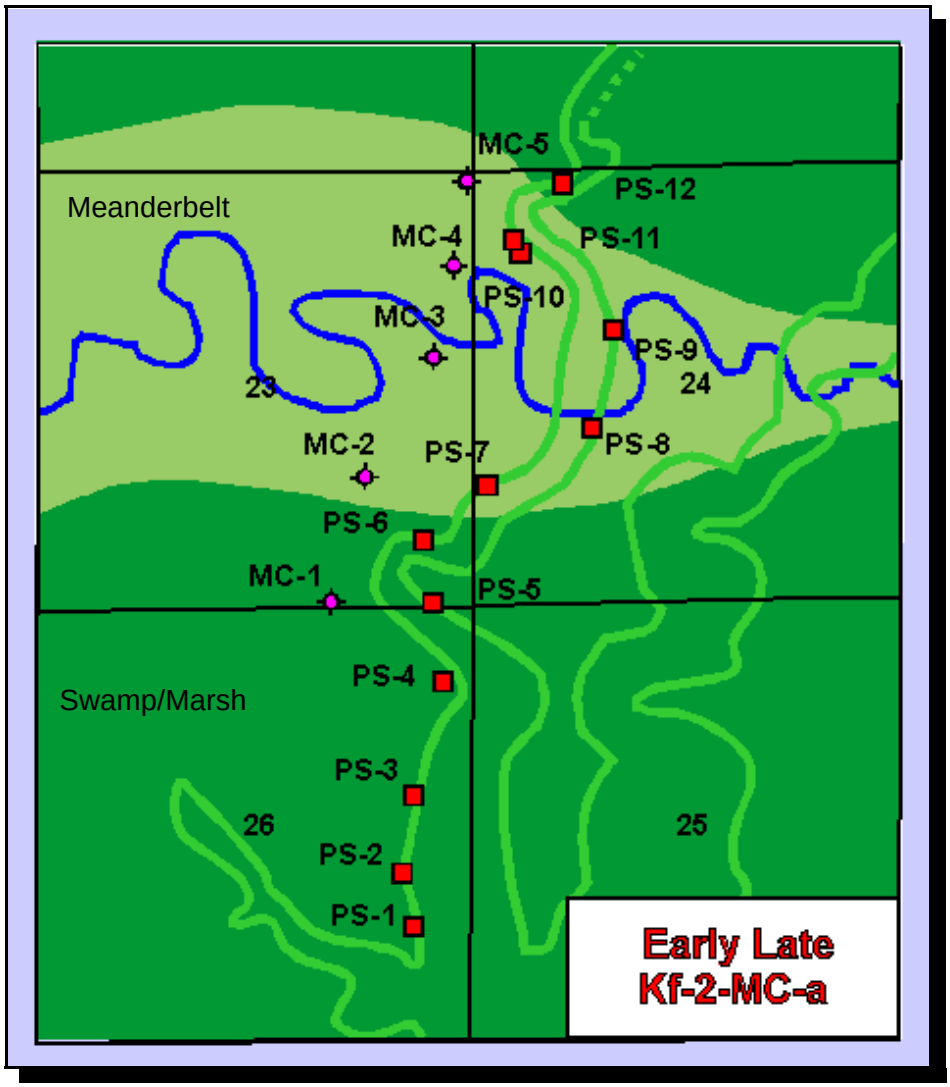


Figure 6-82. Paleogeography of parasequence Kf-2-MC-a at the time of emplacement of the northern meanderbelt.

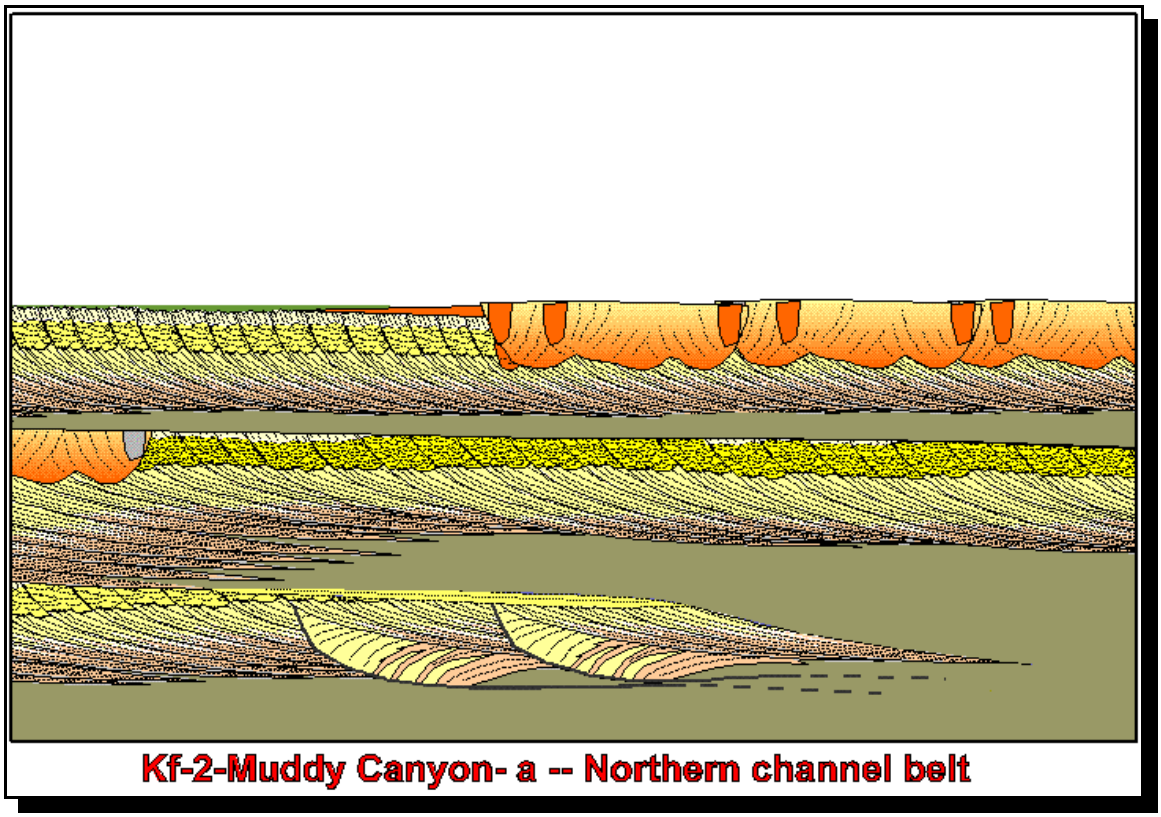


Figure 6-83. Emplacement of the northern meanderbelt of parasequence Kf-2-MC-a.

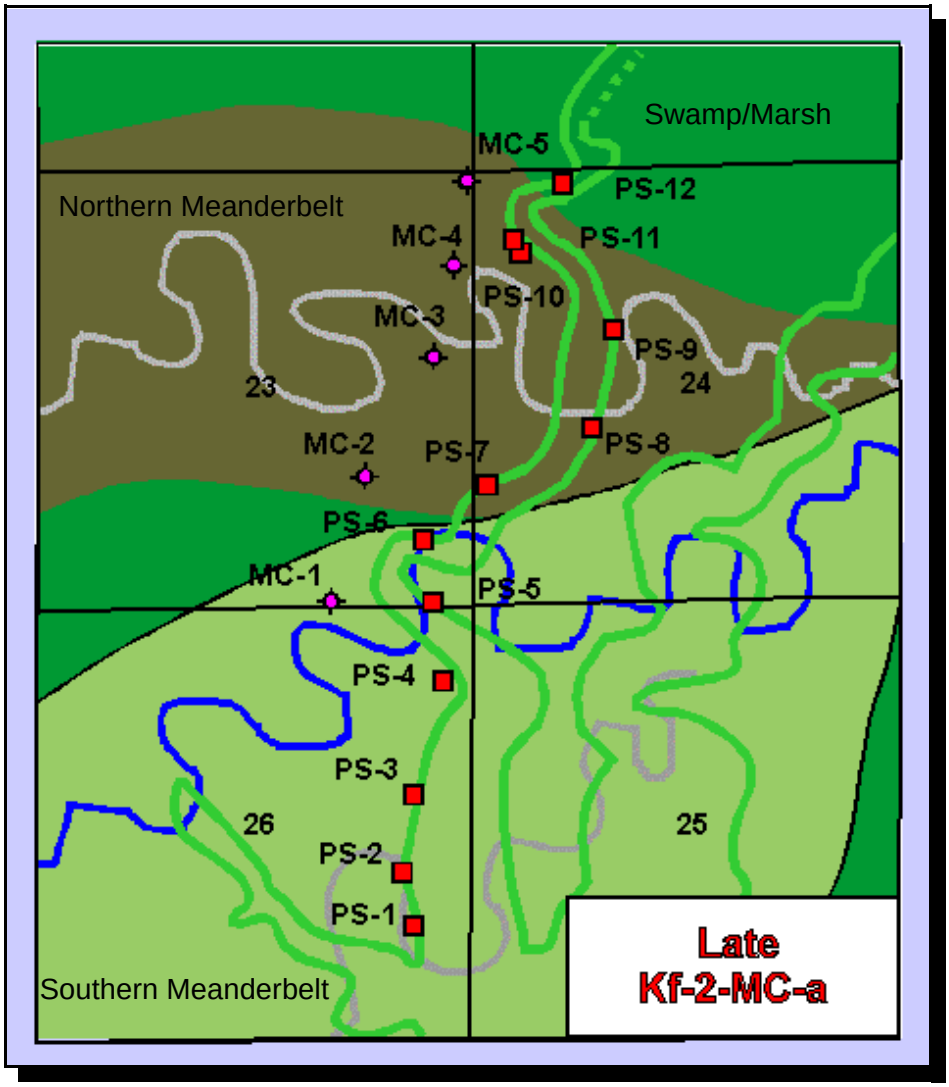


Figure 6-84. Paleogeography of parasequence Kf-2-MC-a at the time of emplacement of the southern meanderbelt.

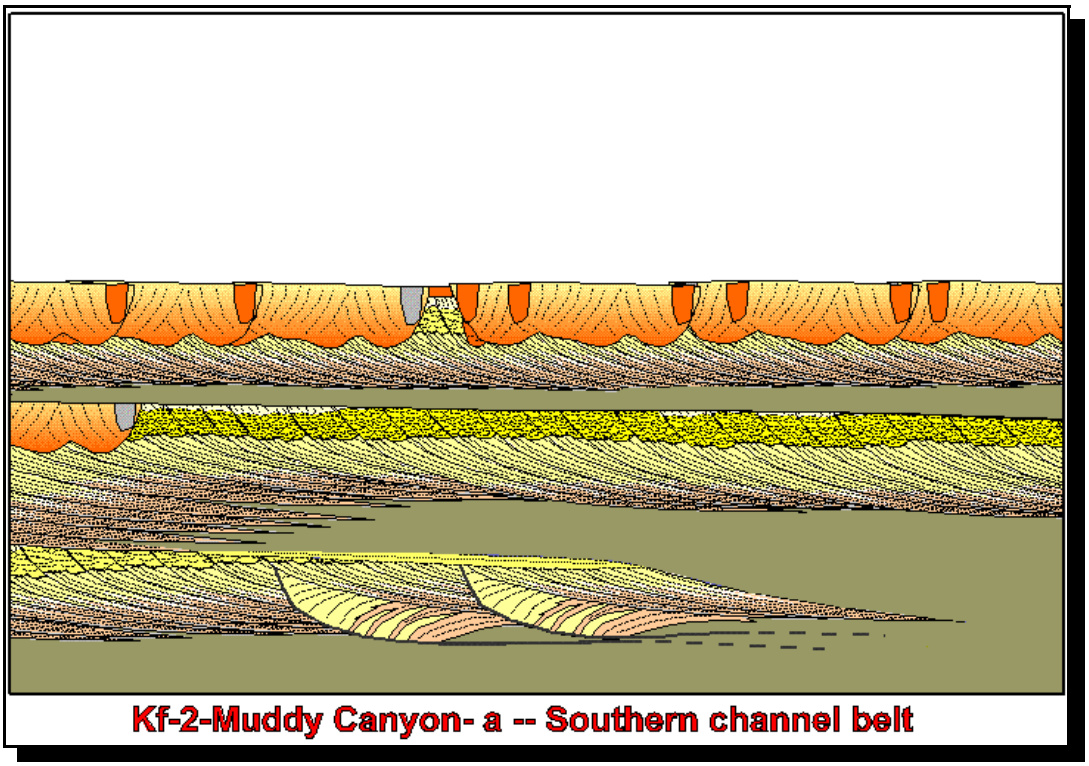


Figure 6-85. Emplacement of the southern meanderbelt of parasequence Kf-2-MC-a.

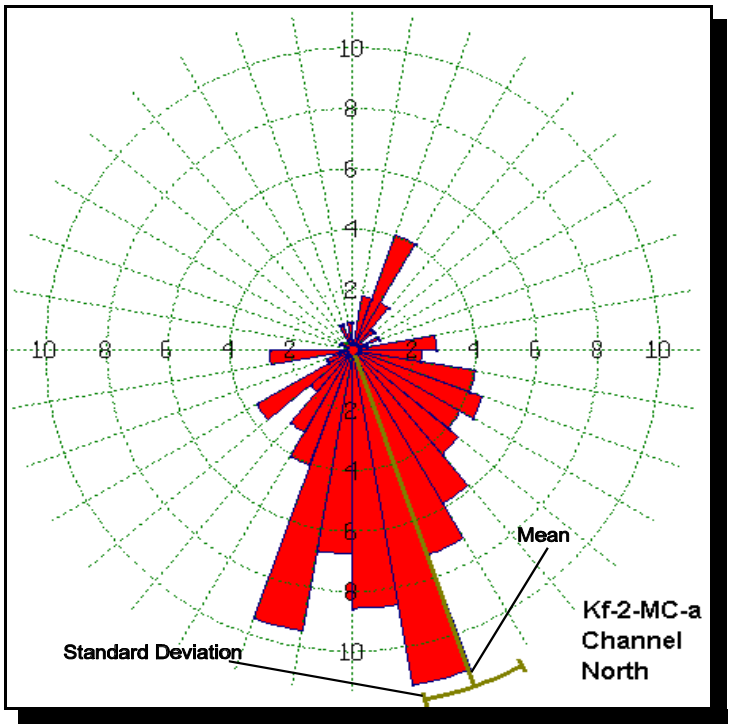


Figure 6-86. Paleocurrent data derived from trough cross-stratification in the northern meanderbelt of parasequence Kf-2-MC-a.

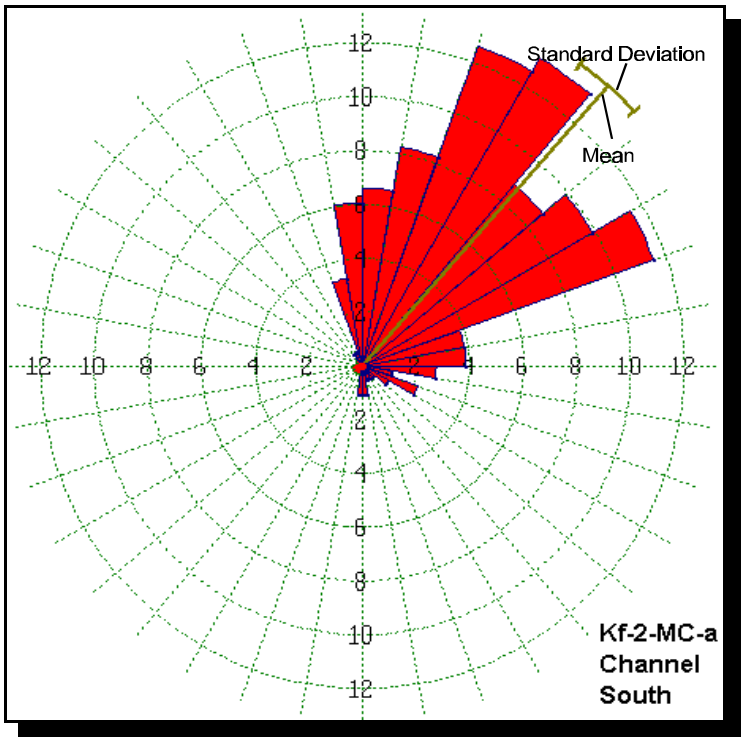


Figure 6-87. Paleocurrent data derived from trough cross-stratification in the southern meanderbelt of parasequence Kf-2-MC-a.

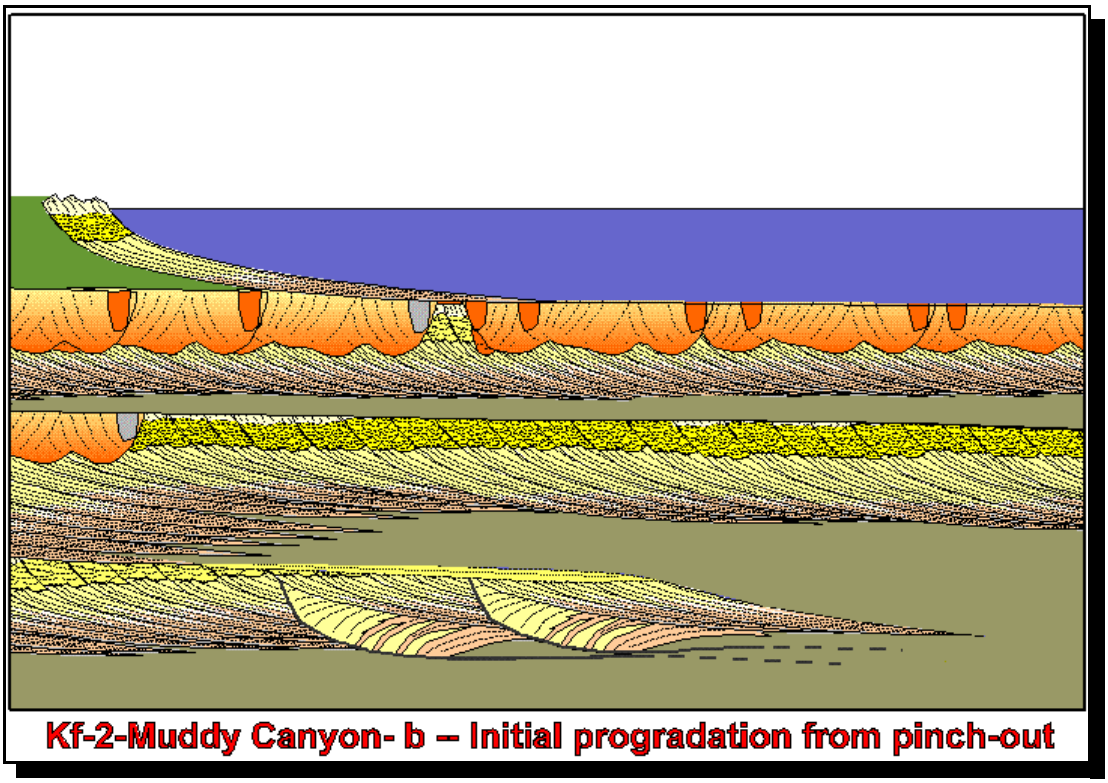


Figure 6-88. Transgression of the sea across the deposits of parasequence Kf-2-MC-a and beginning of progradation of parasequence Kf-2-MC-b.

Kf-2-Muddy Canyon-b

Only the landward most part of parasequence Kf-2-MC-b is present in the Muddy Creek Canyon case-study area (figure 6-8). Its landward pinchout can be seen at the mouth of Miller Canyon, and lies close to drill hole MC-1 (figure 6-9) and to the outcrop in the curve of the canyon opposite the "Lower Gooseneck," where the unit is quite thin. It increases in thickness eastward from its feather edge to about 30 feet (9 m) in Muddy Creek Canyon, but continues to thicken rapidly eastward, reaching 75 feet (23 m) in "Grassy Canyon."

The most striking feature of parasequence Kf-2-MC-b is the presence of numerous bodies of medium-grained sandstone characterized by northward-dipping bedsets up to about 30 feet (9 m) in height (figure 6-59). They were deposited by tidal inlets migrating along the coast. The inclination of the large-scale surfaces (figure 6-58) indicates that migration of the inlets was toward the north (figure 6-89). Trough cross-stratification in the inlet deposits (figure 6-61) preserves a dominant eastward direction of transport (figure 6-90), which represents the ebb direction. Variation in transport direction, however, is fairly high. Tidal inlet deposits are distinguished in cores from drill holes MC-2, MC-3, and MC-4. The emplacement of the earlier inlet deposits and some of the tidal channels behind them are shown diagrammatically in figures 6-91 through 6-93.

Tidal inlet deposits are found only with about a mile of the landward pinchout of parasequence Kf-2-MC-b. This relationship has been observed in other units of the Ferron, although no other parasequence contains such an abundance of inlet deposits as parasequence Kf-2-MC-b. Rise of relative sea level during the transgression that ended parasequence Kf-2-MC-a and during the early phase of progradation of parasequence Kf-2-MC-b created, and maintained, a lagoon behind the shoreline. Exchange of water between the lagoon and the seaway maintained the inlets. When the rate of rise of relative sea level decreased, the lagoon filled, the volume of the tidal prism diminished, and the inlets were abandoned. No inlet deposits have been observed in parasequence Kf-2-MC-b east of "Grassy Canyon."

In the "Lower Reach" of the canyon, the top of parasequence Kf-2-MC-b has been replaced by trough cross-stratified, medium-grained, white sandstone that includes abundant *Ophiomorpha*. These deposits are interpreted the be the tidal channels that lay behind the inlets, but they were not studied in detail. They can, however, be distinguished on some of the photomosaics. Progradation of the shoreline following filling of the lagoon that lay behind the parasequence Kf-2-MC-b shoreline and abandonment of the inlets is shown in figure 6-94. Channel deposits, generally consisting of current-rippled, fine-grained sandstone, cut the top of parasequence Kf-2-MC-b in many places. Near the "Upper Gooseneck," and in drill hole MC-5, most of parasequence Kf-2-MC-b has been replaced by a large channel belt of late Kf-2 age (figure 6-95). The emplacement of this channel belt and deposition of younger strata are shown in figures 6-96 and 6-97.

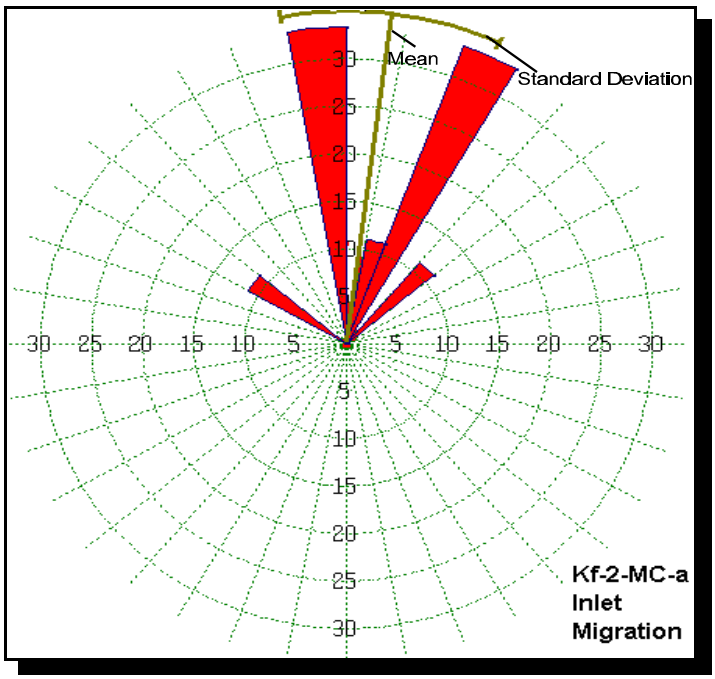


Figure 6-89. Direction of inclination of large-scale, planar-tabular cross-stratification representing lateral migration of tidal inlets in parasequence Kf-2-MC-b.

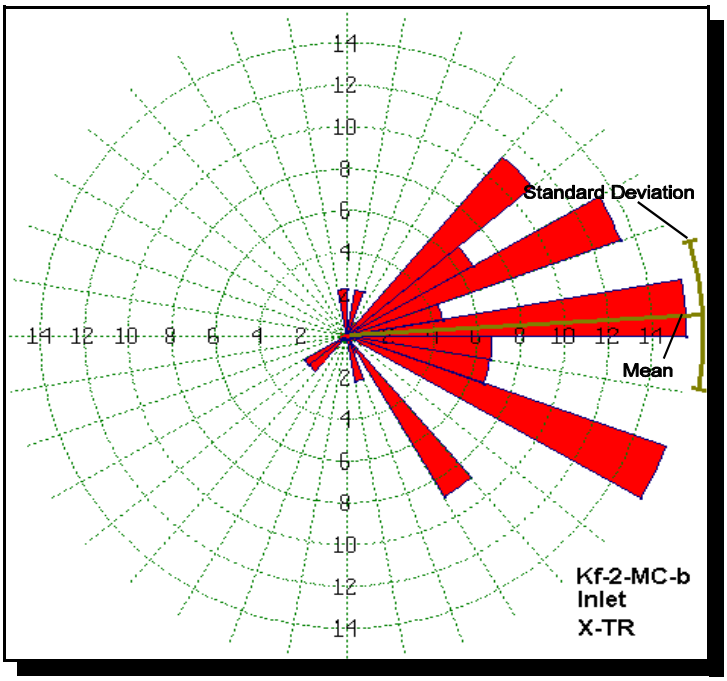


Figure 6-90. Transport direction indicated by trough cross-stratification in tidal inlets of parasequence Kf-2-MC-b.

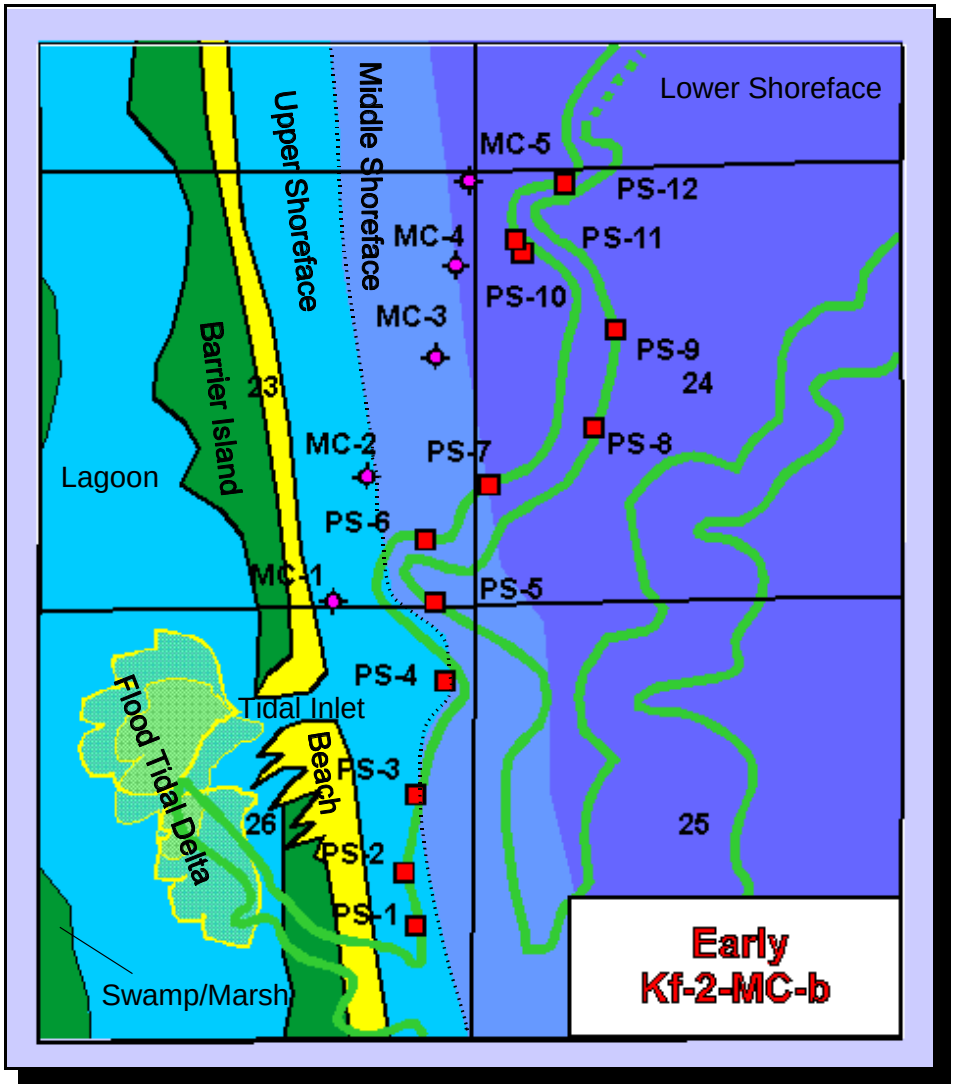


Figure 6-91. Paleogeography at the peak of transgression and the beginning of progradation of parasequence Kf-2-MC-b. The western edge of the barrier island sandstone body represents the landward pinchout of the parasequence.

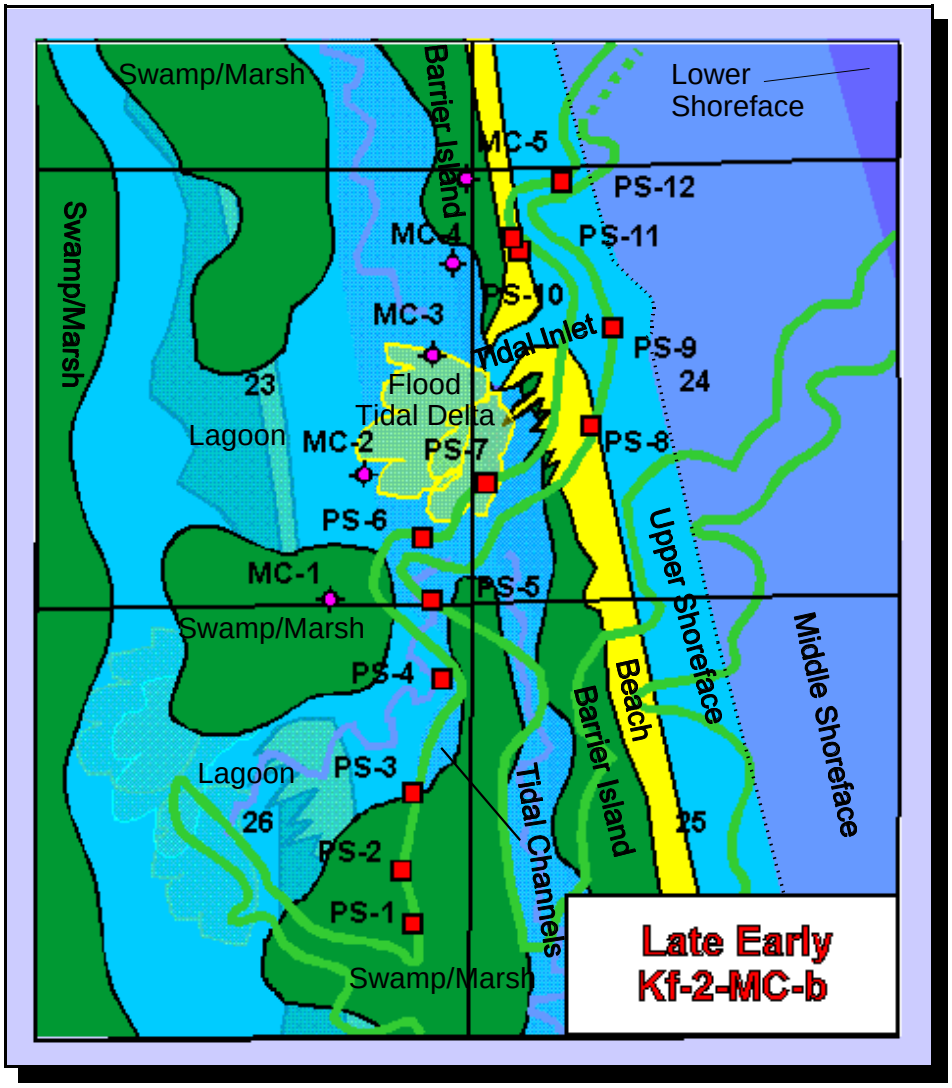


Figure 6-92. Paleogeography of the earliest phase of progradation of parasequence Kf-2-MC-b.

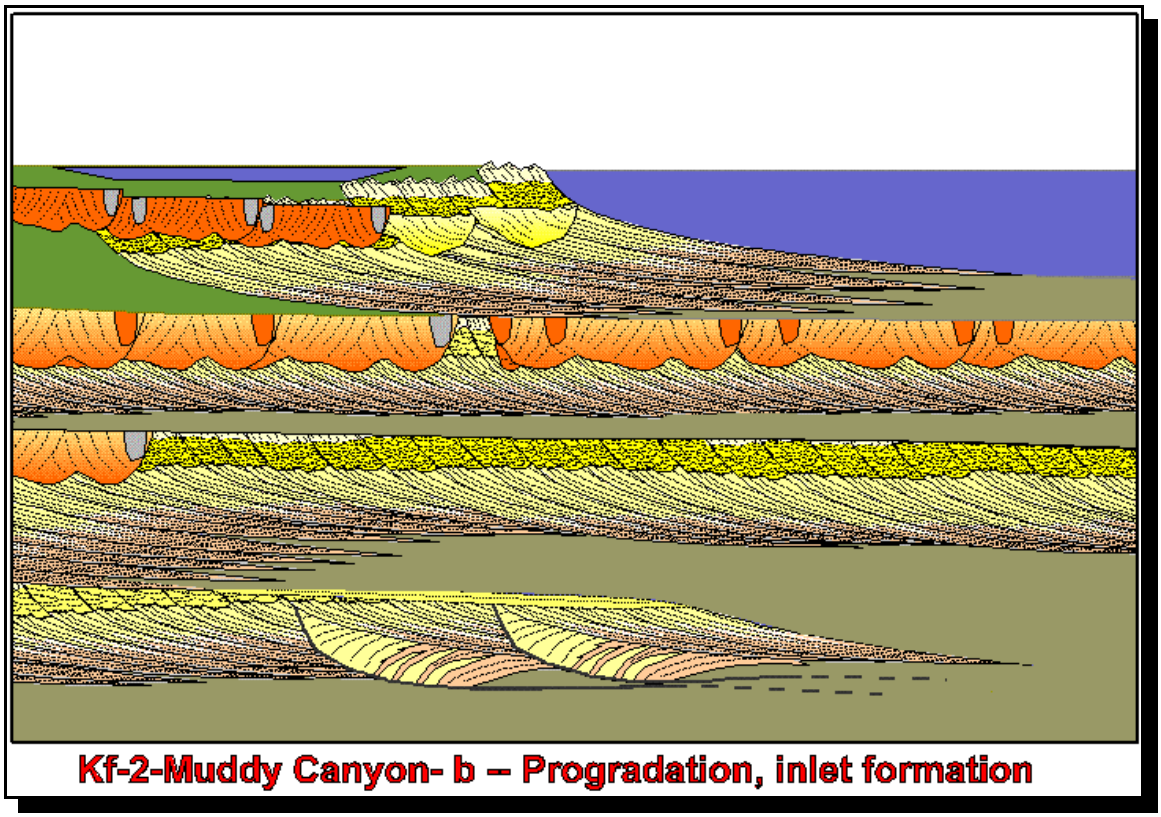


Figure 6-93. Emplacement of inlet bodies in the landward part of parasequence Kf-2-MC-b.

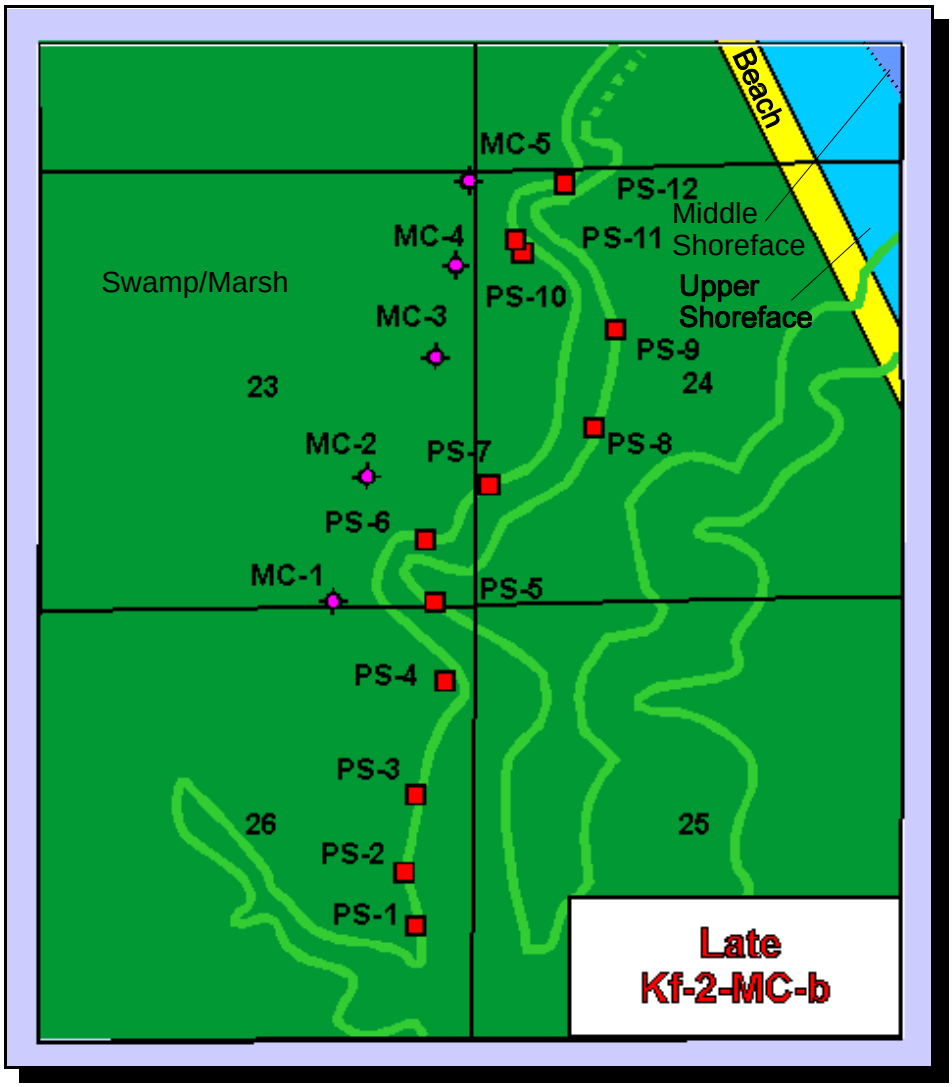


Figure 6-94. Paleogeography of the prograding, wave-dominated shoreline of parasequence Kf-2-MC-b when the shoreline was positioned near the eastern edge of the case-study area. Lagoons and tidal inlets did not exist in the area at this time.

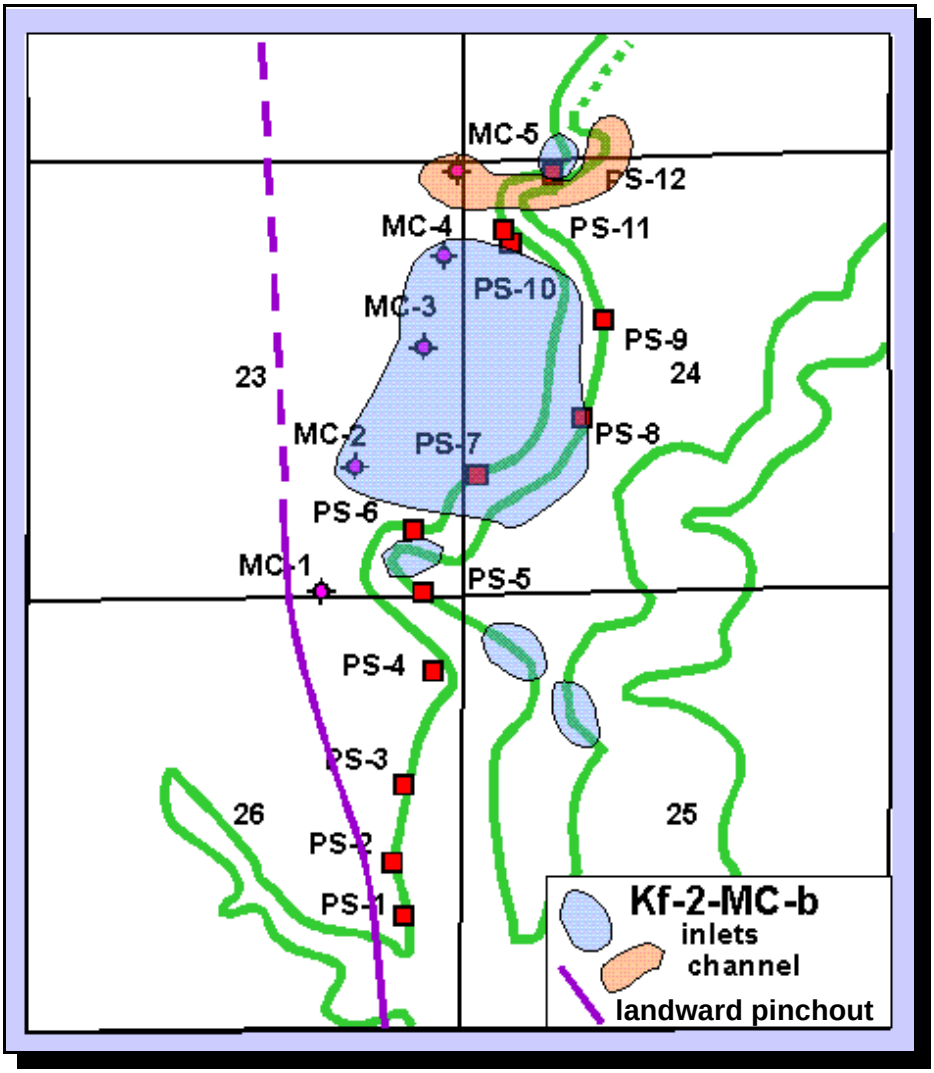


Figure 6-95. Areas where tidal inlets occur in parasequence Kf-2-MC-b and location of a channel belt that cross-cuts Kf-2-MC-b in the northern part of the area.

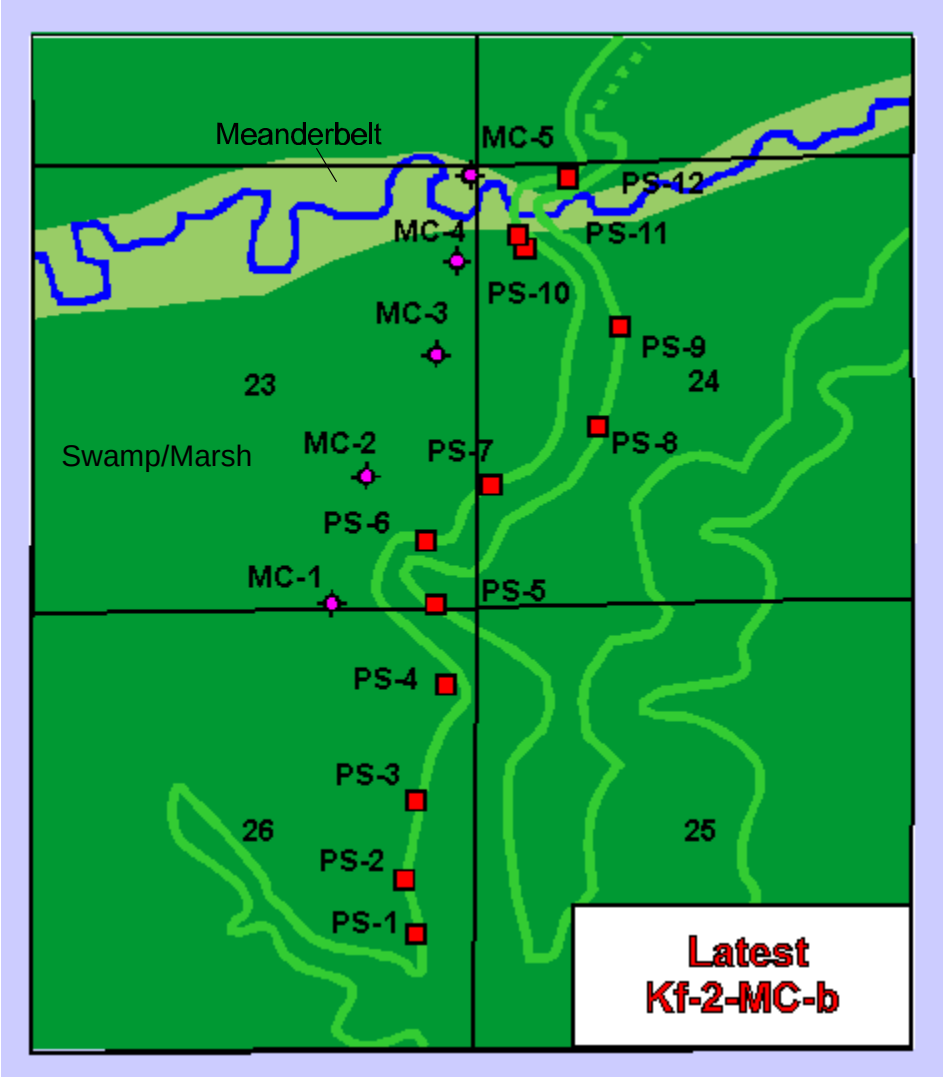


Figure 6-96. Paleogeography of parasequence Kf-2-MC-b at the time the channel belt identified in the northern part of the case-study area was active.

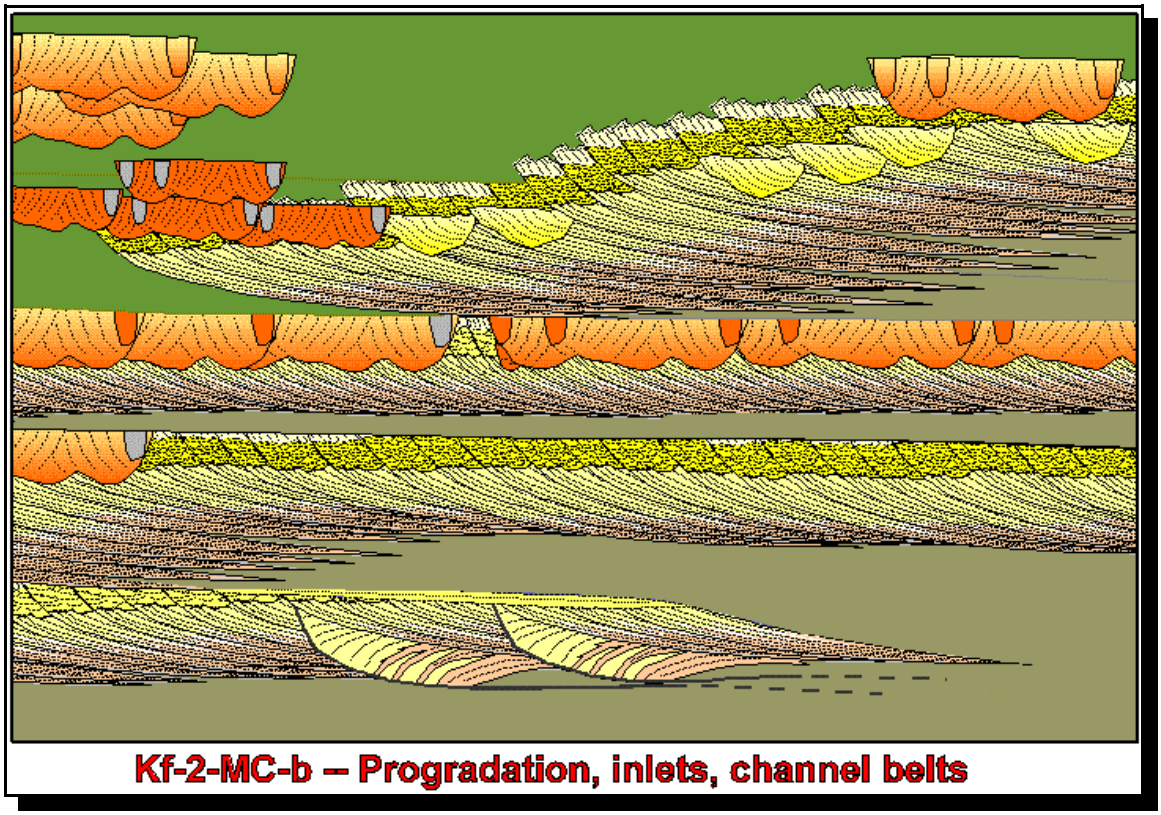


Figure 6-97. Emplacement of the channel belt that cross-cuts parasequence Kf-2-MC-b.

CHAPTER VII
GEOLOGIC FRAMEWORK OF THE IVIE CREEK CASE-STUDY AREA

P.B. Anderson, T.C. Chidsey, Jr., T.A. Ryer, Ann Mattson, and R.D. Adams

Introduction

The Ivie Creek case-study area (figure 7-1) was selected to develop a detailed geological and petrophysical characterization, at well-sweep scale or smaller, of the primary reservoir lithofacies typically found in a fluvial-dominated deltaic reservoir. Sedimentary structures, lithofacies, bounding surfaces, and permeabilities measured along closely spaced traverses were combined with drill-hole data to develop a three-dimensional view of the reservoirs within the area.

The Ivie Creek case-study area contains abrupt facies changes in the Ferron delta-front sandstones or parasequence sets. The Ferron Sandstone in the Ivie Creek case-study area consists of two regional scale parasequence sets, the Kf-1 and Kf-2 (figure 7-2). In the Ivie Creek case-study area, the Kf-1 parasequence set consists of one parasequence with two named bedsets, Kf-1-Ivie Creek[a] (Kf-1-Iv[a]) and Kf-1-Ivie Creek[c] (Kf-1-Iv[c]). The older bedset has been interpreted as a fluvial-dominated delta deposit which changes from proximal to distal from east to west. The Kf-2 parasequence set represents wave-modified deposits. Each type of deltaic system produces differing geometries that can be characterized by geologic parameters for exploration or modeling efforts.

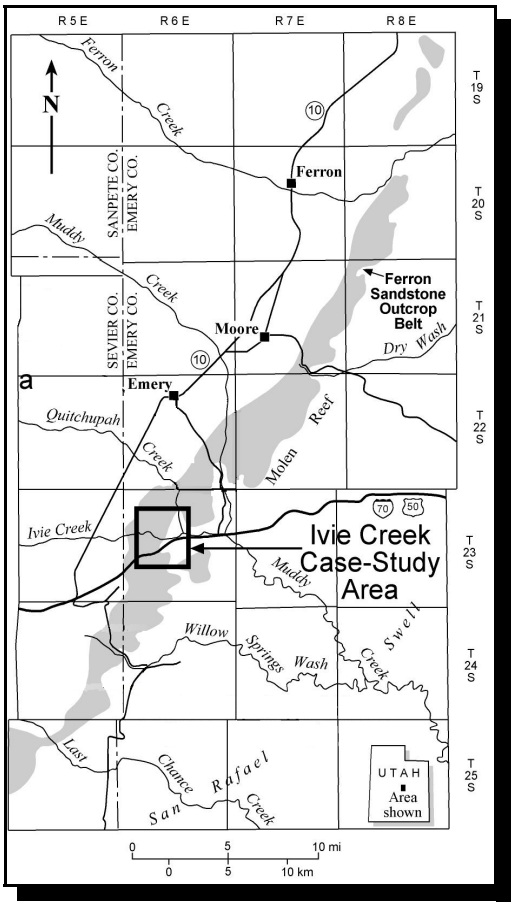


Figure 7-1. Location map of the Ferron Sandstone project area (outcrop belt is shaded) showing the Ivie Creek case-study area.

The objectives of this study were therefore, to determine: (1) how variations in sedimentary structures and lithofacies influence both compartmentalization and permeability, and (2) how bounding surfaces can be identified from core and geophysical well-log data and, (3) ultimately, how such features should be considered in oil field development and secondary or enhanced oil recovery programs.

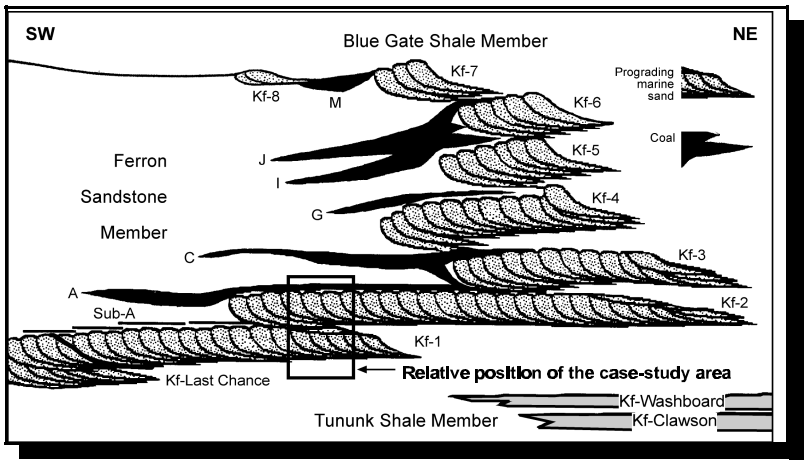


Figure 7-2. Diagrammatic cross section showing relative positions of Ferron parasequence sets with their associated coal zones (black), and the relative stratigraphic position of the Ivie Creek case-study area within the Ferron Sandstone (from Ryer, 1991; Anderson and others, 1997). The diagram has no scale.

Location

The Ivie Creek case-study area is located in the central part of the project area (figure 7-1), about 6 miles (9.7 km) south of the town of Emery, Utah, in the center of T. 23 S., R. 6 E., Salt Lake Base Line (SLBL), Emery County. The Ferron Sandstone outcrops straddle Interstate 70 (I-70). A small stream, Ivie Creek, flows just north of the interstate highway, hence the name Ivie Creek case-study area.

Within the study area, outcrops along Ivie Creek, Quitchupah Creek, "Scabby Canyon," and the I-70 road-cut, and UGS drill holes provide information in three dimensions on rock bodies of the Kf-1 and Kf-2. Access to the area is excellent because of proximity to I-70. The "Ivie Creek amphitheater" is an informal name applied to a broad, curving area of cliffs north of I-70 where the most detailed work was conducted (figure 7-3).

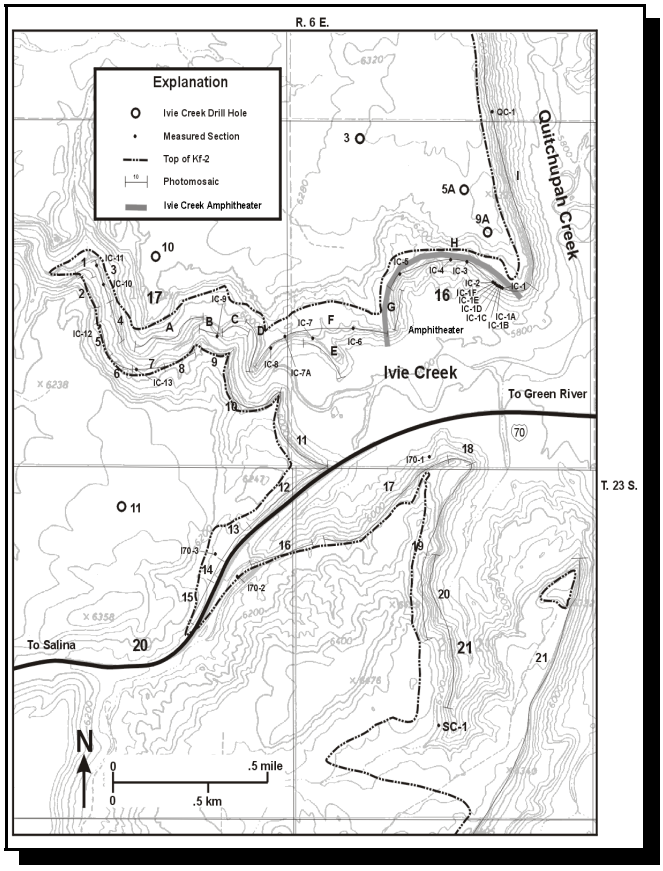


Figure 7-3. Data collection point locations in the Ivie Creek case-study area.

Methods

Surface and subsurface data (figure 7-3) were collected to: (1) map variations in lithofacies, sedimentary structures (size, geometry, orientation/dip, and percent of sedimentary structures), and bedding types, (2) characterize bounding surfaces both between and within sandstone bodies, and (3) merge with permeability transect data. These data consisted of measured stratigraphic sections (23), paleocurrent measurements (about 400), and scaled interpreted photomosaics (21), logged drill-hole cores (4), and geophysical logs (five sets).

Field methods: Field work for the project took place from April to October, 1994 and 1995. Sections were measured using a Jacob's Staff or by directly measuring a units thickness with a tape on the mostly vertical outcrops. Description of the individual units in the measured sections included the following information: (1) primary and secondary lithologies, composition, color, and grain size of the rocks; (2) size, shape, and degree of induration of the beds; (3) sedimentary structures, biologic structures (trace fossils), and fossils in the rocks; and (4) bounding surfaces and depositional environment of the unit. Most of these parameters were recorded on a measured section form designed for its ability to be entered into a computer database for later manipulation (see Appendix B, Field Methods - Digital Measured Sections). Sections were correlated to interpret stratigraphy, lithofacies, depositional environment, and define reservoir components in the statistical and reservoir-modeling parts of the project.

Measured section locations were chosen during the first field season to develop a general geologic characterization of the case-study area. In the second season, the Kf-1-Ivie Creek[a] bedset in the "amphitheater" became the focus of sections measured. Each section was located on photomosaic coverage and plotted on a topographic map.

Paleocurrent measurements were taken both during the measurement of sections and opportunistically during photomosaic annotations. Paleocurrent measurements taken while measuring a section are tied to the specific unit of each section. The data have also been compiled by bedset and parasequence, and plotted as rose diagrams (Anderson and others, in press). Measurements plotted according to bedset and parasequence give an overall indication of the direction of progradation. Measurements plotted according to depositional units within a bedset or parasequence give direction of sediment transport of that depositional component (for example, distributary channels, mouth bars, or parts of the delta front). In addition, paleocurrent measurements from wave ripples were plotted separately from measurements taken from unidirectional current ripples and cross-beds. Wave-ripple measurements provide information on direction of waves impinging on, and modifying, the delta front. Unidirectional measurements provide information on depositional processes that delivered sediments to the delta, and can be used in modeling fluid flow in reservoirs. All lithologic and paleocurrent data were entered into a database using codes from field forms, and then computer software was used to generate a hard-copy measured section (Anderson and others, in press).

Photomosaics played a key role in developing a geologic understanding and our data set. Photomosaics were constructed for the entire case-study area (see Appendix B, Field Methods - Photomosaics). Measured sections, permeability transects (see Chapter 8 for details on permeability transect methodology), and line work on photomosaics were scaled, both vertical and horizontal. The methods and techniques used to do this are described in more detail in Appendix B, Field Methods - Scaling.

Drill-hole program: The drill holes in the Ivie Creek case-study area were located downdip 200 to 1,200 feet (60-265 m) from the Ferron outcrop to provide data for a three-dimensional (3-D) morphologic interpretation of individual lithofacies and to capture the various reservoir changes in the Kf-1 and Kf-2 parasequence sets (figure 7-3). The drill holes were permitted, drilled, logged, and plugged. Where hole conditions allowed, drill holes were logged with sonic, density, neutron, focused resistivity, spectral gamma ray, and dipmeter tools. Cuttings were described and tied to

existing wells in the area to pick tops and core points. A total of 586 feet (179 m) of core was recovered and described from the Kf-1 and Kf-2 parasequence sets. Descriptions of the individual units in the core sections include the following information: (1) primary and secondary lithology, composition, color, and grain size of the rocks; (2) size, shape, and degree of induration of the beds; (3) sedimentary structures, biologic structures (trace fossils), and fossils in the rocks; and (4) bounding surfaces and depositional environment of the unit. Sections were correlated to interpret the stratigraphy and lithofacies. Geophysical logs and core logs of the project drill holes can be found in (Anderson and others, in press). Continuous-core logging of the core recovered from the Ivie Creek hole numbers 3, 5A, and 9A was conducted using a computer-interfaced multisensor track which simultaneously recorded natural gamma, density (via gamma-ray attenuation), and magnetic susceptibility. These data were used to determine porosity and clay content. Data from this logging exercise are found in Chapter 8, Petrophysical Characteristics of the Ivie Creek Case-Study Area.

Surface elevation and isopach maps: Contour maps of various stratigraphic contacts and isopach maps of selected intervals were constructed from points picked along the continuum of scaled line work on the photomosaics and from picks in project drill holes. The datum for all project contour and isopach mapping is the contact between the Kf-1 and Kf-2 parasequence set. This datum was "flattened" by simply assuming it was horizontal and measuring up or down from this line on the scaled line work derived from the photomosaics. The Kf-1/Kf-2 boundary was assigned an arbitrary elevation of 100 feet (30 m). There was no attempt to reconcile the true elevation of the contact. Using this method the present structural dip of the beds is removed from the mapping. On a contour map, elevations less than 100 feet (30 m) represents a surface which lies below the Kf-1/Kf-2 boundary, and elevations greater than 100 feet (30 m) represent a surface which lies above the same boundary. Mattson (1997) used a kriging algorithm to create our project contour and isopach maps.

Stratigraphy

The Ferron Sandstone in the Ivie Creek case-study area consists of two regional-scale parasequence sets, the Kf-1 and Kf-2 (figures 7-2 and 7-4 [see detailed regional cross section in Anderson and others, in press]). The Kf-1 represents fluvial-dominated delta deposits which change from proximal to distal. In the Ivie Creek case-study area, two bedsets (see Chapter 4, Regional Stratigraphy, for a definition of bedset) are present within the Kf-1 parasequence set: the Kf-1-Iv[a] and Kf-1-Iv[c] (figures 7-4 and 7-5). Kf-1 prograded from the south-southeast to the north-northwest as fluvial-dominated delta lobes represented by two bedsets. Most of the sediments in Kf-1 cycles accumulated as delta lobes, sourced from a point. Locally, the pods of sediment in Kf-1 cycles indicate deposition in a protected environment such as a bay. The Kf-1 lies conformably upon the Tununk Shale Member of the Mancos Shale. The Kf-1 is the second parasequence set from the base of the "upper" Ferron (the Kf-Washboard and Kf-Clawson lie within the "lower" Ferron). The first parasequence set has feathered into the Tununk Shale before reaching the Ivie Creek case-study area.

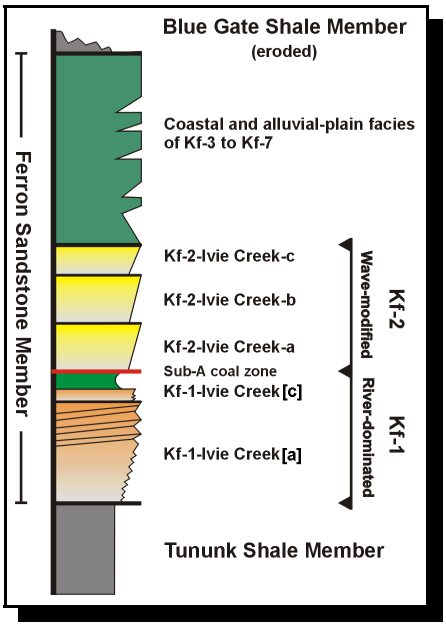


Figure 7-4. Ivie Creek case-study area stratigraphy.

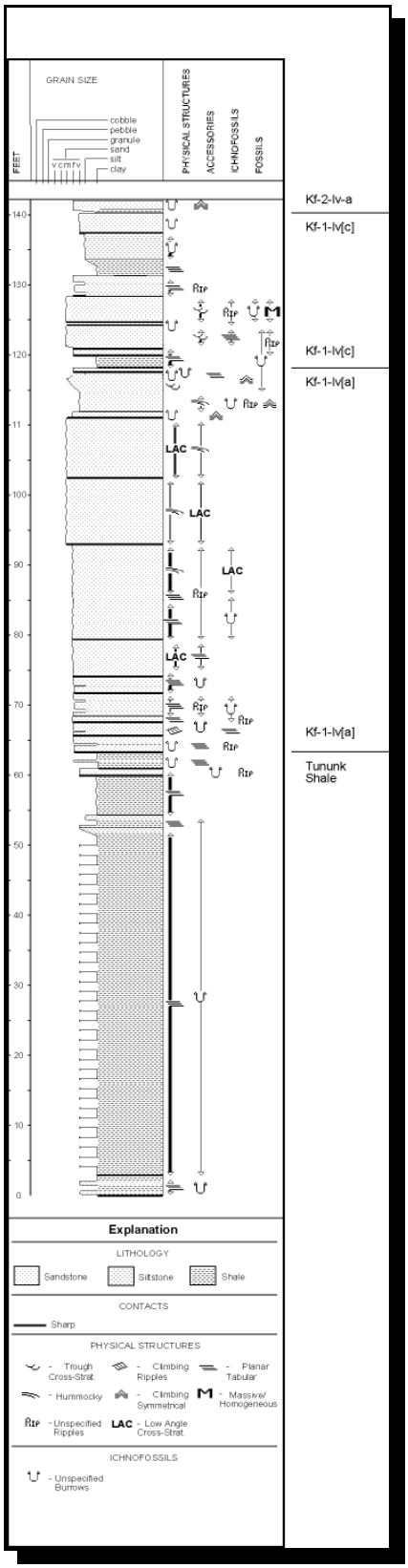


Figure 7-5. Stratigraphic section from the Ivie Creek amphitheater of Kf-1 (originally at a scale of 1 inch = 10 feet [2.54 cm = 3 m]) showing lithology, nature of contacts, sedimentary structures, ichnofossils, and bedset designations.

The sediment source of Kf-2 switched to west from the east-southeast source of Kf-1 deposition. The Kf-2 contains more and cleaner sand, indicating a more wave-influenced environment of deposition. The Kf-2 parasequence set contains three parasequences: the Kf-2-Ivie Creek-a (Kf-2-Iv-a), Kf-2-Ivie Creek-b (Kf-2-Iv-b), and Kf-2-Ivie Creek-c (Kf-2-Iv-c) (figure 7-6). These parasequences show less lateral variation in lithofacies than the Kf-1 bedsets, due to greater wave influence. Within the case-study area, there is little lateral variation in thickness of sand-rich Kf-2 lithofacies, even when lateral change occurs from one depositional subfacies to another. Kf-2 cycles accumulated in sheet-like bodies that pinchout laterally forming a wedge due to wave-action along the delta front. The contact between the Kf-1 and Kf-2 is generally drawn at the top of the Sub-A coal zone in the Ivie Creek case-study area (figure 7-7). The top of the Kf-2 lies near the top of the C coal, and includes all of the A coal zone and delta-plain strata which separates the A and C coal zones (see Kf-3-MA in stratigraphic Appendix A for additional details). Above the Kf-2 parasequence set is coastal-plain and alluvial-plain facies which have not been divided into parasequence sets, but represent the landward equivalent of the marine portions of Kf-3 through Kf-7 (see figure 7-7).

The stratigraphy of the Ivie Creek case-study area is displayed in a series of cross sections which incorporate both surface measured sections and drill-hole data developed as part of this project. These cross sections are available as UGS Open-File Report by Anderson and Chidsey, (in press). A detailed, diagrammatic regional cross section and all photomosaics (PM-) are found on CD-Rom in Anderson and others (in press).

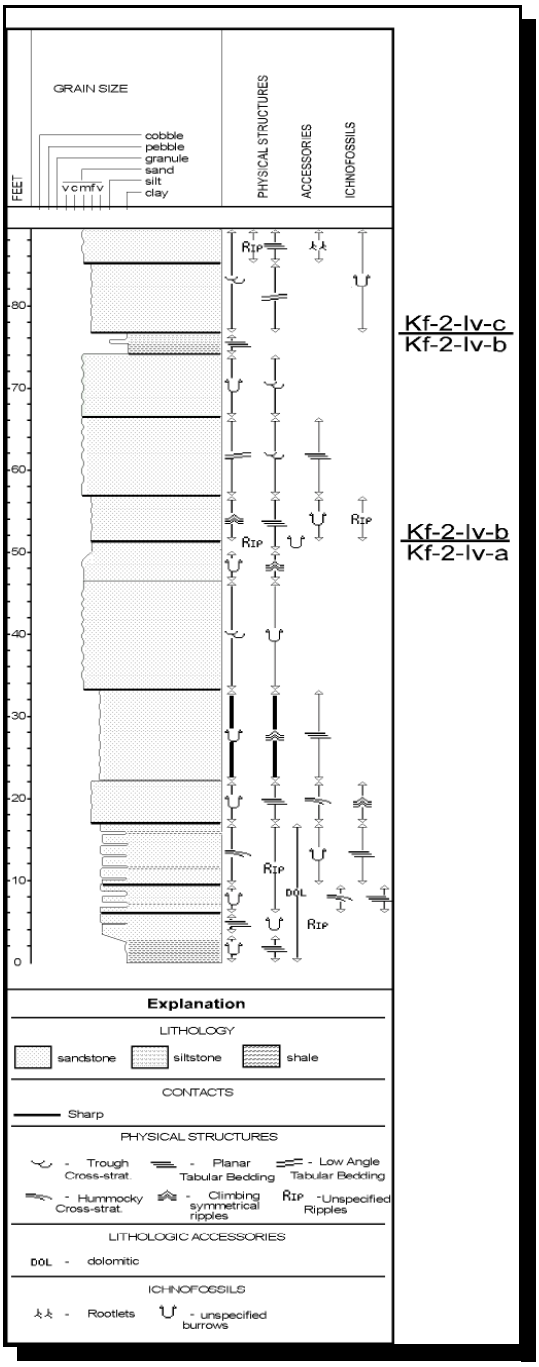


Figure 7-6. Stratigraphic section from Ivie Creek Canyon of Kf-2 (originally at a scale of 1 inch = 10 feet [2.54 cm = 3 m]) showing lithology, nature of contacts, sedimentary structures, ichnofossils, and parasequence designations.

Kf-1-Iv[a] Bedset

The Kf-1-Iv[a] bedset can be traced on outcrop photomosaics to its landward most position in mid-Blue Trail Canyon (see PM-IC3) and seaward into mid-Quitchupah Canyon (see PM-IC43). The distance from landward to seaward pinchout along a depositional dip

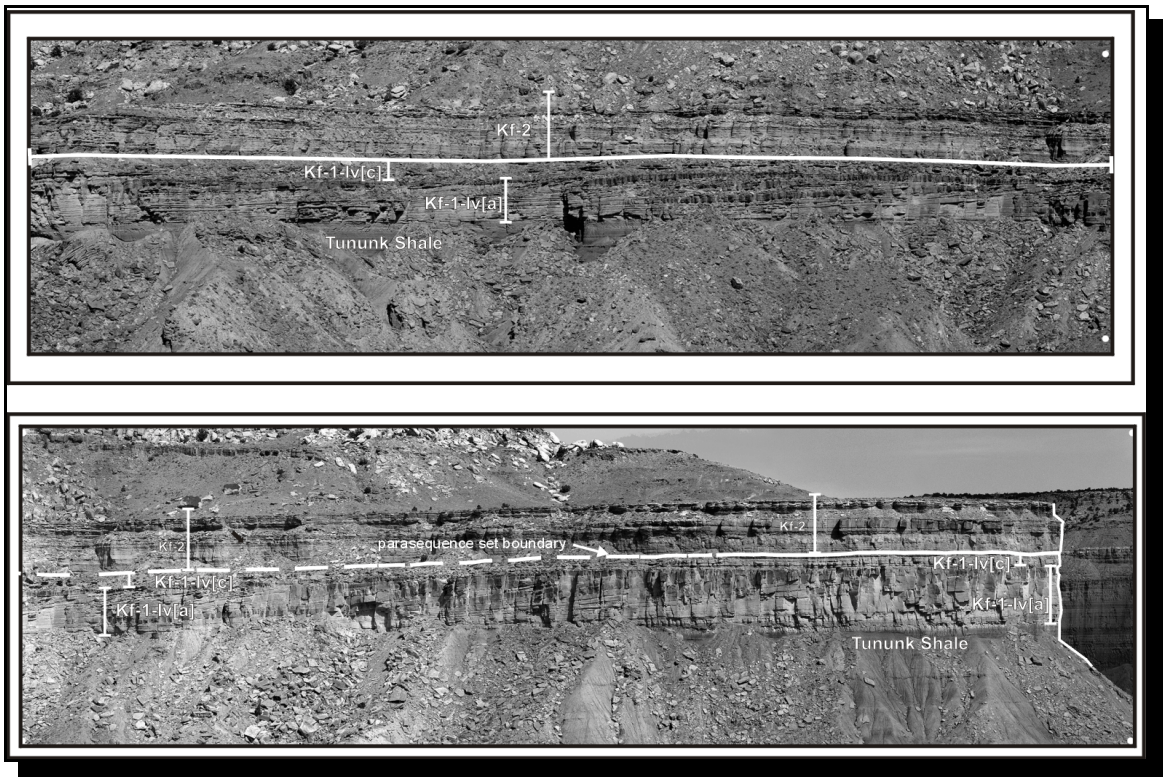


Figure 7-7. Photomosaic of Ferron parasequence sets, view to the north, of the Ivie Creek area displaying contrasting delta-front architectural styles (top is left panel, bottom is right panel). The heavy, white, horizontal line is a parasequence-set boundary separating Kf-1 and Kf-2 and drawn on top the Sub-A coal zone. Kf-1-Iv[a] has steeply inclined (10 to 15E) clinoforms representing fluvial-dominated deposition. Kf-2 has gently inclined (< 3E) clinoforms representing wave-modified deposition. Outcrop in photomosaic located in SW1/4NE1/4 section 16, T. 23 S., R. 6 E., Salt Lake Base Line, Emery County, Utah.

line is about 1.5 miles (2.4 km). Although the photo-documentation of the landward pinchout is poor, the unit clearly does not exhibit offset into the non-marine lithofacies and hence has been designated a bedset instead of a parasequence. This bedset thins rapidly to the west (see PM-IC36) as well as to the more typical seaward direction of north. This is anomalous for Ferron delta lobes.

The contour map on the top of the Kf-1-Iv[a] bedset shows the fluvial-dominated deltaic lobes dipping to the north-northwest (figure 7-8A), in the direction of progradation. The Kf-1-Iv[a] bedset is a fan-like deposit which thickens to the east (figure 7-8B) and was deposited into an area with minimal wave influence, therefore, the primary bed forms are preserved (figure 7-9).

Delta-front sandstones of a modified Gilbert delta make up these sand-rich deposits which changes from proximal to distal (where the sandstone pinches out) east to west across the Ivie Creek case-study area. Smaller sedimentary packages than the bedset are recognized within Kf-1-Iv[a]. Figure 7-10 illustrates these smaller units. In descending order they are: (1) subcycle, (2) clinoform, and (3) bounding layer.

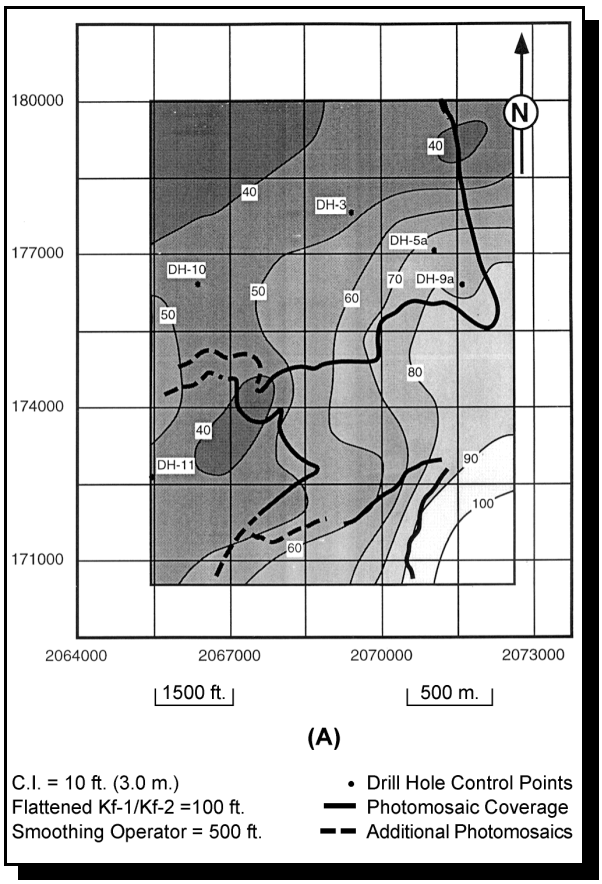


Figure 7-8. (A) Contour map of the top of Kf-1-Iv[a] using the parasequence set boundary between Kf-1 and Kf-2 as a datum with an arbitrary elevation of 100 feet assigned to the datum. Values less than 100 feet are below the contact. The map shows a sloped surface at the top of the Kf-1-Iv[a] to the west.

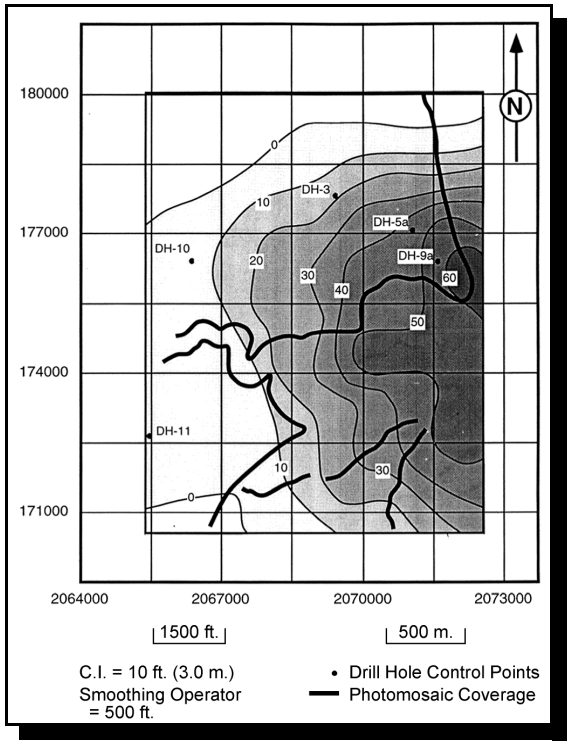


Figure 7-8. (B) Isopach map of Kf-1-Iv[a] in feet. State Plane coordinates are used in both maps.

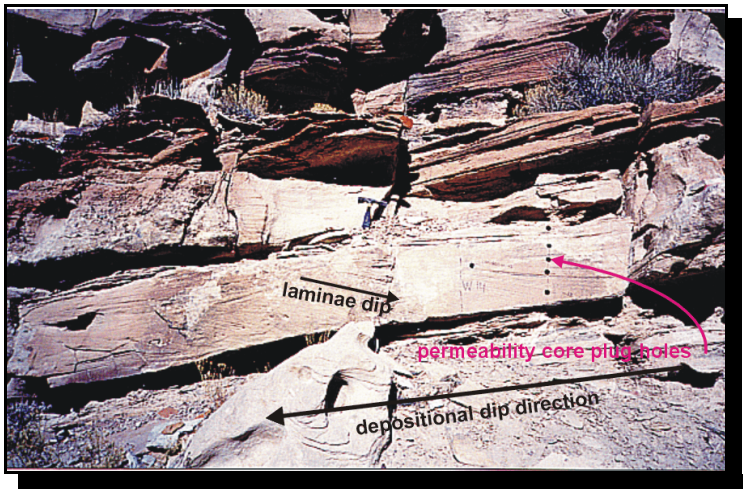


Figure 7-9. Low-angle cross-beds are the primary sedimentary structure dominant in the proximal portions of the Kf-1-Iv[a] bedset. The general direction of the depositional dip is from right to left. Note the gentle up depositional dip inclinations of many laminae in the bed below the hammer. Holes in the rock are from outcrop permeability plugs taken in the unit. Location is near the top of transect 3 (see figure 7-3).

Subcycle definition: A **subcycle** divides the bedset into a smaller recognizable coarsening-upward, bed-thickening-upward unit. The mappable extent of the subcycle is distinctively smaller than the bedset. It is possible that the unit's formation is in response to a localized relative sea-level change (perhaps compaction related), or to a change in sediment supply.

Clinoform definition: The Kf-1-Iv[a] bedset was the focus of much of the geologic investigation which fed into the development of a geologic model used in flow simulation. Using photomosaics the architectural elements of the Kf-1-Iv[a] were quantified as off-lapping packages of beds here referred to as clinoforms.

Clinoform is used to identify a group of beds which are inclined seaward in an *en echelon* pattern and generally separated from one another by a distinctive bounding surface observable on outcrop. The clinoforms are visually defined on photomosaics of the outcrop (figures 7-7, 7-11, and PM-IC41). The clinoform shape is defined on the photomosaics based on a slightly more recessive break in the cliff face chiefly along the bounding surfaces which define the clinoform. General lithofacies categories, described in detail later, were assigned to clinoforms (polygons) on the scaled photomosaic panels: clinoform proximal, clinoform medial, clinoform distal, and clinoform cap.

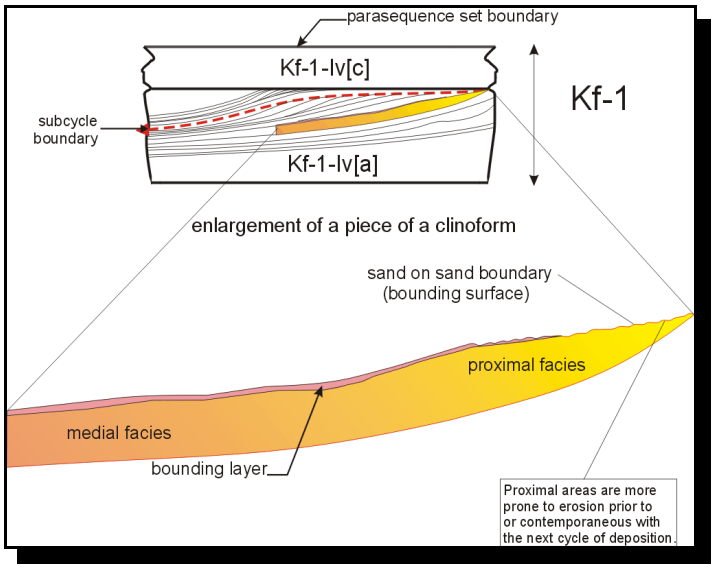


Figure 7-10. Stratigraphic nomenclature and hierarchical units of the Kf-1-Iv[a] bedset, Ivie Creek case-study area.

Clinoform boundaries in the Kf-1-Iv[a] bedset identified on photomosaics were digitized and scaled to: (1) provide internal consistency for spatial relationships of field data, (2) correct all data (photomosaics) for distortions, (3) tie to a common datum (the Kf-1/Kf-2 parasequence set

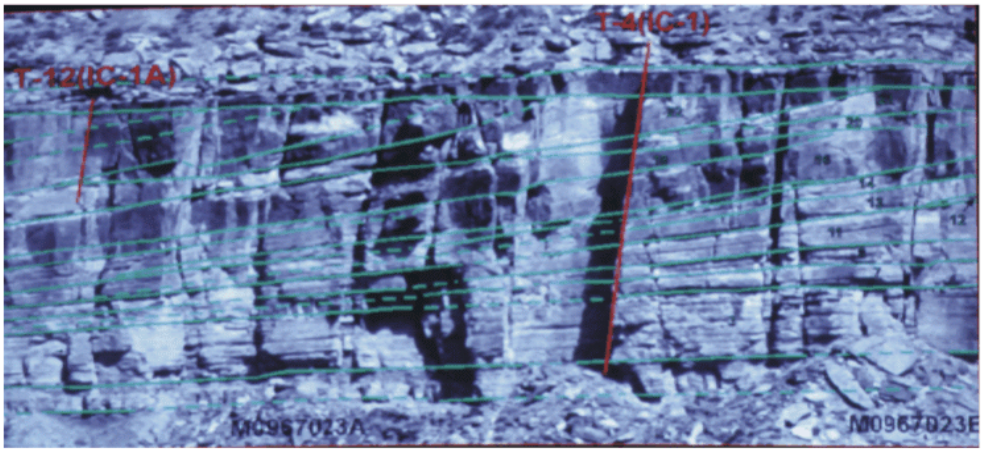


Figure 7-11. Inclined bedforms (clinoforms) in Kf-1-Iv[a] at the Ivie Creek amphitheater, Ivie Creek case-study area, defined by the inclined gray (green) lines. These lines represent the bounding elements of the clinoform -- bounding layers. Vertical (red) lines are permeability transects.

boundary), and (4) provide a framework for scaled cross sections. Graphic logs along permeability transects and measured sections were adjusted to fit the scaled line work to form the base for construction of cross sections and the three-dimensional model of the reservoir architecture. Utilizing tie points on the panels that were identified in the field, the elevation profile picks were positioned on the 7.5 minute topographic maps.

Bounding layer definition: The term **bounding surface** was used to describe the line on the photomosaics which separated one clinoform from another. Upon closer examination, it is clear that the line work representing the boundaries of clinoforms are drawn on a unit that generally does have some thickness on outcrop. In order to clarify this difference, the term **bounding layer** is used to describe the thin rock layer which creates the erosive contrast on the cliff face and is appropriately called a bounding surface at the scale of the subcycle or bedset. The bounding layer is defined by the base of the overlying clinoform and by the top of the underlying main sand body of the genetically associated clinoform. The bounding layer is important as an element of the flow characteristics of a clinoform-type reservoir because it generally contains beds and laminae which are finer grained, mud and carbonaceous-detritus rich, and probably have distinctly lower permeability than the main sand body of the clinoform.

The measured section data, photomosaics, and overlaying line work (which defines the clinoforms and lithofacies), and permeability transect data were used to target specific clinoforms for study. Bounding layers were described with the following information: location (plotted on the photomosaic), type of bounding surface (between what lithofacies), thickness of the bounding layer, slope profile, detailed description of lithology, a general description of the rocks above and below the bounding layer, photographs of the layer and the overlying and underlying rock, and geologists' in-field opinion of the cause of the recessive break in the cliff face.

Descriptive field data were gathered to better define the characteristics potentially effecting flow across clinoform-to-clinoform boundaries. The emphasis was on bounding layers in portions of the clinoforms which are designated proximal or medial lithofacies. It was assumed that the distal lithofacies in the clinoforms are all similar in permeability and essentially act as strong baffles or barriers to flow.

Clinoform characteristics: The basal Kf-1-Iv[a] bedset of the Kf-1 is characterized by clinoform geometries that dip basinward. Clinoforms in the delta front dip 10E-15E, and shale-out laterally within a mile (1.6 km) down depositional dip. The clinoforms change characteristics from the shallower water, more proximal locations, to the deeper water, more distal locations (figure 7-12A). Clinoform facies designations were based on sedimentary structures (figure 7-12B), grain size (figure 7-12C), bedding thickness, inclination angle, and stratigraphic position. The abrupt end of the medial facies in figure 7-10 (end of shading) is representative of most of the contacts between proximal, medial, and distal clinoform facies used in this study. Polygon-shaped packages of rock are necessary for reservoir modeling and simulation. In reality, the transition from medial to distal (as well as medial to proximal) is gradational.

As the bounding layers are followed on outcrop up the inclined surface of the clinoform, the last visible evidence of the bounding layer is often one or several laminae of carbonaceous material forming a very slight recess in the outcrop. On rare occasions the bounding layer does not reach the upper termination of the clinoform, resulting in a true sand-on-sand contact between clinoforms.

The generally abrupt nature of the contact between the clinoform below and the bounding layer above raises the question: which clinoform is the bounding layer most closely related to? Most of the bottoms of clinoforms (top of the underlying bounding layer) exhibit a smooth, sharp, concave up

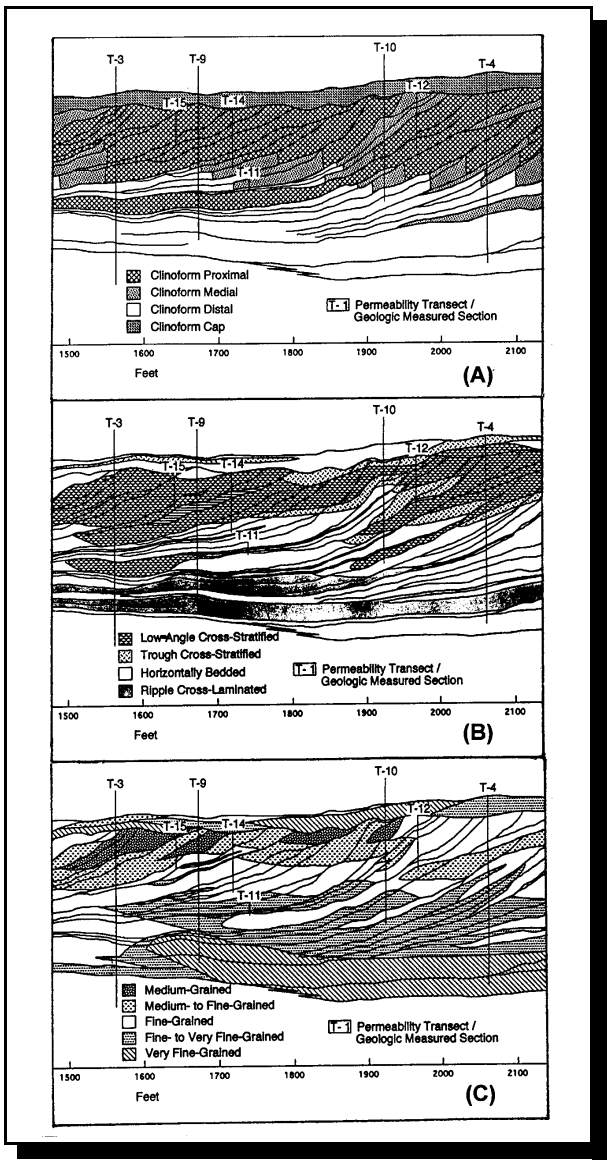


Figure 7-12. Scaled cross sections, oriented west to east, of the Kf-1-Iv[a] bedset from the Ivie Creek amphitheater based on a portion of the interpreted photomosaic. Vertical lines represent permeability transect locations. (A) Cross section showing clinoform lithofacies assigned to the Kf-1-Iv[a] bedset. (B) Dominant sedimentary structure distribution within clinoform facies. (C) Average grain size distribution within clinoform facies.

contact. Occasionally erosional truncation of the underlying bounding layer (figure 7-13) and/or the underlying clinoform (figure 7-10) is evident, particularly in the more proximal part of the clinoforms, hence, the conclusion that the bounding layer is more closely related to the depositional episode of the underlying clinoform. Sand-on-sand contacts represent either an area of no deposition of the finer-grained sediment during the waning stage of deposition of the underlying clinoform or, an area of erosion prior to, and associated with the deposition of the next clinoform.

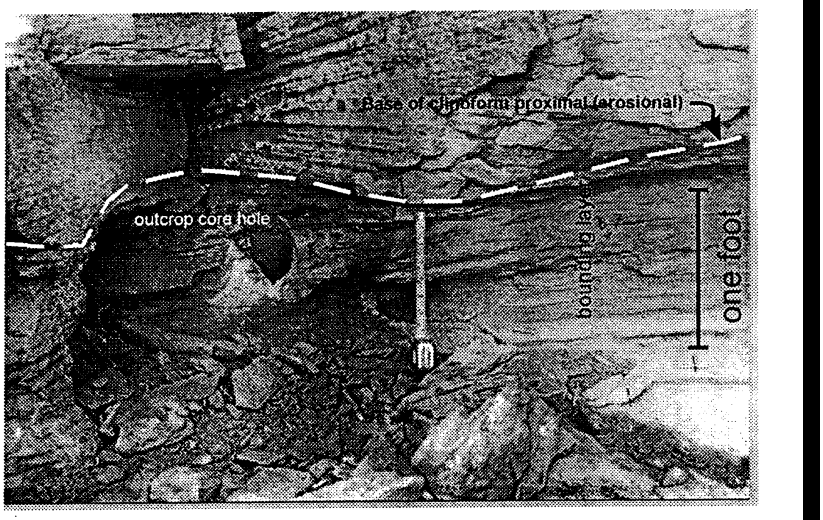


Figure 7-13. Low-angle cross-beds preserved in the proximal portion of Kf-1-Iv[a] cut into the underlying bounding layer at location B-7 (see figure 7-14 for measurement locations).

The abrupt end of clinoform sand-dominated deposition is interpreted to represent the temporary change in sand distribution at the delta. During the temporary cessation of rapid sedimentation the small amount of wave energy at the delta front continues to move and rework some bed load sediments. Suspended load (and associated carbonaceous debris) is "raining down" on the delta front almost continuously. Mud, silt, and carbonaceous debris dominance in the deeper water portions of Kf-1-Iv[a] indicates the ability of wave-energy to winnow the "fines" to deeper and lower energy environments. The presence of the bounding layer/clinoform couplet is indicative of high frequency depositional cyclicity during deposition of the subcycle.

Characteristics of clinoform bounding layers: The lower surface of the bounding layer is generally sharp, but occasionally is gradational over a thin interval. Most of the bounding layers examined contained two common elements: (1) they are finer-grained, less cemented, and less resistant than the overlying and underlying clinoforms, and (2) they contain laminations of carbonaceous material, which are consistently poorly cemented and more easily eroded, hence, are expressed as recesses on outcrop. The bounding layer ranges in thickness from less than an inch to a few feet thick. The unit generally decreases in grain size in a down-depositional-dip direction with a corresponding increase in thickness. The bounding layers generally range from fine-grained sandstone to mudstone, and commonly contain bedding planes with laminae rich in carbonaceous debris. The bounding layer is chiefly horizontal to slightly irregular bedded with minor oscillation ripples and flaser bedding. Bed thickness is generally thin to laminated. Occasionally some portion of the bounding layer contains gypsum veinlets which are probably related to weathering since they have not been observed in bounding layers examined in core. The lithologic nature of the bounding layer is generally very similar to the clinoform distal facies.

Bounding layer thicknesses were measured at 23 locations (figure 7-14) and are summarized in table 7-1. The clinoform facies above and below each measure point is also listed in table 7-1. The bounding layer is believed to be genetically related to the underlying clinoform. Based on this assumption, the mean thickness and range for the bounding layer which is underlain by clinoform proximal facies is 0.358 feet (0.109 m) (0.05 to 1.05 feet [0.02-0.32 m]) and for the clinoform medial facies is 0.600 feet (0.183 m) (0.11 to 1.63 feet [0.03-0.5m]). Only one measurement was taken at the clinoform distal facies location (B-1). Table 7-2 is a summary of the thickness changes on a single bounding layer. With the limited number of data points common to the same bounding layer, there is high variability in the thickness to length ratio.

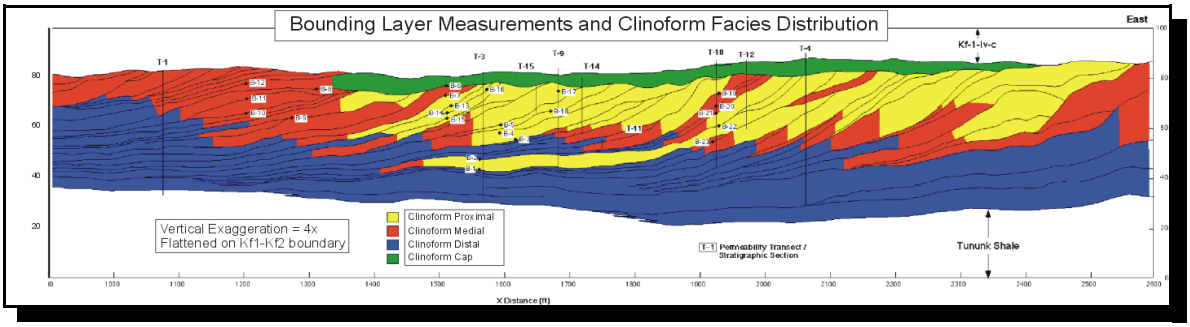


Figure 7-14. Bounding layer measurement locations and clinoform facies distribution, Ivie Creek amphitheater.

The focus of the outcrop activities was on the bounding layers associated with clinoform proximal and medial facies. These two facies have the best reservoir characteristics. As the bounding layer is tracked seaward, or down the clinoform, it becomes essentially indistinguishable from the underlying and overlying clinoform distal facies. Another way to state this is the bounding layer is a tongue of clinoform distal facies which separates clinoform proximal-proximal facies, clinoform proximal-medial facies, and clinoform medial-medial facies.

The mapping of the bounding layer thickness is based on an estimate of thickness from a "best guess" examination of the detailed outcrop photomosaics and bounding layer measurements from the field (figure 7-15). The bounding layer thickness is broken into three thickness categories: (1) < 0.25 feet (0.08 m), (2) > 0.25 (0.08 m) and < 0.75 feet (0.23 m), and (3) > 0.75 feet (0.23 m).

Close inspection of the photography and associated line work, and outcrop observations (figure 7-11) reveals the presence of bounding layers within the designated clinoforms. These internal layers are very similar in nature to those found defining the exterior of the enclosing clinoform. Generally these layers are less continuous than the bounding layers that define the clinoform. These internal bounding layers should have similar permeability characteristics to those found external to the clinoform.

Recognition of a bounding layer in the subsurface is essential in transferring knowledge from the outcrop analog to producing reservoirs. Using the detailed outcrop descriptions of these layers, cores from the drill holes back of the outcrop at Ivie Creek were examined to identify bounding layers. Unfortunately, no proximal facies were encountered in any of the drill holes. The most highest energy facies are found in cores of drill hole Ivie Creek no. 9A and are medial facies. Core from this hole was examined in detail and several bounding layers identified.

Table 7-1. Bounding layer measurements and characteristics.

Measurement ID	Thickness (in feet)	Clinoform Facies	
		Above the layer	Below the layer
B-1	0.63	Proximal	Distal
B-2	0.40	Proximal	Proximal
B-3	0.05	Proximal	Proximal
B-4	0.17	Internal-proximal*	Internal-proximal
B-5	0.35	Proximal	Proximal
B-6	0.26	Cap	Medial
B-7	0.86	Medial	Proximal
B-8	1.25	Medial	Medial
B-9	0.70	Medial	Medial
B-10	0.26	Medial	Medial
B-11	0.38	Medial	Medial
B-12	0.49	Medial	Medial
B-13	0.13	Proximal	Proximal
B-14	0.54	Proximal	Proximal
B-15	1.63	Proximal	Medial
B-16	0.19	Proximal	Proximal
B-17	0.08	Internal-proximal	Internal-proximal
B-18	1.05	Proximal	Proximal
B-19	0.11	Proximal	Medial
B-20	0.50	Medial	Medial
B-21	0.07	Medial	Proximal
B-22	0.40	Proximal	Proximal
B-23	0.40	Medial	Medial

* Internal-proximal is “bounding layer” character with a clinoform

Table 7-2. Tabulation of thickness changes along specific bounding layers.

From ID to ID	Change in thickness (feet)	Distance between points	Clinoform facies from pt. to pt.	Ratio thickness/length
B-6 to B-8	0.99	200 feet	medial-medial	.0046
B-16 to B-14	0.35	72 feet	prox.-prox.	.0049
B-22 to B-2	0	375 feet	prox.-prox.	0
B-23 to B-1*	0.23	356 feet	medial-distal	0.0007

*jump of one clinoform up at B-1

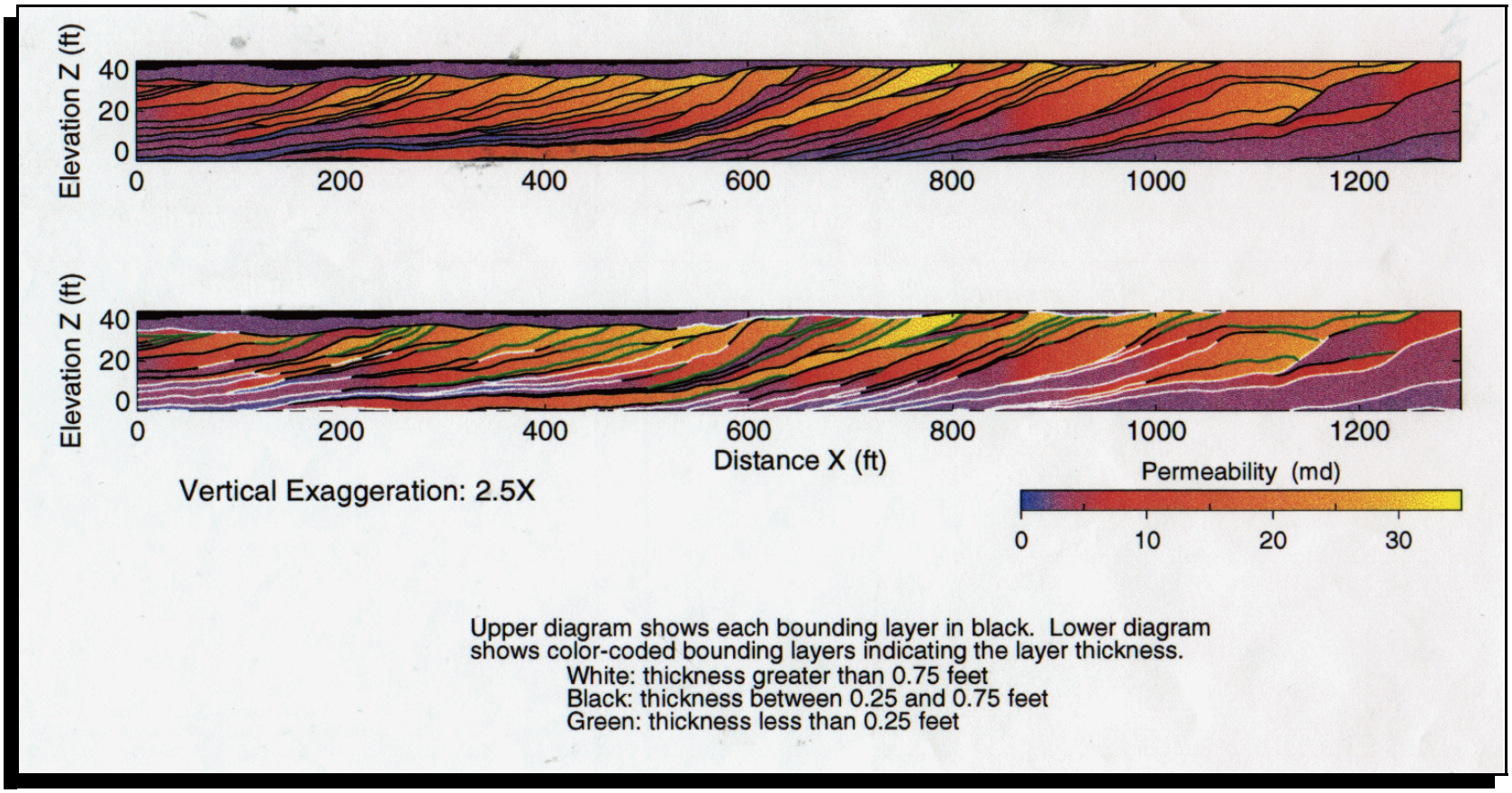


Figure 7-15. Ivie Creek, 40-acre (98.8-ha) spacing model estimating bounding layer thicknesses.

The identification of bounding layers in the core is interpretive. It is impossible to correlate individual bounding layers from outcrop into the subsurface, even with the close proximity of the drill holes to the outcrop (figure 7-3), but similar features in core to those observed on outcrop can be identified.

Kf-1-Iv[c] Bedset

The Kf-1-Iv[c] bedset is sand rich and varies in thickness within the case-study area. In contrast to the Kf-1-Iv[a], delta-front subtle clinoforms of the lower units in the bedset dip less than 5E. Thinning of sand-rich lithofacies occurs in both up-depositional-dip and down-depositional-dip directions due to lateral lithofacies changes. The lower section of the Kf-1-Iv[c] laps onto the more distal parts of the Kf-1-Iv[a] in the western part of the case-study area (see PM-IC43) and represents the distal portion of another delta lobe, probably originating from the southwest. This lower section may be completely absent in some locations as a result of erosion and/or non-deposition (figure 7-16). It also includes a channel sandstone body, lenticular in cross section, deposited by a northwesterly flowing stream (figure 7-16).

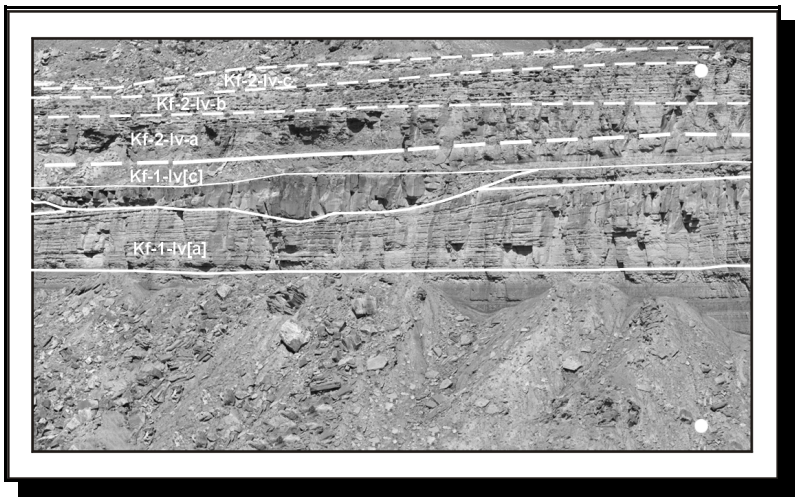


Figure 7-16. Photomosaic, view to the north, of Ferron parasequences in the Ivie Creek case-study area displaying Kf-1-Iv[a] clinoforms and a Kf-1-Iv[c] distributary channel. The Kf-1-Iv[a] contains more clinoform distal facies than observed to east on figure 7-7. Outcrop in photomosaic located in SW1/4NE1/4SW1/4 section 16, T. 23 S., R. 6 E., Salt Lake Base Line, Emery County, Utah.

The uppermost section of the Kf-1-Iv[c] is continuous across the entire Ivie Creek area and indicates wave and fluvial influences (figures 7-7 and 7-16). It is capped by unidirectional, trough cross-bedded sandstone. The Kf-1-Iv[c] contains slump or rotated block features near the mouth of Ivie Creek (see PM-IC36). It thickens to the north as the Kf-1-Iv[a] pinches out. In the amphitheater area, above the cross-bedded sandstone, are 10 to 15 feet (3-6 m) of bay-fill deposits. These deposits consist of carbonaceous mudstone; thin, rippled-to-bioturbated sandstone and siltstone; fossiliferous mudstone to sandstone; oyster coquina; and ash-rich coal. Although no contacts are mapped in the immediate Ivie Creek area, the upper portion of this bay interval is related to a younger marine progradation found north and east of the Ivie Creek area (Kf-1-Cowboy Canyon). The uppermost carbonaceous mudstone or ash-rich coal is the Sub-A coal zone. The coal zone shows considerable variation in thickness (0 to 1 foot [0-0.3 m] in thickness) and intertongues with underlying bay deposits. A flooding surface has been identified at the top of the Sub-A. The boundary with the overlying Kf-2 parasequence set is drawn at this flooding surface.

The Kf-1-Iv[c] thickens dramatically from east to west across the Ivie Creek case-study area (figure 7-17). On the west, the Kf-1-Iv[c] has onlapped Kf-1-Iv[a]. It represents a slightly younger episode of progradation filling space that Kf-1-Iv[a] delta left unfilled, likely due to avulsion of the sediment source. At the mouth of Ivie Creek Canyon, it is anomalously thick due to large slump features or rotated blocks (see PM-IC36). Failure of the rotated blocks is consistently toward the north to northwest, the direction that the delta lobe appears to have prograded. The abundance of rotated blocks, which are relatively rare entities elsewhere in the Ferron, in this particular area may be related to a zone of flexure in the foreland basin, the axis of which is to the northwest. More rapid subsidence toward the northwest may have encouraged failure of the delta-front in that direction.

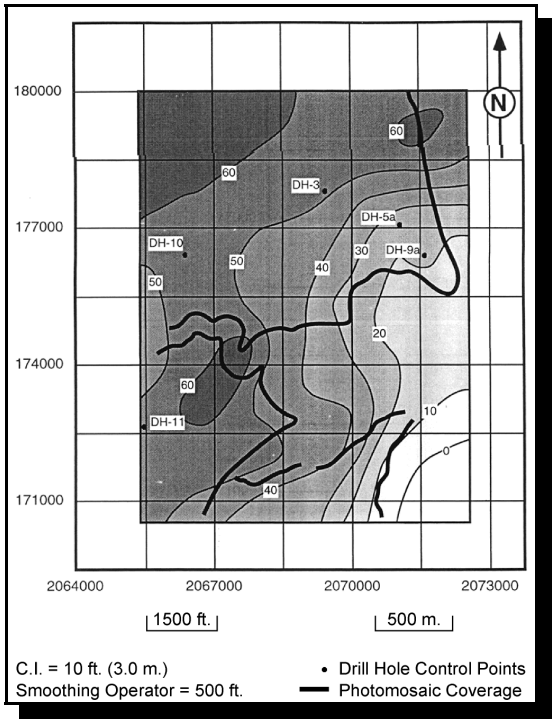


Figure 7-17. Isopach map of Kf-1-Iv[c] bedset (State Plane coordinates).

Kf-2-Iv-a Parasequence

The oldest parasequence of the Kf-2 parasequence set in the Ivie Creek area is the Kf-2-Iv-a. It is separated from overlying Kf-2-Iv-b parasequence by a surface that was initially interpreted to be a "marine-flooding surface" because it appeared to separate two vaguely upward-coarsening depositional sequences. Truncation of channel deposits in the lower part of Ivie Creek Canyon has subsequently been recognized at the top of Kf-2-Iv-a, confirming the initial interpretation of a flooding surface and parasequence status.

The base of the Kf-2-Iv-a parasequence consists of interbedded sand and minor shale deposited in prodelta to lower shoreface environments (see PM-IC17, right end). These deposits are thin, typically less than 10 feet (3 m) thick. In some places along the basal contact of the parasequence a thin (1 foot [0.3 m]) bed of transgressive deposits is present just above the Sub-A coal zone. The prodelta and lower shoreface deposits are overlain by a 0.5-to 1-foot-(0.2-0.3-m-) thick zone of highly carbonaceous to coaly sandstone which grades into 20 to 30 feet (6-9 m) of very fine-grained, silty, and slightly carbonaceous sandstone representing a middle shoreface environment. The unit is intensely bioturbated. The flooding surface and parasequence boundary at the top of the unit is difficult to recognize because there is frequently no offset in facies with the overlying Kf-2-Iv-b. Kf-2-Iv-a becomes thin and downlaps onto the parasequence set boundary a short distance to the east, near "Junction Point" (see PM-IC40).

The Kf-2-Iv-a parasequence thickens (to 50 feet [15 m]) west across the area. Near the mouth of Ivie creek Canyon, it consists of a thin sequence of lower shoreface heterolithics overlain by about 28 feet (8.5 m) of middle-shoreface deposits (see PM-IC17, right end). Farther up the canyon to the west, a distributary channel deposit has cut into the upper half of the shoreface deposits. The coarser (medium-grained) channel is easy to distinguish from the darker-colored shoreface deposits (see PM-IC32, left side). Possible foreshore deposits are found near the last outcrop of the Kf-2-Iv-a in the creek bottom of Ivie Creek (see PM-IC25).

Kf-2-Iv-b Parasequence

In the Ivie Creek amphitheater, the Kf-2-Iv-b parasequence was deposited in a middle shoreface environment. Kf-2-Iv-b exhibits gently seaward inclined beds which are very conspicuous when viewed from west to east along the outcrop. The parasequence has at least two sub-cycles of grain size coarsening and bed thickening upward (see PM-IC40 and IC41). This same architecture is clearly exposed on the south side of I-70 (see PM-IC10 and IC11). The Kf-2-Iv-b parasequence consists of horizontally bedded, silty sandstone at the base (middle shoreface) and unidirectional, trough cross-bedded sandstone toward the top (distributary channel to mouth-bar deposits). These units are generally intensely bioturbated.

In Ivie Creek Canyon, Kf-2-Iv-b is dominated by unidirectional, trough cross-bedded sandstone of a 24-foot-thick (7.3 m) mouth-bar complex (figure 7-18) which continues farther up the canyon and is present in core from the UGS drill hole Ivie Creek no. 11, 0.5 mile (0.8 km) to the southwest. The unit thickens slightly from west to east in the study area, unlike to underlying parasequence.

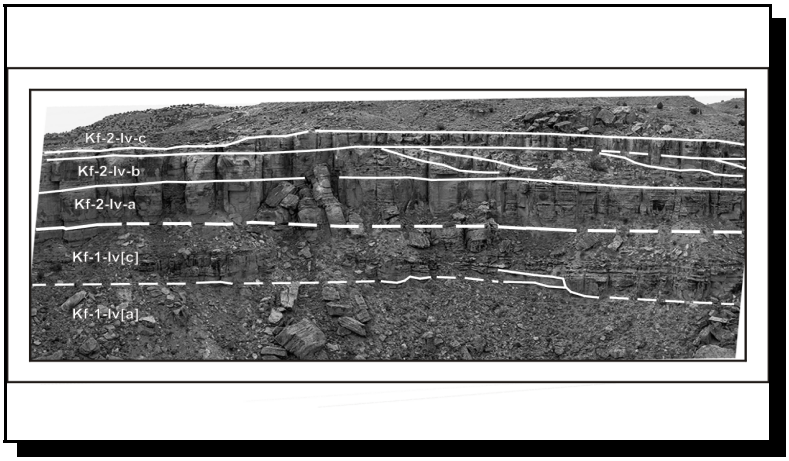


Figure 7-18. Photomosaic, view to the southwest, of Ferron parasequences in the Ivie Creek case-study area displaying the mud-rich distal, delta-front deposits of the Kf-1 and distributary-mouth-bar deposits of the Kf-2. The Kf-1 has now changed laterally from the sand-rich, proximal delta-front deposit. The distributary-mouth-bar deposits of the Kf-2-Iv-b parasequence are broadly channelized. Outcrop in photomosaic located in SE1/4SE1/4 section 17, T. 23 S., R. 6 E., Salt Lake Base Line, Emery County, Utah.

Kf-2-Iv-c Parasequence

The Kf-2-Iv-c parasequence is separated from the underlying Kf-2-Iv-b parasequence by a siltstone to shale interval which varies in thickness across the east portion of the Ivie Creek case-study area. Generally, the entire parasequence fines from west to east. In the Ivie Creek amphitheater, Kf-2-Iv-c is interpreted as a bay-fill deposit (although it is devoid of body fossils). At the top of this sequence is a thin, medium-grained carbonaceous sandstone, which may represent the migration of a low-energy beach (foreshore deposits) across the bay fill prior to capping by coastal-plain deposits and deposition of the overlying A-coal zone (which is locally burned).

The type area of Kf-2-Iv-c is the mouth of Ivie Creek Canyon (figure 7-18). This unit undoubtedly warrants designation as a parasequence inasmuch as the associated transgressive surface is clearly recognizable both in Ivie Creek Canyon and to the south in the I-70 road cut (see figure 4-14, Chapter 4, Regional Stratigraphy). The landward pinchout of the marine facies of Kf-2-Iv-c trends just slightly east of south toward I-70 (see figure 4-15, Chapter 4, Regional Stratigraphy).

The shoreline sandstone unit displays some interesting and unusual changes at the mouth of Ivie Creek Canyon, changing over a distance of about 300 feet (90 m) from a strongly wave-modified shoreface unit (see PM-IC32) to a much lower wave energy unit that contains mud interbeds and finer sand, and that has a silvery-gray color on outcrop (see PM-IC41). This change suggests a change from a coast directly facing the sea to one that was sheltered from wave energy. The facies content of this shoreline unit is a wave-modified coast, probably shoreface in the proximal part, transforming to a low-wave-energy bay. There is evidence for bay-head deltas and tidal channels feeding the bay to the northeast, in Quitchupah Canyon (see PM-IC43).

In Ivie Creek Canyon, Kf-2-Iv-c forms a 10-foot (3.1-m) cliff. Excellent upper shoreface facies are exposed. The top of the unit is rooted by the overlying coastal-plain vegetation. Root casts are commonly visible at the top of this unit. Just a short distance up the canyon, there is a thin, but well developed, carbonaceous shale at the top of Kf-2-Iv-b, with the flooding surface for Kf-2-Iv-c immediately above (see PM-IC30, left side).

An interesting feature of the Kf-2-Iv-c parasequence contour map (figure 7-19) is the structural high in the southern portion of the map with closure around the 180 foot contour. This closed high is the result of differential compaction around the sides of a large distributary channel, previously described by Barton, 1994 (figure 7-20). This distributary system dominates the unit in "Scabby Canyon," south of I-70.

Facies

A general description of the facies used in the Ferron regional work is provided in Chapter 3. The following descriptions are more finely defined and were used in the description and analysis for this case study.

Distributary Complex

The distributary complex facies is characterized by a predominance of sandstone and trough cross-stratification (see PM-IC24, parasequence Kf-2-Iv-a) which is typically unidirectional (figure 7-21). In places, this facies can be subdivided into distributary channel, distributary mouth-bar, and clinoform facies. This facies is often characterized by the complex geometry of bedding and large-scale bounding surfaces which are related to cut and fill processes in contrast to the flat to very gently inclined surfaces of the lower delta-front (figure 7-22).

Distributary Channel

The distributary channel facies is common in river-dominated delta-fronts and is also found within the wave-modified shoreline of the Ivie Creek case-study area (figures 7-16 and 7-23). It is characterized by channels with high height-to-width ratios, and unidirectional trough cross-stratified and current ripple cross-laminated deposits. Channel fills are sandstone dominated, but heterolithic channel fills are also found. In sand filled channels, the grain size is often coarser than the surrounding delta-front or shoreface and fines up. Troughs in the channel base generally contain mud rip-up clasts, woody fragments, and rare sharks' teeth. This facies grades seaward into the distributary-mouth bar facies.

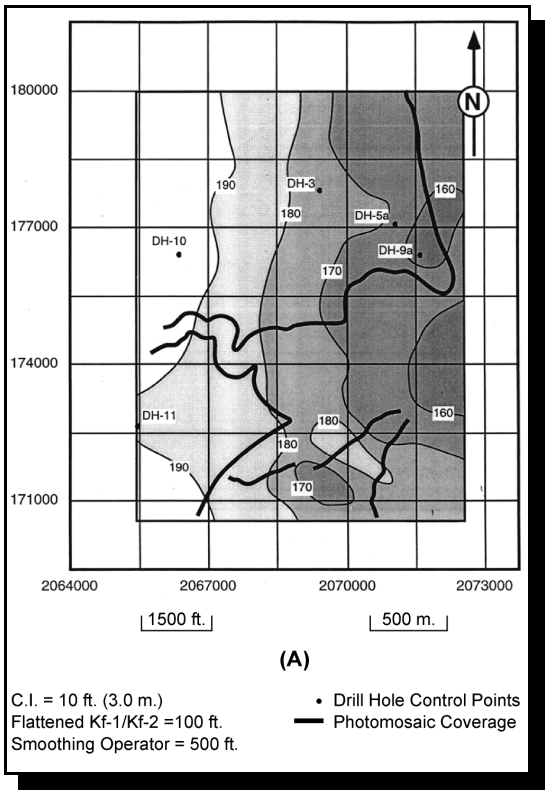


Figure 7-19. (A) Contour map of the top of Kf-2-Iv-c using the parasequence set boundary between Kf-1 and Kf-2 as a datum with an arbitrary elevation of 100 feet assigned to the datum. Values more than 100 feet are above the contact. The map shows a sloped surface at the top of the Kf-2-Iv-c parasequence to the east, in the direction of progradation.

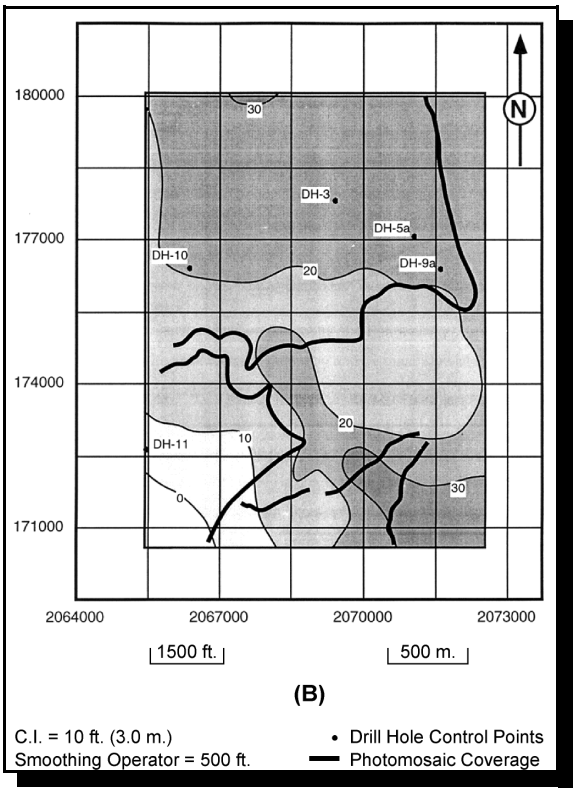


Figure 7-19. (B) Isopach map of Kf-2-Iv-c in feet. State Plane coordinates are used in both maps.

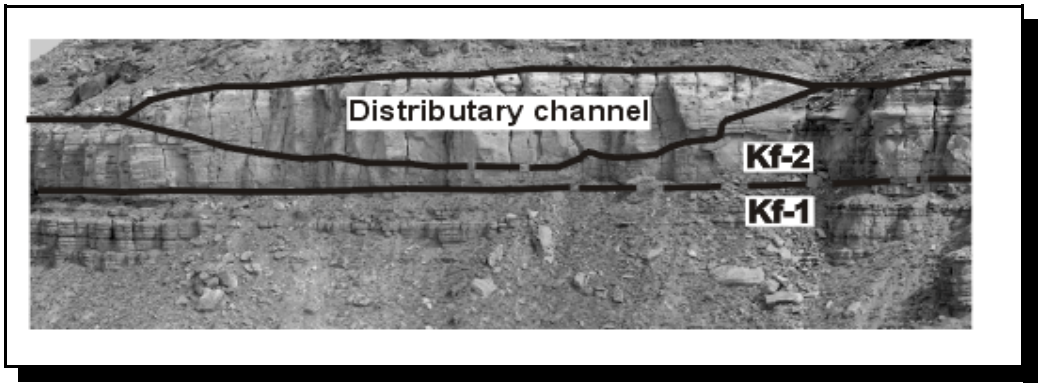


Figure 7-20. Photomosaic near I-70, view to the south, showing both Kf-1 and Kf-2. A major distributary channel (center of photo) associated with the Kf-2-Iv-c parasequence has cut down to near the base of the Kf-2-Iv-a parasequence. Outcrop in photomosaic located in NW1/4NE1/4NW1/4 section 21, T. 23 S., R. 6 E., Salt Lake Base Line, Emery County, Utah.

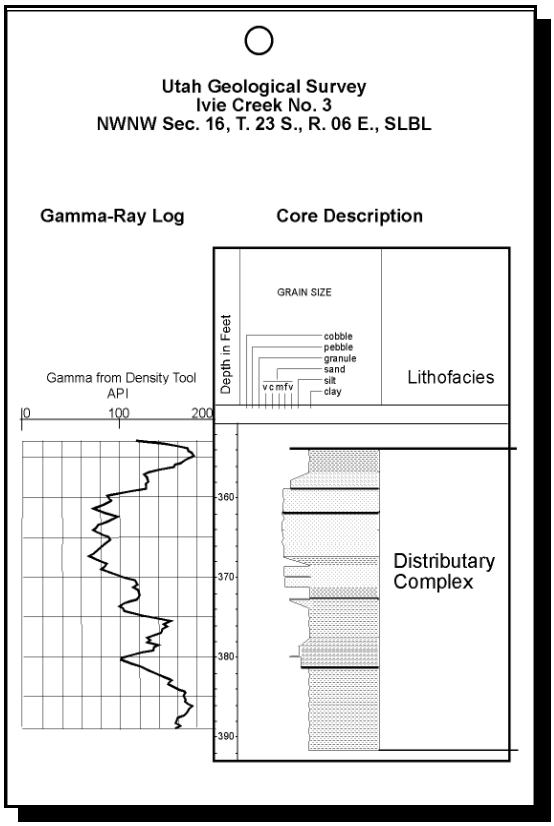


Figure 7-21. Example of the Ferron Sandstone reservoir gamma-ray type log and core description for the distributary complex facies.

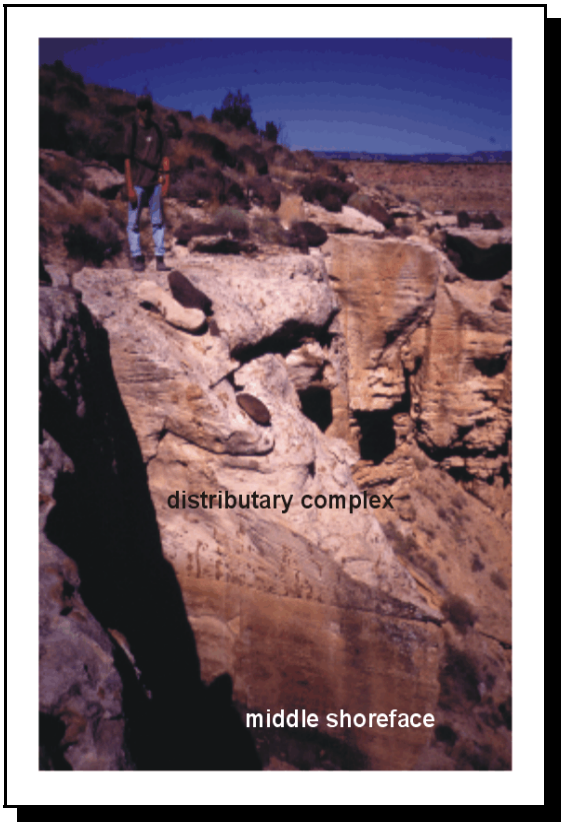


Figure 7-22. Distributary complex facies cut into the shoreface. The lighter colored distributary complex facies, below the geologist, is dominated by unidirectional trough cross-stratification. The underlying middle shoreface is dark brown. Note the burrowing which is iron-stained, just above the scoured base and contact with the middle shoreface. Location is near the mouth of Corbula Canyon, center of section 4, T. 24 S., R. 6 E., Salt Lake Base Line.

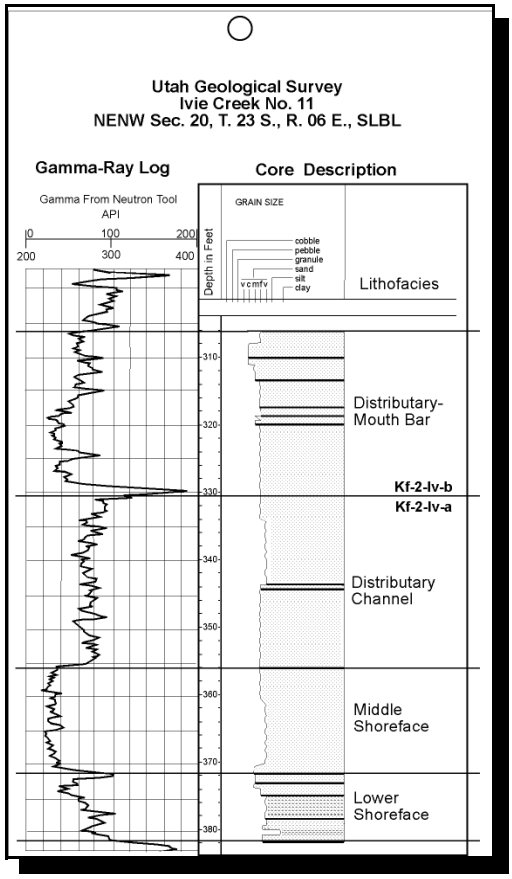


Figure 7-23. Example of the Ferron Sandstone reservoir gamma-ray type log and core description for the distributary-mouth bar, distributary channel, middle shoreface, and lower shoreface facies.

Distributary-Mouth Bar

The distributary-mouth bar facies is found in the upper parts of delta-front sequences of Kf-2, and is associated with distributary channels (figures 7-18 and 7-23). This facies is characterized by fine-grained or coarser, trough cross-stratified sandstone, with moderate, to intense burrowing developed in areas that had lower flow velocities and decreased sedimentation rate; some intervals between trough sets are completely bioturbated. *Ophiomorpha* is common; escape burrows are less common. Paleoflow directions show a strong offshore component with the amount of scatter increasing with increased wave influence and distance from the distributary channel. Major bed boundaries are inclined in a seaward direction (see PM-IC12, parasequence Kf-2-Iv-b). Traced laterally and seaward, the facies commonly grades into middle shoreface or lower delta-front facies (fluvial-dominated shoreline).

Clinoform Facies

The clinoforms change characteristics from the shallower water, more proximal (near the shoreline) locations to the deeper water, more distal locations (figures 7-5 and 7-24). Four clinoform facies are designated within the Kf-1-Iv[a] bedset: clinoform proximal (cp), clinoform medial (cm), clinoform distal (cd), and clinoform cap (cc). Clinoform facies were based on grain size, sedimentary structures, bedding thickness, inclination angle, and stratigraphic position. Facies cp, cm, and cd are assigned to clinoforms only, and facies cc is a bounding facies above the clinoforms (Anderson and others, 1997; Chidsey, 1997).

Clinoform proximal (cp): Facies cp is sandstone, mostly fine to medium grained. The chief sedimentary structure is low-angle cross-stratification with minor horizontal and trough cross-stratification and rare hummocky bedding. The facies is dominantly thick- to medium-bedded, well to moderately indurated, with permeabilities ranging from 2 to 600 millidarcies (md) and a mean of about 10 md. The inclination of bed boundaries is generally greater than 10E. This facies is interpreted to be the highest energy, and most proximal to the sediment supply. The steep inclinations are interpreted to represent deposition into a relatively localized deep portion of an open bay environment. The dominance of low-angle cross-stratification, along with inclinations within the bed or clinoforms in an up-depositional dip direction, indicates the influence of on-shore wave energy (figure 7-9).

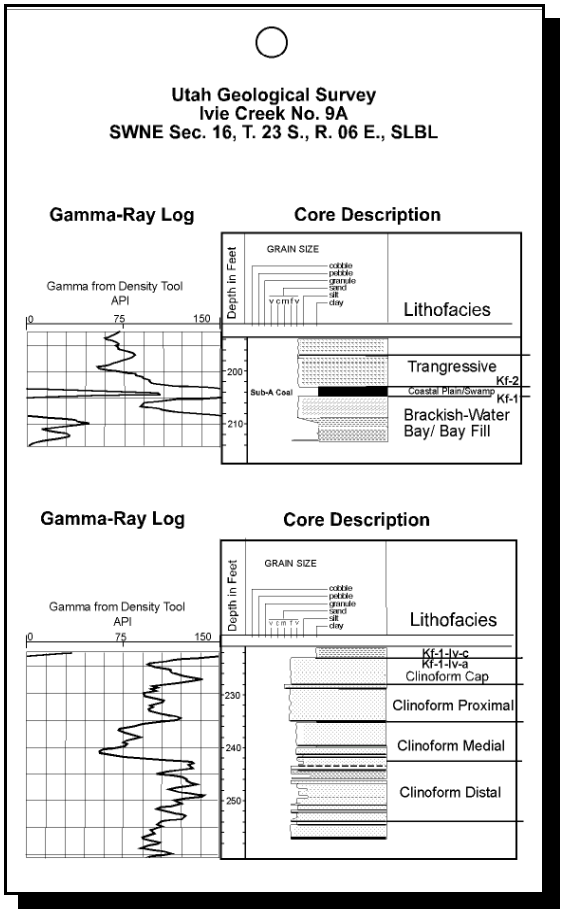


Figure 7-24. Example of the Ferron Sandstone reservoir gamma-ray type log and core description for the clinoform distal, medial, proximal, and cap facies; and the brackish-water bay/bay fill, coastal plain/swamp, and transgressive facies.

Clinoform medial (cm): Facies cm is dominantly sandstone with about 5 percent shale. The sandstone is primarily fine grained with slightly more fine- to very fine-sized grains than fine- to medium-sized grains. Horizontal beds dominate with some rippled, trough, and low-angle cross-stratified beds (figure 7-25). Bed thicknesses range from laminated to very thick, but most are medium. The beds are generally well to moderately indurated, but are occasionally noted as friable. The permeability values range from non-detectable to 100 md with the mean about 3 md. Inclination on the clinoform boundaries is between 2° and 10E. The facies is generally transitional between facies clinoform proximal and distal. Clinoform medial is occasionally present at the erosional truncation, or off-lapping boundary, of the clinoforms, with no visible connection to facies clinoform proximal.

Clinoform distal (cd): Facies cd is sandstone (sometimes silty) and about 10 percent shale. The sandstone grain size is dominantly fine to very fine grained, with considerable variation (figure 7-26). Sedimentary structures in this facies are chiefly horizontal laminations and ripples in medium to thin beds. Induration of the beds ranges from well cemented to friable. Average facies permeability is just at the detection limit of 2 md, but ranges up to 80 md. This facies is gradational with facies cm and represents the deepest water and lowest energy deposition within the clinoform. It can be traced distally into prodelta to offshore facies.

Clinoform cap (cc): Facies cc is sandstone, generally very fine to fine grained. The beds are horizontal, with some trough and low-angle cross-stratification in thick to medium beds (figure 7-27). Burrowing is rare. The sandstone is mostly well indurated, with permeabilities ranging from non-detectable to 100 md and a mean of about 2 md. Clinoform cap facies are present stratigraphically above the subcycle line (truncated clinoforms), where the line is near the top of the parasequence and bed boundaries show little to no inclination. This facies is interpreted to represent an eroded and reworked delta top.



Figure 7-25. Clinoform medial facies exposed just east of permeability transect 1 (T1) at the Ivie Creek amphitheater. The facies is dominated by horizontal bedding as found in the thicker bedded units. The recessive parts of the outcrop are typically ripple laminated and finer grained than the resistant sandstone beds. Hammer for scale.



Figure 7-26. Clinoform distal facies in the Ivie Creek amphitheater. The base of the Ferron Sandstone is exposed at the base of the heterolithic sequence of interbedded sandstone, siltstone, and mudstone. Ripple and planar bedding are common. Hammer in the lower right for scale.

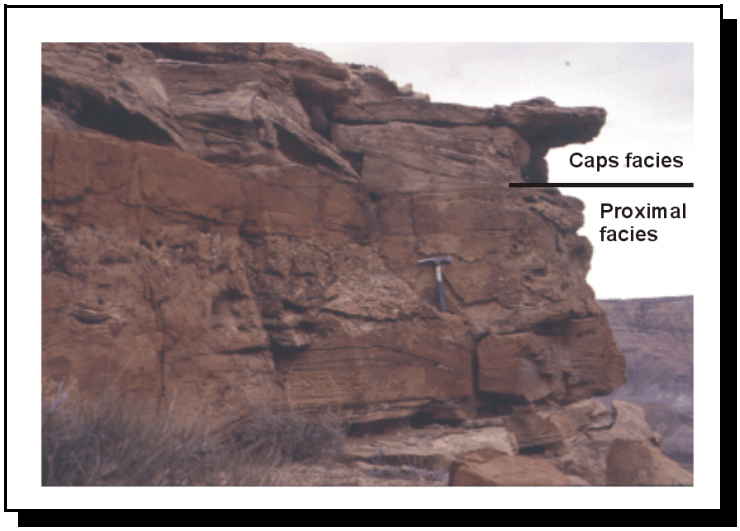


Figure 7-27. Clinoform cap facies with trough cross-bedding exposed at the top of the photo. The hammer sandwiched between two hard reddish-beds, is within the underlying clinoform proximal facies. Kf-1-Iv[a] bedset in the Ivie Creek amphitheater.

Brackish-Water Bay/Bay Fill

The brackish-water/bay-fill facies consists of heterolithic mudstone to sandstone, coarsening and bed thickening up, with wave ripple to horizontal laminations which are sparse to intensely burrowed. The presence of a brackish-water fauna (*Crassostrea, Corbula securis, Lucinid, Caryo corbulais*, aff. *Varia*, and *Serrthid*), is the distinguishing characteristic of this facies. This fauna is present within "dirty" sandstone, siltstone, mudstone, and carbonaceous mudstone. Oyster coquinas commonly are found within this facies (figure 7-28). Typically the rocks are rich in carbonaceous debris. The facies is often under and/or overlain by coastal plain facies (the top is often rooted), and may grade into shoreface deposits below (figure 7-24).



Figure 7-28. Oyster coquina containing brackish-water fauna within carbonaceous mudstone. Core from UGS drill hole Ivie Creek no. 11.

Coastal Plain/Swamp

The coastal plain/swamp facies is represented by a sequence of non-marine rocks dominated by mudstone, carbonaceous mudstone, and siltstone with minor sandstone (see PM-IC13, left side). Coal is commonly interstratified with the other rock types (figures 7-24, 7-29, and 7-30). These rocks are interpreted as inter-fluvial environments along a low gradient coast.

Transgressive

The transgressive facies consists of siltstone and very fine- to fine-grained sandstone with an erosional base. Lag deposits are common and bioturbation is extensive throughout the facies. Transgressive units are 8 feet (2.4 m) or less in thickness (figure 7-24). This facies represents a significant marine-flooding event (onset of Kf-2) with the base usually being a parasequence set boundary (figures 7-29 and 7-30).

Shoreface

Shoreface is the relatively steeply dipping zone from the subaerial beach to a poorly defined point where the slope flattens on the sea floor. Wave energy is sufficient to move sand-sized grains in this zone. At the seaward end of the shoreface is the prodelta facies. This mud-dominated facies represents the area just seaward of the dominant influence of wave-energy and typically interfingers with the lower shoreface defined below.

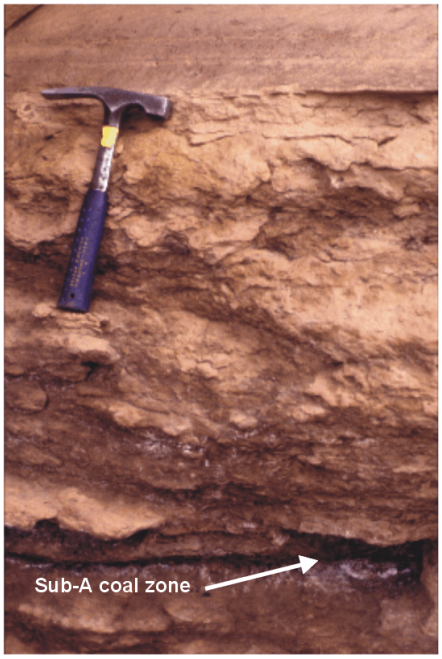


Figure 7-29. Thin transgressive unit (Kf-2) above the thin carbonaceous bed which is part of the Sub-A coal zone (Kf-1) and set boundary between Kf-1 and Kf-2 in the Ivie Creek area. This is near the seaward downlap of the Kf-2-Iv-a parasequence in the Ivie Creek amphitheater. Hammer for scale.

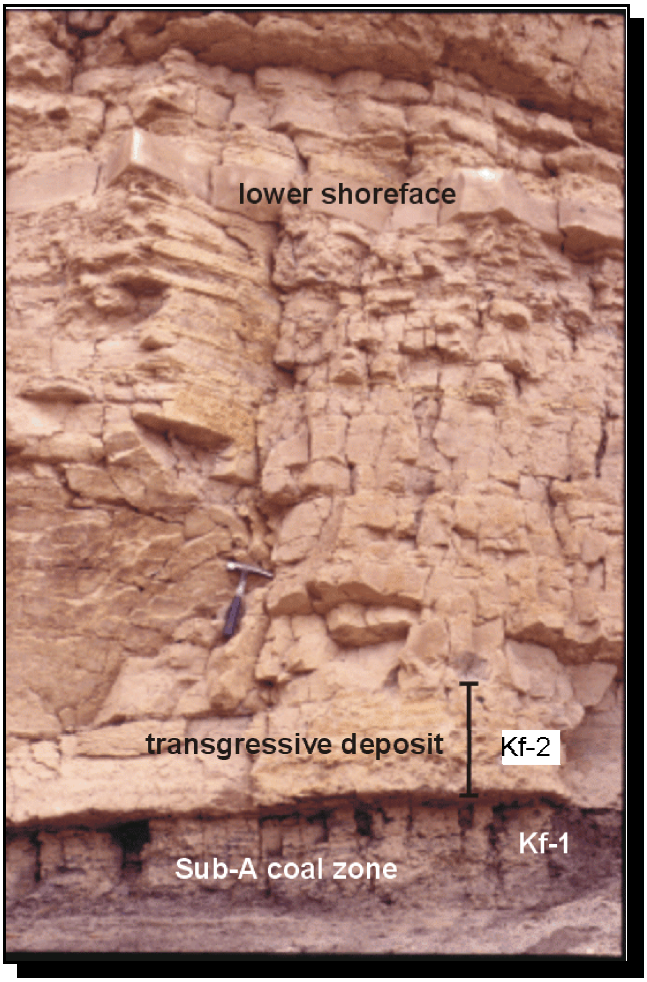


Figure 7-30. Lower shoreface facies found above the Kf-1/Kf-2 parasequence set boundary in the Ivie Creek case-study area. Typically the facies consists of interbedded very fine-grained sandstone, siltstone, and shale, and coarsens and bed thickens upward. This is stratigraphically the lowest facies in the wave-modified delta deposits in the area.

Lower shoreface: The lower shoreface facies consists of thinly interbedded shale to siltstone and very fine- to fine-grained sandstone (see PM-IC15, center). Wave ripples to horizontal laminations dominate this facies (figure 7-30). Burrowing is generally found on the top of thin sandstone beds and the shale is often bioturbated. This facies is very similar to the transition facies but sandstone is more abundant than shale and siltstone (figure 7-23). Hummocky stratification is common.

Middle shoreface: The middle shoreface facies is very fine- to fine-grained sandstone composed of hummocky, swaley, and planar laminations with minor ripple laminations (figure 7-31). This facies is generally thick, representing 50 percent or more of the shoreface sequence (figure 7-23). The most common burrow types are *Thalassinoides* and *Ophiomorpha* and the amount of burrowing varies from moderate to bioturbated.

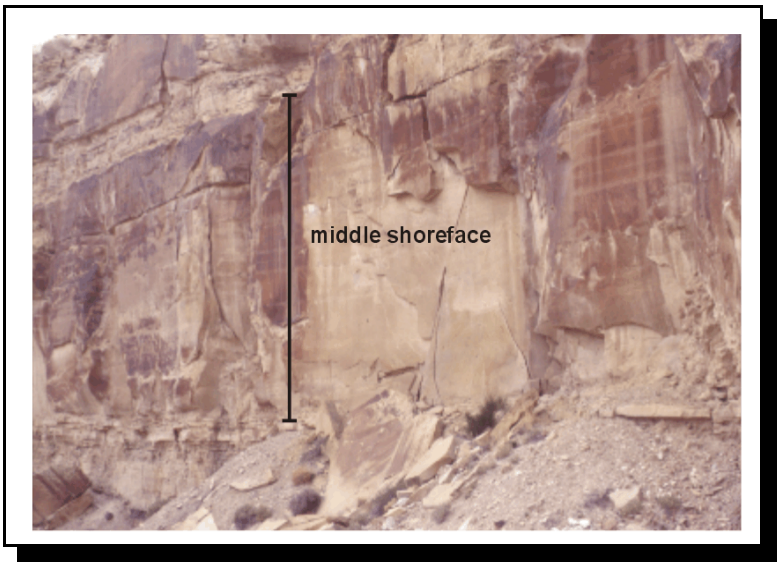


Figure 7-31. Middle shoreface facies usually form a vertical cliff and consist of very fine- to fine-grained sandstone which is horizontally bedded and often moderately burrowed to bioturbated. Note the horizontal bedding indicated by the light horizontal lineations in the photograph. Parasequence Kf-2-Iv-a near permeability transect 20 (T20), Ivie Creek case-study area.

Upper shoreface: The upper shoreface facies is characterized by fine- to medium-grained multidirectional to bimodal cross-stratified sandstone (figure 7-32), in sets that are occasionally separated by planar laminations, and generally moderate to well sorted. This facies is about 10 feet (3 m) thick (figure 7-33), but greater in the vicinities of the landward pinchouts of the parasequences, where the upper shoreface may reach 20 feet (6.1 m) in thickness. The facies is slightly to moderately burrowed, with *Ophiomorpha* as the most common trace fossil. This facies is one of the most permeable in the Ferron.

Foreshore: The foreshore facies consists of fine- to medium-grained sandstone with planar to inclined bedding, slightly to intensely burrowed, and sometimes rooted (figure 7-32). This facies is not always present at the top of the shoreface sequence but when present ranges up to a few feet in thickness (figure 7-33).

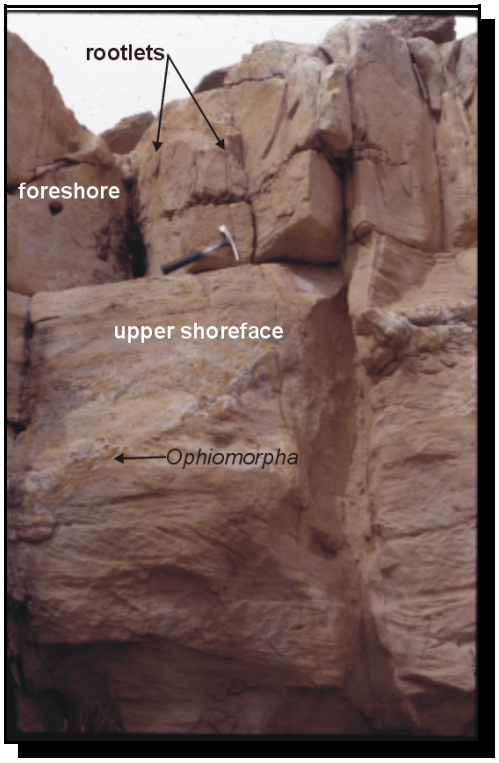


Figure 7-32. Upper shoreface and foreshore facies exposed near permeability transect 17 (T17) in Ivie Creek Canyon. The hammer marks the boundary between the two facies. Note the cross-beds in the base of the upper shoreface, typical of this facies. *Ophiamorpha* is common in both facies. The foreshore bedding is horizontal to sometimes slightly inclined. Note the vertical rootlets penetrating the facies and originating from the overlying A coal.

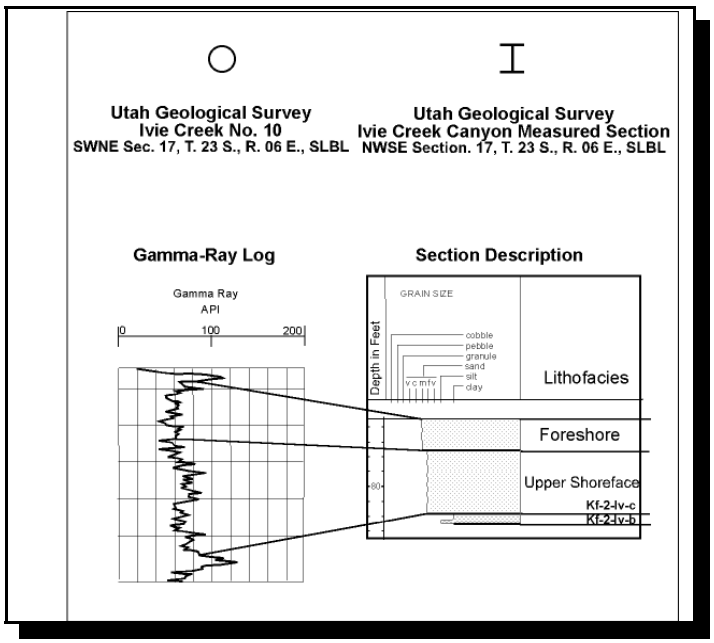


Figure 7-33. Example of the Ferron Sandstone reservoir gamma-ray type log and core description for the upper shoreface and foreshore facies.

Paleogeography and Depositional Processes

Kf-1-Iv[a] Bedset

The Kf-1-Iv[a] bedset in the Ivie Creek case-study area records an episode of delta-lobe progradation into a deeper water, fully marine bay. However, the main delta was probably located to the east and northeast (Anderson and others, 1997; Chidsey, 1997). That delta allowed a protected embayment to develop in the northwest part of the case-study area. The direction of delta-lobe progradation into the protected bay, west-northwest, is somewhat unique for the Ferron Sandstone. The direction of progradation is well constrained by control from outcrops in the Ivie Creek case-study area (see figure 7-3). Inclination of these outcropping clinoforms is away form a point located in space at about the intersection of I-70 and the trend of Quitchupah Canyon. The clinoform outcrops together form an arcuate feature (convex surface to the northwest), which is interpreted as a fluvial-delta complex.

Figure 7-34 A-E is a series of paleogeographic maps of the Ivie Creek case-study area at about the time the delta lobe prograded into the Ivie Creek amphitheater. The distributary complexes/delta front, shallow marine, and deep marine environments produced the clinoform proximal, medial, and distal facies respectively. Based on the geometry of the clinoform deposits, the source for the delta lobe is believed to be from the southeast. Outcrops to the southeast of the case-study area, on the north side of Mesa Butte, contain numerous distributary-channel deposits at the top of the Kf-1. The Kf-1-Iv[a] bedset changes from 60-foot- (18-m-) thick sand-dominated delta deposits to less than 10 feet (3 m) of shale and siltstone as it is traced from the mouth of Quitchupah Creek to the entrance into the narrow canyon of Ivie Creek, near the west line of section 16 (figure 7-3).

Figure 7-35 contains a series of cartoons illustrating an interpretation of the depositional history of a portion of the lower subcycle of Kf-1-Iv[a] at the Ivie Creek amphitheater area. These diagrammatic cross sections step through time. Figure 7-36 is a companion to figure 7-35 and shows the map view of each time step. Time Step 1 begins during active progradation of delta deposits and after the establishment of a major delta-front deposit prograding into the area. At the base of this illustration on figure 7-35 is a line which represents more typical inclinations of delta-front deposits in the Ferron Sandstone. Note the steeper angle on the delta profile of Kf-1-Iv[a]. Minor erosion of the uppermost portion of the delta-front (clinoform proximal facies) is portrayed in Time Step 2. Time Steps 3 to 6 illustrate the addition of several clinoforms with some minor erosion. At the scale of the illustrations in figure 7-35, the bounding layers were not specifically depicted, but are deposited with each clinoform.

At Time Step 7, a significant change in deposition occurs. Either a relative rise of sea level at this location (most likely caused by minor tectonics or compaction and subsidence of the delta lobe), or a change in the wave-energy regime of the bay resulted in reworking of the previous upper portion of the delta and deposition of the cap facies during Time Step 8. It is likely that this change, marked by the clinoform cap facies, was related to a change in the volume, or point of discharge, of sediments as well. The recognition of an overall fining of the Kf-1-Iv[a] bedset at this stratigraphic level points to some change in the depositional regime. This event marks the base of the next subcycle.

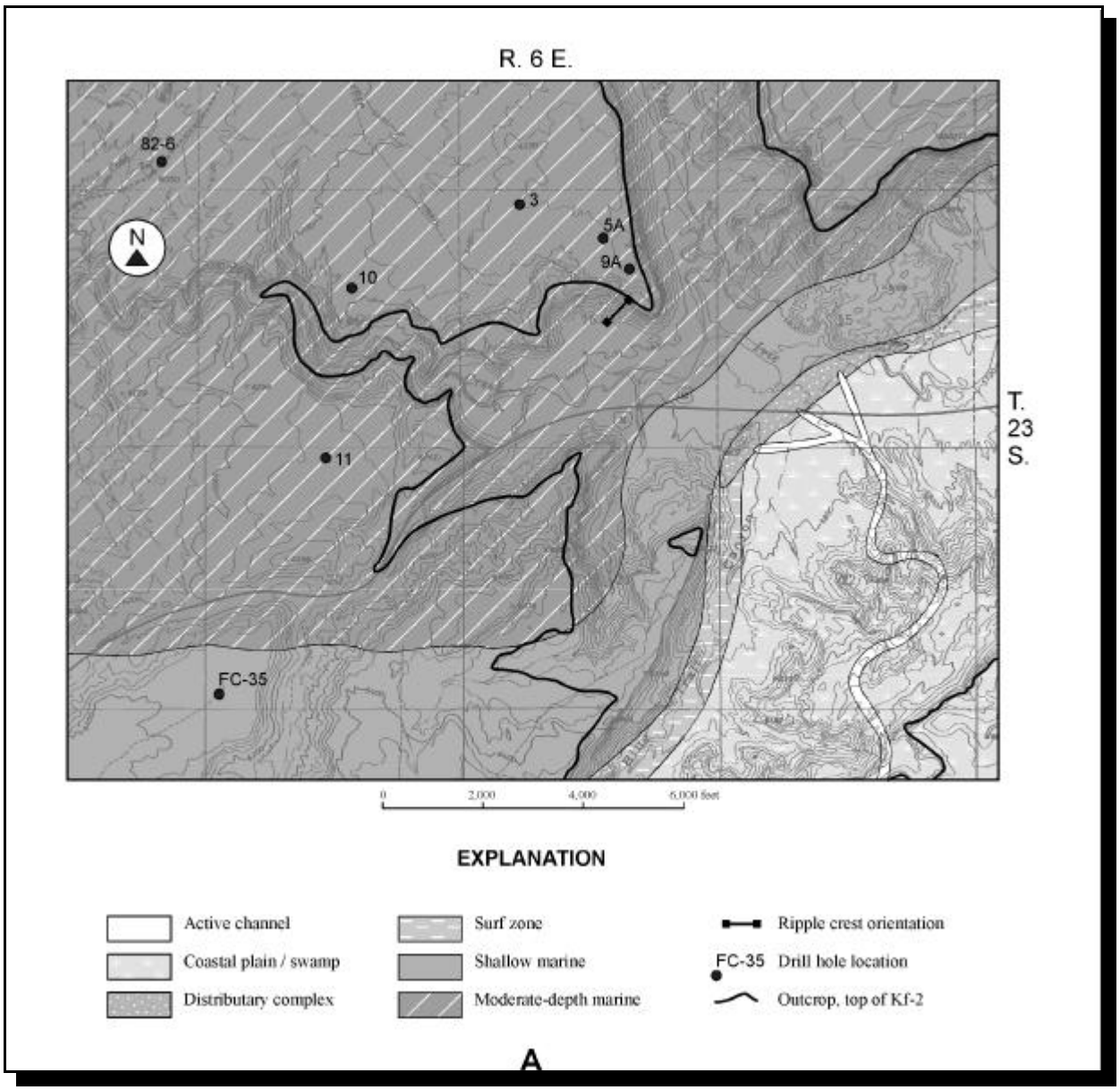


Figure 7-34A. Paleogeographic interpretation of the first of five time steps of the Kf-1-Iv[a] bedset. River channels flowing from the south and southeast deposited sands into a protected embayment in the northwest part of the area.

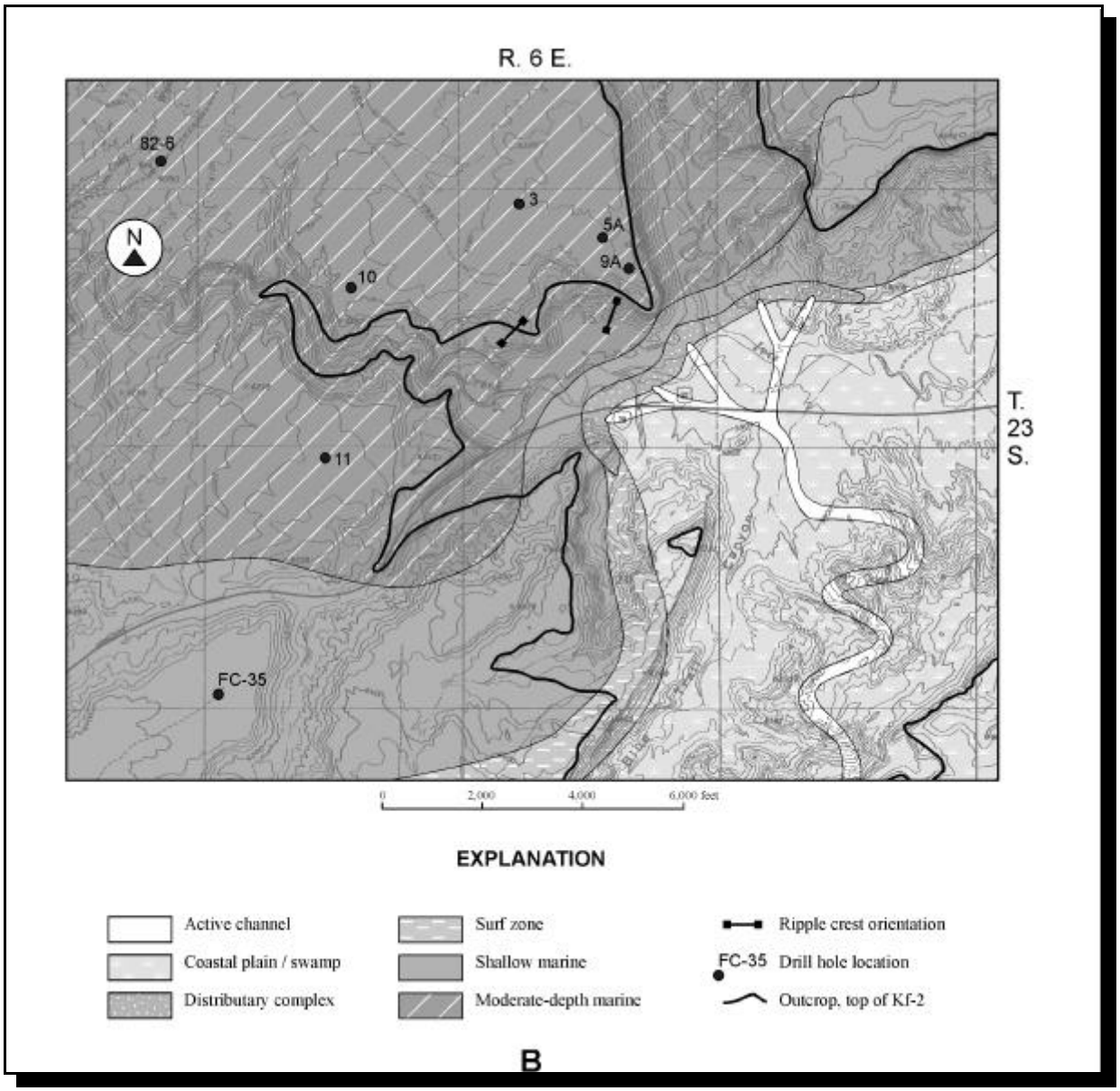


Figure 7-34B. Paleogeographic interpretation of the second of five time steps of the Kf-1-Iv[a] bedset.

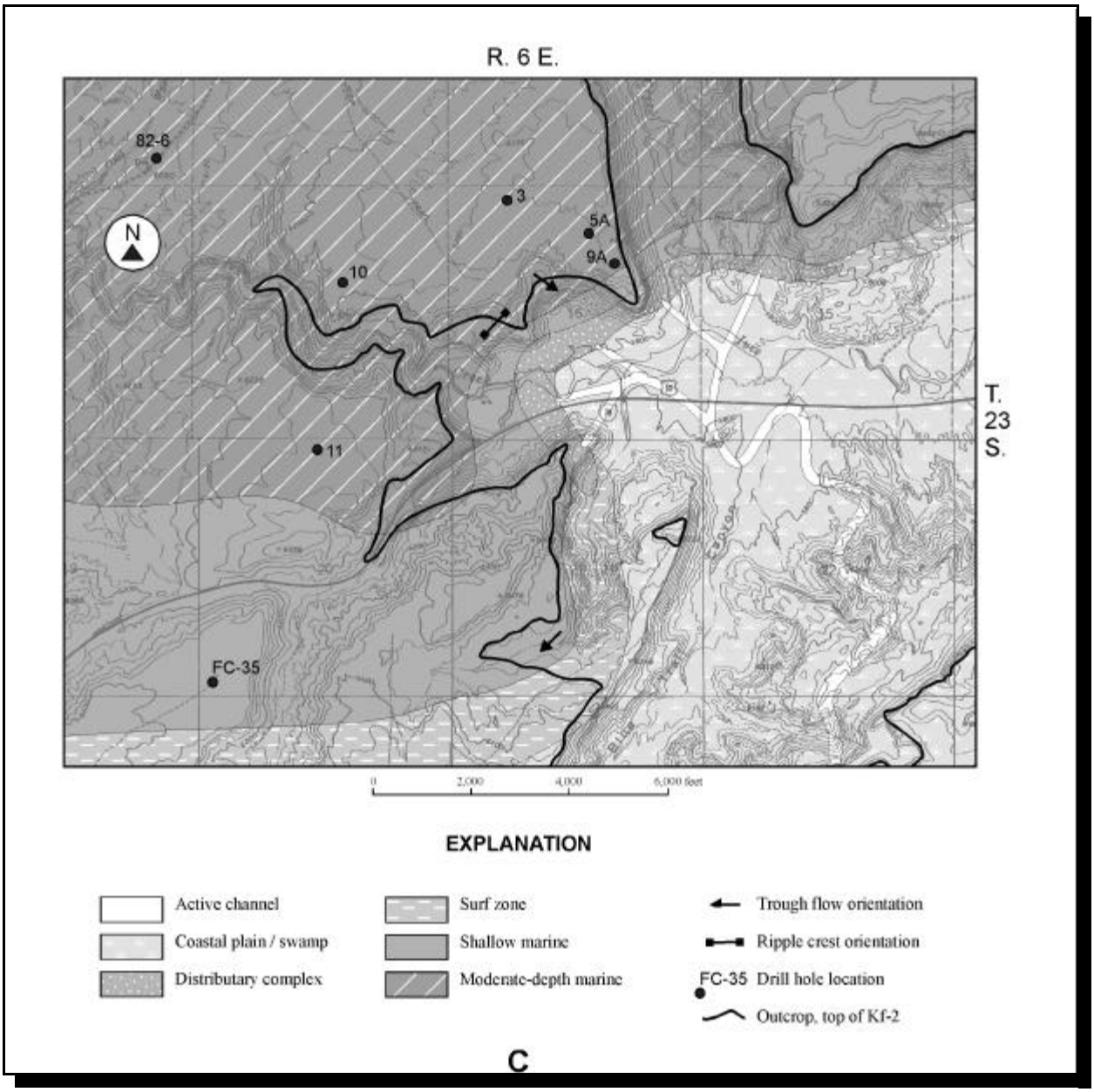


Figure 7-34C. Paleogeographic interpretation of the third of five time steps of the Kf-1-Iv[a] bedset.

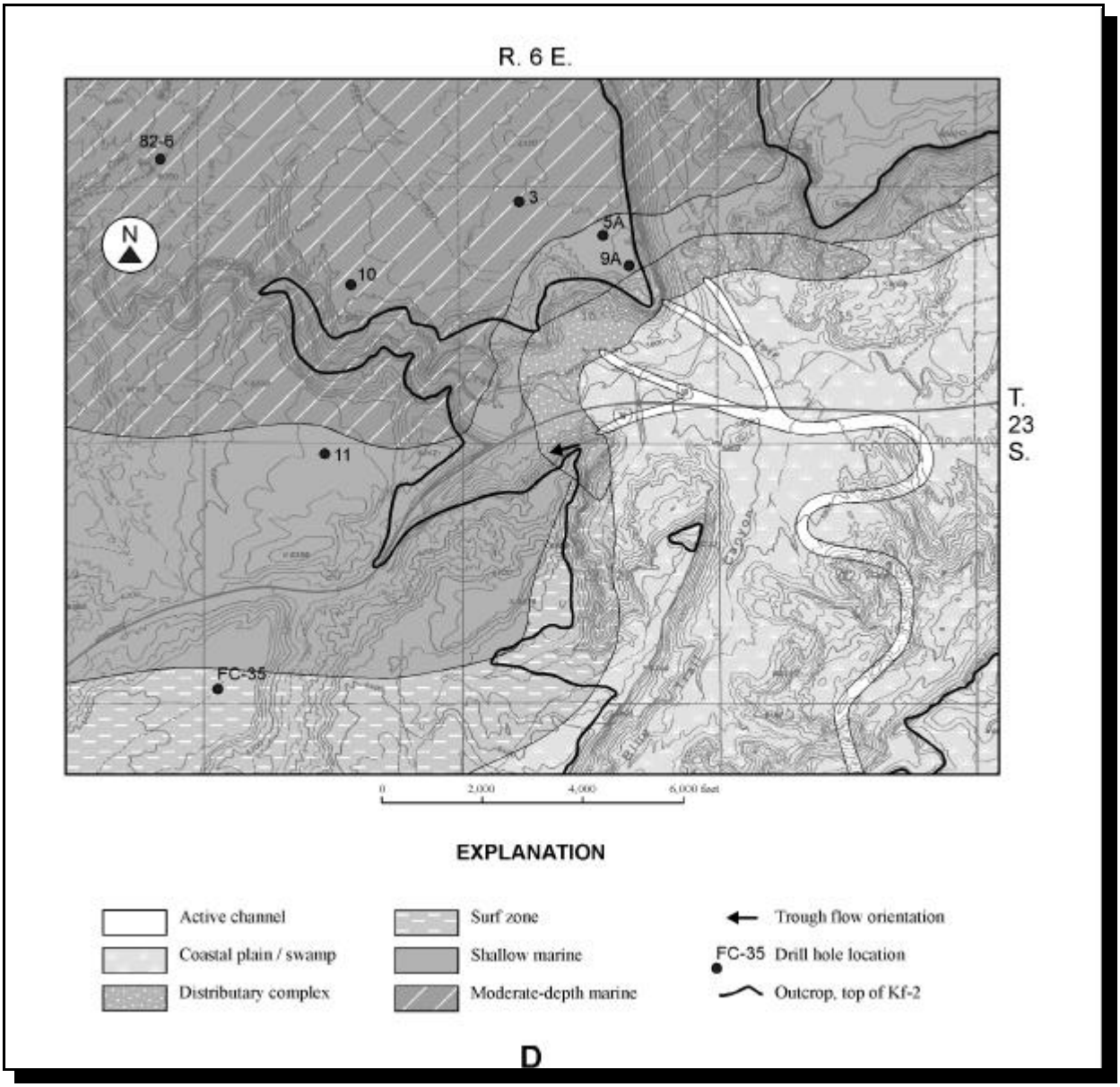


Figure 7-34D. Paleogeographic interpretation of the fourth of five time steps of the Kf-1-Iv[a] bedset.

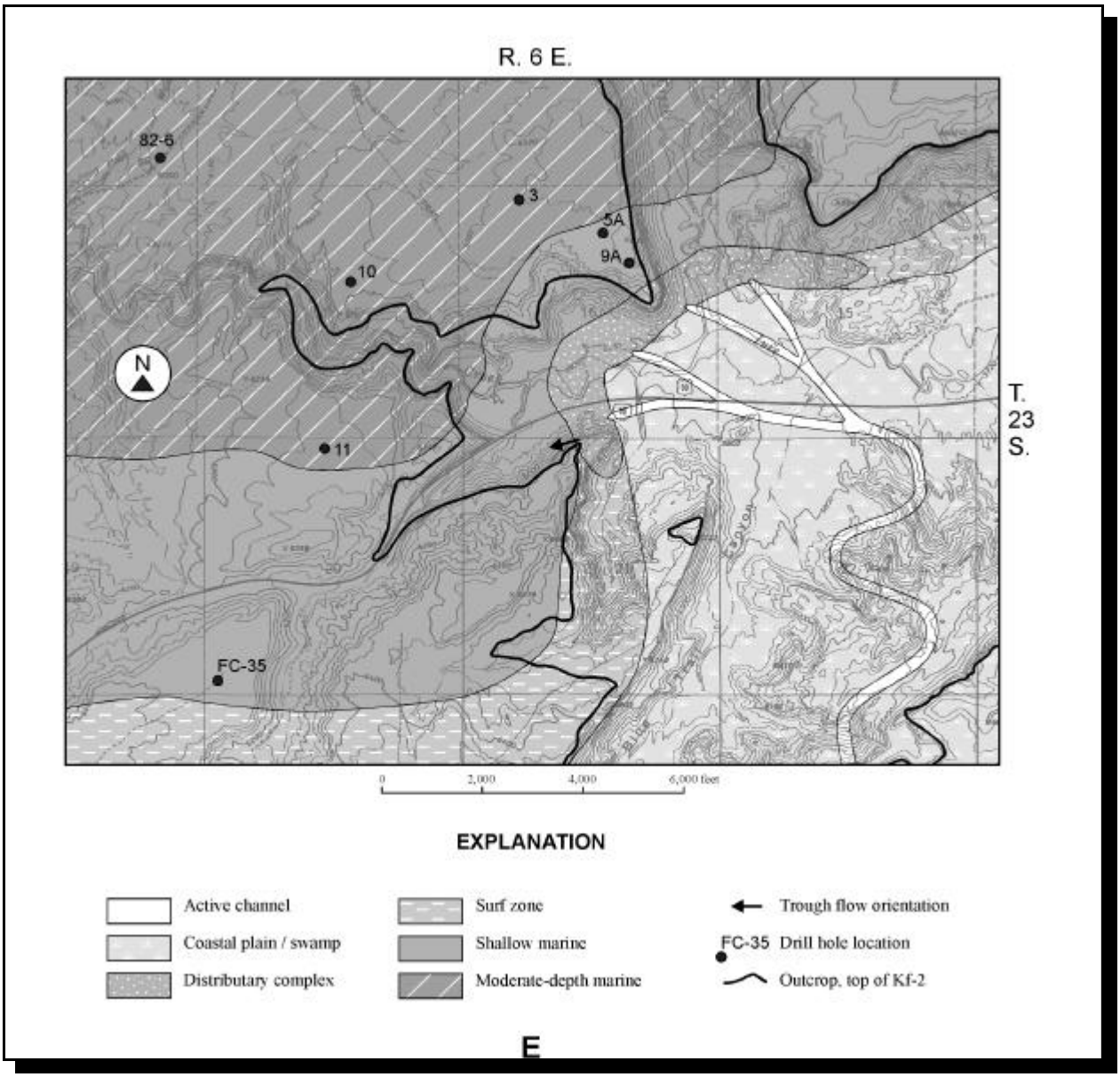


Figure 7-34E. Paleogeographic interpretation of the fifth of five time steps of the Kf-1-Iv[a] bedset.

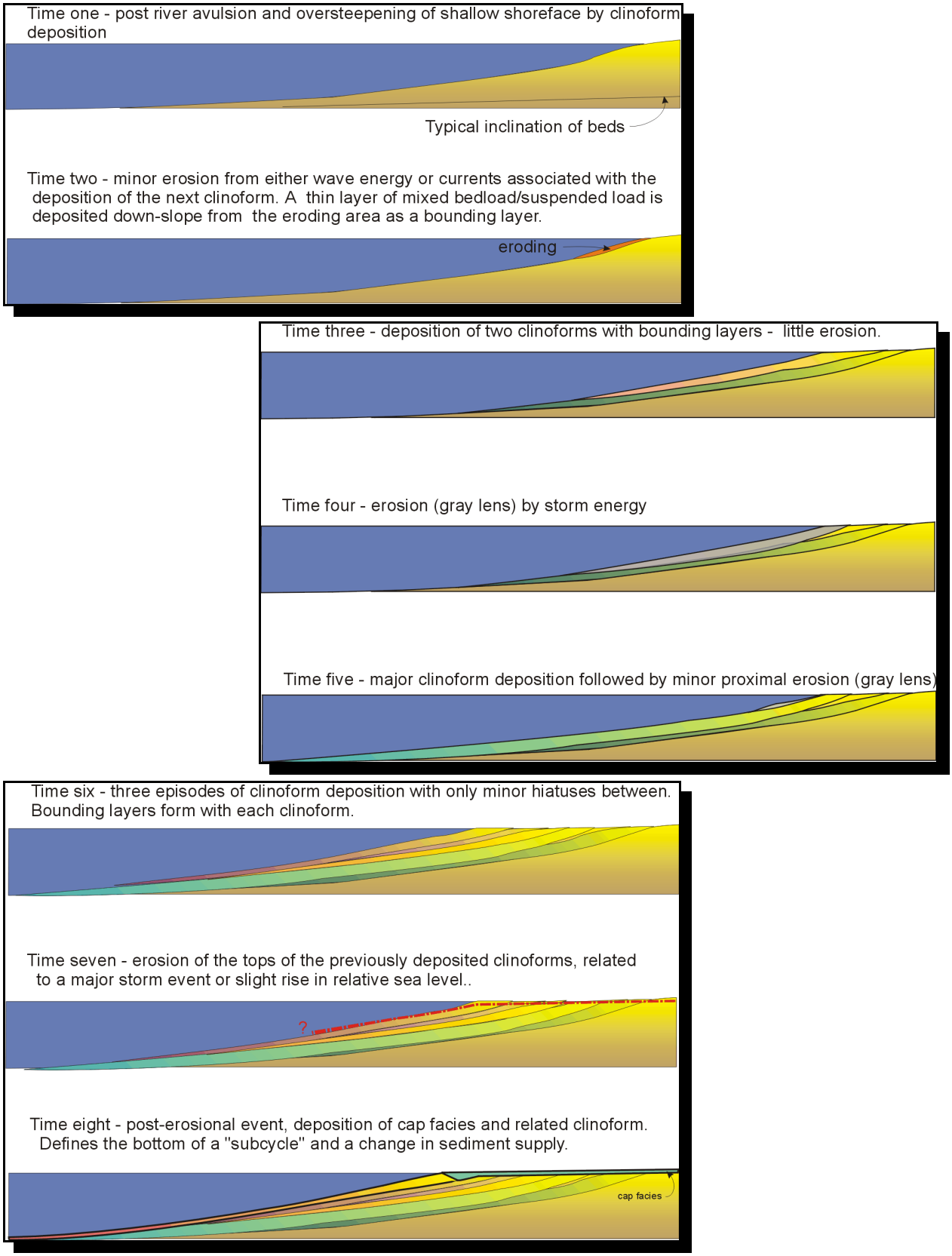


Figure 7-35. Diagrammatic cross sectional view of clinoform depositional time steps in the Ivie Creek case-study area.

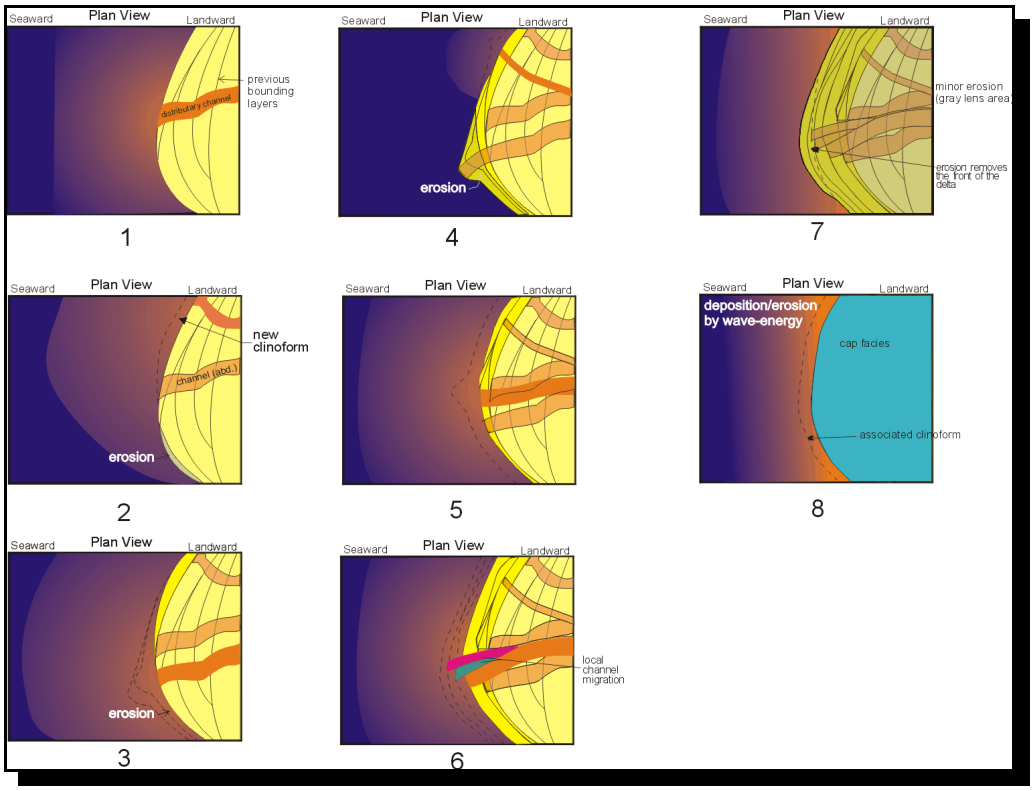


Figure 7-36. Plan view of eight time steps during deposition of the lower subcycle of the Kf-1-Iv[a] bedset. These views emphasize the switching of a distributary channel. Changes in the of amount wave energy or sediment reaching the shore also influenced clinoform cyclicity.

Distributary channel switching is the most probable mechanism for clinoform cyclicity in figure 7-36; however, no distributary channel deposits have been located juxtaposed to the clinoforms. This association shown on figures 7-35 and 7-36 is conjectural. Either these channels were located just landward of the clinoforms found on outcrop and have been removed by erosion, or they were present within the clinoforms but were located in areas presently eroded away. Either way, wave energy within the bay must have played an important role in distributing the sediment along the delta front. Low-angle cross-stratification common in the clinoform proximal facies typically shows inclinations of cross-laminae in an up depositional dip direction, an unlikely direction for fluvial-generated bed forms. Some of these structures have characteristics similar to hummocky bedding, indicating the influence of oscillating wave energy during deposition.

Kf-1-Iv[c] Bedset

In the amphitheater area, this unit is separated from the underlying Kf-1-Iv[a] bedset by a distinctive break in slope (see PM-IC41). Interbedded shale and siltstone are responsible for the slope change. Several channel sandstone deposits are present in the area, and one occurs very near the contact with the unit below (see PM-IC38). These were small distributary channels feeding the prograding shoreline of Kf-1-Iv[c] seaward of the amphitheater. The typical fluvial-deltaic deposits

outcrop to the northeast of the amphitheater on the west side of Quitchupah Canyon (see PM-IC42 and 43). Here, the deposits can be traced northward into distal deltaic facies.

Across Quitchupah Canyon the tie to the section in the amphitheater is more difficult. Directly across from "Junction Point" the unit has been identified (see PM-IC62), but poor outcrops toward "Cowboy Point" and north into Quitchupah Canyon made mapping difficult, and the unit is not defined on mosaics in these areas. Fluvial-deltaic marine rocks which lie below the Kf-1-CC parasequence in upper Quitchupah Canyon may be the Kf-1-Iv[c] bedset. These rocks exhibit steep inclinations (see PM-IC56 and 58) similar to those seen at Junction Point in the Kf-1-Iv[a] bedset.

Channel deposits at the base of the Ferron, and probably in the Kf-1-Iv[c] bedset, or slightly younger, indicate that the water depth during the first regressive deposition was on the order of 15 to 20 feet (5-6 m) deep in this area of Quitchupah Canyon (figure 7-37). The paleogeography of these earliest progradational deposits was a series of small deltas prograding into shallow seas. The geometry and architecture are often characterized by steeper inclinations in the delta-front. The combination of shallow water, rapid deposition, and relatively low wave energy created a unique environment which preserved steeper clinoforms in the delta-front deposits of the first regression into the Tununk sea.

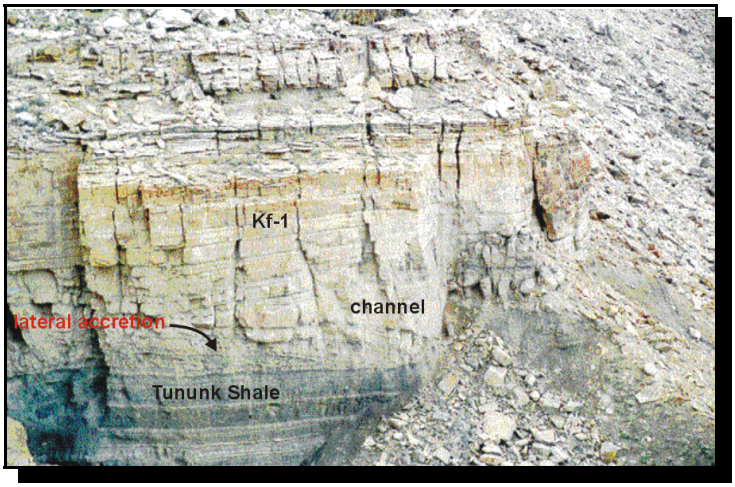


Figure 7-37. Ferron-Tununk contact in upper Quitchupah Canyon. The first regressive unit is the Kf-1-Iv[a] bedset. Note the inclined heterolithics which are stratigraphically equivalent to the channel-shaped sandstone body to the right. This is an indication of the shallow water depths which existed during the earliest deltaic deposition of the Ferron in the Quitchupah Canyon area. This is very near the seaward pinchout of the Kf-1 parasequence set.

Kf-2-Iv-a Parasequence

The shoreline orientation of the Kf-2-Iv-a parasequence rotated to the west to become primarily north-south (figure 7-38). This unit downlaps onto the parasequence set boundary in the Ivie Creek case-study area (see PM-IC40). A similar stratigraphic relationship to the underlying unit is exposed south of I-70 (see PM-IC9), and just south of "Hoodoo Point" (see PM-RC29). Perhaps the downlapping of this unit is related to growth of a peripheral bulge at this location in the foreland basin. The westernmost exposure of Kf-2-Iv-a is in Ivie Creek Canyon where the facies is distributary-mouth bar. This indicates that the shoreline was probably not to far to the west. Drill hole Ivie Creek no. 11 contained distributary-mouth bar facies in the unit, but interpretation of drill holes farther west indicate the shoreline has been crossed and only non-marine deposits exist there.

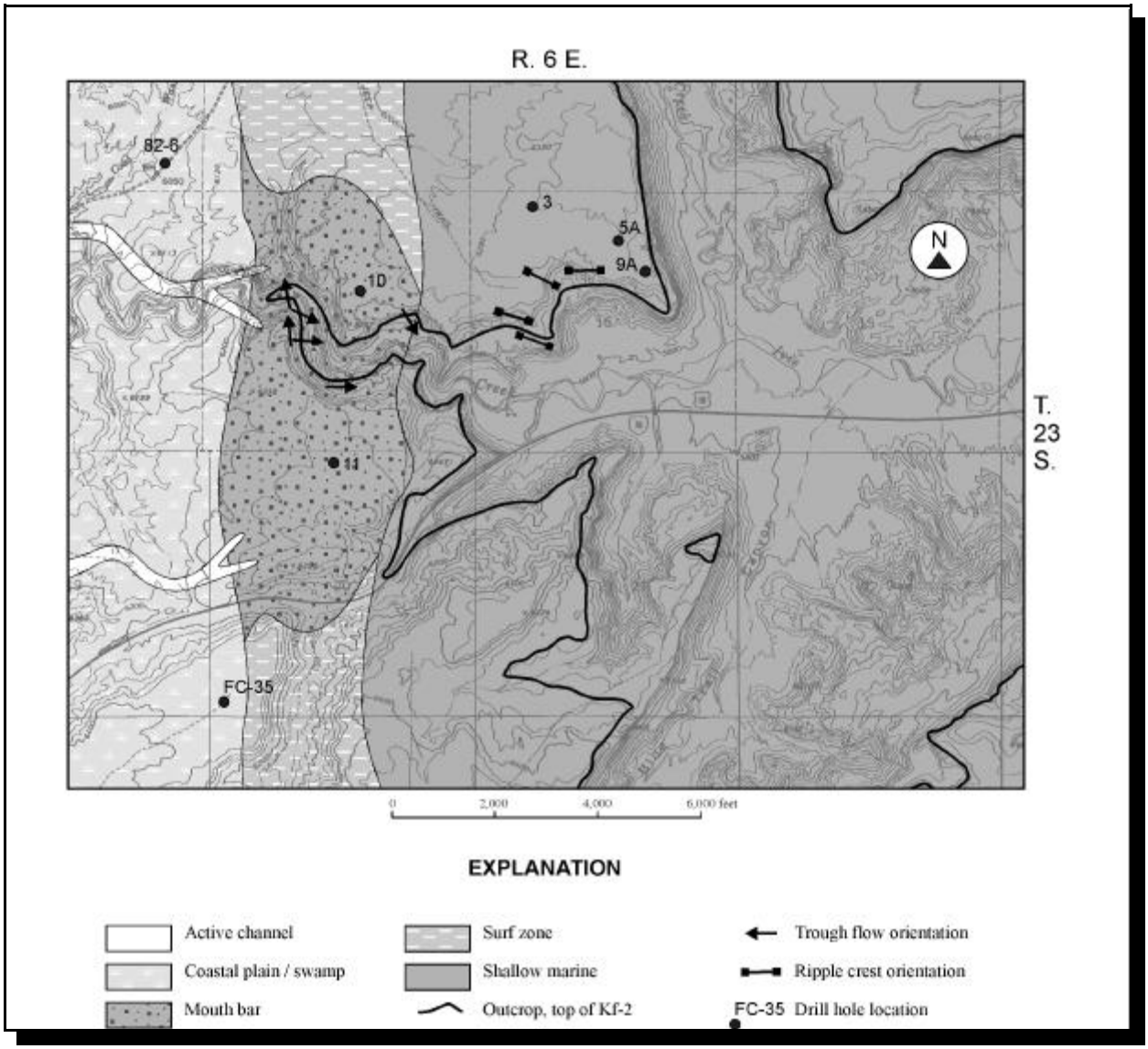


Figure 7-38. Paleogeographic interpretation of the Kf-2-Iv-a parasequence.

Kf-2-Iv-b Parasequence

Like the preceding unit, the shoreline orientation during deposition of the Kf-2-Iv-b parasequence was generally north-south. In the landward exposures at Ivie Creek Canyon, the unit is dominated by distributary-mouth bar and distributary channels (see PM-IC32) associated with wave-modified delta deposits (figure 7-39). Farther seaward, the distributary-mouth bar deposits give way to middle shoreface deposits. Seaward (east) of the Ivie Creek area, a well-developed lower shoreface is present at the base of the unit. Several subcycles of upward coarsening, middle shoreface or distal, mouth-bar deposits can be identified in the eastern Ivie Creek case-study area (see PM-IC41 and IC10), probably related to the proximity of the sediment distribution point and wave energy through the history of progradation. Several wave-ripple crest measurements were taken in the area and have a consistent east-west orientation (figure 7-39), perhaps indicating a shoreline parallel longshore drift. Paleoflow of several of the distributary channels indicate a general northerly trend in the local area.

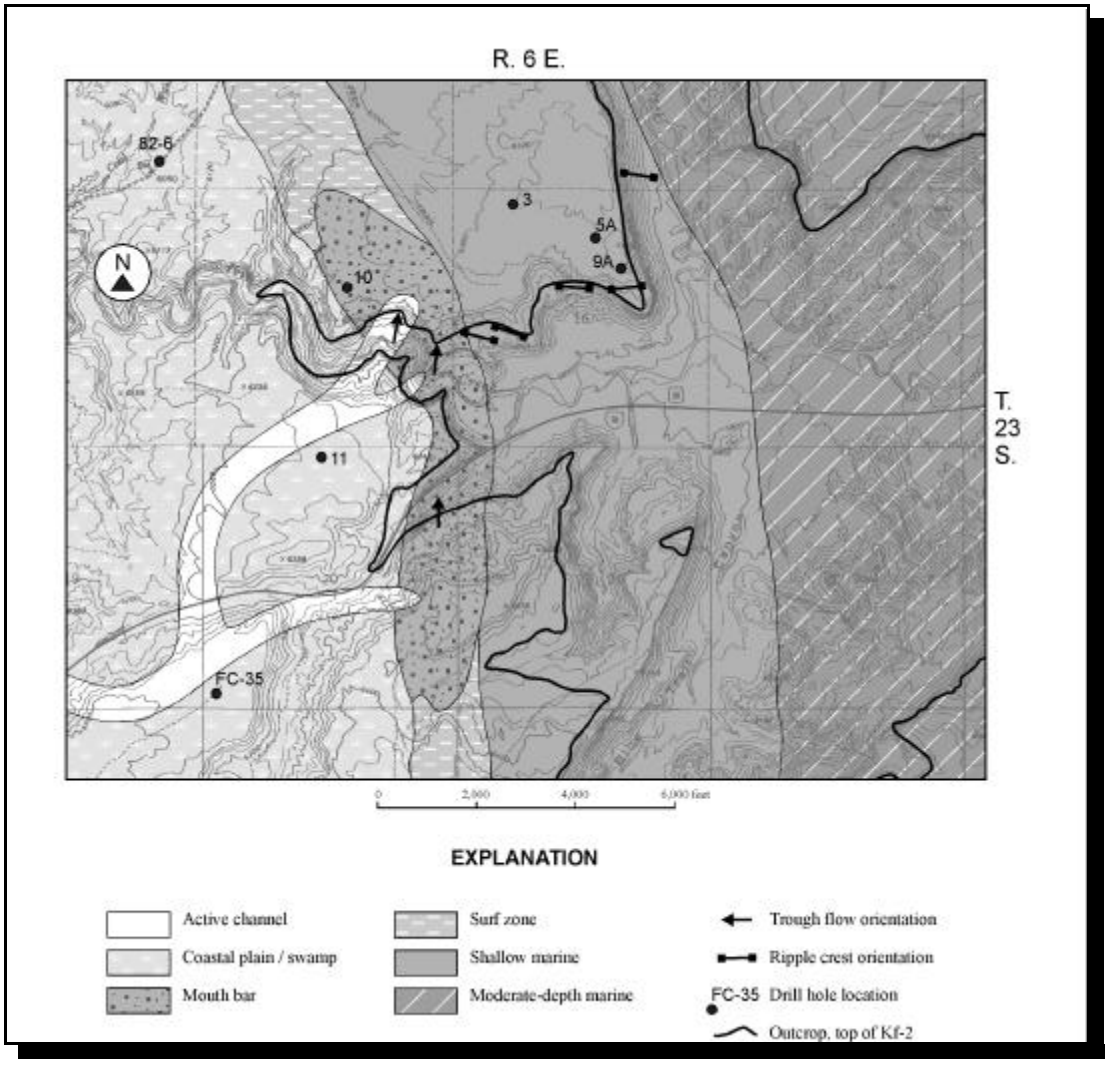


Figure 7-39. Paleogeographic interpretation of the Kf-2-Iv-b parasequence.

At the I-70 road cut, a new drainage channel was cut through solid rock to accommodate storm runoff. This cut provides superb views of Kf-2-Iv-b mouth-bar deposits. From the downstream end of the drainage channel, cross-bedded, mouth-bar deposits can be visually followed into distal bar or middle shoreface deposits to the east.

Kf-2-Iv-b has abundant soft-sediment deformation features which occur throughout the area in specific stratigraphic intervals. These features are particularly evident south of I-70, near the mouth of Scabby Canyon and in Quitchupah Canyon (figure 7-40). The proximity to the seismically active thrust belt, and the occurrence in specific stratigraphic intervals, indicates a potential cause may be disturbance by earthquakes shortly after deposition.



Figure 7-40. Soft-sediment deformation from the lower Kf-2-Iv-b on the east side of Quitchupah Creek. The "rib cage" like feature is caused by the more cohesive rippled beds which are rolled during an episode of soft-sediment deformation, probably related to seismic events in the thrust belt to the west. Similar deformation is common at this stratigraphic interval in the surrounding outcrops.

Kf-2-Iv-c Parasequence

The shoreline of this unit is well exposed in the western portion of the Ivie Creek case-study area, both at the top of the I-70 road cut (see figure 4-14, Chapter 4, Regional Stratigraphy), and in Ivie Creek Canyon (figure 7-41A). Connecting these two points creates a line bearing of just west of north. Wave-dominated delta deposits with a well-developed foreshore and upper shoreface are found east of the landward pinchout throughout the narrow portion of Ivie Creek Canyon. This wave-dominated coast prograded to a point just beyond where Ivie Creek breaks through the Coal Cliffs today. This point is indicated on figure 7-41A by the change from surf zone to shallow marine depths. It is here that the character of the rocks change dramatically within about 100 feet (33 m) horizontally (see PM-IC36, right side).

Typical shallow shoreface deposits intertongue with thin- to medium-bedded, horizontal to rippled, very fine- to fine-grained sands, which grossly coarsen up. We have interpreted these deposits as a bay-fill sequence. Some event must have shut off the main wave energy of the coast and partially restricted the flow along the coast. Figure 7-41B illustrates our vision of the paleogeography of the area. The figure places a surf zone on the east side of Quitchupah Canyon. This is supported by a well-developed shoreface on the south end of "Cowboy Mesa" at the same stratigraphic interval. The transition from bay-fill to shoreface on the east side of the bay is either poorly exposed or eroded so this part of the interpretation is somewhat tentative. Some distributary channels are present in outcrops in Ivie Creek Canyon (figure 7-41B) and on the west side of Quitchupah Canyon a bay-head delta is present in the Kf-2-Iv-c parasequence (see PM-IC43).

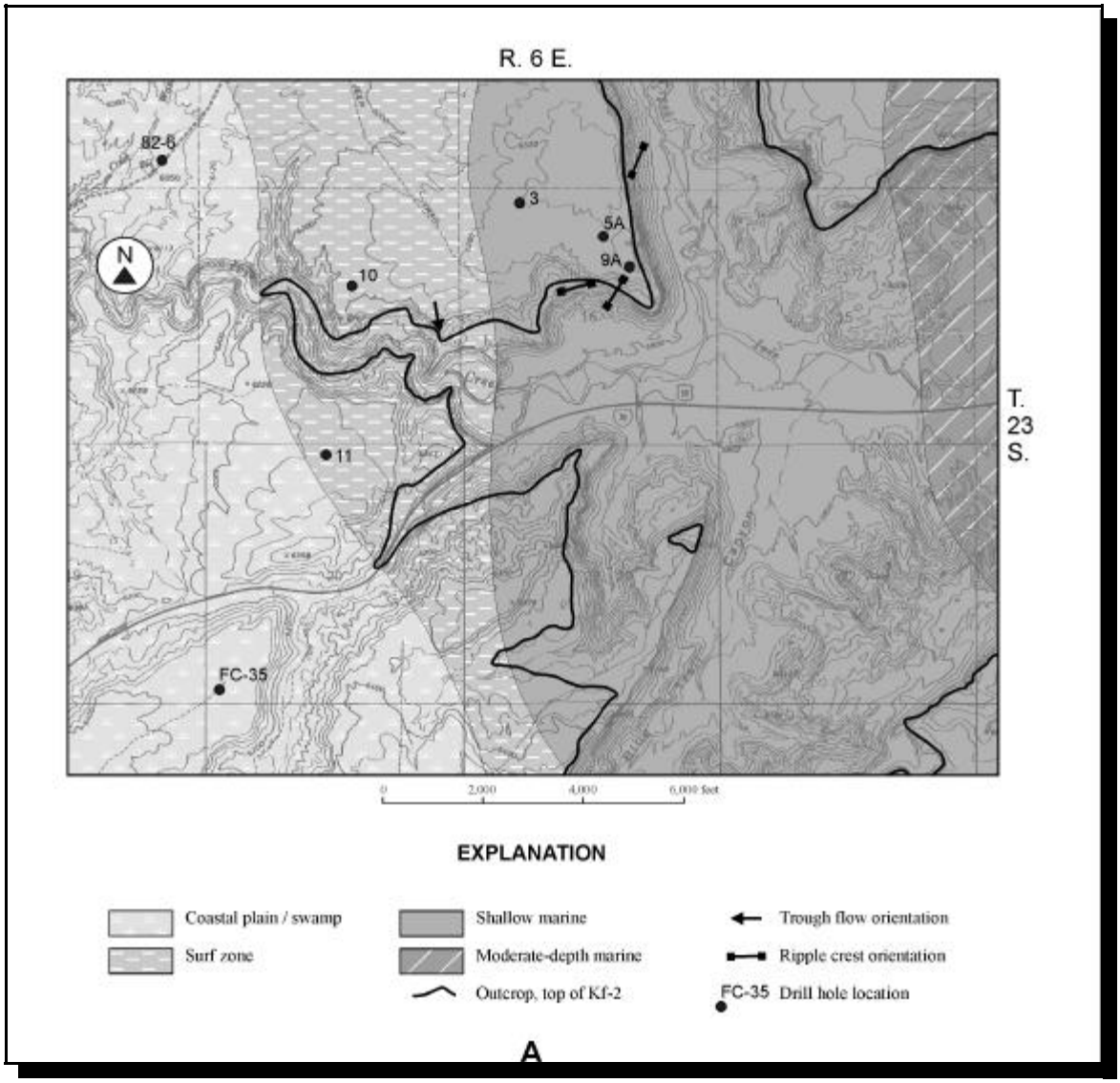


Figure 7-41A. Paleogeographic interpretation of the first of four time steps of the Kf-2-Iv-c parasequence.

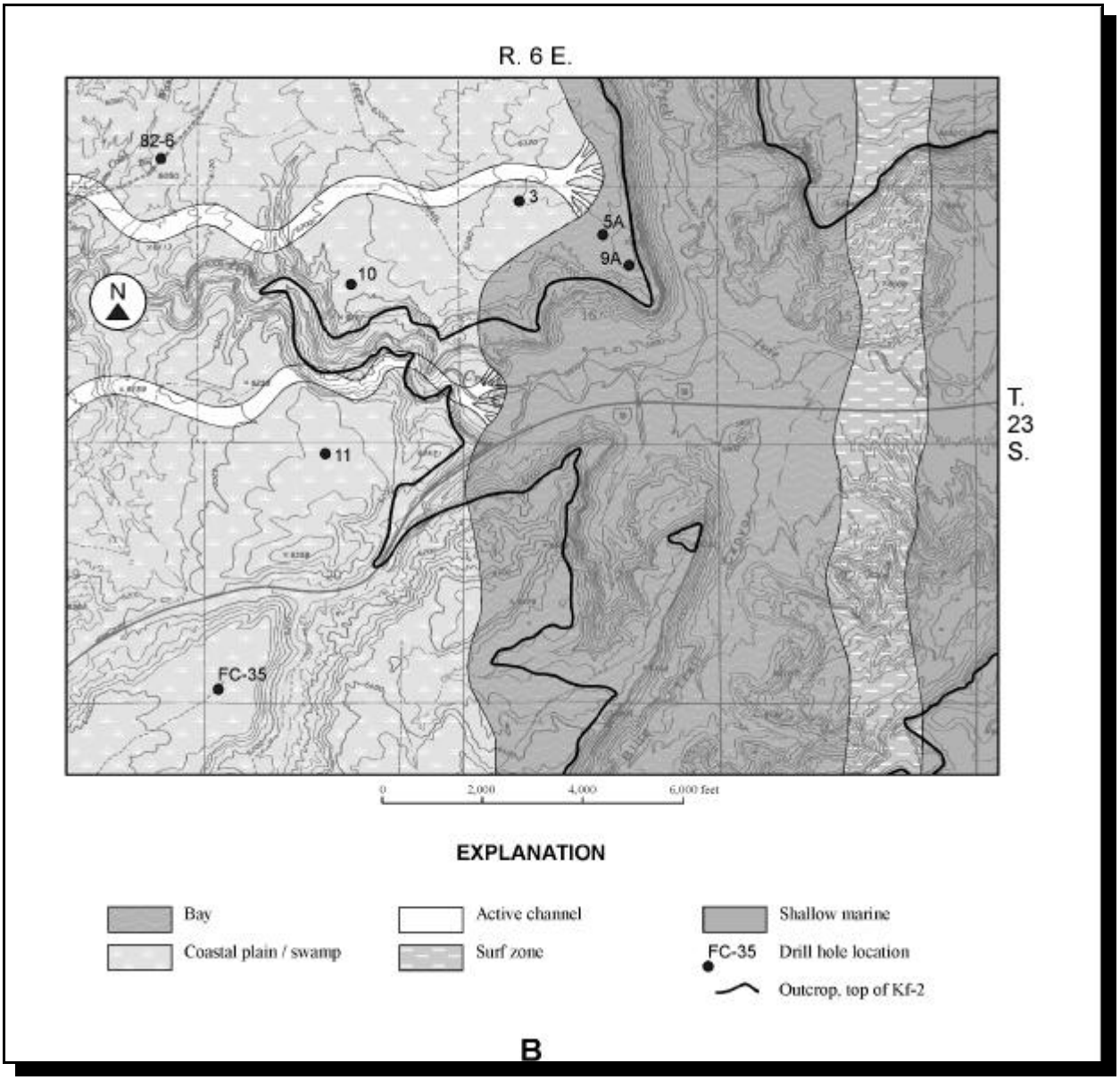


Figure 7-41B. Paleogeographic interpretation of the second of four time steps of the Kf-2-Iv-c parasequence.

A large meanderbelt channel system cut into the top of the Kf-2-Iv-c parasequence just south of the immediate Ivie Creek case-study area (figure 7-41C), in the vicinity of "Scabby Canyon." The channel system flowed to the northeast, but much of this Ferron channel system has been removed by erosion. These deposits are well exposed in the west side of "Scabby Canyon" (see PM-IC6). A late-stage episode of lateral channel migration across the top of the Kf-2-Iv-c delta-plain deposits is recorded by scours into the meanderbelt deposits (figure 7-41D). The best example of this channel system is exposed on the south side of I-70, just east of the road cut (figure 7-20; see PM-IC10 and 11). The Texas Bureau of Economic Geology has taken numerous permeability measurements from this channel (Barton, 1994; White and Barton, 1998, 1999; Knox and Barton, 1999). This same channel system is exposed in the road cut on the north side of I-70, but the channel orientation and the nature of its exposure in the cut face do not present the classic channel shape exhibited in the southern exposure. The meanderbelt and younger channel systems feed the continued progradation of Kf-2-Iv-c and stratigraphic equivalents to the east and northeast.

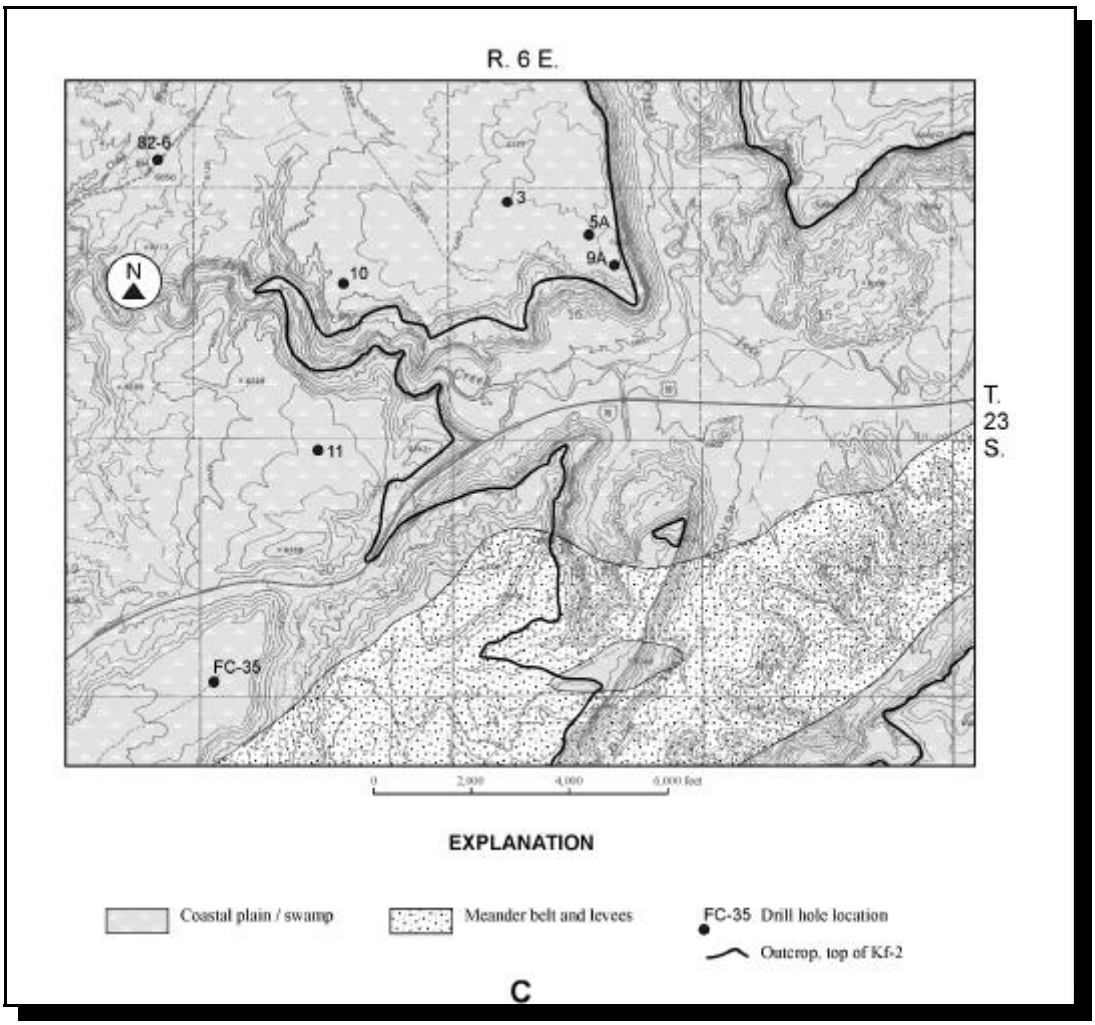


Figure 7-41C. Paleogeographic interpretation of the third of four time steps of the Kf-2-Iv-c parasequence.

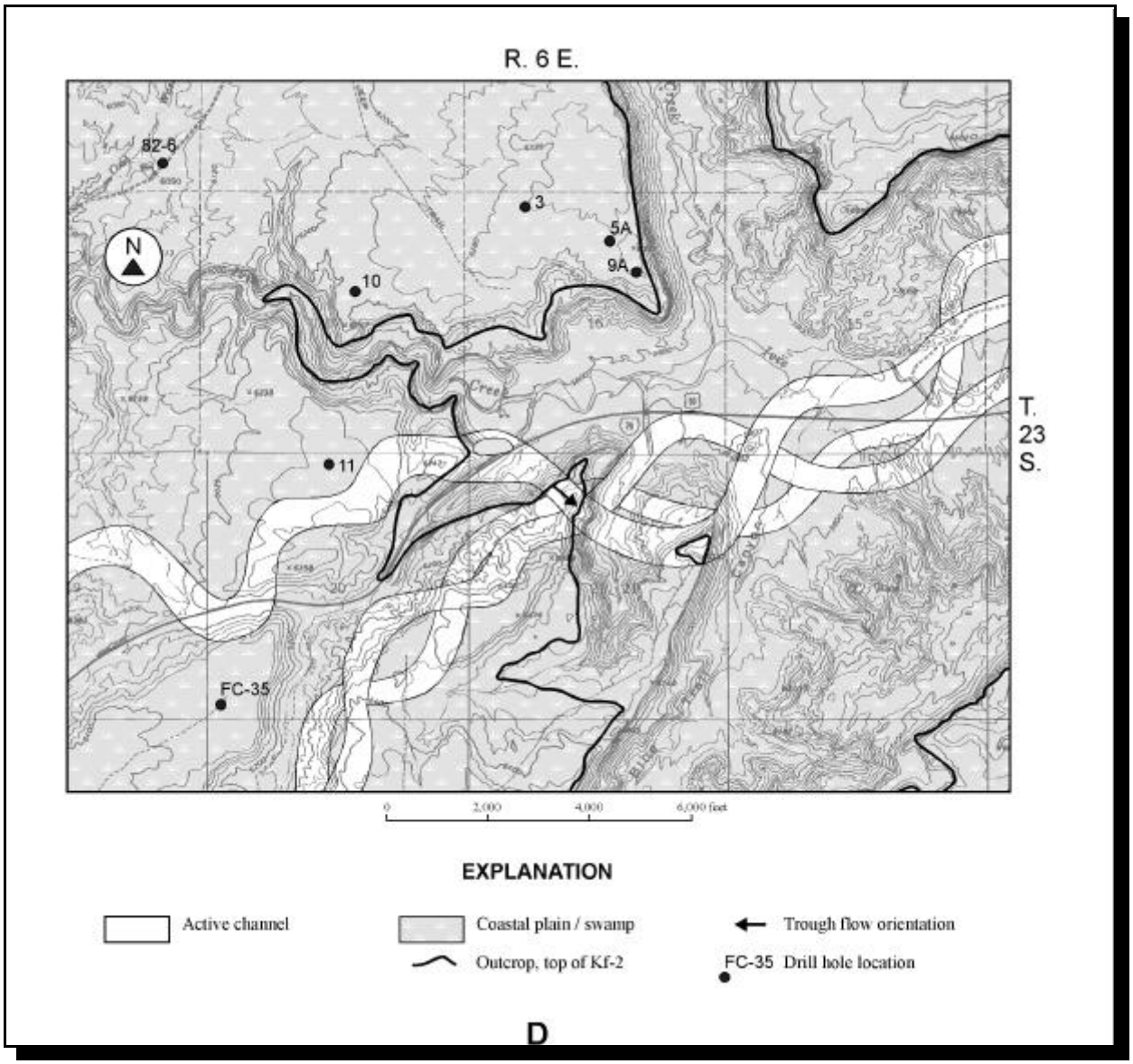


Figure 7-41D. Paleogeographic interpretation of the fourth of four time steps of the Kf-2-Iv-c parasequence.

CHAPTER VIII
PETROPHYSICAL CHARACTERISTICS OF THE IVIE CREEK CASE-STUDY AREA

R.D. Jarrard, M.A. Chan,
C.B. Forster, and S.H. Snelgrove

Introduction

A large quantity of permeability and other petrophysical data were collected and analyzed from outcrop exposures in the Ivie Creek case-study area. These data were integrated into a reservoir characterization model that can assist in subsequent reservoir-simulation work. Five drill holes near the cliff exposures provided core and geophysical logs through the sedimentary sections of primary interest. Most importantly, the data from the cores and logs provide a continuous basis for determining the detailed vertical variation in reservoir properties that cannot easily be seen on outcrop. Measurements and description of sedimentary structures, lithofacies, bounding surfaces, along with petrophysical data from core plugs, were collected along closely spaced outcrop traverses (both vertical and horizontal) and combined with drill holes data to develop a three-dimensional view of the reservoirs.

Mini-Permeameter Measurements

Outcrop permeability testing, when combined with detailed geologic mapping, improves the understanding of the lateral variability in permeability for specific bedform types. Vertical permeability transects provide a coarse profile of vertical permeability variations. These variations can be used to correlate the lateral permeability transects with the geological mapping. Additional detailed data was provided from the nearby drill holes. Twenty-two permeability transects, 18 vertical and four sub-horizontal (parallel to bedding), were made on the outcrop at the Ivie Creek case-study area (figure 8-1).

Methods

Permeability transect locations were jointly chosen by the geological and engineering teams to include the majority of the lithofacies present in the Kf-1 and Kf-2 parasequence sets. Data from these transects were used to determine the statistical structure of the spatially variable permeability field within the delta fronts, to investigate how geological processes control the spatial distribution of permeability, and to evaluate permeability measurement techniques. Measured stratigraphic sections were tied to the permeability transects (Anderson and others, in press). Empirical relationships were developed between mini-permeameter measurements made in the field and laboratory-determined permeabilities. The resulting transforms were used to estimate the relative permeability values to be used as parameters in single-phase reservoir models.

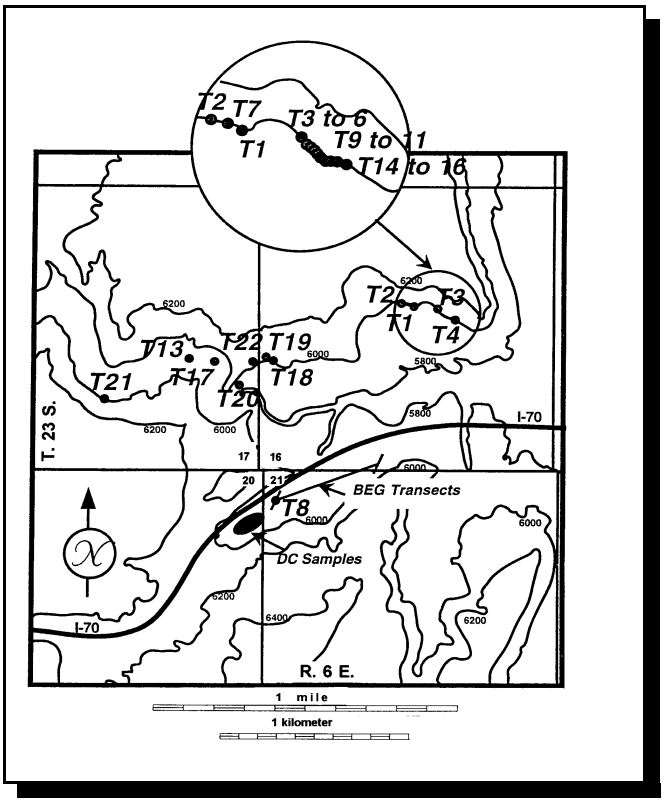


Figure 8-1. Location of 22 permeability transects (vertical and parallel to bedding) in the Ivie Creek case-study area, sections 16, 17, 20, and 21, T. 23 S., R. 6 E., Salt Lake Base Line, Emery County, Utah. BEG transects refers to the location of permeability transects conducted by the Texas Bureau of Economic Geology. The DC Samples was a series of plugs collected to study the influence of cross-bedding and soft-sediment deformation structures on anisotropy.

Measurement intervals (station spacing) on all of the vertical transects are 0.3 feet (0.1 m). Core plugs were collected at 3.0-foot (1-m) spacing along the horizontal transects. Core plugs roughly 0.75 inches (1.9 cm) in diameter and 1 to 3 inches (2.5-7.6 cm) long were drilled from the outcrop at each transect station (where possible) to ensure that permeability measurements could be made on fresh, unweathered rock surfaces. Drilling experience and examination of the core plugs indicate that chemical weathering extends into the rock less than 0.5 inches (1.3 cm). Whole plugs were typically recovered only from sandstone beds greater than 2 inches (5 cm) thick. Useful plugs could usually not be obtained from thinner sandstone beds or from thinly bedded sandstones, siltstones, and mudstones. Core-recovery ranged from 50 to nearly 100 percent. Where core plugs could not be recovered, small rock samples were taken, except where the outcrop was buried under colluvium. Each sample was washed then dried in an oven for two days in an effort to ensure that all moisture was removed from the samples prior to testing.

Permeability was measured in the laboratory on the unweathered end of the core plugs after the unweathered end was trimmed flat with a rock saw. The thin disks trimmed from the plug ends were saved for possible future petrographic analysis. At those stations where a good hole was drilled but a broken core was recovered, permeability was measured in the hole. Prior to measuring field permeability in a core hole, the back of the hole was prepared using a screwdriver and a rock hammer to chip away rough spots, providing a flat surface for the mini-permeameter probe tip. The hole was rinsed out with water and allowed to dry for at least 24 hours prior to permeability testing. The hole was also "cleaned" by a blast of compressed gas immediately before testing.

An electronic miniprobe permeameter (EMP), also referred to as the mini-permeameter, supplied by the Mobil Exploration/Producing Technical Center was used to make laboratory core holes (figure 8-2). This instrument has an accuracy of 1 to 12 percent and a precision of 1 to 3 percent on homogenous core plugs with permeabilities ranging from 1 to 4,500 millidarcies (md)

permeability measurements on the trimmed, whole core plugs and to make field measurements in (J.R. Garrison, Jr., Mobil, verbal communication, 1994). A rack was used to secure the probe in the laboratory; an expansion packer was used to secure the probe in a core hole in the field. In both cases, an air-actuated piston pushes the probe tip against the center of the sample, providing a air-tight coupling between the probe tip and the rock. A subset of 220 core plugs was tested using Mobil's Hassler cell equipment. All test results were compiled in a spreadsheet and plotted in graphical form. A total of 1,954 permeability tests were performed on 1,622 core plugs taken along the transects.



Figure 8-2. The electronic miniprobe permeameter measuring permeability in a core hole in the Ivie Creek case-study area. Photo by R.D. Adams, Utah Geological Survey.

Laboratory permeability testing was also performed on 3-inch- (7.6-cm-) wide slabbed conventional cores from drill holes using Mobil's stage-mounted, automated mini-permeameter. The distance between measurement points along the core ranged from 0.03 to 0.05 feet (0.9-1.5 cm). Core was selected for slabbing and testing after a series of reconnaissance mini-permeability tests were performed on segments of whole core. Detailed permeability data (1,939 measurements) were collected from approximately 110 feet (34 m) of slabbed core obtained from Ivie Creek Nos. 3, 5A, and 9A drill holes (see figure 7-2, Chapter 7, Geologic Framework of Ivie Creek Case-Study Area). These samples were tested for comparison to the other portions of the delta-front rocks. Overall, the results are similar to those obtained from outcrop-derived core plugs.

In performing the field and laboratory testing, we collected sufficient information to compare the results of *in-situ* testing (k-hole) to laboratory tests performed on core (k-plugs) collected from the holes tested in the field (figure 8-3). Several stations were occupied multiple times in the field in order to obtain statistics to verify the precision of the mini-permeameter. In addition, several stations from which good whole core plugs were recovered were also field tested

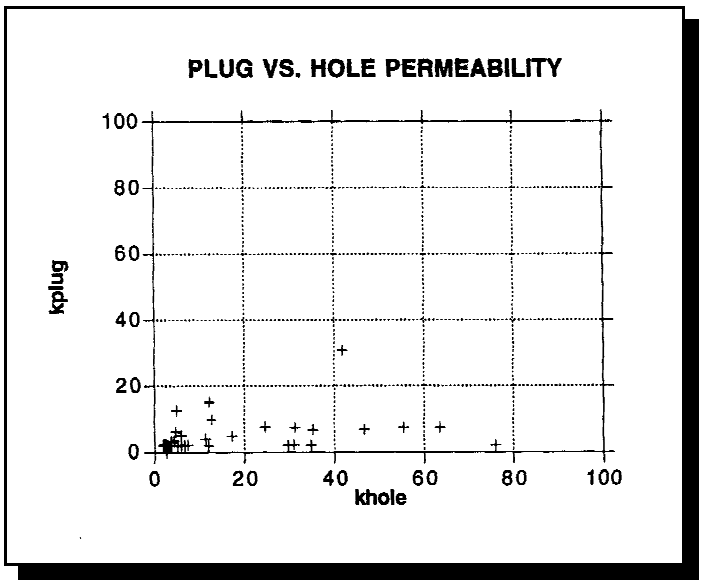


Figure 8-3. Comparison of results in millidarcies, of mini-permeameter tests on core plugs (kplug) collected from holes where *in-situ* tests (khole) were also conducted.

were tested two ways. First, the samples were tested after only brushing off the drill cuttings (unprepared). Second, each sample was washed then dried in an oven for two days in an effort to ensure that all moisture was removed from the samples prior to testing. Apparently, for the samples tested, sample preparation method has little impact on permeability test results (Chidsey and Allison, 1996).

Outcrop core-plug sampling of both the Kf-1 and Kf-2 parasequence sets shows that at least 14 percent porosity is required to obtain measurable permeabilities with the mini-permeameter. Data shown in figure 8-4 are grouped to illustrate that grain-size variations appear not to influence the relationship between permeability and porosity. Further results and data from the permeability collection in the Ivie Creek case-study area can be found in Allison (1995); Chidsey and Allison (1996); Anderson and others (in press); and Forster and others (in press).

in the core hole to provide a comparison between field and laboratory measurements of permeability. The *in-situ* tests produce generally larger permeability values. We suspect that this effect might result from differences in surface preparation; the core plugs are trimmed with a saw while testing surfaces in the *in-situ* holes are chipped to a roughly flat surface. Because *in-situ* testing requires a large field commitment (in time and field personnel) and appears to provide overestimates of rock permeability, we continued to emphasize the collection of core plugs for subsequent laboratory testing.

Due to difficulties in accessing portions of the Ivie Creek amphitheater the cliff face, 20 core plugs were collected from blocks on talus slopes that appear to have fallen from the Kf-1-Iv[a] bedset in the eastern part of the case-study area. Samples

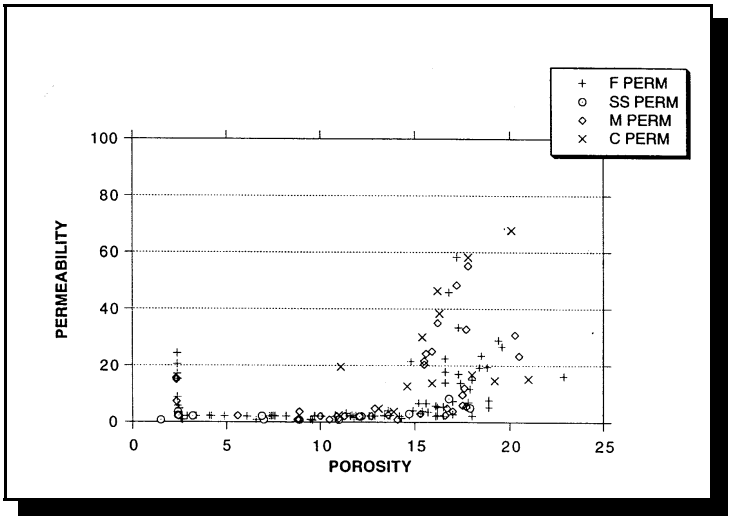


Figure 8-4. Comparison of permeability (in millidarcies) and porosity (in percent) values obtained from core plugs collected from outcrop; values grouped by grain size (F = fine grained, SS = silty/shaley, M = medium grained, and C = coarse grained).

Kf-1-Iv[a] Bedset

Permeability transects, as a group, span all clinoform facies of the Kf-1-Iv[a] bedset (figure 8-5). A large percentage of the rock tested apparently has a permeability lower than the resolution of the mini-permeameter (approximately 2 md). Overall, permeabilities in Kf-1-Iv[a] sandstones are relatively low; less than about 50 md. A clear increase in permeability exists within the clinoform beds from distal to proximal transects (T2 to T4). Although permeability values are below instrument resolution, the horizontal transects' results suggest that there is a definite permeability structure that may correspond to mappable variations in lithology and grain size.

Transect T9 had much higher permeability rocks where values for several core plugs exceeded 300 md. More than 50 percent of the cores yielded permeability values in the 10 to 40 md range. Although permeability results obtained for transects T12, T14, T15, and T16 did not generally exceed 100 md, more than 50 percent of the cores yielded permeability values in the 10 to 40 md range. These results, as expected, indicate higher-permeability regions are present in the clinoform proximal facies. Transects T10 and T11 yielded lower-permeability results that conform to the expectation that more clinoform medial facies contain relatively low permeability rocks.

Kf-2 Parasequence Set

In Kf-2 sandstones, permeabilities are locally much higher than Kf-1-Iv[a]; in excess of 80 md. North-to-south permeability measurements show little variation within the distributary-mouth bar deposits of the Kf-2-Iv-b and the upper shoreface/foreshore deposits of the Kf-2-Iv-c. This is clearly seen for example, when comparing the results of transects T8 and T20, which are separated by a distance of 0.5 mile (0.8 km) (figure 8-6). However, significant differences in permeability exist from west-to-east in the Kf-2-Iv-b and Kf-2-Iv-c as a result of transitions from distributary-mouth bar and upper shoreface/foreshore deposits to middle shoreface. Such a change can be seen by comparing the results obtained at transects T20 and T1, which are separated by a distance of 0.6 mile (1.0 km) (figure 8-7). The distance between transects T20 and T1 indicates that permeability transitions can occur at typical interwell distances.

Core plugs were also collected from several locations in the Kf-2 to examine the two-dimensional (2-D) and three-dimensional (3-D) permeability anisotropy associated with specific sedimentary structures. The DC series of plugs (figure 8-1) were collected to study the influence of cross-bedding and soft-sediment deformation structures on anisotropy. Permeability anisotropy is less than one order of magnitude and may range from 2 to 5.

Petrophysics: Overview

Subsurface geological interpretations, whether based on geophysical data or on drilling, can be guided by case studies that combine stratigraphic concepts with transforms linking geological to geophysical variables. The primary goal of the petrophysical task was to establish these transforms and their causal underpinnings. An essential aspect of this task was determining interactions between the diagenesis and petrophysics of the Ferron Sandstone. An additional objective was to examine the reliability of a common assumption: that geophysical properties and

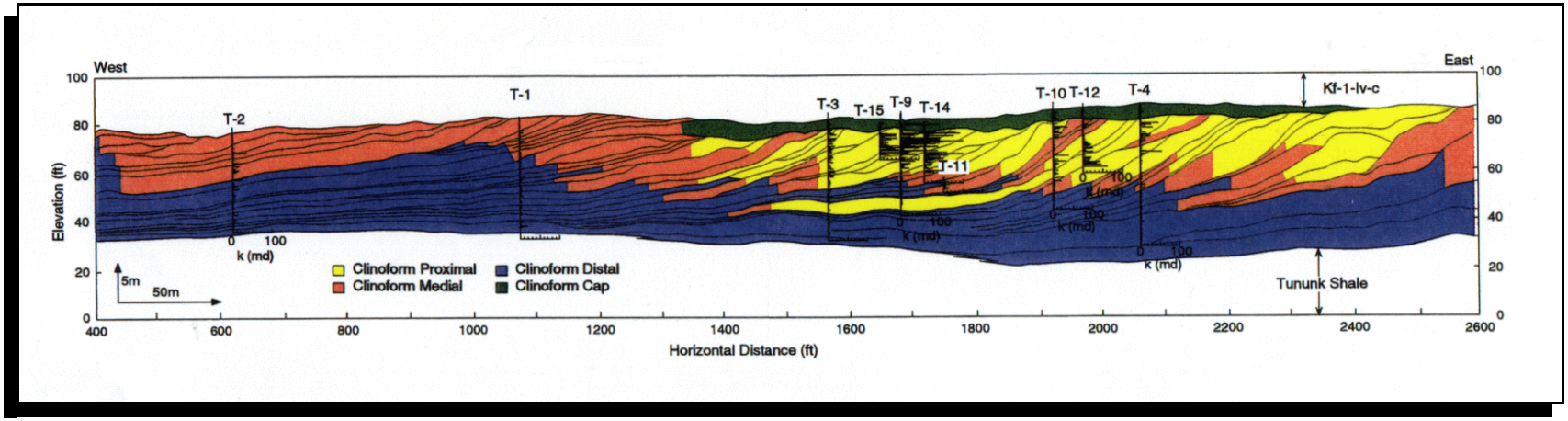


Figure 8-5. East-west permeability distribution along transects in the clinoform facies of the Kf-1-Iv[a] bedset, eastern Ivie Creek amphitheater.

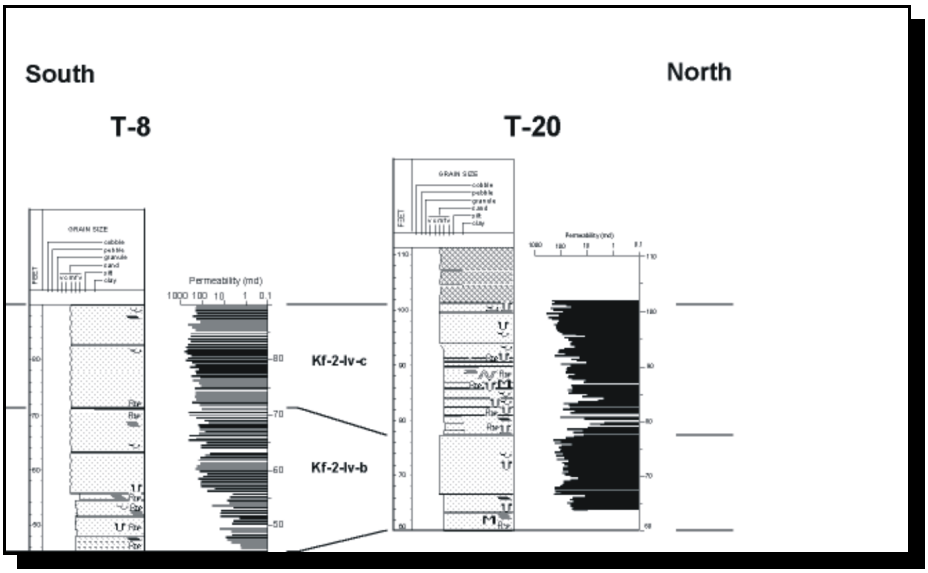


Figure 8-6. North-south permeability distribution along transects T-20 and T-8 in distributary-mouth bar and upper shoreface/foreshore deposits of the Kf-2-Iv-b and c parasequences, Ivie Creek case-study area.

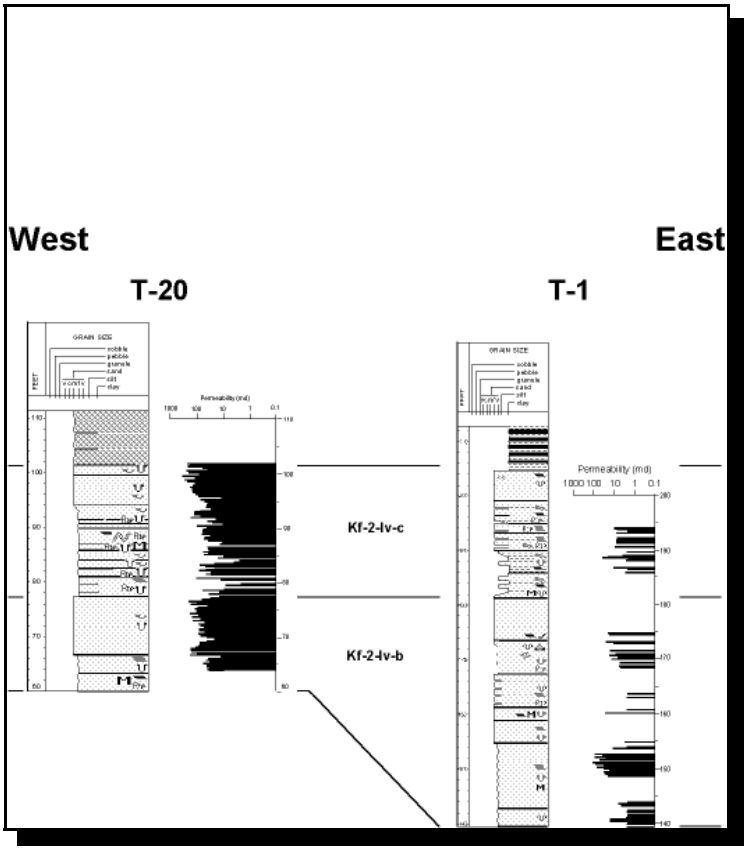


Figure 8-7. East-west permeability distribution along transect T-20 in the distributary-mouth bar and upper shoreface/foreshore deposits and along transect T-1 in the middle shoreface deposits, Kf-2-Iv-b and c parasequences, Ivie Creek case-study area.

relationships observed on outcrop are representative of those operating in the subsurface. We examined the possibility that the process that generates outcrop exposures--exhumation resulting from uplift and erosion--may overprint the original patterns of velocity, porosity, and permeability developed in the subsurface. Petrophysical overprints potentially may result either from diagenetic processes or from mechanical rebound, the rock expansion caused by pressure release. In contrast to most previous studies of diagenetic influences on petrophysical properties, the emphasis here is on dissolution rather than on cementation. Previous research on rebound has concentrated mainly on engineering and soils applications (Terzaghi, 1965), and on cores (Hamilton, 1976), rather than on *in-situ* sedimentary rocks.

Sampling and Measurements

Outcrop exposures offer the opportunity to examine lateral stratigraphic and petrophysical variations at a much higher resolution than is feasible or cost-effective with wells. Concepts and patterns based on these high-resolution studies can then be applied to actual exploration plays, where data coverage is more limited and interpolation is essential.

In two field seasons (1994 and 1995), we took a total of 722 oriented core plugs from the Ferron outcrop, using a portable rock drill with water as coolant. The core samples were 1.2 to 3.1 inches (3-8 cm) long and 1 inch (2.5 cm) in diameter. Sampling was conducted along more than a dozen near-vertical traverses (figure 8-8), some accessible on foot and others by rock-climbing gear. A vertical sample spacing of 6 to 12 feet (2-4 m) was usually chosen in order to sample all major lithologic units. We did not, however, sample shale units on outcrop, because they were too weathered.

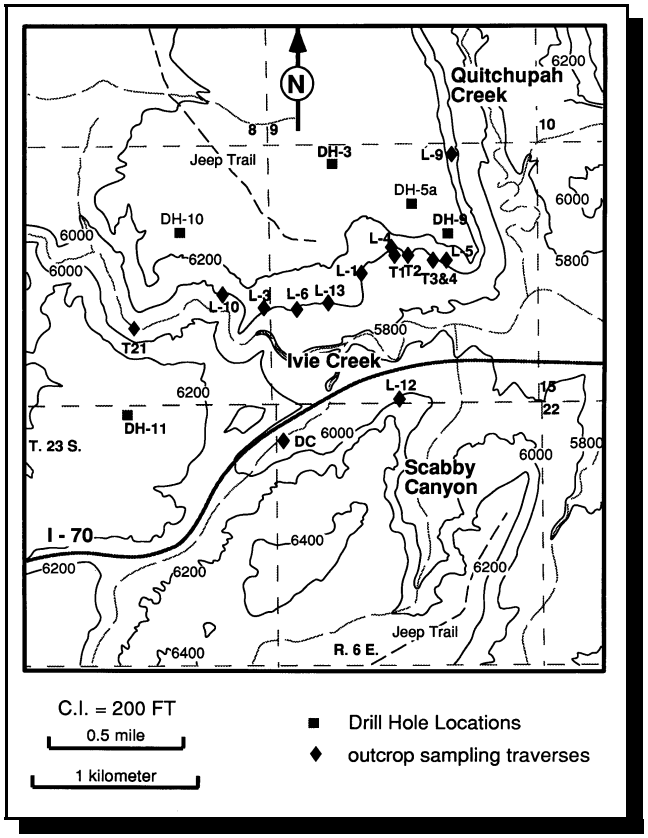


Figure 8-8. Map of the Ivie Creek case-study area showing UGS drill-hole locations and outcrop sampling traverses.

Nearly all core samples--from both outcrops and drill core--were drilled horizontally. However, at 79 sample locations, a 3-D set of three samples (horizontal, vertical, and 45E diagonal) was collected for detection of petrophysical anisotropy.

Petrophysical sampling during the third season concentrated on drill cores, particularly those from our Ivie Creek drilling program. The UGS drilled five wells on the plateau adjacent to Ivie Creek, at distances of 325 to 1,300 feet (100-400 m) from the outcrops, to delineate 3-D Ferron stratigraphy more thoroughly than is possible from outcrops alone (figure 8-8). The Kf-1 and Kf-2 sandstones were cored at four of these drill holes. We took 86 core plugs and 11 3-D sets from UGS Ivie Creek drill hole Numbers 3, 9, and 11. Shale units in these drill-hole cores

were unweathered and therefore could be sampled, unlike outcrop shales. We undertook a database search for any Ferron cores at UGS Geological Sample Library and U.S. Geological Survey (USGS) Denver Core Repository, to find samples from wells deep enough to have experienced minimal development of secondary porosity. We identified three suitable wells with cores at USGS repository and took 28 core-plug samples from the best two wells.

Of these plug samples, 471 were analyzed using the Geoscience Evaluation Module (Sondergeld and Rai, 1988, 1993a, 1993b) at Amoco Production Company. Measurements were collected in three batches so that results from earlier batches could guide sample selection for later batches. For each sample, P-wave and two S-wave velocities were measured for both dry and water-saturated states, at the following pressures: 250, 484, 750, 1,000, 1,500, 2,000, 3,000, 4,000, and 5,000 pounds per square inch (psi) (1.72, 3.34, 5.17, 6.90, 10.3, 13.8, 20.7, 27.6, and 34.5 Mpa). Porosity, matrix density, and bulk density were measured by helium porosimeter and mercury immersion. Porosity was also measured along with air permeability at a pressure of 1,000 psi (6.9 Mpa). Magnetic susceptibility was measured on a 1 kilohertz (Khz) susceptibility bridge. Infrared spectroscopy gave approximate concentrations of the following 14 mineral components: quartz, feldspars (orthoclase, oligoclase, albite, and intermediate plagioclase), carbonates (calcite, dolomite, siderite), clays (illite, kaolinite, chlorite, and smectite), pyrite, and anhydrite.

Geophysical well logs of caliper, density, and gamma ray were run in all UGS Ivie Creek five drill holes. The Kf-1 and Kf-2 units were above the water table at all drill holes, but the lower portions of Ivie Creek Numbers IC-3 and IC-11 could be saturated so that sonic logging was feasible. For cores from three drill holes, we used the USGS continuous-core system to measure velocity of whole-core samples, plus continuous-core magnetic susceptibility and gamma-gamma density.

Analysis of Ferron Well Logs

The Ferron Sandstone today exhibits an immense range of exhumation: along its northern and western extent it is still buried by 9,800 to 11,200 feet (3,000-3,400 m) of sedimentary rocks, about the same as the previous maximum burial depth of the entire Ferron Sandstone. Overburden thickness decreases rapidly to the east and south, and the Ferron Sandstone crops out over a broad region (figure 8-9). In order to extend our understanding of Ferron diagenesis and petrophysics to a much broader region than that represented by the Ivie Creek outcrops and drill holes, we analyzed Ferron well logs from the deep subsurface (figure 8-9).

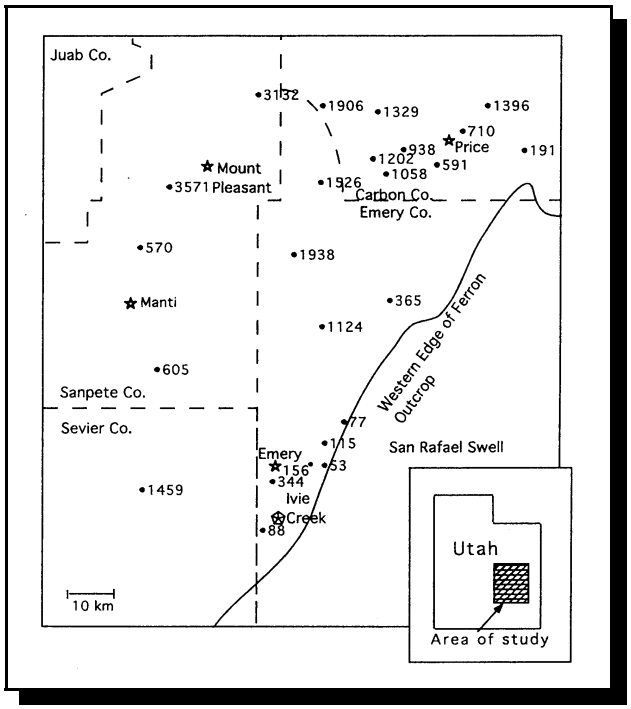


Figure 8-9. Map of east-central Utah, showing Ferron Sandstone locations considered in this study. Solid dots are wells with both sonic and density logs from the Ferron; adjacent numbers are average depth of the Ferron data, in meters. Stars are towns. Starred pentagon is the Ferron outcrop at the Ivie Creek case-study area, where core plugs were obtained.

Coal and petroleum companies have drilled more than 500 wells through the Ferron Sandstone (Hucka and others, 1995; Tripp, 1989). Most of these wells have density logs, but few have sonic logs. Only 31 wells satisfy the criterion that both sonic and density logs were run in the Ferron. Of these, we discarded six because of neutron/density crossover or other evidence (Tripp, 1989) of gas presence. These gas sandstones were avoided because gas causes density-based porosity to be overestimated and velocity to plummet. We discarded one additional well, plus portions of several other wells, because of poor or dubious log quality. Twenty-four wells survived these selection and rejection criteria: all appear to have good quality sonic and density logs of water-saturated Ferron Sandstone beds.

Wells penetrating the Ferron typically encounter 56 to 1,060 feet (17-323 m) of alternating sandstones, shaly sands, shales, and coals (Ryer and McPhillips, 1983). At each of the 24 wells, we identified sandstone or slightly shaly sandstone beds based on the gamma-ray log, then picked average sonic travel time and density for 2 to 20 beds (an average of 7.5), or relatively homogeneous portions of beds. Sonic travel time (Fseconds/foot) was converted to velocity (feet/second [or km/s]). To convert density to porosity, an estimate of grain density is needed. As described later, core-plug petrophysical data provided that estimate.

Diagenesis and Porosity of the Ferron Sandstone

Petrography

Recent petrographic work on Ferron Sandstone samples includes studies by Fisher and others (1993a) and Barton (1994). They noted compositional differences between distributary channels and delta-front deposits. The distributary channel sandstones were not as well sorted, contained more feldspar, and were classified as quartz-rich arkoses. The delta-front deposits ranged from quartz arenites for the reworked, distributary mouth-bar sandstones, to subarkoses and arkoses for the delta-front sandstones. The more reworked the sediments, the fewer feldspar and lithic fragments were present. The work of this study corroborates these previous observations and considers differences between parasequences (in Kf-1 and Kf-2), other facies, and new mini-permeameter permeability data (Mattson and Chan, 1996; Snelgrove and others, 1996; Mattson, 1997).

Thirty-eight thin sections were made from a suite of samples encompassing the dominant lithofacies in the Kf-1 and Kf-2 of Ivie Creek case-study area. Thin sections were not made of the mudstone or low-permeability facies due to difficulties in distinguishing mineralogies of fine-grained sediments in thin section.

For 18 thin sections from outcrop plugs of fluvial-dominated Kf-1-Iv[a] bedset (table 8-1), the following grain parameters were estimated: 14 framework grain compositions, two types of matrix, six types of cement, and porosity. The textural aspects of grain size, rounding, sorting, and contacts were also estimated. In subsequent samples (final tally of table 8-2), the focus was more on examination of the major categories of grain size, grains, cement, porosity, and the potential relationships among various sedimentary structures, facies or parasequence set(s) (both fluvial-dominated Kf-1-Iv[a] bedset and wave-modified Kf-2 parasequences). In table 8-2, the categories

Table 8-1. Compositional estimates for selected permeability plug thin sections. Ferron samples are from the Kf-1 in the Ivie Creek case-study area and can be keyed to studies of Snelgrove and others (1996) and Mattson (1997). Texture abbreviations for (1) grain size: vf = very fine-grained sand, f = fine-grained sand, m = medium-grained sand, and cg = coarse-grained sand; (2) rounding: r = rounded, sr = subrounded, sa = subangular, a = angular; and (3) sorting: poor = poorly sorted, mod = moderately sorted, and well = well sorted. Permeability measurements are from Snelgrove and others (1996). Sedimentary structure abbreviations: hor = horizontally laminated, ripple = ripple cross-laminated, lac = low-angle cross-stratified, and tro = trough cross-stratified. Facies code abbreviations: cp = clinoform proximal, cm = clinoform medial, and cd = clinoform distal.

Samples	1	2	3	4	5	6	7	8	9	10	11	12	13	14	15	16	17	18
	T1-101	T2-50	T2-73	T2-78	T2-159	T2-161	T3-30	T3-149	T4-54	T9-72	T9-75	T9-82	T9-86	T12-41	T12-47	T14-8	T14-14	T14-19
GRAINS (100%)	93	83	90	80	77	84	85	88	80	84	84	83	87	85	88	88	85	85
Qtz- monoxlin	60	50	38	36	54	60	53	50	50	35	35	50	55	40	55	55	30	55
Qtz- polyxlin	6	3	6	5	3	5	12	12	10	30	25	5	7	10	2	2	20	2
Kspar/microcline	6	6	2	2	3	5	18	19	7	10	10	10	7	10	5	5	10	5
Plag	2	1	1	2		1	2	2	7	10	10	5	5	10	5	5	10	5
Clay Altered Frags	6	6	2	2	3	2	6	6	10	10	10	10	5	10	10	10	20	10
CO3 Altered Frags	6	30	5	13	8	2	2		2	5	12	15	5	15	10	10	6	10
Muscovite		2	3	2	3	1		2		2	3	2	1	1			1	
Blotite	2		10	7		1		2		2	2	1	1					
Clorite					3		1						2				1	
Glauconite			1			2					1	2		1				
Heavy mins	1			1					2									
Iron Opaques	1		2		3	2		2	2									
Organic matter			9	2	8	1												
Other		6			3							2			3	3		3
MATRIX	7	1	20	13	8	1	2	2	2		2	5	10	3	10	10	2	10
protomatric (clay)	2	1	14	13	8	1	2	2	2		2	5	2	3	4	4	2	4
pseudomatrix	5		6				3		8				8		6	6		6
CEMENT (100%)	5	15	8	10	15	15	12	10	8	8	8	12	10	10	10	8	8	10
carbonate/calcite	15	43	40	15	20	23	43	28	10	20	40	20	18	30	20	20	15	20
dolomite rhombs	45	50	30	85	55	35	25	30	50	10	10	20	20	30	50	50	20	50
qtz overgrowths	15	2				2	2	2	5	10	10	5	2	5			5	
Iron cement	20	5	30			25	15	20	15	10	10	30	30	5	20	20	30	20
gypsum	5				25													
kaolinte porefill/repl.						15	15	10	20	50	30	30	30	30	10	10	30	10
POROSITY (100%)	2	2	2	10	8	1	3	2	12	8	8	5	3	5	2	4	7	5
primary	50	50	50	15	25	50	25	50	15	25	25	25	25	25	25	25	25	25
secondary	50	50	50	85	75	50	75	50	85	75	75	75	75	75	75	75	75	75
TEXTURES																		
GRAIN SIZE	vf-f	vf-f	slt-vf	slt-vf	slt-vf	vf-f	f-crse	vf-med	f-med	vf-f	vf-m	vf	vf-m	vf-f	slt-m	vf-f	f-m	vf-f
ROUNDING	r,sr,sa	r,sr,sa	sa,a	sr,sa	sa,a	sr,sa,a	sr,sa,a	sr,sa,a	sr,sa,a	r,sr,sa	r,sr,sa	sr,sa	sr,sa	sr,sa	sr,sa	sr,sa	sr,sa	sr,sa
SORTING	mod-well	mod	poor	mod	mod	mod-well	mod	poor	mod	poor	poor	mod	poor	poor	poor	mod-well	mod	mod-well
COMMENTS																		
Facies Code	cd		cm	cm	cd	cd		cd	cp	cp	cp	cp	cp	cp	cp	cp	cp	cp
Sed Structure		hor	ripple	ripple	ripple	ripple	tro	horiz	tro	lac	lac	hor	hor	tro	tro	lac	lac	hor
Permeability, md	2.2	2.1	36.4	2.3	12.7	2	3.4	3.4	31.7	565.4	74	96.3	8.6	16	4.8	9.5	101	6.5

Table 8-2. Summary porosity estimates with permeability measurements for drill-hole (DH) samples and permeability plugs of table 8-1 (T samples). Kf numbers indicate the parasequence set (fluvial-dominated Kf-1 vs. wave-modified Kf-2) with more detailed units from measured sections (Mattson, 1997). Asterisk (*) indicates units outside of the Kf-1 units. Facies codes are listed in table 8-1 and also include additional facies: dmb = distributary-mouth bar, dic = distributary channel, msf = middle shoreface, and ldf = lower-delta front. Grain size and sedimentary structure abbreviations are given in table 8-1 caption. Additional sedimentary structures are: bio = bioturbated, and hcs = hummocky cross-stratified. Permeability measurements from DH samples are from automated stage-mounted mini-permeameter equipment. Measurements for T samples are mini-permeameter plugs taken in the field (Snelgrove and others, 1996).

Name	Feet	Kf-lv	Parasequence Unit No.	Facies Code	Grain Size	Sedimentary Structures	Perm (mD)	Grain (%)	Cement (%)	Porosity (%)	Description
C11	356.3	2	30	dic	cg	tro	72.0	85	-5	<10	base of distributary channel
C11	351.3	2	30	dic	cg	tro	146.30	85	<5	<15	mid distributary channel–good porosity, large pores secondary solution of carbonates
C11	348.8	2	30	dic	cg	tro	36.90	85	<5	<10	mid to upper distributary channel
C11	345.2	2	27	dic	mfg	hor	23.20	85	<5	<10	channel top
C11	342.8	2-a	28	dic	mfg	tro low	109.80	80	<5	<15	base of mouth bar–coarse sandstone; similar to W11 339.4, but more lithics, good porosity
C11	339.4	2	28	dic	fg	hor	20.20	80	<5	<15	mid bar–coarse-grained, little to no cement
C11	332.0	2-b	27	msf	fg	bio	25.10	90	<5	<10	mid bar, burrowed–clean arenite, qtz-rich good porosity
C11	321.6	2	26	dmb	vf	bio	87.30	90	<5	-10	mid bar, burrowed–clean arenite, qtz-rich good porosity
C11	312.0	2	22	dmb	mf	tro	18.30	90	<5	<5	bar top, moderately burrowed–more clay cement
C11	360.9	2-a	51	msf	fvf	hor	39.70	85	-5	-10	middle shoreface–clean sandstone, less Fe & organics, some large spots of cc cement
C3	376.0		42	ldf	m	tro		85	<10	-5	base of 1a?
C3	362.4		38	bay	fvf	rip		85	-15	<5	rippled to wavy 1a top–lots of carbonated cement
C3	285.5	2	18	bay	fvf	rip		95	<5	<5	wave rippled #2–very fine-grained, more qtz-rich
C3	306.5	2	23	msf	fvf	rip	13.96	90	<5	<10	climbing ripple crest–moderate porosity
C3	297.3	2	21	msf	f	hcs?	6.05	85	<10	<10	possible hcs
C3	323.7	2	28	msf	fvf	hcs?	11.87	90	-5	<10	possible hcs–relatively clean, more qtz-rich

Table 8-2 continued

Name	Feet	Kf-lv	Parasequence Unit No.	Facies Code	Grain Size	Sedimentary Structures	Perm (mD)	Grain (%)	Cement (%)	Porosity (%)	Description
C9	221.5	1	29	ldf	mc	tro		90	-5	-5	
C9	231.6	1	35	cp	fvf	hor		90	-5	<5	
C9	255.6	1	53	cd	fvf	hor	3.38	90	-5	-5	
C9	262.0	1	59	cd	f	hor	4.31	90	-5	<5	red freckled bed–more repl. CO_3, dolomite rhombs
T4	117.0	1[a]	15	dp	f	hor-lac	0.79	85	<10	-5	Proximal clinoform–0 permeability (why?)–pervasive Fe cement, isolated porosity?
T4	114.0	1[a]	15	dp	f	hor-lac	0.59	85	<10	-5	Proximal clinoform–0 permeability (why?)–pervasive Fe cement, squashed RF, isolated porosity?
T1	101.0	1[a]		cd	fvf		2.20	95	-	<2	medial, unit 11, redbed
T2	50.0	1[a]		?	fvf	hor	2.10	85	-	<2	capping unit 1b
T2	73.0	1[a]		cm	fvf	rip	36.40	90	<10	<2	medial, silty
T2	78.0	1[a]		cm	fvf	rip	2.30	80	-	<15	medial, silty–much like T2-73, sample has fractures?
T2	159.0	1[a]		cd	fvf	rip	12.70	85	<15	<10	distal
T2	161.0	1[a]		cd	fvf	rip	2.00	95	-	<2	distal
T3	30.0	1[a]		?	m	tro	3.40	85	<10	<5	U1c capping ?
T3	149.0	1[a]		cd	f	hor	3.40	90	-	<5	not red, distal
T4	54.0	1[a]		cp	f	lac	31.70	80	-	<15	proximal–coarser
T9	72.0	1[a]		cp	m	lac	565.40	80	-	-15	proximal, blow out–cleaner sandstone
T9	75.0	1[a]		cp	m	lac	74.00	85	-	-10	proximal, blowout–squashed RF
T9	82.0	1[a]		cp	f	lac	96.30	90	-	-5	proximal, blow out
T9	86.0	1[a]		cp	f	lac	8.60	90	-	<10	proximal, blow out
T12	41.0	1[a]		cp	f	tro	16.00	85	<5	-10	
T12	47.0	1[a]		cp	f	tro	4.80	90	-	<5	squashed RF
T14	8.0	1[a]		cp	mf	lac	9.20	85	<5	<10	non blow out
T14	14.0	1[a]		cp	mf	lac	10.10	85	<10	<10	non blow out
T14	19.0	1[a]		cp	f	hor	6.50	85	<10	<10	non blow out
T2	79.0			cp	sltst						

of grains, cement, and porosity total 100 percent. For the detailed examinations of table 8-1, individual parameters within each category are rescaled to sum to 100 percent of that particular category. Note that "matrix" is treated as a grain type and the sum of its subcategories (clay protomatrix and pseudomatrix) equals the "matrix" value. Because all values on the table are visual estimates, there is probably a 10 to 20 percent margin of error in these estimates.

These thin-section examinations indicate that all Ferron samples fall within a broad category of quartz arenites to quartzo-feldspathic arenites. Compositionally, these sandstones would be classified as submature to mature. Framework grains consist of monocrystalline quartz, polycrystalline quartz, K-feldspar/microcline, plagioclase, carbonate- and clay-altered rock fragments, muscovite, biotite, chlorite, glauconite, heavy minerals, iron opaque minerals, organic matter, other indistinguishable grains, and matrix (either proto- or pseudomatrix). The categories are approximately listed in decreasing order of abundance. Cement types in the samples consist of carbonate cement, dolomite rhombs (a replacement), quartz overgrowths, iron oxide cement, kaolinite pore fill and replacement, and gypsum vein fill (which is probably a surface weathering phenomenon).

The sandstone samples range from very fine to medium with some silt and coarse sand fractions. Most samples are poorly to moderately well sorted, with varying degrees of rounding. Kf-2 shoreface sandstones (hummocky cross-stratified, horizontal laminated, or burrowed facies) tend to be the "cleanest." Kf-1 samples are typically "dirtier" and show more lithics and altered grains with a higher degree of compaction, probably due to rapid sedimentation fed by fluvial-dominated deltas.

Porosity values are variable, averaging 5 to 10 percent and occasionally as high as 15 percent. Although complete discrimination between primary and secondary porosity is difficult, little primary porosity appears to remain in any of the samples. Many of the samples have undergone substantial reduction of primary porosity by compaction. Squashed rock fragments and point to concavo-convex grain contacts are common, indicating moderate to strong compaction. Much of the original porosity was likely occluded by early carbonate cement, and then later dissolution of those same carbonate phases (carbonate, dolomite, and possibly siderite) created secondary porosity in the same intergranular spaces. Evidence of secondary porosity development is shown by dissolution of carbonate mineralogies, and typically this secondary porosity development is patchy and unevenly distributed. Where secondary porosity is abundant, surviving cements consist primarily of quartz and kaolinite, with some interspersed minor carbonate and/or iron oxide cement (figure 8-10).

The diagenesis of the sandstone samples is complex. Several diagenetic stages or events are evidenced by the varying cement types. Quartz overgrowths are generally an early diagenetic stage. Calcite cement and dolomite rhombs are middle diagenetic stages, followed by late phases of iron/hematite staining or replacing of the carbonate minerals (such as the dolomite rhombs). Some grains are altered to clay and/or replaced by carbonate. Final stages of diagenesis are dissolution of those same carbonate phases and development of microfractures.

Based on our thin-section petrography, it is difficult to fully evaluate the effect of weathering. For the most part, the outcrop plugs have permeabilities and porosities comparable to samples from adjacent drill holes. However, identical beds from the outcrop and from unweathered drill-hole cores have not been sampled and compared. Poikilotopic cements were

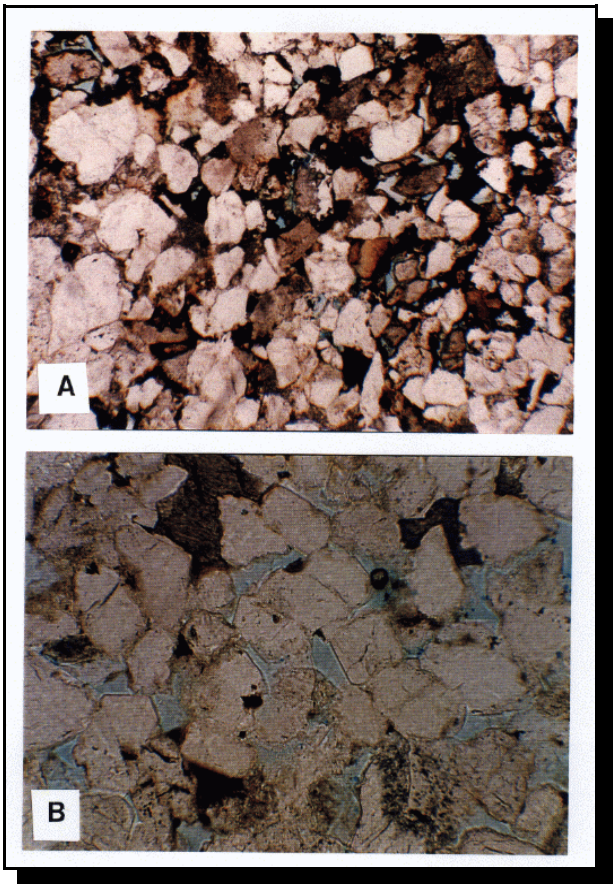


Figure 8-10. Polarized-light photomicrographs of fluvial-dominated Kf-1 sandstone. A. Sample T4 117, showing localized secondary porosity development (porosity shown in light gray [blue]) at right from dissolution of cements; field of view ~ 1.9 mm across. B. Sample DH11 321.6, showing more uniform secondary porosity development (corresponding to higher permeability, see table 8-2) from dissolution of cements; field of view ~ 0.8 mm across.

observed in the most weathered outcrop samples, but such features were not noted in the cored samples away from the outcrop faces.

Surprisingly, some of the samples with relatively high permeability were very fine-grained sandstones with fairly low porosity, as visually noted from the thin sections (for example, T2-73). Generally those samples do have relatively little cement compared with other samples. Another possible explanation is that localized porosity, perhaps along some bedding/parting planes, may locally produce very high permeability. Porosity localization occasionally was observed (for example, T9-82). The two outcrop samples with lowest permeability (T4-117 and T4-114) have pervasive iron oxide cement, yet there is still visible porosity in thin section (figure 8-10); the cause of their very low permeabilities is not evident in thin sections.

The thin section examinations suggest several generalizations concerning relationships among grain size, sorting, depositional energy, and facies. Samples with coarser grain sizes (generally fine to medium or coarse) have more and larger pores. Coarser grained sandstones tend to be more quartz rich and are relatively "cleaner," with less matrix. Organic matter may form small-scale permeability barriers, and coarser grained samples with better porosity generally contain less organic matter. Fine-grained samples tend to have more organic matter, reduced porosity, and more concavo-convex grain contacts.

Overall, it appears that reservoir potential is well correlated to facies. Coarse-grained distributary channel, proximal clinoform, burrowed bar, and shoreface deposits seem to have the best permeabilities and porosities. Wave-modified (reworked) Kf-2 sandstones are generally better sorted and cleaner and may have higher porosities and good permeabilities in the coarser sand grain sizes. Fluvial-dominated deposition, as in the Kf-1 samples, implies less sorting and more rapid sedimentation fed by rivers. These Kf-1 samples thus have a corresponding decrease in both porosity and permeability. Although diagenesis is pervasive and complex, the original intergranular pore spaces that filled with early cements are the same sites that were later dissolved to form secondary porosity.

Controls on Porosity: Evidence from Ivie Creek Core Plugs

Atmospheric-pressure porosities (in porosity units or volume percentage of pores) of core plugs were measured in two ways. Pycnometer porosity, or Boyle's Law porosity, is calculated from grain density and dry density. Saturated porosity is calculated from saturated and dry densities. Because the latter considers only pore space accessible to water, it is slightly lower than pycnometer porosity (maximum difference 2 porosity units at high porosities) and is most appropriate for our subsequent considerations of seismic response of saturated rocks.

Ivie Creek core-plug porosities average 13.0 percent (standard deviation 4.0 percent, range 1.7 to 20.9 percent). Cross plots of porosity versus abundance of individual minerals show, surprisingly, no significant correlation with clay content, at least among these low-clay samples. Similarly, porosity is not correlated with abundance of other minerals, with one exception: carbonate content. Increasing carbonate content (here summing concentrations of calcite, dolomite, and siderite, based on infrared spectroscopy) is strongly associated with porosity reduction (figure 8-11A). Carbonate-free samples have porosities of about 12 to 19 percent, probably reflecting the porosity of these samples at the time that carbonate cementation initiated. The carbonate content of the near-zero-porosity samples is not 12 to 19 percent as expected for simple pore filling, but considerably higher. Thin sections show that carbonate is present not merely as pore filling but also sometimes as feldspar alteration and replacement; thus carbonate contents can exceed primary porosities.

A correlation between porosity and carbonate content can be either primary (reflecting early carbonate precipitation) or secondary (reflecting earlier carbonate filling of pores followed by later carbonate dissolution). The latter is indicated by petrographic observations that the highest-porosity samples have secondary porosity (Figure 8-11B). This secondary porosity is intergranular, not vugular or crack porosity.

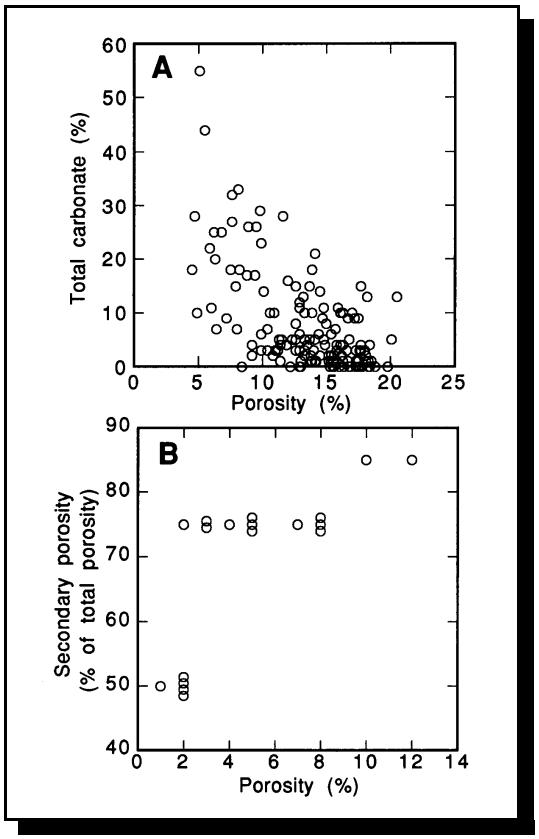


Figure 8-11. A. Cross plot of core-based analyses showing that total carbonate increases with decreasing porosity. B. Cross plot of total porosity versus percentage of the porosity that is secondary, based on thin sections. These two patterns suggest that porosity reduction was caused mainly by carbonate cementation, and the current high porosities are mainly secondary porosities generated by carbonate dissolution.

The controls of cementation and dissolution on Ferron porosity impact the conversion between bulk density and porosity. Bulk density is a function of mineral and fluid components:

Eq. 8-1 $\tilde{n}_b = \tilde{n}_f ö + \tilde{n}_{ma}^{(1-ö)}$

where ö = fractional porosity, $\tilde{n}_f$ = fluid density, and $\tilde{n}_{ma}$ = matrix (or grain) density. For sandstones and slightly shaly sandstones such as these, a single matrix density of 2.65, corresponding to quartz, is usually appropriate for all porosities. Carbonates, however, have higher matrix densities (2.71 for calcite, 2.88 for dolomite, and 3.9 for siderite). Consequently, a plot of matrix density versus porosity shows matrix densities of 2.70±0.05 for the lowest-porosity (carbonate-rich, figure 8-11A) rocks, dropping to the 2.65 value of quartz at porosities of about 18 percent (carbonate-free, figure 8-11A). Linear regression indicates that the dependence of matrix density on 1,000 psi (6.9 Mpa) porosity is $\tilde{n}_{ma} = 2.719 - 0.406ö$ (R = 0.62). Combining this equation with Eq. 8-1, and using a value of 1.02 g/cc for $\tilde{n}_f$, gives:

Eq. 8-2 $$\tilde{n}_b = 2.719 - 2.105ö + 0.406ö^2,$$

or

$$ö = 2.592 - 1.232 \bullet \text{sqrt}\,(0.0154 + 1.624\tilde{n}_b)$$

To convert density logs of Ferron sandstones to porosities, Eq. 8-2 is more appropriate than Eq. 1.

Effects of Exhumation on Ferron Porosities

The 179 paired Ferron log picks of velocity and porosity are plotted as a function of depth in figures 8-12A and 8-12B. Two features are evident on these plots: (1) heterogeneous porosities and velocities at each depth, and (2) gradual porosity increase and velocity drop with decreasing depth (increasing exhumation). The wide ranges for porosity and velocity are an advantage in defining velocity/porosity relationships, but they partially obscure the changes with depth. Systematic changes with depth are more evident on plots of three-well averages of porosity and velocity, along with 95 percent confidence limits (Figures 8-12C and 8-12D).

Only two very deep wells survived our rejection criteria. The deepest (~11,800 feet [3,600 m]) has porosities of 2 to 4 percent, and the shallower one (~10,200 feet [3,100 m]) has porosities of 4 to 8 percent (figure 8-12A). These differences are comparable to heterogeneity within wells; they do not provide strong evidence of porosity increase associated with initial exhumation. Porosities for the two wells suggest that pre-exhumation porosities of the Ferron were 4±4 percent. Shallower than 5,900 feet (1,800 m), where the abundance of well data is much higher, the systematic increase in porosity with continuing exhumation is more reliably indicated.

Porosity increase accelerates as the Ferron is progressively exhumed, leading to a porosity/depth trend that is approximately logarithmic (Figure 8-12C). By the time the Ferron has reached near-surface depths (70 to 460 feet [20-140 m]), average porosity has increased to 9.3±2.4 percent (95 percent confidence limits). Outcrop samples are even more porous than these log-based well porosities: average porosity of our 162 batch-1 Ivie Creek outcrop samples is 13.0±0.6 percent, and 90 percent of the 59 outcrop samples from nearby Muddy Creek Canyon have porosities within the range 12 to 20 percent (Miller and others, 1993a).

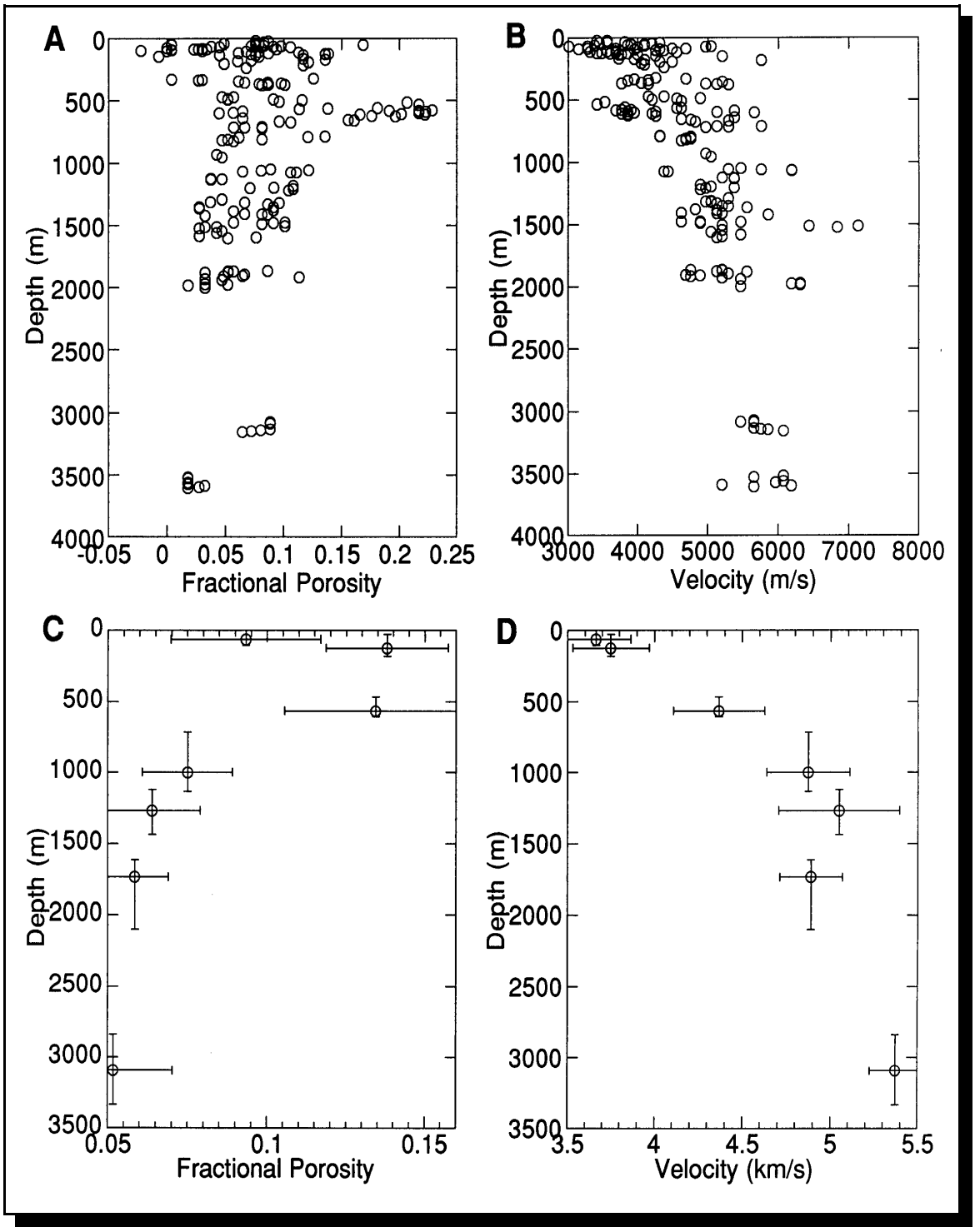


Figure 8-12. Fractional porosity (A) and velocity (B) of individual Ferron beds, based on well logs at the wells of figure 8-9. Note both the heterogeneity at a given depth and the systematic changes with depth. Variation of average Ferron porosity (C) and velocity (D) with depth, based on three-well adjacent-depth averaging of data from (A) and (B), respectively.

Many authors have emphasized the influence of provenance and depositional environment on sandstone diagenesis and development of secondary porosity (Hayes, 1979; Stonecipher and others, 1984). Could the regional variations in Ferron porosities be caused by lateral changes in lithology? The general sedimentary pattern of fining and thinning eastward (Ryer and McPhillips, 1983; Tripp, 1989) could cause higher primary porosities in more deeply buried western sediments than in shallower, eastern sediments, but observed present porosities exhibit the opposite pattern.

Increase in Ferron porosities is not correlated with subsurface variations in fracturing (Tripp, 1991b, 1993b,1993c). Nor could fractures explain the magnitude of the increase: macrofracture and microfracture porosity is seldom more than 1 to 2 percent. Porosity increase is inevitable because of elastic expansion of pores due to pressure release (Domenico and Mifflin, 1965), but this unloading-curve effect is far too small to account for the observed porosity changes.

Secondary Porosity in the Ferron Sandstone

Carbonate dissolution can account for the presence and magnitude of depth-dependent porosity increases of the Ferron. The petrographic and petrophysical studies discussed previously demonstrate that outcrop samples have secondary porosities that result from carbonate dissolution. The depth dependence of Ferron porosities implies a relationship between exhumation and this dissolution of carbonate cement. Its origin might be either a direct influence of exhumation on calcite solubility or an indirect link between exhumation and fluid flow. In either case, determining the origin of Ferron secondary porosities is an essential prerequisite to identifying implications for secondary porosity of other exhumed sandstones.

Once thought to be relatively rare, intergranular secondary porosity has increasingly been recognized as being comparable to primary porosity among sandstones globally (Schmidt and McDonald, 1979). Secondary porosity often occurs below the depths at which primary porosity is destroyed, as a consequence of kerogen breakdown at temperatures of greater than 100EC (Schmidt and McDonald, 1979; Surdam and others, 1984). Maturation generates both carbon dioxide (Hunt, 1979) and organic carboxylic acids, and both can induce dissolution of carbonates, perhaps the most frequent cause of secondary porosity (Schmidt and McDonald, 1979). Organic acids may also induce silicate dissolution (Hayes, 1979; Surdam and others, 1984), which can be as important as carbonate dissolution among immature sandstones (Hayes, 1979).

Cementation or dissolution rate depends on both calcite solubility (Garrels and Christ, 1965) and fluid flow rate (Maxwell, 1960). For significant dissolution of a formation to occur, substantial fluid flux is required; ion diffusion is insufficient (Hayes, 1979; Bjørlykke, 1984). This flux can come from dewatering of adjacent shales (Hayes, 1979), smectite/illite transition (Surdam and others, 1984), or meteoric water (Bjørlykke, 1984). Galloway (1984) emphasized the impact of hydrologic regime--either meteoric, compactional, or thermobaric–on diagenetic history. He noted that basins commonly undergo a temporal evolution from one hydrologic regime to another, with associated diagenetic changes. A very common hydrologic evolution is from early compaction flush to later meteoric flush (Harrison and Tempel, 1993).

The Ferron Sandstone appears to demonstrate the impact of meteoric flux on its late-stage diagenetic history. Flow rates in regional ground-water-flow systems nearly universally decrease rapidly with subsurface depth (Freeze and Witherspoon, 1967), compatible with the strong depth dependence that we observe for carbonate dissolution in the Ferron Sandstone. The maximum depth of meteoric leaching depends on many factors: potential gradients, permeability, and the rates of recharge, flow, reactions, and solubility change (Schwartz and Longstaffe, 1988; Bjørlykke, 1994). The 6,500-foot (2,000-m) depth of Ferron secondary porosity enhancement is compatible with the 9,800-foot (3,000-m) maximum depth of meteoric flow in other regions with comparable head (Toth, 1980).

The modern hydrologic regime of the Ferron Sandstone is dominated by recharge in the Wasatch Plateau and Book Cliffs at the west and northern margins of the study area of figure 8-8, with discharge near the Ferron outcrop (Lines and Morrissey, 1983). Whereas topography slopes downhill to the east and southeast of these recharge regions, stratigraphic dips of the Ferron and other strata are to the west and northwest. Consequently, meteoric flux is not simply downslope in the subsurface. Confined by relatively impermeable, bracketing shales, ground water moves up along Ferron sandstone beds toward the eastern outcrops (Lines and Morrissey, 1983).

This upward flux of meteoric waters into discharge areas is orders of magnitude faster than the rate of exhumation. For example, Lines and Morrissey (1983) report a carbon-14 age of 28,000 years for a fluid sample from 1,475 feet (450 m) in the subsurface, whereas only about 20 feet (6 m) of erosion would occur in this time period if the erosion rate were steady-state at 6,500 feet (2,000 m) per 10 m.y. Thus upward meteoric flux, not exhumation, probably generates an increase in carbonate solubility responsible for late-stage carbonate dissolution within the Ferron Sandstone. Upward flow of meteoric water can be an extremely effective mechanism for development of secondary porosity, because of the combination of high flow rates (compared to other types of fluid flow) and cooling-induced increase in calcite solubility (Bjørlykke, 1994).

Ground-water flow at Ferron outcrops contrasts with the large-scale meteoric flux, which is upward and eastward within Ferron Sandstone beds. At Ferron outcrops such as Ivie Creek, rainwater percolates downward through the vadose zone to the water table and is discharged at the deeply incised canyons (Lines and Morrissey, 1983). Near and above the water table, carbon dioxide buildup from decaying organic matter can enhance carbonate leaching (Bjørlykke, 1994), and this mechanism probably accounts for the porosity increases among outcrop samples that we previously noted. Although the Ivie Creek and Muddy Creek Canyon outcrop samples are mostly different Ferron parasequences and partly different facies, the 12 to 20 percent porosities of generally carbonate-free Muddy Creek Canyon sandstones (Miller and others, 1993a, 1993b) are remarkably similar to the 12 to 19 percent porosities of carbonate-free Ivie Creek case-study area sandstones.

The Ferron hydrologic analysis of Lines and Morrissey (1983) is confined to relatively shallow depths (less than 1,650 feet [<500 m]) and to the south-central portion of figure 8-9. The patterns of secondary porosity development seen in our study suggest that upward flow along the Ferron beds is pervasive and that this meteoric flow extends to about 6,500 feet (2,000 m) subsurface depth.

Velocity of the Ferron Sandstone

Controls on Velocity: Evidence from Ivie Creek Core Plugs

In one of a classic series of papers, Biot (1962) developed a general theoretical description for the viscoelastic responses of fluid and mineral framework of a porous medium. The Biot theory, though rigorous and powerful for sensitivity studies, requires specification of 13 to 16 parameters, a formidable hurdle for most geophysical studies of sound propagation. Gassmann (1951) described the special case in which behavior is elastic and fluid is driven neither into nor out of the porous medium; friction, attenuation, and frequency dependence can be neglected, allowing compressional velocity to be specified largely in terms of dynamic elastic moduli. In the Gassmann (1951) model, velocity is affected by porosity both explicitly and through the effect of porosity on shear modulus, frame bulk modulus (Hamilton, 1971), and bulk density (Eq. 8-1). Consequently, for sedimentary rocks in general, porosity is the dominant control on velocity.

Recognizing this porosity dominance, Wyllie and others (1956) introduced an empirical relationship between porosity and velocity that has been used successfully in much of the petroleum industry (particularly by log analysts) for 40 years. Raymer and others (1980) and later Erickson and Jarrard (1999) proposed revised porosity-velocity relationships that are much more accurate than the Wyllie equation at high porosities. At moderate porosities, such as in the Ferron Sandstone, the differences between models are minor, and we use the Wyllie equation in this study as a familiar, reasonably accurate reference. The simplicity of these models is their virtue, but they fail under a variety of conditions:

1. atypical cementation, because they assume average cementation in which changes of frame modulus are implicit in changes of porosity;

2. porosities greater than about 25 percent, with an error that increases rapidly with further porosity increase;

3. anisotropy, which is particularly strong in shales;

4. pore aspect ratio of non-unity (for example, cracks);

5. pore fluids other than water (for example, the bright-spot effect of gases is not predicted); and

6. pressure dependence of velocity, for both overburden pressures and excess pore pressures.

Of these potential problems, our Ferron analysis must be particularly alert to numbers 1 and 6. Cementation is representative of rocks with secondary rather than primary porosity. Pressure dependence is also a potential concern: overpressures are absent, but overburden pressures have plummeted during exhumation. In contrast, porosities are within the range

appropriate for the time-average equation, pores are filled with water (we have avoided gas-bearing sands), and microcracks are present but probably volumetrically minor from the standpoint of anisotropy and pore aspect ratio.

In rocks with extremely low porosities, microcracks can constitute a significant proportion of total porosity. In contrast, the contribution of microcracks to Ivie Creek porosities is minor: the median difference between porosity measurements at atmospheric pressure and 1,000 psi (6.9 Mpa) is 0.6 percent, much smaller than the average 13.0 percent total porosity. It does not follow, however, that microcracks have a minor influence on P-wave velocity. Virtually all core samples, regardless of lithology, exhibit patterns of increasing P-wave velocity with increasing pressure (Nur, 1971; Bourbié and others, 1987), attributable to closing of microcracks. In-situ stress relaxation generates and opens these microcracks. Because Ivie Creek outcrops have been exhumed from 9,800 feet (3,000 m) in the subsurface to ground level, open microcracks are expected, and our laboratory measurements of velocity and porosity confirm their presence (figure 8-13).

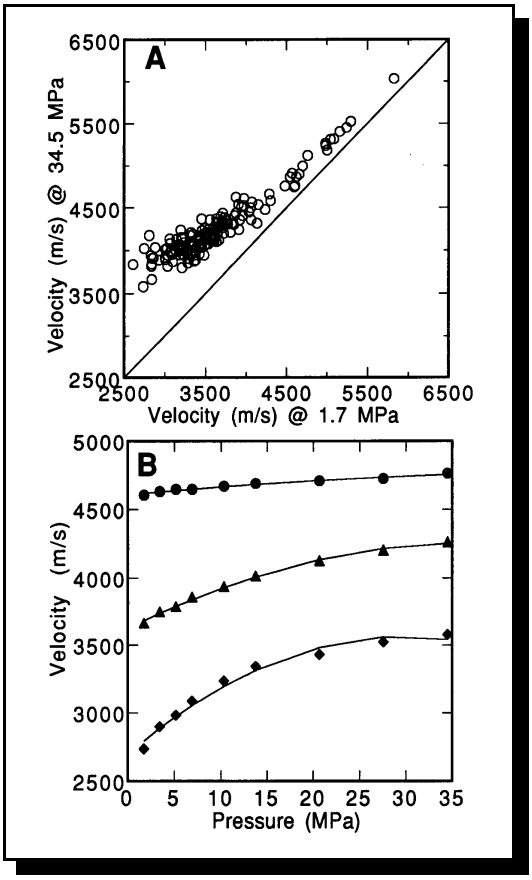


Figure 8-13. A. Comparison of the lowest-pressure and highest-pressure measurements of compressional-wave velocity of core plugs. B. Pressure dependence of velocity for three representative samples. All sample velocities are sensitive to pressure change, due to closing of microcracks, and this effect is most marked in the lowest-velocity samples.

Core-plug compressional velocities at the highest measured pressure are plotted as a function of porosity in figure 8-14D. This pressure, 5,000 psi (34.5 Mpa), is comparable to the pressure at 9,800 feet (3,000 m), the maximum depth to which the Ferron Sandstone has been buried. Also plotted in figure 8-14D is the time-average equation (Wyllie and others, 1956) for sandstone (V_{ma} = 19,360 feet/second [5,950 m/s]). This relationship fits these data moderately well, as does a revised equation by Raymer and others, (1980). As previously observed with matrix density versus porosity, we might expect a porosity dependence of matrix velocity. If so, the higher matrix velocities of carbonates would cause a systematic offset of the highest-carbonate points in figure 8-14D to velocities above the sandstone line. The highest velocities are consistent with this expectation: they are found in samples with less than 25 percent carbonate and are compatible with typical limestone matrix velocities of about 21,150 feet/second (6,450 m/s).

Shaly sandstones are generally better fit by a function of both porosity and clay content than by the time-average equation (Castagna and others, 1985; Han and others, 1986). Clay minerals affect velocity not only indirectly by changing sediment porosity, but directly by decreasing frame bulk modulus and aggregate bulk modulus. For the Ferron samples, however, the shaly-sand relationships of Castagna and others (1985) and Han and others (1986) are no more successful than the time-average equation in predicting velocity. Furthermore, velocity

residuals from the time-average equation (observed velocity minus that predicted from porosity based on the time-average equation) are not correlated with clay content. We conclude that the effect of clay content on velocity can be neglected for the Ferron sandstones and moderately shaly sandstones. This surprising result probably is attributable to overprinting of the original pattern of intergrain contacts by thorough cementation followed by leaching. It raises an important question: are the shaly-sand velocity models relevant to rocks (like the Ferron) with secondary porosity?

Effects of Exhumation on Ferron Velocities

Whenever exhumation causes development of secondary porosity, then velocity decrease is also expected, because velocity is primarily dependent on porosity. Figures 8-12B and 8-12D confirm that Ferron velocities do exhibit a strong depth dependence. Indeed, the velocity drop at the shallowest depths appears to be even stronger than the associated porosity increase (figure 8-12C).

We can use cross plots of porosity versus velocity to separate porosity effects from other factors that may control velocity. Figure 8-14 shows that the observed velocity variations are mostly attributable to variations in porosity. The log data from deeper than about 1,800 feet (550 m) (figure 8-14B) fit Wyllie and others' (1956) time-average relationship for sandstone matrix fairly well. Several points with near-zero porosity fall far above the time-average prediction for sandstone; their velocities imply a high carbonate content, presumably from the combination of carbonate cementation and carbonate replacement that is seen in these sandstones.

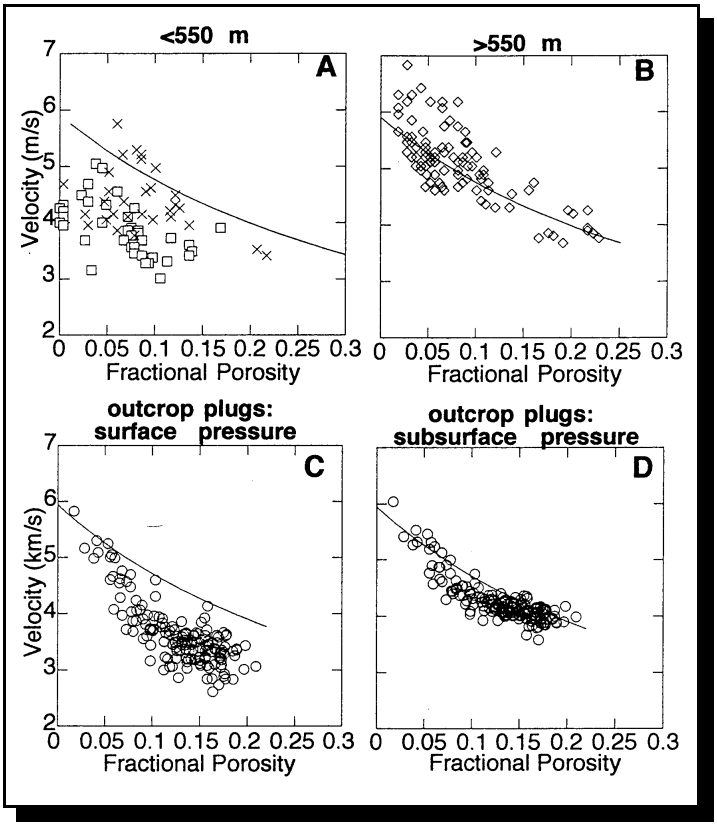


Figure 8-14. Velocity/porosity patterns from core-plug and log measurements. (A) and (B): Ferron log-based velocities and porosities from figure 8-13, showing systematic changes of the velocity/porosity relationship with sample depth. Data from deeper than 1,800 feet (550 m) are consistent with the empirical relationship of Wyllie and others (1956), whereas shallower data are systematically lower in velocity than one would expect based on their porosities. Squares: data from shallower than 500 feet (150 m). Crosses: data from depths between 500 to 1,800 feet (150 -550 m). Outcrop core-plug measurements made at 250 psi (1.7 Mpa) (C) exhibit a similar velocity/porosity relationship to that of low-pressure (shallow burial) log data (A). In contrast, outcrop core-plug measurements made at 5,000 psi (34.5 Mpa) (D) are compatible with both high-pressure (greater than 1,800 feet [>550 m] burial) log data (B) and with the Wyllie and others (1956) relationship, indicating that pressure increase has closed microcracks.

For Ferron sandstones that have been exhumed to within 1,800 feet (550 m) of ground level, porosity is no longer the only control on velocity; often, it is not even the main control. Figure 8-14A shows that the entire velocity/porosity relationship is systematically offset toward lower velocities for these shallow-burial data. The time-average relationship forms a lower bound to these data: a few data fit this prediction, but most points--and particularly those at the lowest porosities--are offset by 3,200±1,600 feet/second (1,000±500 m/s) below the time-average predictions. For the depth interval 0 to 500 feet (0-150 m), the offset is even larger (figure 8-14A): all are below the time-average predictions, averaging about 5,000 feet/second (1,500 m/s) too low, and most have velocities less than those observed at 500 to 1,800 feet (150-550 m).

These systematic depth-dependent changes in the porosity/velocity relationship indicate that exhumation-induced pressure release decreases velocity. The effect cannot be either an elastic expansion of porosity or development of secondary porosity, because the entire porosity/velocity relationship is offset. Decrease in frame bulk modulus must be responsible. All bulk moduli are pressure dependent, but frame bulk modulus is particularly so. This influence has been thoroughly studied for shallow (less than 160 feet [<50 m]) unconsolidated sediments, where the primary causes of depth-dependent velocity changes are porosity decrease and pressure-induced increase in shear modulus and frame bulk modulus (for example, see the excellent summary by Stoll, 1989). Increased overburden pressure increases the number and area of interparticle contacts, thereby increasing shear modulus and frame bulk modulus, and this increased framework stiffness increases velocity. Stoll (1989) cautions, however, that cementation and other changes occurring during lithification will tend to make the complex moduli less dependent on overburden pressure."

The pressure dependence of frame bulk modulus is evident within lithified cores when velocity is measured as a function of pressure. As increased pressure closes microcracks, reduction in total porosity is trivial (Han and others, 1986). Initial microcrack porosities of less than 0.5 percent are sufficient to cause pressure-dependent velocity variations of 5 to 50 percent, indicating that the primary effect of pressure on velocity is through its impact on frame bulk modulus, not on porosity or density (Walsh, 1965; Nur and Murphy, 1981; Bourbié and others, 1987).

Can the measured pressure dependence of plug velocities account for the observed log-based changes in velocity and in velocity/porosity relationship? Figures 8-14A and 8-14C compare velocities and porosities for lowest-pressure core-plug measurements to those for shallow (less than 1,800 feet [<550 m]) log data. Log velocities for 500 to 1,800 feet (150-550 m) are comparable to core-plug velocities for the same porosity; the core-plug pressures of 250 psi (1.72 Mpa) are comparable to or lower than log pressures of 250 to 900 psi (1.7-6.2 Mpa) for these depths. Both are systematically lower than Wyllie and others' (1956) time-average relationship, but we have already seen that pressure increase can reclose microcracks and remove this discrepancy (figure 8-14D). The shallowest log data (65 to 460 feet [20-140 m]) are even lower in velocity than the 500 to 1,800 foot (150-550 m) log and 250 psi (1.72 Mpa) core-plug data (figure 8-14A); the core-plug measurements do not extend to pressures low enough for comparison to these shallowest log data.

Do Velocity Logs See Secondary Porosity?

Log analysts often generalize that sonic logs do not see secondary porosity, particularly secondary porosity in carbonates (Schlumberger, 1972, 1989; Ellis, 1987; Winkler and Murphy, 1995), and that one can therefore estimate the amount of secondary porosity ($ö_{sec}$) by comparing sonic ($ö_{son}$) and neutron-density ($ö_{nd}$) porosities: $ö_{sec} = ö_{nd} - ö_{son}$. These generalizations assume that secondary porosity consists of either fractures or vugs. Sonic logs do not simply measure average velocity, because the tools record only the fastest of many compressional-wave paths between source and receiver. For vertically traveling waves in a vertically fractured rock, waves paralleling fractures will arrive sooner than waves from within fractures. Thus, the measurement does not see some fractures, particularly large-scale fractures that are separated by substantial zones of unfractured rock. Similarly, waves traversing isolated large vugs arrive later than waves whose paths encounter no vugs.

Large fractures and vugs are, however, merely two of many kinds of secondary porosity. Among sandstones, a more common type of secondary porosity than either large-scale fractures or vugs is that encountered by the Ferron logs: intergranular secondary porosity, created by dissolution of carbonate (or other) cement, replacement carbonates, or detrital minerals (Schmidt and McDonald, 1979). Both Ferron core-plug velocity measurements and sonic logs clearly see this secondary porosity (figures 8-12 and 8-14). Indeed, they appear to respond to this porosity in the same manner as to primary intergranular porosities, based on their fits to the time-average equation (figure 8-14). The agreement of Ferron data with Wyllie and others' (1956) time-average equation suggests that the frame bulk moduli for the Ferron are comparable to those of other sandstones of similar total porosity, despite the difference in porosity origin.

Is it reasonable to assume that core-plug and log measurements would be equally sensitive to microfractures? Two mechanisms might generate a greater sensitivity to microfractures for plug than for log velocities: (1) plug velocity measurements are made at a much higher frequency than log velocity measurements, and higher-frequency measurements are likely to be more sensitive to tiny defects; and (2) these plug velocity measurements are horizontal and therefore routinely cross microfractures, whereas log velocity measurements are vertical and parallel microfractures. Both possibilities can be investigated by comparing whole-core and log measurements for drill hole IC-3. This drill hole has continuous core, with greater than 99 percent recovery, throughout the Kf-1 and Kf-2 parasequence sets of the Ferron. These cores were run through the U.S. Geological Survey gamma-gamma density logger, obtaining porosities every 2 centimeter along core. The equivalent down-hole interval was logged with a BPB gamma-gamma density tool. The two density data sets agree (figure 8-15A).

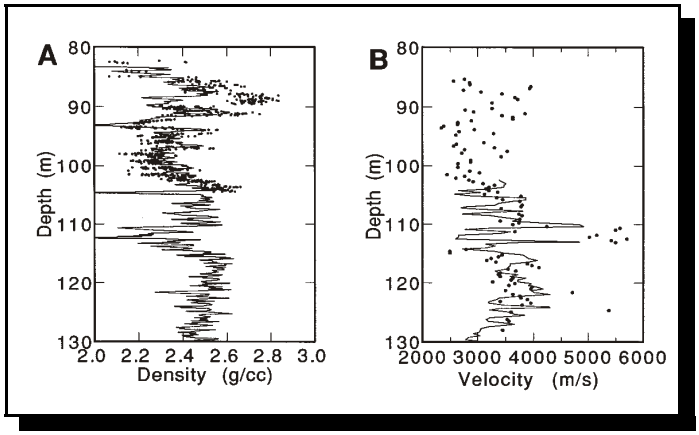


Figure 8-15. Comparison of log (line) and core (dots) measurements for density (A) and velocity (B) at Ivie Creek drill hole IC-3.

At this well we also made 113 horizontal measurements of whole core velocity, using transducers with a frequency of 500 Khz, the same as for plug velocity measurements and much higher than the frequency of about 25 Khz employed in sonic logging. For part of the same depth interval, we were able to retain water in the hole long enough to run sonic logs. Rock velocities for air-filled pores (cores) are expected to be lower than those for water-filled pores (logs); for Ferron core plugs, this difference is 1,000 to 1,600 feet/second (300-500 m/s). Log and whole-core velocity data for drill-hole IC-3 show good agreement (figure 8-15B). Log velocities may be slightly lower than core velocities, but the need to bias core measurements toward better cemented, less attenuating samples may be responsible. Log velocities certainly are not higher than core velocities, as would be expected if sonic logs were less sensitive to microfractures than are horizontal core velocity measurements.

Bourbié and others (1987) suggested that acoustic properties of heterogeneous media can be understood in terms of the concept of minimum homogenization volume. If the wavelength of compressional waves is substantially greater than the diameter of the minimum homogenization volume, then the wave sees an effective average porosity and may be insensitive to the geometry of the microscopic heterogeneities. This concept can account for the observed variety of responses to secondary porosity. The minimum rock volume required to homogenize porosity depends on the type of porosity: perhaps less than a cubic centimeter for microcracks and for primary and secondary intergranular porosity, and perhaps cubic meters for rocks with large open fractures or vugs. Thus, core plugs and sonic logs respond similarly to both microfractures and intergranular secondary porosity. Rocks with intergranular porosity have a velocity/porosity relationship that is independent of the origin of that porosity--primary or secondary.

Permeability of the Ferron Sandstone

Controls on Permeability: Evidence from Ivie Creek Core Plugs

Ferron Sandstone permeability is very closely related to porosity, with a linear relationship between porosity and the logarithm of permeability (figure 8-16) that is roughly similar to those found from other high-porosity sedimentary rocks. That relationship, however, varies so much between formations in different parts of the world that it must be locally determined (Nelson, 1994). Our relationship for the Ferron Sandstone is much better than we had anticipated based on the Texas Bureau of Economic Geology (TBEG) measurements (Miller and others, 1993a) or our own porosity/mini-permeameter data, and it extends to permeabilities far below the 2-md threshold for useful mini-permeameter measurements. This relationship means that permeability can be estimated for all core-plug samples for which porosity is measured. Furthermore, density logs from the Ivie Creek drill holes can provide continuous records of down-hole permeability variations. We used equation 8-2 to convert IC-3, IC-11, and IC-10 density logs to porosity. Based on the transform from porosity to permeability (figure 8-16), we then converted IC-3, IC-11, and IC-10 porosity logs to permeability.

Effects of Exhumation and Outcrop Exposure on Ferron Permeability

Whenever exhumation causes development of secondary porosity, then permeability increase is also expected, because permeability is primarily dependent on porosity. We can use cross plots of porosity versus permeability to separate porosity effects from other factors that may affect permeability (for example, weathering, microcracks, clay content). Figure 8-16 shows that the observed permeability variations are mostly attributable to variations in porosity. Similar patterns are observed for outcrop samples, shallow subsurface samples from Ivie Creek, and deep subsurface samples. This correspondence indicates that the primary impact of exhumation on permeability is through porosity enhancement. Outcrop exposure does not diagenetically modify the pattern, as evidenced by the similarity among three groups of samples (figure 8-16): mature, natural outcrops, a road cut less than a few decades old, and wells (both shallow and deep).

Comparison of atmospheric-pressure porosity measurements to those made at 1,000 psi (6.9 Mpa) shows that the atmospheric-pressure porosities are systematically higher than the 1,000 psi (6.9 Mpa) data by up to 1 percent. Thus, it is likely that atmospheric-pressure measurements of permeability, such as the TBEG data and all mini-permeameter data, are increased slightly (relative to 1,000 psi [6.9 Mpa] measurements) by microcrack opening. However, intergranular porosity and associated intergranular permeability are much larger than this minor effect.

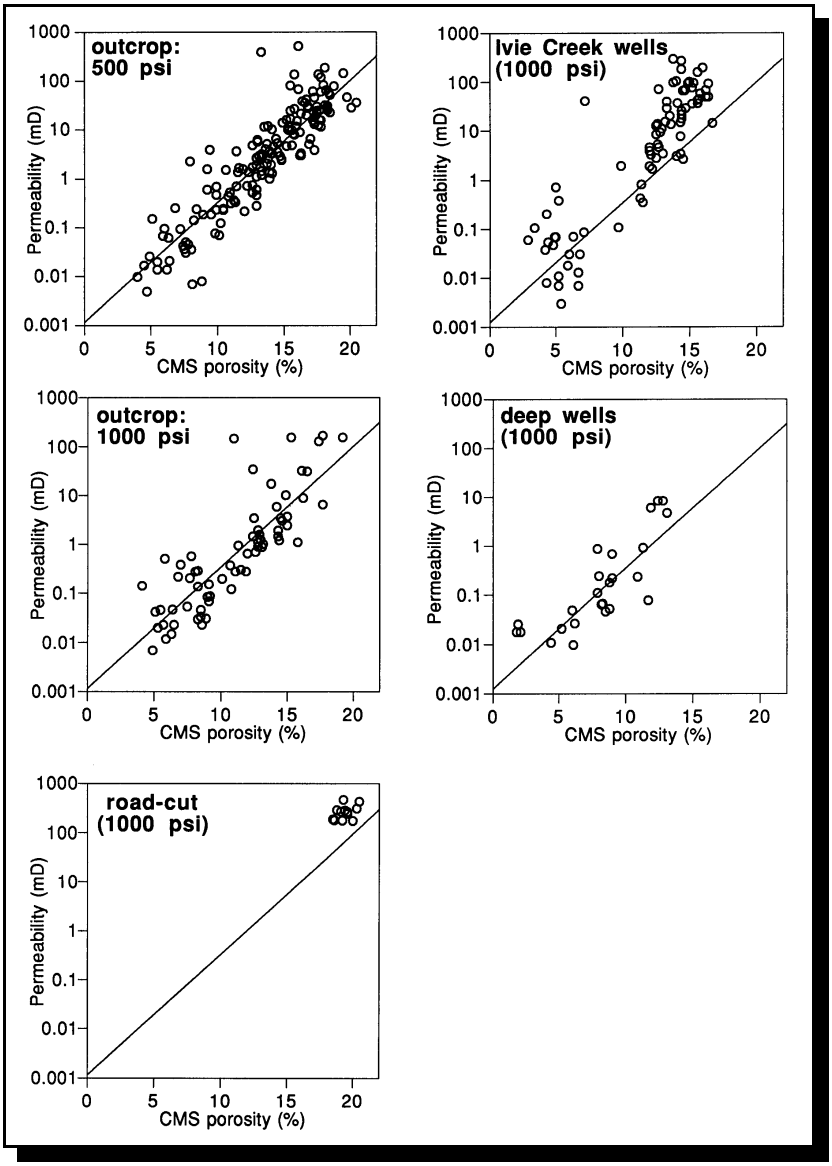


Figure 8-16. Porosity/permeability pattern for core-plug samples from the Ferron Sandstone. The reference line is based on linear regression of the 500 psi (3.44 Mpa) outcrop data.

Ferron Sandstone permeability (k) is related to fractional porosity (ö) by:

Eq. 8-3 $\ln(k) = -6.657 + 56.6*ö \quad (R = 0.921)$

This relationship is based on all data from the first batch of Amoco measurements, excluding four anomalous points (inclusion of those points has only a minor effect on the result). Residuals from this relationship can be examined, in order to search for second-order influences on permeability. Cross plots of these residuals against mineral concentrations show, remarkably, no significant correlation with clay content. This observation does not imply that shaly samples have the same permeability as sandy ones; indeed, as described elsewhere, shaly bedsets in the Kf-1 parasequence set is much lower in permeability than sandy parasequences of the Kf-2 parasequence set. It indicates, however, that the relationship between clay content and permeability is entirely indirect: shaly samples have lower porosity and therefore lower permeability. The only significant correlations between porosity residuals and mineralogy are subtle positive correlations between permeability residuals and both quartz and orthoclase, and a subtle inverse correlation with dolomite. An inverse correlation with kaolinite, noted in the initial batch of outcrop samples and attributed to kaolinite lining of pores, is not evident in drill-hole samples.

Not all Ferron Sandstone beds share in the porosity increase associated with exhumation (figure 8-12A). Even at near-surface depths, a few beds have porosities comparable to those at 9,500 to 11,100 feet (2,900-3,400 m). The standard deviation of porosities increases with exhumation, indicating a heterogeneity of the process that generates this porosity increase. Fluid flux and resulting dissolution are focused at the meter scale of individual beds. Hayes (1979) and Bjørlykke (1984) have predicted that leaching often might concentrate secondary porosity in beds that have the highest primary porosity, because fluid flux is localized within the most permeable (coarsest grained) beds. Ferron outcrop studies at the Ivie Creek and other areas indicate that grain size is positively correlated with permeability (Mattson and Chan, 1996; Barton and Tyler, 1991). Our outcrop petrophysical data show that permeability is very strongly dependent on porosity ($R = 0.92$; figure 8-16), and thin sections demonstrate that the porosity is largely secondary (figure 8-10B). These observations imply that grain size has influenced the entire history of Ferron porosity evolution: (1) early mechanical compaction left coarse-grained sandstones with higher porosity and permeability than fine-grained sediments; (2) carbonate precipitation reduced all porosities and permeabilities but did not obscure this grain-size dependence; and (3) dissolution enhanced this grain-size dependence because fluid flow and associated dissolution were concentrated in the most permeable, coarsest-grained sediments. Consequently, Ferron outcrop stratigraphy can provide useful clues to fluid-flow patterns in other deltaic formations, despite its complex diagenetic history.

Permeability Anisotropy

Anisotropy is a variable that needs to be considered in fluid-flow modeling. It is also a much broader petrophysical concern because anisotropy can be caused by either mineral alignment (for example, platy, subhorizontal clay minerals) or by microfractures (usually one set

of vertical microfractures), because both affect fluid flow, and because large-scale anisotropy can be estimated by seismic methods. Permeability anisotropy at the parasequence level is obvious in the reservoir modeling studies (see Chapter 10, Reservoir and Fluid-Flow Modeling of the Ivie Creek Case-Study Area). Based on abundance of finely laminated sediments, particularly in the bedsets of the Kf-1 parasequence set, substantial permeability anisotropy might also be expected at the scale of individual core plugs.

The Amoco suite of anisotropy petrophysical measurements for Kf-1 and Kf-2 was undertaken on 38 3-D sample sets, consisting of adjacent horizontal, vertical, and 45 degree diagonal measurements. Figure 8-17 compares permeabilities within these sets. As expected, vertical permeabilities are lower than horizontal ones, but this difference is surprisingly small: usually a factor of two or less, in contrast to the more than four orders of magnitude variation in permeability attributable to porosity variations. This magnitude of anisotropy is comparable to the impact on permeability of changing porosity by only about 1 percent. Indeed, companion samples often vary in porosity by this much due to local heterogeneity. Porosity variations among samples of an individual 3-D set can be corrected for, by normalizing each set of permeability data to an equivalent effective porosity, but this correction accomplishes only minor improvement. Diagonal permeabilities are not significantly higher than horizontal permeabilities.

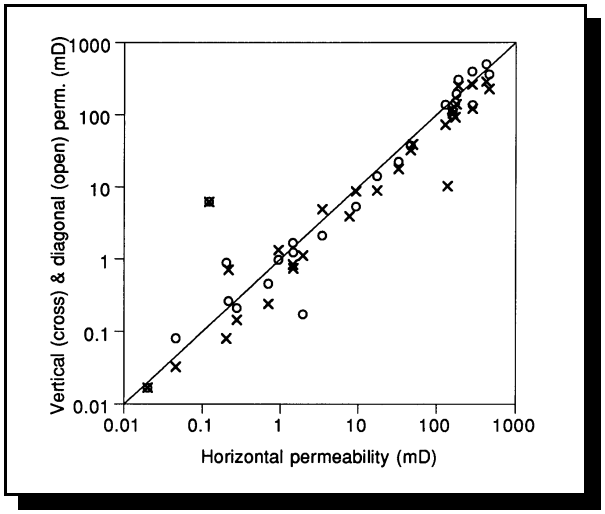


Figure 8-17. Relationship between horizontal permeability and both vertical (crosses) and diagonal (open circles) permeability, based on 3-D sets of adjacent core-plug samples from Kf-1 and Kf-2.

The subtlety of plug-scale permeability anisotropy means that it can be neglected in reservoir modeling. This anisotropy is much less than is often determined for shaly sands from other regions, probably because Ferron permeabilities are associated with leaching-induced intergranular secondary porosity, rather than mechanical compaction-induced primary porosity. Ferron permeability, like Ferron velocity, lacks the sensitivity to clay content that is characteristic of primary porosities.

Implications for Estimating Amount of Exhumation from Velocity or Porosity Changes with Depth

Normal mechanical compaction and consolidation of siliciclastic sediments causes porosity to decrease and velocity to increase with increasing depth. If lithologies and pore pressures are relatively uniform laterally, then this process generates a characteristic pattern -- valid throughout a region--of porosity and velocity change with depth. Departures from this

characteristic pattern may indicate overpressures (Hottmann and Johnson, 1965), lithologic changes (Schlumberger, 1989; Japsen, 1993), or exhumation (Magara, 1976).

Various procedures have been proposed for using velocity/depth or porosity/depth patterns to estimate amount of exhumation at a well. All assume that uplift does not modify porosity or velocity. The Ferron sandstones are a dramatic illustration of the problem: all of their major velocity and porosity changes with depth (figure 8-12) result from processes--pressure release and/or dissolution of carbonate cement--ignored by traditional exhumation estimation techniques. Both processes accelerate as beds are brought closer to the ground surface, causing the amount of erosion and exhumation to be substantially underestimated. Focusing on shales does not avoid the problem; shales also undergo carbonate cementation and dissolution, as well as pressure-dependent velocities. Furthermore, exhumation of impermeable shales may sometimes generate abnormally low fluid pressures (Neuzil and Pollock, 1983), presumably resulting in velocity change.

Conclusions

This petrophysical study challenges the reliability of a common assumption: that geophysical properties and relationships observed in outcrop are representative of those in the deep subsurface. We find that the processes that generate outcrop exposures--uplift, erosion, and exhumation--can overprint patterns of velocity, porosity, and permeability developed in the subsurface.

Thin-section examinations showed that little, if any, primary porosity appears to remain in any of the Ferron outcrop samples. A complex diagenetic history culminated with the development of substantial secondary porosity as a result of carbonate dissolution. This secondary porosity is intergranular, not vugular or crack porosity. Petrophysical measurements confirm that decreasing carbonate content is strongly associated with porosity increase. Surprisingly, clay-mineral content has only a minor direct correlation with petrophysical properties.

Ferron porosities in deep wells suggest that pre-exhumation porosities were 4±4 percent. Porosity increase accelerated as the Ferron was progressively exhumed. By the time portions of the Ferron reached near-surface depths, average porosity had increased to 9.3±2.4 percent, and outcrop samples are even more porous (13.0±0.6 percent). This pattern of secondary porosity development differs from the diagenetic pattern commonly observed in deeply buried, but not exhumed, sandstones: growth of secondary porosity below the depths at which primary porosity is destroyed. The Ferron Sandstone, like sedimentary rocks in several other foreland basins, appears to demonstrate the impact of meteoric flux on late-stage diagenetic history. Upward meteoric flux provides a combination of high flow rates and cooling-induced increase in calcite solubility that is probably responsible for late-stage carbonate dissolution within the Ferron Sandstone. The patterns of secondary porosity development seen in our study suggest that upward flow along the Ferron beds is pervasive, and that this meteoric flow extends to depths of about 6,000 feet (2,000 m).

Whenever exhumation causes development of secondary porosity, then velocity decrease is also expected, because velocity is primarily dependent on porosity. Depth-dependent changes

in both velocity and porosity are observed in geophysical well logs of the Ferron Sandstone. Cross plots indicate that the velocity drop at depths of less than 1,800 feet (<550 m) is even stronger than expected from the associated porosity drop. Core-plug measurements indicate that the pressure dependence of velocity accounts for these log-based observations of changes in velocity and in velocity/porosity relationship. The lowest-pressure core-plug measurements have a velocity/porosity pattern similar to that for shallow (less than 1,800 feet [<550 m]) log data, and the highest-pressure core measurements are consistent with deep log data. We conclude that pressure decrease associated with exhumation has opened microcracks; laboratory velocity measurements at high pressure reverse this process.

Log analysts often generalize that sonic logs do not see secondary porosity, particularly vugular porosity in carbonates and fracture porosity. Among sandstones, however, the most common type of secondary porosity is that encountered by the Ferron logs, intergranular secondary porosity created by dissolution. Ferron core-plug velocity measurements and sonic logs clearly see this secondary porosity, responding in the same manner as for primary intergranular porosity. Comparison of whole-core and log measurements at drill hole IC-3 showed consistency for both density and velocity, indicating that these two measurement scales are equally sensitive to microfractures.

Permeability in the Ferron Sandstone is strongly dependent on porosity. The effect of mineralogy on permeability is indirect, associated with the influence of grain size on porosity evolution. Grain size has affected the entire diagenetic history of the Ferron Sandstone: the coarsest sands retained highest permeabilities during compaction and cementation, and they experienced the greatest permeability enhancement during late-stage expansion of secondary porosity. At the scale of core plugs, permeability anisotropy is relatively minor.

CHAPTER IX
STATISTICAL ANALYSIS, IVIE CREEK CASE-STUDY AREA

Ann Mattson, M.A. Chan, C.B. Forster, and P.B. Anderson

Introduction

Geostatistics are a set of tools that offers a method to describe spatial continuity (Isaaks and Srivastava, 1989). These tools include the semi-variogram that quantifies spatial distribution and various stochastic methods to populate data within a volume (Srivastava, 1994). Traditional statistics deal only with data populations as a whole, and do not take spatial distribution into account. In geology it is critical to understand not only the summary statistics of a population, but also its spatial distribution. Stochastic methods rely on a set of rules to generate data distributions such that each output obeys the summary statistics of the input data.

The geostatistical objectives of the Ferron Sandstone outcrop analog project are: (1) derive relationships between permeability and geology, (2) establish an architectural framework based on facies maps, (3) study the spatial distribution of various parameters, and (4) map variables in both a stochastic and deterministic manner.

Previous geostatistical research can be broken down into three broad categories with some overlap: (1) outcrop analog studies, (2) subsurface studies, and (3) theoretical studies. Outcrop analog studies typically extend into the subsurface by utilizing drill-hole data. Subsurface studies may also include new theories for distributing model parameters within a volume. Theoretical studies usually make reference to field applications.

Some important recent outcrop analog studies that used geostatistical techniques similar to the Ferron Sandstone project include: (1) the San Andres Formation, an upward shoaling carbonate ramp deposit (Grant and others, 1994); (2) the Gypsy Sandstone, a meandering river deposit (Doyle and Sweet, 1995); (3) the Hawkesbury Sandstone, a braided stream deposit (Liu and others, 1996); (4) a fluvial-deltaic, Yorkshire cliff face that was mapped deterministically and stochastically as input to groundwater transport modeling (McKenna and Poeter, 1994); (5) sandstone-body and shale-body dimensions for the Salt Wash Member of the Morrison Formation (Robinson and McCabe, 1997); and (6) Chaunoy field modeling based on sequence stratigraphy, geostatistical simulations, and production data (Eschard and others, 1998). These studies take an approach similar to the Ferron project, but none of them continue through to reservoir simulation or incorporate as many different scales of data (petrographic to outcrop and subsurface) as this study.

Various subsurface geostatistical modeling studies have predicted heterogeneity, facies, and architecture distribution between wells by integrating geologic data with wireline and seismic data. These subsurface studies were able to: (1) match the production history of oil and gas wells (Begg and others, 1994; and Dull, 1995), (2) pick in-fill well locations for existing fields (Hohn and others, 1993a, b), (3) improve model accuracy by incorporating widespread "soft" data such as seismic (Bashore and others, 1987), and (4) predict interconnectedness of sand bodies (Fielding and Crane, 1987; and Fogg, 1989).

Theoretical overviews that summarize much of the development of geostatistical literature include: (1) Gorell (1995), a very general overview; (2) Srivastava (1994), on geostatistical methods; and (3) Isaaks and Srivastava (1989), a comprehensive text on applied geostatistics. Research papers that compare existing methods or develop new methods include: (1) Rhea and others (1994), kriging compared to conditional simulation as a tool to trace long distance oil migration within a sedimentary basin; (2) MacDonald and Aasen (1994), developed a truncated Gaussian field with a linear trend to predict facies tract distribution in shoreface reservoirs; and (3) Liu and others (1996), developed an application of the Levy-stable method to distribute highly variable permeability data without dividing the reservoir into facies.

The Ferron Sandstone project pulls data from outcrop, subsurface, and microscopy and integrates it through geostatistical analysis into a reservoir simulation. Other studies do not integrate all of these various data types. In particular, none of the previously cited studies used subsurface data that was close to the outcrop locale, and all the studies except Liu and others (1996) mapped a single outcrop. By incorporating more data sources we sought to better quantify reservoirs heterogeneity. Possessing the ability to improve reservoir characterization allows the oil and gas industry to: (1) identify reservoir trends, (2) increase recoverable reserves, (3) reduce development costs, and (4) increase production rates.

Characterization of Geology and Permeability

Variations in facies, stratigraphic thickness, sedimentary structures, and permeability data were quantified through statistical and geostatistical analysis. The statistical variability of these parameters was needed to define individual petrophysical units within the Ivie Creek case-study area, and to predict the three-dimensional distribution of each unit. The statistical modeling is an important step to develop procedures for "scaling up" from the observational scale to the typical reservoir scale.

Characterization work was devoted to: (1) displaying in illustrations the deterministic permeability of the Kf-1-Iv[a] bedset, (2) testing the permeability data set for log-normality, (3) analyzing permeability controls for the Kf-1-Iv[a] bedset and the Kf-2-Iv-a, -b, -c parasequences (hence referred to as Kf-2 parasequences), and (4) defining the architecture of the units. Statistical analysis of this work required quantification of field data (figure 9-1) and synthesis of defined facies.

Methods

The UGS database, composed of geological and petrophysical megascopic observations within the defined facies, was used to generate graphical representations showing the spatial distribution of sedimentary structures, megascopic grain size, sand/shale ratios, and facies. Statistical analyses of geological characteristics included: pie charts and relative percentage bar plots. Statistical analyses of permeability data included: (1) summary statistics (mean, median, and others) for each parasequence and facies type, (2) histograms, (3) cumulative probability plots, (4) cross plots, and (5) semivariograms (Mattson, 1997).

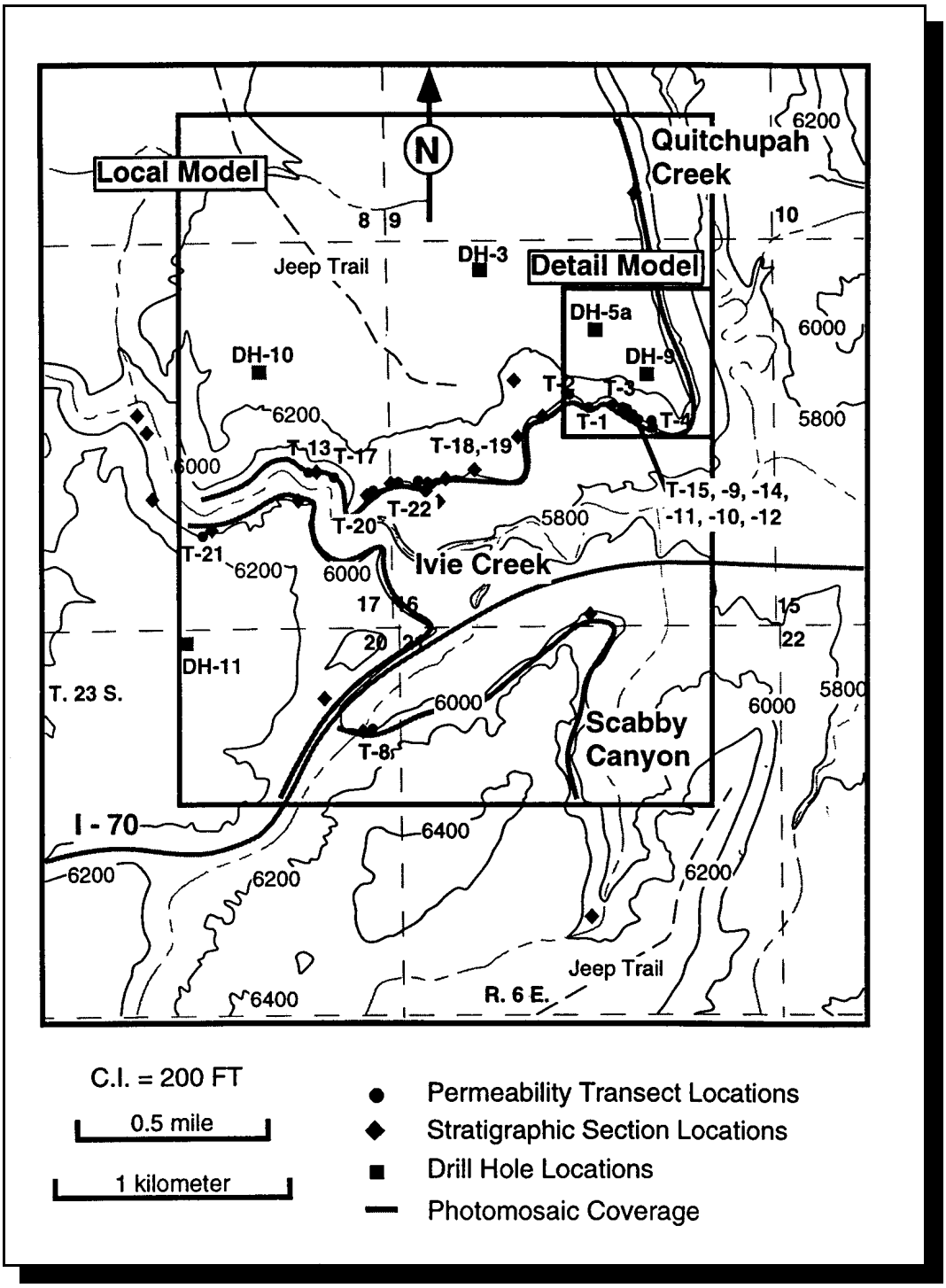


Figure 9-1. Ivie Creek case-study area, database locations.

Summary statistics and pie charts comprise the geologic information used to quantify lithologic characteristics. The summary statistics include percentage of features observed within a facies, bedset, or a parasequence. These percentages are calculated by summing the net footage of each feature through the parasequence using unit thickness and structure percent. Pie charts provide a graphical representation of the summary data. The parasequence sets are analyzed separately to compare the fluvial-dominated system (Kf-1-Iv[a] bedset) to the wave-modified system (Kf-2 parasequences).

The Lilliefors test was used to analyze the permeability data set for log-normality since it could handle the large number of data points involved, and is considered to be one of the more robust tests available. Of the 41 categories (combinations of facies, sedimentary structure, and average grain size) that permeability data were divided into, only nine categories met the criteria of log normality. Categories failed due to two factors: (1) the large number of data points constrain the cumulative probability curve to such a degree that even small deviations away from a log-normal distribution will result in test failure; and (2) the limits of the permeability instruments create step-function increases in the cumulative probability curves at 0.5 and 2.0 md. The influence of the second factor was evident when the Kf-1-Iv[a] bedset permeability data was modeled to remove instrument effects.

In order to perform reservoir simulation of a three-dimensional facies model, the model must be populated with petrophysical data. The approach taken by this project, populated each facies with the geometric mean of the permeability data for that facies type. The geometric mean of the permeability data was chosen because it is believed to reflect the effective permeability of units where bedding and fluid flow are in non-orthogonal directions.

Kf-1-Iv[a] Bedset Geologic Summary

The fluvial-dominated Kf-1-Iv[a] bedset thins and becomes more distal toward the northwest. Clinoform beds in this bedset have inclinations which vary from 28E proximally to 0E distally. Within these clinoform bodies, four facies were defined based on similarities in average grain size, sedimentary structure, lithology, bed size, angle of inclination, and position within a clinoform bedform (figure 9-2, table 9-1). The four clinoform facies are (see Chapter VII, Geologic Framework of the Ivie Creek Case-Study Area): proximal, medial, distal, and cap. The change from clinoform proximal to clinoform distal facies represents a decrease in depositional energy within an individual bedform. The change is characterized by decreases in: sandstone to shale ratio, average grain size, bed thickness, and inclination angle between beds. Sedimentary structures pass from low-angle,

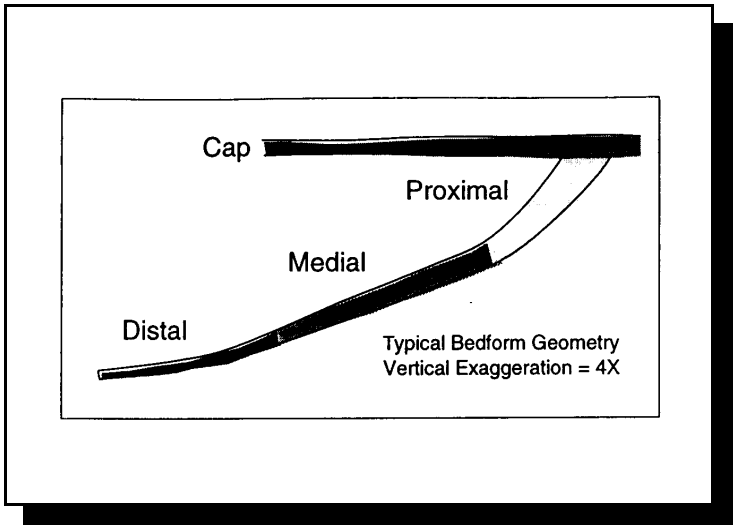


Figure 9-2. Typical clinoform facies distribution. The diagram has no scale.

cross-stratified and trough cross-stratified beds to ripple cross-laminated and horizontal beds down dip within a clinoform body. In contrast, biostructures increase in abundance as depositional energy decreases. The clinoform cap facies represents a laterally-continuous zone of reworked sediment that truncates the tops of the clinoform bedforms.

Table 9-1. Clinoform facies summary (Mattson, 1997).

Property*		Cap**	Proximal	Medial	Distal
Lithology		ss - 99% other - 1%	ss - 100%	ss - 94%, sh - 5% other - 1%	ss - 62%, sh - 31%, st - 7%
Grain Size Sandstone		mfg to vfg (fvf 49%)	med to fvf (fin 49%)	mfg to vfg (fvf 36%)	mfg to vfg (vfg 39%)
Sedimentary Structures	Major	hor - 30%, lac - 28%, bio - 24%	lac - 60%	hor - 80%	hor - 59%
	Minor	tro - 15%	hor - 26%, tro - 10%	rip - 7%, bio - 6%	rip - 21%, bio - 16%
Bed Thickness		thk to mtn (thk - 35%)	ver to mtn (tkm - 28%)	thk to lam (med - 33%)	tkm to tnl (tnl - 49%)
Induration		wel to mfr (wel - 60%)	wel to mfr (wlm - 68%)	wel to fri (wel - 38%)	wel to fri (mfr - 37%)
Angle of Inclination†		0 to 2E	10.0 ± 0.76E	6.0 ± 0.55E	2.1 ± 0.30E
Deposition		Truncates & overlays tops of clinoform packages, represents an eroded & reworked delta top	Highest energy, proximal to sediment input source, localized basin in open bay with some wave influence	Moderate energy, usually transitional between proximal & distal	Lowest energy, continuous with medial, deepest water, traces distally into prodelta facies

* Properties cutoff at 5 percent; this does not apply to properties angle of inclination nor deposition.
** All abbreviations found in Appendix B, field methods, page B-2.
† Values reported as arithmetic mean ± 95 percent confidence limit; this does not apply to clinoform cap.

Low-angle, cross-stratified sedimentary structures are common within the Kf-1-Iv[a] bedset. These beds are composed of fine- to medium-grained sandstones, and the laminae are inclined at a few degrees in the up-dip direction to the bedform bounding surfaces. These structures are found primarily in the clinoform proximal facies, and are believed to be related to development of a fair-weather, swash-bar along the actively prograding part of the delta front. Similar features have been described in coarse-grained Gilbert-type deltas in southern Italy (Massari, 1996) where they are thought to be formed by anti-dunes. The energy level of the Ferron system for Froude numbers at depths of a few tens of meters for the clinoforms do not appear to be high enough to cause anti-dunes, thus the exact origin of these features is unknown. However, they represent a higher energy portion of the system.

To characterize the clinoform beds, measurements were taken of: (1) the overall length of the clinoform body, (2) the inclination angle from datum at quartiles along the body, and (3) the vertical thickness at quartiles along the bedform (figure 9-3A). Some interesting observations arise from the quantitative analysis of the inclination angle data. Upon visual inspection, inclination angles appear to be the same for the Ivie Creek amphitheater and Quitchupah Canyon for a given clinoform facies. However, when the inclination angles are averaged, the initial angles found in Quitchupah Canyon (~14E) are steeper than those in the amphitheater (~11E).

The other parameters necessary to create a typical clinoform shape are the length and thickness of the body. Clinoform lengths range from 40 feet (12.2 m) to greater than 2,000 feet (610 m). A plot of thickness as a function of quartile shows that the first quartile is the thickest part of the clinoform (figure 9-3B). Quartile thickness as a function of clinoform facies decreases from proximal facies to distal facies. The thickness data combined with the inclination angle data present a two-dimensional picture of the geometry of a typical clinoform.

Clinoform facies can also be described as a function of position within a clinoform body. For the clinoform bodies analyzed, the dominant facies at the initial position (see figure 9-3a) in a bedform are proximal (~ 55 percent) and medial (~ 45 percent). At the final position (see figure 9-3a), the dominant facies is distal (~ 60 percent). The facies percentage at each quartile can provide rules to populate clinoform bodies with facies data.

When clinoform facies, permeability, and geometric data are brought together, a “typical clinoform” is constructed. This is a two-dimensional building block that may be used to create a reservoir simulation model based on clinoform facies.

Of the sections measured within the Kf-1-Iv[a] bedset, the clinoform facies are broken down as follows (in percentage of the thickness in the measured sections): distal facies ~ 50 percent, medial and proximal facies ~ 20 to 25 percent each, and cap ~ 6 percent (figure 9-4). In terms of lithology, 80 percent of facies are sandstone. The clinoform cap, proximal, and medial facies are almost 100 percent sandstone, and the distal facies is more than 60 percent sandstone with the balance composed of shale and siltstone (figure 9-4). In terms of average megascopic grain size, sub-equal parts of the units are very fine-grained, fine- to very-fine grained, and fine-grained. Lesser percentages are medium- to fine-grained and medium-grained. The average grain size of each facies decreases as the facies becomes more distal (figures 9-5 and 9-6). The sedimentary structures observed are dominated by horizontal beds which equal about 50 percent of all the structures. The proximal facies is dominated by low-angle, cross-stratified beds; the medial facies by horizontal beds; and the distal facies by horizontal beds, but with an increased volume of ripple cross-laminated beds and bioturbation (figures 9-5 and 9-6). The range of bed sizes varies widely within each facies, but overall, the bed size decreases distally (figure 9-7). Induration also varies widely within each facies, but overall, the degree of cementation decreases distally (figure 9-7).

Facies panels (facies, sedimentary structures, and grain sizes) for the Ivie Creek amphitheater were used to generate a deterministic distribution of permeability. Each of three panels was divided into 4 feet by 4 feet (1.2 x 1.2 m) blocks, and a number code was assigned for each attribute (for example clinoform proximal [CP] facies = 2). These attribute values were entered into a computer with accompanying spatial coordinates. The rules for assigning permeability values to each block were calculated from the transect data. Geometric mean permeability values were calculated for all

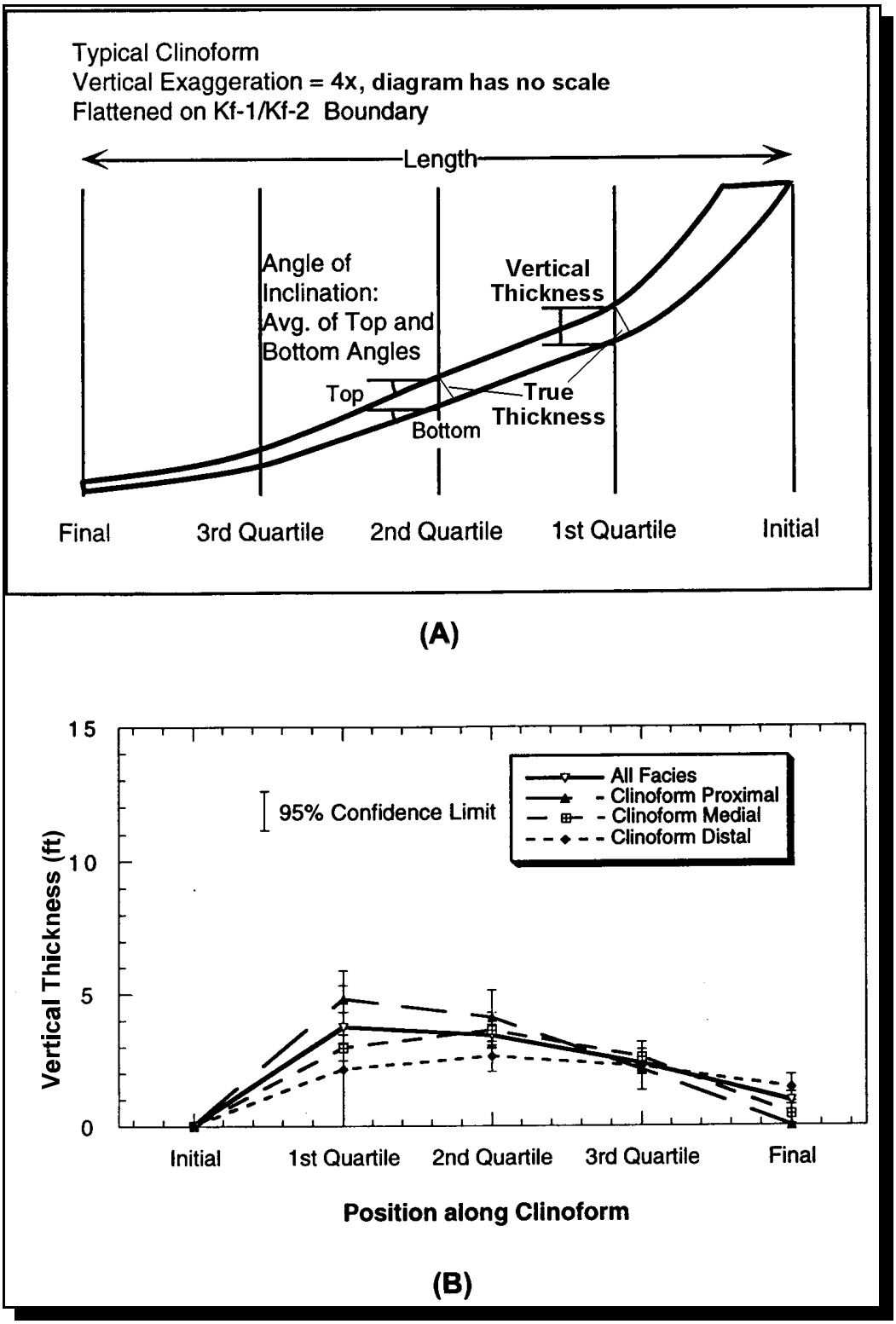


Figure 9-3. (A) Diagram of measurements used for clinoform characterization. (B) Bedform thickness vs. position along clinoforms in the Kf-1-Iv[a] bedset, Ivie Creek amphitheater.

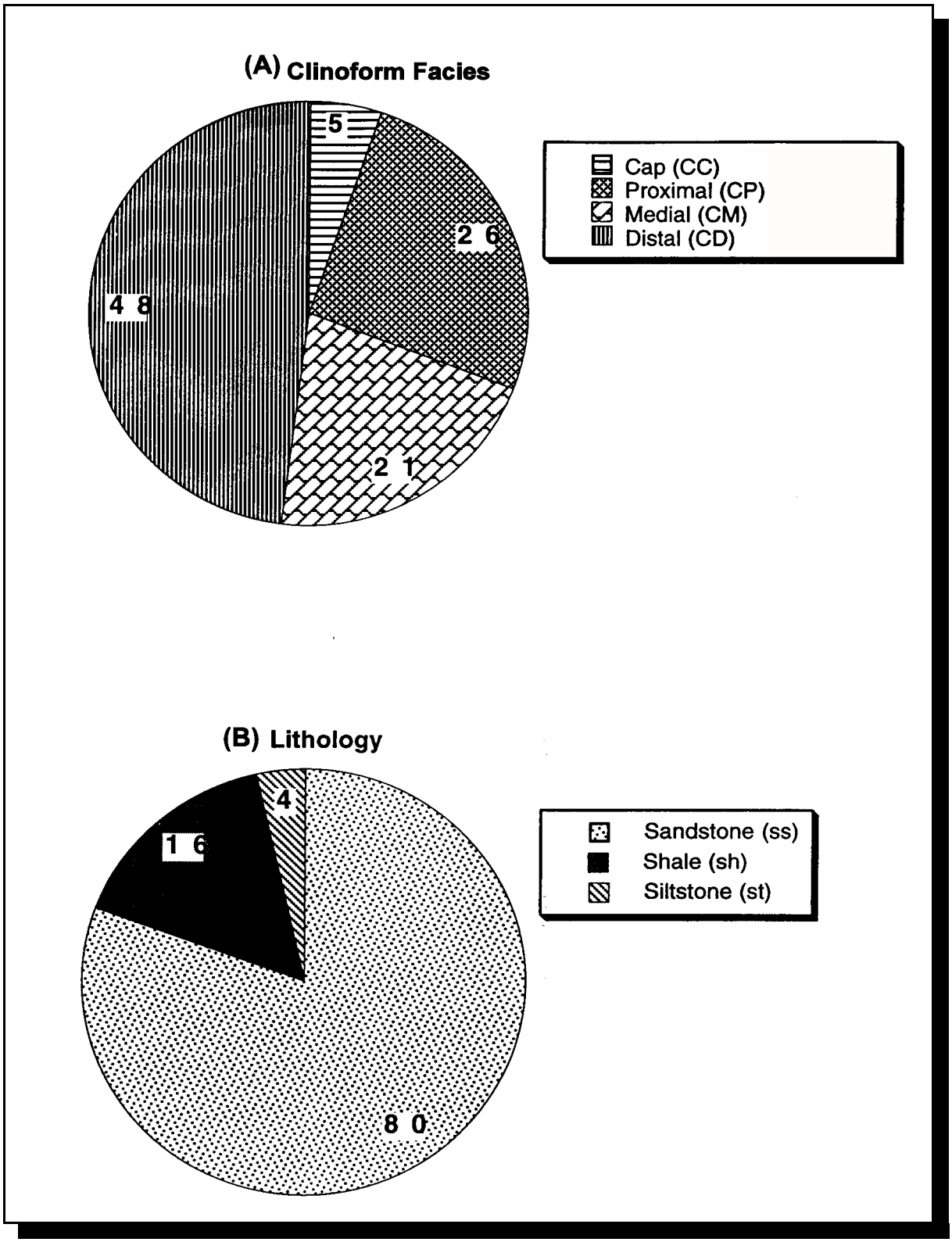


Figure 9-4. Kf-1-Iv[a] bedset detail model, summary of: (A) clinoform facies, and (B) lithology. Numbers in sectors are percentage of each component.

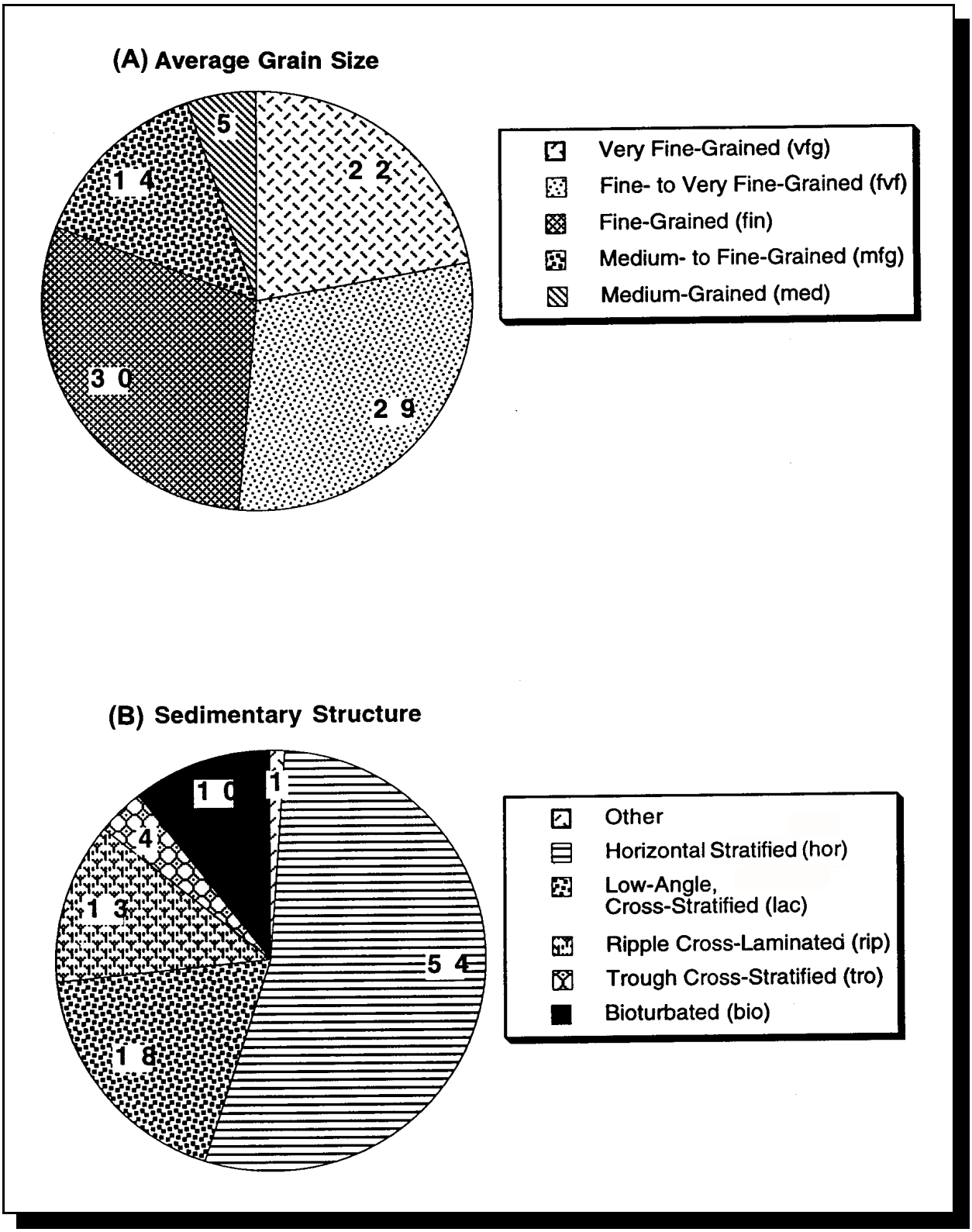


Figure 9-5. Kf-1-Iv[a] bedset detail model, summary of: (A) average grain size, and (B) sedimentary structure. Numbers in sectors are percentage of each component.

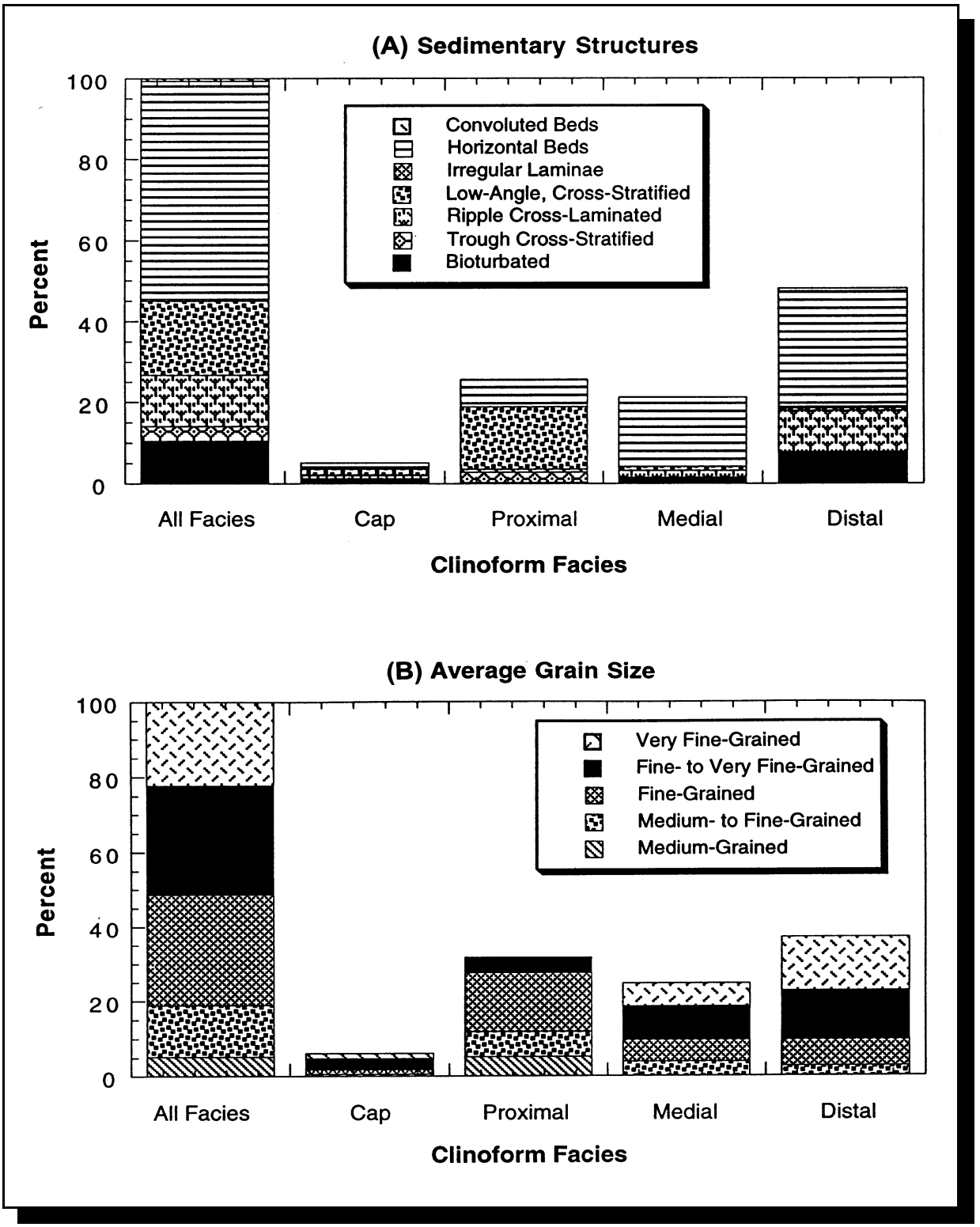


Figure 9-6. Statistical analyses of the clinoform facies from the Kf-1-Iv[a] bedset: (A) histogram showing relative frequency of sedimentary structure versus facies, and (B) histogram showing grain-size distributions (megascopic observations) in each facies.

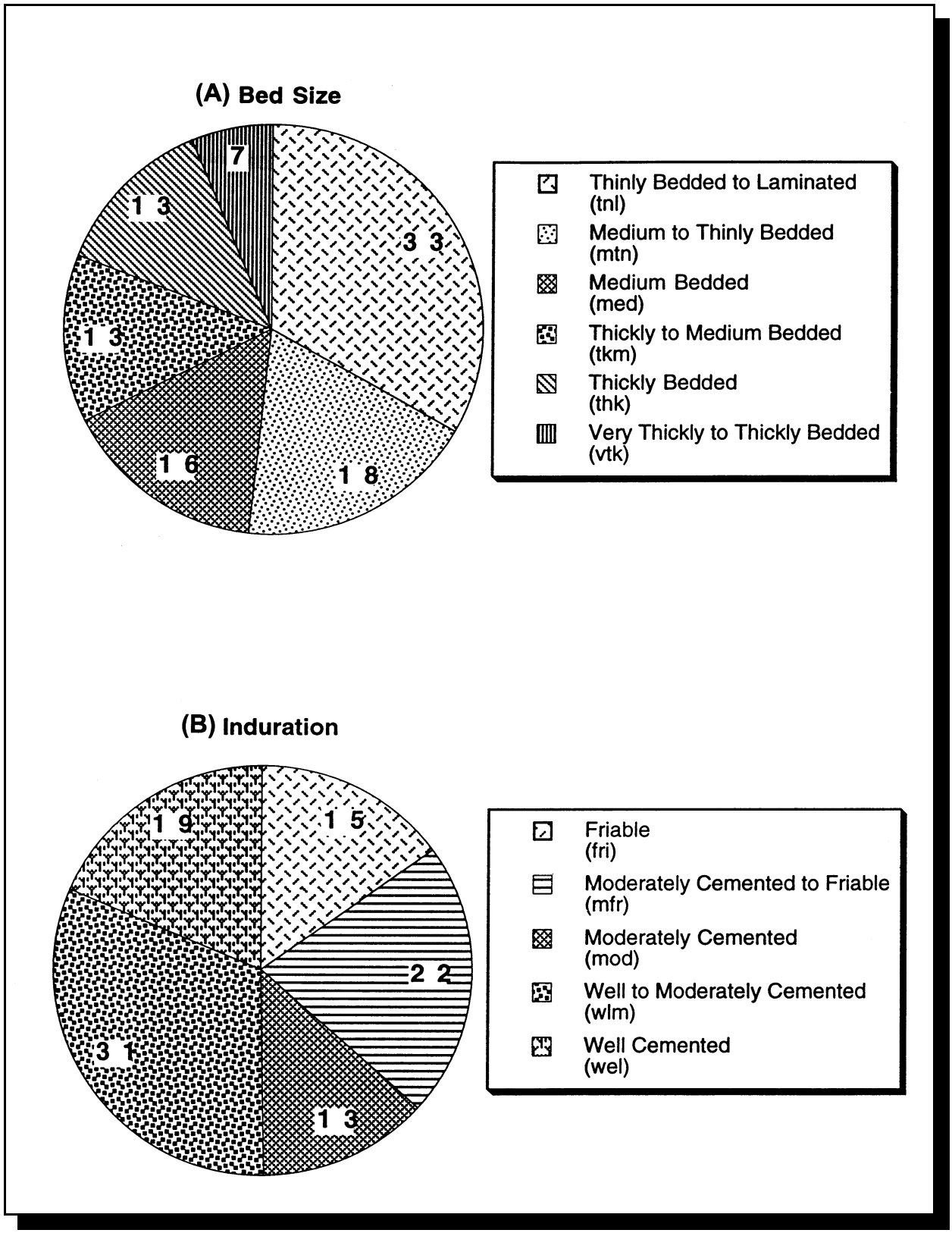


Figure 9-7. Kf-1-Iv[a] bedset detail model, summary of: (A) bed size, and (B) induration.

known combinations of facies, sedimentary structures, and grain size. The results of statistical analyses of sedimentary structures and grain sizes were applied to the four facies assigned to the clinoforms of the Kf-1-Iv[a] bedset (see figure 7-10, Chapter VII, Geologic Framework of the Ivie Creek Case-Study Area). Each clinoform facies in the Kf-1-Iv[a] bedset is characterized by a particular suite of geologic features as shown in the summary plots of figure 9-6 and the cross sections on figures 7-10B and C in Chapter VII.

Kf-2 Parasequence Set Geologic Summary

The wave-modified Kf-2 parasequences are composed of three prograding parasequences and described by 14 facies. The oldest parasequence, Kf-2-Iv-a, is primarily composed of lower and middle shoreface facies. The very fine-grained sandstones are most common (38 percent of total sandstones), and also have the highest degree of bioturbation (51 percent). The middle parasequence, Kf-2-Iv-b, is dominated by the middle shoreface facies, but has a significant proportion of distributary-mouth bar facies. The sandstones are mostly fine-grained (37 percent) and exhibit a lesser degree of bioturbation than the Kf-2-Iv-a. The youngest parasequence, Kf-2-Iv-c, is dominated by bay-fill facies, but also contains the highest percentage of upper shoreface and foreshore facies. These near-shore sandstones have the coarsest grain sizes, ranging up to medium-grained. Horizontal stratification is dominant over bioturbation. These properties, as measured over the limited region of the Ivie Creek case-study area, support the hypothesis of a progradational system.

A wider range of facies is used to describe Kf-2 parasequences than the Kf-1-Iv[a] bedset. In a wave-modified delta, the marine facies range from prodelta to foreshore (figures 9-8 and 9-9). The transition from prodelta to foreshore is characterized by increases in sandstone to shale ratio, average grain size, bed size, and degree of cementation. All of these facies exhibit a fairly high degree of bioturbation, about 50 percent, but the sedimentary structures range from horizontal and ripple cross-laminated in the prodelta to trough cross-stratified in the upper shoreface. The distributary-mouth bar facies is almost 100 percent medium- to fine-grained sandstone, dominated by trough cross-stratification. The beds tend to be thick and well to moderately cemented. In contrast, the highly bioturbated distal facies is fine-grained sandstone and siltstones. Channels are present in the meander-belt and the distributary channel facies. These facies are predominantly trough cross-stratified, medium- to fine-grained sandstone that are relatively thick bedded and well cemented. The marginal marine facies include the bay-fill and bayhead delta. These facies are heterolithic with a high percentage of fine-grained sandstone that is bioturbated and horizontally bedded. The nonmarine facies include the coastal plain and swamp units, with the diagnostic presence of coal. In comparison to the Kf-1-Iv[a] bedset, Kf-2 parasequences have: (1) lower percent shale (figure 9-8), (2) coarser average grain size (figure 9-10), (3) higher percentage of trough cross-stratification, (4) higher degree of bioturbation (figure 9-10), and thicker bed size and less well cemented (figure 9-11).

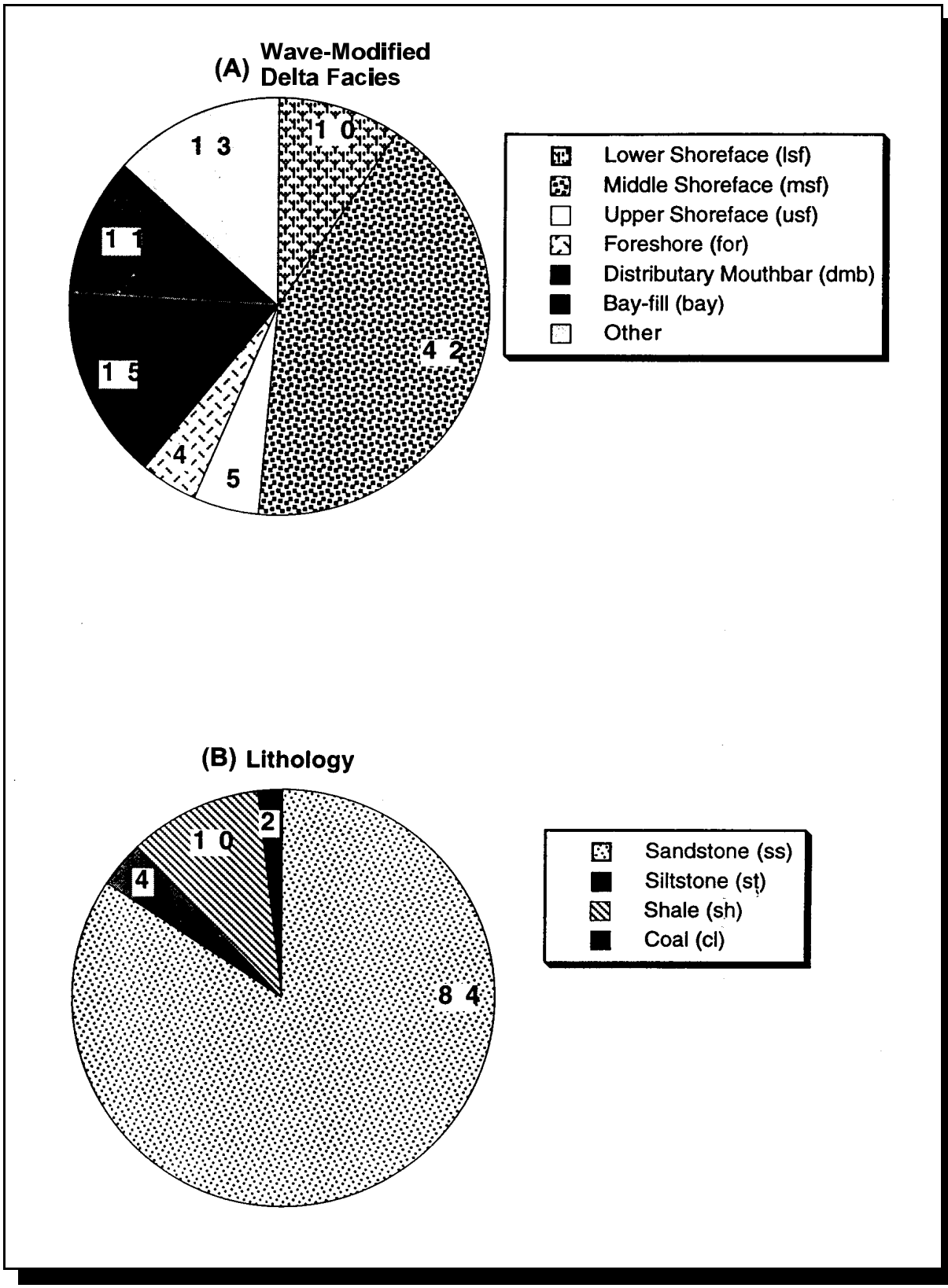


Figure 9-8. Kf-2 local model, summary of: (A) wave-modified delta facies, and (B) lithology.

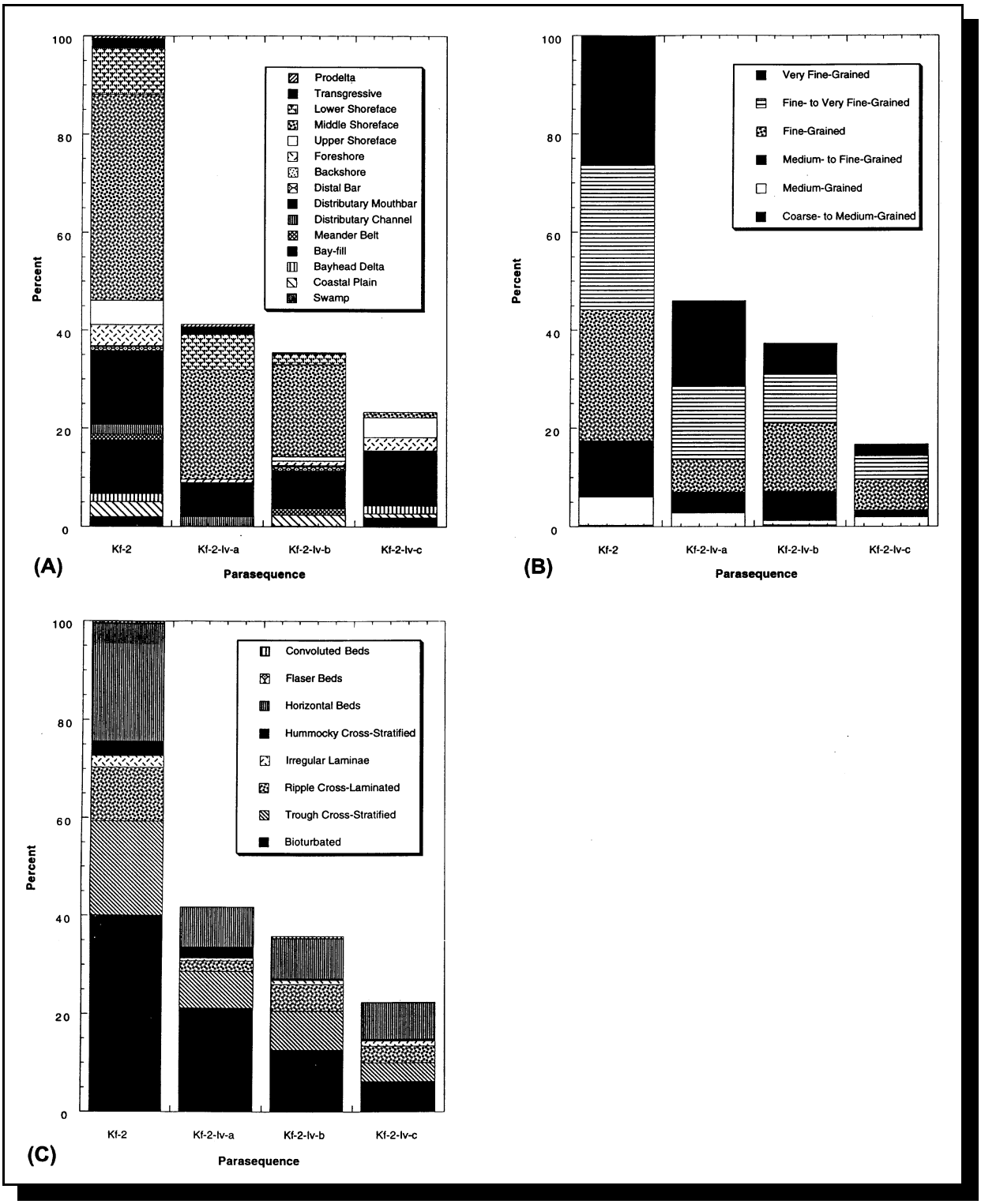


Figure 9-9. Statistical analyses of the Kf- 2 parasquence set as a whole and the three parasequences within it (Kf-2-Iv-a, b, and c), Ivie Creek case-study area: (A) histogram showing facies distribution, (B) histogram showing grain-size distributions (megascopic observations), and (C) histogram showing relative frequency of sedimentary structures.

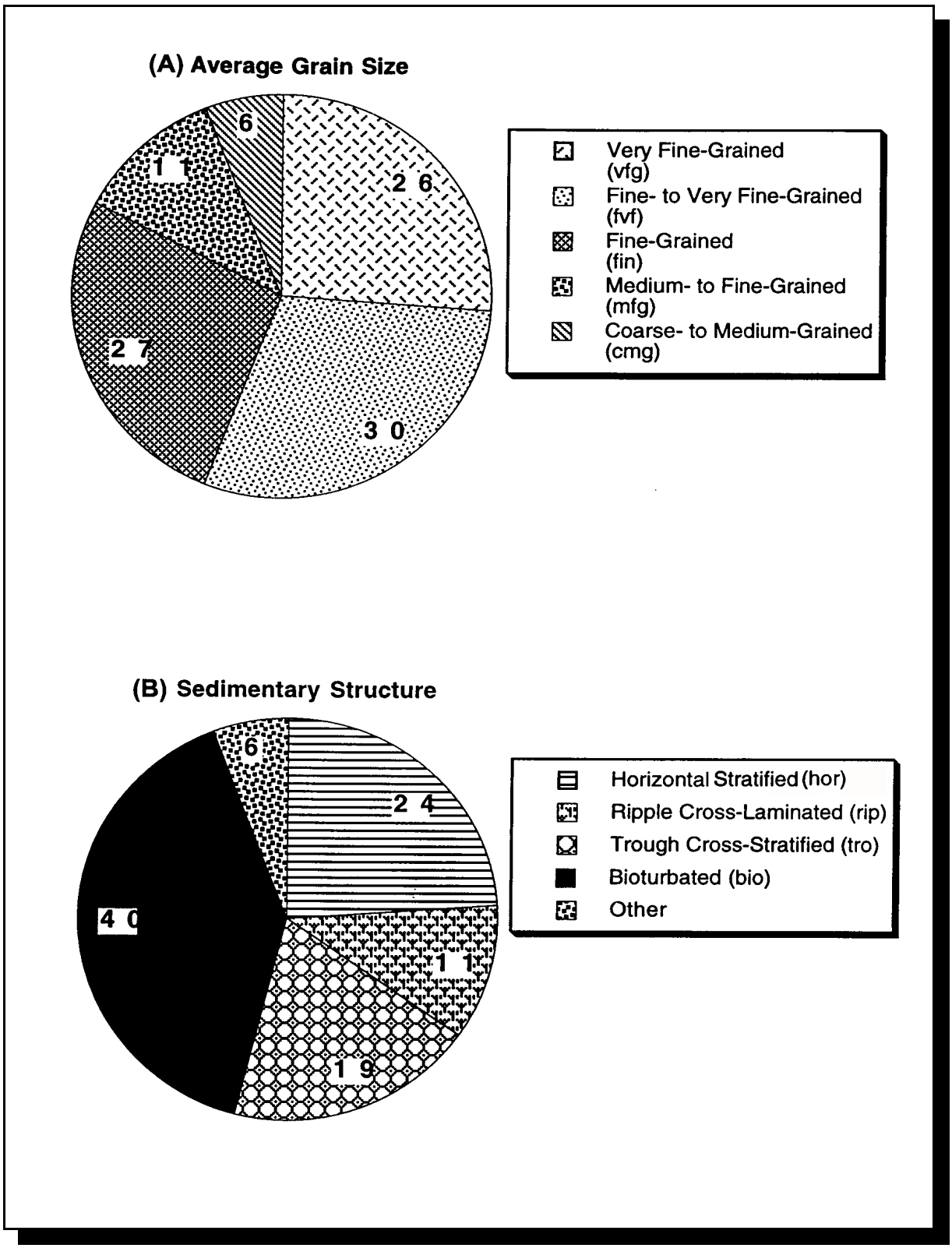


Figure 9-10. Kf-2 local model, summary of: (A) average grain size, and (B) sedimentary structure.

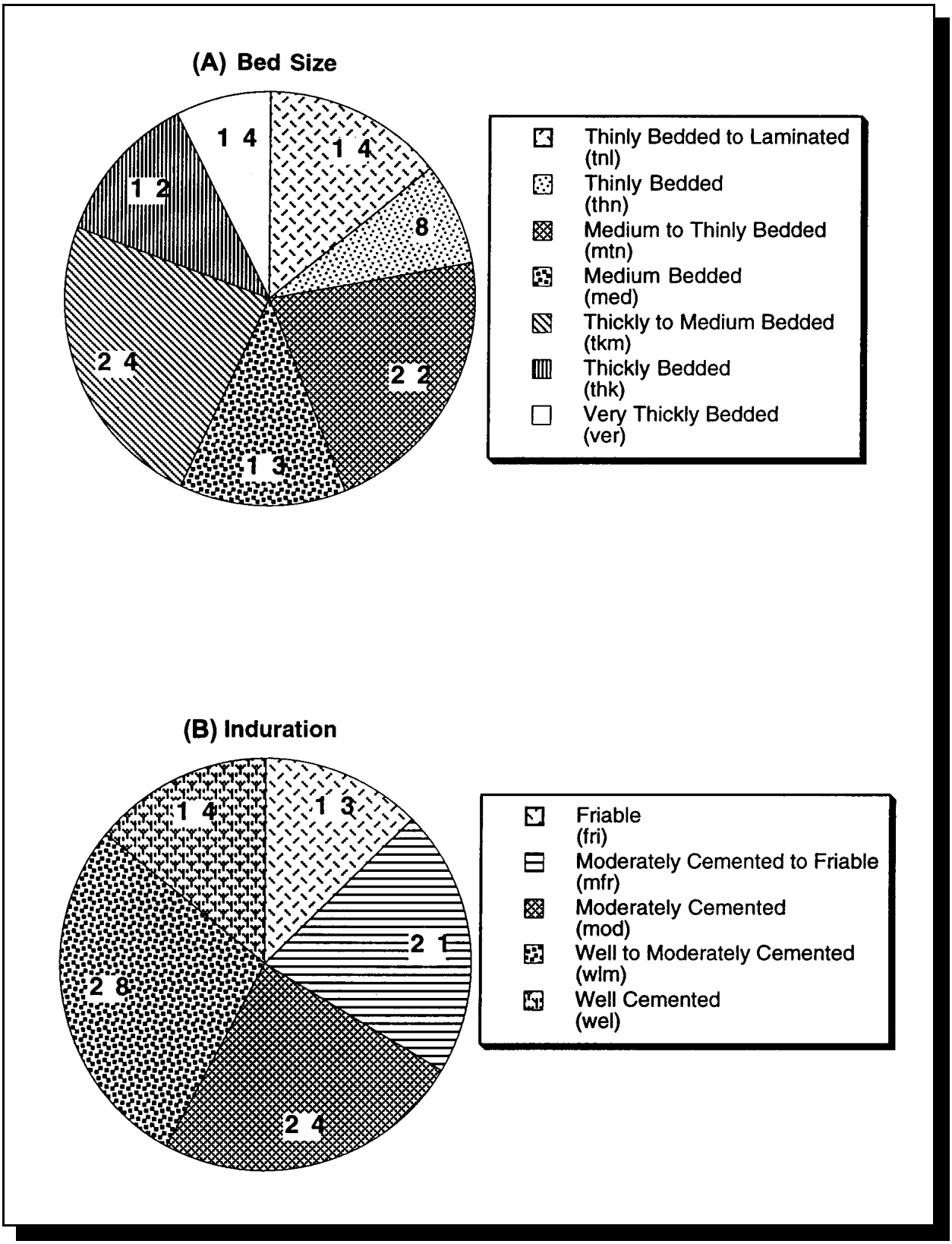


Figure 9-11. Kf-2 local model, summary of: (A) bed size, and (B) induration.

Permeability Summary

Two objectives of the permeability analysis were to derive relationships between geology and permeability and to describe the spatial distribution of permeability. Analysis of the permeability relationships is presented in statistical cumulative probability plots and cross plots. The cross plots analyze arithmetic and geometric means, coefficient of variation for each mean, median, range, and count for permeability as a function of parasequence, parasequence set, facies, and other geologic features. Cumulative probability curves of the permeability data provide distribution functions to use in simulation models and to visually analyze normal or log-normal behavior. Cross plots show the relationship between two independent parameters such as percent sandstone and average permeability. Separate analyses of the fluvial dominated Kf-1-Iv[a] bedset and the wave-modified Kf-2 system allow comparison of these deltaic members.

Kf-1-Iv[a] Bedset Permeability Analysis

In general, the permeability values for the Kf-1-Iv[a] bedset are quite low compared to permeabilities of reservoir facies in many oil and gas production fields due to the very fine-grained nature of the Kf-1. The highest permeability values measured in the clinoform proximal facies are, on average, less than 50 md. This facies is described as having the highest depositional energy, coarsest average grain size, and lowest shale percentage. The coefficient of variation (coefficient of variation = standard deviation/mean) of permeability in the clinoform proximal and medial facies is about half that of the clinoform distal and cap facies, indicating a lower degree of variability relative to the mean. The clinoform proximal facies is the most important reservoir facies within the fluvial-dominated, Kf-1-Iv[a] bedset.

The lowest permeability values are measured in the clinoform distal facies, with most values below 5 md. This facies is described as representing the lowest depositional energy, finest average grain size, and highest shale percentage. The coefficient of variation of the geometric mean permeability of this facies is the highest, indicating a higher degree of variability relative to the mean. The clinoform medial facies is intermediate to these end members, with most values below 15 md. The clinoform cap has very few measurements, but averages 2 md.

Cross plots of mean permeability versus percent sandstone show a logarithmic increase in permeability with a linear increase in percent sandstone (figure 9-12). Regressions of the geometric mean and arithmetic mean of permeability with respect to percent sandstone have coefficients of determination (r^2) of 0.79 and 0.73 respectively. The coefficient of determination measures the proportionate decrease in the variability of y data points (percent sandstone) with the introduction of more x data points (permeability). This coefficient ranges between zero (no correlation between x and y) and one (perfect correlation between x and y) (Neter and Wasserman, 1974). These coefficients of determination indicate a strong relationship between percent sandstone and permeability.

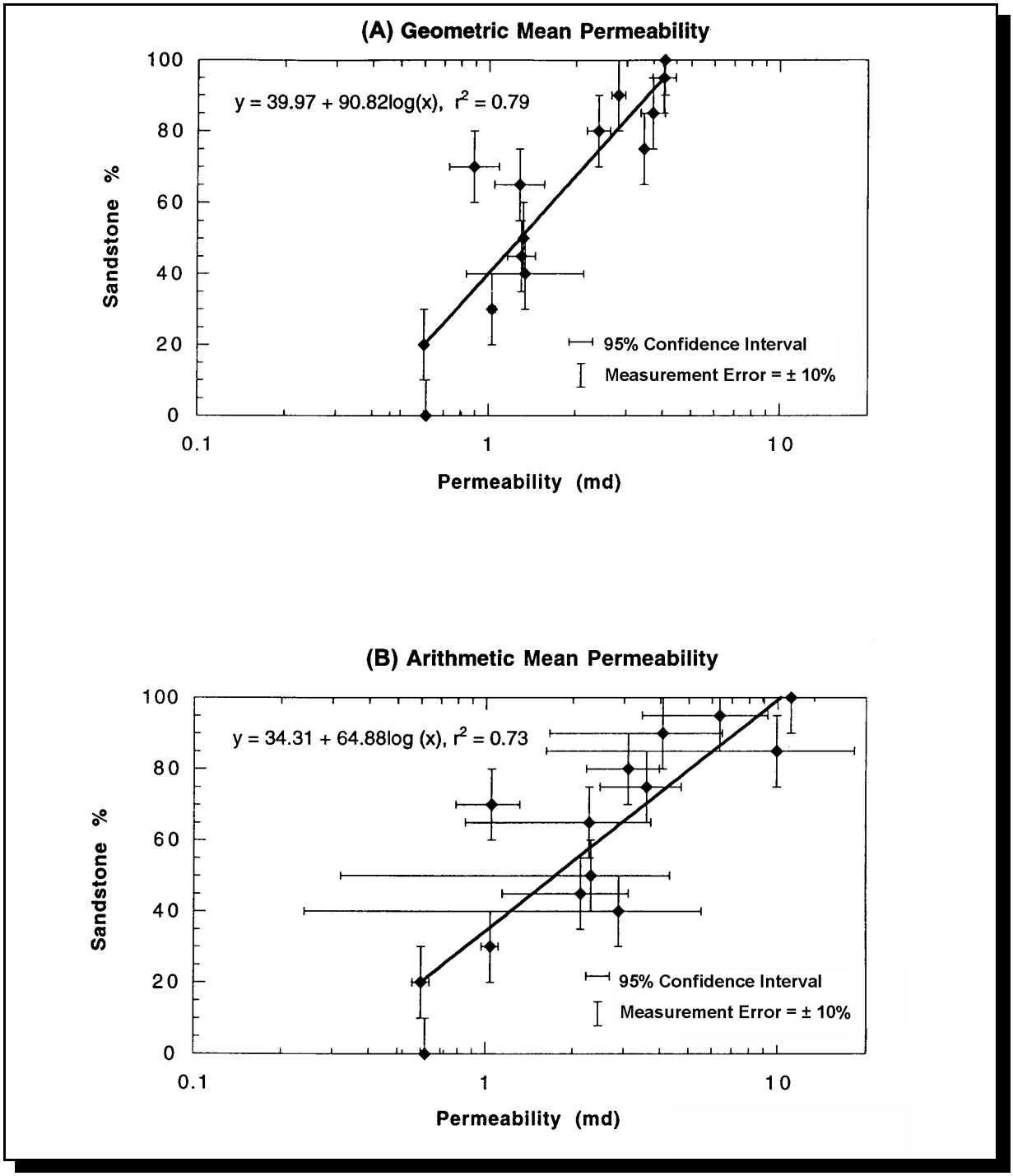


Figure 9-12. Kf-1-Iv[a] bedset detail model, permeability vs. percent sandstone for: (A) geometric mean, and (B) arithmetic mean.

Permeability is directly related to depositional energy as implied by sedimentary structure, average grain size, and lithology. Low-angle, cross-stratified sandstones have the highest mean permeability (7.8 md geometric mean) and ripple cross-laminated ones the lowest (1.43 md). Correspondingly, medium-grained sandstones have the highest mean permeability (21.0 md) and very fine-grained sandstones the lowest mean (1.27 md). In general, permeability decreases with increasing shale percentage and therefore with decreasing depositional energy.

The cumulative probability plots of permeability versus clinoform facies (figure 9-13), average megascopic grain size (figure 9-14), and sedimentary structure (figure 9-15) plot as relatively straight lines on log-normal plots. This agrees with the general assumption that permeability distribution as a function of geologic facies behaves log-normally (Rhea and others, 1994; Liu and others, 1996; Barton, 1994). The curves show a decrease in average permeability as: (1) facies become more distal; (2) average grain size decreases; (3) and depositional energy decreases as indicated by sedimentary structure. Permeability does not appear to correlate to bed size or induration.

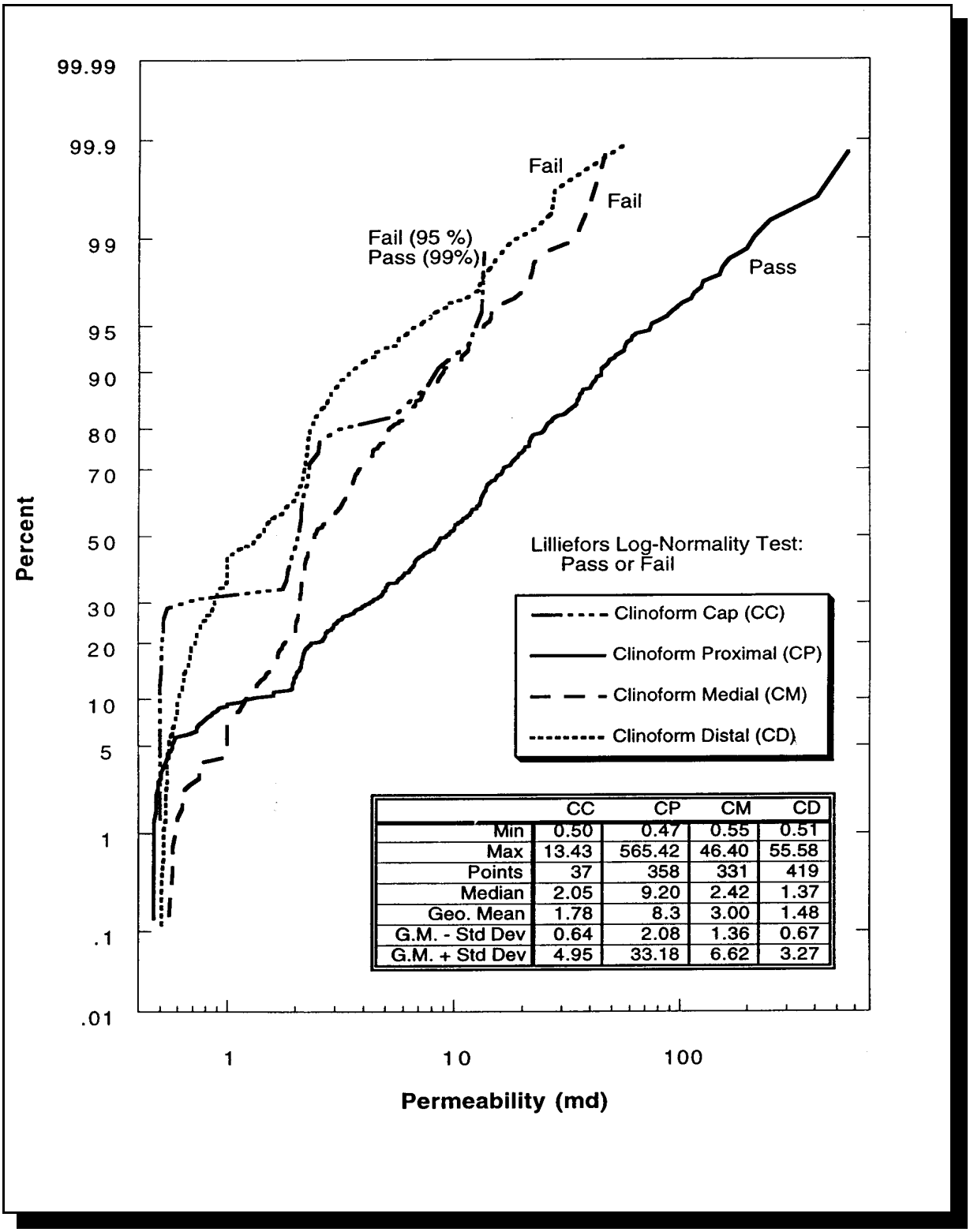
The cumulative probability curves of permeability versus clinoform facies are relatively straight lines (figure 9-16) implying a log-normal distribution as discussed earlier. The step functions observed in the curves appear to coincide with the resolution limits of the permeability instruments. Based on this assumption, the low data values should follow a log-normal distribution curve when extrapolated from the higher permeability data. Adjusting the low permeability raw data to fit the curve is a means to "correct" for the step functions and produce model data. The model data as compared to the raw data have: (1) a lower mean, (2) a greater separation between the mean for each facies, and (3) permeability values that represent an instrument with no measurement limitations. The model data was selected to provide another realization of permeability data to use in reservoir simulation.

Deterministic permeability panels consisted of two models (figure 9-17). The first model incorporated clinoform proximal, medial, and distal facies as the sole control on permeability distribution (figure 9-17A). The second model incorporated clinoform facies, sedimentary structure, and average grain size to distribute permeability values (figure 9-17B). Each block in the model was populated with the geometric mean of the permeability data.

Kf-2 Parasequence Set Permeability Analysis

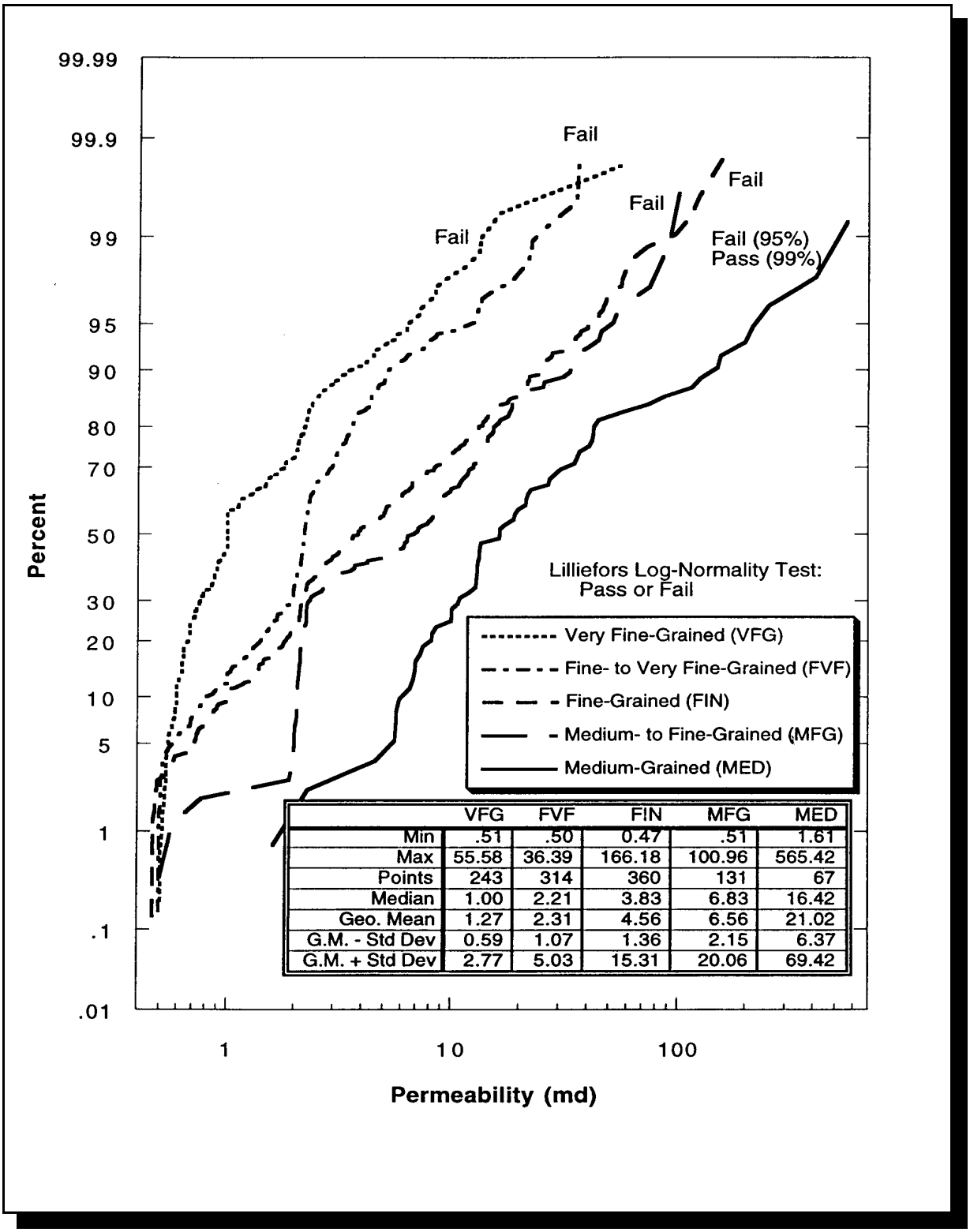
Eight facies were sampled in Kf-2 permeability analysis: transgressive, lower shoreface, middle shoreface, upper shoreface, foreshore, distal bar, distributary-mouth bar, and bay-fill. However, seven other facies were not sampled: prodelta, backshore, distributary channel, meander belt, bayhead delta, coastal plain, and swamp. The lack of data in these seven facies is due to: (1) sampling methods, (2) permeability core plug recovery rates during cliff-face drilling, and (3) lack of potential reservoir facies. Thus, it is not possible to fully characterize all facies of the Kf-2 parasequence set.

Permeability values for Kf-2 parasequences (0.34 to 1,121 md) have twice the range of the Kf-1-Iv[a] bedset (0.47 to 565 md). The volumetrically most important reservoir facies are the distributary-mouth bar and upper shoreface. These facies have the highest permeability values (up to 1,121 md), the highest percent of sandstone (100 percent), the coarsest average megascopic grain size (fine- to medium- to fine-grained), highest percent of trough cross-stratified sedimentary structures (60 to 80 percent), and the lowest degree of bioturbation (12 to 50 percent). A relatively



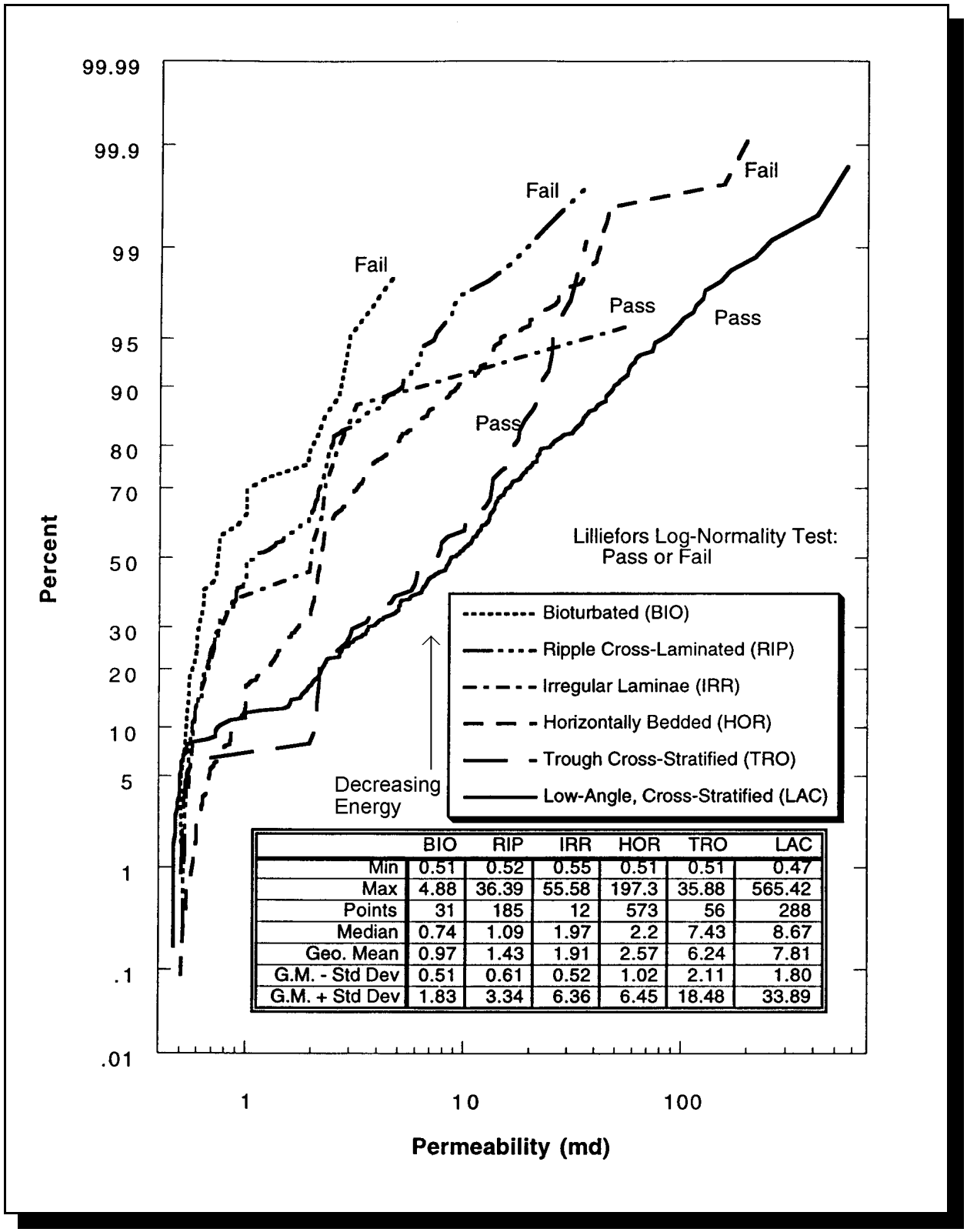
	CC	CP	CM	CD
Min	0.50	0.47	0.55	0.51
Max	13.43	565.42	46.40	55.58
Points	37	358	331	419
Median	2.05	9.20	2.42	1.37
Geo. Mean	1.78	8.3	3.00	1.48
G.M. - Std Dev	0.64	2.08	1.36	0.67
G.M. + Std Dev	4.95	33.18	6.62	3.27

Figure 9-13. Kf-1-Iv[a] bedset detail model, cumulative probability curves: facies vs. permeability.



	VFG	FVF	FIN	MFG	MED
Min	.51	.50	0.47	.51	1.61
Max	55.58	36.39	166.18	100.96	565.42
Points	243	314	360	131	67
Median	1.00	2.21	3.83	6.83	16.42
Geo. Mean	1.27	2.31	4.56	6.56	21.02
G.M. - Std Dev	0.59	1.07	1.36	2.15	6.37
G.M. + Std Dev	2.77	5.03	15.31	20.06	69.42

Figure 9-14. Kf-1-Iv[a] bedset detail model, cumulative probability curves: average grain size vs. permeability.



	BIO	RIP	IRR	HOR	TRO	LAC
Min	0.51	0.52	0.55	0.51	0.51	0.47
Max	4.88	36.39	55.58	197.3	35.88	565.42
Points	31	185	12	573	56	288
Median	0.74	1.09	1.97	2.2	7.43	8.67
Geo. Mean	0.97	1.43	1.91	2.57	6.24	7.81
G.M. - Std Dev	0.51	0.61	0.52	1.02	2.11	1.80
G.M. + Std Dev	1.83	3.34	6.36	6.45	18.48	33.89

Figure 9-15. Kf-1-Iv[a] bedset detail model, cumulative probability curves: sedimentary structure vs. permeability.

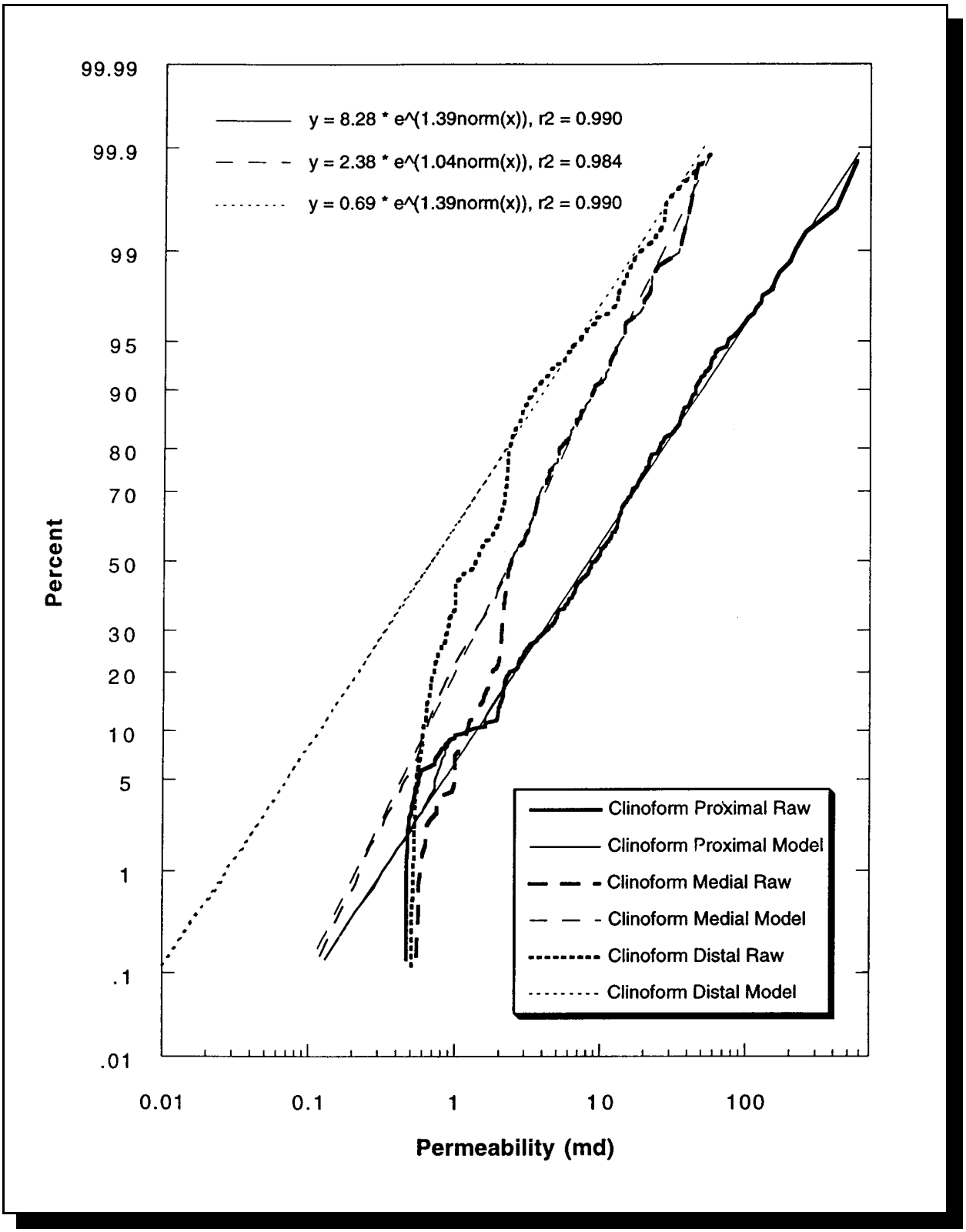


Figure 9-16. Kf-1-Iv[a] bedset detail model, cumulative probability curves: facies vs. permeability for model and raw data.

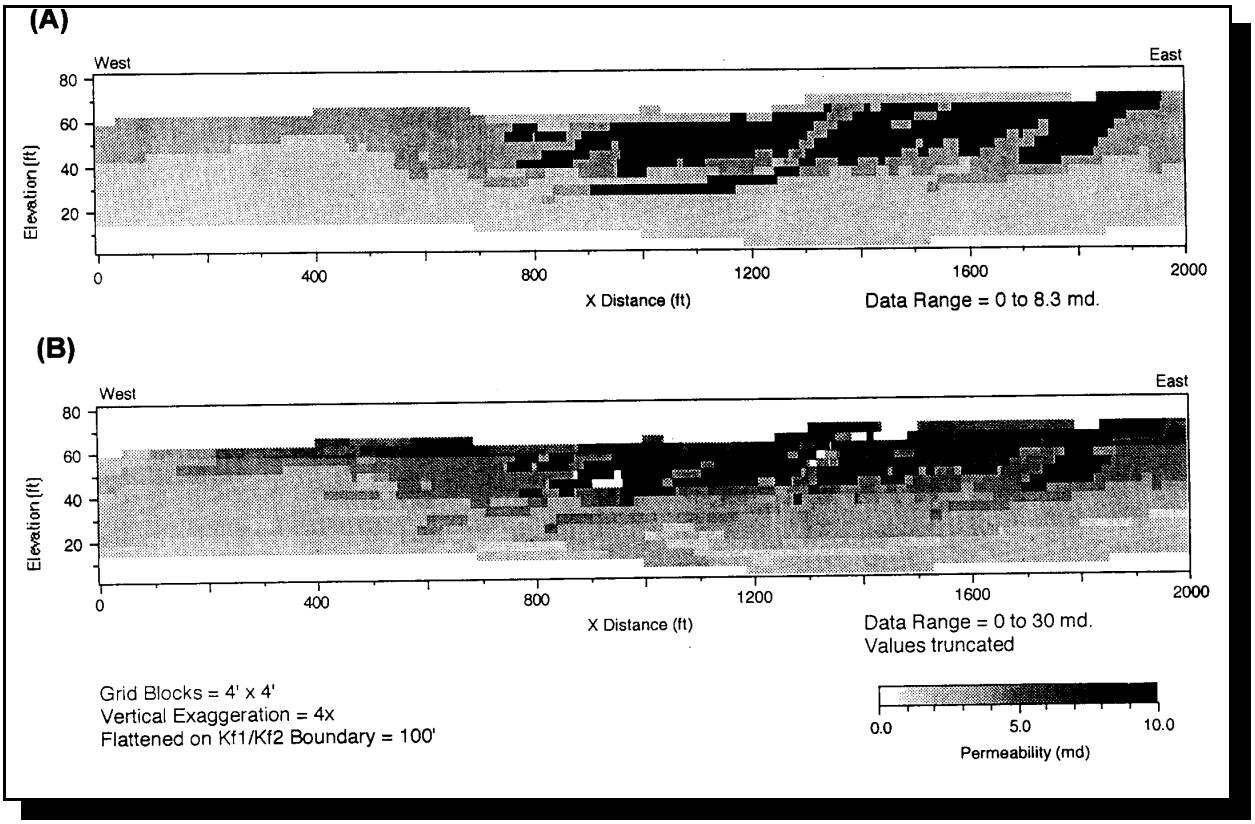


Figure 9-17. Ivie Creek amphitheater two-dimensional deterministic model for the Kf-1-Iv[a] bedset. (A) Geometric mean permeability distribution incorporating only facies. (B) Geometric mean permeability distribution incorporating facies, sedimentary structure, and average grain size.

high degree of sorting due to higher depositional energy may be inferred from the geologic observations. The transgressive, lower shoreface, and bay-fill facies have the lowest permeability values (less than 52 md). These facies have the lowest percent of sandstone (42 to 76 percent), the finest average grain size (up to fine- to very fine-grained), the highest percent of ripple cross-laminated (about 15 percent) and horizontal bedded (10 to 40 percent) sedimentary structures, and the highest degree of bioturbation (32 to 87 percent). A relatively low degree of sorting is inferred for these facies. The coefficient of variation of permeability is low for the distributary-mouth bar, upper shoreface, and foreshore; all potential reservoir facies. The low permeability facies, such as the transgressive and lower shoreface, exhibit slightly higher coefficients of variation indicating higher variability relative to the mean.

Cross plots of mean permeability versus percent sandstone show a logarithmic increase in permeability with a linear increase in percent sandstone (figure 9-18). Regressions of the geometric mean and arithmetic mean with respect to percent sandstone have coefficients of determination (r^2) of 0.38 and 0.46 respectively. The coefficients for the Kf-2 parasequence set are lower than those measured for the Kf-1-Iv[a] bedset (0.79, 0.73), but they still imply a weak correlation between permeability and percent sandstone.

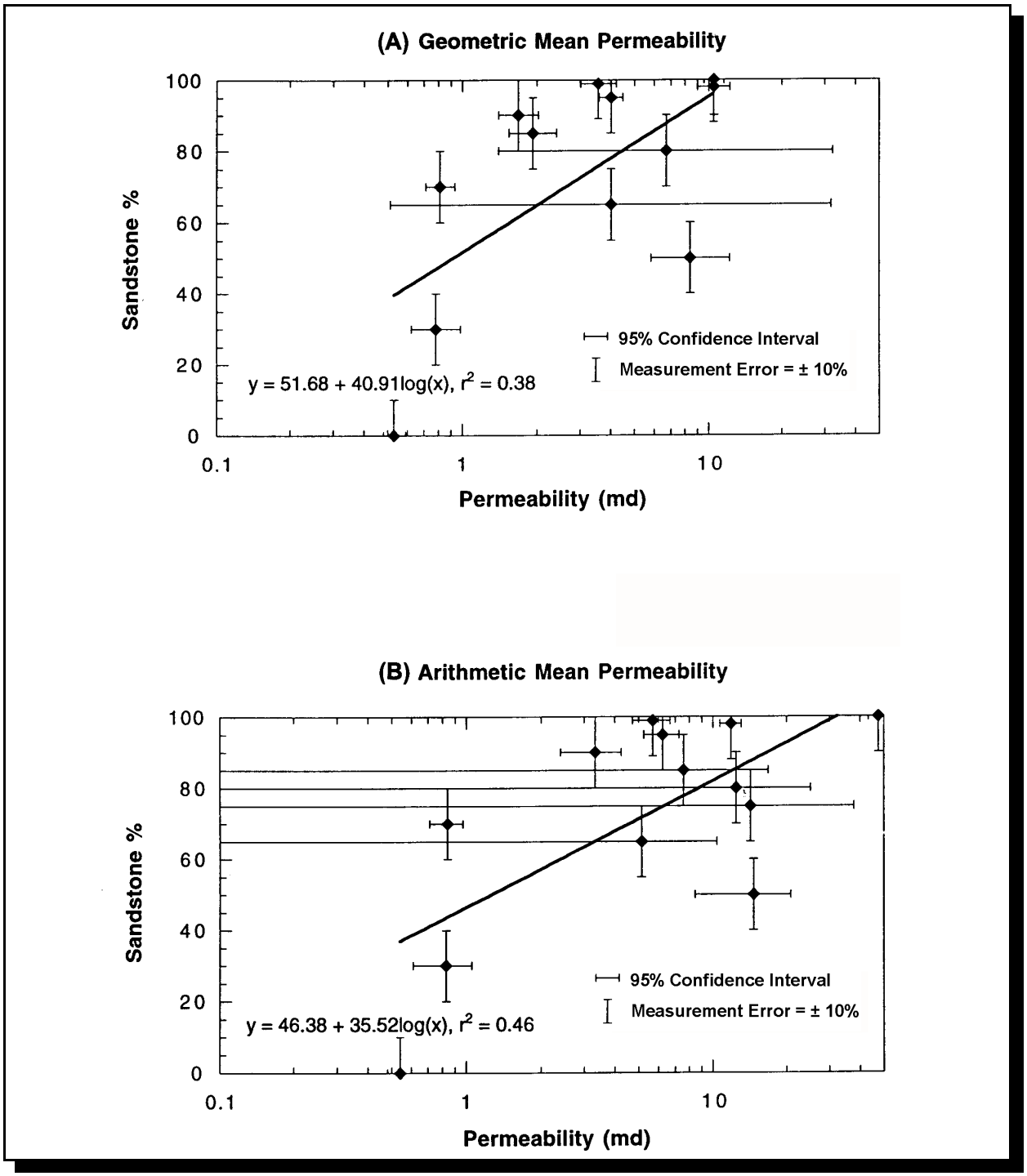


Figure 9-18. Kf-2 local model, permeability vs. percent sandstone for: (A) geometric mean, and (B) arithmetic mean.

The cumulative probability plots of permeability versus parasequence, facies, average grain size, and sedimentary structure (figures 9-19 through 9-22) mimic these obtained for the Kf-1-Iv[a] bedset. The cumulative curves of Kf-2 are shifted to slightly higher permeability values, reflecting the coarser average grain size of the parasequences. The geometric mean permeability values increase from 3.13 md for the Kf-1-Iv[a] bedset to 4.72, 6.82, and 44.12 md for the Kf-2-Iv-a, -b, and -c parasequences respectively. The curves also appear to exhibit log-normal behavior and have the same step function increases at about 0.5 md and about 2.0 md as observed in the Kf-1-Iv[a] bedset plots.

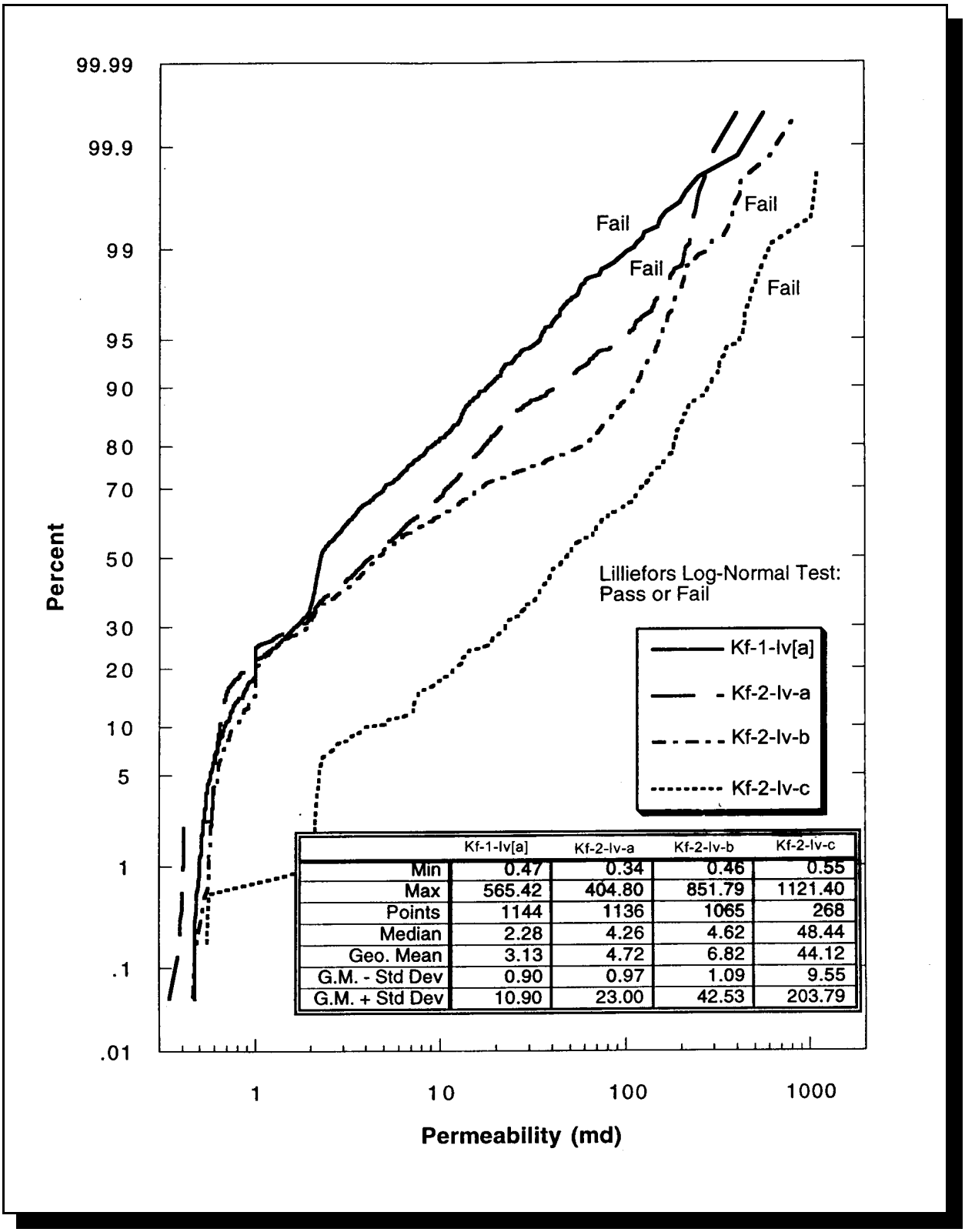
The plot of permeability versus individual parasequence (figure 9-19) demonstrates an increase in permeability from the oldest to the youngest parasequence. The lowest permeabilities of Kf-2 are found in the Kf-2-Iv-a parasequence, and the highest in the Kf-2-Iv-c. The trend implies progradation within Kf-2. As facies become more distal, the curves show a decrease in average permeability (figure 9-20), average megascopic grain size (figure 9-21), and depositional energy of a sedimentary structure (figure 9-22). To simplify the cumulative probability plot of sedimentary structure versus permeability, genetically similar structures were grouped together. The observations in Kf-2 parasequences reinforce the trends observed in the Kf-1-Iv[a] bedset.

Controls on Permeability

In the preceding data analysis, a strong relationship exists between geologic parameters and permeability. The permeability range is ultimately controlled by the energy of the depositional setting. Low energy deposits yield low permeability values and vice versa. In this study, the primary geologic parameters related to permeability are average grain size, lithology, and sedimentary structure. Another important textural parameter that was not measured in this study is sorting, but it may be inferred from these other parameters.

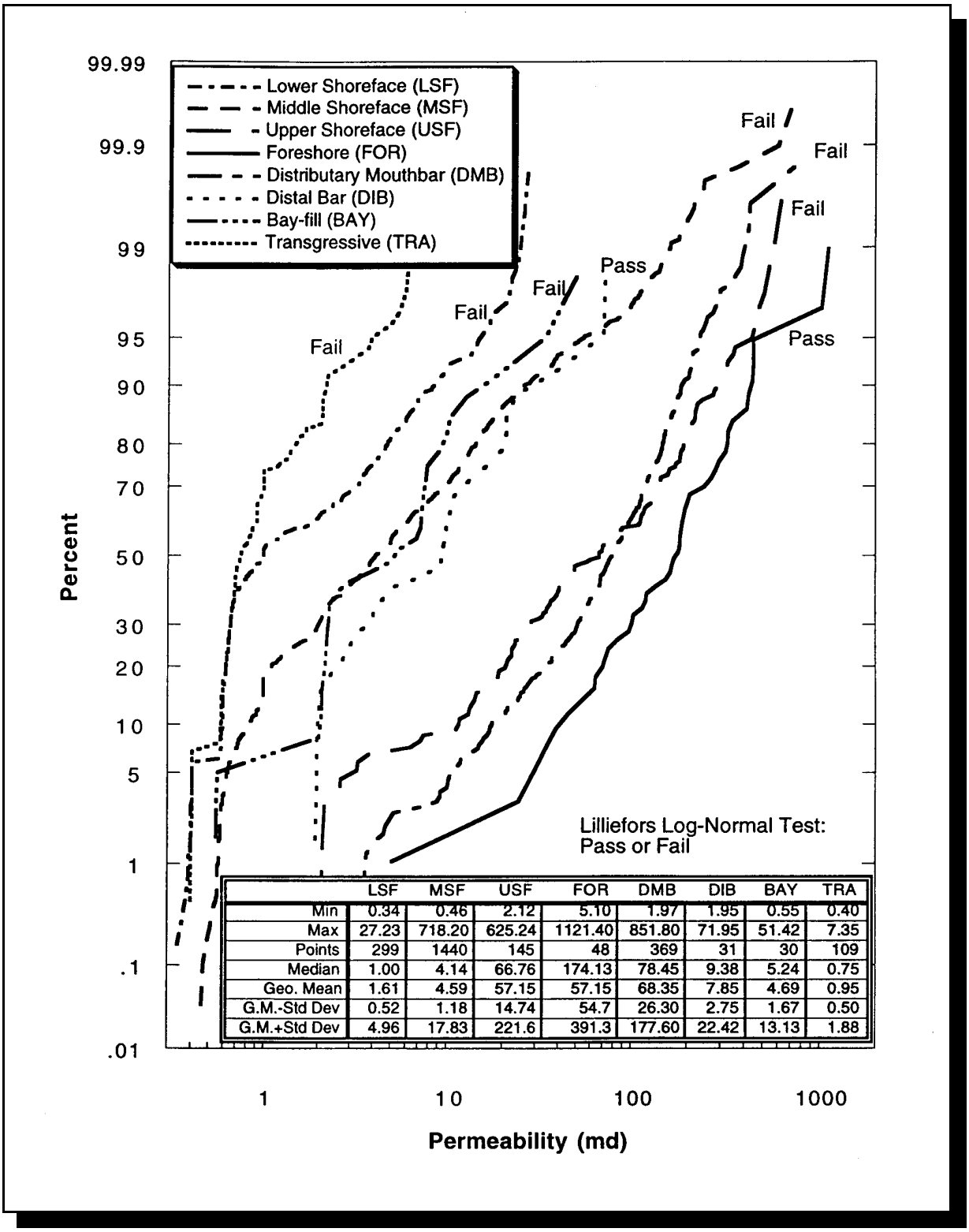
Other work (for example, Barton, 1994; Doyle and Sweet 1995; Liu and others, 1996) indicates that average grain size is the primary control on permeability, and sorting and lithology are secondary controls. Barton (1994) further hypothesized that 90 percent of permeability variations are due to four variables, in decreasing order off importance: (1) grain size, (2) sorting, (3) mineralogical composition, and (4) porosity. A relative degree of sorting can be inferred from depositional energy. In the scope of this study, high energy implies relatively well sorted deposits, and low energy implies relatively unsorted deposits. If average grain size were the only control, no variation in permeability would be predicted for different sedimentary structures for a given average grain size. However, variations do exist. For a given average grain size, high-energy sedimentary structures, such as trough cross-stratification and low-angle, cross-stratification, all have higher average permeabilities than do lower energy sedimentary structures, such as horizontally bedded or ripple cross-laminated probably due to sorting. These generalizations are only based on units described as 100 percent sandstone to eliminate the influence of lithology.

Lithology also plays a significant role in permeability. An increase in percent siltstone or shale corresponds to a decrease in permeability (figures 9-12 and 9-18). Again, this phenomenon relates back to depositional energy. If the inferred depositional energy is high, the unit tends to be better sorted and ranges up to 100 percent sandstone. If the inferred depositional energy is low, the unit is poorly sorted and more heterolithic.



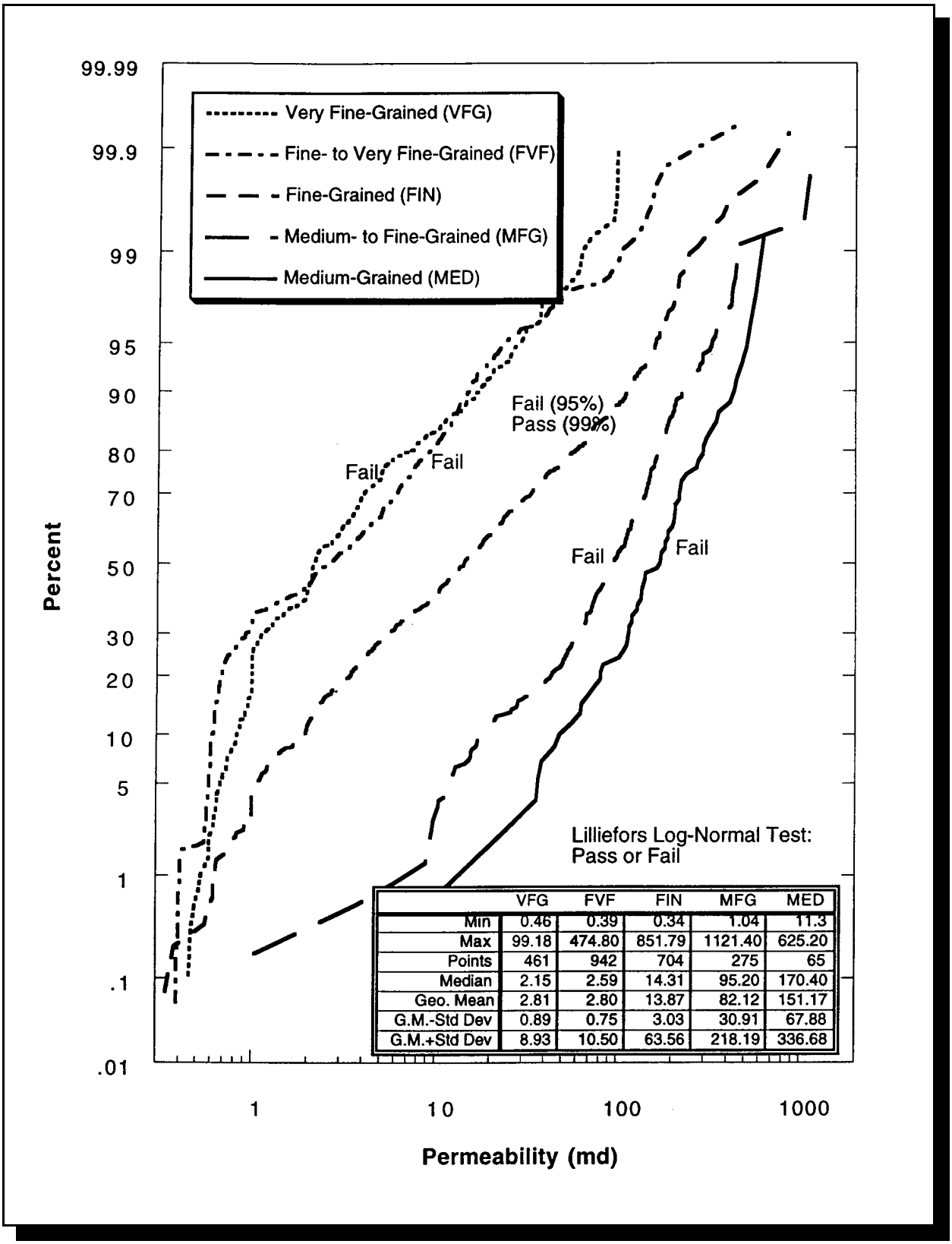
	Kf-1-Iv[a]	Kf-2-Iv-a	Kf-2-Iv-b	Kf-2-Iv-c
Min	0.47	0.34	0.46	0.55
Max	565.42	404.80	851.79	1121.40
Points	1144	1136	1065	268
Median	2.28	4.26	4.62	48.44
Geo. Mean	3.13	4.72	6.82	44.12
G.M. - Std Dev	0.90	0.97	1.09	9.55
G.M. + Std Dev	10.90	23.00	42.53	203.79

Figure 9-19. Kf-1-Iv[a] bedset and Kf-2 detail and local models, cumulative probability curves: parasequence vs. permeability.



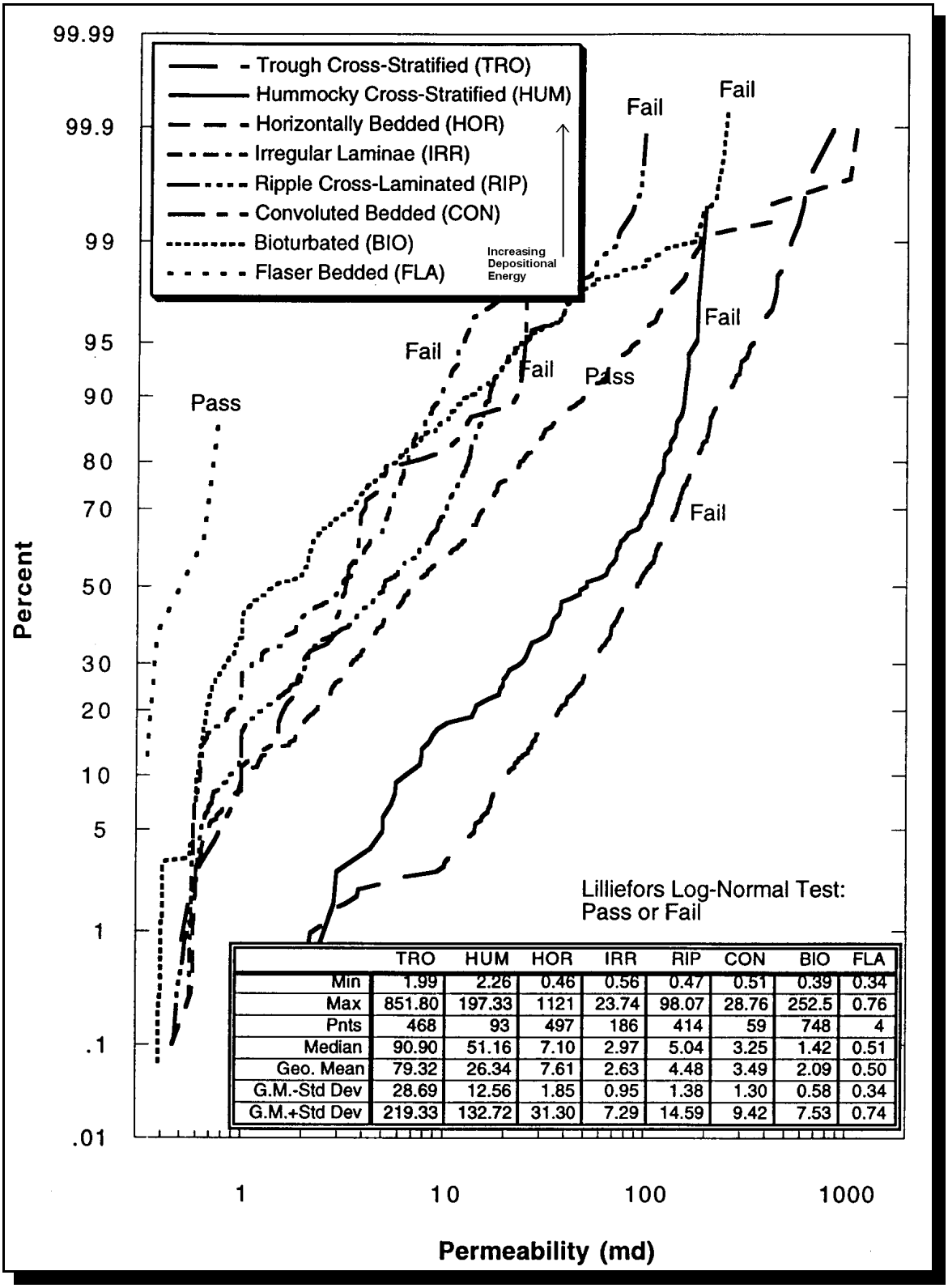
	LSF	MSF	USF	FOR	DMB	DIB	BAY	TRA
Min	0.34	0.46	2.12	5.10	1.97	1.95	0.55	0.40
Max	27.23	718.20	625.24	1121.40	851.80	71.95	51.42	7.35
Points	299	1440	145	48	369	31	30	109
Median	1.00	4.14	66.76	174.13	78.45	9.38	5.24	0.75
Geo. Mean	1.61	4.59	57.15	57.15	68.35	7.85	4.69	0.95
G.M.-Std Dev	0.52	1.18	14.74	54.7	26.30	2.75	1.67	0.50
G.M.+Std Dev	4.96	17.83	221.6	391.3	177.60	22.42	13.13	1.88

Figure 9-20. Kf-2 local model, cumulative probability curves: facies vs. permeability.



	VFG	FVF	FIN	MFG	MED
Min	0.46	0.39	0.34	1.04	11.3
Max	99.18	474.80	851.79	1121.40	625.20
Points	461	942	704	275	65
Median	2.15	2.59	14.31	95.20	170.40
Geo. Mean	2.81	2.80	13.87	82.12	151.17
G.M.-Std Dev	0.89	0.75	3.03	30.91	67.88
G.M.+Std Dev	8.93	10.50	63.56	218.19	336.68

Figure 9-21. Kf-2 local model, cumulative probability curves: average grain size vs. permeability.



	TRO	HUM	HOR	IRR	RIP	CON	BIO	FLA
Min	1.99	2.26	0.46	0.56	0.47	0.51	0.39	0.34
Max	851.80	197.33	1121	23.74	98.07	28.76	252.5	0.76
Pnts	468	93	497	186	414	59	748	4
Median	90.90	51.16	7.10	2.97	5.04	3.25	1.42	0.51
Geo. Mean	79.32	26.34	7.61	2.63	4.48	3.49	2.09	0.50
G.M.-Std Dev	28.69	12.56	1.85	0.95	1.38	1.30	0.58	0.34
G.M.+Std Dev	219.33	132.72	31.30	7.29	14.59	9.42	7.53	0.74

Figure 9-22. Kf-2 local model, cumulative probability curves: sedimentary structure vs. permeability.

A weaker correlation exists between permeability and induration, and permeability and bed size. Beds that are thin or laminated tend to have lower permeabilities than beds which are thick. Units that are well- to moderately cemented tend to have higher permeabilities than units described as friable. The exception is very well-cemented units that tend to have the lowest permeabilities of all.

Of the geologic parameters measured in the field, average grain size, lithology, and sedimentary structure show the strongest correlation with permeability. The highest permeability values correspond to geologic units with the highest depositional energy, for example, coarsest grain size, 100 percent sandstone, trough cross-stratified units.

All of these relationships are dependent on the assumption that diagenesis has not obliterated or destroyed the primary grain size, fabric, and sorting. In initial petrographic studies for this Ferron Project (see Chapter VIII, Petrophysical Characteristics of the Ivie Creek Case-Study Area), it appears that permeability is still a function of primary fabrics and textures. Secondary porosity (the dominant pore space for permeability) seems to have dissolved cements where depositional porosity was originally filled, thus preserving the relationship of permeability and relative energy.

Kf-1-Iv[a] Bedset vs. Kf-2 Parasequences: Comparison of Characteristics

The fluvial-dominated Kf-1-Iv[a] deltaic bedset can be contrasted to the wave-modified Kf-2 deltaic parasequences. The differences between the deltaic depositional conditions influence the range and distribution of permeability. The fluvial-dominated system exhibits lower overall permeability values (geometric mean = 3.1 md). In contrast, the wave action reworked the delta front of the wave-modified system, thus sorting the material and improving the overall permeability of the system (geometric mean = 7.1 md). The sorting also decreased the variability of the permeability values, concentrating shale in low depositional energy facies, and increasing the average grain size and permeability of the reservoir facies.

The primary reservoir facies are the clinoform proximal facies in the Kf-1-Iv[a] bedset, and the distributary-mouth bar and upper shoreface in Kf-2. Secondary reservoir facies include the clinoform medial in the Kf-1-Iv[a] bedset, and the foreshore and middle shoreface in Kf-2. The cumulative grain size plot (figure 9-23), shows similar curves for clinoform proximal and upper shoreface, but the permeability curve for clinoform proximal is shifted to lower values (figure 9-24). Likewise, the clinoform medial grain size curve is similar to the middle shoreface, but the permeability curve for clinoform medial is shifted to lower values. This implies that average grain size is not the sole control on permeability; sorting and textural maturity are probably also factors. The wave action of Kf-2 parasequences improves the sorting and increases the percent sandstone in the facies, which in turn increases the permeability of the facies.

The overall shape and distribution of cumulative probability curves of permeability versus geologic parameters (for example, facies) for analog field studies are believed to be applicable to subsurface reservoirs that were deposited under similar conditions, but not the absolute values (Barton, 1994). The suite of permeability curves would shift to higher or lower permeability values depending on the average grain size, lithologic composition, and diagenesis of the reservoir.

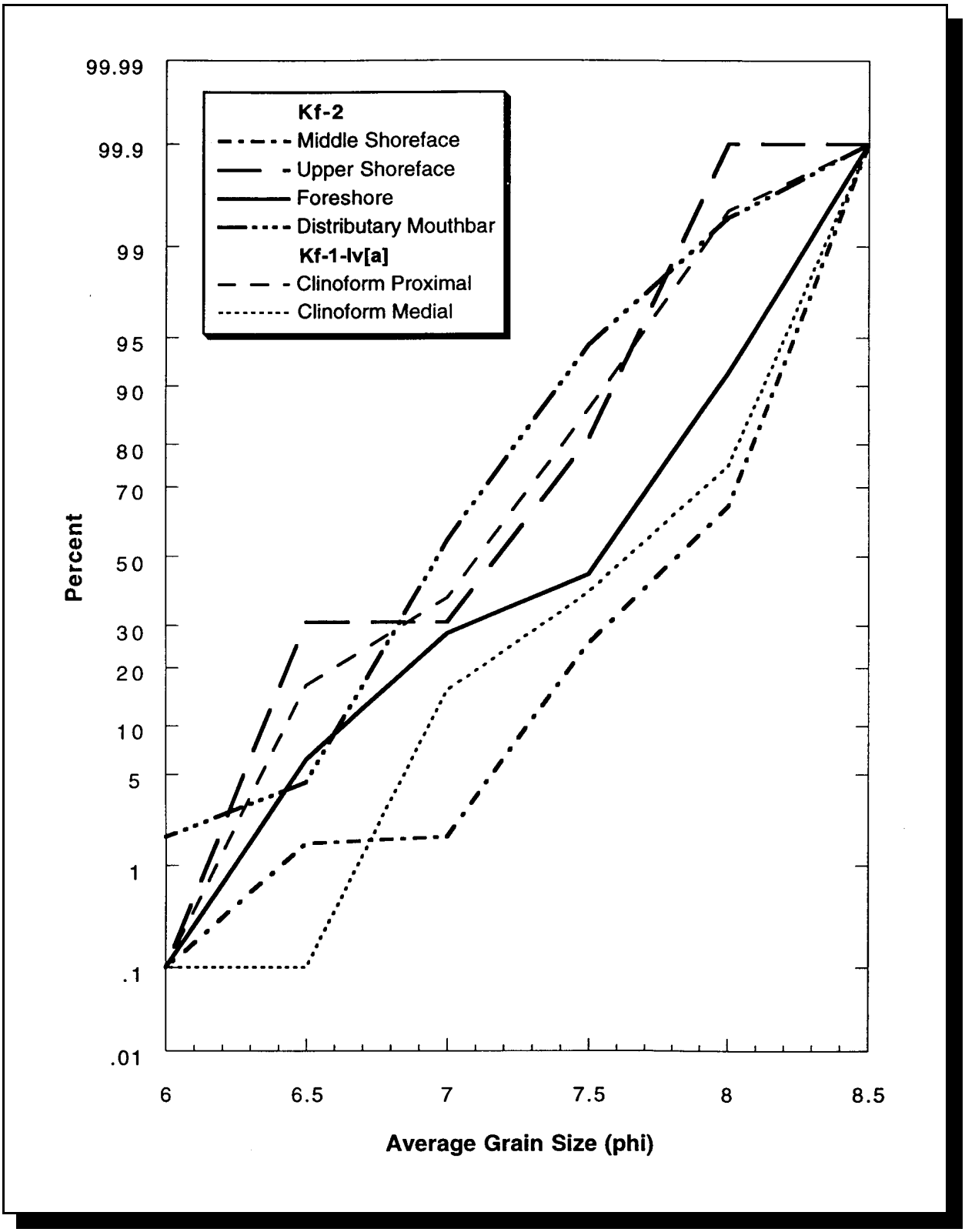


Figure 9-23. Kf-2 and Kf-1-Iv[a] bedset potential reservoir facies: facies vs. cumulative grain size.

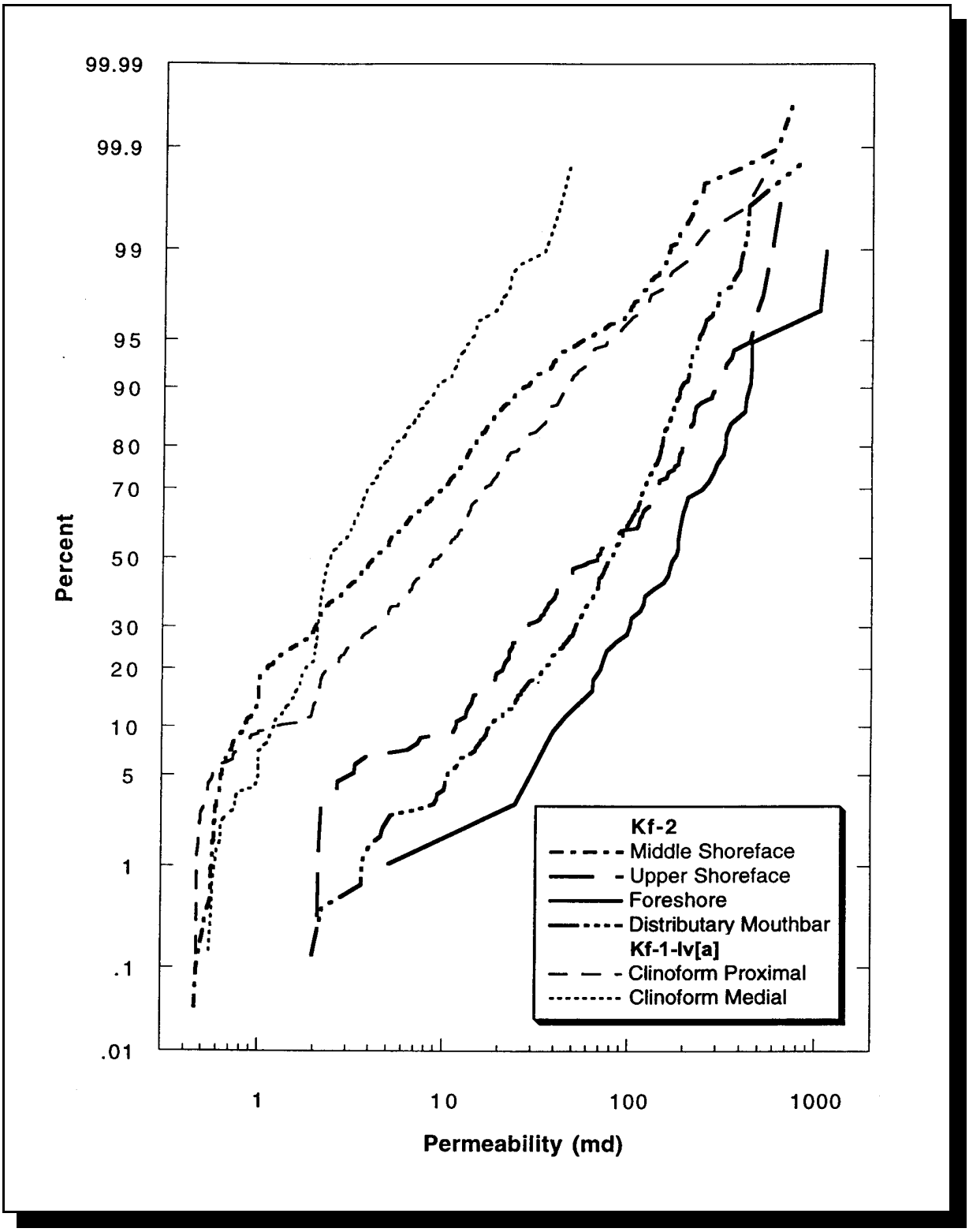


Figure 9-24. Kf-2 and Kf-1-Iv[a] bedset potential reservoir facies: facies vs. permeability.

Wave action along the delta front also produced tabular bedforms as opposed to the dipping, clinoform shapes of the fluvial-dominated system. Tabular bedforms have less complex internal geometry than clinoform bedforms, and generally provide more simple targets for hydrocarbon production. The wave action formed the tabular beds, improved sediment sorting in the proximal facies, and decreased the occurrence of thin shale beds that act as permeability barriers. These thin shale beds are more common in the fluvial-dominated facies, especially between clinoform bedforms, and they would act as baffles and/or barriers to hydrocarbon production. Thus, each deltaic system needs special consideration of the depositional conditions and processes, resulting geometries, and sorting to optimize hydrocarbon recovery.

Conclusions

Heterogeneities in two fluvial-deltaic members of the Cretaceous Ferron Sandstone are quantified for reservoir characterization. Permeability shows a strong correlation to lithology, average grain size, and sorting (as inferred from other geologic parameters). Although the rocks have undergone diagenesis, the original depositional relationships are not obliterated because secondary porosity development appears to have paralleled depositional porosity by dissolution of earlier cements.

The fluvial-dominated Kf-1-Iv[a] bedset is characterized by four clinoform facies: proximal, medial, distal, and cap. Overall, the clinoform facies have a geometric mean permeability of 3.1 md, and are fine-grained sandstones with clinoform proximal and medial facies being potential reservoir facies. Within these potential reservoir facies, low-angle, cross stratification, and horizontal beds are the predominant sedimentary structures.

The wave-modified Kf-2 parasequences are characterized by delta-front facies with tabular geometries, and are generally medium- to fine-grained sandstones with geometric mean permeability of 7.1 md. Potential reservoir facies are distributary-mouth bar, upper shoreface, foreshore, and middle shoreface. The higher Kf-2 permeability values are interpreted to be a function of the higher depositional energy from waves that produced better sorting in coarser grain sizes.

Permeability can be approximated by a log-normal distribution with respect to facies, sedimentary structure, and average grain size. These relationships establish probability distribution functions that could be input into reservoir simulation. The probability functions could be applied to analogous delta systems although the absolute values of the curves should be evaluated where depositional environment, average grain size, and geometry information is available.

The Ferron outcrop and drill-hole data set provides an excellent opportunity to quantify facies relationships and statistical measures of heterogeneity for fluvial-deltaic bedsets and parasequences. This study further emphasizes the need to understand the depositional energy, as reflected in sorting, and depositional process to correctly evaluate and populate reservoir simulation models. Careful analysis of the depositional environment is an essential prerequisite to applying the results of any analog study to the subsurface. From analysis of a large data base of several types of field (for example, lithology, facies, average grain size, and sedimentary structures) and lab measurements (for example, permeability), recurring themes are repeated, emphasizing the most important controls of depositional grain size and relative sorting (both as a function of facies).

CHAPTER X
RESERVOIR MODELING AND FLUID-FLOW SIMULATION, IVIE CREEK CASE-STUDY AREA

C.B. Forster, S.H. Snelgrove, and J.V. Koebbe

Introduction

Detailed, two- and three-dimensional petrophysical and fluid flow modeling at the Ivie Creek case-study area (figure 10-1) is based on data from two sources: (1) the stratal architecture on outcrop, derived mainly from cliff-face photomosaic panels; and (2) permeability measurements made on core plugs extracted from the outcrop and from slabbed borehole cores. Descriptions of the procedures used to establish the outcrop architecture and to measure permeability, and an analysis of the permeability measurements, are contained in Mattson (1997), and Chapter VII (Geologic Framework of Ivie Creek Case-Study Area), Chapter VIII (Petrophysical Characteristics of the Ivie Creek Case-Study Area), and Chapter IX (Statistical Analysis, Ivie Creek Case-Study Area) of this report. These topics are reviewed only briefly here. The key objective of the flow-simulation studies is to evaluate the impact of outcrop-based geology on numerical simulations of reservoir performance.

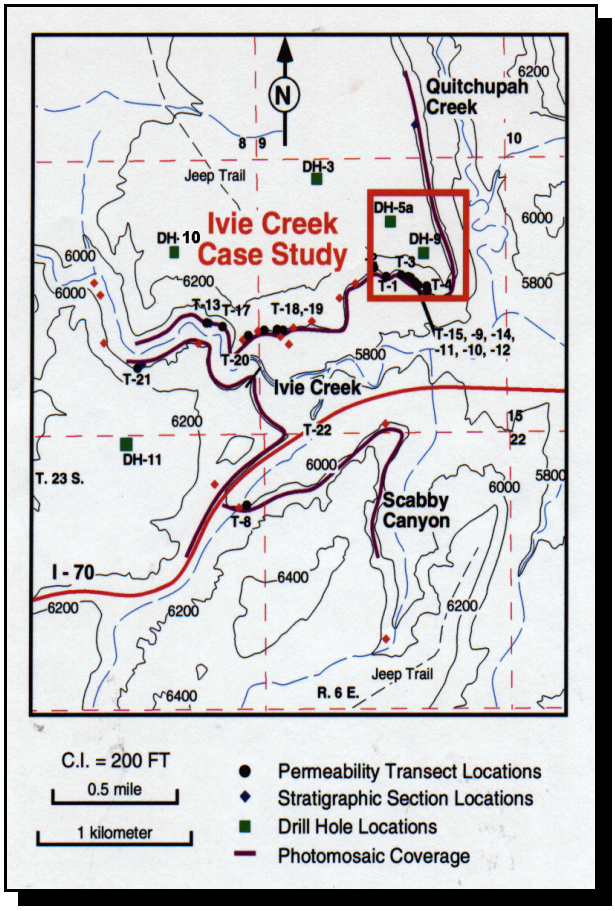


Figure 10-1. Location of Ivie Creek case-study area.

The stratal architecture exposed at Ivie Creek consists of the juxtaposition of many variants of a single architectural element, the clinoform, and indicates prograding, shallow-marine deposition of a fluvial-dominated delta-front system (figure 10-2). The sandstone beds within each sigmoid-shaped clinoform body record an episode of deposition, followed by partial erosion. Depositional episodes were likely related to variations in the sediment load carried by the distributary channel(s) feeding the delta front, and by upstream channel switching. Clinoform bodies are inclined seaward, arranged *en echelon*, and are usually separated from each other by a thin (less than 1 foot thick [< 0.3 m]) mudstone and siltstone bounding layer. The resulting architecture provides the spatial framework for distributing permeability and porosity within numerical models of this delta-front reservoir analog.

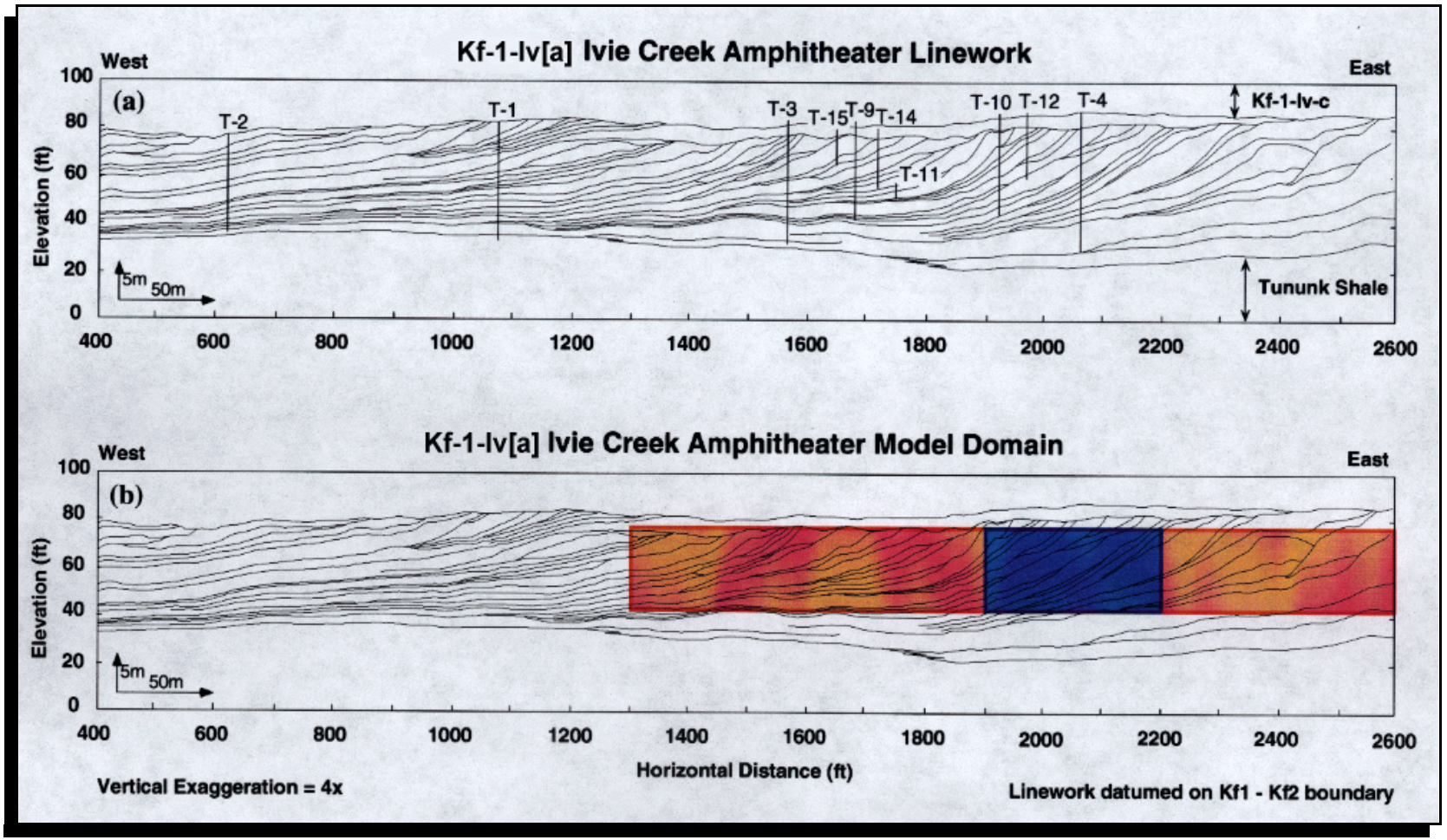


Figure 10-2. (a) Linework interpretation of Ivie Creek case study architecture (from Chidsey and Allison, 1996; Mattson, 1997). The labeled vertical lines are locations of permeability transects. (b) The shaded area indicates the extent of gridded modeling domain used in fluid-flow simulations. The sub-domain shaded in darker gray was used in permeability upscaling experiments.

Underlying this approach is the assumption that the similar geometry shared by individual clinoforms indicates that they were deposited under the influence of similar hydrodynamic and geological processes. The interplay between these processes results in a characteristic spatial distribution within each clinoform of sediment grain sizes, sedimentary structures, and sediment mineralogy. These factors, in turn, are key controls on primary porosity and permeability. Those parts of a clinoform deposited in high energy hydrodynamic conditions with an ample supply of coarse, angular quartz grains would be expected to produce comparatively high porosity and high permeability rocks. Lower energy conditions which favor the deposition of smaller grains and tabular clay particles yield lower permeability deposits. In short, since individual clinoforms were originally deposited under conditions similar to those in which every other clinoform was deposited, all clinoforms exhibit similar spatial patterns of primary porosity and permeability (Weber, 1978).

Trends in permeability and porosity are difficult to establish at the Ivie Creek case-study area because of the strategy used to collect core plug samples from the outcrop (discussed below). However, most clinoforms at Ivie Creek show a systematic decrease in grain size and a clear succession of sedimentary structures in the direction of depositional dip. This trend indicates a transition from a high energy depositional setting proximal to the sediment source to a low energy depositional setting distal to the source. A corresponding, but weak, progression from high permeability and porosity to lower permeability and porosity exists within clinoforms, even though much of the primary porosity has been modified by diagenesis.

A gridded, two-dimensional (2-D) digital model of the stratal architecture was generated by interpreting a photomosaic of the exposed cliff-face in the Ivie Creek amphitheater. Individual clinoforms are preserved in the digital model, and are the basis for developing two- and three-dimensional permeability models of the case study. Each clinoform is assumed to result from a similar set of depositional conditions, and thus to exhibit similar trends in permeability. The validity of this approach is based on the discussion above.

Permeability distributions within a clinoform are assigned in the models by first subdividing the clinoform into facies. The mean permeability of each facies, derived from permeability measurements made on plugs extracted from the outcrop, is then used to assign permeability throughout each clinoform. An empirical relationship that relates permeability and porosity at the Ivie Creek case-study area is used to compute porosity values from permeability.

Several petrophysical models are constructed, each a different representation of the degree to which individual clinoforms are surrounded by thin, siltstone and mudstone bounding layers. Numerical simulations of a waterflood in a two-phase (oil and water) system illustrate the impact the bounding layers might have on reservoir performance. The fraction of the original in-place oil that is ultimately recovered is only slightly affected by the various bounding layer models. The timing of production, however, is closely related to the spatial configuration of the bounding layers. A permeability upscaling study performed using a sub-region of one the permeability models indicates that none of the simple averaging methods (arithmetic, harmonic, and geometric) are appropriate for deposits of this type. An upscaled permeability model obtained using a perturbation technique, however, yields simulation results similar to those obtained using the detailed permeability model.

Three-dimensional (3-D) petrophysical models are created in several steps as described by Chidsey and Allison (1996), Chidsey (1997), Mattson (1997), and briefly described here. Eight detailed vertical cross sections containing clinoform geometry and facies are derived from outcrop and drill hole control (figure 10-1). Two cross sections correspond to the south and east facing

outcrops (including the Ivie Creek amphitheater cliff-face, used in the 2-D modeling studies), four define the sides of the modeling domain, and two (tied to drill holes) cut diagonally across the block. Computational constraints prevent the level of detail contained in the gridded cross sections from being incorporated in the computational grid of the 3-D flow-simulation model. Thus, the facies grid contained in the detailed vertical sections are coarsened to match the scale of the computational grid. The dominant clinoform facies type found within each computational block is assigned in the coarsened model as an attribute for the whole block. Facies data from these coarsened vertical sections are transferred to horizontal slices created throughout the modeling domain and the facies are interpolated between control points. The permeability of a grid block is defined as the arithmetic mean of the permeability values obtained for the specific clinoform facies assigned to the block. The resulting model (Reference Case) is consistent from layer to layer, and agrees with our hypothesis that sediment deposition created arcuate lobes sourced from the east-southeast. An isotropic permeability tensor is assumed for each grid block in the Reference Case.

Three other 3-D petrophysical models are developed to examine whether any significant improvement might be made by including outcrop-based information in numerical waterflood simulations. The first model (Anisotropic Case) is obtained by estimating 3-D permeability anisotropy from the 2-D permeability modeling and applying the result to the facies-based model described above. The second model (Layered Case) is a simple, isotropic, layered model derived by re-sampling the gridded facies architecture of the Reference Case at the four corners of the model domain. Using only these data represents a conventional, and simplified, approach to building a reservoir model given borehole data obtained at a 40-acre (16.2-ha) spacing. The third, and simplest model (Homogeneous Case) is constructed by assigning a single value of isotropic permeability throughout the model domain.

Numerical simulations are performed using the TETRAD-3D finite-difference reservoir simulation software, provided for use in the project courtesy of Mobil Exploration and Producing Company. This package allows the implicit pressure/explicit saturation (IMPES) solution technique to be used to minimize computational requirements. However, when simulation runs involving large changes in oil saturation through time cannot be treated explicitly, a fully implicit solution method is used. All simulations involve two fluids, oil and water. The bulk of the 2-D simulations were completed before 3-D modeling began. Thus, differences in the model parameterization between the 2-D and 3-D modeling efforts reflect changes in thinking that occurred as the project evolved.

Two-Dimensional Modeling

Developing a Gridded Architecture Model

The architectural framework of the Kf-Iv-1[a] bedset was established by the geologic field team. The framework was built using a cliff-face photomosaic of the case-study area, augmented by careful field checking. The interpretation is based on the thin (typically less than 1 foot [<0.3 m), mudstone and siltstone bounding layers which often separate individual clinoforms. These layers are generally less resistant to weathering than the sandstone clinoforms, producing recessive breaks in the cliff-face. The breaks are clearly seen on the photomosaic, highlighting the prograding clinoform architecture of the cliff face. The architecture is sometimes difficult to interpret in the proximal portion of the outcrop, where the bounding layers separating adjacent clinoforms are often

absent. Interpretation is also challenging in the distal region, where clinoforms thin and become increasingly finer-grained, approaching the character of a bounding layer. Indeed, clinoforms and bounding layers are indistinguishable in the most distal reaches of the outcrop. The linework representation of the architecture is shown in figure 10-2a (Mattson, 1997). Figure 10-2b indicates the portion of the case study eventually used in 2-D flow simulations, denoted the "model domain" in subsequent discussions.

The linework was digitized and rectified as described by Mattson (1997). Rectification corrects for distortion in the linework interpretation caused by projecting the cliff-face, which has spatial depth, onto the 2-D image of the photomosaic.

As discussed above, the digital petrophysical model is constructed by treating each clinoform individually. The underlying assumption is that the spatial configuration of petrophysical properties within a particular clinoform is similar to that in all other clinoforms. Thus, a single set of rules can be used to assign properties within any particular clinoform. This approach requires that each clinoform be represented as a closed polygon, analogous to the piece of a puzzle, and that all such polygons completely fill the model domain.

Several steps are needed to transform the rectified, digitized linework into a structure suitable for developing a numerical model. First, gaps in the linework due to minor digitizing errors and interpretation uncertainty are repaired (closed), enabling each clinoform to be represented as a polygonal body. Next, individual clinoform boundaries are established by cutting the appropriate line segments from the digitized linework and joining them to form a closed polygon. Finally, the entire model domain is gridded so that petrophysical properties can be assigned to rectangular grid blocks within each clinoform.

Figure 10-3 shows a small portion of the digitized linework and illustrates how gaps in the linework are repaired. The gaps must be eliminated so that clinoform boundaries can be represented as closed polygons. The arrows in figure 10-3a indicate breaks in the linework due to digitizing errors. These errors are manually fixed by extending the lines along trend, as shown in figure 10-3b, so that they terminate against another line. The circles indicate gaps caused by interpretation uncertainty, where the clinoform boundary could not be established either from the photomosaic or from field checking. These particular examples are from the thin, fine-grained, distal portions of the affected clinoforms, where it is difficult to distinguish a clinoform from a bounding layer. A similar problem often occurs in the proximal reaches of a clinoform, where the bounding layer is thin or nonexistent. These gaps are repaired either by terminating a line against another line (as in the two upper circles), or by extending the line to the domain boundary. The decision to either terminate or extend a line is dictated mainly by geological principles, although at times modeling convenience is also a consideration.

The linework derived from the photomosaic was digitized without regard to individual clinoforms. Instead, the longest continuous line segments possible were digitized in order to expedite the digitizing process. As a consequence, any single digitized line usually contains portions of the boundary of many different clinoforms. In order to treat clinoforms individually, the boundary of each clinoform in the modeling domain is constructed by cutting the appropriate line segments from the digitized linework and joining them to form a closed polygon. The concept behind a computer program written to accomplish this task is depicted using the sub-domain shown in figure 10-4. Four digitized lines (labeled 1a35, 1a36, 1a37, and 1a50) contribute to the boundary of the gray clinoform in figure 10-4a). The lines also contribute to the boundaries of other clinoforms, in particular the clinoform to the right and below the gray clinoform (other lines, and hence clinoforms,

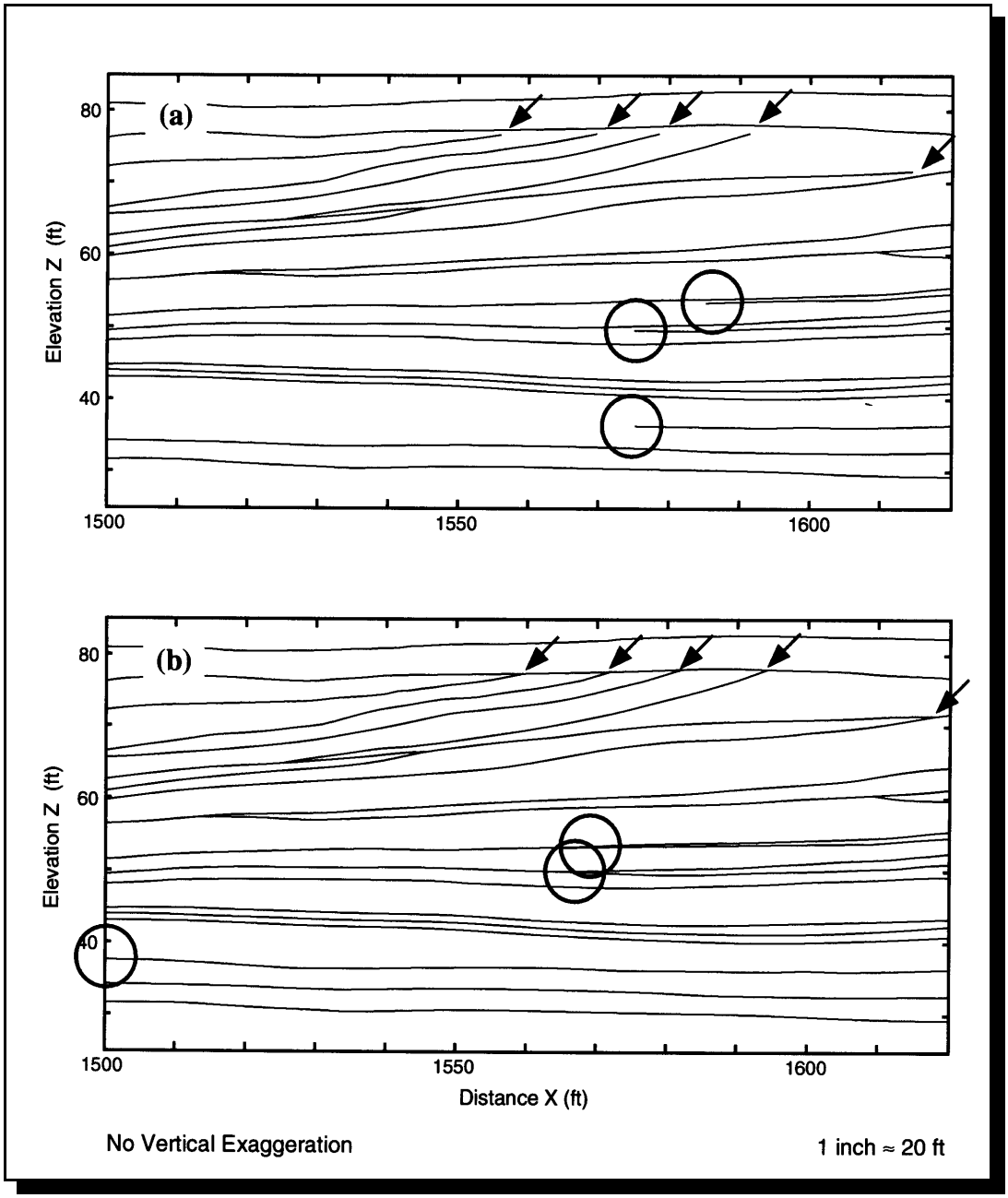


Figure 10-3. Digitized linework repair in a portion of the modeling domain. In (a) some lines do not terminate against other lines or extend to a boundary. In (b) the linework is repaired. Arrows indicate simple digitizing errors; circles indicate ambiguity in the interpretation.

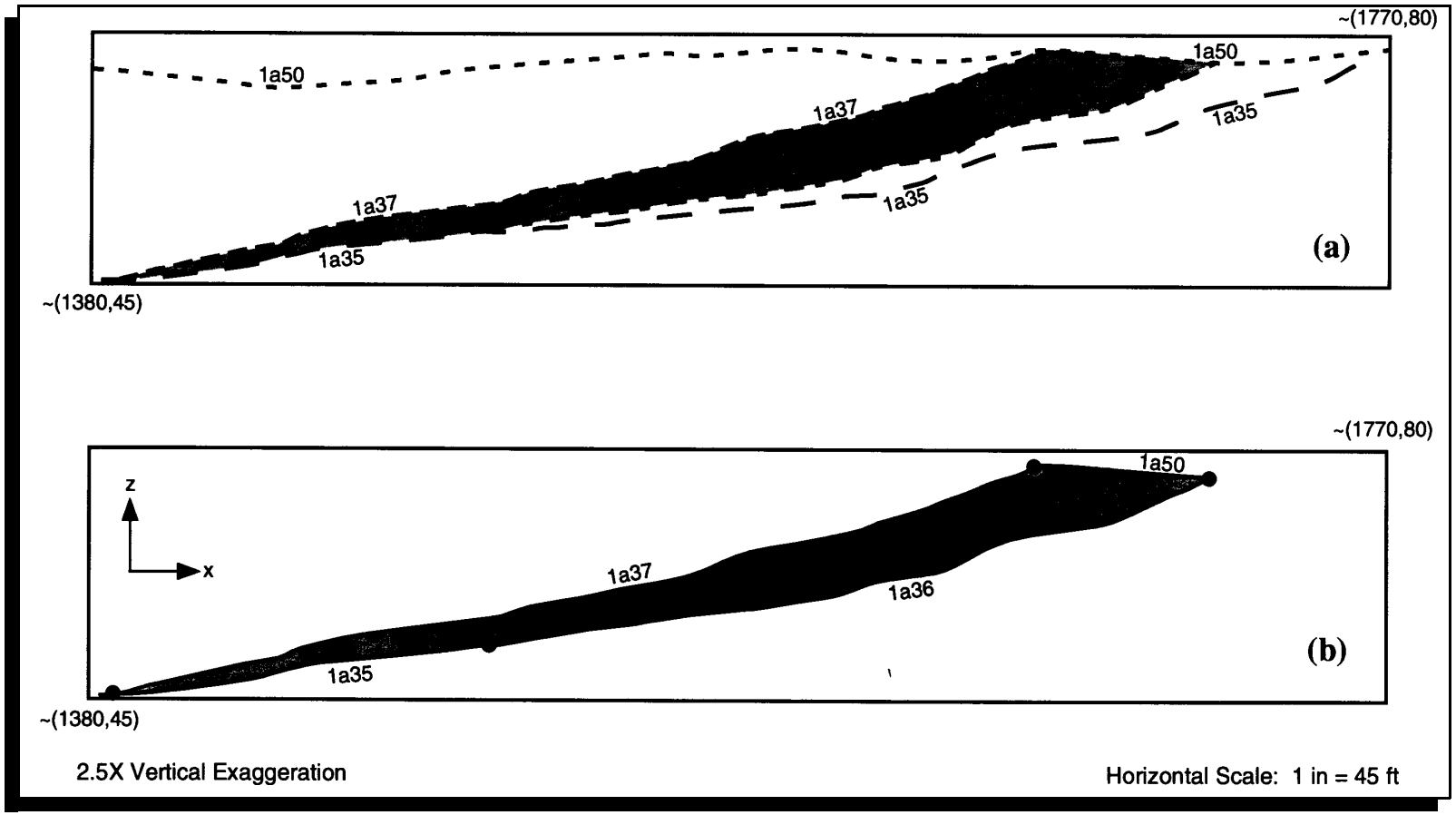


Figure 10-4. Extracting the boundary of an individual clinoform from the digitized linework. (a) Shows that four digitized lines contribute to the boundary of the clinoform indicated by the gray shading. (b) Shows the portions of each of the lines that were cut and joined to form the boundary of the clinoform.

in the sub-domain are omitted for the sake of clarity). Also note that part of the boundary is shared by the two clinoforms. The closed circles in figure 10-4b show where each of the lines in figure 10-4b is cut and joined to form the boundary of the gray clinoform.

The closed polygon defining the boundary of a clinoform simply specifies the shape of the clinoform. It does not provide a way to associate an attribute, such as permeability, to regions on the interior of the clinoform. Gridding imposes a structure on the modeling domain that can be used to assign attributes to specific regions within every clinoform in the domain. It is a crucial step, allowing the linework representation of the case study architecture to be used in conjunction with fluid-flow modeling. The clinoforms in figure 10-5a are shown in their gridded form in figure 10-5b. The shading in figure 10-5b indicates varying values of permeability, although any attribute can be represented in this way. A computer program designed to allow different gridding increments in the x and z directions was written to accomplish this step. The grid increments used to construct figure 10-5, x = 2.5 feet (0.8 m) and z = 0.5 feet (0.2 m), are the same as those used in fluid-flow simulations. Simple rectangular gridding is used because subsequent flow modeling is performed using finite-difference flow simulation software.

Each clinoform is gridded with respect to the modeling domain shown in figure 10-2. The domain is 1,302.5 feet (397 m) long in the x-direction and 40 feet (12 m) high in z. The gridding increments are x = 2.5 feet (0.8 m) and z = 0.5 feet (0.2 m), resulting in nx = 521 grid blocks in x and nz = 80 blocks in z, for a total of 41,680 grid blocks. The domain is sized to capture the transition from highest to lowest values of permeability at the interwell scale. The grid-block dimensions are sized to allow a reasonably detailed description of the bounding layers, while at the same time keeping the number of blocks small enough that the computational resources available to the project would not be overwhelmed.

Distributing Permeability Within Clinoforms

The original intent of the project was to construct a permeability model of the case-study area by merging the case-study architecture with outcrop-based permeability measurements, and then apply geostatistical methods to distribute permeability throughout the model domain. Our ability to follow this approach was inhibited by inexperience and by the steep, broken terrain of the outcrop, which made the collection of core plugs very difficult. Most of the outcrop was inaccessible except by rope, so the locations of permeability profiles were dictated by safety concerns. Plugs were therefore taken along widely spaced vertical profiles, as shown in figure 10-2 (the vertical sample spacing was 0.3 feet [9.1 cm]). As a result, parts of many clinoforms were sampled, but no single clinoform contained enough well-distributed measurements to adequately characterize the spatial structure of permeability within it. Plausible estimates of permeability trends and correlation lengths were not feasible. With the benefit of retrospect, the ideal approach would be to characterize several clinoforms with well distributed measurements. This alternative approach would enable us to identify permeability trends and correlation lengths, provide data for testing the assertion that a spatial trend exist within each clinoform (from proximal high permeability to distal low permeability), and that a similar trend applies to all clinoforms. The results of such a test could be used to build the case study permeability model in a more rigorous fashion.

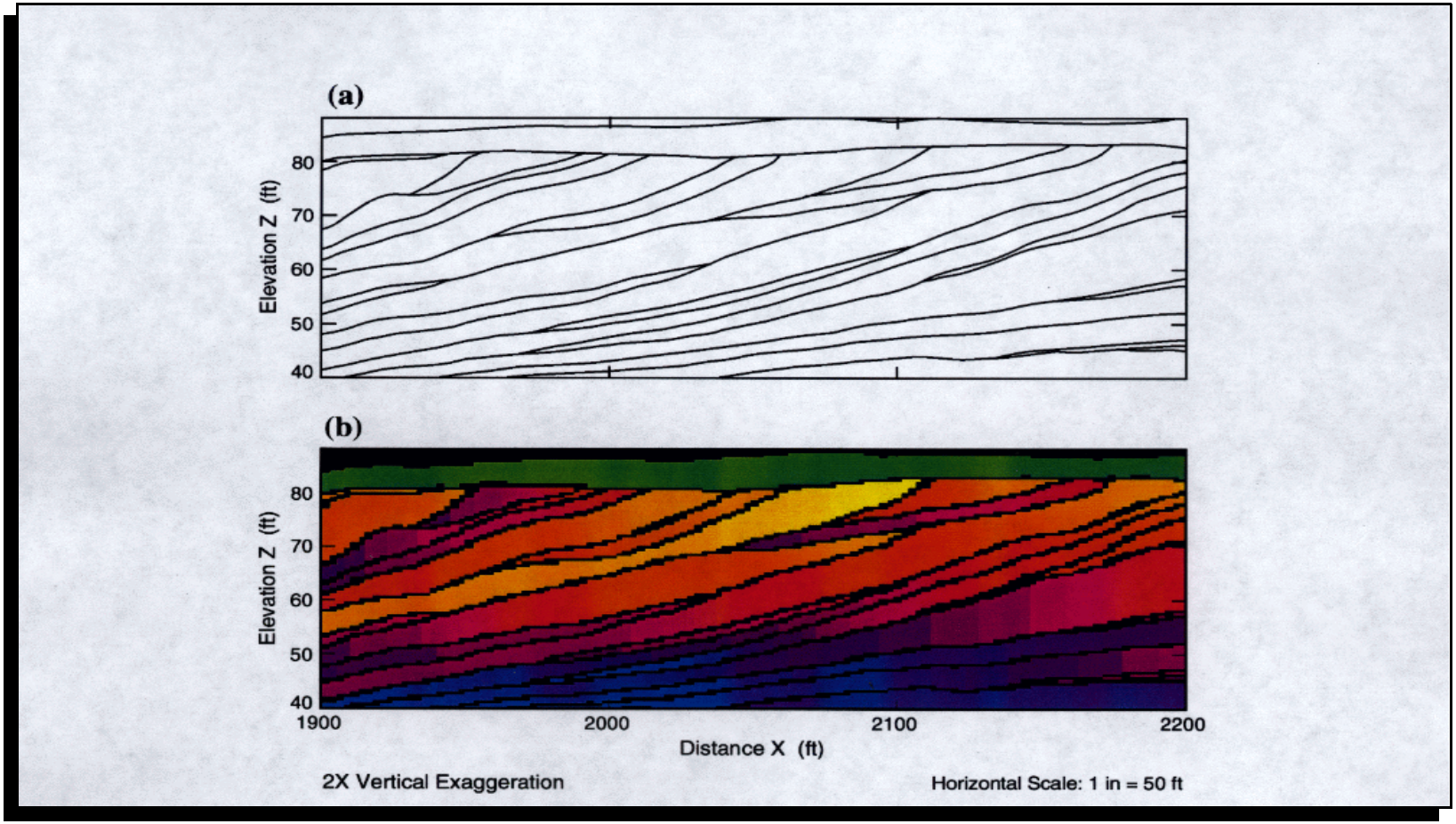


Figure 10-5. Sub-domain showing: (a) closed polygons enclosing individual clinoforms and (b) gridded clinoforms. The polygons in (a) are simply lines in the plane. The grid in (b) allows petrophysical properties, represented here in black and as shades of gray, to be assigned to throughout the modeling domain. This sub-domain was used in subsequent permeability upscaling experiments.

Relationships between absolute permeability and clinoform facies described by Chidsey and Allison (1996), Chidsey (1997), and Mattson (1997) are used to surmount the problem of incomplete permeability characterization within a clinoform. Each clinoform in the gridded model domain is populated with permeability using the simple approach illustrated in figure 10-6 and 10-7. Each clinoform is subdivided into three facies (distal, medial, and proximal) based on average grain size, sedimentary structure, lithology, bed thickness, angle of bed inclination, and position within the clinoform (Chidsey and Allison, 1996; Chidsey, 1997; Mattson, 1997). An example of this procedure, together with permeability histograms of measurements grouped by facies, are shown in figure 10-6. The arithmetic mean of permeability of a particular facies is assigned to the grid cell at the mean x-coordinate of that facies (figure 10-7). Absolute permeability in any other grid cell is calculated by linear interpolation or extrapolation, based on the x-coordinate of the cell. A lower limit of 0.1 millidarcies (md) is imposed on the extrapolation in the distal part of a clinoform, while an upper limit of 500 md is imposed on the extrapolation in the proximal part of a clinoform (however, the maximum calculated permeability is only 33.9 md). These limits roughly correspond to the minimum and maximum permeability measurements in the respective facies. Note that this scheme imparts only a horizontal permeability trend within a clinoform, since the interpolation or extrapolation is based solely on x coordinates. The data do not support defining vertical permeability trends at specified x coordinate locations, thus this possibility is not included in the models.

The approach described above is possible only when a clinoform is "complete" in the sense that it contains each of the three clinoform facies types: proximal, medial and distal (Mattson, 1997). However, only 18 of the 66 clinoforms in the model domain are complete; the remaining 48 clinoforms are "incomplete," containing only one or two of the clinoform facies. Incomplete clinoforms are the result of erosion or non-deposition of a particular facies. Table 10-1 lists the possible combinations of facies that can be preserved in a clinoform, and the corresponding number of clinoforms of each combination type incorporated in the model domain.

Table 10-1. Facies preservation in model domain clinoforms.

Facies Preserved*	Number of Clinoforms
Complete	18
Proximal	8
Medial and Proximal	5
Medial	13
Distal and Medial	19
Distal	3

* Does not include cap facies, which is present in only one clinoform.

Absolute permeability is distributed within incomplete clinoforms using the average length ratios R_{mp} and R_{md} computed from the complete clinoforms. These ratios are defined as:

Eq. 10-1 $$R_{mp} = \frac{1}{N}\sum_{i=1}^{N}\frac{Lm_i}{Lp_i}$$

and

Eq. 10-2 $$R_{mp} = \frac{1}{N}\sum_{i=1}^{N}\frac{Lm_i}{Ld_i}$$

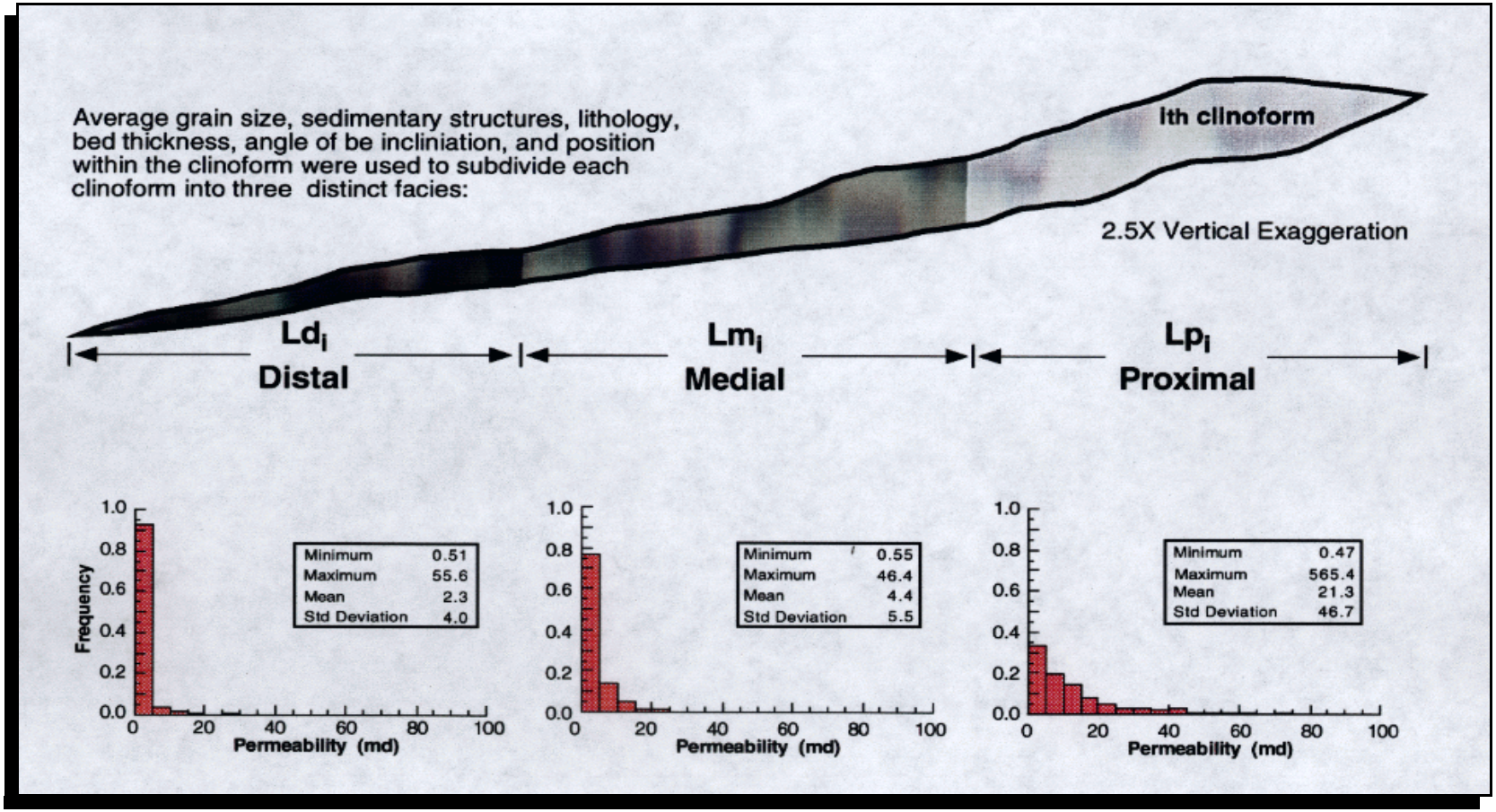


Figure 10-6. Method used to subdivide each clinoform into distinct facies, and histograms of permeability measurements pooled by facies.

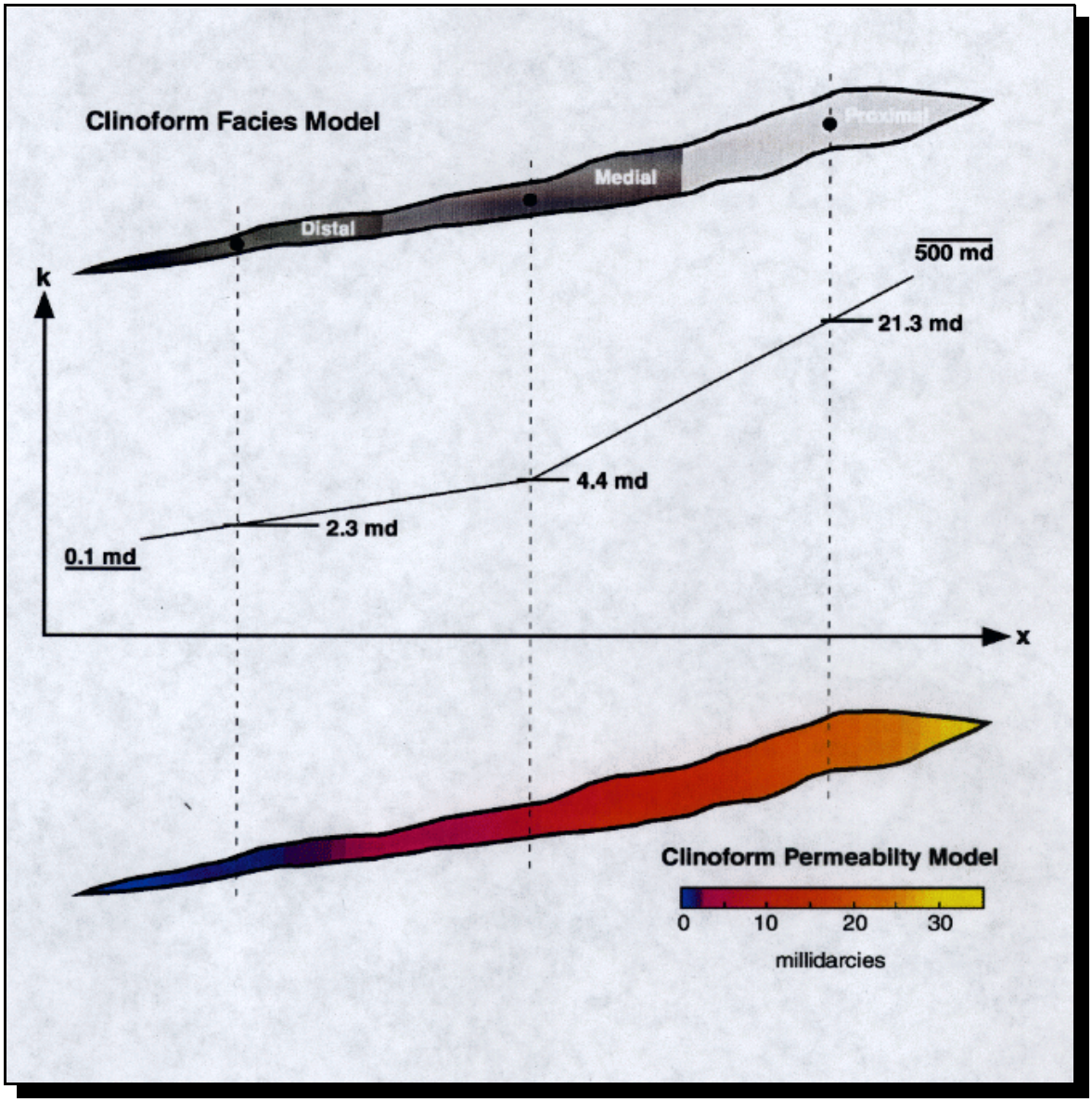


Figure 10-7. Method of populating a clinoform with permeability.

where N = 18, and Lp_i, Lm_i, and Ld_i are as shown in figure 10-6. R_{mp} = 0.823 is the average ratio of *x*-distance spanned by the medial facies to the *x*-distance spanned by the proximal facies. R_{md} = 0.383 is the average ratio of x-distance spanned by the medial facies to the x-distance spanned by the distal facies. The ratios are used to compute the length of the "missing" facies so that the linear interpolation/extrapolation method outlined above for populating complete clinoforms with permeability can be applied to incomplete clinoforms. For example, consider the kth incomplete clinoform in which the distal and medial facies are preserved but the proximal facies is absent. The estimated x-distance Lp_k spanned by the missing proximal facies is computed in:

$$\text{Eq. 10-3} \qquad Lp_k = \frac{Lm_k}{R_{mp}}$$

With this computed length Lp_k, interpolation of permeability between the medial and proximal facies can be performed as discussed earlier. A similar approach is used for incomplete clinoforms in which a facies other than proximal is missing.

Petrophysical Models Used for Flow Simulation

Figure 10-8 shows the four permeability models built for subsequent use in flow simulation studies (the black region in the top left of each model represents null grid blocks that are inactive during numerical flow simulations). Each is a different portrayal of the extent to which bounding layers surround individual clinoforms. At one extreme, no bounding layers separate clinoforms (figure 10-8a): all contacts between adjacent clinoforms are sandstone-on-sandstone. At the other extreme, every clinoform in the model domain is completely encased by bounding layers (figure 10-8d). Between these extremes, and presumably closer to reality, are two models in which bounding layers are absent over a portion of the modeling domain. The first of these models is based on the detailed interpretation of bounding layers described in Chapter 7, Geologic Framework of the Ivie Creek Case-Study Area, and is shown in figure 10-8b. The second (figure 10-8c), is built by assuming that a sandstone-on-sandstone contact exists between two neighboring clinoforms wherever the proximal facies of the two clinoforms are adjacent. The permeability tensor is taken to be isotropic in all models. A single relative permeability curve, from Odeh (1981), is used in the flow simulations.

Boundary layers are assigned a constant permeability of 0.01 md. This is lower than any permeability measured in the project, and an order of magnitude lower than the smallest permeability permitted within a clinoform. Selecting this plausible value provides enough contrast between boundary layer permeability and clinoform permeability to compare the impact that various boundary layer configurations have on reservoir performance.

No thickening of bounding layers is considered, although field observations indicate that boundary layers thicken in the depositional dip direction. The thickness of the modeled bounding layers is nominally 0.5 feet (0.2 m), the z-dimension of the model grid blocks. Greater thicknesses occur where bounding layer grid blocks are "stacked" as a result of the conversion from polygonal to gridded clinoforms, and where the bounding layers of adjacent clinoforms intersect.

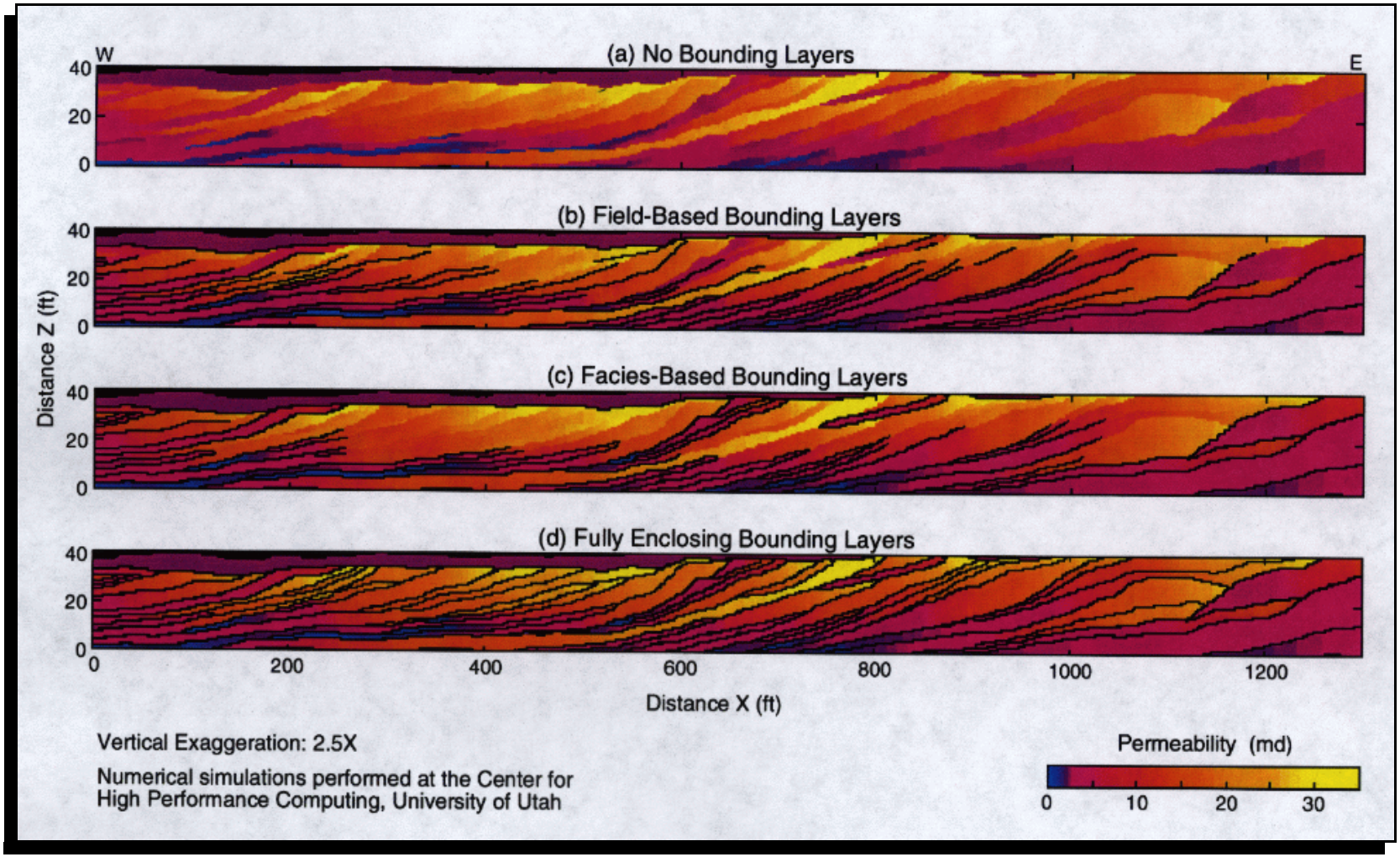


Figure 10-8. Permeability models used in subsequent flow-simulation study. (a) No bounding layers enclose clinoforms. (b) Partial bounding layer model derived from photomosaic and field work. (c) Partial bounding layer based on adjacent proximal facies. (d) Bounding layers completely enclose clinoforms.

Porosity ö is computed from absolute permeability k using the empirical relationship obtained from permeability and porosity measurements of case-study outcrop plugs (and previously reported in Chapter 8, Petrophysical Characteristics of the Ivie Creek Case-Study Area):

Eq. 10-4 $\ddot{o} = (\log_{10} k + 2.64)/22.72$

where ö is fractional porosity and k is absolute permeability. Porosity is computed from the permeability model in which bounding layers are absent (figure 10-8a). This porosity model is used in all numerical flow simulations, regardless of the permeability model used, in order to facilitate comparisons between the flow simulation results of the four permeability models. Note that different porosity models, derived from and used with each permeability model, would yield different pore volumes. The different pore volumes, in turn, would produce different estimates of original oil in place (OOIP) and also affect the timing of water breakthrough in waterflood simulations.

Two-Dimensional Flow Simulation Studies

The effect of permeability layering imparted to the model reservoir by juxtaposing clinoform facies, and the impact of bounding layer configuration on reservoir performance is studied by simulating a waterflood in each of the petrophysical models illustrated in figure 10-8 and discussed in the previous section. The flow simulations involve two fluid phases, water and oil. Water injection begins at the start of the simulations, without any period of primary production. Injection is accomplished by a vertical well completed in all active grid cells on the left (west) side of the model. The water injection rate is 10 stock tank barrels (stb)/day (1.6 m^3) (approximately 0.007 pore volumes/day). Production is from a vertical well completed in all active grid blocks on the right (east) of the model, subject to a 3,500 pounds per square inch absolute (psia) (24,133 Kpa) bottom-hole pressure constraint. The time period simulated is three years (1,095 days). Simulation experiments indicate that reversing the positions of the injector and producer has only a minor impact, and does not materially affect the main results of the study.

The total pore space in each model is 8145 cubic feet (231 m^3), yielding an average fractional porosity for the entire model domain of about 0.16. Initial oil saturation in all models is 0.70, with an initial reservoir pressure of 5,000 psia (34,475 Kpa). OOIP is 1,003 stb (160 m^3). Other key reservoir and fluid properties are listed in table 10-2. These properties, the pressure-volume-temperature (PVT) properties of the reservoir fluids (Appendix C), as well as the relative permeability curve and capillary pressure curve used are taken from Odeh (1981).

Table 10-2. Key reservoir and fluid properties.

Parameter	Description	Value
Pi	Initial reservoir pressure	5000 psia
Oil gravity	API oil gravity	45° API
S_{wc}	Connate water saturation	0.30
S_{or}	Residual oil saturation	0.15
c_f	Formation compressibility	2×10^{-6} psi^{-1}
c_o	Oil compressibility	1×10^{-4} psi^{-1}
c_w	Water compressibility	5×10^{-5} psi^{-1}
μ_o	Oil viscosity	2.5 cp
μ_w	Water viscosity	1.0 cp

The modeling results are presented as a set of figures showing the spatial distribution of oil saturation in each petrophysical model, from model **a** to **d** (for example, figures 10-8a to 10-8d), at a series of time steps. Figure 10-9 shows oil saturation at 180 days after the start of water injection. Figure 10-10 shows oil saturation at 365 days, figure 10-11 at 540 days, and figure 10-12 at 730 days. The arrangement of the oil saturation plots in each figure is consistent with the arrangement of the permeability models, **a** through **d**, displayed in figure 10-8. Production curves presented in figure 10-13 summarize the production performance of each petrophysical model.

A common, though hardly surprising, feature of the simulation results obtained from each of the four petrophysical models is the tendency for the injected water to preferentially invade the upper, higher permeability part of the domain. This tendency is enhanced by the absence of bounding layers surrounding either all or part of the clinoforms comprising the domain architecture. Model **a** contains no bounding layers to impede flow; the preferred flow in the upper part of the domain simply reflects the higher permeabilities due to the juxtaposition of proximal facies. In models **b** and **c**, the water invasion is enhanced by the absence of bounding layers in the proximal parts of clinoforms, combined with the presence of bounding layers surrounding the medial and distal parts of clinoforms. Water flow is impeded in the lower part of the domain by the low permeability bounding layers between adjacent clinoforms, while in the upper part of the domain flow is enhanced because bounding layers are nearly absent.

The partial bounding layer models enhance the permeability stratification imparted to the model by the *en echelon* juxtaposition of clinoforms and the resulting arrangement of clinoform facies. A finger of high water saturation extends into the upper domain, so that near and behind the water front only about half the reservoir thickness is involved in the flood. The tendency for water to override the lower part of the domain is diminished in model **d**, where all clinoforms are completely enclosed by bounding layers. In this case, bounding layers surround and retard flow through the proximal, higher permeability facies concentrated in the upper part of the domain. The finger of high water saturation in the upper part of the model is much shorter in **d** that in **a** through **c**, so that just behind the water front a greater vertical proportion of the reservoir is involved in the flood.

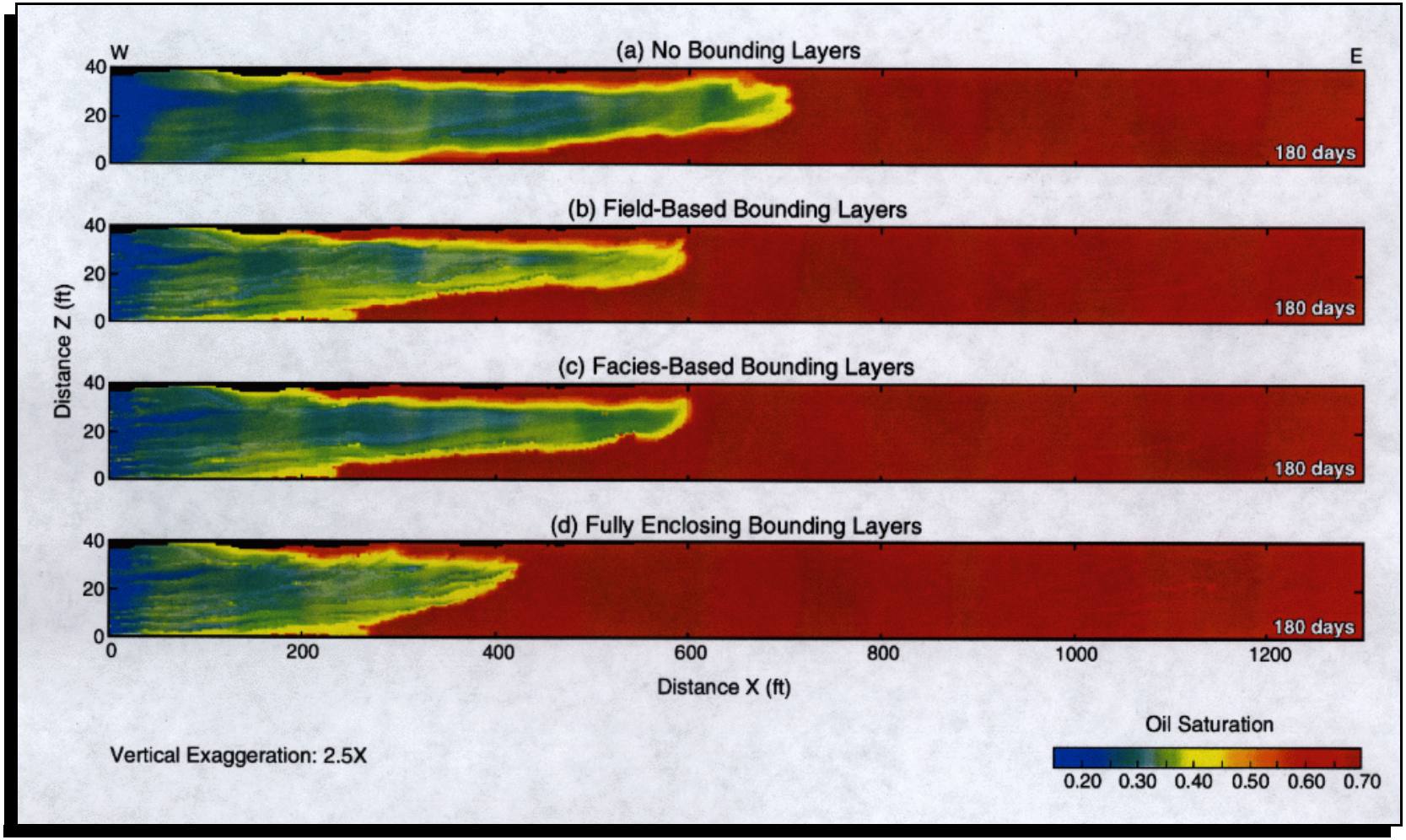


Figure 10-9. Oil saturation at 180 days after the start of water injection along the left-hand side of the modeling domain.

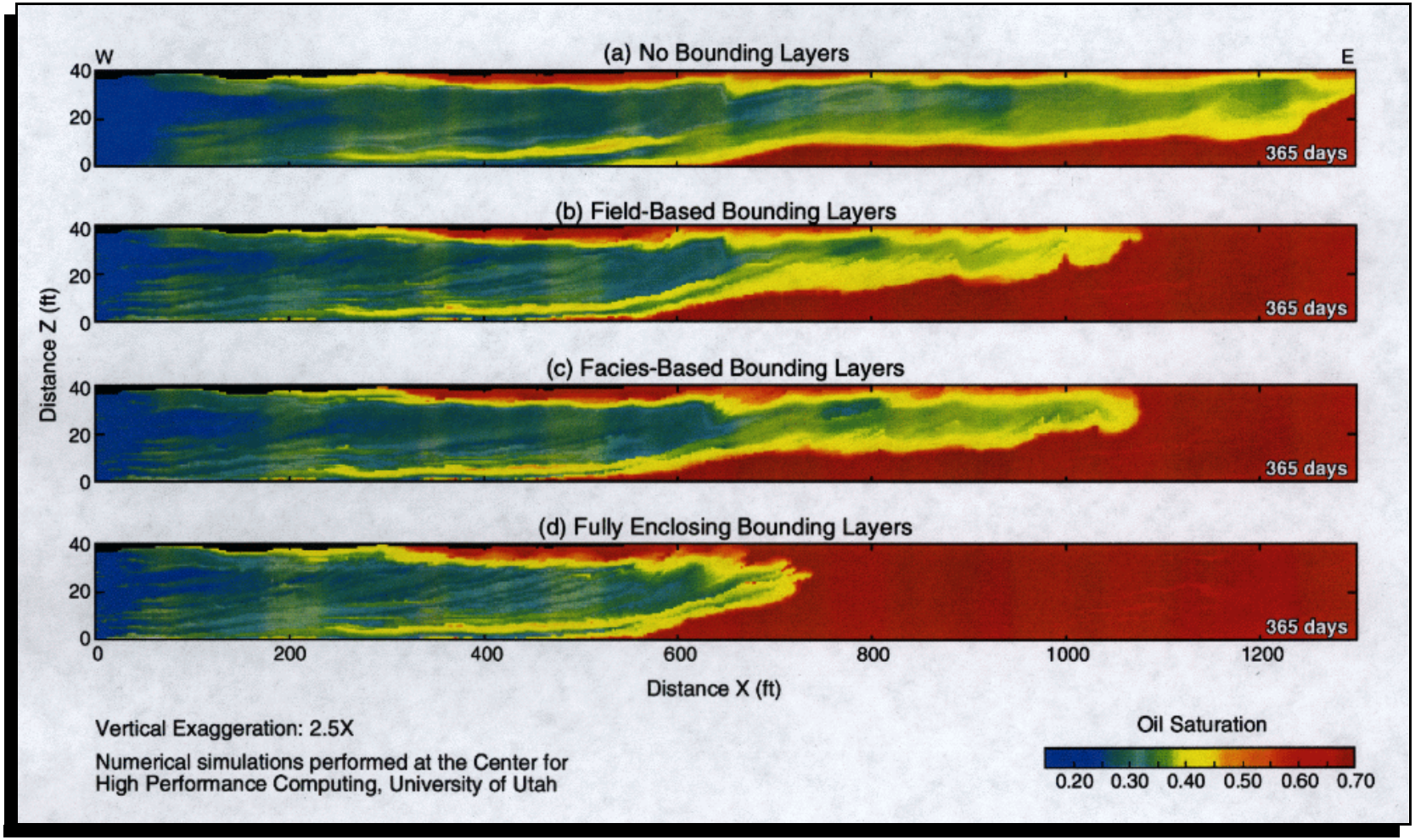


Figure 10-10. Oil saturation at 365 days after the start of water injection along the left-hand side of the modeling domain.

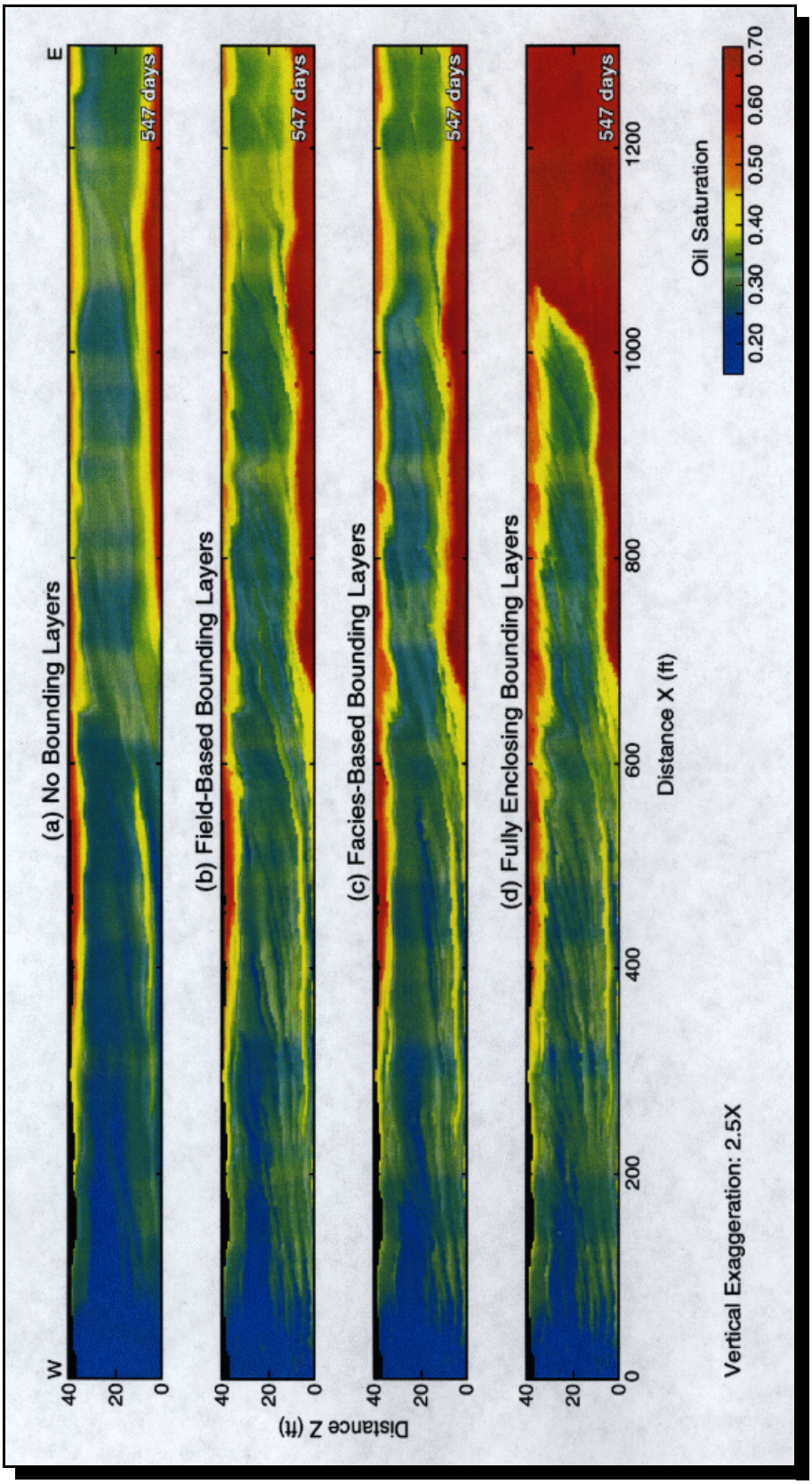


Figure 10-11. Oil saturation at 547 days after the start of water injection along the left-hand side of the modeling domain.

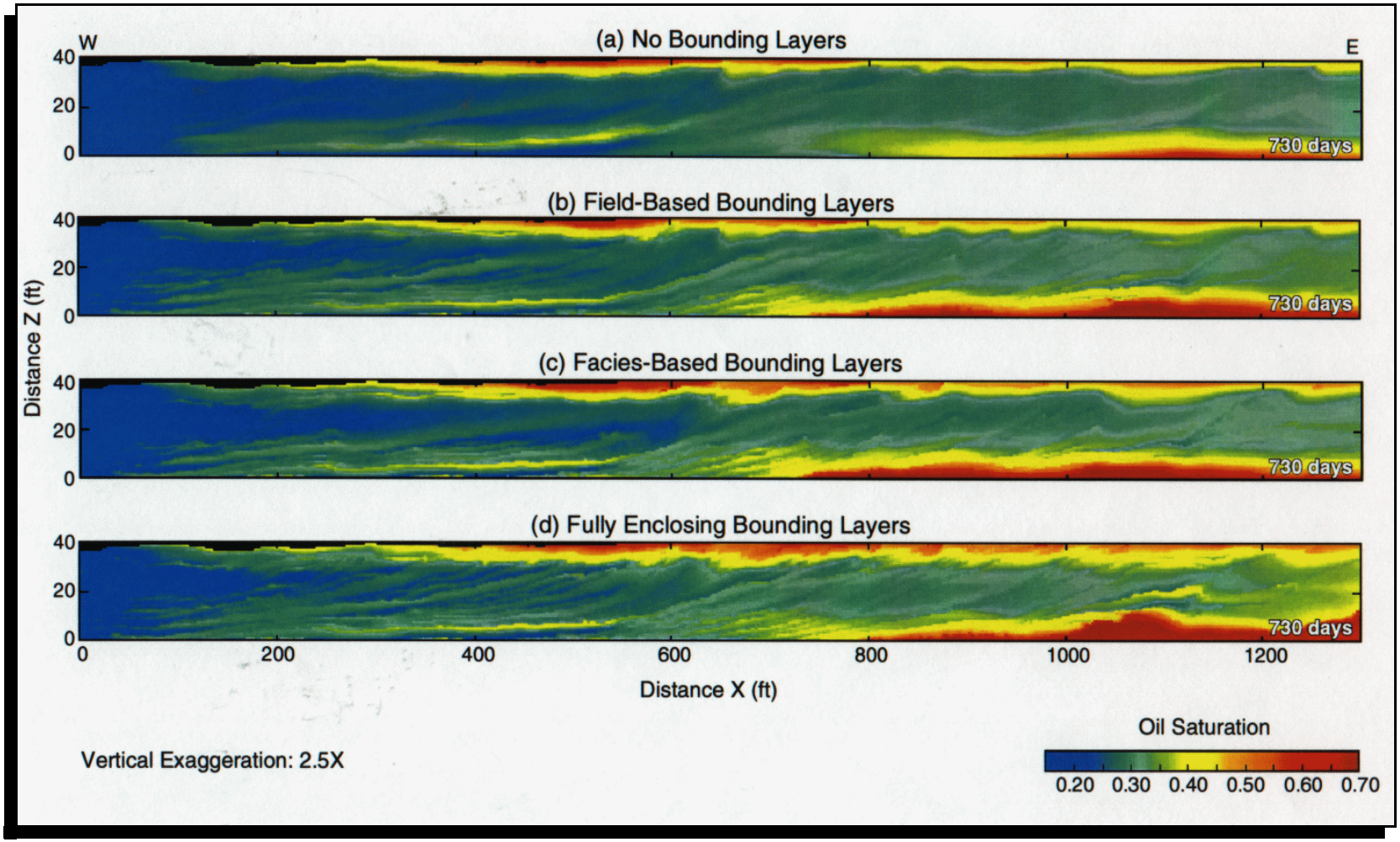


Figure 10-12. Oil saturation at 730 days after the start of water injection along the left-hand side of the modeling domain.

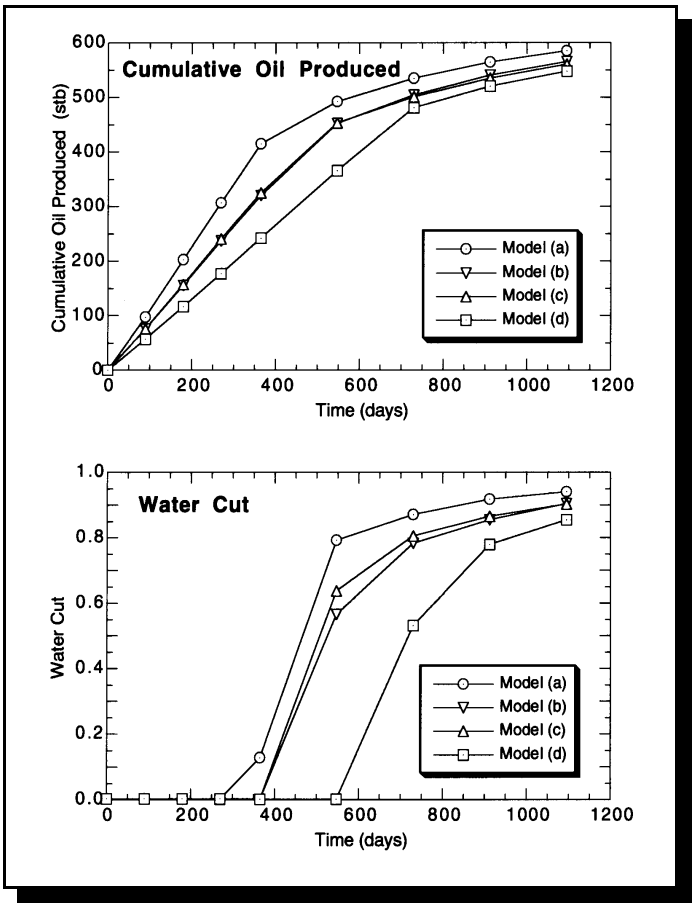


Figure 10-13. Cumulative production and water cut curves for the four petrophysical models. OOIP is 1,003 stb for all models.

The facies-based bounding layer model in figure 10-8c is used to estimate effective horizontal and vertical absolute permeability, and thus permeability anisotropy, for the model domain. The computed permeability anisotropy is used in the 3-D modeling work discussed more fully in a later section.

Total oil recovery from each model after three years of production is similar (figure 10-13). Cumulative production ranges from a high of 585 stb (93 m^3) (0.58 of OOIP) from model **a** to a low of 548 stb (87 m^3) (0.55 of OOIP) from model D; models B and C yield cumulative production, respectively, of 565 stb (90 m^3) (0.56 of OOIP) and 560 stb (89 m^3) (0.558 of OOIP). At any fixed time after the start of production, model **a** has the highest cumulative production and model **d** the lowest. These results are expected, since the more realistic permeability configurations of models **b** and **c** are intermediate between the extremes represented by models **a** and **d**. The shape of the production curves in figure 10-13 suggest that the differences in cumulative production between the models would persist even for considerably longer production times. The curves also suggest that the incremental additions to cumulative production would be small, and possible only under the penalty of high water cut conditions, as discussed below.

Although cumulative production from each of the four models is similar after three years, it is clear from figure 10-13 that bounding layer configuration has a large impact on the timing of oil production and water breakthrough. Water breakthrough occurs first in model **a**, at about 365 days. Water cut ([water produced]/[total fluids produced]) climbs rapidly, to nearly 0.80 at 547 days. In contrast, breakthrough in model **d** occurs at about 547, and a water cut of 0.80 is reached after approximately 1,000 days. Models **b** and **c** exhibit similar water breakthrough curves, with breakthrough between 365 days and 547 days; a water cut of 0.80 is reached at roughly 800 days.

These modeled production results have clear economic consequences. For example, model **a** yields a pessimistic estimate of the time to water breakthrough, and an optimistic estimate of cumulative production at a fixed time after the start of water injection. Note that at 365 days cumulative production from model **a** is 415 stb (66 m^3), nearly 30 percent higher than the 320 stb

(51 m^3) produced from model **b**. Economic calculations based on model **a** would result in high cash flow early in the operation of the field, and a short lifetime of operation if the decision to abandon the field is based on water cut. Conversely, predictions based on model **d** would indicate a prolonged period of low water cut production at low production rates.

There are only minor differences in the production curves for models **b** and **c**, suggesting that the facies-based approach to modeling the extent of bounding layers is a good approximation to the model based on field observations. If this method is to be used, it is crucial that good estimates of clinoform dimensions and the relative lengths of the facies comprising clinoforms be obtained by comparing downhole information to similar facies mapped in outcrop analogs.

Several issues that would likely have an impact on the performance of the modeled reservoir were not explored in the study. These include:

- Bounding layer thickness typically increases in the depositional dip direction. Including this observation in the permeability models, combined with the absence of bounding layers between the proximal facies of adjacent clinoforms would increase the apparent stratification of flow exhibited by models **b** and **c**. Water invasion in the lower part of the model domain would be diminished, enhancing the finger of high water saturation advancing in the upper part of the domain.

- Flow between adjacent clinoforms is likely retarded by permeability anisotropy in bounding layers. Modeling bounding layer anisotropy is difficult, however, because the principal directions of the permeability tensor are probably aligned parallel (maximum permeability) and perpendicular (minimum permeability) to bedding rather than coincident with coordinate axes. Moreover, the bedding orientation of a particular bounding layer varies in space. Bounding layer bedding at Ivie Creek is near horizontal in the distal part of a clinoform, but may reach up to 10° proximally. The effect of anisotropy is likely to enhance the stratification of flow, as in the case of increasing boundary layer thickness discussed above.

- Different relative permeability and capillary pressure curves for the clinoform interiors and bounding layers are not used. Differences in capillary pressure between the two regions may result in the flow of oil from the bounding layers to the clinoform interiors, even though the bounding layers retard the flow of oil induced by hydrodynamic forces.

Permeability Upscaling (Homogenization)

Full field simulations are impractical using the grid block size (2.5 feet x 0.5 feet [0.8 x 0.2 m], yielding 41,680 grid blocks) used in the 2-D Ivie Creek modeling. A 3-D model of the same thickness (40.5 feet [12.3 m]) and of areal extent equal to the squared length (13,002 $feet^2$ [1,208 m^2], slightly less than 40 acres [16.2 ha]) of the 2-D model would require nearly 22,000,000 grid

blocks. Permeability upscaling, or homogenization, addresses this issue by attempting to find the equivalent permeabilities of a group of large grid blocks which will yield the same simulation results as those obtained using many smaller grid blocks. Coarser gridding can then be used to discretize the problem domain.

Two-dimensional permeability upscaling experiments are conducted using a computer program developed by Koebbe (1995). The program is a flow-based averaging scheme which yields homogenized absolute permeability using a perturbation method applied to the equations for flow in a porous medium. The method provides a homogenized, full tensor, absolute permeability. It does not address the issue of upscaling relative permeabilities, and thus is not a "pseudo-function" approach (for example, Kossack and others, 1990).

The portion of the 2-D modeling domain highlighted in figure 10-2 and shown detail in figure 10-5 is used in the upscaling experiments. Fluid and reservoir properties are the same as those used in the previous 2-D modeling, except that the injection and production rates are adjusted to reflect the smaller domain size. In addition, the porosity is fixed at 50 percent.

Four grid block sizes are used in the upscaling experiments: the original 2.5 foot x 0.5 foot (0.8 x 0.2 m) blocks, denoted 1x1; blocks scaled by a factor of 2 in both x and z (5.0 feet x 1.0 feet [1.5 x 0.3 m]), denoted 2x2; blocks scaled by a factor of 4, denoted 4x4; and blocks scaled by a factor of 8, denoted 8x8. An upscaled, absolute permeability tensor is obtained by supplying the homogenization program with the scaling factor and the detailed, 1x1 permeability model. Water injection simulations were then run with the TETRAD-3D simulator on a model domain discretized at the larger grid spacing and populated with the upscaled permeabilities. Off-diagonal terms of the upscaled permeability tensor were ignored because TETRAD-3D assumes that the grid axes are parallel to the principal directions of the permeability tensor. Upscaled permeabilities are also computed by taking the harmonic and geometric means of the permeabilities within the larger grid blocks. Water injection simulations are also run using the permeabilities obtained by these simple averaging techniques.

Cumulative production and water cut curves obtained from the upscaling experiments are shown in figure 10-14. Also shown for reference are the results of water injection into a homogeneous domain with a permeability of 8 md, the arithmetic mean of the permeabilities in the 1x1 model. Results are presented for harmonic averaging, geometric averaging, and perturbation method homogenization.

Harmonic averaging tends to emphasize lower permeabilities. It is the appropriate averaging technique for computing the effective permeability for a stratified medium when flow of a fully saturating, single-fluid phase is perpendicular to the stratification. When used to upscale the permeabilities in the small Ivie Creek sub-domain, both cumulative production and water cut are underestimated. The production estimates are very sensitive to grid block size, and degrade dramatically as the size of the grid block increases: in the 8x8 case, cumulative production after three years of simulated waterflooding is only 70.2 stb (11.2 m^3), compared with 383.2 stb(60.9 m^3) in the 1x1 case; water cut at three years is 0.20, compared with 0.98 in the 1x1 case. This occurs because a grid block is more likely to contain low permeability values as the size of the grid block increases.

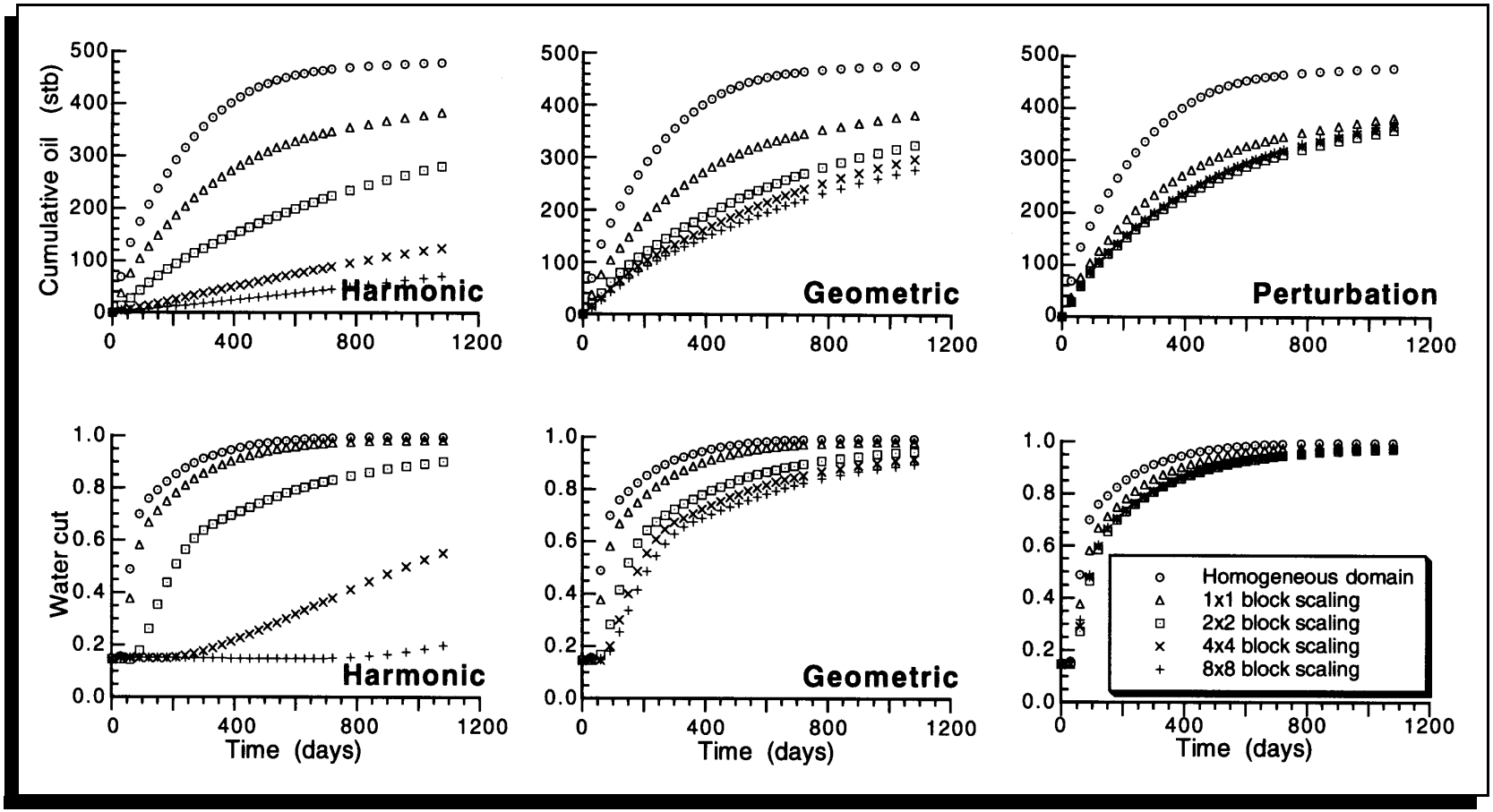


Figure 10-14. Results of permeability upsealing experiments. Top row: cumulative oil production plots obtained using harmonic, geometric, and perturbation method averaging at various block sizes. Bottom row: corresponding water cut plots.

Geometric averaging yields a number intermediate between arithmetic and harmonic averaging. It is considered a 'quick and dirty' upscaling method after the work of Warren and Price (1961), who found it to be the best estimator of bulk permeability for a medium in which permeabilities are distributed randomly and without spatial correlation. Cumulative production and water cut are both underestimated when geometric averaging is used to upscale permeabilities, as was the case with harmonic averaging. However, production estimates are less sensitive to grid block size than with harmonic averaging. Cumulative production in the 8x8 case is 278.1 stb (44.2 m^3) and water cut is 0.90 after three years of simulated waterflooding.

Permeability upscaling by the perturbation method also leads to lower simulated values of cumulative production and water cut. However, the simulated results are better than those obtained using either harmonic or geometric permeability. Cumulative production is 372.0 stb (59.1 m^3) and water cut is 0.97 after three years of simulated waterflooding. In addition, the computed results are far less sensitive to grid block size than they are when harmonic or geometric permeability averaging is used. Indeed, production estimates obtained in the 8x8 case are actually better than those obtained from the 2x2 or the 4x4 case. This surprising result warrants further attention, which we are unable to provide in this study.

Not shown are the results obtained using simple arithmetic averaging as an upscaling method. Experiments performed using a model in which clinoform interiors have a constant permeability indicate that arithmetic averaging leads to simulation results that overestimate production estimates. Production estimates tend towards the results obtained from the homogeneous model as the size of the grid block increases.

Summary and Conclusions

Two-dimensional petrophysical and fluid-flow modeling at the Ivie Creek case-study area is based on the outcrop architecture along with permeability measurements made on core plugs extracted from the outcrop and on slabbed core from drill holes.

The clinoform is the main architectural element observed at the site. Each sigmoidal clinoform consists of sandstone bedsets which record an episode of delta-front deposition followed by partial erosion. Clinoforms are inclined seaward, arranged *en echelon*, and are usually separated from each other by a thin (less than 1 foot [< 0.3 m]) mudstone and siltstone bounding layer. The resulting architecture provides the spatial framework for modeling the configuration of petrophysical properties, and the subsequent numerical simulation of two-phase (oil and water) fluid flow.

A gridded, digital model of the site architecture preserves individual clinoforms, and is the basis for distributing absolute permeability throughout the modeling domain. Permeability modeling is accomplished by subdividing each clinoform into three facies (distal, medial, and proximal). The arithmetic means of permeabilities grouped by facies are used to linearly interpolate or extrapolate permeability throughout a particular clinoform. A method based on ratios of mean lengths of the three facies was developed to handle those clinoforms in which all three facies are not present. Resulting clinoform permeabilities in the modeling domain range from 0.1 md to 33.9 md. Bounding layer permeability is a constant 0.01 md.

Four permeability models are built for the flow-simulation studies. Each portrays a different extent to which constant thickness bounding layers surround individual clinoforms. At one extreme, no bounding layers separate clinoforms and all contacts between adjacent clinoforms are sandstone-on-sandstone. At the other extreme, every clinoform in the model domain is completely encased by bounding layers. Between these extremes, and presumably closer to reality, are two models in which bounding layers are absent over a portion of the modeling domain. One of the intermediate models is based on field observations. The other is obtained by assuming that the bounding layer between clinoforms is thin or absent where the proximal facies of two neighboring clinoforms are adjacent. The same porosity model, obtained using an empirical relationship between permeability and porosity for the case study, was used together with each of the four permeability models in subsequent flow simulations.

The production performance of each reservoir model was studied by simulating a waterflood in each of the reservoirs. Water injection began at the start of the simulations, without a period of primary production. A single relative permeability curve and a single capillary pressure curve were used in all simulations. In addition, absolute permeability tensor was considered to be isotropic. The simulations run for a time period of three years (1,095 days).

All models exhibit a common, unsurprising feature: preferred flow of the waterflood in the upper, higher permeability portion of the models. This is caused by the juxtaposition of proximal facies, which imparts a stratified permeability structure to the models. This effect is most pronounced in the two models in which bounding layers are absent between proximal clinoform facies.

The timing of oil production and water breakthrough is sensitive to the nature of the bounding layers. Earliest breakthrough occurs, at roughly 365 days, in the model without bounding layers. This model also yields the highest cumulative production at any fixed time after the start of water injection: after three years 0.583 of the OOIP is produced. The longest time to breakthrough occurs in the model in which bounding layers completely enclose clinoforms, at between 547 and 730 days. This model also yields the lowest cumulative production at any fixed time after the start of water injection: after three years 0.546 of the OOIP is produced. The two models with partial bounding layers are similar to one another, and yield simulation results between those of other two models. In these intermediate cases water breakthrough occurs between 365 days and 547 days, while after three years of production about 0.561 of the OOIP is produced. Economic calculations based on cumulative oil production and time to water breakthrough will clearly be affected by the type of bounding layer model used.

Permeability upscaling experiments indicate that common averages (arithmetic, harmonic, and geometric) are inadequate approaches to upscaling absolute permeability in this depositional environment. An upscaling technique based on perturbation analysis yields simulation results similar to those obtained with detailed permeability models.

Three-Dimensional Modeling

Model Domain

The 3-D model grid is 2,000 feet by 2,000 feet (610 x 610 m) in plan view and 60 feet (18 m) thick (figure 10-15). The domain contains 150,000 rectilinear grid blocks each 20 feet by 20 feet (6 x 6 m) in plan view and 4 feet (1.2 m) thick. Thus, there are 15 layers each with a grid of 100 by 100 blocks. The southeast corner of the model lies just outside the point where the cliff that bounds the north side of Ivie Creek meets the cliff that bounds the west side of Quitchupah Canyon (figure 10-16).

Production Strategies and Wellbore Configurations

A simple 5-spot pattern (figure 10-15) containing a central, vertical water injection well and four vertical oil production wells is used to model a waterflood scenario for most simulations. In these cases a maximum injection rate of 1,516 stb (241 m^3) of water are injected per day. In one additional case, a 9-spot pattern containing a central injection well (maximum injection rate of 1,516 stb water per day) and eight production wells (figure 10-15) is simulated. In all cases the wells are assumed to be completed across the entire thickness of the reservoir. A wellbore radius of 0.25 feet (7.62 cm) is specified for both injection and production wells. Wellbore skin effects are assumed negligible.

Physical Properties

Initial Conditions: A hypothetical, but plausible, set of initial reservoir conditions are selected for the 3-D fluid-flow modeling. Each model run started at the same initial oil and water saturations (0.5 for each fluid), rather than modeling primary production prior to performing a waterflood. This approach provides a straightforward basis for comparing the relative differences in reservoir performance. Note that an initial oil saturation of 0.7 is assigned in the 2-D simulations described in the previous section. A uniform initial fluid pressure of 5,000 psi (34,475 Kpa) and an isothermal temperature of 166E F (60E C) are also assumed throughout the model domain. A minimum bottom-hole pressure of 2,685 psi (18,513 Kpa) (corresponding to the bubble-point pressure of black oil) is specified at the water injection well. This constraint prevents the reservoir pressure from falling below the bubble-point pressure, ensuring that gas is not released from solution and restricting the simulation to only two phases (oil and water).

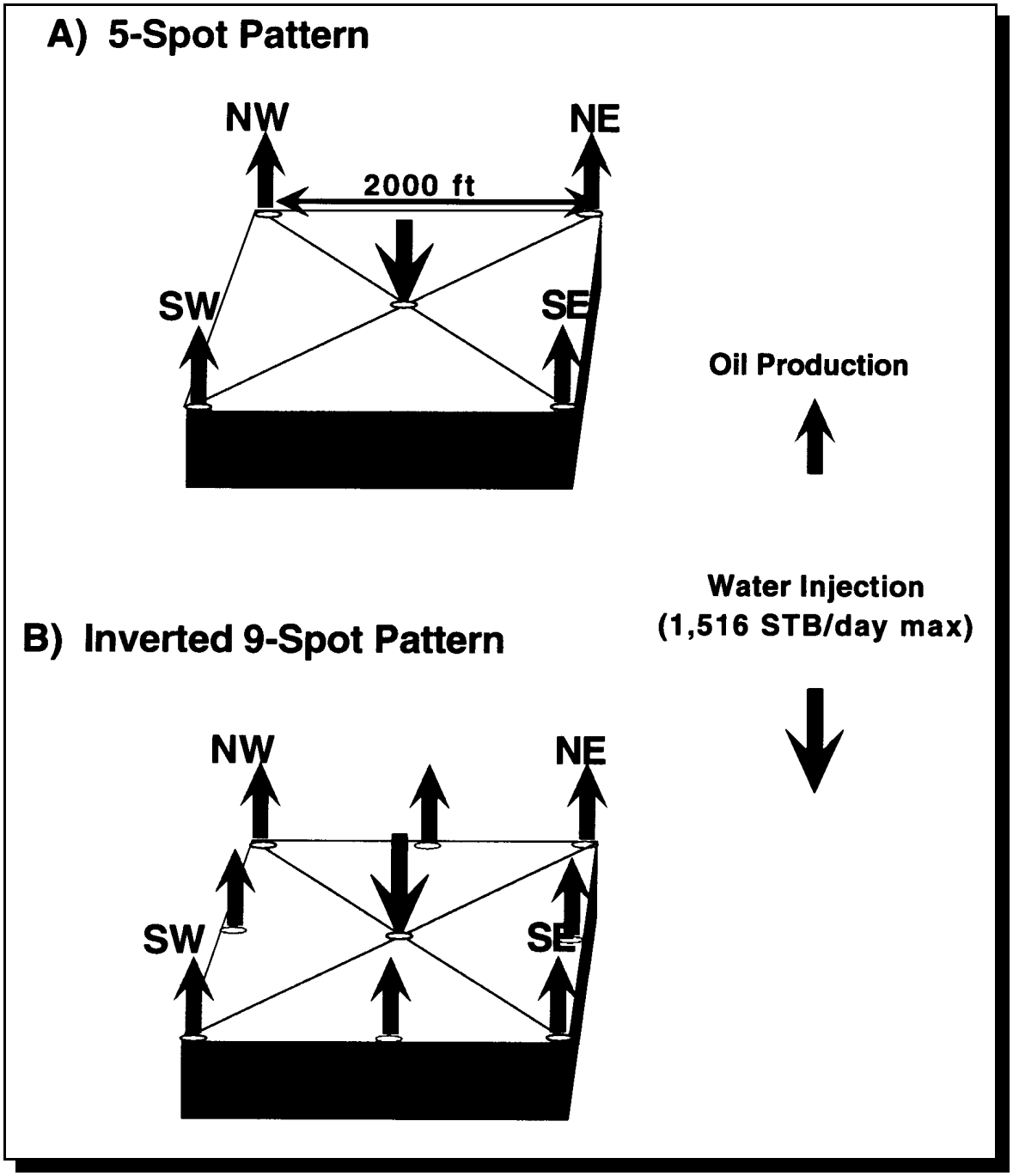


Figure 10-15. Schematic diagram showing well patterns used in simulated reservoir production.

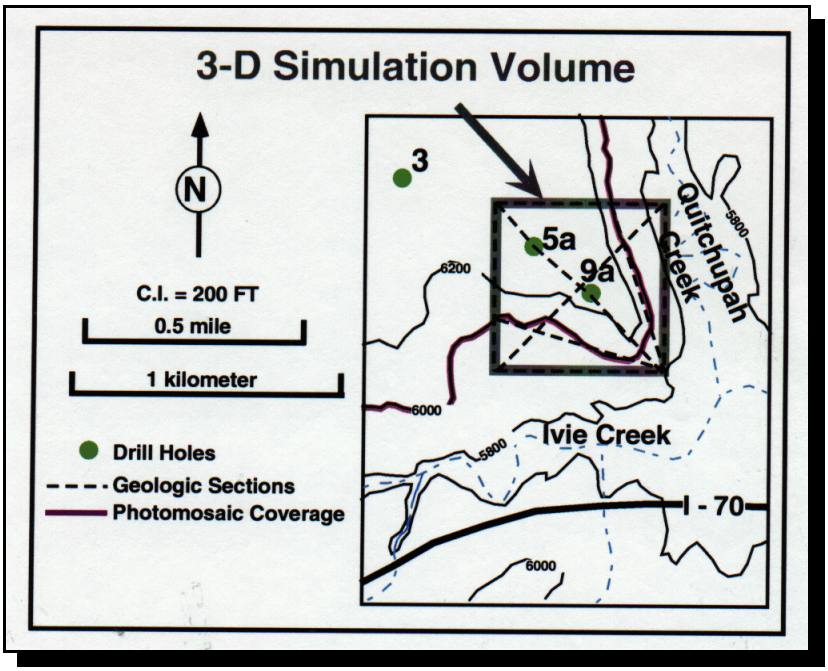


Figure 10-16. Location map showing the relationship between the 3-D simulation volume, cliff-face outcrops, drill holes, and geological cross sections.

Absolute Permeability: The distribution of clinoform facies described in previous sections is used to construct the different permeability structures simulated within the model domain. The reference permeability structure is derived from the 3-D clinoform facies structure (proximal, medial, and distal facies). Each facies is assigned an absolute permeability equal to the arithmetic mean of the permeability measurements made in that facies. These mean permeability values, listed in table 10-3 are the same as those used to construct the 2-D, trending permeability models discussed in the previous section (figure 10-7). The proximal facies is assigned a permeability of 21 md, the medial facies is assigned 4 md, and the distal facies is assigned 2 md. The fourth facies (clinoform cap) and the fifth facies (overlying Kf-1-Iv[c] bedset) are assigned permeabilities of 3 and 0.01 md, respectively. The base of the model is assumed to mark the upper boundary of the low-permeability Tununk Shale. Four different permeability structures (Reference Case, Homogeneous Case, Layered Case, and Anisotropic Case) are constructed, representing four different ways that drill-hole data might be used to interpolate absolute permeabilities within the model domain (figure 10-17).

The 'Reference Case' (figure 10-17) is defined as the most detailed permeability structure constructed for the model domain. Because a unique permeability and a unique porosity is associated with each clinoform facies type, these parameters are also shown in the facies distributions illustrated in the vertical and horizontal sections of figure 10-18. The maps and sections shown in figure 10-18 are taken directly from the detailed, 3-D facies structure. The horizontal sections (labeled with reference to their height, in feet, above the base of the model) show three of the 15 layers involved in the fluid-flow simulator. The vertical sections are constructed along the two diagonals that extend between opposite corners of the model domain and intersect at the central water injection well (figure 10-15). Only isotropic permeability values are assigned in the Reference Case. Thus, although facies-based permeability variations are included in the permeability structure, the bulk anisotropy imparted by the shaley bounding layers discussed under 2-D modeling is not included.

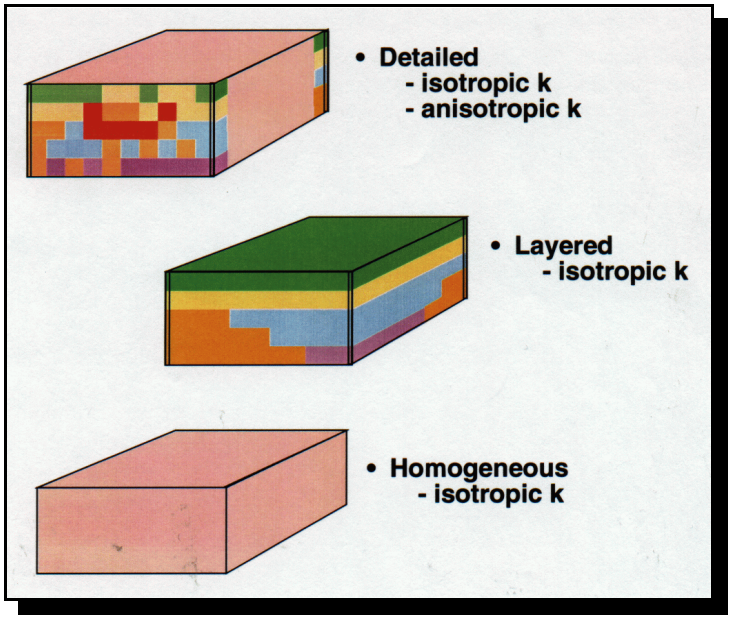


Figure 10-17. Schematic diagram showing the four permeability structures considered in the 3-D reservoir simulations, Reference case (detailed isotropic and anisotropic.

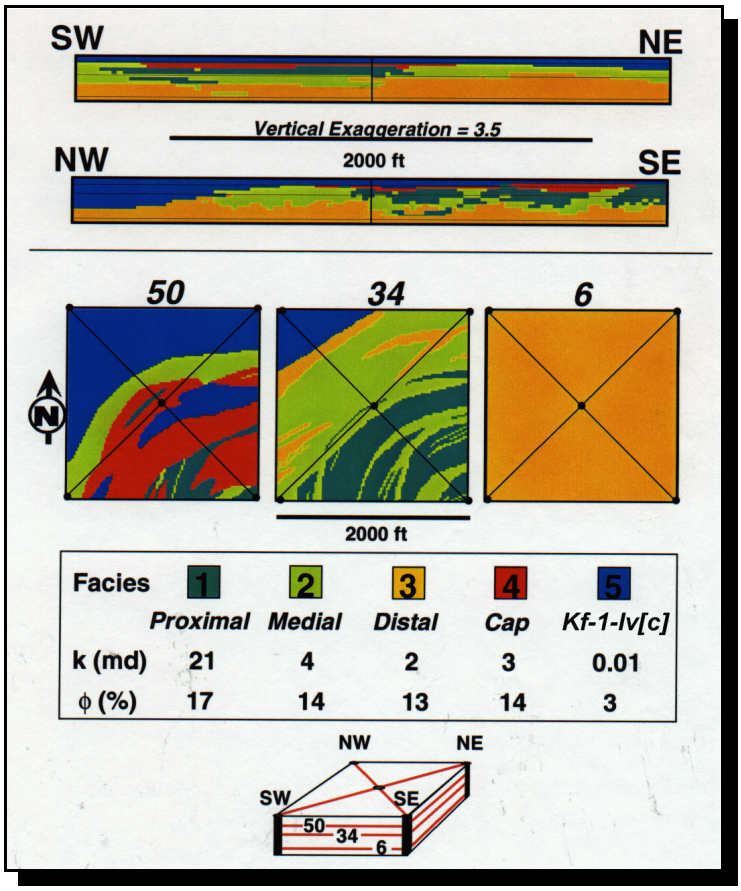


Figure 10-18. Isotropic permeability structure used in 3-D simulation studies.

The 'Anisotropic Case' includes the same level of detail as the 'Reference Case,' however, anisotropic permeabilities are assigned at each gridblock in an effort to incorporate the possible impact of the shaley bounding layers discussed and modeled in the previous section on 2-D modeling. The 2-D modeling results indicate that these features can play an important role in controlling oil production. The bulk effect of the shaley bounding layers is crudely approximated in a four-step process of building an anisotropic permeability structure outlined in Appendix C and shown in figure 10-19. Note that a radial character is imparted to the anisotropic permeability structure that is, in turn, superimposed on the heterogeneous facies structure incorporated in the Reference Case (figure 10-18). In addition, it is important to recognize that the 'rules' used to create the Anisotropic Case yield a wider range of permeability values than are included in the corresponding Reference Case. One consequence of our approach to constructing the Anisotropic Case is that both north-south permeability (k_{NS}) and west-east (k_{WE}) respectively, are less than the isotropic k values assigned at the south and east boundaries of the model domain (figure 10-20). Elsewhere, using a radial anisotropy ratio of k_{arc}/k_r (permeability k in annular direction [k_{arc}] perpendicular to radial permeability [k_r]) equal to 10 can yield either smaller or larger values of both k_{NS} and k_{WE}. It is clear, however, that important elements of the original permeability heterogeneity are retained. The 'Layered Case' is a simplified permeability structure constructed by sampling the vertical distribution of facies found at each of the four corners of the Reference Case. This sampling mimics the facies data that might be collected by drilling wells at the four locations. With this information in hand, a simple geological model is constructed by assuming that each facies has a tabular character. The resulting permeability structure (figure 10-21) has a layered appearance that mimics some of the gross features of the Reference Case (figure 10-18).

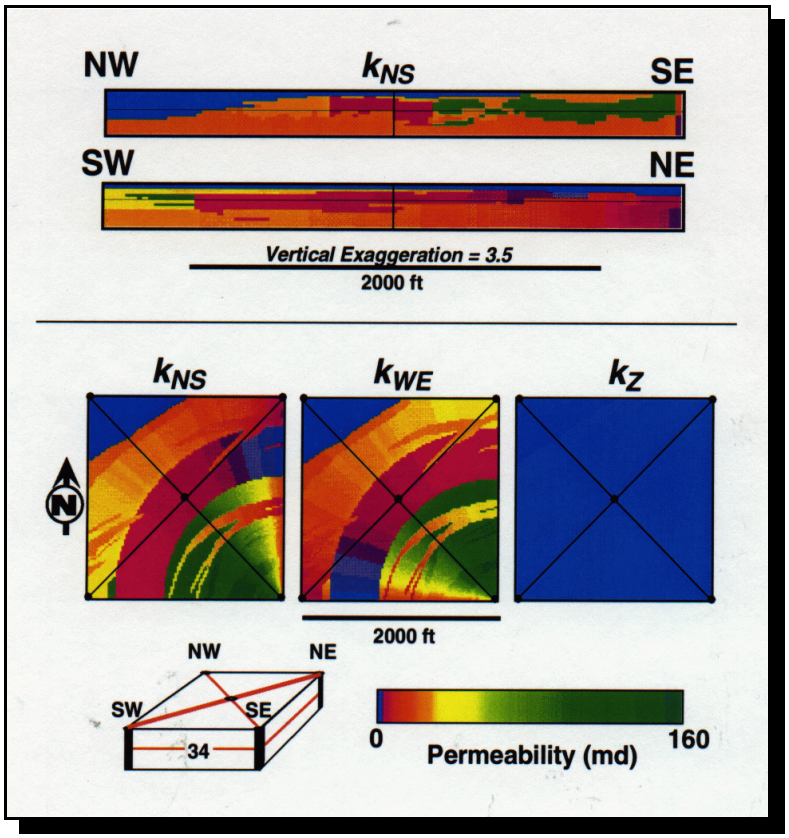


Figure 10-19. Anisotropic permeability structure used in 3-D simulation studies. This structure is used in an effort to preserve the impact of thin, fine-grained bounding layers that often separate adjacent clinoforms.

The simplest permeability structure is provided by the 'Homogeneous Case.' In this case the harmonic mean of all permeabilities assigned in the Reference Case (permeability of 3.8 md and porosity of 14 percent) is assigned throughout the model domain.

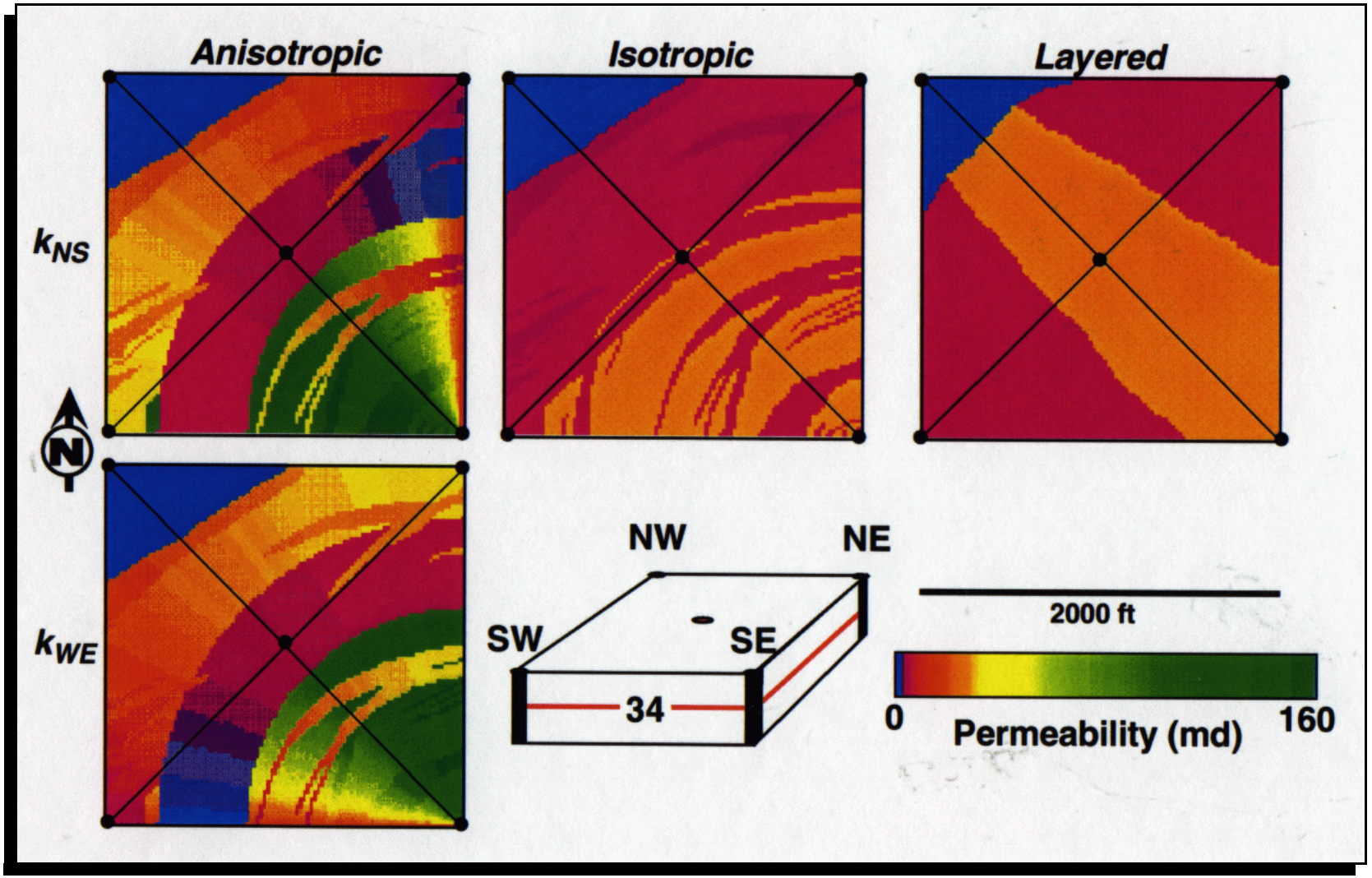


Figure 10-20. Plan view comparisons of the layer corresponding to z = 34 feet for each of the permeability models used in the 3-D simulations.

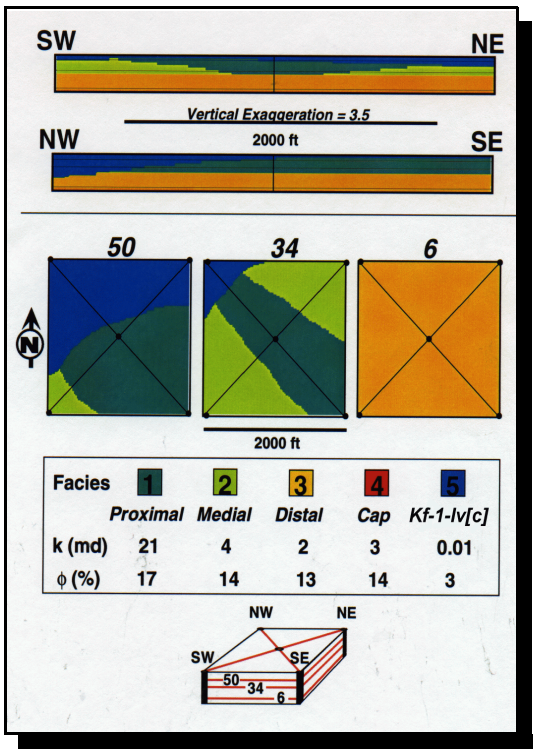


Figure 10-21. Simple layered permeability structure used in 3-D simulation studies.

Porosity: Porosity is defined throughout each model domain using a functional relationship between porosity ö and absolute permeability k. Because each facies type is assigned a single permeability value, a single porosity value is also assigned to each facies. Permeabilities and porosities measured on representative core plugs collected from the Ivie Creek field area suggest a reasonable correlation between porosity and permeability (see Chapter 8, Petrophysical Characteristics of the Ivie Creek Case-Study Area). The empirically derived relationship was given in Eq. 10-4. Because we assume negligible reservoir consolidation by matrix subsidence, a coefficient of reservoir matrix compressibility is not required. Permeability and porosity as a function of facies type are shown in table 10-3.

Table 10-3. Permeability and porosity for each clinoform facies.

Facies	Permeability (md)	Porosity (%)
Proximal	21.3	17
Medial	4.4	14
Distal	2.3	13
Clinoform Cap	3.0	14
Kf-1-lv[c]	0.01	3

Relative Permeability: Computed reservoir performance can depend strongly on the character of relative permeability relationships used to represent variations in permeability as a function of oil saturation (S_o) or water saturation (S_w). Although absolute permeabilities derived from outcrop provide good insight regarding the permeability structure of the Ivie Creek case-study area, we concluded that measuring the relative permeability characteristics of outcrop-derived samples would yield only limited new insight regarding relative permeabilities at reservoir conditions. As a consequence, plausible relative permeability relationships are derived from previous measurements of relative permeabilities for the Ferron Sandstone (Barton and Tyler, 1991, 1995; Fisher and others, 1993a, 1993b; Barton, 1994) and Berea Sandstone (Honarpour and others, 1986).

Developing oil-water relative permeability relationships for the Ferron Sandstone involves a two-step process. First, brine-air relative permeability relationships available for both Berea and Ferron rocks are compared to develop a transformation that relates the characteristics of the Berea

Sandstone to those of the more poorly sorted Ferron Sandstone. Once the transformation relationship is developed, oil-water relative permeability data for the Berea Sandstone is transformed into an oil-water relative permeability relation for Ferron Sandstone using the Brooks-Corey relations. Ultimately, relative permeability relationships for oil (k_{ro}) and water (k_{rw}) are derived for each facies included in the model domain. The approach used to derive the relative permeability relationships is outlined in Appendix C.

Fluid Properties: Fluid properties are defined to be consistent with an initial reservoir fluid pressure of 5,000 psia (34,475 Kpa). Wherever possible fluid properties (Appendix C) were specified to be the same as those used to conduct the black oil simulations performed for the Society of Petroleum Engineers Comparative Solution Project (Odeh, 1981). A two-phase oil/water system is assumed.

Three-Dimensional Flow Simulation Results

Two-phase fluid-flow simulations are used to explore how the four different permeability structures might influence oil production. In each case production is initiated with a waterflood rather than starting with an initial period of primary production.

Oil saturations obtained for a 5-spot production pattern in the Reference Case at times of 1, 3, and 10 years after the start of water injection are shown in three horizons (figure 10-22) and two vertical cross sections (figure 10-23). The detailed heterogeneities included in the Reference Case clearly influence the progress of the waterflood. Note that the low permeability clinoform cap facies (Kf-1-Iv[c] bedset) that dips down into the northwest quadrant of the model causes a localized increase in oil saturation to 70 percent from the initial value of 50 percent. The distribution of oil saturation at early times is clearly influenced by the details of the permeability structure. Higher permeabilities assigned in the proximal facies cause the waterflood to break through first at the southeast corner production well, followed soon after by breakthrough at the southwest corner.

A 9-spot pattern of wells (figure 10-15) is simulated to evaluate the relative merits of infill drilling using a regularized pattern of production wells. Oil saturations obtained at times of 1, 3, and 10 years after the start of water injection are shown in figures 10-24 and 10-25. Although the simulation results clearly indicate an increased sweep efficiency relative to the Reference Case, localized areas with increased oil saturation indicate regions where oil is likely to remain in the reservoir after production is halted. If the radial geometry assumed when building the permeability structure can be identified through analysis of bedding orientations logged in the initial 5-spot pattern, then a more efficient pattern of wells might be devised.

A 5-spot pattern simulated in the simple Layered Case is used to illustrate how an incomplete understanding of the facies architecture might contribute to uncertainty in assessing reservoir performance. The layered permeability structure has a much reduced level of heterogeneity than that of the Reference Case (figures 10-18, 10-20, and 10-21). As a consequence, a more uniform sweep of the reservoir is achieved in the Layered Case (figures 10-26 and 10-27). The low permeability clinoform cap facies encountered in the northwest corner of the

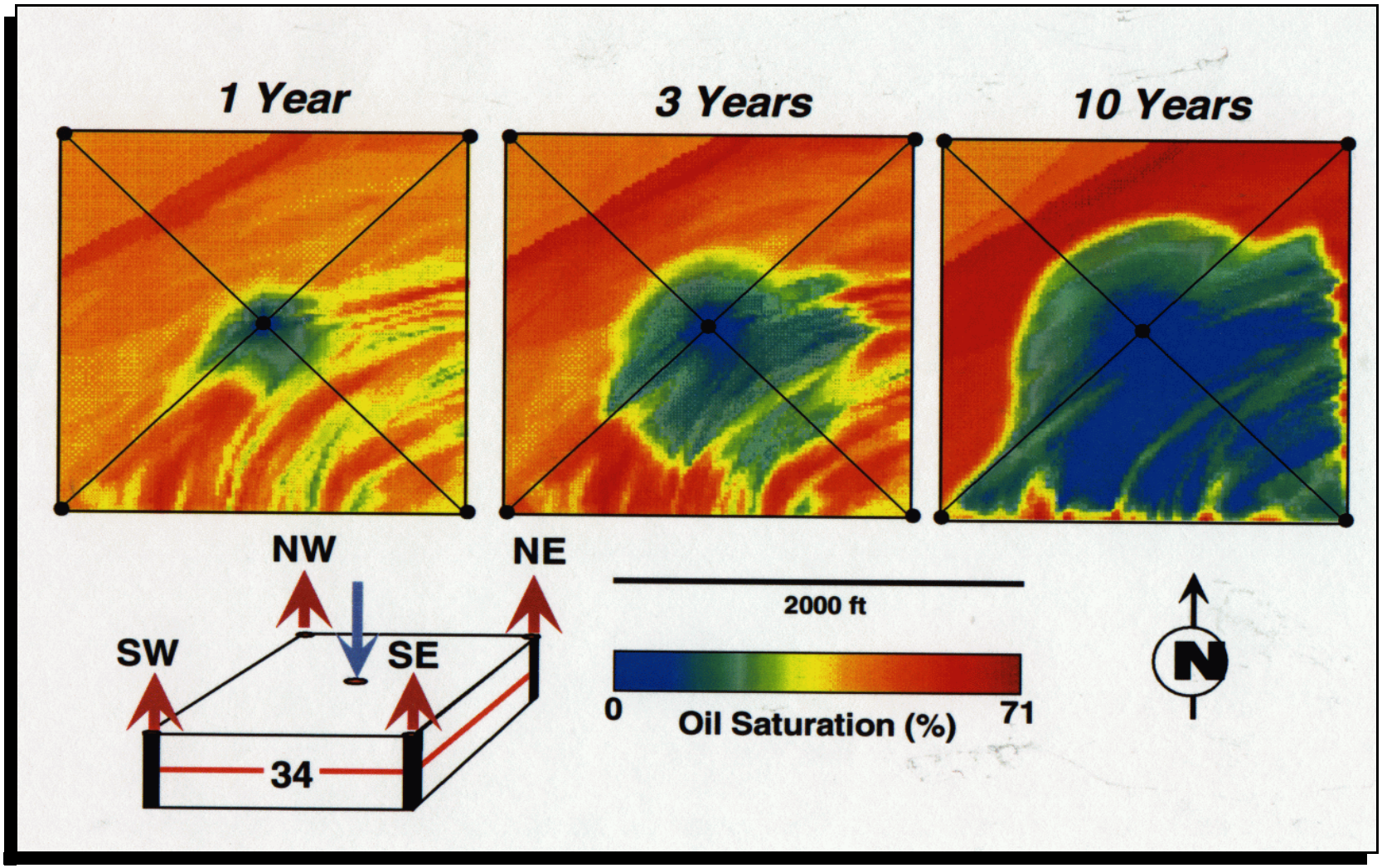


Figure 10-22. Computed oil saturation at 1, 3, and 10 years after the start of water injection, layer z = 34 feet, isotropic permeability model.

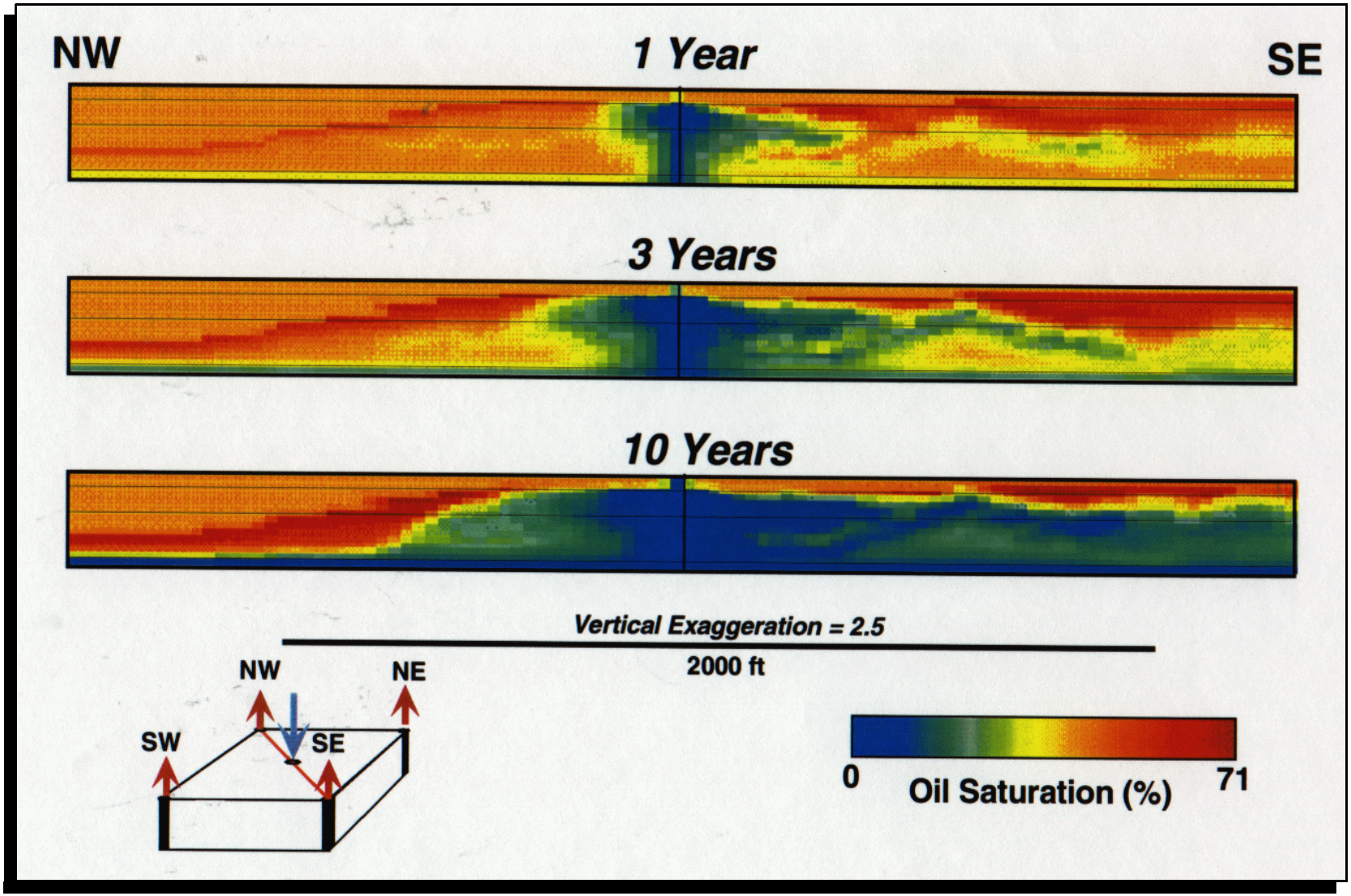


Figure 10-23. Computed oil saturation at 1, 3, and 10 years after the start of water injection, vertical section along the northwest-southeast diagonal, isotropic permeability model.

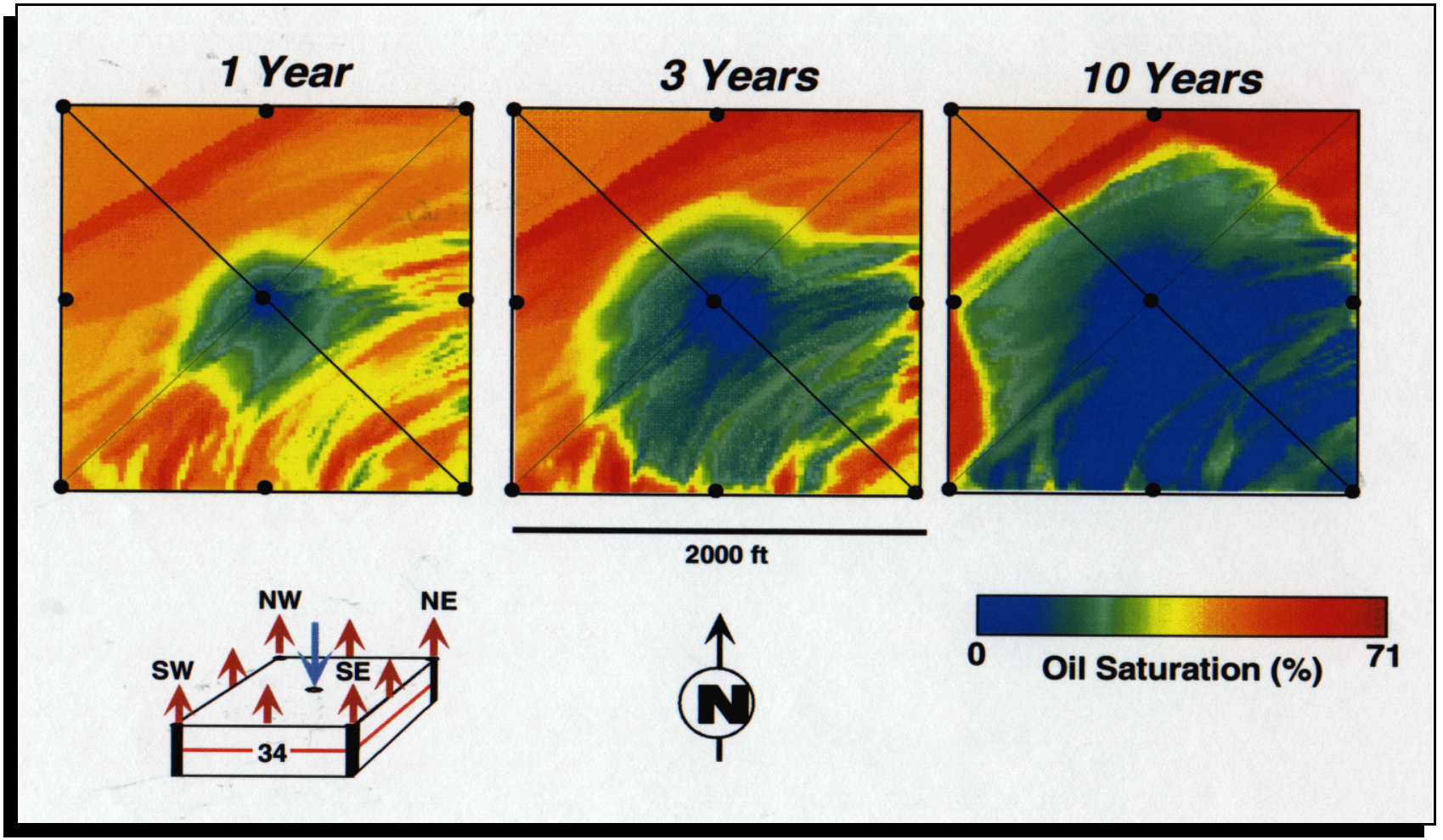


Figure 10-24. Computed oil saturation at 1, 3, and 10 years after the start of water injection for the 9-spot production scenario, layer z = 34 feet, isotropic permeability model.

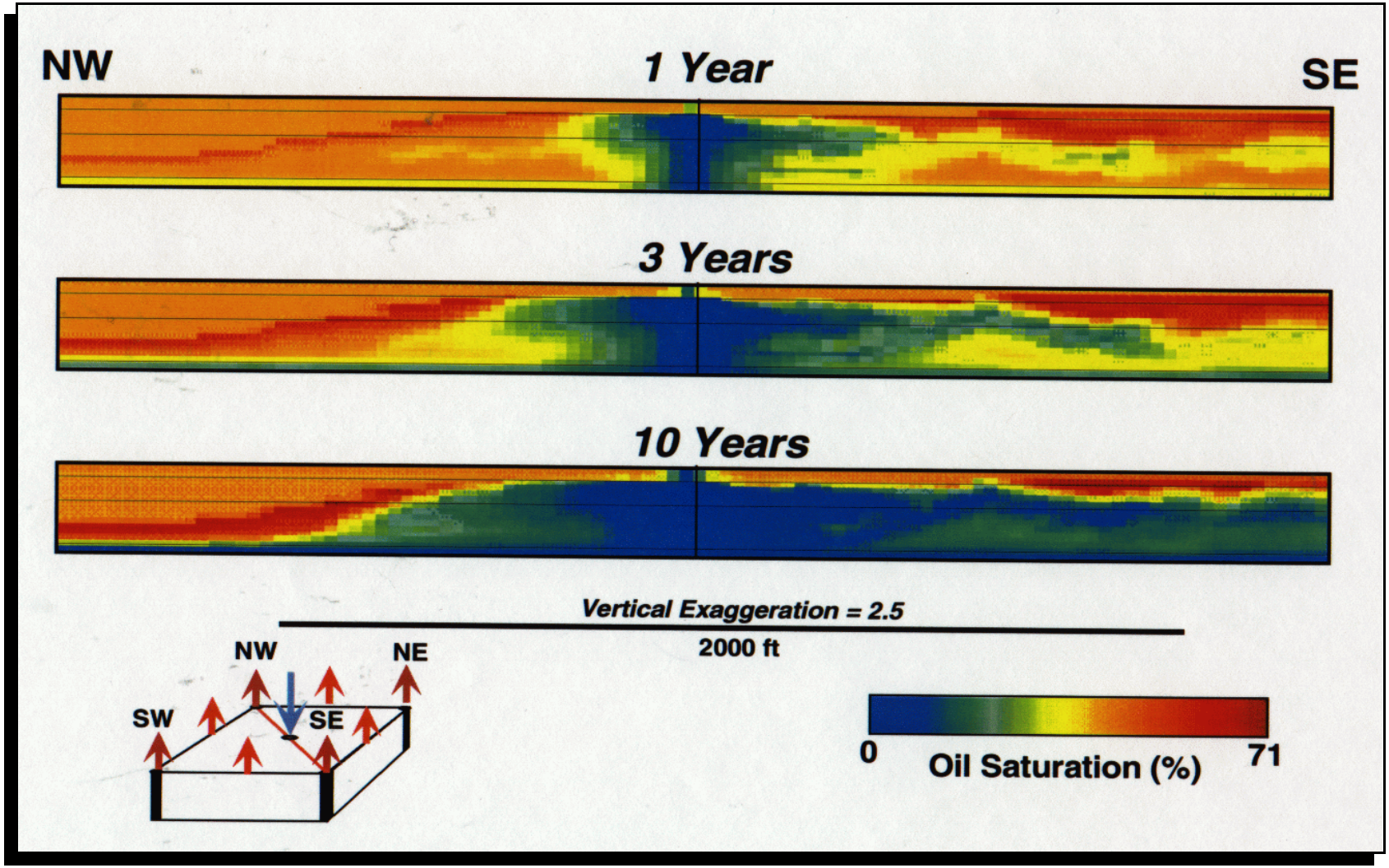


Figure 10-25. Computed oil saturation at 1, 3, and 10 years after the start of water injection for the 9-spot production pattern, vertical section along the northwest-southeast diagonal, isotropic permeability model.

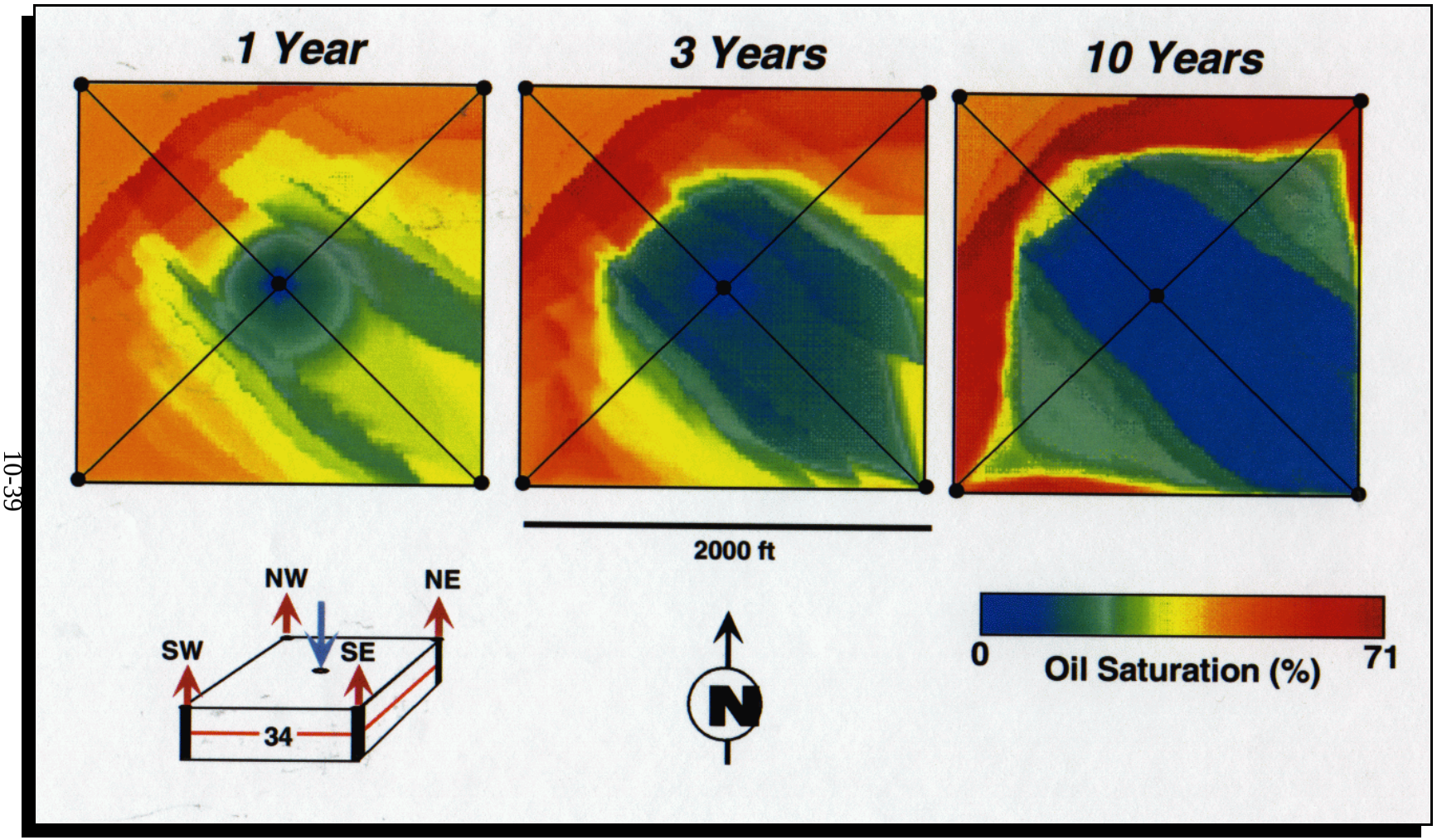


Figure 10-26. Computed oil saturation at 1, 3, and 10 years after the start of water injection for the 5-spot production scenario, layer z = 34 feet, layered permeability model.

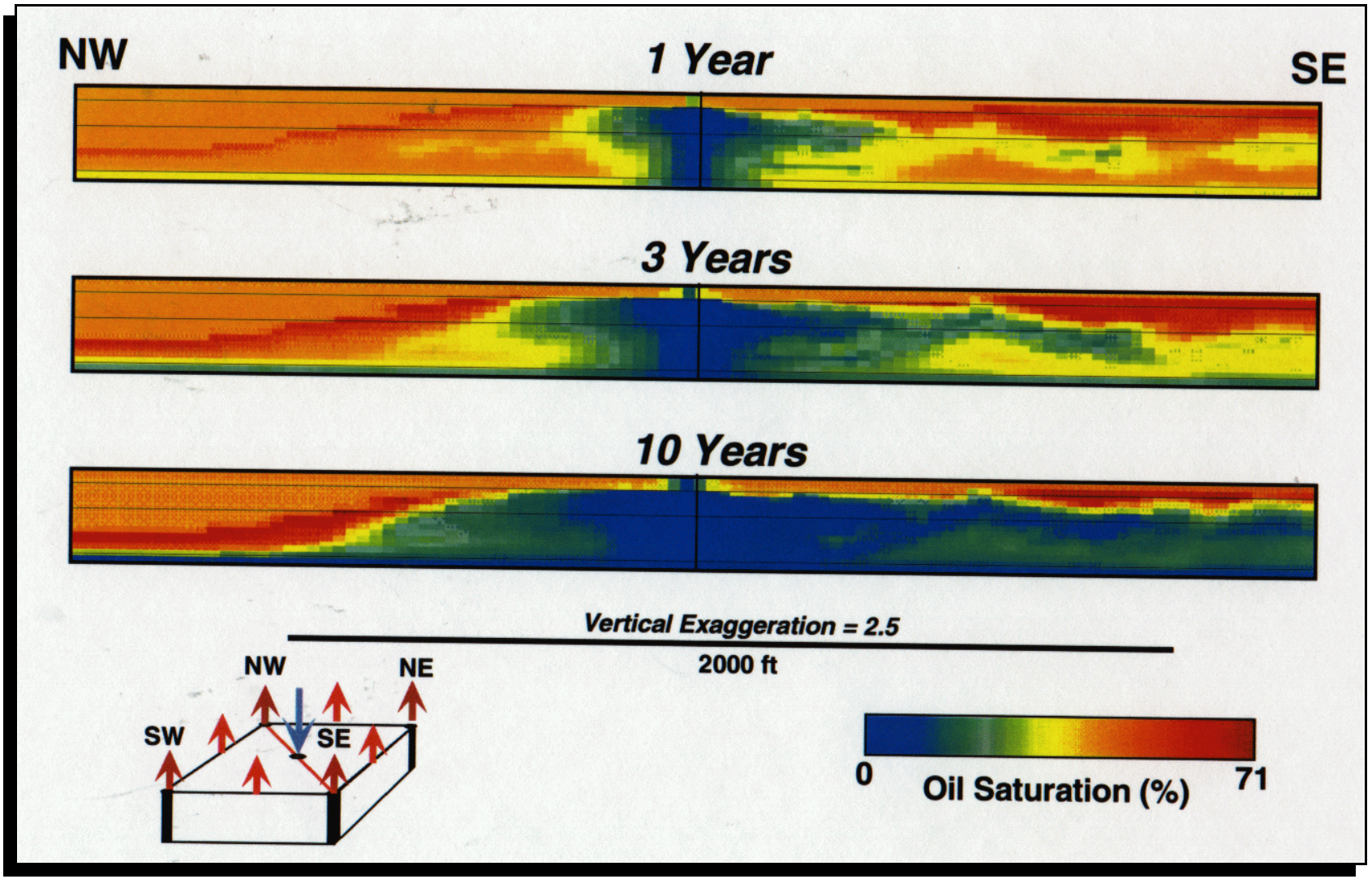


Figure 10-27. Computed oil saturation at 1, 3, and 10 years after the start of water injection for the 5-spot production patter, vertical section along the northwest-southeast diagonal, layered permeability model.

model domain, however, produces a region of enhanced oil saturation similar to that found in the Reference Case. Although the graphical results suggest a qualitative similarity in production characteristics for both the Reference and Layered Cases, a later section uses plots of cumulative oil production and water cut to more quantitatively illustrate the differences between the simulation results.

Results obtained by simulating the 5-spot pattern in the Anisotropic Case are shown in figures 10-28 and 10-29. Recall that the higher permeabilities built into this case reflect the relatively high radial anisotropy ratio (k_{arc}/k_r) of 10 used in the model. We suspect that this choice yields an upper limit for the possible effect of the bulk anisotropy imparted to each facies type by the lower permeability bounding layers found within each facies. Additional numerical experiments with a variety of anisotropy ratios are required, however, to more fully evaluate this hypothesis. Given the anisotropic permeability structure shown in figure 10-19 the modeling results show enhanced and more uniform sweep when compared to results obtained in simulating the isotropic Reference Case (figures 10-22 and 10-23). Note that the zones of increased oil saturation computed in the Reference Case are not found in the Anisotropic Case. This result likely reflects the overall enhanced permeability of the Anisotropic Case combined with the heterogeneous structure imparted to permeabilities found within each facies type. The homogeneous facies simulated in the isotropic Reference Case lack the high permeability pathways that can enhance oil production and reduce the volume of residual oil. Although the permeabilities assigned within each facies of the Anisotropic Case attain relatively high values, the internal heterogeneity seems more realistic than the homogeneous permeabilities of each facies modeled in the Reference Case. Developing a radially anisotropic permeability structure might be motivated by two factors. First, dipping shaley drapes that might form low permeability bounding layers are identified in drilling logs. Second, analysis of dips associated with the shaley drapes suggest a radially symmetric character with a likely position for the point of origin of the sediments.

Discussion

Quantitative Comparison of 3-D Simulation Results: Simulation results presented in the previous section are quantitatively summarized in plots of cumulative oil production (figure 10-30) and water cut (figure 10-31). Although not discussed in the previous section, results obtained for the Homogenous Case are also shown in (figures 10-30 and 10-31). Table 10-4 summarizes the cumulative oil production obtained for each case after 10 years of waterflooding. Water cut shown in figure 10-31 is computed as the volume of water produced divided by the total volume of oil plus water produced.

Table 10-4. Cumulative oil production after 10 years of waterflooding.

Model	Mean k (md)			Mean	OOIP	10 Yr Recovery	10 Yr
	k_{WE}	k_{NS}	k_z	ö (%)	(MSTB)*	(% OOIP)	Water Cut
Reference		4		18	3.0	17	.65
Homogeneous		4		14	3.0	17	.55
Layered		5		18	3.2	25	.68
Anisotropic	5	5	5	18	3.0	26	.90
9-Spot - Reference		4		18	3.0	26	.85

* MSTB = thousand stock tanks barrels.

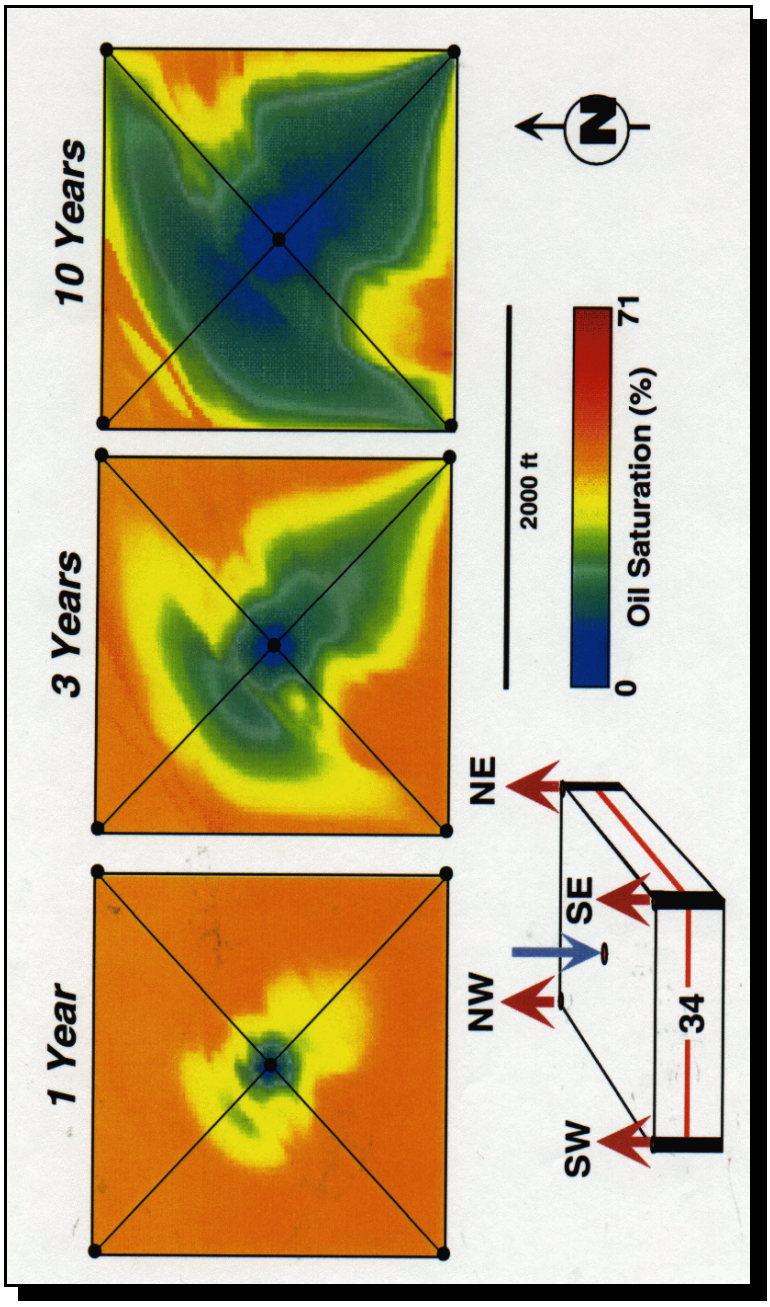


Figure 10-28. Computed oil saturation at 1, 3, and 10 years after the start of water injection for the 5-spot production scenario, layer z = 34 feet, anisotropic permeability model.

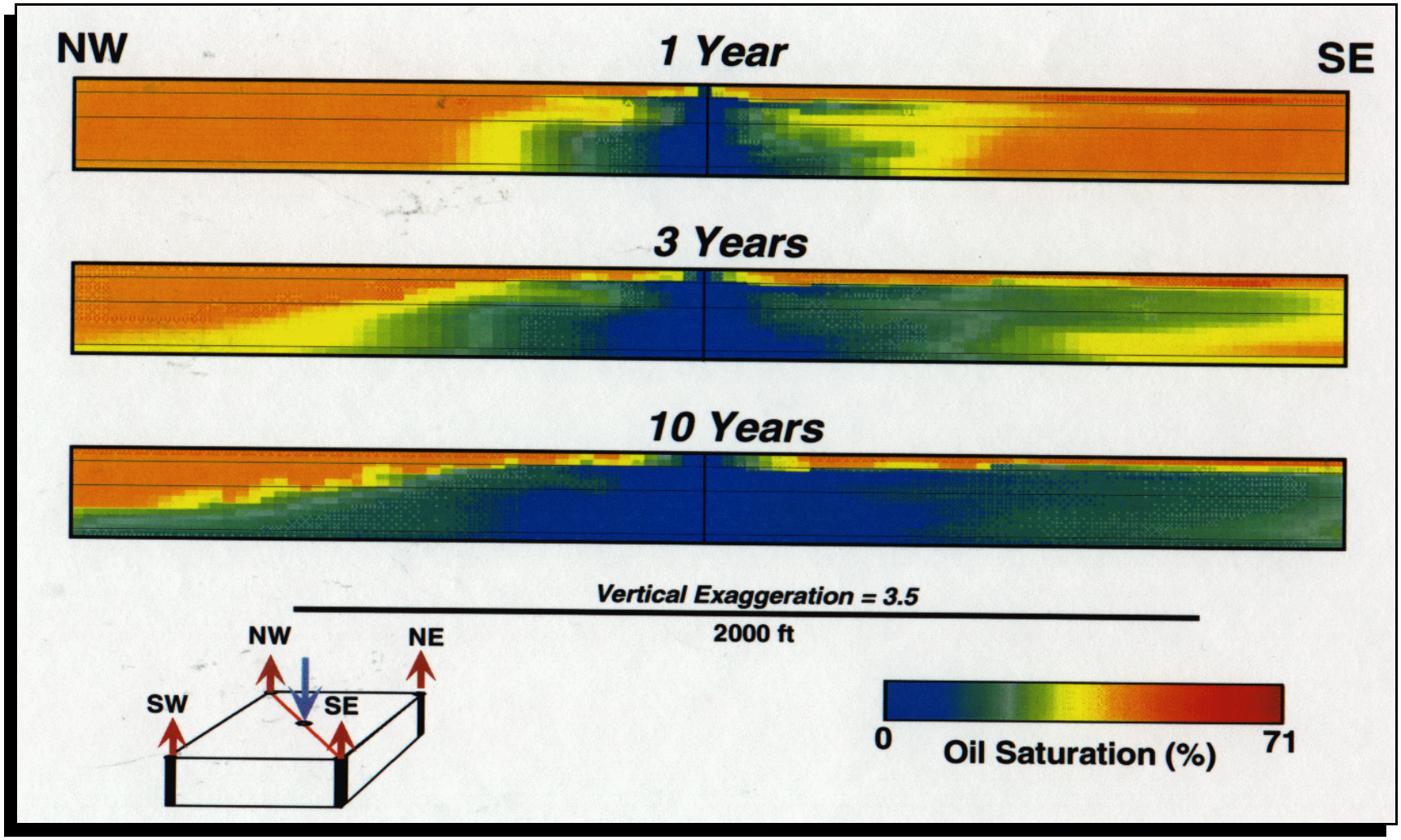
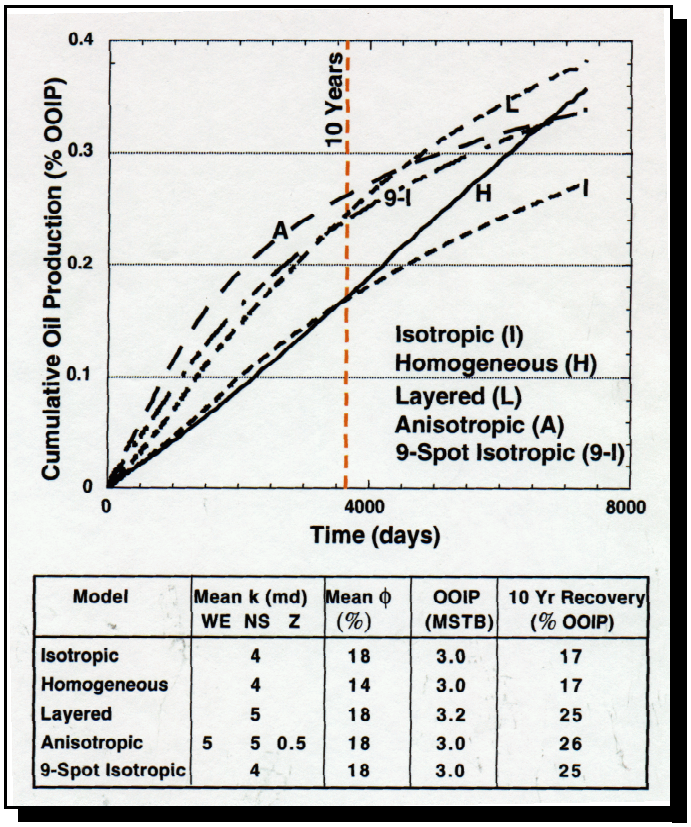


Figure 10-29. Computed oil saturation at 1, 3, and 10 years after the start of water injection for the 5-spot production pattern, vertical section along the northwest-southeast diagonal, anisotropic permeability model.



Model	Mean k (md) WE NS Z	Mean ϕ (%)	OOIP (MSTB)	10 Yr Recovery (% OOIP)
Isotropic	4	18	3.0	17
Homogeneous	4	14	3.0	17
Layered	5	18	3.2	25
Anisotropic	5 5 0.5	18	3.0	26
9-Spot Isotropic	4	18	3.0	25

Figure 10-30. Plot of cumulative oil production against time for each of the permeability models used in the 3-D simulations.

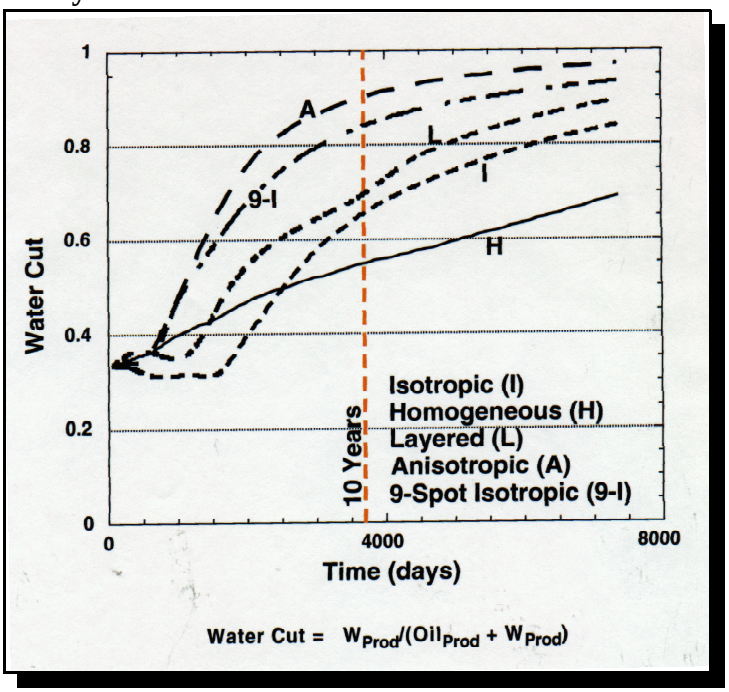


Figure 10-31. Plot of water cut against time for each of the permeability models used in the 3-D simulations.

The cumulative oil production from both the Reference and Homogeneous Cases is remarkably similar (17 percent of OOIP) for the first 10 years of water flooding (figure 10-30). After 10 years of production, however, the homogeneous case yields an increasingly large deviation from the oil recovery obtained for the heterogeneous Reference Case. Although computed cumulative oil production is similar during the first 10 years for both the Reference and Homogeneous Cases, the plot of cumulative water cut (figure 10-31) reveals markedly different water production (65 percent and 55 percent water cut, respectively). The inherent heterogeneity imparted by the facies-based petrophysical properties of the Reference Case yields less water cut in the first four years of production while much greater water cut is produced at later times. This result suggests that even a relatively coarsely defined heterogeneity in petrophysical properties can have a significant impact on oil production economics. For example, the northwest quadrant of the Homogeneous Case has higher permeability than that of the Kf-1-Iv[c] bedset facies included in this region of the Reference Case (figure 10-18). Increased sweep efficiency in this region of the Homogeneous Case likely accounts for the primary differences between the two simulation results. Early breakthrough at the southeast corner yields a marked increase in water cut for the Reference Case at the five year mark.

Let us assume that the Anisotropic Case represents an upper limit for realistically distributing petrophysical properties within the 3-D model domain. Thus, depending upon the radial anisotropy ratio (k_{arc}/k_r) assigned to each facies type, it appears that both the Homogeneous and Reference Cases could yield moderate to severe underestimates of the volume of oil that might be produced from fluvial-deltaic reservoirs with architectures similar to that exposed in the Ivie Creek outcrops. This result strongly suggests that reasonable efforts should be made to incorporate the impact of the shaley bounding layers in reservoir simulators. Developing appropriate empirical rules for defining values of bulk anisotropy associated with different architectural styles might provide a workable approach. It is important to note that the underestimate of total oil produced in the Reference and Homogeneous Cases is derived at reduced cost in terms of water cut. Results obtained for the Anisotropic Case consistently yield much higher values of cumulative water cut. Attempting to represent clinoformic sandy bodies and shaley bounding layers as layered facies (for example, Layered Case) provides little improvement over the other approaches used to represent the 3-D structure of petrophysical properties. The model results suggest that after 10 years of waterflooding, estimates of cumulative oil production could range between 17 to 26 percent depending on the approach used to represent the reservoir architecture. Breakthrough of the waterflood is much earlier in the Layered Case, in part, due to the more uniform distribution of petrophysical properties in the Layered Case. In the absence of a comprehensive understanding of the producing reservoir, it seems reasonable to expect a range of uncertainty in estimating cumulative oil production on the order of ±40 percent. A similar range of uncertainty is indicated for estimates of cumulative water cut. The Layered Case provides much higher oil production than that of both the Reference and Homogeneous Cases.

Comparing saturation plots of figures 10-22 through 10-25 indicates that the 9-spot pattern yields improved sweep efficiency. This result appears to be obtained with increased costs expressed as larger values of water cut.

Comparing 2-D and 3-D Simulation Results: It is valuable to compare the results of the very detailed 2-D simulation results to those obtained in the 3-D simulations. Although the comparison is complicated by the fact that somewhat different initial conditions and relative permeability properties were used in each case, a qualitative comparison can be made between the 3-D Reference Case and the 2-D simulations.

Figure 10-32 shows the analogous permeability structures defined for the 2-D and 3-D model domains. Section A-A' extracted from the 3-D model corresponds exactly with the 2-D section constructed along the Ivie Creek amphitheater outcrop. Note that the bounding layers fully encase the sandy bodies in this version of the 2-D model. Although the facies-based permeabilities used in the 3-D case do not incorporate the detailed internal permeabilities of sandy bodies and their shaley bounding layers, the overall permeability structure of the 2-D case is preserved in the 3-D structure of section A-A' (figure 10-32). Recognizing the general radial character of the 3-D permeability structure section C-SE is extracted to obtain a reasonable analog for the fluid-pressure gradients imposed between the injection and production wells of the 2-D case (figure 10-32). Comparing the permeability structure of the 2-D, A-A', and C-SE sections shows that similar permeability structures are obtained in each case. The corresponding C-SE permeability structures obtained for the Layered and Anisotropic cases are shown in the vertical sections of figures 10-21 and 10-19, respectively.

Oil saturations computed in the 2-D case and the corresponding 3-D Reference, Layered, and Anisotropic Cases are shown in figure 10-33. Although somewhat different time steps are available for presenting the results (two years in the 2-D case and three years in the 3-D case), the overall appearance of the simulation results is similar for each case. Closer inspection of figure 10-33, however, suggests that results obtained for the 3-D Anisotropic Case are most similar to the 2-D simulation results. The primary difference between the 2-D results and those obtained for the Reference and Layered Cases is the lack of a zone of enhanced saturation near the top of the reservoir as the production well is approached. The upper region of the 2-D case is likely better swept than the corresponding 3-D Reference and Layered Cases because the proximal facies contains permeability values higher than the average value used in the 3-D cases (figure 10-33). Apparently the reduced permeability provided by the shaley bounding layers does little to moderate the effect of the enhanced proximal facies permeabilities. Thus, the simulation results suggest that the impact of the lower permeability shaley bounding layers might reasonably be represented by assigning characteristic, but variable, values of bulk anisotropy for each facies. Additional numerical experiments are required, however, to more fully explore the implications of this result.

Conclusions

Oil production by waterflooding a 2,000 foot by 2,000 foot by 60 foot (610 m x 610 m x 18 m) analog reservoir volume with a 5-spot pattern of wells is simulated for four, 3-D permeability/porosity structures based on outcrop studies in the Ivie Creek case-study area. Each permeability/porosity structure represents different approaches taken to preserve the geologic details that might influence oil production. An unusually fine 3-D grid (150,000 nodes with 20 foot [6 m]

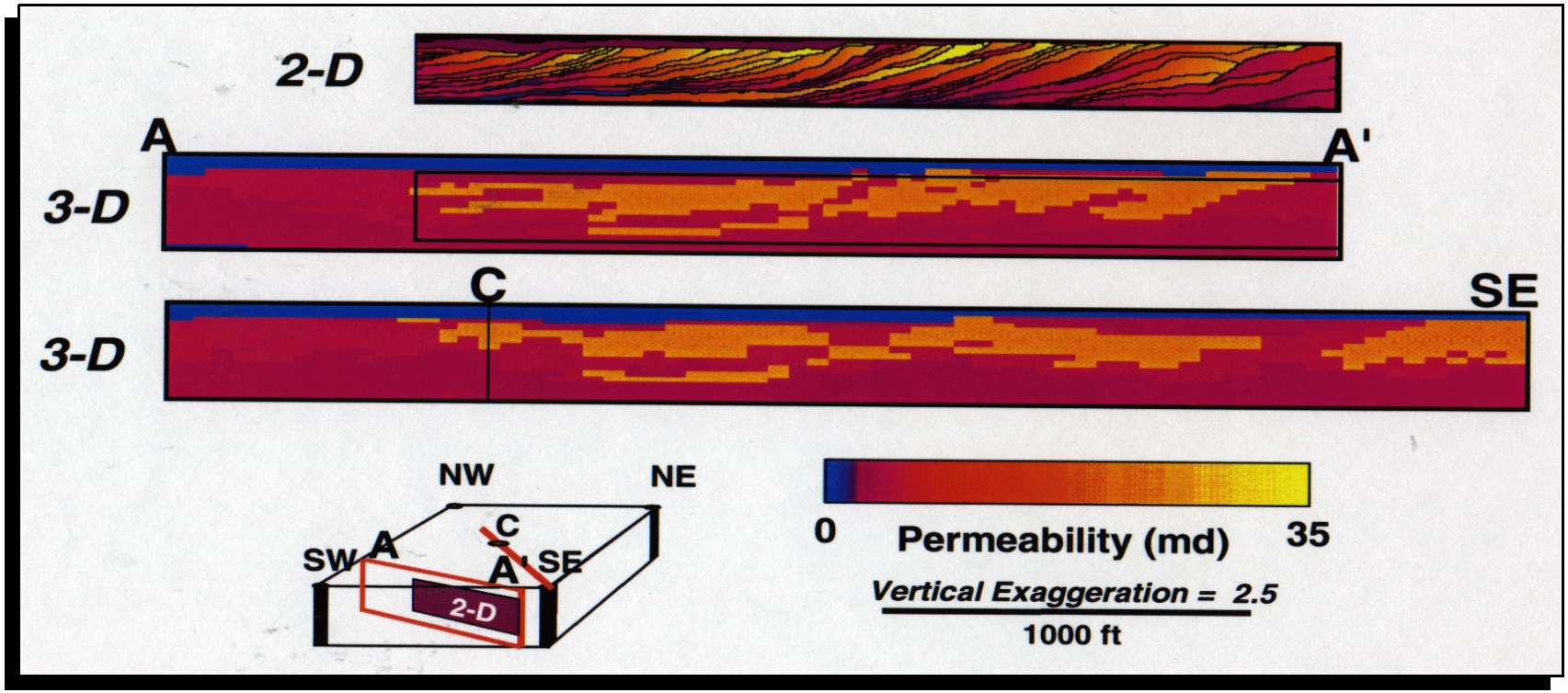


Figure 10-32. Comparison of the permeability structures for corresponding 2-D and 3-D modeling domains. Vertical section A-A' is extracted from the 3-D isotropic permeability model at an orientation parallel to the 2- model domain.

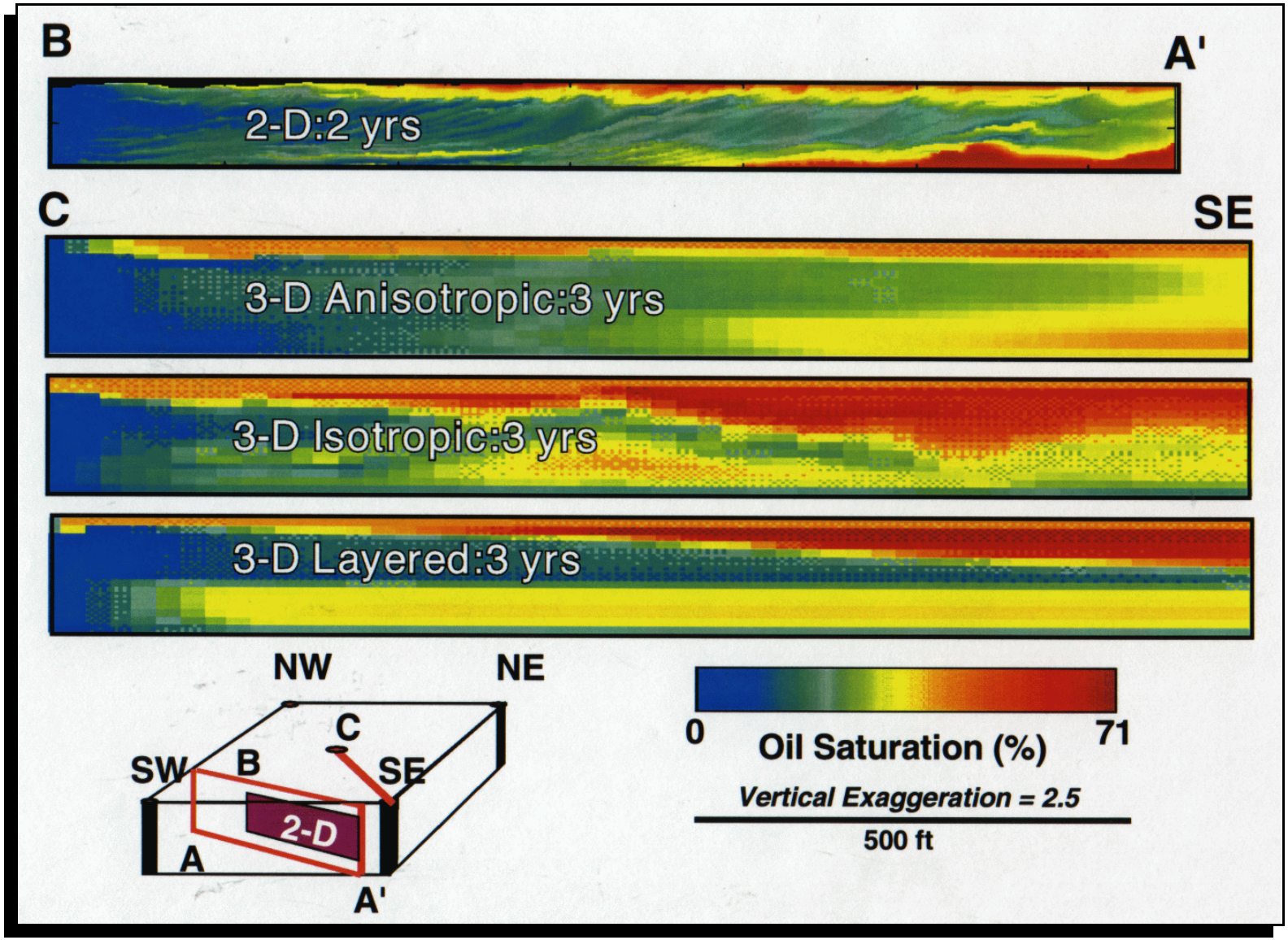


Figure 10-33. Comparison of oil saturations computed in the 2-D and 3-D simulations.

spacing in both horizontal directions and 4 foot [1 m] spacing in the vertical direction) is developed to preserve the features observed in outcrop. Computational constraints would generally not permit reservoir-scale simulations to incorporate such small grid blocks. The Reference Case represents a geologist's best estimate of the 3-D geometry of clinoform-related facies mapped on two intersecting cliff-face exposures and encountered in behind-the-outcrop drill holes. Although the overall geometry of each of four facies types is preserved, the internal variations in stratigraphy and petrophysical properties explored in the 2-D simulations are not retained. It is unlikely that such a detailed model could be developed with confidence based on subsurface data alone. The Layered Case is a simplified permeability structure constructed by sampling the vertical distribution of facies found at each of the four corners of the Reference Case without any benefit of the detailed stratigraphic insight that might be provided by outcrop analog studies. This case represents a structure that might reasonably be inferred by a reservoir geologist in the absence of information regarding the environment of deposition that created the clinoforms observed in outcrop. The simplest model contains a homogeneous, isotropic permeability structure numerically equivalent to the bulk average permeability of the Reference Case. The most complicated model is an idealized anisotropic permeability structure intended to capture the effect of the dipping shale drapes identified within each facies but not incorporated in the isotropic Reference Case.

Although simulated distributions of oil and water saturation appear fairly similar at each point in time, plots of cumulative oil recovery and water cut reveal significant differences in the production response of each analog reservoir model. For example, although the isotropic Reference Case and the Homogeneous Case each produce about 17 percent of OOIP after 10 years of production, the Homogeneous Case severely underestimates the water cut predicted using the Reference Case (0.55 for the Homogeneous Case and 0.65 for the Reference Case). Meanwhile, after 10 years of production the Layered Case severely over predicts oil recovery (25 percent of OOIP for the Layered Case and 17 percent for the Reference Case) with a relatively small increase in water cut (0.68 for the Layered Case and 0.65 for the Reference Case). These differences in production response (primarily inferred from computed water cut) suggest that every effort should be made to develop permeability models that preserve the effect of the clinoform-related facies observed in outcrop. Given the lack of detail typically available from subsurface data and current computational constraints, however, it is likely that these effects will usually be approximated within larger simulation grid blocks than used in this study.

Simulations performed to produce oil from the Reference Case with an inverted 9-spot pattern suggest only a possible advantage over the 5-spot pattern. Although 10-year oil recovery is much improved with the 9-spot pattern (25 percent OOIP for the 9-spot pattern and 17 percent for the 5-spot pattern) the resulting water cut is much less attractive (0.85 for the 9-spot pattern and 0.65 for the 5-spot pattern). The reservoir-specific economics of drilling additional producer wells, and the desired timing of production must be known before the relative economic advantages of either approach can be fully identified.

Even without attempting to incorporate the effect of shale drapes within each clinoform-related facies, it is clear that the overall facies geometry exerts a significant impact on oil production. Analogous fluid-flow simulations performed with the more finely gridded 2-D permeability models

indicate that relatively thin shale drapes within each clinoform-related facies can have a significant impact on oil production and water cut. The possible impact of the shale drapes is crudely approximated in the 3-D permeability model by computing anisotropic permeability tensors for each node that reflect the characteristic radial geometry associated with the inferred depositional environment. The results of this effort are somewhat ambiguous because we are restricted to using a 5-point differencing scheme that cannot represent the off-diagonal terms of permeability tensors oriented in directions other than those of the simulator coordinate axes. We are convinced, however, that reasonable estimates of vertical and horizontal anisotropy can be made for the Ivie Creek case-study area using the 2-D permeability structures. Additional simulations with higher-order differencing schemes or finite element models are required to properly evaluate the advantages of adopting this approach.

Recommendations

The following are recommendations for additional 3-D modeling and reservoir fluid-flow simulations:

- Additional numerical experiments should be performed using the 3-D permeability/porosity models. Digital files containing the three heterogeneous permeability models developed as input to the reservoir simulator are available from the Utah Geological Survey (Appendix C). The detailed, isotropic, heterogeneous Reference Case model provides a foundation for assessing different approaches for 3-D upscaling. In addition, the clinoforms mapped in the Ivie Creek case-study area have slopes much steeper than typically observed at other locations in the same geologic environment. Possible differences in computed oil production and water cut, as a function of clinoform slope, can be explored by 'stretching' the x and y coordinates of the permeability models while maintaining a constant vertical scale and well spacing.

- Ground-water hydrology testing methods should be used to perform wellbore-to-wellbore (interwell) scale, shallow *in situ* tests of permeability anisotropy in well-understood, unfractured, and water-saturated sandstone analogs. Such data sets, combined with detailed numerical fluid-flow simulations, would help substantially to develop and evaluate methods for assigning permeability anisotropy at simulator grid-block scales. Unfortunately, the few outcrop analog studies that include behind-the-outcrop drill holes have been carried out where the drill holes fail to reach the water table and fracturing is common. One viable strategy could integrate detailed 3-D ground penetrating radar (GPR), high resolution seismic, detailed drill-hole logging, and shallow interwell testing in closely spaced holes drilled in modern unconsolidated analogs near mappable cliff-face exposures.

- Commercial software available for building stochastic 3-D permeability models (for example, Heresim3D™) should be used in an effort to mimic the detailed, isotropic, heterogeneous Reference Case. Such an exercise would provide a sound basis for evaluating how the commercial software results might best be tuned to work with clinoform-related facies. Fluid-flow simulations performed using the stochastic model would provide insight into the level of uncertainty that might be associated with extrapolating from sparse wellbore data in producing reservoirs. Although Heresim3D™ has been used to create detailed 3-D clinoform structures similar to those of the Ivie Creek case-study area (Joseph and others, 1993), the results of any fluid-flow simulations are not reported.

- Additional effort should be expended to quantify how permeability anisotropy associated with shale drapes found within the clinoform-related facies might be incorporated at appropriate scales in numerical fluid-flow simulations. The formal homogenization method applied in the 2-D modeling should yield improved estimates of upscaled bulk anisotropy if applied to 3-D volumes on the order of 200 by 200 feet (61 x 61 m) in plan and 60 feet (18 m) thick. Higher order differencing and finite element methods are needed, however, in fluid-flow simulations used to test different methods for computing effective 3-D permeability anisotropy at grid-block scales. Ongoing outcrop-based study of lateral accretion, point-bar deposits in the Ferron Sandstone will provide an improved data base for exploring how to work with clinform sandstone geometries with shale drapes.

- Simulations performed in this 3-D study have not fully accounted for the possible variations in relative permeability and capillary pressure curves associated with different, clinoform-related facies types. Additional fluid-flow simulations would aid in establishing the relative importance of these effects as compared to the obvious impact of facies geometry illustrated in this study.

Implications of Reservoir Analog Modeling Results for Oil Reservoir Exploration and Development

Geehan (1993) notes that development planning can be strongly influenced by heterogeneities that cannot be correlated between wells or mapped with seismic data. Yet, such heterogeneities are difficult to include in the performance prediction models needed to establish optimal well spacing, the economic viability of horizontal wells, and estimate hydrocarbon recovery factors. Outcrop analog studies help to define which heterogeneities should be preserved in performance prediction models, and provide a foundation for estimating the range of uncertainty implicit in predicted oil recoveries. Outcrop analog studies help to address two issues of concern: (1) the geometry of architectural elements that might be distinguished with high-resolution sequence stratigraphy, and (2) the internal permeability structure of different architecture types. Both issues can be addressed

using outcrop-to-simulation studies like the Ivie Creek case study. Outcrop studies typically provide only a 2-D view of architectural elements and permeability structure. Even with two, nearly orthogonal cliff faces and several behind-the-outcrop drill holes, it is still difficult to unequivocally resolve the 3-D facies architecture in the Ivie Creek case-study area. Significant 3-D insight is derived, however, in more recent outcrop-based studies where we use high-resolution, 3-D GPR to establish the 3-D geometry of architectural elements observed in adjacent cliff faces (Thurmond and others, 1997; Snelgrove and others, 1998). The resulting data sets provide a sound basis for constructing geologically plausible permeability models using wellbore and seismic data from producing reservoirs. The Ivie Creek project provides an outcrop-to-simulation case study that adds to the growing suite of reservoir analogs available to constrain geological and petrophysical models used in reservoir simulation studies.

Spacing of Vertical Wells

The 3-D simulation results show that creating a 9-spot pattern through infill drilling within our analog reservoir significantly boosts oil recovery at the expense of increased water cut. If shale drapes could be explicitly included in the 3-D model, as they are in the 2-D models, we would expect to see a different response because interwell connectivity would likely be reduced. Unfortunately, we lack the outcrop-based information required to estimate the geometry of sandy bodies as viewed in a vertical section that traces an annular transect between the two cliff-face outcrops. If the spacing between shale drapes is short in the annular transect, then a significant increase in compartmentalization should be expected that, in turn, may cause the 9-spot pattern to perform better than the 5-spot pattern. Forster and Snelgrove are currently working on a new outcrop analog study in the Ferron Sandstone where high-resolution, 3-D GPR surveys, combined with two cliff-face exposures, are yielding 3-D insight regarding the shapes and sizes of sandy bodies bounded by shale drapes in a lateral accretion, point-bar deposit.

Viability of Horizontal Wells

Economides and others (1989) and Geehan (1993) suggest that the economic viability of horizontal wells depends upon the ratio of horizontal permeability k_h to vertical k_v permeability within the volume swept by an individual well. For example, horizontal wells are most likely to be effective when the vertical permeability approaches that of the horizontal permeability. In attempting to estimate 3-D anisotropy we used our detailed 2-D permeability models to compute ratios of k_h/k_v in a radial direction that corresponds to the orientation of the cliff-face exposures. Using this approach we found that permeability ratios vary as a function of facies type and position relative to the sediment source. Unfortunately, we lack a sound basis for attempting to compute permeability ratios in the annular direction. It is clear, however, that steeply inclined clinoforms are more likely to provide the permeability ratios needed to justify horizontal wells because the steeply dipping shale drapes tend to reduce bulk permeability in the horizontal direction. Creating 3-D permeability models with different clinoform slopes by ‘stretching’ the x and y coordinates provides

a basis for computing and plotting the corresponding variations in k_h/k_v that could be used to assess the viability of horizontal production wells.

Oil Recovery Estimates

The 2-D simulation results show similar magnitudes of ultimate oil production for each permeability model, but different water breakthrough times. The 3-D simulation results, however, show different 10-year and ultimate oil recoveries as well as different water cut patterns. This confirms that it can be misleading to use 2-D simulation results to predict oil recovery and water cut in a reservoir with the internal 3-D geometry inferred at the Ivie Creek site. It is clear, however, that a more complete assessment of oil production from the Ivie Creek analog reservoir would require explicit inclusion of the shale drapes in the 3-D permeability model in the same way that they are included in the 2-D model. We lack both the data and computational capacity to perform such an analysis.

We suggest above that the 2-D simulation results should not be used to predict oil recovery for the corresponding 3-D case. The 2-D results, however, are valuable in that they clearly show that the timing of oil production and water breakthrough can be affected by both facies geometry and internal shale drapes. Furthermore, the comparison of permeability averaging methods performed using the 2-D permeability models suggests that the clinoform geometry observed in outcrop is poorly approximated by traditional averaging approaches. A formal, flow-based homogenization method (Koebbe, 1995) performs much better in preserving the impact of the dipping shale drapes. Because we are restricted to using a 5-point differencing scheme, however, we are unable to fully exploit the inherent strength of the homogenization approach as it should be applied in a 3-D context.

Application to Reservoir Studies

In their description of an integrated study of the Meren E-01/MR05 sands in the Niger Delta, Cook and others (1999) provide a good, real world foundation for explaining how outcrop-to-simulation work similar to our Ivie Creek case study might aid reservoir studies. Located in offshore Nigeria, the reservoir comprises interstratified sandstones and shales deposited in shoreface to shelf environments. Cook and others (1999) combined geological attribute information obtained from well logs with depositional environment information inferred from sequence stratigraphic analysis. Using a sequence stratigraphic approach with 1-foot (0.3-m) vertical resolution provides an opportunity to match outcrop analogs to the reservoir by comparing not only the geometries and distributions of depositional features, but also sediment supply and accommodation rates (as expressed by sandy body geometries and fine scale bedding statistics [Geehan, 1993]).

Although Cook and others (1999) did not incorporate an outcrop analog model in their analysis, their subsurface studies provide the information needed to evaluate the possible match to an analog reservoir and to exploit a suitable analog. Cook and others (1999) constructed variograms to characterize permeability structure in terms of sand quality and sea/baffle quality using wellbore

data obtained from each parasequence. Increased confidence in the variograms could be derived if a matching outcrop analog were available to provide a quantitative, observation-based assessment of both characteristics. In addition, outcrop-based observations would aid in assessing the likelihood that sandy bodies with inclined shaly drapes similar to those observed in the Ivie Creek case-study area might be found between sub-horizontal flooding surfaces. Thus, although shale volumes might be computed from gamma-ray logs, dipmeter logs, an outcrop analog would aid in identifying the possibility of dipping beds.

Cook and others (1999) developed a 14.5-million cell geological model that contains too many nodes to be used in practical numerical fluid-flow simulations. As a consequence, Cook and others (1999) used an in-house homogenization software package that incorporates the approach of Durlofsky and others (1995) to upscale the geological model to a 250,000 node simulation model that explicitly retained the flooding surfaces defined by high-resolution sequence stratigraphic mapping. The homogenization approach adopted by Cook and others (1999) is similar to the flow-based homogenization approach implemented by Koebbe (1995) and used in our study.

Outcrop-Based Reservoir Analog Studies

Outcrop-to-simulation studies performed for the Ivie Creek case-study area provide valuable insights that we have been incorporating in subsequent outcrop analog studies in the Ferron Sandstone and elsewhere. For example, we now target formations where the top surface of the analog facies is available for detailed mapping, GPR surveys, and comprehensive continuous core drilling. The drill core enables us to quantify the possible effects of weathering on the outcrop permeability measurements, and provides a base for closely spaced mini-permeability measurements throughout the section of interest. The drill core provides a complete record of all facies in the section, including those that are weathered out of the nearby cliff faces. The GPR surveys provide detailed 3-D geometries that cannot be fully characterized even with two orthogonal cliff-face exposures.

Although we used a deterministic approach to building the 3-D permeability model for the Ivie Creek case-study area, stochastic approaches should be used to estimate the uncertainty that results from our inability to fully map the detailed 3-D geometry of outcrop analogs. Joseph and others (1993) illustrate how a stochastic modeling technique might be used to create geologically plausible clinoform architectural elements similar to those observed in the Ivie Creek case-study area. Before constructing the stochastic model, Joseph and others (1993) built a deterministic model using Heresim3D^{TM} and included inferences regarding environments of deposition and all available outcrop data from exposures of the Roda deltaic complex in Spain. The deterministic model provides a reference for evaluating the success of the stochastic model built with a random genetic simulation approach. In attempting to mimic typical reservoir contexts, only a subset of the data incorporated in the deterministic model are used in building the stochastic model. Because insufficient data are available to apply a completely geostatistical approach, a genetic model is used to simulate the accumulation of sedimentary bodies that produce the clinoform architecture observed in outcrop. Sufficient data are available for the Ivie Creek case-study area, and new Ferron outcrop sites to perform similar comparative studies.

REFERENCES

Allison, M.L., compiler, 1995, Geological and petrophysical characterization of the Ferron Sandstone for 3-D simulation of a fluvial-deltaic reservoir - annual report for the period September 29, 1993 to September 29, 1994: U.S. Department of Energy, DOE/BC/14896-6, 49 p. (Ch-8).

Allred, L.D., and Coates, R.L., 1980, Methane recovery from deep unminable coal seams, *in* Proceedings of the first annual symposium on unconventional gas recovery: Society of Petroleum Engineers Reprint 8962, p. 307-312 (Ch-2).

---1982, Methane recovery from deep coalbeds in the Book Cliffs, *in* Proceedings of the 1982 SPE/DOE unconventional gas recovery symposium: Society of Petroleum Engineers Reprint 10819, p. 245-252 (Ch-2).

Anderson, P.B., 1991a, Landward pinch-out of Cretaceous marine nearshore clastics in the Ferron Sandstone Member of the Mancos Shale and Blackhawk Formation, east-central Utah; potential stratigraphic traps: Utah Geological Survey Contract Report 91-12, 110 p. (Ch-2).

---1991b, Comparison of Cretaceous landward pinch-outs of nearshore sandstones: wave- versus river-dominated deltas, east-central Utah, *in* Chidsey, T.C., Jr., editor, Geology of east-central Utah: Utah Geological Association Publication 19, p. 283-300 (Ch-2).

Anderson, P.B., and Ryer, T.A., 1995, Proposed revisions to parasequence-set nomenclature of the Upper Cretaceous Ferron Sandstone Member of the Mancos Shale, central Utah [abs.]: American Association Petroleum Geologists Bulletin, v. 79, no. 6, p. 914-915 (Ch-2).

Anderson, P.B., Chidsey, T.C., Jr., and Ryer, T.A., 1997, Fluvial-deltaic sedimentation and stratigraphy of the Ferron Sandstone, *in* Link, P.K., and Kowallis, B.J., editors, Mesozoic to Recent geology of Utah: Provo, Brigham Young University Geology Studies, v. 42, pt. 11, p. 135-154 (Ch-5, Ch-7).

Anderson, P.B., McClure, Kevin, Chidsey, T.C., Jr., Ryer, T.A., Morris, T.H., Dewey, J.A., Jr., and Adams, R.D., in press, Photomoasics and measured sections from the Cretaceous Ferron Sandstone Member of the Mancos Shale, Emery and Sevier Counties, east-central Utah: Utah Geological Survey Open-File Report, compact disk (Ch-3, Ch-4, Ch-5, Ch-7, Ap-A, Ap-B).

Armstrong, R.L., 1968, Sevier orogenic belt in Nevada and Utah: Geological Society of America Bulletin, v. 79, no. 4, p. 429-458 (Ch-1).

Barton, M.D., 1994, Outcrop characterization of architecture and permeability structure in fluvial-deltaic sandstones, Cretaceous Ferron Sandstone, Utah: Austin, University of Texas, Ph.D. dissertation, 255 p. (Ch-1, Ch-2, Ch-3, Ch-4, Ch-7, Ch-8, Ch-9, Ch-10).

Barton, M.D., and Tyler, Noel, 1991, Quantification of permeability structure in distributary channel deposits Ferron Sandstone, Utah, *in* Chidsey, T.C., Jr., editor, Geology of east-central Utah: Utah Geological Association Publication 19, p. 273-282 (Ch-2, Ch-8, Ch-10).

---1995, Sequence stratigraphy, facies architecture, and permeability structure of fluvial-deltaic reservoir analogs - Cretaceous Ferron Sandstone, central Utah: University of Texas, Bureau of Economic Geology, Field Trip Guidebook, August 21-23, 1995, 80 p. (Ch-2, Ch-10).

Bashore, W.M., Langan, R.T., Tucker, K.E., and Griffith P.J., 1987, Geostatistical integration of crosswell data for carbonate reservoir modeling, McElroy field, Texas: *in* Stoudt, E.L., and Harris, P.M., editors, Hydrocarbon reservoir characterization: Society for Sedimentary Geology (SEPM) Short Course No. 34, 199-225 p. (Ch-9).

Begg, S.H., Kay Alex, Gustason, E.R., and Angert, P.F., 1994, Characterization of complex fluvial-deltaic reservoir for simulation, *in* 69th Annual Technical Conference and Exhibition of the Society of Petroleum Engineers: Society of Petroleum Engineers Reprint 28398, p. 37-384 (Ch-9).

Bhattacharya, J.P., 1998, Wave-influenced deltas [abs.]: American Association of Petroleum Geologists Annual Convention Extended Abstracts, v. I, p. A-64 (Ch-3, Ch-4).

Biot, M.A., 1962, General theory of acoustic propagation in porous dissipative media: Journal Acoustical Society of America, 34, p. 1254-1264 (Ch-8).

Bjørlykke, K., 1984, Formation of secondary porosity: how important is it? *in* McDonald, D.A., and Surdam, R.C., editors, Clastic diagenesis: American Association of Petroleum Geologists Memoir 37, p. 277-286 (Ch-8).

---1994, Fluid-flow processes and diagenesis in sedimentary basins, *in* Parnell, J., editor, Geofluids - origin, migration and evolution of fluids in sedimentary basins: Geological Society of America Special Publication 78, p. 127-140 (Ch-8).

Bohor, B.F., and Triplehorn, D.M., 1993, Tonsteins - altered volcanic-ash layers in coal-bearing sequences: Geological Society of America Special Paper 285, 44 p. (Ch-2).

Bourbié, T., Coussy, O., and Zinszner, B., 1987, Acoustics of porous media: Paris, Education Technology, 334 p. (Ch-8).

Bunnell, M.D., and Hollberg, R.J., 1991, Coal beds of the Ferron Sandstone Member in northern Castle Valley, east-central Utah, *in* Chidsey, T.C., Jr., editor, Geology of east-central Utah: Utah Geological Association Publication 19, p. 157-172 (Ch-2).

Campbell, C.V., 1967, Lamina, lamina-set, bed and bedset: Sedimentology, v. 8, no. 1, p. 7-26 (Ch-4).

Castagna, J.P., Batzle, M.L., and Eastwood, R.L., 1985, Relationships between compressional-wave and shear-wave velocities in clastic silicate rocks: Geophysics, v. 50, p. 571-581 (Ch-8).

Chidsey, T.C., Jr., compiler, 1997, Geological and petrophysical characterization of the Ferron Sandstone for 3-D simulation of a fluvial-deltaic reservoir - annual report for the period October 1, 1995 to September 30, 1996: U.S. Department of Energy, DOE/BC/14896-15, 57 p. (Ch-7, Ch-10).

Chidsey, T.C., Jr., and Allison, M.L., compilers, 1996, Geological and petrophysical characterization of the Ferron Sandstone for 3-D Simulation of a fluvial-deltaic reservoir - annual report for the period October 1, 1994 to September 30, 1995: U.S. Department of Energy, DOE/BC/14896-13, 104 p. (Ch-8, Ch-10).

Clifton, H.E., Hunter, R.E., and Phillips, R.L., 1971, Depositional structures in the non-barred high-energy nearshore: Journal of Sedimentary Petrology, v. 41, no. 3, p. 651-670 (Ch-5).

Coleman, J.M., 1976, Deltas - processes of deposition and models for exploration: Champaign, Continuing Education Publication Company, Inc., 102 p. (Ch-5).

Coleman, J.M., Roberts, H.H., Murray, S.P., and Salama, M., 1981, Morphology and dynamic sedimentology of the eastern Nile delta shelf: Marine Geology, v. 42, p. 301-326 (Ch-2).

Cook, G., Chawathé, L.D., Legarre, H., and Ajayi, E., 1999, Incorporating sequence stratigraphy in reservoir simulation - an integrated study of the Meren E-01/MR-05 sands of the Niger Delta: Proceedings of Society of Petroleum Engineers 15th Symposium on Reservoir Engineering, SPE 51892, p. 147-159 (Ch-10).

Cotter, Edward, 1971, Paleoflow characteristics of a Late Cretaceous river in Utah from analysis of sedimentary structures in the Ferron Sandstone: Journal of Sedimentary Petrology, v. 41, no. 1, p. 129-138 (Ch-2).

---1975a, Deltaic deposits in the Upper Cretaceous Ferron Sandstone, Utah, *in* Broussard, M.L.S., editor, Deltas, models for exploration: Houston Geological Society, p. 471-484 (Ch-1, Ch-2, Ch-3, Ap-A).

---1975b, Late Cretaceous sedimentation in a low-energy coastal zone: the Ferron Sandstone of Utah: Journal of Sedimentary Petrology, v. 45, p. 669-685 (Ch-1, Ch-2, Ch-3).

---1976, The role of deltas in the evolution of the Ferron Sandstone and its coals: Brigham Young University Geology Studies, v. 22, pt. 3, p. 15-41 (Ch-2, Ch-4, Ap-A).

Cross, C.W., and Spencer, A.C., 1899, Description of the La Plata quadrangle [Colorado]: U.S. Geological Survey Geologic Atlas of the United States, Folio 60 (Ch-2).

Davidson-Arnott, R.D.G., and Greenwood, Brian, 1976, Facies relationships on a barred coast, Kouchibouguac Bay, New Brunswick, Canada, *in* Davis, R.A., Jr., and Ethington, R.L., editors, Beach and nearshore sedimentation: Society for Sedimentary Geology (SEPM Special Publication 24, p. 149-168 (Ch-5).

Davis, L.J., 1954, Stratigraphy of the Ferron Sandstone, *in* Grier, A.W., editor, Geology of portions of the high plateaus and adjacent canyon lands, central and south-central Utah: Intermountain Association of Petroleum Geologists, Fifth Annual Field Conference Guidebook, p. 55-58 (Ch-2).

Davis, F.D., and Doelling, H.H., 1976, Methane content of Utah coals - first annual report to the U.S. Bureau of Mines: Utah Geological and Mineral Survey Open-File Report 23, 34 p. (Ch-2).

---1977, Methane content of Utah coals: second annual report to the U.S. Bureau of Mines (Carbon County): Utah Geological and Mineral Survey Open-File Report 24, 26 p. (Ch-2).

Davis, R.A., and Hayes, M.O., 1984, What is a wave-dominated coast?: Marine Geology, v. 60, p. 313-329 (Ch-5).

Diamond, W.P., and Levine, J.R.,1981, Direct method determination of the gas content of coal: procedures and results: U.S. Bureau of Mines Report of Investigations 8515, 36 p. (Ch-2).

Doelling, H.H., 1972, Central Utah coal fields: Sevier-Sanpete, Wasatch Plateau, Book Cliffs and Emery: Utah Geological and Mineral Survey Monograph Series, no. 3, 570 p. (Ch-2, Ch-3).

Doelling, H.H., Smith, A.D., and Davis, F.D., 1979, Methane content of Utah coals, *in* Smith, Martha, editor, Coal studies: Utah Geological and Mineral Survey Special Study 49, p. 1-43 (Ch-2).

Domenico, P.A., and Mifflin, M.D., 1965, Water from low-permeability sediments and land subsidence: Water Resources Research, v. 1, p. 563-576 (Ch-8).

Dott, R.H., Jr, and Bourgeois, Joanne, 1982, Hummocky stratification - significance of its variable bedding sequences: Geological Society of America Bulletin, v. 93, no. 8, p. 663-680 (Ch-5).

Doyle, J.D., and Sweet, M.L., 1995, Three-dimensional distribution of lithofacies, bounding surfaces, porosity, and permeability in fluvial sandstone - Gypsy Sandstone of northern Oklahoma: American Association of Petroleum Geologists Bulletin, v. 79, no. 1, p. 70-96 (Ch-9).

Dull, D.W., 1995, Reservoir characterization and the application of geostatistics to three-dimensional modeling of a shallow ramp carbonate, Mabee San Andres field, Andrews and Martin Counties, Texas, *in* Stoudt, E.L., and Harris, P.M., editors, Hydrocarbon reservoir characterization: Society for Sedimentary Geology (SEPM) Short Course No. 34, p. 155-197 (Ch-9).

Durlofsky, L.J., Behrens, R.A., Jones, R.C., and Bernath, A., 1995, Scale up of heterogeneous three dimensional reservoir descriptions: Proceedings of 1995 Society of Petroleum Engineers Annual Technical Conference and Exhibition, SPE 30702, p. 147-159 (Ch-10).

Eaton, J.G., 1990, Stratigraphic revision of Campanian (Upper Cretaceous) rocks in the Henry Basin, Utah: Mountain Geologist, v. 27, no. 1, p. 27-38 (Ch-2).

Economides, M.J., McLennan, J.D., Brown, E., and Roegiers, J., 1989, Performance and stimulation of horizontal wells: World Oil, v. 208, no. 6, p. 41-77 (Ch-10).

Edson, D.J., Jr., Scholl, M.R., Jr., and Zabriskie, W.E., 1954, Clear Creek gas field, central Utah: Intermountain Association of Petroleum Geologists Guidebook, 5th Annual Field Conference, p. 89-93 (Ch-2).

Ellis, D.V., 1987, Well logging for earth scientists: New York, Elsevier, 532 p. (Ch-8).

Erickson, S.N., and Jarrard, R.D., 1999, Velocity/porosity relationships for siliciclastic sediments and rocks: Journal Geophysical Research, in review (Ch-8).

Eschard, Rémi, Lemouzy, Pierre, Bacchiana, Claude, Désaubliaux, Guy, Parpant, Jacques, and Smart, Brian, 1998, Combining sequence stratigraphy, geostatistical simulations, and production data for modeling a fluvial reservoir in the Chaunoy field (Triassic, France): American Association of Petroleum Geologists Bulletin, v. 82, no. 4, p. 545-568 (Ch-9).

Fielding, C.R., and Crane, R.C., 1987, An application of statistical modeling to the prediction of hydrocarbon recovery factors in fluvial reservoir sequences: *in* Ethridge, F.G., Flores, R.M., and Harvey, M.D., editors, Recent developments in fluvial sedimentology: Society for Sedimentary Geology (SEPM) Special Publication No. 39, p. 321-327 (Ch-9).

Fisher, W.L., Brown, L.F., Jr., Scott, A.J., and McGowen, J.H., 1969, Delta systems in the exploration for oil and gas: a research colloquium: University of Texas Bureau of Economic Geology, 210 p. (Ch-2).

Fisher, R.S., Barton, M.D., and Tyler, Noel, 1993a, Quantifying reservoir heterogeneity through outcrop characterization - architecture, lithology, and permeability distribution of a seaward-stepping fluvial-deltaic sequence, Ferron Sandstone (Cretaceous), central Utah: Gas Research Institute Report 93-0022, 83 p. (Ch-2, Ch-8, Ch-10).

---1993b, Quantifying reservoir heterogeneity through outcrop characterization - architecture, lithology, and permeability distribution of a landward-stepping fluvial-deltaic sequence, Ferron Sandstone (Cretaceous), central Utah: Gas Research Institute Report 93-0023, 132 p. (Ch-2, Ch-8, Ch-10).

Fogg, G.E., 1989, Stochastic analysis of aquifer interconnectedness: Wilcox Group, Trawick area, east Texas: Austin, University of Texas, Bureau of Economic Geology Report of Investigations No. 189, 68 p. (Ch-9).

Forrester, Robert, 1892, The coal fields of Utah: U.S. Geological Survey Report on Mineral Resources, p. 511-520 (Ch-2).

Freeze, R.A., and Witherspoon, P.A., 1967, Theoretical analysis of regional groundwater flow: 2. effect of water-table configuration and subsurface permeability variation: Water Resources Research, v. 3, p. 623-634 (Ch-8).

Galloway, W.E., 1975, Process framework for describing the morphologic and stratigraphic evolution of deltaic depositional systems, *in* Broussard, M.L., editor, Deltas, models for exploration: Houston Geological Society, p. 87-98 (Ch-2).

---1984, Hydrogeologic regimes of sandstone diagenesis,*in* McDonald, D.A., and Surdam, R.C., editors, Clastic diagenesis: American Association of Petroleum Geologists Memoir 37, p. 3-13 (Ch-8).

Gardner, M. H., 1992, Volumetric partitioning and facies differentiation in Turonian strata of central Utah - field illustrations from the Ferron Sandstone of base level and sediment accommodation concepts: unpublished guidebook, 215 p. (Ch-2).

---1993, Sequence stratigraphy and facies architecture of the Upper Cretaceous Ferron Sandstone Member of the Mancos Shale, east-central Utah: Golden, Colorado School of Mines, Ph.D. dissertation T-3975, 528 p. (Ch-1, Ch-2, Ch-3, Ch-4, Ap-A).

---1995a, Tectonic and eustatic controls on the stratal architecture of mid-Cretaceous stratigraphic sequences, central Western Interior foreland basin of North America, *in* Stratigraphic evolution of foreland basins: Society for Sedimentary Geology (SEPM) Special Publication No. 52, p. 243-281 (Ch-1, Ch-2, Ch-3, Ch-4).

---1995b, The stratigraphic hierarchy and tectonic history of the mid-Cretaceous foreland basin of central Utah, *in* Stratigraphic evolution of foreland basins: Society for Sedimentary Geology (SEPM) Special Publication No. 52, p. 284-303 (Ch-1, Ch-2, Ch-3).

Gardner, M.H., Barton, M.D., and Fisher, R.S., 1994, Sequence stratigraphy, facies architecture, and permeability structure of fluvial-deltaic reservoir analogs - a field guide to selected outcrops of the Upper Cretaceous Ferron Sandstone, central Utah: unpublished guidebook prepared for 1994 American Association of Petroleum Geologists Annual Meeting, Denver, 257 p. (Ch-2, Ch-3).

Garrels, R.M., and Christ, C.L., 1965, Solutions, minerals, and equilibria: New York, Harper and Row, 450 p. (Ch-8).

Garrison, J.R., Jr., and van den Bergh, T.C.V., 1996, Coal zone stratigraphy -- a new tool for high-resolution depositional sequence stratigraphy in near-marine fluvial-deltaic facies - a case study from the Ferron Sandstone, east-central Utah: American Association of Petroleum Geologists Rocky Mountain Section Meeting, expanded abstracts volume, Montana Geological Society, p. 31-36 (Ch-2, Ch-4).

Garrison, J.R., Jr., van den Bergh, T.C.V., Barker, C.E., and Tabet, D.E., 1997, Depositional sequence stratigraphy and architecture of the Cretaceous Ferron Sandstone: implications for coal and coal bed methane resources -- a field excursion, *in* Link, P.K., and Kowallis, B.J., editors, Mesozoic to Recent geology of Utah: Provo, Brigham Young University Geology Studies, v. 42, pt. 11, p. 155-202 (Ch-1, Ch-2, Ch-3, Ch-4, Ap-A).

Gassmann, F., 1951, Elastic waves through a packing of spheres: Geophysics, v. 16, p. 673-685 (Ch-8).

Geehan, G., 1993, The use of outcrop data and heterogeneity modeling in development planning, *in* Eschard, R., Doligez, B., editors, Subsurface reservoir characterization from outcrop observations, Paris, Editions Technip, p. 53-64 (Ch-10).

Gilbert, G.K., 1877, Report on the geology of the Henry Mountains: U.S. Geographical and Geological Survey Rocky Mountain Region Report, 160 p. (Ch-2).

---1885, The topographic features of lake shores: U.S. Geological Survey, 5th Annual Report, p. 69-123 (Ch-2).

Gloyn, R.W., and Sommer, S.N., 1993, Exploration for coalbed methane gains momentum in Uinta Basin: Oil and Gas Journal, May 1993, p. 73-76 (Ch-2).

Gorell, S.B., 1995, Using geostatistics to aid in reservoir characterization: The Leading Edge of Geophysics, Sept. 1995, p. 967-974 (Ch-9).

Grant, C.W., Goggin, D.J., and Harris, P.M., 1994, Outcrop analog for cyclic-self reservoirs, San Andres Formation of Permian basin - stratigraphic framework, permeability distribution, geostatistics, and fluid-flow modeling: American Association of Petroleum Geologists Bulletin, v. 78, no. 1, p. 23-54 (Ch-9).

Gray, R.J., Patalski, R.M., and Schapiro, N., 1966, Correlation of coal deposits from central Utah, *in* Central Utah coals: Utah Geological and Mineralogical Survey Bulletin 80, p. 81-86 (Ch-2).

Gustason, E.R., Ryer, T.A., and Anderson, P.B., 1993, Integration of outcrop and subsurface information for geological model building in fluvial-deltaic reservoirs: unpublished Utah Geological Survey/American Association of Petroleum Geologists Rocky Mountain Section Core Workshop Manual, September 16, 1993, 24 p. (Ch-2).

Hale, L.A., 1972, Depositional history of the Ferron Formation, central Utah, *in* Baer, J.L., and Callaghan, Eugene, editors, Plateau-basin and range transition zone: Utah Geological Association Publication No. 2, p. 115-138 (Ch-1, Ch-2).

Hale, L.A., and Van DeGraff, F.R., 1964, Cretaceous stratigraphy and facies patterns -- northeastern Utah and adjacent areas: Intermountain Association of Petroleum Geologists, 13th Annual Field Conference Guidebook, p. 115-138 (Ch-2).

Hamilton, E.L., 1971, Elastic properties of marine sediments: Journal Geophysical Research, v. 76, p. 579-604 (Ch-8).

---1976, Variations of density and porosity with depth in deep-sea sediments: Journal of Sedimentary Petrology, v. 46, p. 280-300 (Ch-8).

Han, D., Nur, A., and Morgan, D., 1986, Effects of porosity and clay content on wave velocities in sandstones: Geophysics, v. 51, p. 2093-2107 (Ch-8).

Harrison, W.J., and Tempel, R.N., 1993, Diagenetic pathways in sedimentary basins, *in* Horbury, A.D., and Robinson, A.G., editors, Diagenesis and basin development: American Association of Petroleum Geologists Studies in Geology 36, p. 69-86 (Ch-8).

Hay, W.W., Eicher, D.L., and Diner, R., 1993, Physical oceanography and water masses in the Cretaceous Western Interior Seaway, *in* Caldwell, W.G.E., and Kauffman, E.G., editors, Evolution of the Western Interior Basin: Geological Association of Canada Special Paper 39, p. 297-318 (Ch-1).

Hayes, J.B., 1979, Sandstone diagenesis--the hole truth, *in* Scholle, P.A., and Schluger, P.R., editors, Aspects of diagenesis: Society of Sedimentary Geology (SEPM) Special Publication 26, p. 127-139 (Ch-8).

Heward, A.P., 1981, A review of wave-dominated clastic shoreline deposits: Earth Science Reviews, v. 17, p. 223-276 (Ch-5).

Hintze, L.F., and Stokes, W.L., 1964, Geologic map of southeastern Utah: Salt Lake City, University of Utah, College of Mines and Mineral Industries, scale 1:250,000 (Ch-2).

Hohn, M.E., Matchen, D.L., Vargo, A.G., McDowell, R.R., Heald, M.T., and Britton, J.Q., 1993a, Petroleum geology and reservoir characterization of the Big Injun Sandstone (Price Formation) in the Rock Creek (Walton) field, Roane County, West Virginia: West Virginia Geological and Economic Survey Publication B-43, 76 p. (Ch-9).

---1993b, Petroleum geology and reservoir characterization of the Big Injun Sandstone (Price Formation) in the Granny Creek (Walton) field, Clay and Roane Counties, West Virginia: West Virginia Geological and Economic Survey Publication B-44, 91 p. (Ch-9).

Honarpour, M., Koederitz, L., and Harvey, H.A., 1986, Relative permeability of petroleum reservoirs, Boca Raton, Florida, C.R.C. Press (Ch-10, Ap-C).

Hottmann, C.E., and Johnson, R.K., 1965, Estimation of formation pressures from log-derived shale properties: Journal of Petroleum Technology, v. 17, p. 717-722 (Ch-8).

Hoxie, R.L., 1874, Geologic map included in G.M. Wheeler, Annual Report for 1874: U.S. Geological Surveys West of the 100th Meridian, p. 5 (Ch-2).

Hucka, B.P., Sommer, S.N., Sprinkel, D.A., and Tabet, D.E., 1995, Ferron Sandstone drill-hole strip logs, Ferron Creek to Last Chance Creek, Emery and Sevier Counties, Utah: Utah Geological Survey Open-File Report 331, 1417 p. (Ch-8).

Hunt, C.B., 1946, Guidebook to the geology and geography of the Henry Mountains region, *in* Guidebook to the geology of Utah: Utah Geological Society Publication No. 1, 51 p. (Ch-2).

Hunt, J.M., 1953, Composition of crude oil and its relation to stratigraphy in Wyoming: American Association of Petroleum Geologists Bulletin, v. 37, no. 8, p. 1837-1872 (Ch-2).

---1979, Petroleum geochemistry and geology: San Francisco, W.H. Freeman, 617 p. (Ch-8).

Hunter, R.E., Clifton, H.E., and Phillips, R.L., 1979, Depositional processes, sedimentary structures, and predicted vertical sequences in barred nearshore systems, southern Oregon coast: Journal of Sedimentary Petrology, v. 49, no. 3, p. 711-726 (Ch-5).

ICF Resources, Incorporated, 1990, The United States coalbed methane resource: Gas Research Institute Quarterly Review of Methane from Coal Seams Technology, v. 7, no. 3, p. 10-28 (Ch-2).

Irani, M.C., Jansky, J.H., Jeran, P.W., and Hassett, G.L., 1977, Methane emission from U.S. coal mines in 1975, a survey: U.S. Bureau of Mines Information Circular 8733, 55 p. (Ch-2).

Isaaks, E.H., and Srivastava, R.M., 1989, An introduction to applied geostatistics: New York, Oxford University Press, 561 p. (Ch-9).

Japsen, P., 1993, Influence of lithology and Neogene uplift on seismic velocities in Denmark - implications for depth conversion of maps: American Association of Petroleum Geologists Bulletin, v. 77, p. 194-211 (Ch-8).

Joseph, P., Hu, L.Y., Dubrule, O., Claude, D., Crumeyrolle, P., Lesueur, J.L., and Soudet, H.J., 1993, The Roda deltaic complex (Spain) - sedimentology to reservoir stochastic modelling, *in* Eschard, R., Doligez, B., editors, Subsurface reservoir characterization from outcrop observations, Paris, Editions Technip, p. 97-109 (Ch-10).

Kamola, D.L., and Van Wagoner, J.C., 1995, Stratigraphy and facies architecture of parasequences with examples from the Spring Canyon Member, Blackhawk Formation, Utah, *in* Van Wagoner, J.C. and Bertram, G.T., editors, Sequence stratigraphy of foreland basin deposits: American Association of Petroleum Geologists Memoir 64, p. 27-54 (Ch-4).

Katich, P.J., Jr., 1951, The stratigraphy and paleontology of the pre-Niobrara Upper Cretaceous rocks of Castle Valley, Utah: Columbus, Ohio State University, Ph.D. dissertation, 208 p. (Ch-2).

---1953, Source direction of Ferron Sandstone in Utah: American Association Petroleum Geologists Bulletin, v. 37, no. 4, p. 858-862 (Ch-2).

---1954, Cretaceous and Early Tertiary stratigraphy of central and south-central Utah with emphasis on the Wasatch Plateau area: Intermountain Association of Petroleum Geologists, 5th Annual Field Conference Guidebook, p. 42-54 (Ch-2).

Keith, A.C., Hand, J.S., and Smith, A.D., 1990a, Coalbed methane resource map , Castlegate A bed, Book Cliffs coal field, Utah: Utah Geological and Mineral Survey Open-File Report 176 A, 1 plate, 1:100,000 (Ch-2).

---1990b, Coalbed methane resource map, Castlegate B bed, Book Cliffs coal field, Utah: Utah Geological and Mineral Survey Open-File Report 176 B, 1 plate, 1:100,000 (Ch-2).

---1990c, Coalbed methane resource map, Castlegate C bed, Book Cliffs coal field, Utah: Utah Geological and Mineral Survey Open-File Report 176 C, 1 plate, 1:100,000 (Ch-2).

---1990d, Coalbed methane resource map, Gilson bed, Book Cliffs coal field, Utah: Utah Geological and Mineral Survey Open-File Report 176 D, 1 plate, 1:100,000 (Ch-2).

---1991, Coalbed methane resource map, Castlegate D bed, Book Cliffs coal field, Utah: Utah Geological and Mineral Survey Open-File Report 176 E, 1 plate, 1:100,000 (Ch-2).

Knight, L.L., 1954, A preliminary heavy mineral study of the Ferron Sandstone, Utah: Brigham Young University Research Studies, Geology Series, v. 1, no. 4, 31 p. (Ch-2).

Knox, P.R., and Barton, M.D., 1999, Predicting interwell heterogeneity in fluvial-deltaic reservoirs–effects of progressive architecture variation through a depositional cycle from outcrop and subsurface observations, in Schatzinger, R.A., and Jordan, J.F., editors, Reservoir characterization–recent advances: American Association of Petroleum Geologists Memoir 71, p. 57-72 (Ch-4, Ch-7).

Koebbe, J.V., 1995, Documentation and installation guide of HomCode - a code for scaling up permeabilities using homogenization: Logan, Utah State University, Research Report, 413 p. (Ch-10).

Kossack, C.A., Aasen, J.O. and Opdal, S.T., 1990, Scaling up heterogeneities with pseudofunctions: Society of Petroleum Engineers Formation Evaluation, v. 5, no. 9, p. 226-232 (Ch-10).

Kuehnert, H.A., 1954, Huntington anticline, Emery County, Utah: Intermountain Association of Petroleum Geologists, 5th Annual Field Conference Guidebook, p. 94-95 (Ch-2).

Laine, M.D., and Staley, Don, 1991, Summary of oil and gas exploration and production in Carbon, Emery, and Sanpete Counties, east-central Utah, *in* Chidsey, T.C., Jr., editor, Geology of east-central Utah: Utah Geological Association Publication 19, p. 227-235 (Ch-2).

Lines, G.C., and Morrissey, D.J., 1983, Hydrology of the Ferron Sandstone aquifer and effects of proposed surface-coal mining in Castle Valley, Utah: U.S. Geological Survey Water-Supply Paper 2195, 39 p. (Ch-8).

Liu, K., Boult, P., Painter, S., and Paterson, L., 1996, Outcrop analog for sandy braided stream reservoirs: Permeability patterns in the Triassic Hawkesbury Sandstone, Sydney basin, Australia: American Association of Petroleum Geologists, v. 80, p. 1850-1866 (Ch-9).

Lowry, P., and Jacobsen, T., 1993, Sedimentology and reservoir characteristics of a fluvial-dominated delta-front sequence - Ferron Sandstone Member (Turonian), east-central Utah, USA, *in* Ashton, M., editor, Advances in reservoir geology: Geological Society (of London) Special Publication No. 69, p. 81-103. (Ch-3).

Lupton, C.T., 1914, Oil and gas near Green River, Grand County, Utah: U.S. Geological Survey Bulletin 541, p. 115-133 (Ch-2, Ch-4, Ap-A).

---1916, Geology and coal resources of Castle Valley in Carbon, Emery, and Sevier Counties, Utah: U.S. Geological Survey Bulletin 628, 88 p. (Ch-1, Ch-2, Ch-3, Ch-4).

MacDonald, A.C., and Aasen, J.O., 1994, A prototype procedure for stochastic modeling of facies tract distribution in shore face reservoirs, *in* Yarus, J.M., and Chambers, R.L., editors, Stochastic modeling and geostatistics: American Association of Petroleum Geologists Computer Applications in Geology No. 3, p. 241-345 (Ch-9).

Magara, K., 1976, Thickness of removed sedimentary rocks, paleopore pressure, and paleotemperature, southwestern part of Western Canada Basin: American Association of Petroleum Geologists Bulletin, v. 60, p. 554-565 (Ch-8).

Massari, F., 1996, Upper-flow-regime stratification types on steep-face, coarse-grained, Gilbert-type progradational wedges (Pleistocene, Southern Italy): Journal of Sedimentary Research, v. 66, p. 364-375 (Ch-9).

Mattson, Ann, 1997, Characterization, facies relationships, and architectural framework in a fluvial-deltaic sandstone - Cretaceous Ferron Sandstone, central Utah: Salt Lake City, University of Utah, M.S. thesis, 174 p. (Ch-7, Ch-8, Ch-9, Ch-10).

Mattson, Ann, and Chan, M.A., 1996, Facies relationships and statistical measures for reservoir heterogeneities in the Cretaceous Ferron Sandstone, central Utah [abs.]: American Association of Petroleum Geologist Annual Convention Official Program, v. 5, p. A93. (Ch-8).

Maxwell, J.C., 1960, Experiments on compaction and cementation of sand: Geological Society of America Memoir 79, p. 105-132 (Ch-8).

McKenna, S.A., and Poeter, E. P., 1994, Simulating geological uncertainty with imprecise data for groundwater flow and advective transport modeling, *in* Yarus, J.M., and Chambers R.L., editors, Stochastic modeling and geostatistics: American Association of Petroleum Geologists Computer Applications in Geology No. 3, p. 241-345 (Ch-9).

Miall, A.D., 1985, Architectural element analysis - a new method of facies analysis applied to fluvial deposits: Earth Science Reviews, v. 22, p. 261-308 (Ch-5).

Miller, M.A., Holder, John, Yang, H., Jamal, Y., Gray, K.E., Fisher, R.S., and Tyler, Noel, 1993a, Petrophysical and petrographic properties of the Ferron Sandstone: Gas Research Institute Topical Report GRI-93/0219, 257 p. (Ch-8).

Miller, M.A., Yang, H., Holder, J.T., Jounus, M.J., Gray, K.E., and Fisher, R.S., 1993b, Petrophysical properties of Ferron Sandstone during two-phase flow - implications for heterogeneity in Tertiary deltaic reservoirs: Society of Petroleum Engineering Paper SPE 26489, p. 757-762 (Ch-8).

Mitchum, R.M., Jr., Vail, P.R., and Thompson, S., III, 1977, Seismic stratigraphy and global sea level changes, Part 2: the depositional sequence as a basic unit for stratigraphic analysis - global cycles of relative changes of sea level, *in* Payton, C.E., editor, Seismic stratigraphy--applications to hydrocarbon exploration: American Association Petroleum Geologists Memoir 26, p. 53-62 (Ch-4).

Molenaar, C.M., and Cobban, W.A., 1991a, Middle Cretaceous stratigraphy on the south side of the Uinta Basin, east-central Utah, *in* Chidsey, T.C., Jr., editor, Geology of east-central Utah: Utah Geological Association Publication 19, p. 29-43 (Ch-2).

---1991b, Middle Cretaceous stratigraphy on south and east sides of the Uinta Basin, northeastern Utah and northwestern Colorado: U.S. Geological Survey Bulletin 1787-P, 34 p. (Ch-2).

Nelson, P.H., 1994, Permeability-porosity relationships in sedimentary rocks: The Log Analyst, v. 35, no. 3, p. 38-62, (Ch-8).

Neter, J., and Wasserman, W., 1974, Applied linear statistical models: Homewood, IL, Richard D. Irwin, Inc., 842 p. (Ch-9).

Neuzil, C.E., and Pollock, D.W., 1983, Erosional unloading and fluid pressures in hydraulically "tight" rocks: Journal of Geology, v. 91, p. 179-193 (Ch-8).

Nix, T.L., 1999, Detailed outcrop analysis of a growth fault system and associated structural and sedimentologic elements, Ferron Sandstone, Utah: Provo, Brigham Young University, M.S. thesis, 48 p. (Ch-4, Ap-A).

Nur, A., 1971, Effects of stress on velocity anisotropy in rocks with cracks: Journal of Geophysical Research, v. 76, p. 2022-2034, (Ch-8).

Nur, A., and Murphy, W., 1981, Wave velocities and attenuation in porous media with fluids: Proceedings 4th International Conference on Continuum Models of Discrete Systems, Stockholm, p. 311-327 (Ch-8).

Odeh, A.S., 1981, Comparison of solutions to a three-dimensional black-oil reservoir simulation problem: Journal of Petroleum Technology, v. 33, no. 1, p. 13-25 (Ch-10, Ap-C).

Palmer, J.J., and Scott, A.J., 1984, Stacked shoreline and shelf sandstone of La Ventana Tongue (Campanian), northeastern New Mexico: American Association of Petroleum Geologists Bulletin, v. 68, no. 1, pt. 1, p. 74-91 (Ch-2).

Peterson, Fred, and Ryder, T.R., 1975, Cretaceous rocks in the Henry Mountains region, Utah and their relation to neighboring regions, *in* Fassett, J.E., and Wengerd, S.A., editors, Canyonlands country: Four Corners Geological Society Guidebook, 8th Field Conference, p. 167-189 (Ch-2).

Peterson, Fred, Ryder, R.T., and Law, B.E., 1980, Stratigraphy sedimentology and regional relationships of the Cretaceous System in the Henry Mountains region, Utah, *in* Picard, M.D., editor, Henry Mountains symposium: Utah Geological Association Publication 8, p. 151-170 (Ch-1).

Ray, R.M., Brashear, J.P., and Biglarbgi, K., 1991, Classification system targets unrecovered U.S. oil reserves: Oil and Gas Journal, Sept. 30, 1991, p. 89-93 (Ch-2).

Raymer, L.L., Hunt, E.R., and Gardner, J.S., 1980, An improved sonic transit time-to-porosity transform: Transactions of Society of Professional Well Log Analysists 21st Annual Logging Symposium, p. P1-P13 (Ch-8).

Rhea, L., Person, de Marsily, G., Ledoux, E., and Galli, A., 1994, Geostatistical models of secondary oil migration within heterogeneous carrier beds - a theoretical example: American Association of Petroleum Geologists Bulletin, v. 78, p. 1679-1691 (Ch-9).

Roberts, L.N.R., and Kirschbaum, M.A., 1995, Paleogeography of the Late Cretaceous of the Western Interior of Middle North America--coal distribution and sediment accumulation: U.S. Geological Survey Professional Paper 1561, 115 p. (Ch-1).

Robinson, J.W., and McCabe, P.J., 1997, Sandstone-body and shale-body dimensions in a braided fluvial system: Salt Wash Sandstone Member (Morrison Formation), Garfield County, Utah: American Association of Petroleum Geologists Bulletin, v. 81, no. 8, p. 1267-1291 (Ch-9).

Ryer, T.A., 1980, Deltaic coals of the Ferron Sandstone Member of the Mancos Shale--predictive model for Cretaceous coals of the Western Interior, *in* Carter, L.M., editor, Proceedings of the Fourth Symposium on the geology of Rocky Mountain coal: Colorado Geological Survey Resource Series no. 10, p. 4-5 (Ch-2).

---1981a, Deltaic coals of Ferron Sandstone Member of Mancos Shale - predictive model for Cretaceous coal-bearing strata of Western Interior: American Association of Petroleum Geologists Bulletin, v. 65, no. 11, p. 2323-2340 (Ch-1, Ch-2, Ch-3, Ch-4, Ch-5, Ap-A).

---1981b, The Muddy and Quitchupah projects - a project report with descriptions of cores of the I, J, and C coal beds from the Emery coal field, central Utah: U.S. Geological Survey Open-File Report 81-460, 34 p. (Ch-2).

---1982a, Possible eustatic control on the location of Utah Cretaceous coal fields, *in* Gurgel, K.D., editor, Proceedings - 5th ROMOCO symposium on the geology of Rocky Mountain coal: Utah Geological and Mineralogical Survey Bulletin 118, p. 89-93 (Ch-2, Ch-4, Ap-A).

---1982b, Cross section of the Ferron Sandstone Member of the Mancos Shale in the Emery coal field, Emery and Sevier Counties, central Utah: U.S. Geological Survey Map MF-1357, vertical scale: 1 inch = 30 meters, horizontal scale: 1 inch = 1.25 kilometers (Ch-2, Ch-4, Ap-A).

---1984, Transgressive-regressive cycles and the occurrence of coal in some upper Cretaceous strata of Utah, U.S.A.: International Association Sedimentologists Special Publication No. 7, p. 217-227 (Ch-2).

---1987, Distinguishing eustatic and tectonic contributions to major clastic wedges in Cretaceous foreland basin, Wyoming and Utah [abs.]: Geological Society of Canada Annual Meeting, Program with Abstracts, v. 12, p. 86 (Ch-2).

---1991, Stratigraphy, facies, and depositional history of the Ferron Sandstone in the canyon of Muddy Creek, east-central Utah, *in* Chidsey, T.C., Jr., editor, Geology of east-central Utah: Utah Geological Association Publication 19, p. 45-54 (Ch-2, Ch-4, Ch-5).

---1993a, Speculations on the origins of mid-Cretaceous clastic wedges, central Rocky Mountain region, United States, *in* Caldwell, W.G.E., and Kauffman, E.G., editors, Evolution of the Western Interior Basin: Geological Association of Canada Special Paper 39, p. 189-198 (Ch-2).

---1993b, The Ferron Sandstone of central Utah -- an overview, *in* Ryer, T.A., Gustason, E.R., and Anderson, P.B., editors, Stratigraphy and facies architecture of the Ferron Sandstone Member of the Mancos Shale: Utah Geological Survey/American Association of Petroleum Geologists Rocky Mountain Section unpublished field trip guidebook, 9 p. (Ch-2).

---1993c, The Upper Cretaceous Ferron Sandstone of central Utah: an overview [abs.]: American Association of Petroleum Geologists Bulletin, v. 77, no. 8, p. 1459 (Ch-2).

---1994, Interplay of tectonics, eustacy, and sedimentation in the formation of mid-Cretaceous clastic wedges, central and northern Rocky Mountain regions, *in* Dolson, J.C., Hendricks, M.L., and Wescott, S.A., editors, Unconformity-related hydrocarbons in sedimentary sequences: Denver, Rocky Mountain Association of Geologists, p. 35-44 (Ch-2).

Ryer, T.A., and Gustason, E.R., 1993, Ferron delta-front units Nos. 1 and 2, southern part of Muddy Creek Canyon, *in* Ryer, T.A., Gustason, E.R., and Anderson, P.B., editors, Stratigraphy and facies architecture of the Ferron Sandstone Member of the Mancos Shale: Utah Geological Survey/American Association of Petroleum Geologists Rocky Mountain Section unpublished field trip guidebook, 20 p. (Ap-A).

Ryer, T.A., and Lovekin, J.R., 1986, The Upper Cretaceous Vernal delta of Utah--depositional or paleotectonic feature? *in* Peterson, J.A., editor, Paleotectonics & sedimentation in the Rocky Mountain region, United States: American Association of Petroleum Geologists Memoir 41, p. 497-510 (Ch-1, Ch-2).

Ryer, T.A., and McPhillips, Maureen, 1983, Early Late Cretaceous paleogeography of east-central Utah, *in* Reynolds, M.W., and Dolly, E.D., editors, Mesozoic paleogeography of the west-central United States: Society of Economic Paleontologists and Mineralogists, Rocky Mountain Paleography Symposium 2, p. 253-272 (Ch-2, Ch-5, Ch-8, Ap-A).

Ryer, T.A., Dewey, J.A., Jr., and Morris, T.H., 1995, Distinguishing allocyclic and autocyclic causes of parasequence-level cyclicity--lessons from deltaic strata of the Upper Cretaceous Ferron Sandstone, central Utah [abs.]: American Association of Petroleum Geologists Bulletin, v. 79, no. 6, p. 924 (Ch-5).

Ryer, T.A., Phillips, R.E., Bohor, B.F., and Pollastro, R.M., 1980, Use of altered volcanic ash falls in stratigraphic studies of coal-bearing sequences - an example from the Upper Cretaceous Ferron Sandstone Member of the Mancos Shale in central Utah: Geological Society of America Bulletin, v. 91, no. 10., pt 1, p. 579-586 (Ch-2).

Said, Rushdi, 1981, The geological evolution of the River Nile: New York, Springer-Verlag, 151 p. (Ch-2).

Scheihing, M.H., and Gaynor, G.C., 1991, The shelf sand-plume model--a critique: Sedimentology, v. 38, p. 433-444 (Ch-2).

Schlumberger, 1972, Log interpretation volume I–principles: New York, Schlumberger Ltd., 113 p. (Ch-8).

---1989, Log interpretation principles/applications: Houston, Schlumberger Educational Services, 116 p. (Ch-8).

Schmidt, V., and McDonald, D.A., 1979, The role of secondary porosity in the course of sandstone diagenesis, *in* Scholle P.A., and Schluger, P.R., editors, Aspects of diagenesis: Society of Sedimentary Geology (SEPM) Special Publication 26, p. 175-207 (Ch-8).

Schwans, Peter, 1995, Controls on sequence stacking and fluvial to shallow-marine architecture in a foreland basin, *in* Van Wagner, J.C., and Bertram, G.T., editors, Sequence stratigraphy of foreland basin deposits: American Associations of Petroleum Geologists Memoir 64, p. 55-102 (Ch-2).

Schwartz, F.W., and Longstaffe, F.J., 1988, Ground water and clastic diagenesis, *in* Back, W., Rosenshein, J.S., and Seaber, P.R., editors, Hydrogeology, Geology of North America: Geological Society of America, O-2, p. 413-434 (Ch-8).

Shanley, K.W., and McCabe, P.J., 1991, Predicting facies architecture through sequence stratigraphy--an example from the Kaiparowits Plateau, Utah: Geology, v. 19, no. 7, p. 742-745 (Ch-2).

---1995, Sequence stratigraphy of Turonian-Santonian strata, Kaiparowits Plateau, southern Utah, U.S.A. - implications for regional correlation and foreland basin evolution, *in* Van Wagoner, J.C., and Bertram, G.T., editors, Sequence stratigraphy of foreland basin deposits: American Association Petroleum Geologists Memoir 64, p. 103-136 (Ch-2).

Smith, A.D., 1981, Methane content of Utah coals - progress report 1979-1980: Utah Geological and Mineral Survey Open-File Report 28, 9 p. (Ch-2).

---1986, Utah core desorption project , final report: Utah Geological and Mineral Survey Open-File Report 88, 59 p. (Ch-2).

Snelgrove, S.H., Forster, C.B., Mattson, Ann, and Chan, M.A., 1996, Impact of lithofacies architecture and distribution on fluid flow - examples from the Cretaceous Ferron Sandstone, east-central Utah [abs.]: American Association of Petroleum Geologists Annual Convention Official Program, v. 5, p. A132. (Ch-8).

Snelgrove, S.H., McMechan, G., Szerbiak, R.B., Wang, D., Corbeanu, R., Soegaard, K., Thurmond, J., Forster, C.B., Crossey, L., and Roche, K., 1998, Integrated 3-D characterization and flow simulation studies in a fluvial channel, Ferron Sandstone, east-central Utah [abs.]: American Association of Petroleum Geologists Annual Convention Extended Abstracts, v. 2, p. A617 (Ch-10).

Sommer, S.N., Doelling, H.H., and Gloyn, R.W., 1993, Coalbed methane in Utah, *in* Atlas of major Rocky Mountain gas reservoirs: New Mexico Bureau of Mines and Mineral Resources, p. 167 (Ch-2).

Sondergeld, C.H., and Rai, C.S., 1988, Geophysical evaluation module operator's manual: Amoco Research Report T88-E-0033, non-paginated (Ch-8).

---1993a, A new concept in quantitative core characterization: The Leading Edge, July, p. 774-779 (Ch-8).

---1993b, A new exploration tool: quantitative core characterization: PAGEOPH, v. 141, no. 2/3/4, p. 249-268 (Ch-8).

Spieker, E.M., 1946, Late Mesozoic and Early Cenozoic history of central Utah: U.S. Geological Survey Professional Paper 205-D, p. 117-160 (Ch-2).

Spieker, E.M., and Reeside, J.B., Jr., 1925, Cretaceous and Tertiary formations of the Wasatch Plateau, Utah: Geological Society of America Bulletin, v. 36, no. 3, p. 435-454 (Ch-2).

---1926, The Upper Cretaceous shoreline in Utah: Geological Society of America Bulletin, v. 37, no. 3, p. 429-438 (Ch-2).

Sprinkel, D.A., 1993, Wasatch Plateau [WP] play -- overview, *in* Atlas of major Rocky Mountain gas reservoirs: New Mexico Bureau of Mines and Mineral Resources, p. 89 (Ch-2).

Srivasta, R.M., 1994, An overview of stochastic methods for reservoir characterization: *in* Yarus, J .M., and Chambers, R.L., editors, Stochastic modeling and geostatistics: American Association of Petroleum Geologists Computer Applications in Geology No. 3, p. 3-16 (Ch-9).

Stoll, R.D., 1989, Sediment Acoustics: Berlin, Springer-Verlag, 153 p. (Ch-8).

Stonecipher, S.A., Winn, R.D., Jr., and Bishop, M.G., 1984, Diagenesis of the Frontier Formation, Moxa arch - a function of sandstone geometry, texture and composition, and fluid flux, *in* McDonald, D.A., and Surdam, R.C., editors, Clastic diagenesis: American Association of Petroleum Geologists Memoir 37, p. 289-316 (Ch-8).

Surdam, R.C., Boese, S.W., and Crossey, L.J., 1984, The chemistry of secondary porosity, *in* McDonald, D.A., and Surdam, R.C., editors, Clastic diagenesis: American Association of Petroleum Geologists Memoir 37, p. 127-149 (Ch-8).

Swift, D.J.P., 1967, Coastal erosion and transgressive stratigraphy: Journal of Geology, v. 76, no. 4, p. 444-456 (Ch-4).

Tabet, D.E., 1995a, Utah's 1994 coalbed methane gas developments: Utah Geological Survey, Survey Notes, v. 27, no. 2, p. 7-9 (Ch-1).

---1995b, CBM in 'dry county' coalbed gas development expands in Utah: Coalbed Methane Review, issue 3, p. 11-13 (Ch-1).

Tabet, D.E., and Burns, Terry, 1996, Drunkards Wash, *in* Hill, B.G., and Bereskin, S.R., editors, Oil and gas fields of Utah: Utah Geological Association Publication 22 (Addendum): non-paginated (Ch-2).

Tabet, D.E., Hucka, B.P., and Sommer, S.N., 1995, Maps of total Ferron coal, depth to the top, and vitrinite reflectance for the Ferron Sandstone Member of the Mancos Shale, central Utah: Utah Geological Survey Open-File Report 329, 3 plates, 1:250,000 (Ch-1).

---1996, Geology of the Ferron Sandstone coalbed methane "fairway," central Utah [abs.]: American Association of Petroleum Geologists Annual Convention Official Program, v. 5, p. A137 (Ch-1).

Taft, J.A., 1906, Book Cliffs coal field, Utah, west of Green River: U.S. Geological Survey Bulletin 285, p. 289-302 (Ch-2).

Terzaghi, K., 1965, Theoretical soil mechanics: New York, John Wiley, 510 p. (Ch-8).

Thompson, S.L., 1985, Ferron Sandstone Member of the Mancos Shale; a Turonian mixed-energy deltaic system: Austin, University of Texas, M.S. thesis, 165 p. (Ch-2).

Thompson, S.L., Ossian, C.R., and Scott, A.J., 1986, Lithofacies, inferred processes, and log response characteristics of shelf and shoreface sandstones, Ferron Sandstone, central Utah, *in* Moslow, T.F., and Rhodes, E.G., editors, Modern and ancient shelf clastics - a core workshop: Society for Sedimentary Geology (SEPM) Core Workshop No. 9, p. 325-361 (Ch-2, Ch-3).

Thurmond, J., McMechan, G., Soegaard, K., Szerbiak, R., Gaynor, G., Forster, C.B., and Snelgrove, S.H., 1997, Integration of 3-D ground-penetrating radar, outcrop, and borehole data applied to reservoir characterization and flow simulation [abs.]: American Association of Petroleum Geologists Annual Convention Official Program, v. 6, p. A116 (Ch-10).

Toth, J., 1980, Cross-formational flow of groundwater - a mechanism for transport and accumulation of petroleum (the generalized hydraulic theory of petroleum migration), *in* Roberts, W.H., III, and Cordell, R.J., editors, Problems in petroleum migration: American Association of Petroleum Geologists Studies in Geology 10, p. 121-167 (Ch-8).

Triplehorn, D.M., and Bohor, B.F., 1981, Altered volcanic ash partings in the C coal bed, Ferron Sandstone Member of the Mancos Shale, Emery County, Utah: U.S. Geological Survey Open-File Report, 45 p. (Ch-2).

Tripp, C.N., 1989, A hydrocarbon exploration model for the Cretaceous Ferron Sandstone Member of the Mancos Shale, and the Dakota Group in the Wasatch Plateau and Castle Valley of east-central Utah, with emphasis on post-1980 subsurface data: Utah Geological and Mineral Survey Open-File Report 160, 82 p, scale 1:250,000 (Ch-2, Ch-8).

---1990a, Ferron oil and gas field, T. 20-21 S., R. 7 E., Emery County, Utah: Utah Geological and Mineral Survey Open-File Report 191, 23 p., scale 1:24,000 (Ch-2).

---1990b, Wasatch Plateau oil and gas field, T. 13-17 S., R. 6-7 E., Carbon, Emery, and Sanpete Counties, Utah: Utah Geological and Mineral Survey Open-File Report 192, 33 p., scale 1:100,000 (Ch-2).

---1991a, Wasatch Plateau oil and gas fields, Carbon, Emery and Sanpete Counties, Utah, *in* Chidsey, T.C., Jr., editor, Geology of east-central Utah: Utah Geological Association Publication 19, p. 255-264 (Ch-2).

---1991b, Ferron oil and gas field, Emery County, Utah, *in* Chidsey, T.C., Jr., editor, Geology of east-central Utah: Utah Geological Association Publication 19, p. 265-272 (Ch-2, Ch-8).

---1993a, Ferron, *in* Hill B.G., and Bereskin, S.R., editors, Oil and gas fields of Utah: Utah Geological Association Publication 22, non-paginated (Ch-2).

---1993b, Flat Canyon, Indian Creek, East Mountain, *in* Hill B.G., and Bereskin, S.R., editors, Oil and gas fields of Utah: Utah Geological Association Publication 22, non-paginated (Ch-2, Ch-8).

---1993c, Clear Creek, *in* Hill B.G., and Bereskin, S.R., editors, Oil and gas fields of Utah: Utah Geological Association Publication 22, non-paginated (Ch-2, Ch-8).

Tyler, Noel, 1988, New oil from old fields: Geotimes, July, p. 8-10 (Ch-2).

Utah Division of Oil, Gas and Mining, 2000, Monthly production report (December 1999), non-paginated (Ch-1, Ch-2).

Vail, P.R., Mitchum, R.M., and Thompson, S., III, 1977, Global cycles of relative changes of sea level, *in* Payton, C.E., editor, Seismic stratigraphy--applications to hydrocarbon exploration: American Association Petroleum Geologists Memoir 26, p. 83-98 (Ch-2).

van den Bergh, T.C.V., 1995, Facies architecture and sedimentology of the Ferron Sandstone Member of the Mancos Shale, Willow Springs Wash, east-central Utah: Madison, University of Wisconsin, M.S. thesis, 255 p. (Ch-3).

van den Bergh, T.C.V., and Garrison, J.R., Jr., 1996, Channel belt architecture and geometry -- a function of depositional parasequence set stacking pattern, Ferron Sandstone, east-central Utah: American Association of Petroleum Geologists Rocky Mountain Section Meeting, expanded abstracts volume, Montana Geological Society, p. 37-42 (Ch-2, Ch-3).

van den Bergh, T.C.V., and Sprague, A.R., 1995, The control of high-frequency sequences on the distribution of shoreline fluvial reservoir facies: an example from the Ferron Sandstone, Utah [abs.]: American Association of Petroleum Geologists Annual Convention Official Program, v. 4, p. 99A (Ch-2).

Van Wagoner, J.C., 1995, Overview of sequence stratigraphy of foreland basin deposits--terminology, summary of papers, and glossary of sequence stratigraphy, *in* Van Wagoner, J.C., and Bertram, G.T., editors, Sequence stratigraphy of foreland basin deposits: American Association of Petroleum Geologists Memoir 64, p. ix-xxi (Ch-2, Ch-4).

Van Wagoner, J.C., Mitchum, R.M., Posamentier, H.W., and Vail, P.R., 1987, An overview of sequence stratigraphy and key definitions, *in* Bally, A.W., editor, Atlas of seismic stratigraphy: American Association of Petroleum Geologists Studies in Geology 27, v. 1, p. 11-14 (Ch-1, Ch-4).

Van Wagoner, J.C., Mitchum, R.M., Campion, K.M., and Rahmanian, V.D., 1990, Siliciclastic sequences, stratigraphy in well logs, cores and outcrops: American Association of Petroleum Geologists Methods in Exploration, no. 7, 55 p. (Ch-4, Ch-5).

Walsh, J.B., 1965, The effect of cracks on the compressibility of rock: Journal Geophysical Research, v. 70, p. 381-389 (Ch-8).

Walton, P.T., 1954, Wasatch Plateau gas fields, Utah: Intermountain Association of Petroleum Geologists, 5th Annual Field Conference Guidebook, p. 79-85 (Ch-2).

---1955, Wasatch Plateau gas fields, Utah: American Association Petroleum Geologists Bulletin, v. 39, no. 4, p. 385-420 (Ch-2).

Warren, J.E., and Price, H.S., 1961, Flow in heterogeneous porous media: Society of Petroleum Engineering Journal, p. 153-169 (Ch-10).

Weber, K.J., 1978, Influence of common structures on fluid flow in reservoir models: Journal of Petroleum Technology, v. 34, no. 3, p. 665-672 (Ch-10).

Weimer, R.J., 1962, Late Jurassic and Early Cretaceous correlations, south-central Wyoming and northwestern Colorado: Wyoming Geological Association, 17th Annual Field Conference Guidebook, p. 124-130 (Ch-2).

White, C.D., and Barton, M.D., 1998, Comparison of the recovery behavior of contrasting reservoir analogs in the Ferron Sandstone using outcrop studies and numerical simulation: The University of Texas at Austin, Bureau of Economic Geology Report of Investigations No. 249, 46 p. (Ch-7).

---1999, Translating outcrop data to flow models, with applications to the Ferron Sandstone: Society of Petroleum Engineers, Reservoir Evaluation & Engineering (SPE 57482), v. 2., no. 4, p. 341-350 (Ch-7).

Winkler, K.W., and Murphy, W.F., III, 1995, Acoustic velocity and attenuation in porous rocks, *in* Ahrens, T.J., editor, Rock physics and phase relations - a handbook of physical constants: Washington DC, American Geophysical Union, p. 20-34 (Ch-8).

Wyllie, M.R.J., Gregory, A.R., and Gardner, L.W., 1956, Elastic wave velocities in heterogeneous and porous media: Geophysics, v. 21, p. 41-70 (Ch-8).

Other Ferron Project References

Adams, R.D., 1995, The Cretaceous Ferron Sandstone of east-central Utah: a tale of three different morphologies for deltaic parasequences [abs.]: American Association of Petroleum Geologists Bulletin, v. 79, no. 6, p. 914.

Adams, R.D., Chidsey, T.C., Jr., and Laine, M.D., 1995, Integrated multi disciplinary reservoir characterization of a deltaic system-1) architecture and lithofacies of the Cretaceous-age Ferron Sandstone, east-central Utah [abs.]: American Association of Petroleum Geologists Annual Convention Official Program, v. 4, p. 1A.

Adams, R.D., Snelgrove, S.H., and Forster, C.B., 1995, A methodology for obtaining detailed geologic descriptions to constrain 3-D reservoir fluid-flow simulation models in delta-front lithofacies [abs.]: American Association of Petroleum Geologists Bulletin, v. 79, no. 6, p. 914.

Anderson, P.B., 1993, Stratigraphic and sedimentalogic characteristics of the lower portion of the Ferron Sandstone Member of the Mancos Shale along a portion of Muddy Creek, Emery County, Utah [abs.]: American Association of Petroleum Geologists Bulletin, v. 77, no. 8, p. 1441.

Anderson, P.B., Ryer, T.A., and Chidsey, T.C., Jr., 1996, Ferron Sandstone - stratigraphy and reservoir analogs, east-central Utah [abs.]: American Association of Petroleum Geologists Bulletin, v. 80, no. 6, p. 965.

Anderson, P.B., Chidsey, T.C., Jr., McClure, Kevin, Mattson, Ann, and Snelgrove, S.H., in press, Ferron Sandstone stratigraphic cross sections, Ivie Creek area, Emery County, Utah: Utah Geological Survey Open-File Report, 6 plates (Ch-7, Ap-B).

Chidsey, T.C., Jr., 1995, Geological and petrophysical characterization of the Ferron Sandstone in Utah, for 3-D simulation of a fluvial-deltaic reservoir [abs.]: American Association of Petroleum Geologists Bulletin, v. 79, no. 6, p. 916.

Colarullo, S.J., Forster, C.B., Huang, Hongmei, and Mattson, Ann, 1997, From outcrop to simulation in the Ferron Sandstone - 3) impact of 3-D clinoform facies architecture on performance of a fluvial-dominated deltaic-front reservoir [abs.]: Geological Society of America Abstracts with Program, v. 29, no. 6, p. A-465.

Dewey, J.A., Jr., Morris, T.H., and Ryer, T.A., 1995, Constraining reservoir models of fluvial- vs. wave-dominated delta-front sandstones through high resolution and high density sequence stratigraphic analysis, Ferron Sandstone, Utah [abs.]: American Association of Petroleum Geologists Bulletin, v. 79, no. 6, p. 917.

Jarrard, R.D., and Erickson, S.E., 1997, Sandstone exhumation effects on velocity and porosity - perspectives from the Ferron Sandstone [abs.]: American Association of Petroleum Geologists Annual Convention Official Program, v. 6, p. A93.

Mattson, Ann, Chan, M.A., Snelgrove, S.H., Forster, C.B., and Anderson, P.B., 1997, From outcrop to simulation in the Ferron Sandstone - 1) detailed architecture and characterization of a fluvial-dominated deltaic reservoir analog [abs.]: Geological Society of America Abstracts with Program, v. 29, no. 6, p. A-464.

Ryer, T.A., and Anderson, P.B., 1995, Parasequence sets, parasequences, facies distributions, and depositional history of the Upper Cretaceous Ferron deltaic clastic wedge, Utah [abs.]: American Association of Petroleum Geologists Bulletin, v. 79, no. 6, p. 924 (Ch-2).

Snelgrove, S.H., Forster, C.B., Mattson, Ann, and Anderson, P.B., 1997, From outcrop to simulation in the Ferron Sandstone - 2) impact of detailed 2-D clinoform architecture on performance of a fluvial-dominated deltaic-front reservoir [abs.]: Geological Society of America, Abstracts with Program, v. 29, no. 6, p. A-464.

Snelgrove, S.H., Forster, C.B., and Koebbe, J.V., 1995, Integrated multidisciplinary reservoir characterization of a deltaic system-2) developing a petrophysical model for reservoir simulation using data from the Ferron Sandstone, Utah [abs.]: American Association of Petroleum Geologists Annual Convention Official Program, v. 4, p. 90-91A.

U.S. Department of Energy, 1994, Geological and petrophysical characterization of the Ferron Sandstone for 3-D simulation of a fluvial-deltaic reservoir, *in* Contracts for field projects and supporting research on enhanced oil recovery, reporting period October-December 1993: Progress Review No. 77, DOE/BC--94/1, p. 84-86.

---1995a, Geological and petrophysical characterization of the Ferron Sandstone for 3-D simulation of a fluvial-deltaic reservoir, in Contracts for field projects and supporting research on enhanced oil recovery, reporting period January-March 1994: Progress Review No. 78, DOE/BC--94/2, p. 101-103.

---1995b, Geological and petrophysical characterization of the Ferron Sandstone for 3-D simulation of a fluvial-deltaic reservoir, *in* Contracts for field projects and supporting research on enhanced oil recovery, reporting period July-September 1994: Progress Review No. 80, DOE/BC--94/4, p. 40-45.

---1996a, Geological and petrophysical characterization of the Ferron Sandstone for 3-D simulation of a fluvial-deltaic reservoir, in Contracts for field projects and supporting research on enhanced oil recovery, reporting period October-December 1994: Progress Review No. 81, DOE/BC--95/1, p. 112-118.

---1996b, Geological and petrophysical characterization of the Ferron Sandstone for 3-D simulation of a fluvial-deltaic reservoir, *in* Contracts for field projects and supporting research on enhanced oil recovery, reporting period January-March 1995: Progress Review No. 82, DOE/BC--95/2, p. 66-73.

---1996c, Geological and petrophysical characterization of the Ferron Sandstone for 3-D simulation of a fluvial-deltaic reservoir, *in* Contracts for field projects and supporting research on enhanced oil recovery, reporting period April-June 1995: Progress Review No. 83, DOE/BC--95/3, p. 77-81.

---1996d, Geological and petrophysical characterization of the Ferron Sandstone for 3-D simulation of a fluvial-deltaic reservoir, *in* Contracts for field projects and supporting research on enhanced oil recovery, reporting period July-September 1995: Progress Review No. 84, DOE/BC--95/4, p. 112-120.

---1996e, Geological and petrophysical characterization of the Ferron Sandstone for 3-D simulation of a fluvial-deltaic reservoir, *in* Contracts for field projects and supporting research on enhanced oil

recovery, reporting period October-December 1995: Progress Review No. 85, DOE/BC--96/1, p. 74-78.

---1997, Geological and petrophysical characterization of the Ferron Sandstone for 3-D simulation of a fluvial-deltaic reservoir, *in* Contracts for field projects and supporting research on enhanced oil recovery, reporting period January-March 1996: Progress Review No. 86, DOE/BC--96/2, p. 115-120.

Utah Geological Survey, 1995, Ferron project ends first year with a bang!: Utah Geological Survey Petroleum News (July), p. 1-2.

---1996, Ferron sandstone project moves to reservoir simulation stage: Utah Geological Survey Petroleum News (May), p. 2-4.

---1997a, Ferron project in 3-D simulation phase: Utah Geological Survey Petroleum News (April), p. 2-4.

---1997b, Energy news - oil demonstration programs move into advanced phases: Utah Geological Survey, Survey Notes, v. 30, no. 1, p. 10-11.

APPENDIX A
FERRON SANDSTONE STRATIGRAPHIC NOMENCLATURE

Stratigraphic Unit	Stratigraphic Unit Name	Description
Kf	Ferron Sandstone Member of the Mancos Shale Source: Lupton, 1914	Ferron Sandstone is recognized as a member of the Mancos Shale. No type section has been designated. The name is derived from the town of Ferron, but it is clear from Lupton's work that he would have chosen the outcrops farther south, east and south of the town of Emery, as representative of the member where it is most typically developed. The name Ferron Sandstone is presently used on outcrops around the San Rafael Swell, in the Henry Mountains basin, and beneath Castle Valley and the Wasatch Plateau. Controversy exists about whether "Ferron" or "Juana Lopez" is a more appropriate designation for thinly interbedded sandstones and shales of Ferron age on the east side of the San Rafael Swell near Green River and eastward into Colorado.
Kf-Clw	Clawson Unit of Ferron Sandstone Source: Cotter, 1975a	The Clawson unit of the Ferron extends from the northern part of San Rafael Swell southward along its western flank, through Molen Reef, finally feathering out westward toward Muddy Canyon in the "Molen Amphitheater." The Clawson and overlying Washboard units of the Ferron together constitute the "lower Ferron" of Ryer and McPhillips, 1983, and the lower part of the "Hyatti sequence" of Gardner, 1993. They are shelf sandstones with a northern source. Lowering of sea level during middle Turonian time facilitated southward transport of very fine - and fine-grained sand onto a shoal area that marks the eastern hinge of the foredeep developed in front of the Sevier orogenic belt. The shoal may represent a peripheral bulge. In addition to feathering out southward, both the Clawson and Washboard units lose sand content and disappear toward the west in the area stretching from the "Molen Amphitheater" southward to Mesa Butte and westward to the "Tri-Canyon" area and "Cowboy Mesa." A gentle structural flexure has been recognized in this area, suggesting the presence of a down-to-the-west basement fault. The fact that Cretaceous rocks were flexed but not broken by movement on the proposed fault (unlike the younger faults associated with Tertiary extension) suggests that this fault moved during Cretaceous time in response to thrust loading. The westward loss of sand in the Clawson and Washboard units suggest that it was active during lower Ferron deposition. Facies content of shoreline unit: shelf sand body.
Kf-Wsb	Washboard Unit of Ferron Sandstone Source: Cotter, 1975a	The Washboard unit extends from the northern part of San Rafael Swell southward to Mesa Butte, slightly farther than does the underlying Clawson unit. Same origin as Clawson unit comments apply. A dark and organic-rich zone (5 to 20 feet thick [1.5-6 m]) of shale lies just above the Washboard and below the Ferron Sandstone. This zone is traceable from Ferron Creek south into the I-70 area, where its thickness decreases and becomes faintly traceable to the south. Facies content of shoreline unit: shelf sand body.
Kf-LC	Last Chance Unit of Ferron Sandstone (may be a parasequence set?) Source: new name	The type section of the Last Chance unit of the Ferron is at Last Chance Creek, where the shoreline unit, forms vertical cliffs about 165 feet (54 m) high. This is the southern most parasequence (?) in the study area. It appears to be mainly middle shoreface facies, with a few distinct horizontal bedding planes that are continuous for several hundred feet horizontally. The basal contact is sharp. Kf-Last Chance displays inclined bedsets, stacked en echelon that appear to onlap, or possibly downlap against, a surface that may represent a paleotopograhic high, resulting in very rapid seaward thinning to a feather edge. The high may represent the upthrown side of a down-to-the-west fault that was active during Ferron deposition. (A problem with this interpretation is that the thick represented by Kf-LC can be mapped as having a northwest-southeast trend based on limited subsurface data, whereas faults that formed along the eastern hinge of the foredeep would be expected to have a north-south orientation). An unusual dark brown coloration or staining at the base of the unit continues beyond its seaward pinchout and may represent the Washboard interval. No

Stratigraphic Unit	Stratigraphic Unit Name	Description
		contemporaneous channel deposits have yet been identified. Kf-Last Chance corresponds to the upper part of the "Hyatti sequence" of Gardner, 1993. Although we have no "hard data," we believe the unit is part of the Ferronensis sequence based on its position relative to organic-rich bed in the underlying Tununk Shale. Type locality: Limestone Cliffs at Last Chance Creek, NW1/4 section 9, T. 25 S., R. 5 E., SLBL. Landward limit: not known; may be covered by basalt of Fish Lake Plateau. Seaward limit: Limestone Cliffs, SW1/4SW1/4 section 3, T. 25 S., R.5 E., SLBL. Facies content of shorline unit: wave-dominated coast, possibly strand plain.
Kf-1	Kf-1 parasequence set of Ferron Sandstone Source: Ryer, 1981a, 1982a, 1982b	Kf-1 extends from outcrops south of Last Chance Creek to the southeastern side of "Cowboy Mesa" in the southern part of the Coal Cliffs. Its landward limit has not been accurately defined. Seven parasequences are presently recognized. The early parasequences tend to be wave-dominated while the later parasequences have a greater volume of fluvial-dominated facies. Although the control is limited in this set, shoreline orientations are generally northwest to southeast. The seaward pinchout of the set steps seaward about 14 miles (23 km) along the outcrop from the seaward pinchout of the underlying Kf-Last Chance set. The Sub-A coal zone belongs to Kf-1 and generally marks the top of the parasequence set. Only minor amounts of coal are contained in it, most of the coal occurring in the Last Chance area. The seaward limit of coal occurs in the upper half of the canyon of Quitchupah Creek.
Kf-1-Ls	Kf-1-Limestone Cliffs Source: new name	Kf-1-Ls is exposed on the north wall of Last Chance Creek. At Last Chance Creek, the unit is about 15 feet (5 m) thick and overlies the Kf-LC. Based on the style of the parasequences in this set, the landward pinchout of the unit is probably not too far to the south. The unit rapidly thickens to the north (seaward) as the underlying Kf-LC pinches out. Just south of "Killer Canyon" the unit reaches its maximum thickness of about 90 feet (27 m). On photomosaics the unit is dominated by horizontal beds in the upper quarter and en echelon and slightly sigmoidal seaward-inclined beds in the lower three-quarters of the unit. The lower contact with the Tununk Shale is abrupt, with little to no lower shoreface/transition heterolithics. The basal contact and shale below has a distinctive iron-stained brown color. The upper horizontal beds are dominantly sandstone with some interbeds of shale or siltstone. In most cases this upper unit appears to have an erosional lower contact. The seaward pinchout is a few hundred feet north of the cattle trail across the Limestone Cliffs in the SW1/4SE1/4 section 34, T. 24 S., R. 5 E., SLBL, with a minimum depositional dip distance from landward to seaward pinchout of 2.5 miles (4 km). A thin (< 5 feet [2 m]) bed of brown mudstone lies atop the marine sandstone. This brown mudstone is overlain by an equal thickness of black carbonaceous mudstone or coal (this outcrop has not been field checked), and is part of the Sub-A coal zone. Type locality: southern part of Limestone Cliffs, in the center of section 3, T. 25 S., R. 5 E., SLBL. Landward limit: south of Last Chance Creek, position not determined. Seaward limit: Limestone Cliffs, approximately SE1/4SE1/4 section 34, T. 24 S., T. 5 E., SLBL. Facies content of shoreline unit: wave-dominated coast but beginning to show minor wave-modified characteristics in the more distal portions of the outcrops.
Kf-1-Ms	Kf-1-Mussentuchit Source: new name	Kf-1-Ms is exposed for a short distance at the head of Mussentuchit Wash, along the Limestone Cliffs, near the cattle trail across the Limestone Cliffs in the SW1/4SE1/4 section 34, T. 24 S., R. 5 E., SLBL. The landward pinchout is not visible on the Limestone Cliffs because of laterally accreted channels which have scoured out the pinchout. The unit is mainly wave-dominated shoreface deposits and is recognized by its distinct upward-coarsening nature. The seaward pinchout of the unit is exposed in the cliff face in the SW1/4 section 35, T. 24 S, R. 5 E, SLBL. Its maximum exposed thickness is about 60 feet (18 m) in SE1/4SE1/4 section 34, T. 24 S., R. 5 E., SLBL. Approximating the landward pinchout, the overall progradation on outcrop is about 1 mile (1.6 km). Unlike the Kf-1-Ls parasequence in this

Stratigraphic Unit	Stratigraphic Unit Name	Description
		set, the Mussentuchit exhibits a gradual transition at the base of the sand into the underlying Tununk Shale. Type locality: southern part of Limestone Cliffs, along section line between sections 34 and 35, T. 24 S., R. 5 E., SLBL. Landward limit: head of Mussentuchit Wash and Limestone Cliffs, NW1/4NW1/4NW1/4 section 2, T. 25 S., R. 5 E., SLBL. Seaward limit: Limestone Cliffs, approximately SW1/4 section 35, T. 24 S., R. 5 E., SLBL. Facies content of shoreline unit: wave-dominated, with minor channel deposits cut into the top of the unit and interpreted as bay-fill related to flooding of the overlying parasequence.
Kf-1-IC-a	Kf-1-Indian Canyon-a parasequence Source: new name	Kf-1-IC-a is defined in the southern part of Indian Canyon, where the Ferron/Tununk contact reaches the canyon bottom. Only the seaward part of Kf-1-IC-a is exposed in Indian Canyon. The landward limits have been tentatively identified in the Limestone Cliffs and the exact nature of the landward pinchout is obscured by channels within a bay-fill. Although the Limestone Cliff exposures would constitute a better type section, Indian Canyon was chosen because of ease of access and because the relationships between units Kf-1-IC-a, b, and c are quite clear there. A shortcoming of using Indian Canyon as a type section for Kf-l-IC-a is that the unit lacks upper shoreface/foreshore facies in Indian Canyon. A thick, extensively burrowed middle shoreface in Indian Canyon indicates that it was deposited on a wave-dominated coastline. A full suite of shoreface facies are exposed along the Limestone Cliffs confirming the interpretation of wave-dominated shoreline. The seaward feather edge can be projected from the Limestone Cliffs through the subsurface to Indian Canyon and trends generally northwestward. The top of Kf-1-IC-a is cut by meanderbelt deposits belonging to late Kf-1-IC-c found in the Limestone Cliffs exposures. This parasequence of the Kf-1 parasequence set is longer in its dip length and does not exhibit the strong seaward inclination of beds in the shoreface units typical of the earlier two parasequences in the set. Type locality: Indian Canyon, NE1/4NW1/4 section 26, T. 24 S., R. 5 E., SLBL. Landward limit: Limestone Cliffs, SE1/4SE1/4 section 34, T. 24 S., R. 5 E., SLBL. Seaward limit: Indian Canyon, SW1/4SW1/4 section 24, T. 24 S., R. 5 E., SLBL; Limestone Cliffs, SE1/4 section 25, T. 24 S., R. 5 E., SLBL. Facies content of shoreline unit: Wave-dominated coast, probably strand plain. Begins to show signs of moving into a wave-modified facies in the Limestone Cliffs.
Kf-1-IC-b	Kf-1-Indian Canyon-b parasequence Source: new name	Kf-1-IC-b is defined in Indian Canyon at the south end of "The Wall." Landward and seaward limits of Kf-1-IC-b are defined in the Limestone Cliffs. The landward pinchout is not exposed in Indian Canyon; the seaward feather edge is poorly defined in northern part of Indian Canyon owing to similarity of facies content of Kf-1-IC-b and overlying Kf-1-IC-c. The landward most part of the transgressive surface of erosion between these two is a remarkably steep surface well exposed on the east side of Indian Canyon, opposite the south end of "The Wall." The unit is correlated to excellent exposures along the Limestone Cliffs where a "classic" landward pinchout with coastal plain facies above and below the marine sand is well exposed. The wave-dominated unit thickens gradually relative to the older parasequences in the set. Over 50 feet (15 m) of shoreface is exposed in the Limestone Cliffs about 0.25 miles (0.2 km) seaward of the landward pinchout. Distal-delta deposits are recognized in exposures at "Blue Flats Point" (SW1/4SE1/4 section 25, T. 24 S., R. 5 E., SLBL). Here the unit is less than 15 feet (3 m) thick and consists of a convolute bedded silty sandstone not far from its seaward pinchout. This unit cannot be traced on outcrop with confidence either north or south from "Blue Flats Point." Correlation confidence between Limestone Cliffs and Indian Canyon is poor. Type locality: Indian Canyon, east side, just beneath landward pinchout of the overlying Kf-1-IC-c, SW1/4SW1/4 section 24, T. 24 S., R. 5 E., SLBL. Landward limit: Limestone Cliffs, SE1/4 section 34, T. 24 S., R. 5 E., SLBL. Seaward limit: Indian Canyon, NE1/4 section 24, T. 24 S., R. 5 E., SLBL; Limestone Cliffs, C

Stratigraphic Unit	Stratigraphic Unit Name	Description
		section 25, T. 24 S., R 5 E., SLBL. Facies content of shoreline unit: wave-dominated coast, probably strand plain, some indications of transition toward wave-modified in the Limestone Cliffs near the seaward end of the unit.
Kf-1-IC-c	Kf-1-Indian Canyon-c parasequence Source: new name	Defined on the west side of Indian Canyon, Kf-1-IC-c is responsible for forming "The Wall." This unit has been informally divided into an early wave-dominated unit and a later fluvial-dominated unit or bedset. The wave-dominated facies extends from south end of "The Wall" in Indian Canyon northward into Willow Springs Wash, feathering out gradually just north of "Swell Point." Because the unit feathers out seaward so gradually, choosing an exact point on the map for its seaward limit is difficult and arbitrary. The landward pinchout is fairly well exposed on the east side of Indian Canyon, but has been cut out by a channel on the west side. On the Limestone Cliffs, the landward limit of the beach facies is obscured by channel cuts as well. A substantial bay or lagoon existed behind the wave-dominated shoreline unit, as made evident by mudstones bearing oyster shells in Indian Canyon and bay deposits along the Limestone Cliffs. A channel mouth or tidal-inlet deposit that cuts Kf-1-IC-c locally very near its landward pinchout probably connected this body of water with the sea. For over a mile its top is cut by meanderbelt deposits that belong to the younger fluvial-dominated unit (Kf-1-IC-c[d] see below) along outcrops of the Limestone Cliffs. A fluvial-dominated bedset of the Kf-1-IC-c is recognized in the North Fork of Indian Canyon and the northernmost part of "The Wall" in Indian Canyon has been designated Kf-1-IC-c[d] and is described below. Although clearly definable in the field, the boundary between the early wave-dominated Kf-1-IC-c and the late fluvial-dominated Kf-1-IC-c[d] bedset is not a transgressive or "marine-flooding" surface. But the two shoreline sandstone bodies are distinct and locally mappable. The fluvial-dominated delta progarded toward the northwest and represents delta-front deposits in a low-wave-energy setting. The change in depositional style marked by the contact between fluvial-dominated unit and underlying wave-dominated unit is the result of avulsion of a river sytem into the area and transformation of the wave-dominated, straight coastline into a protected bay into which a delta lobe subsequently prograded. At the mouth of Willow Springs Wash, the younger fluvial-dominated unit (Kf-1-IC-c[d]) is well exposed and about 15 feet (3 m) thick. At this location a thin wave-dominated unit is separated by about 15 feet (3 m) of marine shale from the overlying younger delta deposits. This thickening and change to wave-modified facies may indicate an end to the bay associated with the younger fluvial-dominated unit in Willow Springs Wash area. The seaward limit of the parasequence is about a half a mile north of "Corbula Gulch." Type locality: (wave-dominated unit) "The Wall" along the west side of Indian Canyon, SW1/4SW1/4 section 24, T. 24 S., R. 5 E., SLBL; (fluvial-dominated unit) mouth of the North Fork of Indian Canyon, north side, NW1/4NE1/4 section 24, T. 24 S., R. 5 E., SLBL. Landward limit: Limestone Cliffs, approximately SE1/4 section 35, T. 24 S., R. 5 E., SLBL. Seaward limit: north of Corbula Canyon, SW1/4 section 33, T. 23 S., R. 6 E., SLBL. Facies content of shoreline unit: wave-dominated coast, probably, strand plain to fluvial-dominated.
Kf-1-IC-c[d]	Kf-1-Indian Canyon-c[d] Bedset Source: new name	This mappable delta lobe develops out of the top of the Kf-1-IC-c parasequence at the north end of "The Wall" in Indian Canyon (see the above discussion of the Kf-1-IC-c). It is also present, though difficult to distinguish with certainty, on the cliffs east of the mouth of Indian Canyon ("Boot Point"). The "County Line Channel" studied so extensively by Mobil appears to belong to this younger bedset, by correlation of carbonaceous shales and a thin bed of coal within the Sub-A coal zone. Exposures of the unit in the Limestone Cliffs are all fluvial in nature and cut into the underlying shoreface of the wave-dominated Kf-1-IC-c. In Rock Canyon the bedset thickens to about 20 plus feet (6+ m) and gradually changes to more wave-modified facies. In this area the bedset represents the entire thickness of the parasequence. A facies change to a moderately thick wave-dominated unit takes place on the north side of Rock Canyon, where another unnamed bedset comes in on top of the Kf-1-IC-c[d]. In this same area of Rock Canyon the unit thins into the underlying Tununk Shale.

Stratigraphic Unit	Stratigraphic Unit Name	Description
		Type locality: (wave-dominated unit) "The Wall" along the west side of Indian Canyon, SW1/4SW1/4 section 24, T. 24 S., R. 5 E., SLBL; (fluvial-dominated unit) mouth of the North Fork of Indian Canyon, north side, NW1/4NE1/4 section 24, T. 24 S., R. 5 E., SLBL. Landward limit: Indian Canyon, approximately, SE1/4NW1/4 section 24, T. 24 S., R. 5 E., SLBL. Seaward limit: north of side of Rock Canyon, SW1/4 section 5, T. 24 S., R. 6 E., SLBL. Facies content of shoreline unit: began as fluvial-dominated and became wave-dominated coast, probably, strand plain in a seaward direction.
Kf-1-Iv	Kf-1-Ivie Creek parasequence Source: new name	Kf-1-Ivie Creek is a parasequence composed of numerous bedsets although only three are formally named. This parasequence has the most bedsets of any of the Ferron parasequences. Most of the seaward bedsets are fluvial-dominated. Kf-1-Iv derives its name from early work done in the Ivie Creek area near I-70. In subsequent regional work this parasequence is correlated to the south to its landward pinchout just south and west of "Swell Point." The parasequence would have taken its name from the locality near "Swell Point" had the parasequence not been previously named in the Ivie Creek area. Kf-1-Iv has a well-defined landward pinchout on the south-facing cliffs east of Coyote Basin, on the south side of "Swell Point." There, it splits the Sub-A coal zone, one split of carbonaceous mudstone passing below the transgressive surface, and the other passing onto the root-penetrated top of Kf-1-Iv. A tidal- channel deposit rich in oysters, some of which are in growth positions, cuts Kf-1-Iv near its pinchout. The seaward limit of Kf-1-Iv is in Quitchupah Canyon and on the east side of "Cowboy Mesa." The landward part of Kf-1-Iv is strongly wave-dominated. As the parasequence progrades several bedsets evolve and change to wave-modified from fluvial-dominated. A bedset of Kf-1-Iv is tentatively recognized in "Corbula Canyon," on the north side. Its landward edge is poorly defined and could use additional field work. At the mouth of " Corbula" a thick and laterally extensive distributary complex cuts into the older Kf-1-Iv[RC] bedset (see below) and is the chief component of the overlying and younger bedset. Near the landward edge of the unit it has wave-modified characteristics, but because it rapidly becomes fluvial-dominated to the north, with no apparent distinct bedding plane break, it is classified as fluvial-dominated. Bay deposits lie above this bedset and below the Sub-A coal zone. Near the seaward end of this unit, at the head of Blue Trail Canyon, clinoforms with steep inclinations are clearly visible within the unit. The north-south orientation of the outcrop lends itself to have both steep clinoforms and gentle seaward (northward) inclinations in the bedding of the bedset. This unit is found on the west side of Mesa Butte. On the south side of Mesa Butte, a tentative bedset boundary divides wave-dominated from fluvial-dominated facies. This bedset has not been named because its correlation is tentative. A bedset is tentatively defined along the long north-south exposures on the west side of Blue Trail Canyon. Here a bedding plane has been identified on photomosaics to differentiate this bedset from the underlying and unnamed bedset. Above this new bedset is the Ivie Creek[a] (Kf-1-Iv[a]) bedset (see explanation below). This fluvial-dominated unit is clearly gently inclined to the north or seaward along Blue Trail Canyon. Excellent exposures of slump features are found in the middle to northern portions of the canyon. The unit is probably present in exposures on Mesa Butte, to the east, but has not been properly correlated at this time. Above the Kf-1-Iv[c] bedset (see below) is an unnamed portion of the Kf-1-Iv parasequence. This portion extends from near the mouth of Quitchupah Canyon (on the east) into the upper reaches of the canyon where it is no longer exposed due to structural dip to the west. This unit laps onto Kf-1-Iv[c] and thickens rapidly on the west wall of Quitchupah. It represents a multi-cycle depositional event based on a dramatic split into two cycles exposed in the north face of "Cowboy Canyon" at the junction with Quitchupah. Facies are proximal to distal delta-front, representing the fluvial-dominated end member. Inclined clinoform architecture, similar to Kf-1-Iv[a] at Ivie Creek, is well exposed in upper Quitchupah Canyon.

Stratigraphic Unit	Stratigraphic Unit Name	Description
		The unit is capped by fossiliferous brackish-water bay deposits in exposed outcrops within Quitchupah Canyon. The unit thickens from south to north, indicating progradation in a northerly direction. Type Locality: south side of 'Swell Point," CSE1/4 section 8, T. 24 S., R. 6 E., SLBL. Landward limit: south side of "Swell Point," NW1/4SE1/4 section 8, T. 24 S., R. 6 E., SLBL. Seaward limit: north of "Cowboy Point" (S1/2 section 2, T. 23 S., R. 6 E.) and in the upper portion of Quitchupah Canyon. Facies content of shoreline unit: wave-dominated coast; proximal part probably strand plain changing to mainly fluvial-dominated with inclined clinoforms in the distal part.
Kf-1-Iv[RC]	Kf-1-Iv[Rock Canyon] Source: new name	Kf-1-Iv[Rc] is the oldest bedset in the parasequence and is defined by exposures between the landward pinchout of not only the bedset but the Kf-1-Iv parasequence and Rock Canyon. The Kf-1-Iv-[RC] begins as a well-developed wave-dominated unit and is about 45 feet (14 m) thick within a quarter mile of the landward pinchout, near "Swell Point." A large distributary complex occupies the top two-thirds of the unit on the north side of Rock Canyon near "Cut Gulch." From this point to its seaward pinchout the unit is wave-modified. The next overlying and unnamed bedset first appears in "Corbula Gulch." The Kf-1-Iv-[RC] is cut by this overlying bedset at the entrance to "Corbula Gulch" on the north side. The seaward limit of the unit is tentatively identified about 0.5 miles (0.8 km) north of "Corbula Gulch." Type locality: south side of "Swell Point," CSE1/4 section 8, T. 24 S., R. 6 E., SLBL. Landward limit: south side of "Swell Point," NW1/4SE1/4 8, T. 24 S., R. 6 E., SLBL. Seaward limit: north of "Corbula Gulch," S1/2 section 33, T. 23 S., R. 6 E., SLBL. Facies content of shoreline unit: wave-dominated coast; proximal part probably strand plain changing to mainly wave-modified in the distal part.
Kf-1-Iv[a]	Kf-1-Ivie Creek[a] a bedset of Kf-1-Iv Source: new name	Kf-l-Ivie Creek[a] is localized in the Ivie Creek-Quitchupah Canyon area. It has been referred to as Kf-l-Ivie Creek-a (Kf-1-Iv-a) in our early reports of the Ivie Creek case-study area and originally assigned a parasequence level. It is now recognized as a distinctly mappable unit, but without demonstratable evidence of a flooding surface, hence its subsequent classification as a bedset. Kf-1-Iv[a] is characterized by distinctive, steeply inclined clinoform surfaces in the Ivie Creek area (called the "amphitheater"). Mapping the clinoforms reveals an arcuate-shaped delta lobe, having prograded toward the south at the mouth of Blue Trail Canyon, toward the west in the "amphitheater area" north of Ivie Creek, and toward the north in the southern part of Quitchupah Canyon. The clinoforms disappear to the east, across the mouth of Quitchupah Canyon, but exactly how this occurs not clear. It is possible that the odd characteristics of Kf-1-Iv[a] can be attributed to its location at the flexure described for the Washboard-Clawson units. If this flexure marks the hinge of the foredeep, a sag of strata caused by movement of a basement fault, which may have brought about the deep-water bay into which Kf-1-Iv[a] prograded. Meanderbelts, from which its feeder channels came, are situated on the high side of the flexure (east). On the east side of Quitchupah Canyon, along "Cowboy Mesa," this unit is combined with the overlying bedset and mapped as the Kf-1-Iv parasequence. Type locality: amphitheater north of Ivie Creek, SW1/4NE1/4 section 16, T. 23 S., R. 6 E., SLBL. Landward limit: not clearly identified, occurs in mid-Blue Trail Canyon and south of the head of " Scabby Canyon." Seaward limit: west side of Quitchupah Canyon, SE1/4SE1/4 section 9, T. 23 S., R. 6 E., SLBL. Facies content of shoreline unit: fluvial dominated delta deposits.
Kf-1-Iv[c]	Kf-1-Ivie Creek[c] bedset of Kf-1-Iv Source: new name	Kf-1-Iv[c] is a bedset of the Kf-1-Iv parasequence. Early on in the case study work at Ivie Creek the unit was identified as a parasequence. With subsequent work no distinct stratigraphic rise and landward pinchout into continental facies has been identified and hence its designation as a bedset rather than a parasequence. It lies above the Kf-1-Iv[a] bedset with its landward most facies in "Scabby Canyon" and its seaward limit in mid-Quitchupah Canyon.

Stratigraphic Unit	Stratigraphic Unit Name	Description
		In the Ivie Creek area it is dominated by small channels which flowed across the top of fluvial-dominated deltas. These deposits can be correlated to more distal-delta deposits in Quitchupah Canyon, to the north. At the mouth of "Cowboy Canyon" bed boundaries are steeply dipping (10° to 15°) to the west, similar to the Kf-1-Iv[a] bedset at the Ivie Amphitheater. These relatively steep inclinations in major bed boundaries continue a short distance to the north in Quitchupah Canyon. This bedset is rather short in its distance from landward to seaward extent. In Ivie Canyon, this unit becomes the first progradation over the Tununk Shale as the underlying Kf-1-Iv[a] rapidly thins to the west. Excellent growth fault and slump features are exposed in the unit at the mouth of Ivie Canyon. In the Kf-1-Ivie Creek parasequence most of the seaward bedsets are characteristically fluvial-dominated, limited in lateral and dip direction, indicating a complex pattern of smaller delta progradations at the close of this major seaward step in the Ferron Sandstone. Type locality: amphitheater north of Ivie Creek, SW1/4NE1/4 section 16, T. 23 S., R. 6 E., SLBL. Landward limit: mid-'Scabby Canyon," westside, C section 21, T. 23 S., R. 6 E., SLBL. Seaward limit: west side of Quitchupah Canyon, SE1/4 section 9, T. 23 S., R. 6 E., SLBL. Facies content of shoreline unit: fluvial-dominated delta deposits.
Kf-1-CC	Kf-1-Cowboy Canyon Source: new name	The type section of Kf-1-CC parasequence is at the intersection of "Cowboy Canyon" (informal name) and Quitchupah Canyon (east side), at measured section TCC-940825-MS1. The parasequence extends to the south into bay deposits found in the Ivie Creek area and possibly beyond. Its marine correlative bay deposits can be traced on photomosaics to just short of the mouth of Quitchupah Canyon. This sandy brackish-water bay deposit gradually becomes more marine moving north through the canyon. The transition is more rapid on the east side of the canyon than the west, indicating a more north-northwest to south-southeast trend for the shoreline of this unit. On the east side of Quitchupah, the unit has a distinctive thin "white cap" with a thin dirty Sub-A coal above. The "white cap" continues into the upper reach of Quitchupah, as does the coaly zone above. The Sub-A coal zone is present on the west side of Quitchupah, but the distinctive white cap is only observable north of "Burn Canyon." This distinctive "white cap" and the overlying Sub-A coal has not been observed on the south or east sides of Cowboy Mesa. The correlation of this unit to the east on "Cowboy Mesa" is problematic and the unit has not been identified there. The facies of Kf-1 on Cowboy Mesa is fluvial-dominated delta. In Quitchupah, the 5- to 20-foot- (2-6-m-) thick wave-dominated cliff is generally sharp based, thickening to the north before plunging into the subsurface due to structural dip. In the upper portion of Quitchupah, this unit is directly on brackish-water siltstone of the Kf-1-Iv. This unit may represent a short pulse of transgression and associated regressive deposition, concluding bay to peat deposits. The top of this unit is the parasequence set boundary. Type section: mouth of "Cowboy Canyon," SE1/4 section 4, T. 23 S., R. 6 E., SLBL (TCC-940825-MS1, Anderson and others, in press). Landward limit: (gradational with brackish bay) south and west side of Quitchupah Canyon, NE1/4 section 9, T. 23 S., R. 6 E., SLBL. Seaward limit: unknown, outcrop ends in northern Quitchupah Canyon. Facies content of shoreline unit: wave-dominated.
Kf-2	Kf-2 parasequence set Source: Ryer, 1981a, 1982a, 1982b	Kf-2 is characterized by very complicated stratigraphy at the parasequence level. The parasequence set contains 9 parasequences. All but one are seaward stepping. The transgressive surface that marks the boundary between parasequences Kf-2-MC-a and Kf-2-MC-b is extensive enough that it might be justifiable to divide Kf-2 into two parasequence sets (Kf-2-early and Kf-2-late?) utilizing this surface. The associated A coal zone contains thick coal beds south of Willow Springs Wash and in the Quitchupah Canyon area. Much of the thickness of the C coal bed, originally assigned to Kf-3, has recently been determined to belong to the youngest part of Kf-2. The seaward limit of C coal deposition is in the Dry

Stratigraphic Unit	Stratigraphic Unit Name	Description
		Wash area, the lower split of the coal (previously referred to as A coal) extending somewhat farther than the upper split, which occurs in Kf-3. Considering the widespread distribution and substantial thickness of the main A and C coal seams, Kf-2 probably ranks as the most important coal-bearing parasequence set (or sets) of the Ferron. Kf-2 shoreline orientations are primarily north-south during the younger half of its progradational history. This is a departure from the more typical northwest-southeast orientation, but in the late parasequences of the set the orientation appears to come back to the more typical northwest-southeast alignment. The north-south orientation is well documented by several parasequences' landward and seaward pinchouts. Later parasequences in Kf-2 provide some indication of a return to a northwest-oriented shoreline but the evidence is more interpretive. Kf-2 shorelines are dominated by wave-influence rather than rivers. Shoreline types vary between wave-dominated and wave-modified. The tops of the shoreline deposits are commonly "cannibalized" by sand-rich meanderbelts and distributary complexes, but the coast was subject to sufficient wave-energy to rework the sediments. The extensive "cannibalization" of delta deposits brings the question of high-frequency sequence boundaries up for consideration. We have not identified lowstand shorelines in the Kf-2 that can be definitively connected to the channels cutting older shoreline deposits. In a couple of instances, carbonaceous shale is found at the base of isolated scoured channels. These deposits cannot be traced laterally any great distance and leave in question whether they are related to a relative sea-level drop or low accommodation and sediment by-pass. We have chosen not to place any sequence boundaries within this package of rocks although others have (Garrison and others, 1997). The landward pinchout of this set is exposed in only one place, on the north side of Willow Springs Wash in parasequence Kf-2-Ivie Creek-a. Thickening of the unit toward the northeast on to the point that lies north of the mouth of the wash occurs rapidly, surprisingly so since the amount of overall climbing of Kf-2 from here to where it passes beyond the seaward edge of Kf-1 is relatively small. The landward pinchout of the set is cut by a shale-filled channel, possibly of tidal origin. Kf-2 progrades seaward farther than any other parasequence set (31 miles [50 km] along the outcrop). The last parasequence of the set, Kf-2-Molen Seep Wash progrades to the end of the study area, near Ferron Creek. This parasequence's landward limits probably occur to the west and south, beneath the outcrop. At the seaward end of the parasequence set the facies are distal delta, the sandstone content is mixed about 50/50 with shale, and the thickness is on the order of 10 feet (3 m). Type locality: mouth of Willow Springs Wash, north side, CSE1/4 section 18, T. 24 S., R. 6 E., SLBL. Landward limit: mouth of Willow Springs Wash, north side, CSW1/4 section 18, T. 24 S., R. 6 E., SLBL. Seaward limit: Ferron Creek, section 34, T. 19 S., R. 8 E., SLBL. Facies content of shoreline unit: wave-dominated to wave-modified coast.
Kf-2-Iv-a	Kf-2-Ivie Creek-a parasequence Source: new name	Kf-2-Iv-a is distinguished in Ivie Creek. It is separated from overlying Kf-2-Iv-b by a "marine-flooding surface," which separates two vaguely upward-coarsening depositional sequences. Kf-2-Ivie Creek-a is correlated to the south all the way to the north side of Willow Spring Wash, near its mouth. The landward edge of Kf-2-Iv-a occurs in the same area, a short distance west of the mouth. The landward pinchout is cut by a shale-filled channel, possibly of tidal origin. The seaward extent of Kf-2-Iv-a is unusual and occurs as downlap onto the underlying Sub-A coal zone at "Hoodoo Point" and near the junction of Ivie Creek and Quitchupah Creek or "Junction Point." The downlap of this unit onto the top of Kf-1 is not clearly understood. This feature occurs in the area where the progradation orientation of the Kf-1-Iv[a] takes an unusual turn to the west and where the Kf-Washboard

Stratigraphic Unit	Stratigraphic Unit Name	Description
		thins to the west. Perhaps this feature is related to subtle motion on a deep seated fault, causing a slight rise in this area sufficient to create the down lapping relationship and end deposition of Kf-2-Iv-a. A similar relationship occurs in the overlying Kf-2-Iv-b in the Ivie Creek case-study area, although the rise was not sufficient to end deposition completely but simply created a local termination to bedsets. The two points of the seaward end and downlap define a new, almost north-south trend, in the shoreline of Kf-2-Iv-a. This orientation of the shoreline continues through early to middle Kf-2 time. Willow Springs, Coyote Basin, Rock Canyon, and Ivie to Cowboy Mesa all show west to east thickening in the Kf-2. Along the east-facing cliffs south of Coyote Basin, the top of Kf-2-Iv-a has been eroded and replaced by predominantly fine-grained deposits, some of which include "inclined heterolithics" indicative of channel deposition. This scour may be related to the aerially more restricted scour that occurs near the pinchout, or perhaps to a wider scour across the top of much of the Kf-2. Relationships here require more study. To the north, between "Swell Point" and Rock Canyon the unit takes on wave-modified characteristics. A distinct bedding break which can be traced along the outcrop has not been identified, therefore, at present, no new bedset has been defined for this change in facies. Another facies change can be tentatively mapped on the north side of the canyon, between Rock Canyon and "Overhang Point." Here a bedding surface has been identified but not field verified. Type locality: Ivie Creek Canyon, SE1/4 section 17, T. 23 S., R. 6 E., SLBL. Landward limit: mouth of Willow Springs Wash, north side, CSW1/4 section 18, T. 24 S., R. 6 E., SLBL. Seaward limit: near "Hoodoo Point" and near "Junction Point"; sections 16 and 34, T. 23 S., R. 6 E., SLBL. Facies content of shoreline unit: wave-dominated coast probably strand plain, with gradual changes to wave-modified, generally in the more easterly outcrops.
Kf-2-Iv-b	Kf-2-Ivie Creek-b Source: new name	Kf-2-Iv-b takes its name from the Ivie Creek area. No landward pinchout occurs in the type area, but correlation brings the unit into Coyote Basin - "Swell Point." Naming the unit prior to identifying its landward pinchout has displaced the unit's geographic name from its landward pinchout. The unit's landward pinchout is presumed to occur just west of "Swell Point." The pinchout is obscured by channels, which have eroded it, and poor exposures. Similar facies outcrop at Corbula Gulch, to the north, where the landward pinchout is presumed to lie just west of the exposures. The unit rapidly thickens as it approaches "Swell Point." At "Swell Point" Kf-2-Iv-a and Kf-2-Iv-b form an impressive cliff which has a thick upper shoreface and middle shoreface in the upper unit and a thick middle shoreface in the lower unit. These two shoreline units lie one above the other, sharing a contact that sometimes places middle shoreface on middle shoreface, making them essentially indistinguishable. Following the Kf-2-Iv-b towards Coyote Basin, the unit is complexly incised by two channel systems, one of which shows definite tidal influence. In this area most of the stratigraphic thickness of the unit consist of incised channel facies. The uppermost of the channels has a distinctive coarse-grain to gritty white sandstone. This channel system can be traced into the head of "Corbula Canyon" where Kf-2-Iv-b is again composed chiefly of stacked channels. Two landward pinchouts of the unit are mapped in Rock Canyon, about mid-canyon. Here shoreface sands pinchout into bay deposits associated with the flooding event. Connecting these points and the more tentative location near Coyote Basin produces a north-south trend for the shoreline. Between "Corbula Gulch" and "Hoodoo Point" the unit takes on an unusual character of thin bedded, with some shaley to silty interbeds, and a distinct increase in burrowing. The wave energy must have decreased and deposition slowed in this area. Along exposures on the south side of Mesa Butte this unit thins and almost pinches out just north of the "South Point" of Meas Butte. Moving north to Ivie Creek, the Kf-2- Iv-b is tentatively correlated across Quitchupah and around "Cowboy Point," where it feathers out into a thin tongue of Tununk Shale just above

Stratigraphic Unit	Stratigraphic Unit Name	Description
		the last remaining sands of the Kf-1 parasequence set. In the Ivie Creek area the unit consists of three tentatively identified bedsets. Each bedset is upward-coarsening and onlap the underlying parasequence set boundary. These stratal relationships are similar to the seaward pinchout of Kf-2-Iv-a. Similar interbedded and burrowed facies to those near "Hoodoo Point" are found in the "Ivie Creek Amphitheater" area in Kf-2-Iv-b, while in the road cut of I-70 and in outcrops in Ivie Creek Canyon the unit is composed of distributary-mouth-bar facies. Type locality: Ivie Creek Canyon, section 17, T. 23 S., R. 6 E., SLBL. Landward limit: near Coyote Basin on the south side of "Swell Point," SE1/4 section 7, T. 24 S., R. 6 E, SLBL. Seaward limit: just north of "Cowboy Point," approximately C1/4 section 11, T. 23 S., R. 6 E., SLBL. Facies content of shoreline unit: wave-dominated to wave-modified delta.
Kf-2-Iv-c and/or Kf-2-Mi-a	Kf-2-Ivie Creek-c Kf-2-Miller Canyon-a Source: new for Ivie Creek and Gustason and others, 1993 for Kf-2-Miller Canyon-a	The designation of two names for the same parasequence is unfortunate but temporarily unavoidable in our opinion. The type area of Kf-2-Iv-c is the mouth of Ivie Creek Canyon. Its equivalent, Kf-2-Mi-a, was described and named in earlier work (Gustason, and others, 1993) in the Muddy Canyon area. Kf-2-Iv-c is used in the Quitchupah-Ivie Creek canyons area and south to the pinchout. Kf-2-Mi-a is used from the mouth of Quitchupah Canyon, on the south end of "Cowboy Mesa" north to the seaward pinchout. This unit's landward pinchout is clearly recognizable both in Ivie Creek Canyon and to the south in the 1-70 road cut. Exposures southwest of "Hoodoo Point" are tentatively another point along the landward pinchout of this unit. At this location channeling in the underlying unit and at the same stratigraphic horizon obscures relationships. The facies pinching out are wave-modified distributary complex, certainly not as convincing as wave-dominated facies, and the maximum transgression of the shoreline was probably a quarter to half mile farther west. The pinchout of Kf-2-Iv-c near Ivie Creek trends just slightly west of north. Tying this trend to the "Hoodoo Point" area creates a bend to the east from the trend in Ivie Creek. Along the entire length of Blue Trail Canyon the top of the unit is composed of sandstone with inclined bedding to the north. Where the inclination angle is very low the sandstone top appears flat and distinct (near the head of the canyon), but as the inclination increases the top of the sand becomes indistinct and intertongues with muddy rocks that are overlain by the A coal zone. The sand is rooted, burrowed with *Ophiomorpha*, and bedding sets in the middle portion of the canyon are clearly laterally accreted from south to north. The base of this sand is erosional, but sometimes in the upper reaches of the canyon this sand body is disconformable with the underlying middle shoreface. At the mouth of Ivie Creek Canyon the shoreline sandstone unit displays some interesting and unusual characteristics, changing over about 300 feet (100 m) from a strongly wave-dominated shoreface unit to a much lower wave-energy unit which contains mud interbeds and finer sand, and is silvery-gray in color. This transition suggests a change from a coast directly facing the sea to one that was sheltered from wave energy or a bay environment. It can be speculated, however, that Kf-2-Mi-a represents the western margin of a major delta that provided the sheltering from wave energy (see below). The type area of Kf-2-Miller Canyon-a is the mouth of Miller Canyon. At this location only the distal portions of the wave-modified shoreline found farther to the south along "Cowboy Mesa" are exposed. In the "Tri-Canyon" area the boundary between this unit and overlying Kf-2-Mi-b is difficult to recognized in many places, but is very apparent where rotated slump blocks, which are generally restricted to Kf-2-Mi-a are present. The transgressive surface is perfectly apparent where it has beveled the tops of the rotated blocks, which are common enough to facilitate tracing the contact throughout the "Tri-Canyon" area. Its seaward feather-edge can be approximately located in Miller Canyon and in the lower part of Muddy Creek Canyon, near the "Upper Gooseneck." It has a general northeast trend, suggesting that

Stratigraphic Unit	Stratigraphic Unit Name	Description
		this parasequence built northeastward, probably as a deltaic lobe. The deltaic complex from which this lobe built may have provided shelter from wave energy noted for Kf-2-Iv-c. Rotated blocks occur in Kf-2-Mi-a in the Coal Cliffs south of Miller Canyon, in the lower part of Muddy Creek Canyon (Nix, 1999), and are particularly well exposed in "Grassy Canyon." A few are present on the east side of "Dino Head Point" on the western margin of the "Molen Amphitheater." Failure of the rotated blocks is consistently toward the northwest, the direction that the delta lobe appears to have prograded. The abundance of rotated blocks, which are relatively uncommon elsewhere in the Ferron, in the particular area may once again be related to a zone of flexure. Tilting toward the west may have encouraged failure of the delta-front. Type locality: Ivie Creek Canyon (Kf-2-Iv-c), NW1/4SE1/4 section 17, T. 23 S., R. 6 E., SLBL. Landward limit: Ivie Creek Canyon, C section 17, T. 23 S., R. 6 E., SLBL; 1-70 road cut, SW1/4NE1/4 section 20, T. 23 S., R. 6 E., SLBL. Seaward limit: Miller Canyon, NE1/4SW1/4 section 26, T. 22 S., R. 6 E., SLBL; Muddy Creek Canyon, E1/2NW1/4 section 24, T. 22 S., R. 6 E., SLBL. Facies content of shoreline unit: wave-dominated coast, probably shoreface in the proximal part, transforming to low-wave-energy coast, possibly bay shoreline in the east Ivie Creek and west Quitchupah Canyon area, and wave-modified in the "Cowboy Mesa to Tri-Canyon" area.
Kf-2-Mi-b	Kf-2-Miller Canyon-b	Kf-2-Mi-b includes the shoreline sandstone that forms the massive cliffs in the lower parts of Miller and Muddy Creek Canyons. It appears to be a very strongly wave-dominated unit. The landward pinchout of Kf-2-Mi-b has not been located on the outcrop because of erosion by channel deposits. The landward pinchout is tentatively placed along the east face of "Cowboy Mesa" near the section line between sections 2 and 11. Placement of the pinchout in this location means the overlying Kf-2-MC-a parasequence back stepped slightly, another indication this surface is of greater significance than simply a parasequence boundary (see discussion of Kf-2 above). Kf-2-Mi-b thins toward the northeast into "Grassy Canyon" and the "Molen Amphitheater," finally disappearing into marine shale in the southern part of Molen Reef along with overlying Kf-2-MC-a. In Muddy Creek Canyon, it is possible to subdivide Kf-2-Mi-b into two subunits bounded by a distinctive, northward-dipping surface. Both subunits are wave-dominated. The southern subunit, underlying and south of this surface, is moderately wave-dominated; the northern subunit, overlying and north of the surface, is very strongly wave-dominated, displaying unusually thick middle and upper shoreface intervals. The surface that separates these units could be a transgressive surface, but the overlying transgressive surface beneath Kf-2-MC-a has removed any direct evidence. In the absence of compelling evidence to the contrary, it is assumed the surface marks some change of autocyclic origin. Type locality: south side of Miller Canyon near its mouth. Landward limit: along the east face of "Cowboy Mesa," SW1/4SE1/4 section 2, T. 23 S., R. 6 E., SLBL. Seaward limit: Molen Reef, CSE1/4 section 29, T. 22 S., R. 7 E., SLBL. Facies content of shoreline unit: wave-dominated, probably strand plain in proximal part; may include deltaic deposits in medial and distal parts.
Kf-2-MC-a	Kf-2-Muddy Canyon-a Source: Gustason and others, 1993	In its type area Kf-2-Muddy Canyon-a forms ledges and lesser cliffs above the grander cliffs formed by Kf-2-Mi-b throughout most of the lower part of Muddy Creek Canyon and south slightly past "Bear Gulch." Three distinct landward pinchouts points are mapped. Two exposures are on the north and south sides of Meas Butte and a third is found at near the mouth of Quitchupah Canyon on the south side of "Cowboy Mesa." These points indicate the shoreline orientation was north-south. In the Muddy Creek Canyon area there can be no question that the surface that separates Kf-2-MC-a from the underlying Kf-2-Mi-b is a transgressive surface: it places offshore marine shale directly upon upper shoreface sandstone

Stratigraphic Unit	Stratigraphic Unit Name	Description
		and, locally, has planed off small channels within the top of Kf-2-Mi-b. In the this area most of the thickness of Kf-2-MC-a has been cut out by meanderbelt deposits. Although very sandy in some areas, much of the meanderbelt deposit consists of "inclined heterolithics." Two distinct meanderbelt units are distinguished on the basis of paleocurrent directions, the southern one being the younger of the two. At one locality on the west side of Muddy Creek Canyon north of the "Lower Gooseneck," the fluvial erosional surface rises to reveal a fluvial-dominated delta-front sequence. The meanderbelt deposits commonly contain grit-sized sand and broken oyster shell hash, and occasionally brackish -water fossils indicating marine/tidal influence. On the east side of "Dino Head," near the southern mouth of "Pinion Jay Valley," the meanderbelt deposit ends and the delta-front unit, only about 20 feet (6 m) in thickness, appears. It grades from marine mudstone at the base to predominantly sandstone in the upper part and can be traced continuously through the "Molen Amphitheater" to a point where it disappears into marine shale in the southern part of Molen Reef. In the southern exposures the unit is wave-dominated to wave-modified. At the landward pinchout the unit is wave-dominated. Type locality: Southern part of Muddy Creek Canyon, NW1/4SW1/4 section 24, T. 22 S., R. 6 E., SLBL. Landward limit: best exposed on Mesa Butte, near "West Point." Seaward limit: southern Molen Reef, NE1/4SE1/4 section 29, T. 22 S., R. 7 E, SLBL. Facies content of shoreline unit: Full range from wave-dominated to fluvial-dominated delta; fluvial-dominated in Muddy Creek Canyon probably represents a low-wave energy delta that prograded into a protected bay.
Kf-2-MC-b	Kf-2-Muddy Canyon-b Source: Gustason and others, 1993	Kf-2-Muddy Canyon-b was originally defined on the basis of a shoreline sandstone unit that has a distinctive white color found along the "Lower Reach" of Muddy Creek Canyon. The landward pinchout of Kf-2-MC-b occurs in the southern Coal Cliffs just north of "Bear Gulch," at the mouth of Miller Canyon, and is almost reached in the bend opposite the "Lower Gooseneck" in Muddy Creek Canyon. Two very well exposed and distinct landward pinchouts of wave-dominated facies are found on Mesa Butte, near the east side of the mesa. Near the pinchout in the "Tri-Canyon" area, the unit is characterized by large-scale, inclined surfaces that dip to the north, essentially parallel to the trend of the pinchout (that is strike of inclined surfaces is perpendicular to shoreline trend). The surfaces are interpreted to represent a series of tidal inlets that were driven northward by longshore drift. Equivalent flood-tidal delta and lagoonal deposits have been tentatively identified in Miller Canyon and "Bear Gulch." Kf-2-MC-b thickens rapidly eastward, attaining thicknesses in excess of 75 feet (23 m) in "Grassy Canyon." It extends eastward into Molen Reef, where it is a major cliff former, and northward to Dry Wash. From "Molen Point" northward along the Molen Reef a bedset boundary places wave-modified facies over the previous wave-dominated facies. Continuing north the unit changes character as is passes the Emery triangulation station. The marine portion of the unit begins to thin and the overlying non-marine section thickens. The thinnest section of the entire unit occurs near the center of section 21, T. 22 S., R. 7 E., SLBL. From this area to the north the entire unit begins to thicken again, but the non-marine portion thins. Marine section thickening is from addition at the top of the unit. It is in this setting that the next unnamed bedset is tentatively added. The Kf-2 outcrops in the Molen Reef cliffs south of Dry Wash include two distinct upward coarsening units. They appear to constitute distinct bedsets but no clear evidence has yet been found to demonstrate that the boundary between them is or is not a transgressive surface. Perhaps with additional work on the Molen Reef these two units will prove to be parasequences. The areal distribution of this unit is very large compared to most Ferron parasequences. Type locality: southern part of Muddy Creek Canyon, NW1/4SW1/4 section 24, T. 22 S., R. 6 E., SLBL. Landward limit: southern Coal Cliffs north of "Bear Gulch," CSE1/4 section 35, T. 22 S., R. 6 E., SLBL; mouth of Miller Canyon, NE1/4NE1/4 section 35, T. 22 S., R. 6 E., SLBL and SE1/4SE1/4 section 26, T. 22 S., R. 6 E., SLBL; Muddy Creek Canyon, SW1/4SE1/4 section

Stratigraphic Unit	Stratigraphic Unit Name	Description
		23, T. 22 S., R. 6 E., SLBL; Mesa Butte SW1/4 section 23, T. 23 S., R. 6 E., SLBL and NW1/4 section 35, T. 23 S., R. 6 E., SLBL. Seaward limit: just north of Dry Wash, NE1/4NE1/4 section 36, T. 21 S., R. 7 E., SLBL. Facies content of shoreline unit: wave-dominated coast in proximal part, probably strand plain; wave-modified to fluvial-dominated in the north.
Kf-2-DW	Kf-2-Dry Wash Source: new name	Kf-2-Dry Wash is defined on the basis of a shoreline sandstone unit whose landward pinchout crosses the northern edge of the cliffs of the Molen Reef south of Dry Wash and intercepts the cliffs on the north side of the wash, defining a northwest shoreline trend. The northwest shoreline trend represents a return to a more typical orientation for the Ferron. The pinchout is less distinct than most others, possibly because of development of a flood-tidal delta in this area. A large lagoon/bay complex lies landward of the pinchout and can be traced for several miles southward in the Molen Reef outcrops and westward to the limit of Kf-2 outcrops in Dry Wash. Exposures near the landward pinchout on the north side of Dry Wash are poor. The lagoon/bay unit is bracketed by splits of the lower A coal that under- and overlie it. The unit obtains a thickness of about 40 feet (12 m) between Dry Wash and Short Canyon with typical wave-dominated facies in the delta-front. The seaward limit is about 0.5 mile (0.8 km) north of the Short Canyon. Numerous channel deposits, including three large, lenticular channel bodies in Dry Wash and several in the Molen Reef cliffs appear to belong to Kf-2-DW. Type locality: cliffs north of Dry Wash, SW1/4 section 35, T. 21 S., R. 7 E., SLBL. Landward limit: Dry Wash, SW1/4 section 2, T. 22 S., R. 7 E., SLBL and SE1/4 section 34, T. 21 S, R. 7 E., SLBL. Seaward limit: about 0.5 mile (0.8 km) north of Short Canyon, SW1/4 section 18, T. 21 S., R. 8 E., SLBL. Facies content of shoreline unit: wave-dominated, probably strand plain in proximal part.
Kf-2-Ro	Kf-2-Rochester Source: new name	Kf-2-Rochester is named from a locality on the north side of Dry Wash, very near the landward pinchout of the Kf-2-DW. The pinchout of nearshore marine facies occurs in bay-fill deposits. Unlike some units in the Ferron, this one does not rapidly thicken. The unit thickens to about 40 feet (12 m) of shoreface between Dry Wash and Short Canyon. A few small channels cut the shoreface but the thickness and number is significantly less than more landward parasequences. From that point it gradually thins and its seaward pinchout is estimated to be just south of Yellow Seep Wash. Type locality: Cliffs north of Dry Wash, S1/2 section 35, T. 21 S., R. 7 E., SLBL. Landward limit: Dry Wash, SW1/4 section 35, T. 21 S., R. 7 E., SLBL. Seaward limit: about 0.25 mile (0.4 km) south of Yellow Seep Wash, section 8, T. 21 S. R. 8 E., SLBL. Facies content of shoreline unit: wave-dominated.
Kf-2-MSW	Kf-2-Molen Seep Wash Source: new name	Kf-2-Molen Seep Wash is named for exposures in Molen Seep Wash near to top of the Ferron. Its association with the Kf-2 is established by its stratigraphic position relative to a marker bed near the base of the Kf-3. At the head of Molen Seep Wash the outcrop consists of three possible parasequences. The lowest is believed to be the last of the Kf-2-Ro. The overlying two cycles belonging to Molen Seep Wash. This unit may be a small delta on the very northern edge of the "Last Chance Delta" of Cotter (1976). The unit is probably related to a swing to the west in the coastline of the Cretaceous Interior Seaway. The sand thick at the type section has not been directly correlated with parasequences to the south because of gaps in photomosaic coverage but possibly could be correlated with additional outcrop work. Kf-2-MSW is tentatively correlated with a sequence of rocks exposed in the Short Canyon area which lie above the marine Kf-2-Ro. The shallowest water facies in the most western part of Kf-2-MSW outcrop appear to be middle shoreface. The unit is probably wave-dominated to wave-modified but in the absence of more proximal outcrops the unit remains poorly understood. As the unit is traced on the north side of the wash only two cycles are present in mid-canyon, and at the mouth of the wash and the main Ferron outcrop only the top cycle continues toward Ferron Creek.

Stratigraphic Unit	Stratigraphic Unit Name	Description
		Type locality: Molen Seep Wash at top of Ferron Sandstone, SW1/4 section 6, T. 21 S., R. 8 E., SLBL. Landward limit: unknown Seaward limit: north of Dutch Flat, beyond the study area. Facies content of shoreline unit: proximal facies not exposed, probably wave-dominated.
Kf-3	Kf-3 parasequence set of the Ferron Sandstone Source: Ryer, 1981a, 1982a, 1982b	Shoreline sandstones of Kf-3 extend from the "Molen Amphitheater" northward beyond Dry Wash. At present, only two parasequences are distinguished. It is likely that one or more additional parasequences will eventually be defined in the northern part of the area of distribution of Kf-3. Much of the thickness of the C coal bed, previously considered part of Kf-3, has now been reassigned to Kf-2. The uppermost approximately 1 foot (0.3 m) of coal of the C bed, including the thick tonstein bed, extends over the top of Kf-3-MA near the mouth of "Gnat Canyon" in the "Molen Amphitheater." Coal below Kf-3-MA continues to the north. The youngest parasequences (shallow marine portion) of Kf-2 in the Dry Wash area pinchout into this part of the C coal. The C coal is complexly split in the Ivie Creek and I-70 area. The upper part of the seam likely correlates to Kf-3 age. With reassignment of most of the coal of the C zone to Kf-2, Kf-3 becomes one of the leanest parasequence sets in the Ferron with respect to its coal content.
Kf-3-MA	Kf-3-Molen Amphitheater Source: new name	The type area for Kf-3-MA is the large "Molen Amphitheater." The landward pinchout of Kf-3-MA is very well exposed on the cliffs just to the west of the mouth of "Gnat Canyon." This "classic" pinchout occurs in a bed, with about l foot (0.3 m) of coal passing above, and the remaining 6 to 7 feet (2 m) passing below. Only 100 feet (30 m) to the south, there is no trace of the unit within the C coal bed, which carries its full compliment of tonsteins. This is a remarkable situation. In the majority of cases, transgression of the sea across the Ferron coastal/delta plain led to formation of bays or lagoons that are preserved landward of the pinchouts of the subsequently deposited shoreline sandstones. A wedge-shaped deposit of mostly sandstone does occur to the northwest of this landward pinchout, on the east side of "Grassy Canyon" near its mouth. This could be bay-lagoonal deposits related to the Kf-3-MA, but needs further study. The sands are exposed for about 0.25 mile 0.4 km) along the outcrop at the base of the slope composed of marine shale to transition beds of the Kf-4-Mi parasequence and above the C coal zone. At the southwestern most exposure of the unit the beds have been slumped and contorted by some post-depositional event. This slumping has apparently also affected a small portion of the underlying Kf-2-MC-b unit below the coal zones. This is stratigraphically the highest known occurrence of slumping in the Ferron. In the case of Kf-3-MA, the transgressing shoreface cut into and partially eroded a mass of peat. The top of the peat must have lay far enough above sea level to preclude inundation southwest of the shoreline. Peat accumulation was only briefly interrupted, if at all, before progradation of the shoreline occurred. Several well-exposed, lenticular channel deposits filled with "inclined heterolithics" complicate the stratigraphy of Kf-3-MA in the vicinity of its landward pinchout. The shoreline orientation of this parasequence must be north-south. If the orientation were the more typical northwest-southeast the unit should outcrop in Muddy Canyon, but does not. Type locality: at mouth of "Gnat Canyon," NE1/4SW1/4 section 30, T. 22 S., R. 7 E., SLBL. Landward limit: just west of mouth of "Gnat Canyon": CSW1/4 section 30, T. 22 S., R. 7 E., SLBL. Seaward limit: between Dutch Flat and Ferron Creek, section 22, T. 20 S., R. 8 E., SLBL (this is for the Kf-3 undivided). Facies content of shoreline unit: wave-dominated, probably strand plain in proximal part; distal part may include deltaics.
Kf-3-MR	Kf-3-Molen Reef Source: new name	Kf-3-Molen Reef lies above Kf-3-MA in the "Molen Amphitheater," being separated from it by a thin zone of carbonaceous mudstone. The landward pinchout of Kf-3-MR occurs on the floor of "Gnat Canyon" and so is not exposed in the photomosaics, although its position can be determined to within 100 to 200 feet (30-60 m). Kf-3-MR is strongly wave-dominated in its landward part. As is true for Kf-3-MA, channels are numerous in the landward part of Kf-

Stratigraphic Unit	Stratigraphic Unit Name	Description
		3-MR. Kf-3-MA and Kf-3-MR merge to form the Kf-3 cliff along the Molen Reef, but the parasequences have not yet been distinguished there. The clear presence of two pinching wedges of shoreface sands into the C coal zone within a short stratigraphic interval demonstrates a gradual relative rise in sea level punctuated with occasional short but rapid rises. In this case we can demonstrate a flooding surface at the shoreline, but at present cannot trace the flooding surface seaward. Thus, the seaward extent of these two individual parasequences are not known. We have designated these two parasequences as simply the Kf-3 set beyond the Molen Amphitheater. In the Dry Wash to Molen Seep Wash area, the base of the Kf-3 is marked by a persistent and resistant sandstone bed, ranging from 1 to 3 feet (0.3-1 m) in thickness. The bed is generally hummocky cross-stratified and interpreted as a storm deposit. This bed is overlain by typical heterolithic lower shoreface or distal-deltaic deposits. In the Dry Wash area the bed lies atop a 3-foot- (1-m-) thick transgressive deposit. Type locality: "Molen Amphitheater," east of "Gnat Canyon," NE1/4 section 31, T. 22 S., R. 7 E., SLBL. Landward limit: at mouth of "Gnat Canyon," NE1/4SW1/4 section 30, T. 22 S., R. 7 E., SLBL. Seaward limit: not determined for the parasequence but the Kf-3 set pinches out just southeast of Molen, section 22, T. 20 S., R. 8 E., SLBL. Facies content of shoreline unit: wave-dominated coastline, probably strand plain, in proximal part; distal part includes fluvial-dominated deltaics.
Kf-4	Kf-4 parasequence set Source: Ryer, 1981a, 1982a, 1982b	Compared to the parasequence sets that preceded it, Kf-4 thickens very rapidly seaward, indicating a high rate of rise of relative sea level during its deposition. Two parasequences are recognizable, although a third may prove to be distinguishable in the "Fracture Canyon" area. The associated G coal zone only locally contains more than a few feet of coal, probably because peat accumulation could not keep up with the rapid relative rise of sea level that characterized this unit. Carbonaceous mudstones of the G coal zone have been mined to produce a soil conditioner, locally referred to by the trade name "Live Earth," for about 20 years in Miller Canyon.
Kf-4-Mi	Kf-4-Miller Canyon Source: new name	The type area of Kf-4-Mi is the mouth of Miller Canyon, where its shoreline sandstone body forms high cliffs. The landward pinchout of Kf-4-Mi occurs just south of "Bear Gulch," but is somewhat obscured because the upper part of the unit is replaced by a meanderbelt deposit. The meanderbelt deposit is very widespread, being recognized throughout the "Tri-Canyon" area and eastward into the "Molen Amphitheater." The meanderbelt deposit is also relatively coarse grained, being made up of medium- to coarse-grained sandstone that locally includes granules and, rarely, pebbles. One of the unique features of this parasequence is a transgressive deposit that lies just above the flooding surface in the "Tri-Canyon-Molen Amphitheater" and southern Molen Reef area. In most places it lies immediately above the C coal and is up to 8 to 10 feet (2-3 m) thick. The deposit consists of poorly sorted, "dirty" sandstone. It is generally rich in carbonaceous trash, probably the result of minor erosion on the top of the C coal. One easy access point to the deposit is along the Miller Canyon road, at an abandoned coal mine in the C coal. Here the transgressive deposit is about 8 feet (2 m) thick. At "Bear Gulch" the transgressive deposit has thinned to about a foot thick overlain by a 20-plus-foot (6-m+) thick, mainly upper shoreface sandstone. One-half mile (8 km) north the shoreface deposits are about 60 feet (18 m) thick, indicating a rapid relative sea-level rise. One mile (1.6 km) to the north at the mouth of Miller Canyon transition to lower shoreface facies sit atop the transgressive deposit and C coal. The northern limit of the transgressive deposit on the Molen Reef is in section 28, T. 22 S., R. 7 E., SLBL. The landward most part of Kf-4-Mi is strongly wave dominated and this is probably true of the unit as a whole, although it is difficult to tell with the upper part of the unit removed. The seaward limit of the parasequence lies just north of "Molen Point," making this parasequence short in dip length. Type locality: southern Coal Cliffs at the mouth of Miller Canyon, SE1/4SE1/4 section 26, T. 22 S., R. 6 E., SLBL.

Stratigraphic Unit	Stratigraphic Unit Name	Description
		Landward limit: in Coal Cliffs south of "Bear Gulch," SW1/4NE1/4 section 2, T. 23 S., R. 6 E., SLBL. Seaward limit: located about 0.75 mile (1.2 km) northeast of "Molen Point," SE1/4 section 29, T. 22 S., R. 7 E., SLBL. Basic facies content: wave-dominated shoreline--strand plain in proximal part to wave-dominated delta in distal part.
Kf-4-MR	Kf-4-Molen Reef Source: new name	Kf-4-MR is defined on the basis of a shoreline sandstone unit that forms a striking, white wall throughout the "Molen Amphitheater" area. The landward pinchout of Kf-4-MR is well exposed just west of the mouth of "Gnat Canyon," almost directly above the landward pinch-out of Kf-3-MA. Pronounced landward thinning toward the pinchout is also evident in "Pinion Jay Valley" and in the area north of "Molen Point." Kf-4-MR is wave dominated in its landward part. The more distal part, however, may include some lower wave-energy shoreline deposits, some of which may represent fluvial-dominated deltas. It may be that the latter constitute one or more additional, as yet undefined parasequences. The unit thickens rapidly from the landward pinchout and within a mile has become about 90 feet (27 m) thick with a full suite of facies from prodelta to foreshore. The first substantial incised channels into the top of the unit occurs on Molen Reef near the head of Bitter Seep Wash (NE1/4 section 21, T. 22 S., R. 7E., SLBL). In the upper portion of Quitchupah Canyon on the east side, a 4.4-foot-(1.3-m-) thick *Ophiomorpha* burrowed bed outcrops about 25 feet (7 m) stratigraphically above the C coal bed. This sandstone bed can be followed for about a 0.3 miles (0.5 km) in the canyon and is rooted on top and overlain by the G coal zone. Based on the presence of *Ophiomorpha* burrows the bed is interpreted as being marine or marginal marine. It may be a bay or lagoon deposit associated with the landward portion of Kf-4-MR. Similar beds have not been observed in the "Tri-Canyon" area, probably due to erosion by an extensive meanderbelt system at this approximate stratigraphic interval. Little was learned about the seaward end of this parasequence during the study because the unit has been removed by erosion from the face of the Molen Reef north of where "Fracture Canyon" drainage meets the Coal Cliffs (SW1/4 section 15, T. 22 S., R. 7 E., SLBL). Exposures of the unit from this area north to its seaward edge lie principally along the east side of "Fracture Canyon" and the top of the cuesta or dip slope. A thin sandstone bed above the Kf-3 and found at the head of Molen Seep Wash is believed to be the last expression of the unit before it grades to shale. Type locality: Molen Reef, SE1/4SW1/4 section 29, T. 22 S, R. 7 E., SLBL or along white, south-facing wall in "Molen Amphitheater," SE1/4SE1/4 section 30, T. 22 S., R. 7 E., SLBL. Landward limit: mouth of "Gnat Canyon," NE1/4SW1/4 section 30, T. 22 S., R. 7 E., SLBL. Seaward limit: tentatively just north of Molen Seep Wash section 6, T. 21 S., R. 8 E., SLBL; this is certainly the end of the parasequence set. Basic facies content: wave-dominated shoreline--strand plain in proximal part to wave-dominated delta in distal part.
Kf-5	Kf-5 parasequence set Source: Ryer, 1981a, 1982a, 1982b	Kf-5 thickens rapidly seaward from its landward limit in Muddy Creek Canyon. Its seaward feather edge lies in "Fracture Canyon" just south of Dry Wash. Kf-5 has, to date, defied division into parasequences. Almost everywhere, the upper part of the shoreline sandstone of Kf-5 has been cut out and replaced by meanderbelt deposits (among them the channel deposits so extensively studied by the Texas Bureau of Economic Geology in Muddy Creek Canyon, Grassy Valley, and "Cedar Canyon"). It should be noted, however, more emphasis was placed on parasequence sets 1 through 4 than on parasequence sets 5 through 8 during the DOE project. Other workers have broken out parasequences in these sets. The presence of the meanderbelt deposits preclude recognition of the landward pinchouts of any parasequences that Kf-5 contains. Most of the shoreline strata of Kf-5 appear to represent a wave-dominated coast. Kf-5 is relatively short in its exposed landward to seaward distance. It is only found north of "Molen Point" and south of Dry Wash. Based on the approximate position of the landward pinchout of Kf-5 and that of Kf-4, Kf-5 is slightly seaward, but represents a general trend of vertical stacking of parasequence sets. The I coal bed accumulated in a swamp, probably a "raised mire," that existed along the western margin of the Kf-5 meanderbelt that

Stratigraphic Unit	Stratigraphic Unit Name	Description
		trends northward to northeastward across Muddy Creek Canyon. Coal in the I coal zone reaches its maximum thickness in the area at and south of Christiansen Wash, where it combines with the overlying J coal to form a 30-foot (9-m) thick seam. Although the A and C coal zones probably include more coal because of their greater areal distributions, the I coal bed is the only one that has been mined on a large scale. The lower 20 feet (6 m) of coal has been extensively mined by conventional, room-and-pillar techniques at the Emery mine. The upper 10 feet (3 m) of coal, which tends to be higher in sulfur, has been left as roof. Consol estimates that about 100 million tons (100 million MT) of combined I-J coal is strippable in the area south of Emery. Carbonaceous mudstones of the I coal zone are being mined as "Live Earth" south of "Bear Gulch." Type locality: none. Considered to be a parasequence set at present. If Kf-5 is ultimately considered to constitute a single parasequence, a good type section would be the west side of Muddy Creek Canyon, NE1/4SW1/4 section 13, T. 22 S., R. 6 E., SLBL. Landward limit: Muddy Creek Canyon, somewhat obscured because of overlying meanderbelt, approximately C section 24, T. 22 S., R. 6 E., SLBL. Seaward limit: "Fracture Canyon," SW1/4 section 34, T. 21 S., R. 7 E., SLBL. Facies content of shoreline unit: wave-dominated.
Kf-6	Kf-6 parasequence set Source: Ryer, 1981a, 1982a, 1982b	Kf-6 extends from the upper part of Muddy Creek Canyon to Dry Wash. No parasequences are recognized at this time and it is likely that none will be. Contemporaneous channels are rare or absent and all of the shoreline strata of Kf-6 appear to have accumulated along a wave-dominated coast, probably a strand plain. Kf-6 is difficult to study in detail owing to the fact that it is generally exposed only on the lower part of the Molen dip slope and because outcrops are generally poor between the few significant canyons. Both the landward pinchout at the head of Muddy Creek Canyon and the seaward feather edge at Dry Wash, however, are particularly well displayed. Type locality: uppermost part of Muddy Creek Canyon, SE1/4NW1/4 section 13, T. 22 S., R. 6 E., SLBL. Landward limit: uppermost part of Muddy Creek Canyon, SE1/4NW1/4 section 13, T. 22 S., R. 6 E., SLBL. Seaward limit: Dry Wash, NE1/4NW1/4 section 34, T. 21 S., R. 7 E., SLBL. Facies content of shoreline unit: wave-dominated coastline, probably strand plain.
Kf-7	Kf-7 parasequence set Source: Ryer, 1981a, 1982a, 1982b	Kf-7 exposures are found primarily on the western edge of the dip slope. The landward limit of Kf-7 lies somewhere in the vicinity of Christiansen Wash, although it cannot be defined for lack of good outcrop and the fact that it has been cut out by a major meanderbelt deposit. It reaches a seaward feather edge in the northern part of Muddy Creek Canyon. No parasequences are presently distinguished and, because of outcrop limitation, it is likely that none will be. All well exposed parts of the shoreline unit of Kf-7 are of lower and middle shoreface strata. Dominance of hummocky-swaley cross-stratification and planar lamination coupled with moderate bioturbation point to a wave-dominated shoreline. Christiansen Wash demonstrates that a large river was actively feeding sediment to Kf-7 in the area between Christiansen Wash and Miller Canyon. Kf-7 represents a significant change in the stacking pattern from the previous three parasequence sets. It marks the point in the Ferron history when the relative rising sea level began to overtake the rate of sediment supply, resulting in landward-stepping shoreline units. Type locality: west side of Muddy Creek Canyon, NW1/4SW1/4 section 13, T. 22 S., R. 6 E., SLBL. Landward limit: cannot be determined owing to fluvial erosion, approximately at Christiansen Wash, NW1/4 section 33, T. 22 S., R. 6 E., SLBL. Seaward limit: upper part of Muddy Creek Canyon, SE1/4NW1/4 section 13, T. 22 S., R. 6 E., SLBL. Facies content of shoreline unit: wave-dominated.

Stratigraphic Unit	Stratigraphic Unit Name	Description
Kf-8	Kf-8-parasequence set Source: new name	Kf-8 is the stratigraphically highest progradational unit found in the study area. The unit is exposed between Quitchupah Creek, just south of the Browning Mine, and Coal Wash, at the top of the Ferron dip slope. Outcrops of the unit are generally less than 30 feet (9 m) thick and contain hummocky bedded sandstone, troughs with oyster hash (bored shells), and quartzite and carbonate clasts up to cobble size in the sandstone matrix. These deposits lie directly on top of the M coal. From outcrop work and examining coal drill-hole data just west of the outcrops, the unit appears to be lobate in shape, elongated in a east-west direction. Tentative dimensions of the lobe are about 1.5 miles (2.4 km) in depositional dip length and just over 2 miles (3 km) in strike length. The maximum thickness of the unit is found in the subsurface where it is 85 feet (26 m) thick on the east side of section 5, T. 23 S., R. 6 E., SLBL. The base of the unit is generally coarser than the top, indicating both fluvial and marine influences. The thickness of the unit is more erratic than older shoreline units. Differentiation of non-marine deposits from marine rocks are complicated by subsequent marine burrowing into underlying rocks associated with the transgression of the overlying Blue Gate sea. In the Coal Wash area the M coal is overlain by a 3-foot (1-m) thick, medium-grained sandstone bed that is burrowed by *Ophiomorpha* and other unidentified burrows. This sand is overlain by a darker brown sand which is coarser grained and contains abundant oyster shells and occasional coarse gravel clasts of quartzite and limestone. The underlying sand is probably non-marine in origin but the thin dark brown sandstone may represent the more landward portions of Kf-8 or a true transgressive lag deposited at the top of the Ferron as the Blue Gate sea transgressed. Type locality: west side of Quitchupah Canyon, near “Burn Canyon” SE1/4 section 5, T. 23 S., R. 6 E., SLBL. Landward limit: approximately at the south line of section 5, T. 23 S., R 6 E., SLBL, based on drill-hole data and limited outcrops. Seaward limit: poorly understood due to the nature of the outcrop, but probably not beyond the Browning Mine/Christensen Wash area; SW1/4 section 33, T. 22 S., R. 6 E., SLBL. Facies content of shoreline unit: wave-modified; the presence of large clasts at the base of the unit and the unusual facies arrangement indicate some fluvial influence. These large clasts are the source for some or all of the transgressive lag at the top of the Ferron Sandstone.

APPENDIX B
FIELD METHODS

Digital Measured Sections

Measured sections were recorded on a specially designed form for the project (table B-1). This form constrained the description of units to specific parameters but allowed for the input into graphical software and statistical manipulation of the data (see Chapter 9, Statistical Analysis, Ivie Creek Case-Study Area).

Table B-1. Sample measured section form.

Ferron Project Field ID _____ Location _____ Photomosaic frame # _____ Sub-Area _____
Began in: _____ Sheet ___ of ___

Rev. 3/95

Category	Unit	Unit	Unit	Unit	Unit	Unit
Unit Thickness						
1 Lith 1 %						
2 Modifier 1-1						
3 Modifier 1-2						
4 Lith 2 %						
5 Modifier 2-1						
6 Modifier 2-2						
7 Color						
8 Grain Size						
9 Component 1^						
10 Component 2^						
11 Induration						
12 Bed Size						
13 Unit Shape						
14 SedStruc 1 %^						
15 SedStruc 2 %^						
16 SedStruc 3 %^						
17 BioStruc 1 %^						
18 BioStruc 2 %^						
19 BioStruc 3%^						
20 Basal Surf						
21 DepoEnvirn						

Comments: Use brackets to mark text to be excluded from output section.
^Use position code

DOE Ferron Project Lithology Descriptions (use in order listed) - 3/19/95

1&3 Lithology/Prim.& Secon.	Code
coal	coa
conglomerate	con
sandstone	san
siltstone	sil
shale/mudstone	sha
claystone	cla
limestone	lim
dolostone	dol
breccia	bre
volcanic	vol
bone	bon
bentonite	ben
halite	hal
coquina	coq
gypsum	gyp
selenite	sel
anhydrite	anh
alluvium	all
no record	nor
covered	cov

2& 4 Modifier		Code
arkosic	ark	(Memo field)
bentonitic		ben
calcareous/limy		cal
conglomeratic		con
carbonaceous		car
lithic		lit
quartzitic		qua
sandy		san
silty		sil
shaly/muddy		sha
tufaceous		tuf
boney		bon
coaly		coa
fossiliferous		fos

5 Color	**6 Grain Size**	Code
	boulder	bou
	cobble	cob
	granule	gra
	granule to very coarse	gvc
	very coarse grained	vcg
	vc to coarse grained	vcc
	very coarse to medium	vcm
	coarse grained	coa
coarse to medium		cm
	coarse to fine	cof
	medium grained	med
	medium to fine	mfg
	medium to very fine	mvf
	fine grained	fin
	fine to very fine	fvf
	very fine grained	vfg

7 Component Code	Code
rip-up clasts-mud	rip
woody frags	woo
shell hash	she
"coffee grounds"	cof
shells	bod
concretions-calcareous	coc
" ironstone coi	second 5th
" pyrite	cop
plant fossils	pla
rip-up clasts - ironstone rii	

8, Straposition		Code
upper 5th		upp
middle		mid
lowest 5th		low
1,3,5 fifths		two
entire unit		thr
sec		ent
uth 5th	fou	
(Used for 13, 15, 17, 19, & 21)		

9 Induration	Code
Well cemented	wel
Well to moderately	wlm
Moderately cemented	mod
Moderately to friable	mfr
Friable	fri
thick to thinly	ttt
medium bedded .3-1'	med
medium to thinly .03-1'	mtn
thinly bedded .03-.3'	thn
thinly bedded to laminated	tnl
laminated <0.03'	lam

10 Bed Size (in feet)	
very thick > 3	ver
Very thick to thick	vtt
very thick to medium	vtm
thickly bedded 1-3'	thk
thickly to medium .3-3'	tkm

11 Unit Shape	Code
tabular	tab
wavy	wav
wedge	wed
irregular	irr
inclined inc	herringbone x-bedded her
lens	len

12-16 Internal Sed. Struc. %	Code
massive	mas
tabular x-bedding	tab
wedge x-bedding	wed
trough x-bedded	tro
hummocky x-stratified	hum
swaley x-stratified	swa
flaser bedding	fla
cross laminated	cro
ripple cross-laminated	rip
climbing symmetrical ripples	car
climbing asymmetrical ripples	car
planar/flat bedded	pla
horizontal bedded	hor
rhymites	ryt
convoluted/contorted	con
fluid escape bedding	flu
soft sed deformation	sof
sand dikes	san
wave ripples	wav
current ripples	cur
combined-flow ripples	cor
sigmoidal cross bedding	sig
irregular laminae	irr
reverse graded	rev

18-22 Biogenic Struc. %	Code
burrowing	bur
vertical burrows	ver
subhorizontal burrows	sub
horizontal burrows	hor
crawling traces	cra
grazing traces	gra
resting traces	res
rooting	roo
bored	bor
Ophiomorpha	Oh
Thalassinoides	The
Skolithos	Sco
Teichichnus	Tei
Cylindrichnus	Cyl
Arenicolites	Are
Rhizocorallium	Rhi
Terebellina	Ter
Chondrites	Cho
Planolites	Pla
Zoophycos	Zoo

24 Basal Surface	Code
erosional	ero
sharp	sha
irr gradational	gra

25 Depositional Environment	Code
Marine	mar
Non-marine	non
lacustrine	lac
coastal plain	coa
swamp/marsh	swa
eolian	eol
fan	fan
Marginal marine	mar
tidal	tid
high tidal flats	htf
mid-tidal flats	mtf
low tidal flats	ltf
inlets	inl
sand ridges	san
recurved spit	rec
estuarine	est
crevasse splay	cre
lagoon	lag
bay	
Distal bar	dib
pro meander-belt	meb
wash-over fan	was

25 Depositional Environment (cont)	Code
wave-dom. delta	
barrier bar	bar
beach dunes	bea
foreshore	for
upper shoreface	usf
middle shoreface	msf
lower shoreface	lsf
prodelta	pro
turbidite	tur
inner fan	inf
mid-fan	mif
outer fan	ouf
river-dom. delta	riv
delta-front	del
proximal delta-front	
distal delta-front	
Distributary mouth-bar	dmb
Bar crest	bac
abandoned-fill	aba

25 Depositional Environments (cont)		Code
ebb	tidal delta	etd
wav	Swash bar	swb
	Ebb shield esh	
	Ebb spit	ebs
	Delta plain dep	
Backshore	bsh	
	Offshore off	
Bouma sequence	bou	
	Submarine canyon fill	scf
	Back barrier bbr	
	Channel fill (sandy)	chf
	overbank deposits	ove
	braid bar brb	
	Channelized Flow	cha
pdf	point-bar	poi
ddf	anastomosed	ana
	levee lev	bay-fill
flood channel	flc	flood tidal delta flo
	flood ramp flr	Prodelta
	braided bra	
	crevasse splay cre	
	distributary channel	dic
	ebb channel ebc	

MEMO FIELDS:

5 Color **Bedding Plane Structures** **26 Fossils** **27 Comments** **28 References**

Photomosaics

Photomosaics were shot from the ground using 35 mm camera equipment and a telephoto lens. In the narrow portion of Ivie Creek the distance from one canyon wall to the other was too short to allow for the use of a telephoto lens. Normally this photography was shot from a point of approximate equal stratigraphic position from a vantage point on the opposite side of the canyon or cliff face and as perpendicular to the outcrop as possible. The camera position was frequently moved along the outcrop to minimize the angle and distortion of the photograph. Generally, ASA 200, color print film was used and the negatives were commercially scanned and converted to positive images onto a CD-Rom. The digital images were manipulated in a software program to reduce the file size and convert them to black and white. The black and white images were printed to paper for use in the field. The individual digital images were merged into photomosaics. The printed images were annotated in the field and the information transferred visually onto the digital mosaics.

Scaling

In the area of the Kf-1-Iv[a] bedset, for which detailed reservoir models were later developed, dimensional data needed to be determined at a high level of precision. To achieve this, a number of points were surveyed with a laser theodolite followed by reduction of the survey data to yield horizontal and vertical scales for the photomosaics. Elevation profile picks were positioned on the 7.5 minute topographic maps utilizing tie points on rock panels that were identified in the field. The horizontal control is shown as topographic tie points for the photomosaics (Anderson and others, 2000). Vertical scaling is shown on the photomosaics. Location of photomosaics, wells, measured sections, and permeability transects were marked on a summary base map (figure 7-3). The Kf-1-Iv[a] bedset outcrop location was marked and scaled on the base map using field-survey data. This effort included locating all measured points on photomosaics (approximately 200 points, spaced about 100 feet [30 m] apart) and converting these points to state plane X-Y coordinates. The scaled, photomosaic line work was scanned into a well-log digitizing package to produce scaled Ivie Creek reconstructions. Various units seen as open polygons on the reconstructions were closed for integration into the reservoir model. These survey data were reduced to develop x-y-z coordinates used in making the three-dimensional geologic model of the case-study area.

A less precise technique was developed to produce horizontal and vertical scales for photomosaics throughout the rest of the case-study area. Horizontal and vertical scales were produced using a 50-foot (15-m) nylon measuring tape. A 35-to 50-foot-(9-15-m-) thick interval (horizontal or vertical) was measured in the field and the endpoints were recorded on the photomosaics. Measured sections and permeability transects served as an additional vertical scaling device for the photomosaics. Scaled, line cross sections were developed from most of the photomosaics in the Ivie Creek case-study area.

APPENDIX C
RESERVOIR MODELING

Estimating the Effect of Bounding Layers on Grid-Block Anisotropy

A four-step process is used to crudely approximate the hydraulic impact of dipping, shaley bounding layers by computing a grid-block scale bulk permeability anisotropy. This process is based on the assumption that the sandy clinoform bodies discussed in previous sections were deposited in a system with radial geometry. Thus, the lower-permeability shaley drapes that often mark the boundaries between clinoform bodies likely impart a bulk anisotropy to the facies-based permeability structure with the direction of minimum permeability oriented in a radial direction parallel to depositional dip (figure C-1A). The direction of maximum permeability is assumed to be sub-parallel to the annular strike of the bounding layers (figure C-1A). These assumptions lead us to compute radial, annular, and vertical values of bulk permeability based on architectural and permeability data obtained from the Kf-Iv-1[a] bedset.

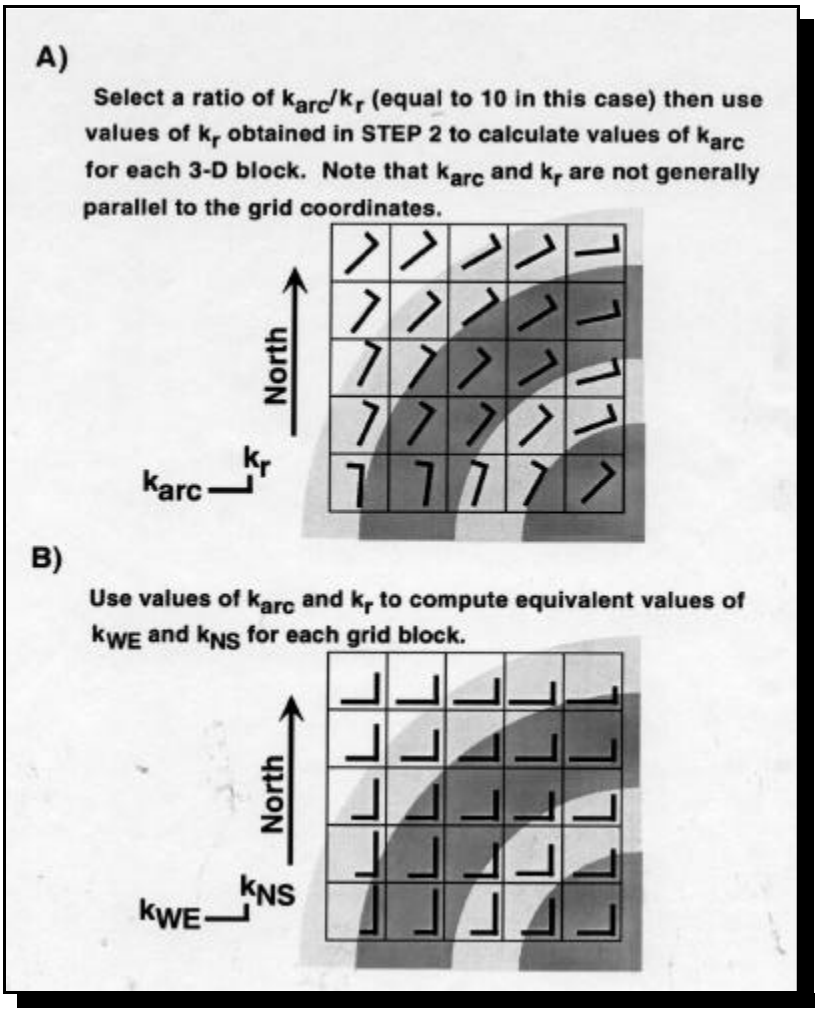
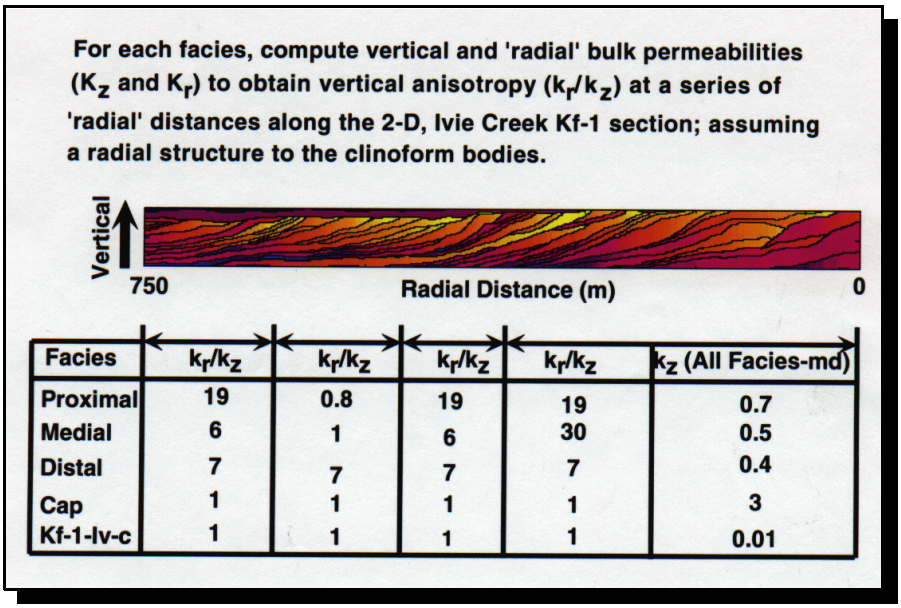


Figure C-1. A) Plan-view schematic showing the assumed orientation of the permeability tensor with respect to the geometry of the depositional system. B) Schematic computed permeability tensors used in 3-D simulations.

Step 1

Using the modeled permeability structure developed for the two-dimensional (2-D) waterflood simulations, vertical (k_z) and radial (k_r) values of bulk permeability are computed for each facies at a series of radial distances (figure C-2). Where the dip of the bounding layers is shallow, values of k_z are estimated using the harmonic mean of the k values identified along individual



Facies	k_r/k_z	k_r/k_z	k_r/k_z	k_r/k_z	k_z (All Facies-md)
Proximal	19	0.8	19	19	0.7
Medial	6	1	6	30	0.5
Distal	7	7	7	7	0.4
Cap	1	1	1	1	3
Kf-1-Iv-c	1	1	1	1	0.01

Figure C-2. Approach used to compute permeability tensor from the 2-D domain.

vertical transects within the modeled permeability structure. Corresponding values of k_r are estimated using the arithmetic mean of k values identified along individual horizons. In the more steeply dipping central region of the 2-D model domain (figure C-2), the harmonic mean of values calculated along both individual horizons and vertical transects yields values of k_r and k_z, respectively. The resulting values of k_z are remarkably uniform within each facies type. Thus, a single value of k_z is assigned to each facies while k_r varies as a function of radial distance from the southeast corner of the model domain.

Step 2

Once Step 1 is completed then values of k_z are distributed throughout the model domain according to the facies specified at each grid block. Knowing k_z, and given the ratios of k_r/k_z associated with each facies type at a specified grid location, values of k_r are computed and then assigned to each grid block. Note that both the clinoform cap and Kf-Iv-1[c] are assumed isotropic, thus k_r/k_z ratios are set equal to one.

Step 3

Values of k_r and k_z are assigned throughout the model domain in Step 2. Assigning values of k_{arc} (k in annular direction perpendicular to k_r), however, requires an estimate of the radial anisotropy ratio, k_{arc}/k_r. This ratio represents the enhancement of k_{arc} relative to k_r as a consequence of incorporating the lower permeability shaley drapes in the bulk permeability values associated with each facies type. Insufficient field-based information, however, is available to compute this ratio. For the example, considered in this report, a ratio of 10 is assumed to illustrate what may represent a relatively large value for k_{arc}/k_r. A schematic of the resulting pattern of permeability anisotropy is shown in plan view for uniform values of k_r and k_{arc} (figure C-1A).

Step 4

Because a five-point differencing scheme is used in the finite difference fluid-flow simulator, the permeability anisotropy derived in radial coordinates must be approximated using a rectangular coordinate system with principal axes of the permeability tensor aligned with the coordinate directions. Figure C-1B is a schematic of the pattern of permeability anisotropy (expressed in terms of k_{NS} and k_{WE}) obtained in plan view for the case shown in figure B-1A. Note that this approach yields k_{NS} equal to k_{WE} along the northwest-southeast diagonal of the model domain (figure C-1B).

Relative Permeability Relationships: 3-D Modeling

Both the Ferron and Berea Sandstones (Honarpour and others, 1986) are water-wet, consolidated porous media. In water-wet rocks, residual oil globules found in large pore spaces tend to block water flow and produce reduced values of relative water permeability, k_{rw}. The resulting k_{rw} vs water saturation (S_w) curve typically exhibits a fairly linear character. In water-wet rocks, however, oil-water relative permeability (k_{ow}) vs S_w curves show a more pronounced curvature. We expect a similar overall relative permeability character for the Ferron Sandstone and therefore use the Berea Sandstone as a proxy for computing plausible oil-water relative permeability relationships for the Ferron sandstone.

The Brooks-Corey relationships are used to compare brine-water relative permeability relationships for both Berea and Ferron Sandstones. Thus, both data sets are fitted using the following relations:

Eq. C-1 $k_{rw} = S_e^{(2+3ë)/ë}$

Eq. C-2 $k_{ro} = (1.0 - S_e)^2 (1.0 - S_e)^{(2+ë)/ë}$

where $S_e = (S_w - S_{wc}) / (1.0 - S_{wc})$ is effective saturation, S_w and S_{wc} are actual and residual (connate) water saturations, and k_{rw} and k_{ro} are relative water and oil permeabilities. In each case, a characteristic value is determined for the fitting parameter, ë. The fitting parameter ë is a measure of the linearity of relative permeability vs saturation curves described by the Brooks-Corey relations. The resulting ratio ($R = ë_{Ferron} / ë_{Berea}$) provides an approximate way to relate the properties of the two rock types. The ratio, R, and the oil-water-gas relative permeability data available for the Berea Sandstone with no gas saturation (Honarpour and others, 1986), are used to generate the Ferron Sandstone relative permeability relationships shown in table C-1.

When assigning relative permeability at block interfaces, a single-point upstream mobility weighting is used. The endpoint mobility ratio, M, for the Ferron Sandstone is defined as the ratio of k_{rw}/F_w to k_{ro}/F_o at residual oil and residual water saturations, respectively:

Eq. C-3 $M = [k_{rw} (\text{for } S_o = S_{ro})/F_w]/[k_{ro}(\text{for } S_w = S_{wc})/F_o] = (0.54/0.31)/(0.70/0.50) = 1.3$

where S_o and S_{ro} are actual and residual oil saturations and F_w and F_o are water and oil viscosities.

Table C-1. Relative permeability and water capillary pressure as a function of water saturation.

k_{rw}	k_{ro}	S_w	P_c (psi)
0.0	0.0	0.6990	2.52
0.1	0.0	0.6990	2.52
0.2	0.0000	0.6990	2.52
0.3	0.0004	0.6990	1.68
0.4	0.0067	0.4339	1.45
0.5	0.0337	0.2282	1.30
0.6	0.1066	0.0919	1.16
0.7	0.2603	0.0210	1.06
0.8	0.5398	0.0009	0.97
0.9	0.5398	0.0	0.87
1.0	0.5398	0.0	0.77

Water capillary pressure P_c (table C-1), or the difference in fluid pressure across the oil-water interface, is obtained from the standard water-wet relation provided by Honarpour and others (1986). In a water-wet reservoir a decrease in water saturation causes a corresponding increase in capillary pressure.

Fluid Properties

Fluid properties are assigned to match those used in the black oil simulations conducted for the Society of Petroleum Engineers Comparative Solution Project (Odeh, 1981).

Fluid Compressibility, Density, and Viscosity

Bulk fluid compressibilities (C_{bw} for water and C_{bo} for oil) are indirectly specified by via the ratio of formation volume factor to reservoir pressure (pounds per square inch [psi]) at the bubble point, P_b, associated with that fluid. At atmospheric pressure, fluid compressibilities for water ($C_w = 3 \times 10^{-6}$ psi^{-1}) and oil ($C_o = 1.5 \times 10^{-5}$ psi^{-1}) combined with formation volume factors for water ($V_w = 1.03$) and oil ($V_o = 1.5$) yield bulk fluid compressibilities for water and oil of -3×10^{-6} and -1×10^{-5}, respectively, where $C_{bw} = -C_w * V_w$ and $C_{bo} = -C_o * V_o$. The density of water and oil are specified as 62.14 and 45.0 (specific gravity = 0.72) lb-m/ft^3, respectively, at stock tank (atmospheric) pressure of 14.7 psia. Water viscosity is assigned a constant value of 0.31 centipoise (cP) while oil viscosity varies as a function of reservoir pressure (table C-2). Black oil viscosities shown in table C-2 vary approximately linearly with pressure. During the course of each simulation TETRAD3D continually updates fluid densities, fluid compressibilities, and oil viscosities to match prevailing fluid reservoir pressures.

Table C-2. Oil viscosity as a function of reservoir pressure.

Pressure (psia)	Oil Viscosity (cP)
14.7	1.040
264.7	0.975
514.7	0.910
1014.7	0.830
2014.7	0.695
2514.7	0.641
3014.7	0.594
4014.7	0.510
5014.7	0.449
9014.7	0.203

Pressure-Volume-Temperature Data

Pressure-volume-temperature (PVT) data relate the volume of oil produced at the ground surface to the volume that the oil occupied while contained in the reservoir. Because reservoir pressures are always maintained above the bubble point pressure, the simulated reservoir never encounters conditions where gas release would be computed. Thus, in the absence of a gas phase in our isothermal simulations, only the pressure-dependant variations in formation volume factors V_o and V_w, and in oil viscosity are required.

Oil and Water Formation Volume Factors vs Pressure

The oil and water formation volume factors (V_o and V_w) represent the way that oil or water expands or contracts while moving from *in situ* pressure conditions to atmospheric pressure at the ground surface. Because *in situ* pressures always exceed the bubble pressure for both oil and water, gas is not released and the fluids only expand during production. The variation in V_o and V_w as a function of reservoir pressure are shown in table C-3.

Table C-3. Oil and water formation volume factors as a function of pressure.

Pressure (psia)	V_o (bbl/stb)	V_w (bbl/stb)
14.7	1.062	1.0410
264.7	1.150	1.0403
514.7	1.207	1.0395
1014.7	1.295	1.0380
2014.7	1.435	1.0350
2514.7	1.500	1.0335
3014.7	1.565	1.0320
4014.7	1.695	1.0290
5014.7	1.827	1.0258
9014.7	2.357	1.0130

bbl/stb = barrels/stock tank barrel

3-D Gridded Data Set

The heterogeneous permeability structures used as input to the 3-D analog reservoir simulations are available in three electronic ASCII text files containing: (1) the isotropic Reference Case, (2) the isotropic Layered Case, and (3) the Anisotropic Case. The grid points represent the block-centered nodes of a 150,000 node finite difference grid with 100 nodes in the x and y directions and 15 nodes in the z direction. The grid origin (0, 0, 0) is located at the bottom, southwest corner of the model volume. Grid spacing is 4 feet (1.2 m) in the z direction and 20 feet (6 m) in the x and y directions. Thus, the node at the bottom southwest corner of the model volume is (10, 10, 2) and the node at the top northeast corner of the model volume is (1990, 1990, 58). The files are set up with 4-column format representing the x, y, and z coordinates and the corresponding permeability value. Porosity values that correspond to the permeability values contained in each file are readily computed for each node using the relationship outlined in the Chapter 8, Petrophysical Characteristics of the Ivie Creek Case-Study Area.